Relicensing Study 3.1.2

Northfield Mountain / Turners Falls Operations Impact on Existing Erosion and Potential Bank Instability Study Report

Volume II – Main Report

Northfield Mountain Pumped Storage Project (No. 2485) and Turners Falls Hydroelectric Project (No. 1889)

Prepared for:

FirstLight™ Power Resources

Prepared by:

Simons & associates

Cardno Shaping the Future

Gomez and Sullivan Engineers

Kit Choi, PhD, PE

APRIL 2017

PREFACE

On October 14, 2016, FirstLight Hydro Generating Company (FirstLight) filed the final report (Volumes I-III) for Study No. 3.1.2 *Northfield Mountain / Turners Falls Operations Impacts on Existing Erosion and Potential Bank Instability* (Study No. 3.1.2) with the Federal Energy Regulatory Commission (FERC, Commission). On December 15, 2016, various stakeholders filed comments on the report, which FirstLight responded to on January 17, 2017. As noted in FirstLight's responsiveness summary, and in response to comments received, FirstLight agreed to re-issue the final report for Study No. 3.1.2 by April 3, 2017.

The contents of this volume remain largely unchanged from the version filed in October 2016, with the following exception:

- **Sites BC1-R and 2L**: As a result of comments received from the stakeholders, FirstLight re-examined all BSTEM input data to ensure that the correct bank geometry was used for each detailed study site. During this review it was discovered that two sites (2L and BC1-R) used the incorrect bank geometry for both the Baseline and S1 (Northfield Mountain idle) scenarios; all other sites used the correct input data and were modeled correctly. In early 2017, BSTEM was re-run at both sites for both scenarios (Baseline and S1) using the correct riverbank geometry. The results of the corrected runs resulted in changes in the amount of erosion at each site, but not the cause(s) of erosion. As such, the findings of the study have not changed from the October 2016 report. Any discussion pertaining to sites BC1-R or 2L (including tables and figures) has been updated to reflect the findings of the corrected runs.

It should also be noted that the quality of images used in a number of sections was improved in response to stakeholder comments received. In the event that this occurred, the content of that section did not change, just the quality of the image.

TABLE OF CONTENTS

LIST OF TABLES

LIST OF FIGURES

LIST OF ABBREVIATIONS

BST	borehole shear-test
BSTEM	Bank Stability and Toe Erosion Model
c	Effective cohesion
ca	Apparent cohesion
cfs	cubic feet per second
cm	centimeter
CO_2	Carbon dioxide
Corps, The	US Army Corps of Engineers
CT	State of Connecticut
CRREL	Cold Regions Research and Engineering Laboratory
CRSEC	Connecticut River Streambank Erosion Committee
CRWC	Connecticut River Watershed Council
D	root diameter, in mm
DBH	diameter at breast height
d_{50}	median particle diameter
ECP	Erosion Control Plan
FCD	Franklin Conservation District
FEMA	Federal Emergency Management Agency
FERC	Federal Energy Regulatory Commission
FirstLight	FirstLight Hydro Generating Company
FIS	Flood Insurance Study
FOV	Field of View concept
FRCOG	Franklin Regional Council of Governments
FRR	Full River Reconnaissance
Fs	Factor of Safety
ft	feet
g	gram
GB	gigabyte
GIS	Geographic Information System
GPS	Global Positioning System
Gomez and Sullivan	Gomez and Sullivan Engineers, DPC
HEC	Hydraulic Engineering Center
HEC-RAS	Hydraulic Engineering Center- River Analysis System
(HYDROs	Laser In-situ Scattering Transmissometry HYDRO unit
Hz	hertz
ILP	Integrated Licensing Process
in	Inch

ISO-NE	Independent System Operator New England
k	erodibility coefficient
kPa	kilopascal
LCCLC	Landowners and Concerned Citizens for License Compliance
LiDAR	Light Detection and Ranging
LISST	Laser In-situ Scattering Transmissometry
m	meter
MA	State of Massachusetts
MADEP	Massachusetts Department of Environmental Protection
MassGIS	Massachusetts Geographic Information Systems Center
mi	mile
mm	milimeter
MPa	Megapascals
MTWT	Monday Tuesday Wednesday Thursday
MWH	megawatt hours
N	Newton
NAD	North American Datum
ND	Non-Detect
NDT	Northrop, Devine, and Tarbell
NEE	New England Environmental
NFM	Northfield Mountain Pumped Storage Project
NGVD	National Geodetic Vertical Datum
NH	State of New Hampshire
NHDES	New Hampshire Department of Environmental Services
NH GRANIT	New Hampshire Geographically Referenced Analysis and Information Transfer System
NMFS	National Marine Fisheries Service
NRCS	Natural Resources Conservation Service
OHWM	Ordinary High Water Mark
PAD	Pre-Application Document
PSP	Proposed Study Plan
QA	Quality Assurance
RMS	Root mean squared
RSP	Revised Study Plan
RTK	Real Time Kinematics
s	second
S&A	Simons and Associates
SD1	Scoping Document

SD2	Scoping Document 2
SPDL	Study Plan Determination Letter
SSC	Suspended Sediment Concentration
StreamSide	Laser In-situ Scattering Transmissometry StreamSide unit.
τ_c	critical shear stress
TFI	Turners Falls Impoundment
T_r	Root tensile strength
TSV	Total Survey Variance
USACE	US Army Corps of Engineers
USDA-ARS	U.S. Department of Agriculture - Agricultural Research Service
USGS	U.S. Geological Survey
WLOG	Wave logger
VT	State of Vermont
VY	Vermont Yankee Nuclear Power Plant
y	year

1 INTRODUCTION

FirstLight Hydro Generating Company (FirstLight) is the current licensee of the Northfield Mountain Pumped Storage Project (FERC No. 2485) and the Turners Falls Hydroelectric Project (FERC No. 1889). FirstLight has initiated the process of relicensing the two Projects with the Federal Energy Regulatory Commission (FERC, the Commission) using FERC's Integrated Licensing Process (ILP). The current licenses for Northfield Mountain and Turners Falls Projects were issued on May 14, 1968 and May 5, 1980, respectively, with both set to expire on April 30, 2018.

As part of the ILP, FERC conducted a public scoping process during which various resource issues were identified. On October 31, 2012, FirstLight filed its Pre-Application Document (PAD) and Notice of Intent with FERC. The PAD included FirstLight's preliminary list of proposed studies. On December 21, 2012, FERC issued Scoping Document 1 (SD1) and preliminarily identified resource issues and concerns. On January 30 and 31, 2013, FERC held scoping meetings for the two Projects. FERC issued Scoping Document 2 (SD2) on April 15, 2013.

FirstLight filed its Proposed Study Plan (PSP) on April 15, 2013 and, per the Commission regulations, held a PSP meeting at the Northfield Visitors Center on May 14, 2013. Thereafter, FirstLight held ten resource-specific study plan meetings to allow for more detailed discussions on each PSP and on studies not being proposed. On June 28, 2013, FirstLight filed with the Commission an Updated PSP to reflect further changes to the PSP based on comments received at the meetings. On or before July 15, 2013, stakeholders filed written comments on the Updated PSP. FirstLight filed a Revised Study Plan (RSP) on August 14, 2013 with FERC addressing stakeholder comments. Included in the RSP was Study No. 3.1.2 *Northfield Mountain/Turners Falls Operations Impacts on Existing Erosion and Potential Bank Instability* (Study No. 3.1.2 or Causation Study). The methodology and scope for Study No. 3.1.2 were approved with modifications by the Commission in its September 13, 2013 Study Plan Determination Letter (SPDL) (FERC, 2013). Those modifications included:

- FirstLight should include analysis of operational changes through the period 1999 to 2013 to identify any correlation between operational changes and observed changes in erosion rates;
- FirstLight should perform its historic geomorphic assessment using available mapping such as 1970 vintage ground survey of the impoundment;
- FirstLight should consult with stakeholders on transect site selection, and;
- FirstLight should employ the RIPROOT module of BSTEM to describe the erodibility of soils and banks;

On August 27, 2013, Entergy Corp. announced that the Vermont Yankee Nuclear Power Plant (VY), located on the downstream end of the Vernon Impoundment on the Connecticut River and upstream of the two Projects, would be closing no later than December 29, 2014. With the closure of VY, it was anticipated that certain environmental baseline conditions would change during the relicensing study period. In their September 13, 2013 SPDL, FERC approved many of the studies or approved them with FERC modification; however, due to the impending closure of VY, FERC did not act on 19 proposed or requested studies pertaining to aquatic resources. The SPDL for these 19 studies was deferred until after FERC held a technical meeting with stakeholders on November 25, 2013 regarding any necessary adjustments to the proposed and requested study designs and/or schedules due to the impending VY closure. FERC issued its second SPDL on the remaining 19 studies on February 21, 2014, approving the RSP with certain modifications. In addition, due to VY's closure and the resulting potential for the increased presence of ice in the Turners Falls Impoundment (TFI) (because of the change in thermal regime with VY closing),

FirstLight filed an addendum to the RSP for Study No. 3.1.2 on September 15, 2014 which detailed protocols for increased investigation of ice as a cause of erosion.

As stated in the RSP, the goals of Study No. 3.1.2 were to evaluate and identify the causes of erosion in the TFI and to determine to what extent they are related to Northfield Mountain and Turners Falls Project operations. In order to accomplish these goals the RSP (p. 3-25) included the following objectives:

- Conduct a thorough data gathering and literature review effort of existing relevant data to identify data gaps;
- Conduct field investigations and field data collection to fill data gaps. Gather the field data required to conduct detailed analyses of the causes of erosion and the forces that control them;
- Develop an understanding of the historic and modern geomorphology of the Connecticut River. A historic geomorphic assessment will be conducted to provide context for analyzing the modern geomorphology of the Connecticut River;
- Identify the causes of erosion present in the TFI, the forces associated with them, and their relative importance at a particular location. Conduct various data analyses to gain a better understanding of these causes and forces;
- Identify and establish fixed riverbank transects that will be representative of the range of riverbank features, characteristics, and conditions present in the TFI;
- Conduct detailed studies and analyses of erosion processes at the fixed riverbank transects;
- Evaluate the causes of erosion using field collected data and the results of the proposed data analyses. This evaluation will include quantifying and ranking all causes present at each fixed riverbank transect as well as in the TFI in general; and
- Develop a final report that will summarize the findings of this study and the methods used.

In order to achieve these objectives, the study methodology was divided into seven tasks:

- Task 1: Data Gathering and Literature Review;
- Task 2: Geomorphic Understanding of the Connecticut River;
- Task 3: Causes of Erosion;
- Task 4: Field Studies and Data Collection;
- Task 5: Data Analyses;
- Task 6: Evaluation of the Causes of Erosion; and
- Task 7: Report and Deliverables

In order to accomplish the goals and objectives of this study, FirstLight assembled a team of technical experts with global experience in the fields of geomorphology, hydrology and hydraulics, geotechnical engineering, water resources engineering, and environmental science. The team of experts included

personnel from: Simons & Associates (S&A), Cardno, The National Center for Computational Hydroscience at the University of Mississippi, and Gomez and Sullivan Engineers, DPC (Gomez and Sullivan). Field support was also provided by New England Environmental (NEE). Key team members included:

- Robert Simons, PhD, PE (S&A, Fluvial Geomorphologist and Hydraulic Engineer);
- Andrew Simon, PhD (Cardno, Fluvial Geomorphologist);
- Yavuz Ozeren, PhD, PE (National Center for Computational Hydroscience and Engineering at the University of Mississippi, Research Scientist);
- Kit Choi, PhD, PE (Geotechnical Engineer);
- Jennifer Hammond (Cardno, Project Engineer);
- Nick Danis, PE (Cardno, Project Engineer);
- Timothy Sullivan, GISP (Gomez and Sullivan, Regulatory Specialist); and
- John Hart (Gomez and Sullivan, Water Resources Engineer)

Thomas Sullivan, PE and Mark Wamser, PE (Gomez and Sullivan, Water Resources Engineers) also provided technical support. The team of professionals were approved by the Massachusetts Department of Environmental Protection (MADEP) in advance of the study commencing. Key personnel listed above have decades of experience on complex river systems around the world. In addition, Andrew Simon, along with his colleagues at the U.S. Department of Agriculture - Agricultural Research Service (USDA-ARS), was the original developer of the Bank Stability and Toe Erosion Model (BSTEM) used as part of this study. Bios for each key team member can be found in Volume III (Appendix A).

In accordance with RSP Task 1, during development of the RSP, and continuing after issuance of FERC's September 2013 SPDL, FirstLight conducted an in-depth literature review and data gathering effort which provided the foundation for this study and allowed for the identification of potential data gaps. Based on the literature and datasets gathered FirstLight was able to conduct a qualitative historic geomorphic assessment of the Connecticut River and TFI (RSP Task 2). The results of the historic assessment provided important context to the study as well as a better understanding of the various hydrologic, hydraulic, geotechnical, and geomorphic dynamics at play in the study reach. Additionally, as part of the initial data gathering and review effort, as well as during development of the RSP, FirstLight developed a list of the potential causes of erosion which may be present in the TFI (RSP Task 3). The preliminary list of potential causes presented in the RSP included (in no particular order):

- Hydraulic shear stress due to flowing water;
- Water level fluctuations due to hydropower operations;
- Boat waves;
- Wind waves;
- Land management practices and anthropogenic influences to the riparian zone;
- Animals;
- Seepage and piping;
- Freeze-thaw; and
- Ice or debris

Based on past experience conducting geomorphic assessments on the Connecticut River and other alluvial rivers, as well as from information gleaned from the preliminary investigation of existing documents and the FRR, the preliminary list of potential causes of erosion was then reviewed and divided in the RSP (p. 3-44) into two categories: 1) potential primary causes of erosion, and 2) potential secondary causes of erosion. From this, the following classifications were developed:

Potential Primary Causes of Erosion

- Hydraulic shear stress due to flowing water
- Water level fluctuations due to hydropower operations
- Boat waves
- Land management practices and anthropogenic influences
- Ice[1]

Potential Secondary Causes of Erosion

- Animals
- Wind waves
- Seepage and piping
- Freeze-thaw

The causes of erosion listed above formed the basis for RSP Tasks 4 (Field Studies and Data Collection), 5 (Data Analyses), and 6 (Evaluation of the Causes of Erosion). While all of these potential causes of erosion were investigated, special emphasis was placed on the potential primary causes of erosion, as discussed in the RSP. The potential primary causes of erosion, and the forces associated with them, were evaluated at a number of fixed riverbank transects located throughout the geographic extent of the TFI.

In accordance with the requirements of the RSP and FERC's SPDL, the fixed riverbank transects where the potential primary causes of erosion were investigated (also referred to as detailed study sites) were selected in collaboration with stakeholders and were presented in the report titled *Study No. 3.1.2 Northfield Mountain/Turners Falls Operations Impact on Existing Erosion and Bank Instability – Selection of Detailed Study Sites – September 2014* (FirstLight, 2014b).[2] Discussion pertaining to the final number of sites and their locations is also included later in this report. Stakeholders consulted during development of the final set of detailed study sites included: the Connecticut River Streambank Erosion Committee (CRSEC), Connecticut River Watershed Council (CRWC), Franklin Regional Council of Governments (FRCOG), Landowners and Concerned Citizens for License Compliance (LCCLC), National Marine Fisheries Service (NMFS), Massachusetts Riverways, and the Franklin Conservation District (FCD) as well as the Massachusetts Department of Environmental Protection (MADEP) and FERC.

Once the final list of detailed study sites was determined, various field data collection efforts were carried out during 2014, with supplemental field work conducted in 2015 and 2016 (ice monitoring). Field activities were conducted in accordance with Task 4 of the RSP as well as the Addendum to the RSP filed with FERC in September 2014.[3] Field data collection efforts are discussed in greater detail in Section 4 of this report. Field data were post processed and prepared for analysis or inclusion in various models throughout late 2014 and into 2015. Following the completion of the various field studies and data collection efforts, as well as completion of all post processing and QA, the field collected data were analyzed and model runs were executed throughout 2015 and into 2016 in accordance with RSP Tasks 5 and 6.

[1] Ice was originally classified in the RSP as a potential secondary cause of erosion, however, due to the closure of VY and the potential for the increased presence of ice in the TFI, and in accordance with the 2014 Addendum to Study 3.1.2 required by the SPDL, it was elevated to a potential primary cause of erosion in 2014.
[2] The *Selection of Detailed Study Sites* report was filed with FERC as part of the *Relicensing Study 3.1.2 Initial Study Report Summary* on September 15, 2014.
[3] The addendum to the RSP, or Ice Addendum, was filed with FERC as part of the *Relicensing Study 3.1.2 – Initial Study Report Summary* on September 15, 2014

The data analyses conducted for this study consisted of a mix of qualitative and quantitative methods based on RSP Tasks 2, 5, and 6 as well as RSP Table 3.1.2-3. Overall, data analyses followed a three-level approach consisting of:

1. Qualitative geomorphic analysis;
2. Quantitative engineering and geomorphic analysis; and
3. Computer modeling

This approach ensures a proper understanding of the physical processes governing bank processes along the reach through the hydraulic action, transport of sediment, river form and response, interaction with infrastructure and/or biologic aspects of riverine morphology or habitat. The three-level approach allows for cumulatively supportive, scientifically justifiable results to be obtained. Each subsequent level of analysis builds on the understanding developed by the previous level. The results of the various analyses discussed in Section 5 were then used to determine the cause(s) of erosion at each detailed study site. These results were then extrapolated throughout the study area resulting in detailed maps identifying the cause, or causes, of erosion at each riverbank segment within the TFI.

Each of the previously mentioned tasks which were identified in the RSP are discussed in greater detail in the ensuing sections and appendices of this report. This includes discussion of: the Geomorphic History of the Connecticut River (Section 2); the Potential Causes of Erosion (Section 3); Field Studies and Data Collection (Section 4); Data Analyses and Evaluation of the Causes of Erosion (Section 5); and a Summary Evaluation of the Causes of Erosion in the TFI (Section 6).

2 GEOMORPHIC UNDERSTANDING OF THE CONNECTICUT RIVER

RSP Task 2 calls for FirstLight to develop a geomorphic understanding of the Connecticut River to fully understand the various processes at work in the TFI. The RSP calls for this task to entail summarizing the historic and modern geomorphology of the Connecticut River, providing background information on the dynamic nature of alluvial rivers, discussing general characteristics of the drainage basin, and comparing the present state of various reaches of the Connecticut River, and/or tributaries, within the TFI. The RSP also requires that analysis and discussion of the historic geomorphology of the Connecticut River be conducted through the review of historic aerial imagery, topographic maps, photographs, surveys, plans, and/or archival studies and literature. Furthermore, in its September 13, 2013 SPDL, FERC recommended that FirstLight perform its historic geomorphic assessment using available mapping such as the 1970 vintage ground survey of the TFI as a base map, comparing it against more recent aerial imagery and available survey data to analyze trends in bank position within the TFI. The goal of the historic assessment was to provide context when discussing the modern geomorphology of the river.

The Connecticut River, which has a very small portion of its drainage area in Quebec, flows in a southerly direction from the Connecticut Lakes in northern New Hampshire, through western Massachusetts and central Connecticut, and into Long Island Sound (Figure 2-1). The river forms the border between New Hampshire and Vermont prior to it entering western Massachusetts. On its journey through New England, the river is impounded by 15 dams, some of which are equipped with hydropower facilities. A few of these dams create impoundments large enough to seasonally re-regulate[4] river flows. The majority of hydropower dams are low-head facilities forming narrow impoundments that experience generally lower water velocities at low flows due to raised water levels and velocities that approach near free-flowing conditions at high flows.

The Connecticut River was once a lake (Lake Hitchcock), formed after the ice melted at the end of the most recent ice age. This history affects current geomorphology and sediments that are found along the bed and banks of the river and is important to understand. The numerous flat terraces found along the Connecticut River were once deposits of fine sediment that settled in the bed of Lake Hitchcock. With the exception of rare segments (such as the French King Gorge located in the TFI), the Connecticut River is an alluvial river. Alluvial rivers consist of banks and bed materials that the river itself transports, deposits, or erodes. As such, alluvial rivers, by definition, are dynamic; thus various riverbank segments along the length of the Connecticut River are eroding as a result of its alluvial nature.

The reach of river extending approximately 20 miles from the Turners Falls Dam in Montague, MA to the Vernon Dam in Vernon, VT is also known as the TFI (Figure 2-2). FirstLight owns and operates the Turners Falls Hydroelectric Project while TransCanada owns and operates the Vernon Hydroelectric Project. The Turners Falls Dam, or a dam of different vintage, has been present at its current location since approximately 1798. The Turners Falls Dam was raised approximately six feet in 1970 during construction of the Northfield Mountain Project to accommodate additional storage volume for the operation of the Project without any significant increase of river flow in the Connecticut River downstream of the dam.

While this study specifically focuses on the TFI, for context it is important to understand the history and geomorphology of the entire Connecticut River, particularly the role of Vernon Dam which forms the upstream boundary of the TFI when discussing the dynamics of the TFI. Riverbank erosion has been a long-standing concern along the Connecticut River due to the proximity of infrastructure, farmland, property, and other valuable resources within the river corridor. Varying degrees of erosion in both free-flowing and

[4] Dams having sufficient storage capacity to store water during periods of high flow thereby reducing flood peaks for release during the low flow season.

impounded reaches of the Connecticut River have been documented over time. To provide context and a better understanding of the dynamics of both the Connecticut River and TFI, this section includes the following discussions:

- Geomorphology of Alluvial Rivers (Section 2.1);
- Geomorphic history of the Connecticut River (Section 2.2);
- Analysis of historic datasets (Section 2.3);
- Geomorphic analysis of tributaries and upland erosion features (Section 2.4);
- Erosion comparison of the TFI and Connecticut River (Section 2.5); and
- Summary of the Geomorphology of the Connecticut River (Section 2.6)

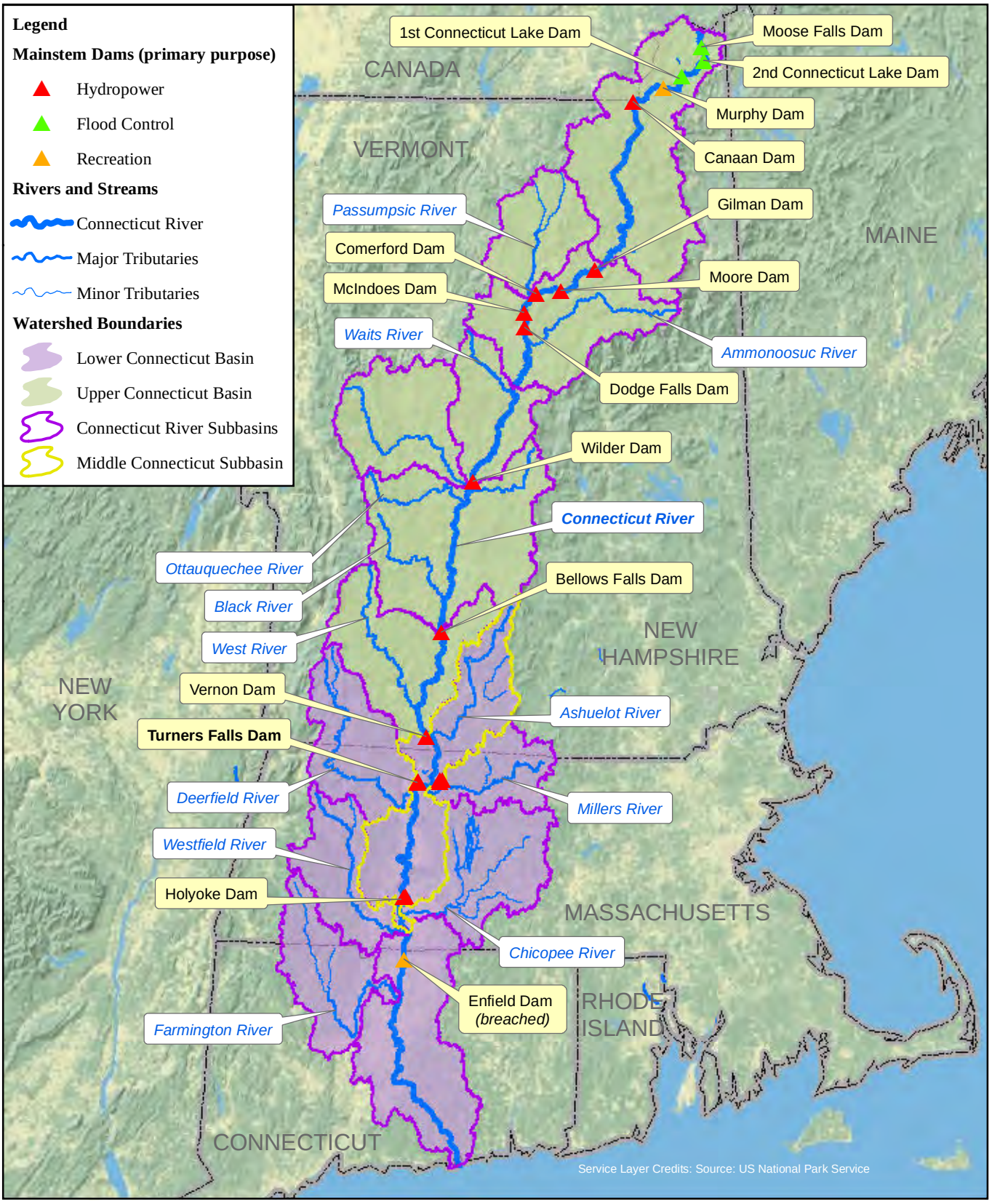

FIRSTLIGHT HYDRO GENERATING COMPANY
Northfield Mountain Pumped Storage Project No. 2485
Turners Falls Hydroelectric Project No. 1889

STUDY 3.1.2

FirstLight Power Resources

N

0 15 30 60 Miles

Figure 2-1
Connecticut River Watershed

Path: W:\gis\studies\3_1_2\maps\final_report\figure_2-1.mxd

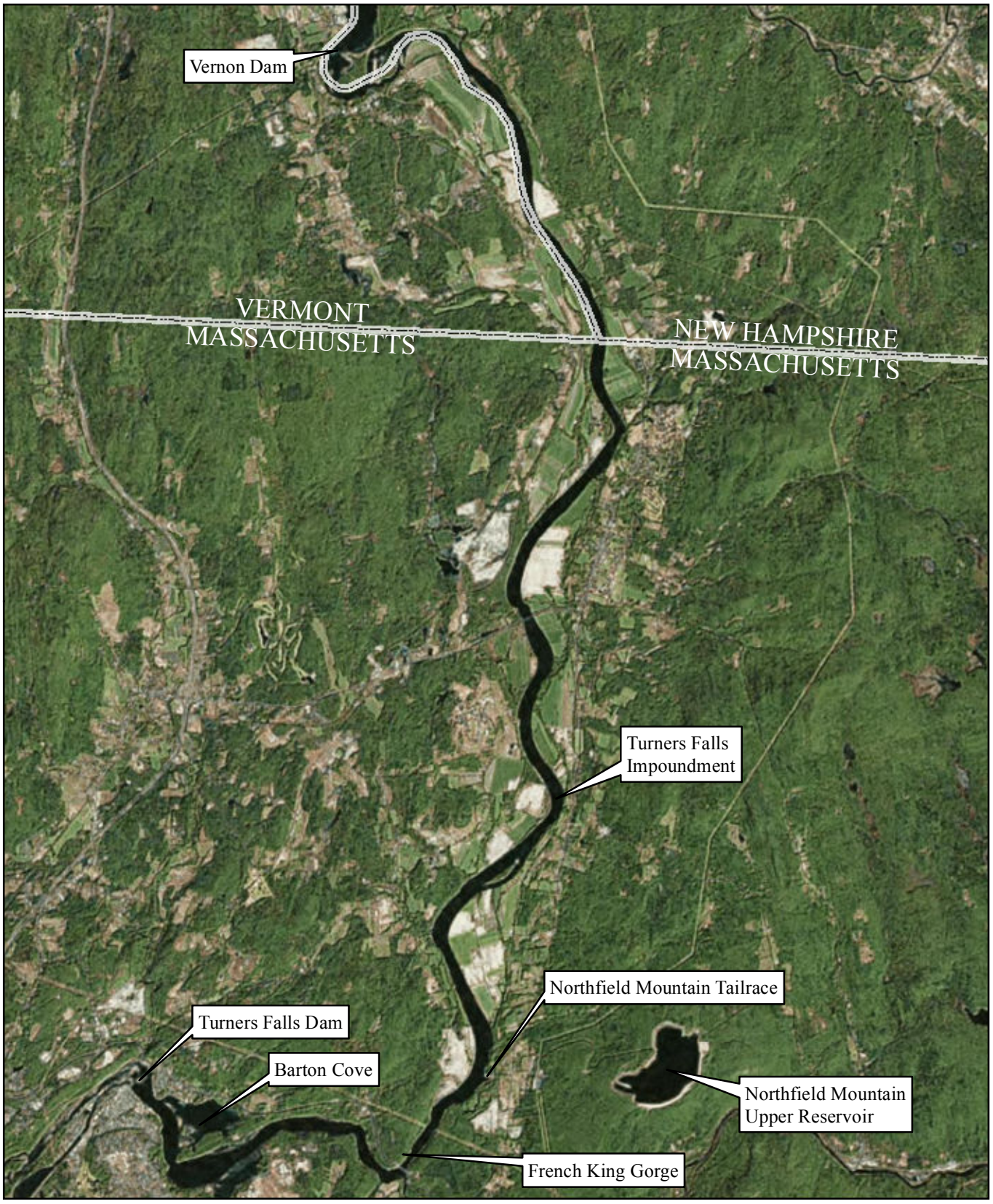

FIRSTLIGHT HYDRO GENERATING COMPANY
Northfield Mountain Pumped Storage Project No. 2485
Turners Falls Hydroelectric Project No. 1889

STUDY 3.1.2

FirstLight Power Resources

N

0 0.75 1.5 3
Miles

Figure 2-2:
Turners Falls Impoundment

Service Layer Credits: Source: Esri, DigitalGlobe, GeoEye, Earthstar Geographics, CNES/Airbus DS, USDA, USGS, AEX, Getmapping, Aerogrid, IGN, IGP, swisstopo, and the GIS User Community

Path: W:\gis\studies\3_1_2\maps\final_report\figure_2-2.mxd

2.1 Geomorphology of Alluvial Rivers

The Connecticut River, with the exception of rare segments, is an alluvial river that was formed following the last ice age. Prior to developing a geomorphic understanding of the river it is important to first understand the nature and geomorphology of alluvial rivers in general. The dynamic nature of alluvial rivers is described in one of the foremost and well-known textbooks, Fluvial Processes in Geomorphology (Leopold *et al*., 1964). Leopold, *et al*. discussed the continual adjustment of river systems by processes of aggradation, degradation, scour, deposition, lateral migration and bank erosion. Even the concept of a river in equilibrium does not mean that a river, so classified, is static and un-changing.

As noted by Leopold, *et al*., the concept of equilibrium in an idealized channel is based on the premise that a natural channel operates in a balance between its ability to transport sediment and the sediment delivered to it from upstream. The former is based on hydraulic characteristics such as stream power or flow energy that determine sediment-transport competence (a measure of the largest size that can be transported) and sediment-transport capacity (the amount of sediment that can be transported for a given flow). This implies that an alluvial stream not only carries sediment but also may entrain and deposit sediment depending on hydraulic characteristics of the flow and the boundary characteristics (shape and resistance) of the channel. If an alluvial stream has excess stream power relative to its sediment load, it will entrain (erode) sediment from its boundary. If it is transporting more sediment than the capacity for a given flow, it will deposit sediment. Erosion may be vertical or lateral and erosion of one bank may be accompanied by deposition on the other side of the channel, maintaining, on average, a relatively constant channel cross-section. Equilibrium does not mean that no erosion occurs but rather that an equilibrium between erosion and deposition is achieved. Based on this concept of equilibrium, the form of the cross-section may not be constant over time and the position of the channel may change, albeit at slow rates. Thus, the processes of erosion and deposition can be characteristics of an alluvial stream in equilibrium so long as the changes do not represent large, systematic adjustments over time and space. Changing position, even while retaining overall average channel geometry, necessarily means riverbank erosion occurs even in such channels that are considered to be in equilibrium.

The concept of the dynamic nature of rivers is confirmed in The Fluvial System (Schumm, 1977), which notes that while it would be convenient if a river were unchanging, an alluvial river generally is changing its position as a consequence of hydraulic forces acting on its bed and banks. Schumm further noted that archaeological, botanical, geological, and geomorphic evidence supports the conclusion that most rivers are subject to constant changes as a normal part of their morphologic evolution (Schumm, 1977; Simon, 1989). These adjustments occur over a variety of temporal and spatial scales ranging from a reach where a single flood hydrograph where scour may occur on the rising limb and deposition may occur on the receding limb, to long periods of time representing the evolution of a channel system.

In summary, as noted by some of the most renowned fluvial geomorphologists, even those river reaches considered to be in "equilibrium" can be expected to move laterally and adjust through processes that include riverbank erosion. Erosion is a natural process, even in channels in equilibrium that cannot and should not be totally controlled.

Examples of natural river dynamics can be found by looking at rivers in the National Parks where no significant development or regulation of rivers for hydropower, agriculture, water supply, navigation, or recreational powerboat use is typically found. Figures 2.1-1 through 2.1-3 show the effect of natural channel dynamics resulting in riverbank erosion on the Yellowstone River in Yellowstone National Park and the Middle Fork of the Flathead River in Glacier National Park. Numerous other examples can be found at National Parks throughout the U.S. It is clear that rivers without significant development and commercial or boat use, and which are protected from such uses, are not exempt from natural geomorphic processes including riverbank erosion. In fact, these rivers can display significant, dynamic geomorphic processes resulting in riverbank erosion. Geomorphic processes include erosion, accretion, lateral migration, avulsion

and shifting of meander bends. All of these natural processes occur in alluvial rivers of all types and sizes, regardless of whether they are found in completely natural settings without external influences or if they are affected by development and anthropogenic uses of various types.

Figure 2.1-1: Yellowstone River – Yellowstone National Park (a)

Figure 2.1-2: Yellowstone River – Yellowstone National Park (b)

Figure 2.1-3: Middle Fork of the Flathead River – Glacier National Park

2.2 Geomorphic History of the Connecticut River

The geomorphic history of the Connecticut River can be divided into two main periods, 1) the recent[5] geomorphic history, and 2) the modern geomorphology. The recent geomorphic history includes the major geomorphic events and processes which occurred approximately 20,000 years ago during and following the last ice age when the river was formed. The modern geomorphology encompasses the processes of the past several centuries when development began expanding throughout the watershed. Various geomorphic processes and events occurred during each of these time periods which continue to impact the Connecticut River watershed today. The geomorphic events and processes associated with these time periods are discussed in greater detail below.

2.2.1 Recent Geomorphic History of the Connecticut River

The Connecticut River has experienced significant changes over the last 20,000 years. During the most recent ice age (approximately 20,000 years ago), the Connecticut River valley was covered by the Laurentide Ice sheet. As the ice progressed to the south, it scraped and pushed rock and soil away from some areas and into mounds in other locations. Thus, the ice redistributed rock and soils throughout the area as well as compressing the underlying rock and soil. As the most recent ice age ended, the melting ice was trapped behind a natural dam which consisted of rock and soil that had been pushed up by the ice as it had advanced. The formation of a natural dam combined with the melting glacial water formed what is known as Lake Hitchcock (Figure 2.2.1-1).

Lake Hitchcock extended from about the middle of what is now the state of Connecticut (Rocky Hill, CT), through Massachusetts, northward through about 80% of Vermont and New Hampshire to St. Johnsbury, VT; a distance of about 200 miles ("Glacial Lake Hitchcock" by Tammy Marie Rittenour). The lateral margins of the lake were confined by the Green Mountains on the west and the White Mountains on the east. As the ice progressively melted northward, water in the lake rose over time creating a large pool of relatively quiescent water. The lake's water surface in the TFI area was likely more than 150 ft. higher than the current level of the Connecticut River; while the lake bottom was likely over 75 ft. higher (Field, 2007).

Glacial melt from the northern extent of the lake combined with inflow from various tributaries resulted in the transport of significant quantities of sediment. As this sediment reached the quieter downstream waters of the lake, velocities rapidly decreased along with sediment transport capacity. This resulted in sediment deposition along the bottom and sides of the lake. Coarser sediment would drop out first with progressively finer sediment making it somewhat further into the lake. Numerous deltas developed along the sides of the lake as well as a somewhat general deposit of finer materials along the bottom. As a result of these processes, the Connecticut River valley bottom is composed of a series of terraces stepping up from the river. As noted in Field, 2007, an example of these type of terrace surfaces is Moose Plain which is located in the vicinity of the TFI (Figure 2.2.1-2). While Moose Plain demonstrates the various terraces neatly along one transect, in most instances this is not the case.

Approximately 14,000 years ago the natural "dam" holding back Lake Hitchcock was broken and the lake began to drain ("Geologic History of the Connecticut River Valley near Greenfield, MA," Richard D. Little). The break was likely the result of instabilities in the natural dam combined with increasing pressure on the dam material. Once the lake began draining it likely eroded through the soil and loose rock until it reached more solid and less erodible rock below. The draining and downcutting of Lake Hitchcock formed what is now the Connecticut River. While some of the deposited lake sediment was probably eroded and transported downstream with the now flowing water, some of the relatively fine deposited sediment (clay, silt and sand) was left behind in the existing Connecticut River valley. Additional erosion and downcutting

[5] The term "recent" is being used in a long-term geomorphic context going back to the last ice age. This is considered recent compared to the numerous geologic ages that preceded this period of time over the life span of the earth.

occurred as the ground beneath the ice and water rebounded vertically from the decreasing load that no longer existed.

Through time the watershed became forested and "normal" riverine dynamic processes took over. As these previous and more dramatic changes faded into the past, geomorphic changes slowed and became less dramatic, however, typical alluvial river dynamics have and will continue. These dynamics are most pronounced in the previously deposited fine sediments that are erodible under normal riverine processes. The fine sediments (clay, silt, and sand) left behind by Lake Hitchcock are prevalent not only along the majority of the Connecticut River's banks but also throughout the TFI. As noted by Field (2007), most of the riverbank sediments in the TFI are naturally susceptible to erosion because, although they are fine grained, they do not contain much silt and clay which would impart additional resistance through cohesive strength into the materials. The sands and sandy loams are relatively erodible. Field (2007) further noted that natural stability is further compromised by past channel incision through older terrace and floodplain surfaces, leading to greater flow energy expended on the banks rather than having the ability to spread out across broad floodplains (Field, 2007).

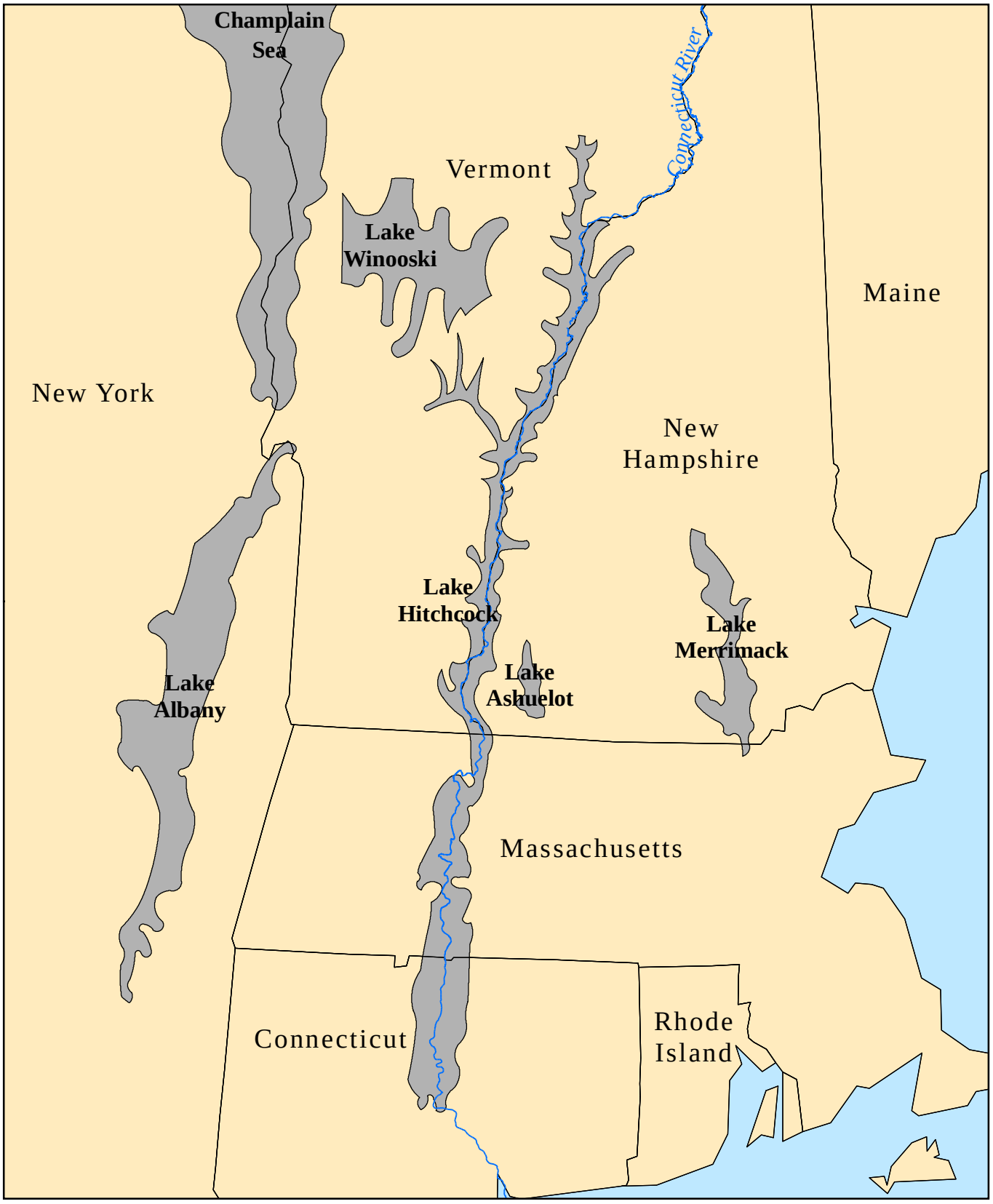

FIRSTLIGHT HYDRO GENERATING COMPANY
Northfield Mountain Pumped Storage Project No. 2485
Turners Falls Hydroelectric Project No. 1889

STUDY 3.1.2

Figure 2.2.1-1:
Lake Hitchcock

FirstLight Power Resources

N

0 15 30 60 Miles

Path: W:\gis\studies\3_1_2\maps\final_report\figure_2_2_1-1.mxd

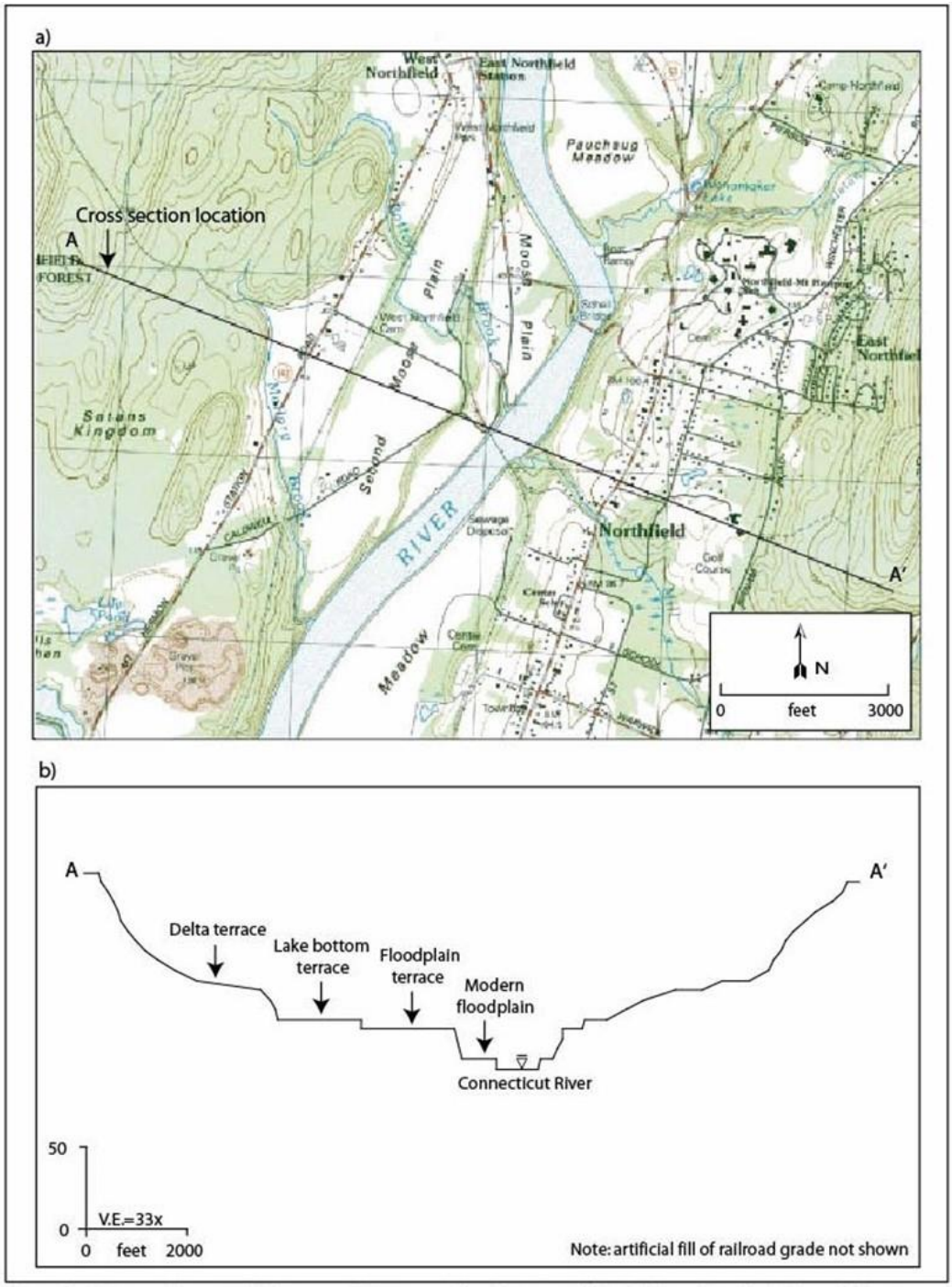

Figure 2.2.1-2: Moose Plain Terraces (Field, 2007)

2.2.2 Modern Geomorphology

In recent centuries, with the expansion of development in the region, the Connecticut River has been used as a means of transporting goods, water supply, waste disposal, recreation, and power generation. As part of this development, several dams were constructed on the Connecticut River for the primary purpose of hydropower production. Table 2.2.2-1 provides a list of the dams located on the Connecticut River. Most of these dams, with the exception of Murphy, Moore and Comerford Dams, are less than 60 feet in height and form relatively narrow, shallow impoundments upstream of the structures. The mainstem dams, and all dams in general, typically reduce the river velocity and trap sediment, the magnitude of which depends on the sediment transport capacity through the impoundment compared to the upstream sediment supply which determines the sediment trapping efficiency.

In addition to the mainstem dams, several United States Army Corps of Engineers (Corps or USACE) flood control dams have been constructed on larger tributaries to the Connecticut River. These facilities were constructed to reduce flood damages that had occurred historically (e.g., damages from the 1936 flood) by reducing peak flows to the Connecticut River and therefore reducing potential flood related damages. Since their construction, the flood control dams have generally been successful in reducing the historic impacts of flood events throughout the Connecticut River watershed, including reducing (but not eliminating) the erosive effects of peak flow events on riverbanks.

The modern geomorphology of the Connecticut River is typical of an alluvial river and is consistent with that described in Section 2.1. As expected of any alluvial river, the Connecticut River has continued to adjust over time through processes of aggradation, degradation, scour, deposition, lateral migration, and bank erosion. Episodic sediment deposition events have been known to occur in the river, such as was observed following Tropical Storm Irene in August 2011. Some sediment deposition also occurs as a result of the spring freshet or other similar high flow events. After such events, while some sediment remains, the river typically erodes some of this deposited material. Since the deposited sediment typically consists of suspended sediment which is fine material (clay, silt and sand), the Connecticut River has the ability to occasionally erode and transport some of this deposited sediment provided by upstream sources or tributaries, such that the overall trend of the river may appear to be more of erosion than deposition. The dynamic nature of the Connecticut River is evident by the fact that riverbank erosion occurs to one degree or another throughout its length in both free-flowing and impounded reaches. While there has been a very long-term tendency towards erosion along the river as the river incised through old lake deposits, it has essentially reached a state of dynamic equilibrium with base level controlled by areas of bedrock or armoring as well as dams along the mainstem.

Over the last several decades numerous studies have been conducted examining riverbank dynamics throughout the Connecticut River watershed as well as the TFI. These studies have ranged from historic analyses and comparisons and geomorphic assessments to hydraulic modeling and riverbank erosion surveys. To understand the modern geomorphology of the Connecticut River and TFI, several of these studies were reviewed and additional analyses were conducted when developing this report. The findings of these analyses are discussed in greater detail throughout the following sections of this report.

Table 2.2.2-1: Connecticut River Dams

Connecticut River Dam *(Upstream to Downstream)*	**Height (ft)**
Moose Falls Flowage	10
Second Connecticut Lake Dam	28
First Connecticut Lake Dam	56
Murphy Dam (Lake Francis)	106
Canaan Dam	27
Lyman Falls Dam	Breached
Wyoming Dam	Breached
Gilman Dam	40
Moore Dam	178
Comerford Dam	170
McIndoe Falls Dam	25
Dodge Falls Dam	28
Wilder Dam	39
Bellows Falls Dam	57
Vernon Dam	60
Turners Falls Dam	35
Holyoke Dam	30
Enfield Dam	Breached

2.3 Analysis of historic datasets

The geomorphic condition of the Connecticut River in general, and TFI specifically, can be further understood by examining available historic maps, aerial photographs, and surveys. Aerial photographs covering the TFI are available over a period of time extending from 1929 to 2014. These photographs provide an important historic perspective over this 80+ year period. Included in this time period were photographs taken along the TFI before and after the construction of the Northfield Mountain Project and associated raising of the Turners Falls Dam.[6] In addition to aerial photographs, historic maps going back over 100 years up through recent LiDAR (Light Detection and Ranging) mapping provide insight as to the recent and existing geomorphology of this section of the river.

Discussion, evaluation, and analysis of these sources of information is presented throughout this section. The purpose of this qualitative assessment is to provide context and important insight as to the condition of the Connecticut River and TFI historically and over recent decades. As such, this section includes the following discussions:

- Historic aerial photographs and maps – limitations (Section 2.3.1)
- Analysis of historic datasets – Connecticut River (Section 2.3.2)
- Analysis of historic datasets – Turners Falls Impoundment (Section 2.3.3)
- Analysis of the 20 erosion sites identified in the Erosion Control Plan (Section 2.3.4)

2.3.1 Historic aerial photographs and maps – limitations

While historic datasets such as aerial photographs and maps provide important historic context, valuable insights, and a better understanding of the geomorphic processes which have occurred over time, there are several significant limitations to comparing historic aerial photographs and maps to present ortho-photos which should be noted.

When mapping or taking aerial photographs over relatively large areas, it is recognized that the surface of the earth is curved while maps are a flat or plane representation of a curved surface. In addition, aerial photographs are taken from the lens of a camera that is vertically above one point on the ground or one small area of each of the photographs that are taken. As such, distortions are often present in the areas of the photograph that are taken farther away from that area that is directly below the camera. This is particularly true around the edges of the photograph depending on any tilt or angle of the line of view of the camera compared to vertical.

A georeferencing process is often utilized to adjust for some of these potential distortions and to bring all sources of information into a common datum. It is well understood that georeferencing or overlaying one mapping dataset onto another can be fraught with issues if not managed properly. One needs to understand how the datasets were compiled, what the resulting accuracies were and what the intended goal of the mapping was to successfully combine them and understand the limitations of the process. Even then the georeferencing process is subject to its own set of errors and accuracy limitations. Historic maps and aerial photographs are often georeferenced to survey data and common features found on more recent ortho-photos.

By their definition, ortho-photos have been reduced to a flat surface, provide a uniform map scale throughout their extent for a given accuracy, and provide a current, truly visual map source over a large

[6] Construction of the Northfield Mountain Project, including raising the Turners Falls Dam, occurred in the late 1960's and early 1970's. Commercial operation of the Northfield Mountain Project began in 1972.

extent. Ortho-photos used for this study typically had an accuracy of 6-10 feet (2-3 meters referenced in the source). When the overlaid dataset also happens to be reduced to a flat surface one can typically find a suitable translation, rotation and scale factor to overlay the mapping. Historic aerial photographs are often more problematic in that it is typically unclear as to how they were generated. Unlike the 2009 or 2014 State of Massachusetts Geographic Information Systems Center (MassGIS) ortho-photos, historic aerials have more than likely not had any rectification performed to correct distortions caused by camera orientation or terrain relief. The transformation of a simple aerial photograph is not as predictable and can be greatly assisted by other factors that confirm the transformation. In the case of the Connecticut River over the last 40 years, several large rock/boulder/bedrock shorelines exist where minimal movement is expected and therefore can be used to confirm the transformation. The results of georeferencing efforts conducted by FirstLight as part of this study typically yielded root-mean-squared (RMS) values less than +/-15 ft.

Other factors to consider when comparing datasets from different vintages is that the top of the riverbank may or may not be well defined and may be difficult to discern from aerial or ortho-photos. At some locations, the top of bank may be a flat terrace whereas the riverbank is steeply sloping so there is an abrupt break in topography. At other locations, a riverbank may just be part of a hillslope that continues sloping upwards, well beyond any limit of high water without any break in topography. In addition, many riverbank areas are densely vegetated so both visibility and topographic accuracy is limited. As a result, determining the historic location of the river often focuses on identifying the edge of the river/water interface.

Although determining the historic position of the river by identifying the edge-of-water is easier than identifying the top of bank, it is not without its own accuracy limitations. Without knowing the specific time and date when each image is taken, the water levels and river conditions are often unknown. Due to varying water levels the question arises as to whether any measured change in river position is due to an actual change in the bank or simply due to the difference in water level. Water levels may change from day to day or even hour to hour while the aerial photographs are being taken; thus, water level conditions may not be consistent within a single set of images. Furthermore, when comparing aerial photographs or edge-of-water datasets from before and after the Turners Falls Dam was raised in 1970, the approximately 6 foot rise in TFI water level would have to be accounted for. Given this, comparing edge-of-water locations from year to year or decade to decade would likely not yield useful or accurate results.

Due to these considerations, if observed changes in river position are within the accuracy limits of the dataset quantitative determinations are not meaningful. To determine if significant changes in riverbank position have actually occurred, the observed change (whether real or perceived) must be of a significant magnitude greater than the accuracy limits of the data. Given that the accuracy limits of the data can be 30 to 40 feet or more depending on their quality, it is often only appropriate to conduct qualitative geomorphic comparison's using historic aerial photographs or maps to provide context or to determine general trends.

As a result of the limitations discussed above, the analysis of historic aerial photographs and maps discussed throughout this report will be limited to a qualitative assessment focused on general geomorphic trends and observations throughout the Connecticut River watershed and TFI. The results of this qualitative assessment provide context in regard to the modern geomorphology of the study area.

2.3.2 Analysis of historic datasets – Connecticut River

In *"Riverbank Erosion on the Connecticut River at Gill, Massachusetts: its Causes and its Timing"* (Reid, 1990) historic maps and datasets from the late 1800's and early to mid-1900's were analyzed to determine geomorphic changes over time. Specifically, this analysis compared historic maps and aerial photographs at several locations along the river.

In the vicinity of Northampton, MA an 1831 map was compared to a 1958 aerial photograph which demonstrated the growth of Elwell Island and a "large amount of retreat of the Hadley (east) bank" (Figure

2.3.2-1) (Reid, 1990). Changes in the bank line were on the order of several hundred feet based on visual comparisons with the overall river width. Comparisons were also made using maps that were surveyed in 1887, 1936, and 1977 (Figure 2.3.2-2). The results of these comparisons showed that the riverbank in the vicinity of Otter Run in the TFI (a tributary to the river in the vicinity of Kidds Island) had retreated some 400 feet between 1887 and 1977. Finally, a comparison of an 1880 map to a 1977 map showed significant erosion progressing over time in a zone of "active erosion" (near the town of Northfield) as well as other locations where the river had moved approximately one river width or on the order of several hundred feet (Figure 2.3.2-3).

Northrop, Devine, and Tarbell (NDT) also examined the possibility of comparing historic maps to evaluate changes in the position of the river over time (NDT, 1991). As part of this effort NDT reviewed work conducted by Reid (1990) and accuracy information from the U.S. Geological Survey (USGS). Several hundred feet of changes in riverbank position were observed at various locations by both NDT and Reid prior to 1944; however, significant changes (beyond the accuracy limits of the datasets) were not observed in the decades since the 1940's. Both Reid and NDT documented much smaller amounts of change in the more recent decades. The observed relatively small changes in recent decades have been confirmed by annual transect surveys at various locations throughout the TFI which have occurred since the 1990's.

As discussed in the previous section, in reviewing the results of these historic comparisons one must take into account the various accuracy limitations of using such old datasets of varying quality. While definitive conclusions or quantitative estimates cannot be drawn from these comparisons, they are still relevant to the analysis. As such, it is clear that significant erosion occurred at various locations along the Connecticut River over time and prior to the 1940's. While erosion continued throughout the watershed following the 1940's it appears to have been reduced to much lower rates, as is discussed in later sections of this report.

When reviewing the historic geomorphology of the Connecticut River, three primary factors are identified as causing the reduction in erosion rates after the 1940's, including: (1) the relative lack of floods in recent decades of the magnitude of those which occurred prior to the 1940's which resulted in substantial erosion and damage (including the flood of 1936); (2) construction of flood control projects throughout the Connecticut River watershed following the flood of 1936; and (3) construction or raising of mainstem Connecticut River dams which reduced river velocities and shear stresses. Each of these potential factors is discussed in more detail below.

The devastating flood of 1936 caused significant damage, erosion, and channel changes to occur throughout New England and, more specifically, the Connecticut River watershed. During a two week period in March of 1936 New England was impacted by a combination of rainfall and snowmelt that totaled over 10 inches. The rainfall and snowmelt, combined with ice jams at certain locations in the river, resulted in the most severe flooding that has ever occurred. The flood of 1936 continues to be the flood of record and also resulted in new flow records from Hartford, CT all the way up to northern New Hampshire which still stand today (Grover, 1937).

Specific to the TFI, the flood of 1936 caused significant erosion and channel change at several locations. As noted in Field (2007), the flood of 1936 spread across the floodplain with enough force that a new channel 20 ft. deep across was cut across Moose Plain and around Schell Bridge. Similar avulsion channels were also observed immediately north of Munns Ferry, across Bennett Meadow near the Rt. 10 Bridge, and on Pine Meadow downstream of Kidds Island; however, only the channel north of Munns Ferry is believed to have formed as a result of the 1936 flood, the others may have been the result of earlier floods (Field, 2007).

Examples of erosion and channel change that occurred during the 1936 flood can be seen by comparing the 1929 to 1939 aerial photographs. As described by Field (2007), an avulsion channel formed behind the Schell Bridge as a result of the flood. Access to this new channel would later be blocked with riprap placed by government works projects in an effort to close the avulsion and maintain the existing channel. Even

decades after the 1936 flood, remnants of the avulsion channel can be seen (Figures 2.3.2-4 – 2.3.2-7) (Field, 2007). Another example of erosion and change resulting from the 1936 flood can be seen by comparing 1929 to 1939 photographs in the vicinity of Stebbins Island down to the confluence with the Ashuelot River (Figures 2.3.2-8 – 2.3.2-9).

In addition to the flood of 1936 there were numerous other historic floods which have been noted, including: 1763, 1854, 1857, 1862, 1869, and 1870 (Hemenway, 1891) as well as 1639 (Kinnison *et al.*, 1938), 1896 (Bain, no date), 1866 (Scott, 2005) and 1824. The 1824 flood was noted to have "washed out the South Hadley Dam, Turners Falls Dam, and the small dam built below the confluence of the Millers River (Pressey, 1910)." Floods of these magnitudes have not occurred since the late 1930's.

As a result of the severe damage associated with the 1936 flood, a series of flood control projects were constructed in the Connecticut River watershed by the USACE. Examination of instantaneous water year flood peaks at the Montague USGS gage show that peak flows have declined in recent decades (Figure 2.3.2-10). While some of this decline in peak flows could be due to natural long-term hydrologic cycles, a significant part of the decline may be attributed to the success of the numerous flood control projects in the watershed. In addition to showing the instantaneous water year peak flow from 1904-2014, Figure 2.3.2-10 also depicts the average peak flow for four time periods as a means of comparison; these time periods include:

- 1904-2014 (representing the entire period of record other than 2015);
- 1904-1960 (pre-flood control through flood control development);
- 1961-2014 (post-flood control period); and
- 2000-2014 (Study 3.1.2 investigation period)

Finally, as mainstem dams were constructed or raised at various locations along the river, the velocities and shear stresses decreased. In a report entitled "Connecticut River Streambank Erosion Study Massachusetts, New Hampshire and Vermont," US Army Corps of Engineers (USACE, 1979), the effect of dams along the mainstem of the river was explained as follows, *"Dams deepened the water and slowed velocities such that bank erosion due to the flowing water was reduced."*

The 1979 study also compared reaches of the river not affected by the dams to those where dams formed narrow pools. An analysis of forces was conducted from a theoretical perspective. Based on this analysis the report found that theoretically the natural river is roughly 1.34 times more susceptible to major bank erosion than impoundments created by dams (USACE, 1979). The Corps then compared the number of erosion sites per mile for the natural segments of the river compared to those impounded by hydropower dams. The results of this analysis found that the number of erosion sites per mile for the natural river was 0.92 while for impounded areas it was 0.68 indicating that the natural river is 1.35 times more susceptible to bank erosion than impoundments (USACE, 1979). The Corps went on to conclude in its report that the presence of impoundments reduces bank erosion on the order of 34% compared to the natural river (USACE, 1979).

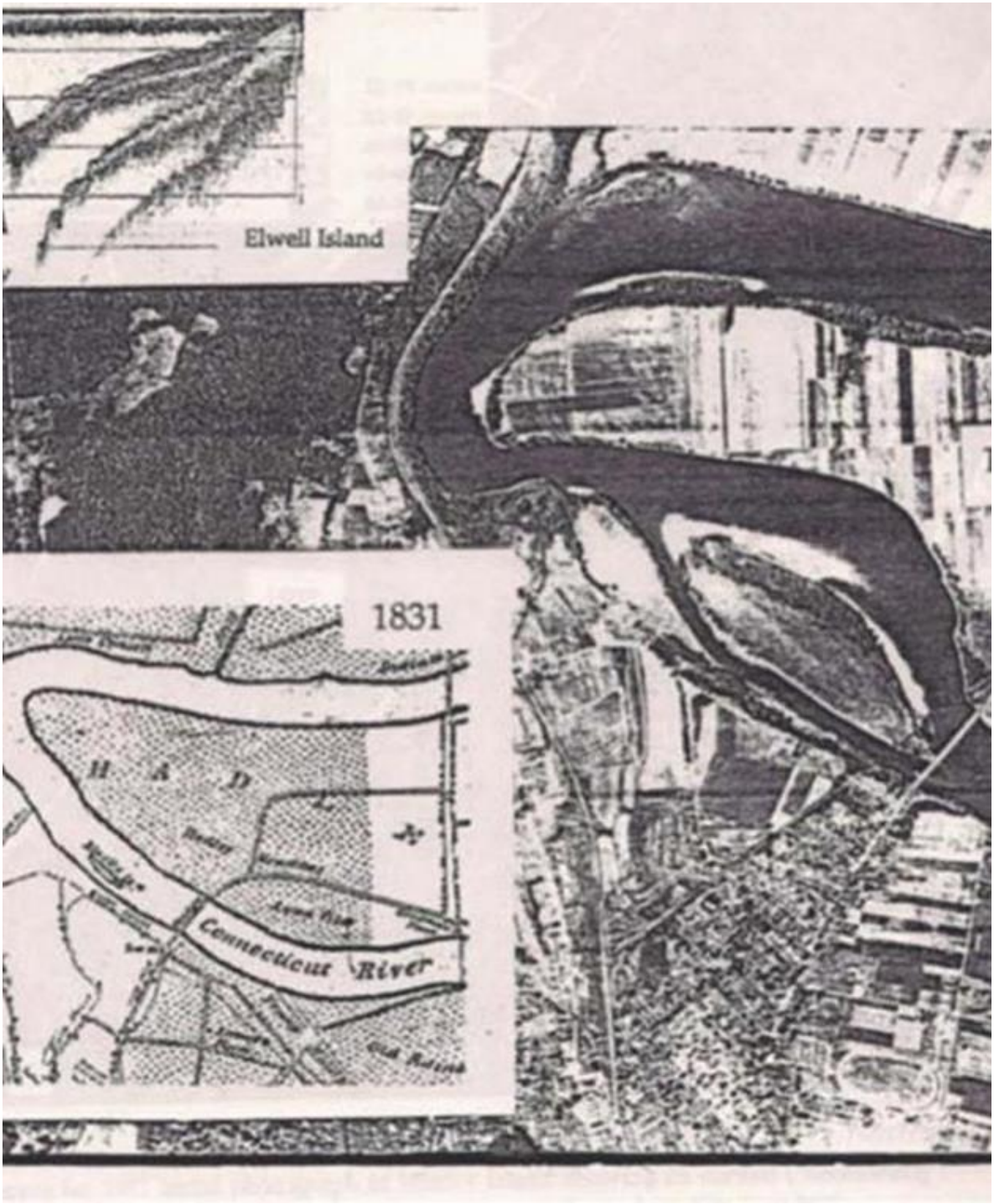

Figure 2.3.2-1 Riverbank Comparison 1831 to 1958 (Reid, 1990)

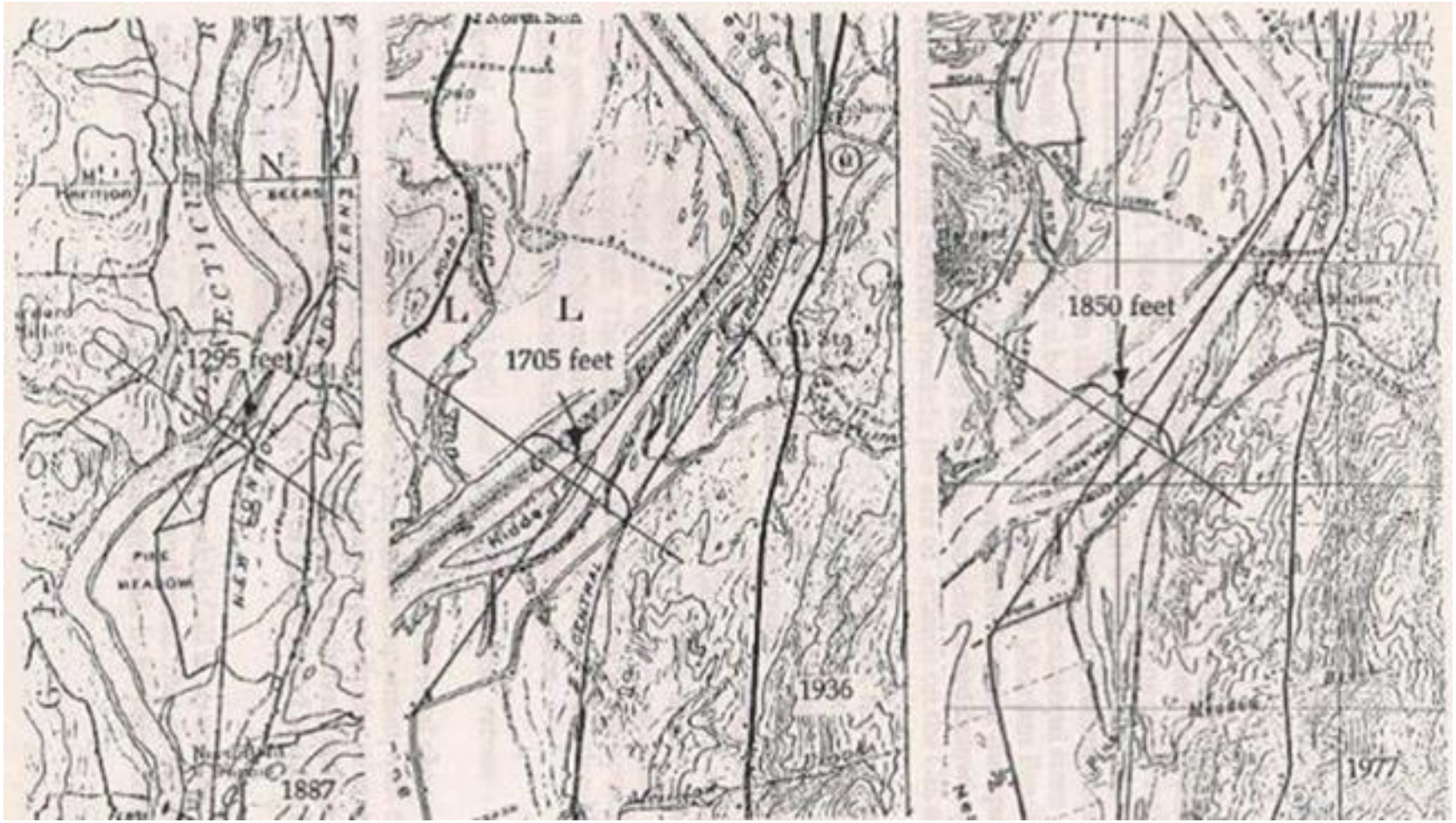

Figure 2.3.2-2 Riverbank Comparison 1887, 1936, and 1977 (Reid, 1990)

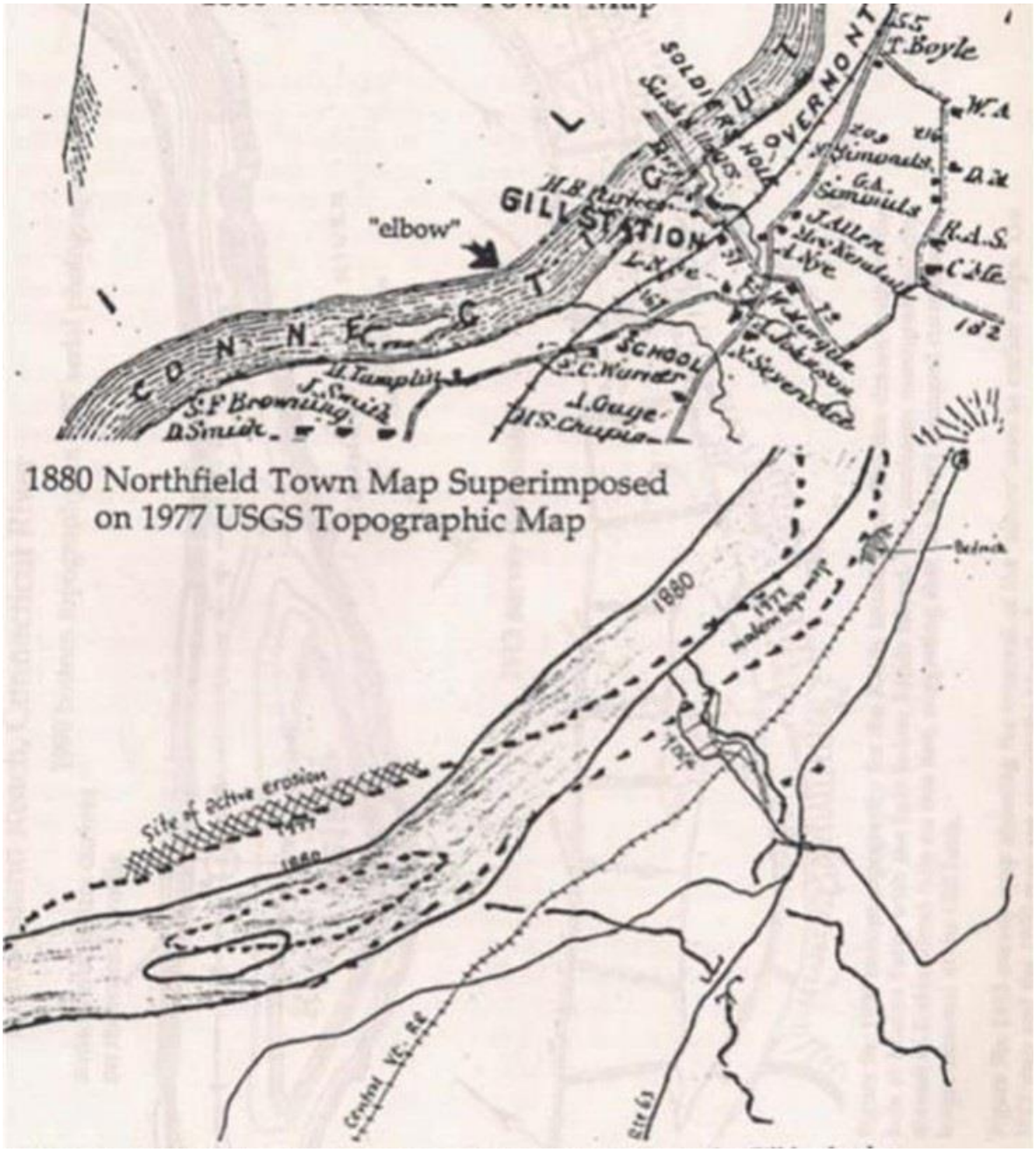

Figure 2.3.2-3 Riverbank Comparison 1880 to 1977 (Reid, 1990)

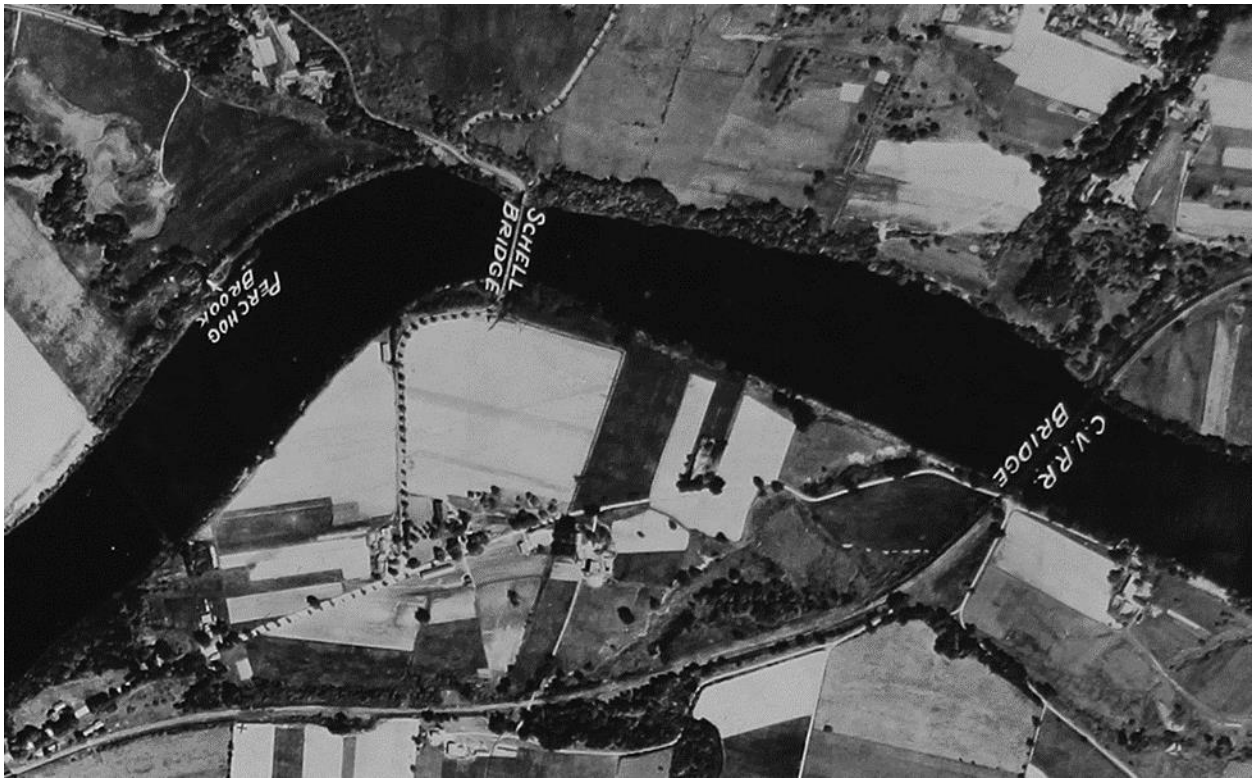

Figure 2.3.2-4 Connecticut River in the vicinity of Schell Bridge, 1929 (a)

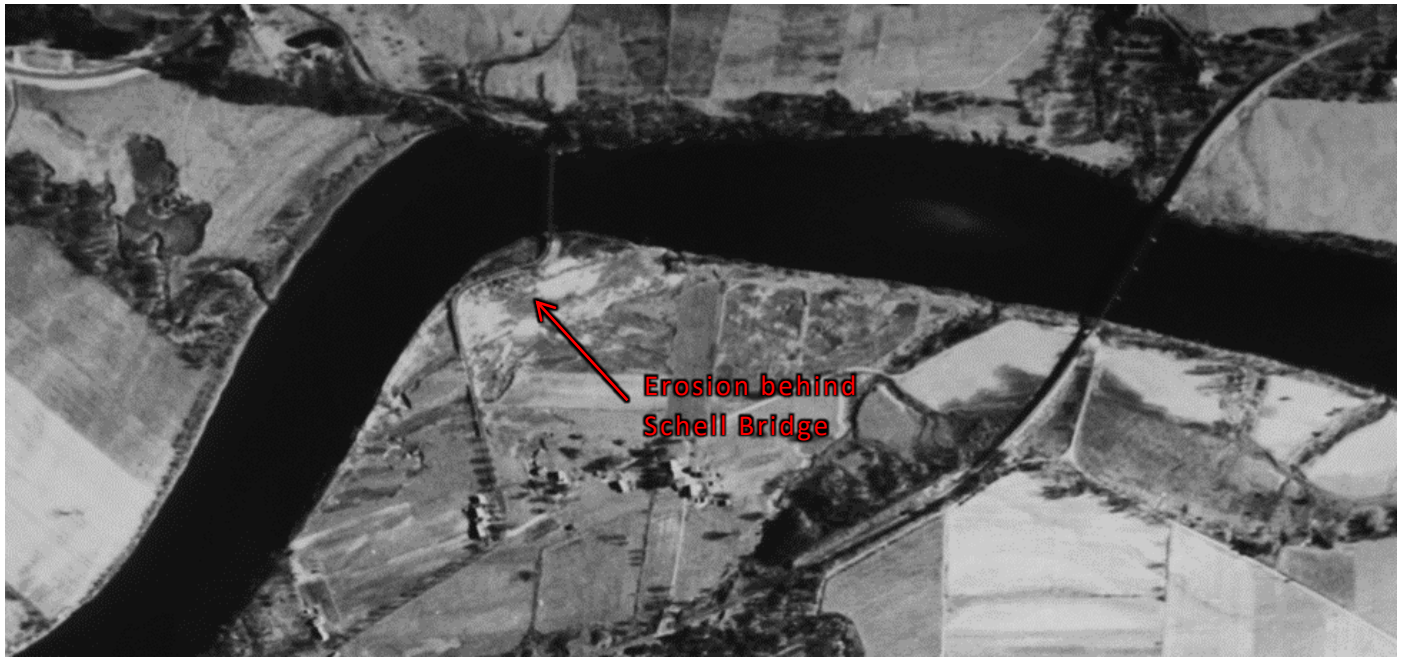

Figure 2.3.2-5 Connecticut River in the vicinity of Schell Bridge, 1939 (b)

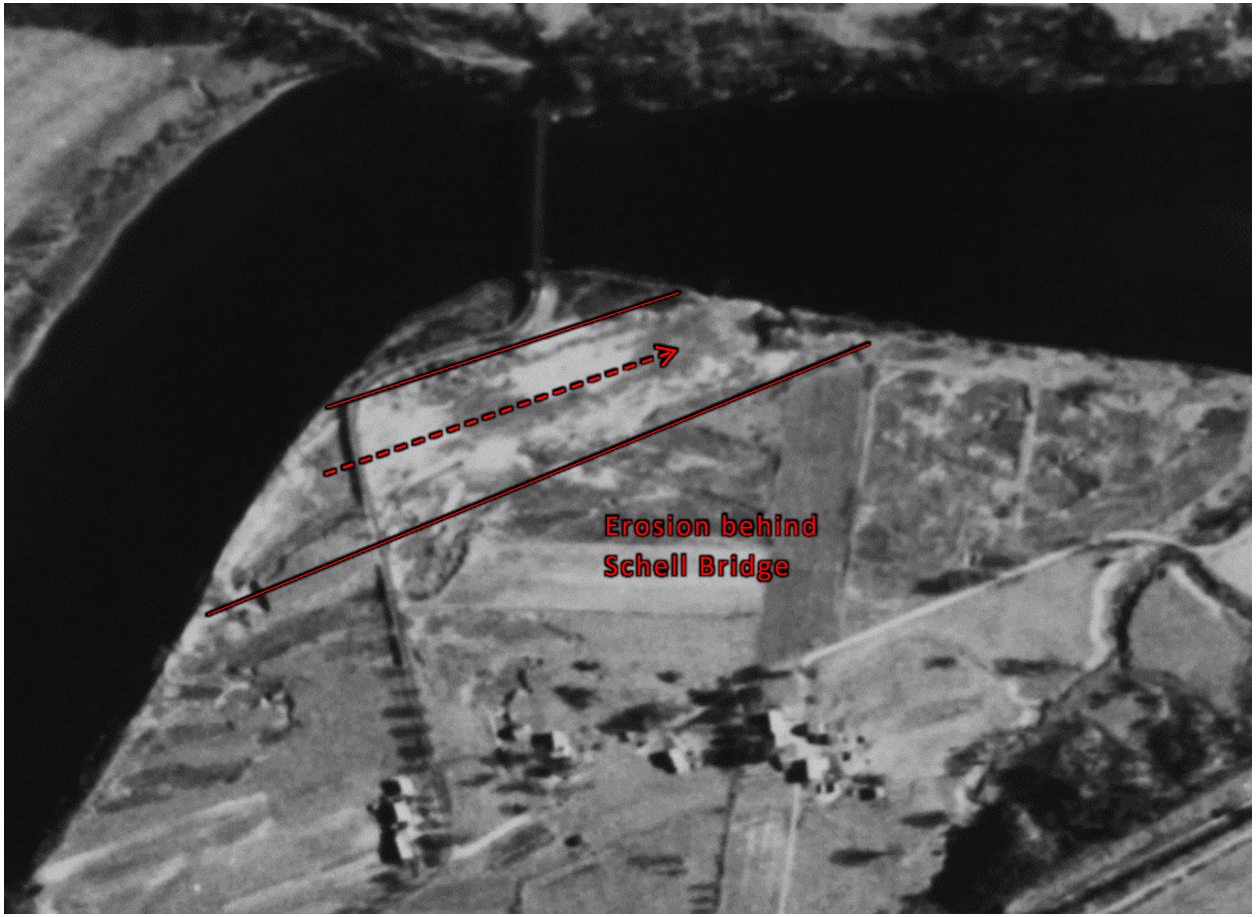

Figure 2.3.2-6 Erosion behind Schell Bridge, 1939 (c)

Figure 2.3.2-7 Abandoned avulsion channel behind Schell Bridge (d) (Field, 2007)

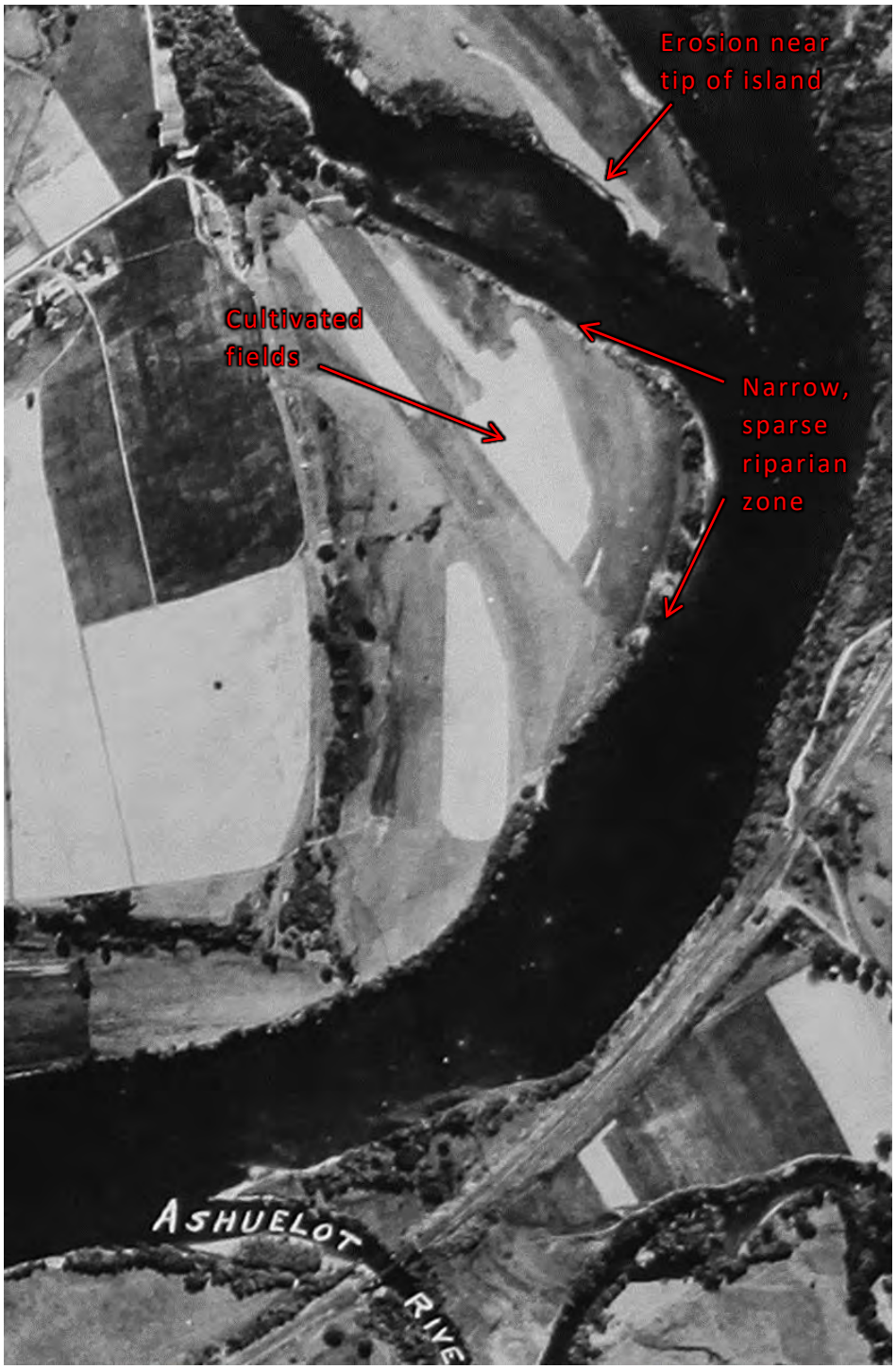

Figure 2.3.2-8 Stebbins Island – Ashuelot River, 1929 (a)

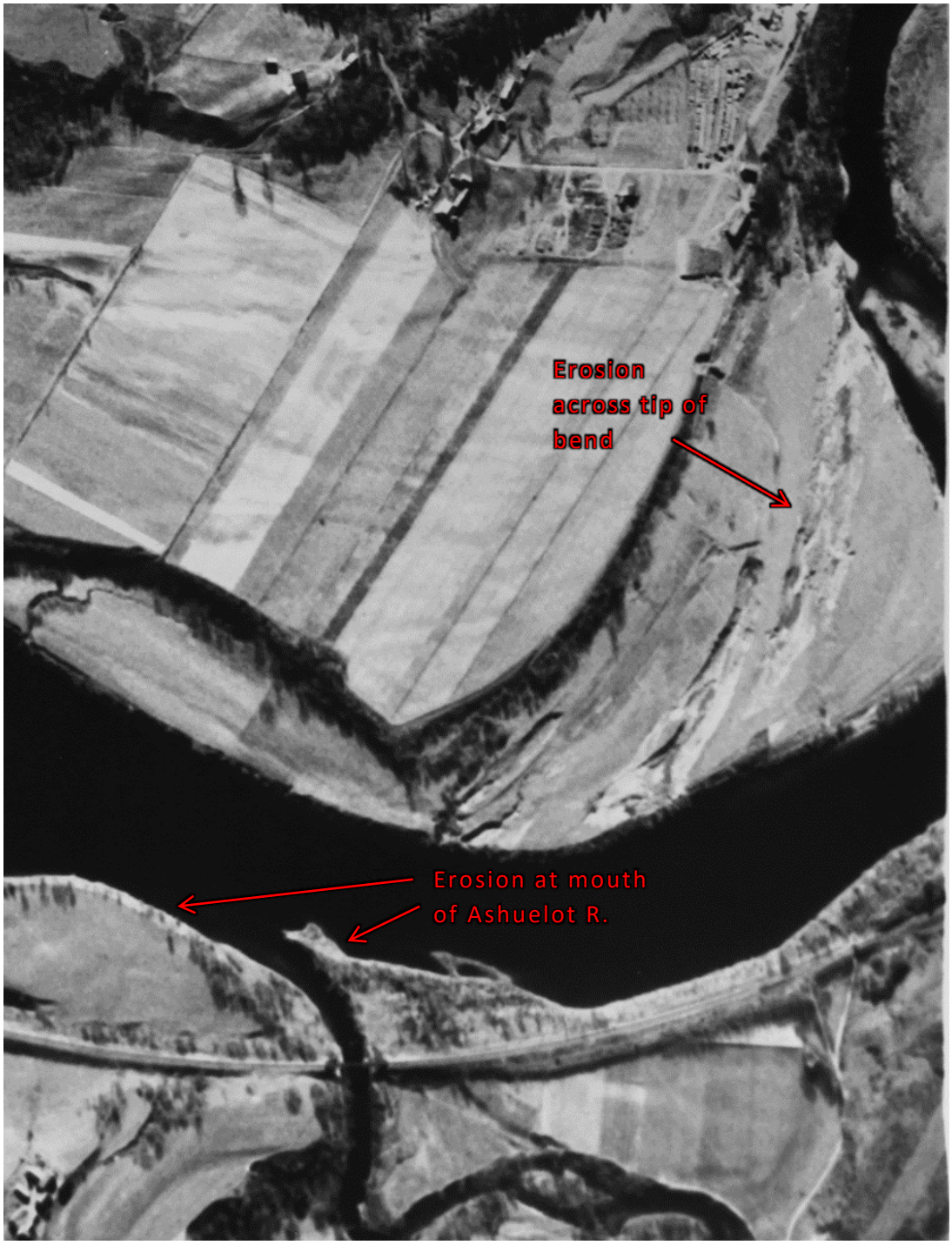

Figure 2.3.2-9 Stebbins Island – Ashuelot River, 1939 (b)

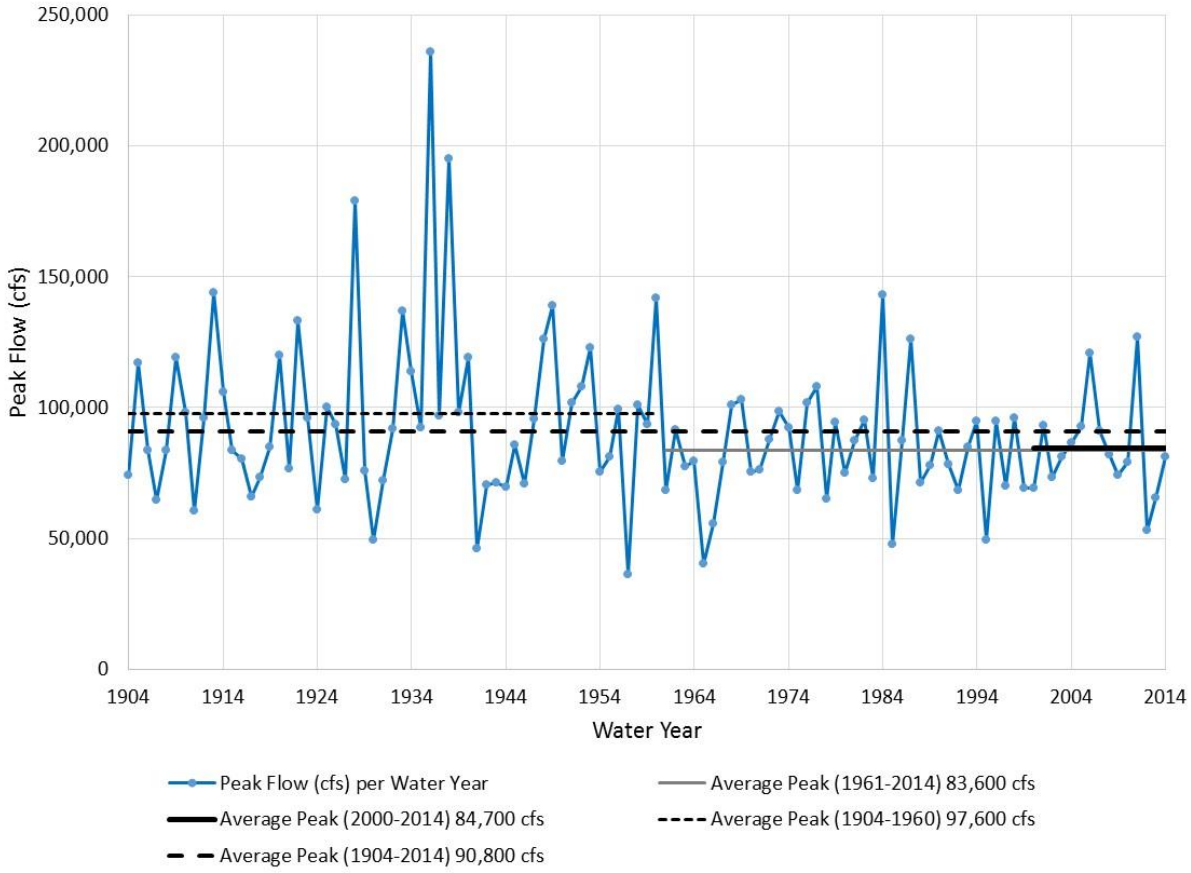

Figure 2.3.2-10 Annual Peak Streamflow – Montague, MA 1904-2014 (USGS)

2.3.3 Analysis of historic datasets – Turner Falls Impoundment

In addition to the historic analysis of the Connecticut River described in the previous section, FirstLight also attempted to conduct a historic geomorphic assessment specific to the TFI. As discussed in the RSP, the goal of this assessment was to provide context when discussing the modern geomorphology of the TFI through the use of available aerial photographs and ortho-photos, historic survey information, and other historic datasets. FERC's September 13, 2013 SPDL further recommended that FirstLight perform the historic geomorphic assessment using available mapping such as the 1970 vintage ground survey data (i.e. the Exhibit K drawings) to analyze trends in bank position within the TFI. In accordance with the RSP and FERC SPDL, FirstLight attempted to use the following datasets when conducting this assessment: 1952, 1961, and 1970 aerial photos, the 1971 Exhibit K drawings, and 2014 ortho-photos obtained from MassGIS and New Hampshire Geographically Referenced Analysis and Information Transfer System (NH GRANIT). Comparison of these datasets were plagued by numerous challenges and limitations which prevented this comparison from yielding any meaningful results.

The first challenge that was encountered when conducting this assessment was relative to the Exhibit K drawings. The original Exhibit K drawings were developed in the late 1960's and early 1970's by Gordon Ainsworth Associates through a combination of aerial imagery, photogrammetry, and ground surveys. The original Exhibit K drawings contained information pertaining to the project boundary, minimum and maximum flow lines, ownership rights, topography, and miscellaneous facility details. National Map Accuracy Standards suggest that this mapping should have been compiled to an accuracy of 1/40th of an inch, which translates to $\pm$10 feet. The original drawings were hand drawn and existed in hard copy format only. FirstLight scanned the hard copy drawings, imported them into ArcGIS, and georeferenced them using coordinates given on the maps in NAD27 Massachusetts State Plane coordinate system.

Upon preliminary review of the drawings, it appeared that the Minimum Flow Line depicted the edge-of-water, however, as the drawings were reviewed more closely that did not appear to be the case. Furthermore, it is unclear how the location of the Minimum Flow Line was identified and what mapping methods were used to develop the original maps. FirstLight also explored the possibility of developing correlations between the Minimum Flow Line depicted on the original Exhibit K drawings and existing surveyed cross-sections of the river to determine the location of the edge-of-water at the time the original drawings were developed, however, that effort proved unsuccessful. The location of the Maximum Flow Line was also reviewed to determine if it could be used to conduct the analysis FERC recommended. Upon review of the drawings it became clear that the Maximum Flow Line would not be an accurate representation of the edge-of-water given that its location extends into the floodplain a far distance from the actual river channel in a number of locations.

Given that the Exhibit K drawings did not contain any information that could be used to determine the edge-of-water, top of bank, or toe of bank they were not useful in conducting a historic geomorphic assessment of the TFI and therefore were not used.

Focus then turned to comparing the 1952, 1961, and 1970 aerial photos with more recent ortho-photos. While the historic aerial photographs were useful for general or site specific observations of the TFI geomorphology at that time, direct comparison of the edge-of-water or riverbank position of the historic photographs with the more recent ortho-photos did not yield useful results given that the historic aerial photographs were taken before the Turners Falls Dams was raised[7] (1952 and 1961) or during construction modifications to the dam (1970). When comparing the 1952 and 1961 historic photos with the more recent ortho-photos it was unclear if changes in the position of the edge-of-water were the result of changes in riverbank position or simply the result of changes in water level due to the raising of the dam. Comparisons

[7] The Turners Falls Dam was raised approximately 6 feet in 1970 as part of the construction of the Northfield Mountain Project.

of the edge-of-water from the 1970 aerial photographs with the more recent ortho-photos also proved to not be useful since the water levels in the TFI were drawn down significantly at the time the 1970 photos were captured to accommodate the construction modifications of the dam.

Due to the limitations discussed above and in Section 2.3.1, a historic geomorphic assessment via comparison of edge-of-water or riverbank position over time was not possible with the available data. While such a comparison did not yield useful results, the historic aerial photographs still provided valuable insights into geomorphic trends when used to examine and compare the condition of specific sites over time. The results of these site specific evaluations and comparisons are discussed in the following section.

2.3.4 Analysis of the 20 Erosion Sites Identified in the Erosion Control Plan

In 1998 a FRR survey was conducted to document riverbank features, characteristics, and conditions throughout the TFI. From this, the Erosion Control Plan (ECP) was developed which identified the 20 most severely eroding sites in the TFI (S&A, 1999). The location of the 20 sites is shown in Figure 2.3.4-1. As part of the historic geomorphic assessment discussed in this section, historic aerial photographs were utilized to evaluate riverbank conditions at the 20 sites identified in the ECP. Table 2.3.4-1 includes a summary of these sites and a comparison of their current status relative to their condition prior to the Turners Falls Dam being raised and the Northfield Mountain Project commencing operation.

Historic aerial photographs from the 1952 and 1961 were analyzed to identify riverbank conditions at each of the 20 most severely eroded sites noted in the ECP. Aerial photographs from these time periods were selected for two main reasons including: (1) they represented conditions in the TFI prior to the raising of the Turners Falls Dam and commencement of Northfield Mountain operations, and (2) they represented riverbank conditions before the shoreline stabilization projects were constructed as part of the ECP. Volume III (Appendix B) contains a full set of figures depicting the conditions at each of the 20 sites identified in the ECP as they appeared in the 1952 and/or 1961.

Based on the results of this analysis it is observed that of the 20 erosion sites identified in the ECP, 14 appear to be eroded prior to raising the Turners Falls Dam and construction/operation of the Northfield Mountain Project. Sites which appear to exhibit erosion in the 1950's and 1960's include:

- Vernon Dam (Site #1)
- Route 10 Bridge (Site #5)
- Flagg (Site #7)
- Kendall (Site #9)
- River Road (Site #10)
- Urgiel Downstream (Site #11)
- Durkee Point (Site #12)
- Split River (Site #13)
- Country Road (Site #14 and #20)
- Stebbins Island (Site #15)
- Kaufhold (Site #16)
- Montague (Site #17)
- Campground Point (Site #18)

Of the 6 remaining sites, one was potentially eroded prior to the Project (Urgiel Upstream - #4), while at the five other sites riverbank conditions are unclear based on the quality of the aerial photographs. Sites where riverbank conditions are unclear include:

- Turners Falls Rod & Gun Club (Site #2)
- Bennett Meadow (Site #3)
- Skalski (Site #6)
- Un-named site (Site #8)
- Davenport or Upper Island (Site #19)

It is significant that a vast majority of the most severely eroded sites identified as part of the 1998 ECP were eroded in the 1952 and 1961 aerial images, prior to raising the Turners Falls Dam and construction of the Northfield Mountain Project.

In addition to the 20 erosion sites identified in the ECP, analysis of the historical aerial photographs revealed several other sites in the TFI that were eroding prior to the raising of the Turners Falls Dam and construction/operation of Northfield Mountain. These additional sites included: the right bank near the downstream end of Stebbins Island, the right bank across from the Ashuelot River confluence, the left bank across from Rock Island, the left bank across from the Mt. Hermon School, the left bank across from Bennett Meadow, and the right bank across from the future location of the Northfield Mountain tailrace. It is instructive to follow what has occurred at these eroded sites over time based on aerial photos, FRRs or other available observations:

- Right bank near downstream end of Stebbins Island: Recent aerial photos and FRR observations show that a narrow zone of riparian vegetation has developed on this previously eroded area indicating natural stabilization is occurring;

- Right bank across from Ashuelot River confluence: A narrow zone of riparian vegetation has become established on this previously eroded bank based on aerial photos and FRR observations;

- Left bank across from Rock Island: Eroded riverbank shown in the 1952 and 1961 aerial photographs now supports a narrow band of riparian vegetation based on recent aerial photographs;

- Left bank across from the Mt. Hermon School: The 1952 and 1961 photographs show eroded conditions with virtually no riparian vegetation. A zone of riparian vegetation becomes established and grows as seen on the 1990's and more recent aerial photographs and confirmed by FRR observations;

- Left bank across from Bennett Meadow: Experimental riverbank protection was placed along this segment of bank by the USACE in the 1970's including articulated blocks on fabric and tires placed in various configurations; and

- Right bank across from Northfield Mountain Tailrace: Rock from the construction of Northfield Mountain was placed at the toe of this eroded riverbank. Vegetation has become established on the upper bank as shown in the series of aerial photographs and FRR observations.

Volume III (Appendix B) includes images of historical aerial photographs depicting erosion in 1952 and 1961 in these areas.

Table 2.3.4-1: Status of the 20 Erosion Sites Identified in the ECP

Site #	Site Name	Current Status (2014)	Pre-Northfield Mtn. Status
1	Vernon Dam	Not selected for stabilization due to extreme hydraulic conditions associated with Vernon spillway	Eroded: Erosion evident in 1952 with continuing erosion through 2008-2010 photos.
2	Turners Falls Rod & Gun Club	Stabilized in 2004	Condition changed considerably due to raised water level and construction of club.
3	Bennett Meadow	Stabilized in 2005	Condition unknown based on aerial photos.
4	Urgiel Upstream	Stabilized in 2001	Potentially eroded: sparse riparian vegetation in 1952 photo.
5	Route 10 Bridge	Not selected for stabilization due to unique hydraulic conditions in the vicinity of the Route 10 Bridge	Eroded: Photos used in this analysis as well as earlier photos from analysis associated with Route 10 bridge show ongoing erosion.
6	Skalski	Stabilized in 2004	Condition unknown based on aerial photos: The left bank of the river in the vicinity of Kidds Island has a band of riparian vegetation in the 1952, 1961 and 1990s photographs. While not apparent in the photographs, erosion had been occurring along this bank and was identified in the ECP and stabilized in 2004 as the Skalski site.
7	Flagg	Stabilized 1999-2000	Eroded: The right bank across from Kidds Island was sparsely vegetated in 1952 and 1961 with ongoing erosion in the 1990s.
8	Un-named	Not selected for stabilization – opposite great meadow	Condition unclear based on aerial photos.
9	Kendall	Stabilized in 2007	Eroded: In 1952 there is some riparian vegetation on the right bank but by the 1961 photograph erosion is evident with no riparian vegetation remaining.
10	River Road	Stabilized in 2003	Eroded: On the inside of the bend along the left bank erosion has occurred over time with the bank moving landward compared to the project boundary line as noted in changes in the bank from the 1952 to 1961 and subsequent photographs.
11	Urgiel Downstream	Stabilized in 2005	Eroded: At a bend in the river upstream of Kidds Island the 1952 photograph shows a reach with some riparian vegetation. The 1961 photograph shows erosion and associated decrease in riparian vegetation.
12	Durkee Point	Stabilized in 2003	Eroded: 1952 and 1961 photographs show erosion and lack of riparian vegetation.
13	Split River	Stabilized in 2009 (Lower Split River) and 2010 (Upper Split River)	Eroded: 1952 and 1961 photographs show erosion and lack of riparian vegetation.
14	Country Road	Stabilized in 2006 (includes site #20)	Eroded: The 1961 photograph shows erosion and a significant reduction in riparian vegetation.

Site #	Site Name	Current Status (2014)	Pre-Northfield Mtn. Status
15	Stebbins Island	Not selected for stabilization	Eroded: Downstream end of island has narrowed through erosion from 1952 to 2008-2010.
16	Kaufhold	Upper Split River stabilized 2010, Bathory-Gallagher stabilized 2012-2013	Eroded: Bathory-Gallagher – Upstream of the tailrace along both banks there was a band of riparian vegetation in the 1952 photograph. By the 1961 photograph the riparian zone appear to have decreased and erosion is evident. Eroded: Upper Split River – 1952 and 1961 photographs show erosion and lack of riparian vegetation.
17	Montague	Stabilized by preventative maintenance in 2008	Eroded: Erosion evident in 1961 photograph.
18	Campground Point	Stabilized by preventative maintenance in 2008	Eroded: Some erosion is evident in the earlier photographs such as 1952 continuing through the 2008 aerial photo
19	Davenport or Upper Island	Not selected for stabilization	Condition unknown based on aerial photos (incomplete imagery available).
20	Country Road	850 ft stabilized in 2006 (included as part of site # 14)	Eroded: The 1961 photograph shows erosion and a significant reduction in riparian vegetation.

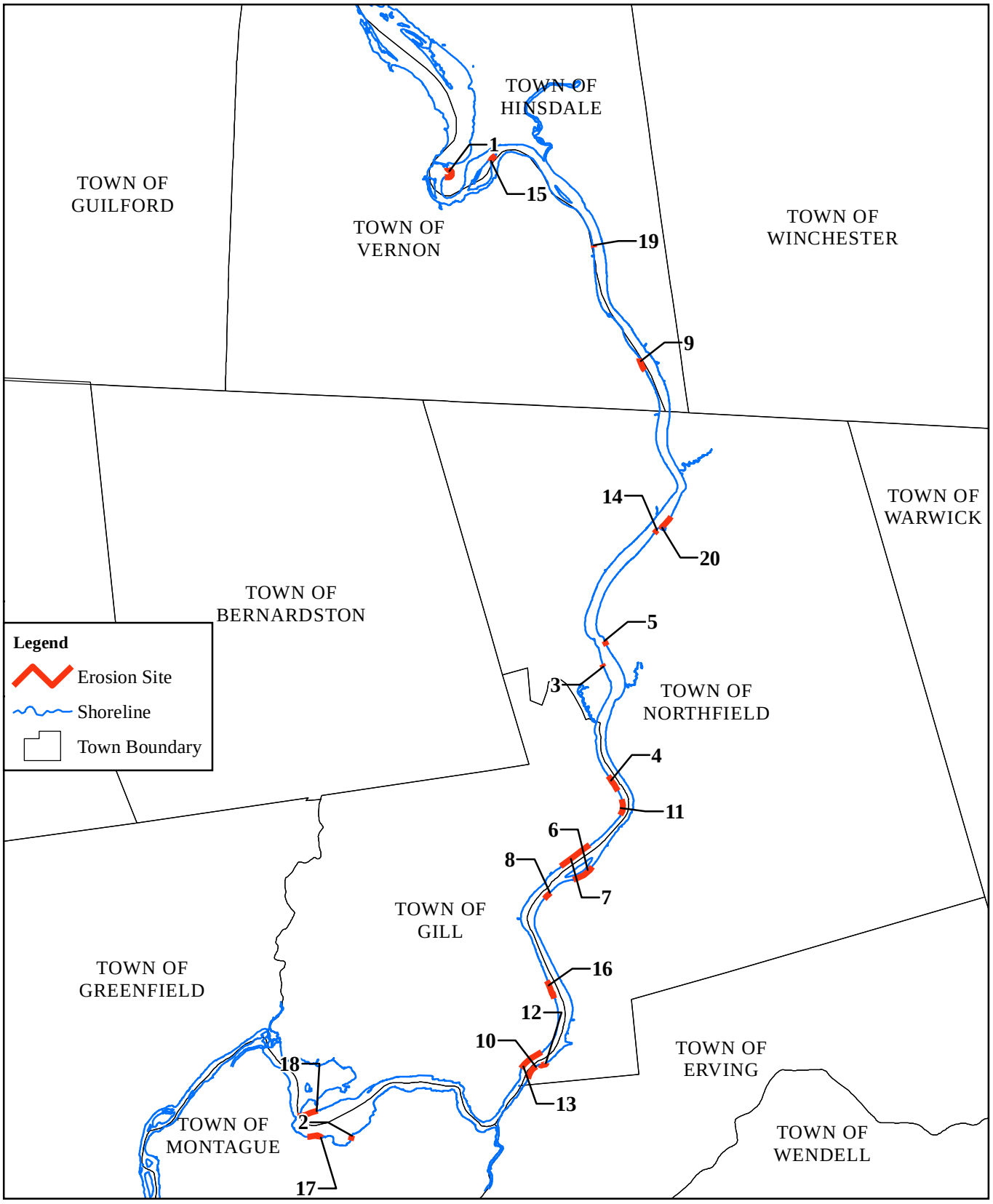

FIRSTLIGHT HYDRO GENERATING COMPANY
Northfield Mountain Pumped Storage Project No. 2485
Turners Falls Hydroelectric Project No. 1889

STUDY 3.1.2

FirstLight Power Resources

N

0 0.875 1.75 3.5 Miles

Figure 2.3.4-1:
Twenty Sites with Highest Erosion Rank (ECP 1998)

Path: W:\gis\studies\3_1_2\maps\final_report\figure_2_3_4-1.mxd

2.4 Geomorphic Analysis of Tributaries and Upland Erosion Features

Tributaries also play an important role in the geomorphology of the Connecticut River and TFI. The energy associated with water flowing from the higher elevations of the surrounding hillsides and mountain ridges tends to erode sediment from the tributary watersheds which is then transported to the mainstem. Inflow and sediment loads from the tributaries can result in both deposition and erosion in the mainstem. For example, during Tropical Storm Irene several inches to a foot or more of sediment was deposited at various locations along the banks of the TFI due to severe erosion farther upstream, particularly from tributaries. Conversely, erosion has been known to occur in the vicinity of various tributary confluences throughout the TFI based on observations of the river at confluences with tributaries and aerial photographs.

The tributaries draining into the TFI have a wide range watershed sizes. The drainage area at the Vernon and Turners Falls Dams are 6,266 mi^2 and 7,163 mi^2, respectively, a difference of 897 mi^2. The two main tributaries to the TFI are the Millers and Ashuelot Rivers which have drainage areas of 390 mi^2 and 420 mi^2 at the confluence with the Connecticut River (combined 810 mi^2) respectively. The combined drainage area of the two tributaries accounts for 88% of the drainage between the Vernon and Turners Falls Dam's. Figure 2.4-1 to Figure 2.4-4 depict these tributaries. The Millers and Ashuelot Rivers have eroded down to stable beds consisting of rock such that little additional erosion of the beds of these two tributaries is possible. Other tributaries are quite steep with beds consisting of gravel, sand or finer material which are erodible and are in the process of erosion, incision, and channel widening. The other TFI tributaries include 16 named and 20 unnamed tributaries which account for the remaining 87 mi^2. The 16 named TFI tributaries include:

- Ashuelot River
- Newton Brook
- Pauchaug Brook
- Bottom Brook
- Mill Brook
- Mallory Brook
- Millers Brook
- Roaring Brook
- Bennett Brook
- Merriam Brook
- Otter Run
- Ashuela Brook
- Dry Brook
- Pine Meadow Brook
- Fourmile Brook
- Millers River

Figure 2.4-5 denotes the tributaries of the TFI. Erosion is often the dominant process at the confluence of tributaries and the Connecticut River/TFI as channels are often cut through the riverbanks as the tributary flows into the mainstem. To the extent tributaries are eroding, incising and expanding; the tributary erosion evolution as it interacts with riverbanks of the mainstem at the confluence may extend the tributary erosion processes to the mainstem in localized areas. As a tributary enters the main river, flow in the tributary can attack the side of the riverbank through which it flows. As a result the main riverbank can be attacked from the main river on the front side of the bank as well as on the side from the tributary. When a tributary meanders as it approaches the main river, flow in the tributary can also attack the back side of the main riverbank.

In addition to tributaries, upland erosion features have also been observed to contribute to riverbank erosion in the TFI. Upland erosion features, if they connect to the main river act as small tributaries. In such cases an upland erosion feature can attack the side or back of the main riverbank as does a tributary. Analysis of LiDAR data and USGS maps indicate that several upland erosion features are present throughout the study area. These upland erosion features have been observed to form drainage patterns that also contribute inflow to the TFI. To more closely examine the potential impact these upland erosion features and drainage patterns

may have on the geomorphology of the TFI, contours derived from LiDAR data[8] of the study area were overlaid on current ortho-photos. Observations made from the LiDAR data were compared against photos collected in the field during the 2013 FRR and subsequent field work associated with this study. Volume III (Appendix C) contains examples of the upland erosion features identified during this analysis.

Further observations of the locations of tributaries and upland erosion features in the TFI finds that a number of the 20 most severely eroded sites identified in the ECP, as well as some erosion sites selected for stabilization in recent years, are located in the immediate vicinity of these features. Table 2.4-1 examines the 20 sites identified in the ECP plus 5 sites recently recommended for stabilization. Of these 25 sites, 16 are directly adjacent to tributaries or upland erosion features. At the 9 remaining sites other factors adversely affect riverbank stability. Two have unusual and extreme hydraulic conditions (S&A, 2012a), four have a very narrow riparian zone adjacent to agricultural activity, one is located at a very narrow tip of an island, while the remaining two have other factors contributing to erosion.

Table 2.4-1: Review of Erosion Sites Identified in the ECP Compared to their Proximity to Tributaries or Upland Erosion Features

Site #/ Name	Presence of tributaries /upland erosion features	Observations
Vernon Dam	No	While there are no tributaries/upland erosion feature, erosion is caused by the rapid current, turbulence and eddying caused by the Vernon Dam gates that release water from the left side of the structure near the bank.
Rod & Gun Club	Yes	Topography shows ravine and alluvial fan shaped feature along with disturbance due to development (road, boat dock).
Bennett Meadow	No	Agricultural terrace with little to no riparian zone (see ECP, site 3).
Urgiel upstream	Yes	Topography modified by stabilization but upstream and downstream upland erosion/damage features can be seen and aerial photo and field observations indicate such features. Seepage through area was observed. Linear erosion feature extends through part of site and extends upstream several hundred feet (unknown cause but downslope from ponds.
Route 10 Bridge	No	Extreme hydraulic conditions with eddying and strong currents from rocky point across river between old and new bridges. One upland erosion/drainage feature. Adjacent to agricultural field with narrow riparian zone.
Skalski	Yes	Next to tributary.
Flagg	Yes	Tributary (Otter Run Brook) splits two sections of stabilization.

[8] LiDAR data of the Connecticut River was collected by US Imaging from April 26-28, 2013 (leaf off) during normal river flows. The data was collected using an Optech M-300 Orion LiDAR Sensor and Integrated CS-10000 Digital CameraAircraft– Cessna T210N – N6258YQA. The LiDAR data was checked against the independently obtained QA/QC points throughout the project area and was found to have a Root Mean Square Error (RMSE) for the sample (RMSEz) of 6.1cm (vertical). The digital imagery was checked against more than 60 photo targets and Photo ID points along the project corridor and was found to have better than 12 cm horizontal standard deviation.

Site #/ Name	Presence of tributaries /upland erosion features	Observations
ECP Site #8	Yes	Tributary and several upland erosion features in the vicinity. Adjacent to gravel pit/quarry and downgradient from Sawyer Ponds.
Kendall	No	Agricultural field, adjacent to abandoned railroad bridge with failed concrete pier which fell into the river and directs current towards riverbank.
River Road	Yes	Site of gully activity
Urgiel downstream	Yes	Modified topography from stabilization changed landscape but observations indicate drainage paths and wetlands uplands from site exist as does seepage through area.
Durkee Point	Yes	Adjacent to tributary.
ECP Site #13	Yes	Transition between ag, hillside, drainage and trail to river.
Country Road	Yes	Tributary flows around from behind stabilized section and joins river on the downstream end of stabilization.
Stebbins Island	No	Narrow, downstream tip of island.
Bathory/Gallagher Upper Split River	No	Agricultural terrace with narrow riparian zone.
Montague	Yes	Numerous upland erosion features.
Campground Point	No	Steep slope with road above and topographic irregularities which could be associated with upland erosion features.
ECP Site #19 (Right bank d/s Upper or Davenport Island)	No	Agricultural terrace with narrow riparian zone.
Country Road	Yes	Tributary flows around from behind stabilized section and joins on the downstream end of stabilization.
Bonnette Farm	Yes	Adjacent to Ashuelot River.
Segment 12 (2013 FRR)	Yes	Numerous upland erosion features.
Segment 75 (2013 FRR)	Yes	Adjacent to tributary
Segment 87 (2013 FRR)	Yes	Adjacent to tributary
Shearer	Yes	Adjacent to tributary

Figure 2.4-1: Ashuelot River – Hinsdale, NH (September 2015)

FIRSTLIGHT HYDRO GENERATING COMPANY
Northfield Mountain Pumped Storage Project No. 2485
Turners Falls Hydroelectric Project No. 1889

STUDY 3.1.2

N

0 500 1,000 2,000 Feet

Figure 2.4-2: Aerial View of the Ashuelot River Flowing into the Connecticut River

Path: W:\gis\studies\3_1_2\maps\final_report\figure_2_4_2.mxd

Figure 2.4-3: Millers River Confluence with Connecticut River (during Tropical Storm Irene)

FIRSTLIGHT HYDRO GENERATING COMPANY
Northfield Mountain Pumped Storage Project No. 2485
Turners Falls Hydroelectric Project No. 1889

STUDY 3.1.2

FirstLight Power Resources

N

0 500 1,000 2,000 Feet

Figure 2.4-4: Aerial View of the Millers River Flowing into the Connecticut River

Path: W:\gis\studies\3_1_2\maps\final_report\figure_2_4_4.mxd

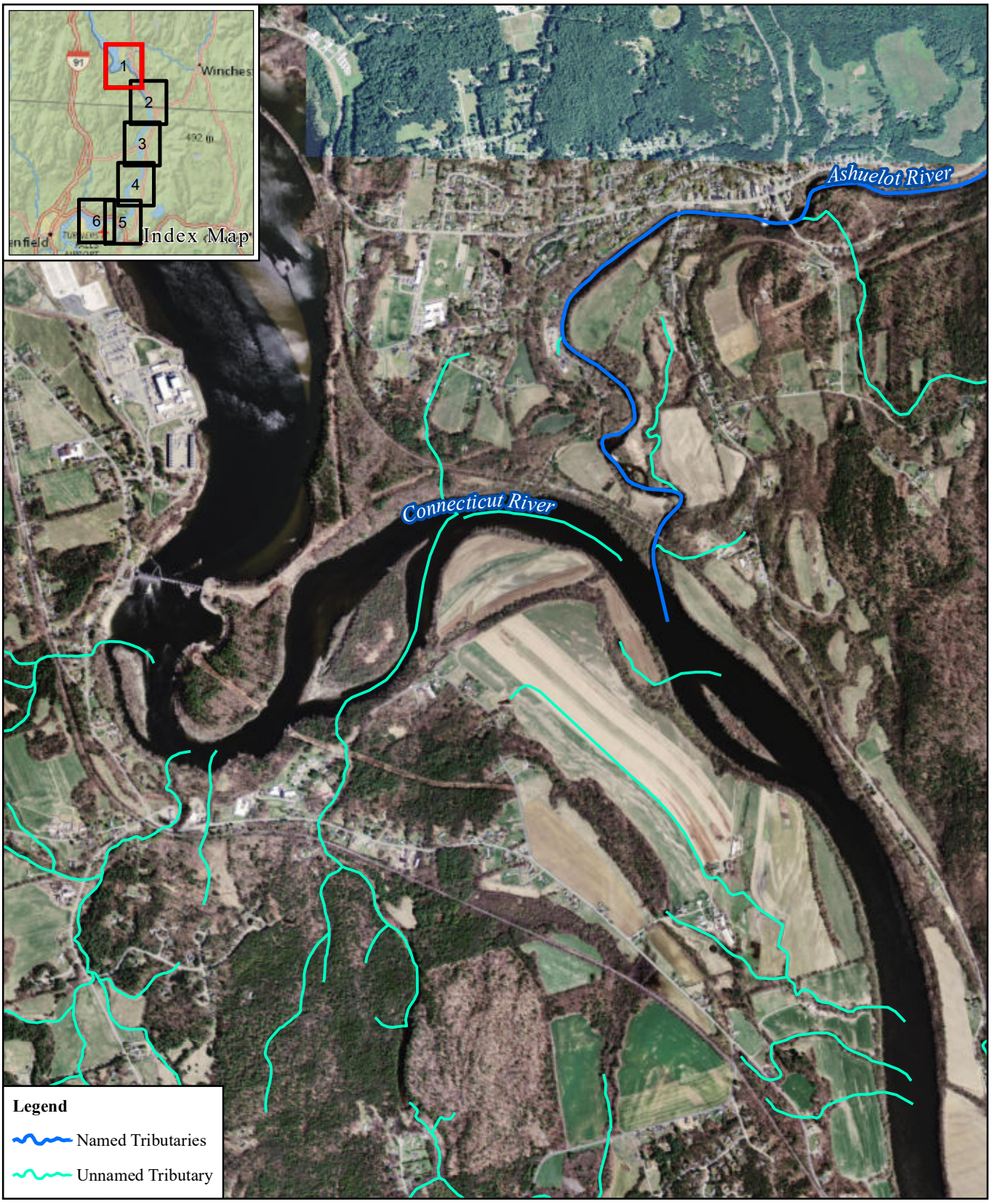

FIRSTLIGHT HYDRO GENERATING COMPANY
Northfield Mountain Pumped Storage Project No. 2485
Turners Falls Hydroelectric Project No. 1889

STUDY 3.1.2

FirstLight Power Resources

N

0 1,000 2,000 4,000 Feet

Figure 2.4-5: Turners Falls Impoundment Tributaries Map 1

Path: W:\gis\studies\3_1_2\maps\final_report\figure_2_4_5.mxd

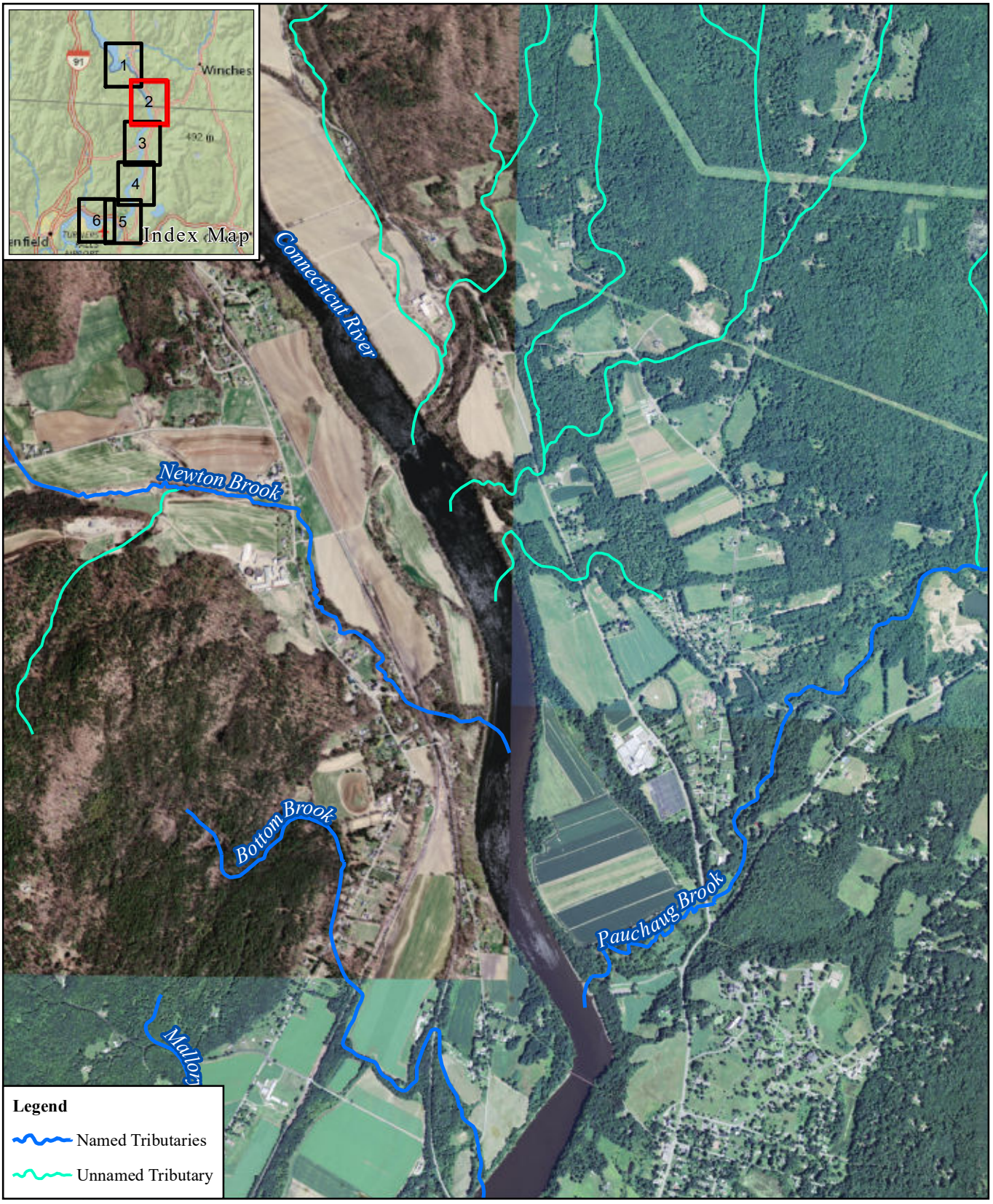

FIRSTLIGHT HYDRO GENERATING COMPANY
Northfield Mountain Pumped Storage Project No. 2485
Turners Falls Hydroelectric Project No. 1889

STUDY 3.1.2

FirstLight Power Resources

N

0 1,000 2,000 4,000 Feet

Figure 2.4-5: Turners Falls Impoundment Tributaries Map 2

Path: W:\gis\studies\3_1_2\maps\final_report\figure_2_4_5.mxd

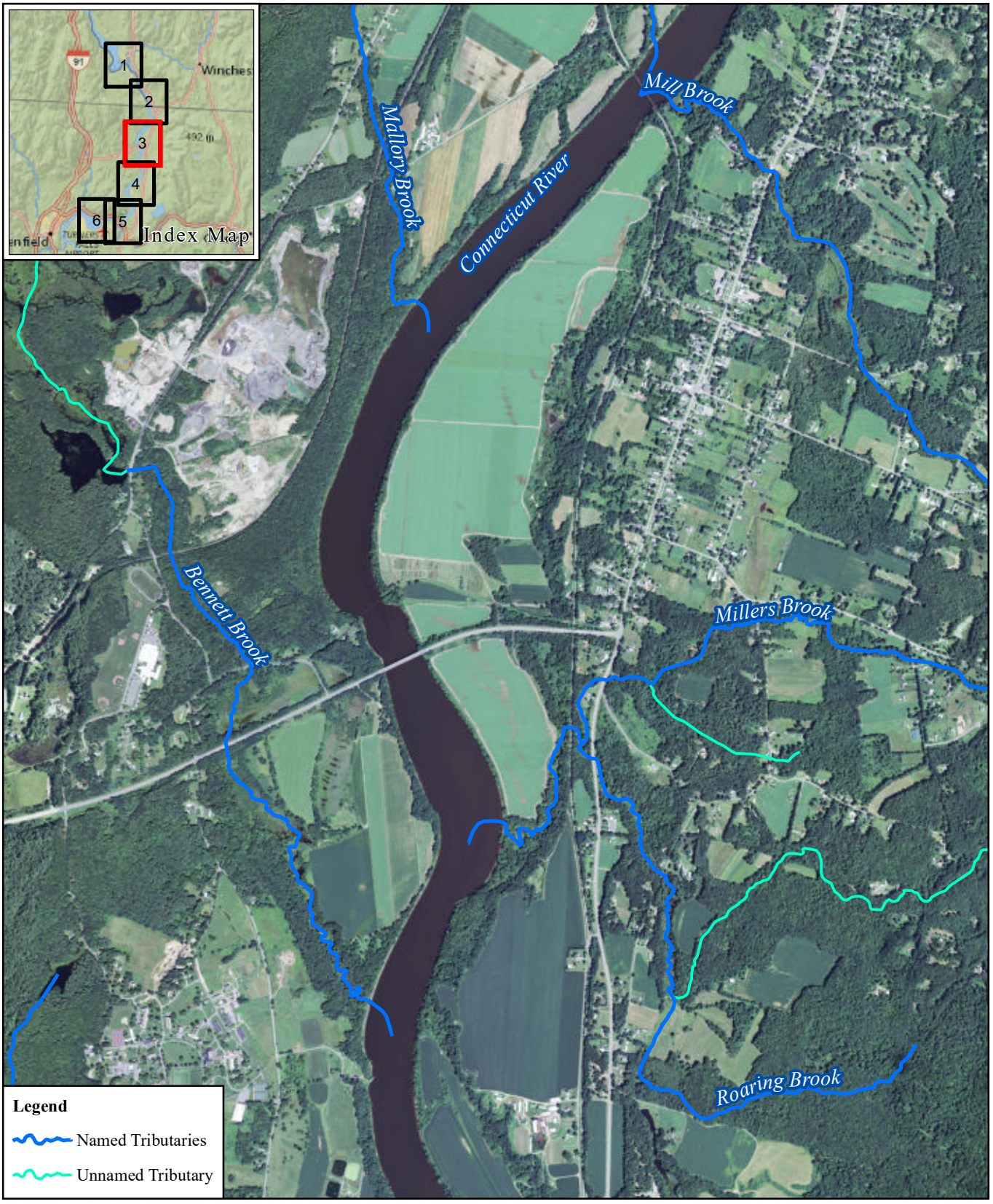

FIRSTLIGHT HYDRO GENERATING COMPANY
Northfield Mountain Pumped Storage Project No. 2485
Turners Falls Hydroelectric Project No. 1889

STUDY 3.1.2

FirstLight Power Resources

N

0 1,000 2,000 4,000 Feet

Figure 2.4-5: Turners Falls Impoundment Tributaries Map 3

Path: W:\gis\studies\3_1_2\maps\final_report\figure_2_4_5.mxd

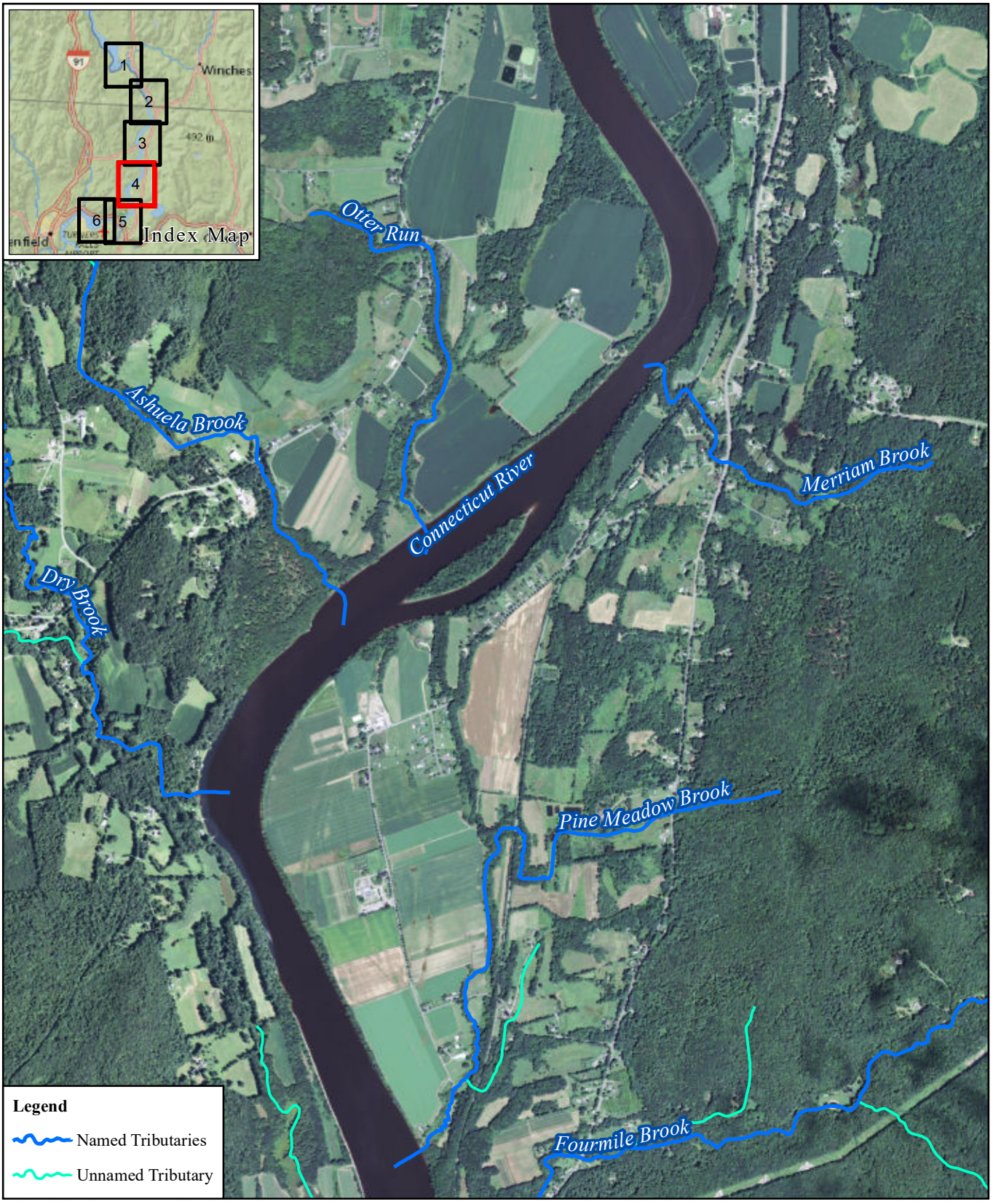

FIRSTLIGHT HYDRO GENERATING COMPANY
Northfield Mountain Pumped Storage Project No. 2485
Turners Falls Hydroelectric Project No. 1889

STUDY 3.1.2

FirstLight Power Resources

N

0 1,000 2,000 4,000 Feet

Figure 2.4-5: Turners Falls Impoundment Tributaries Map 4

Path: W:\gis\studies\3_1_2\maps\final_report\figure_2_4_5.mxd

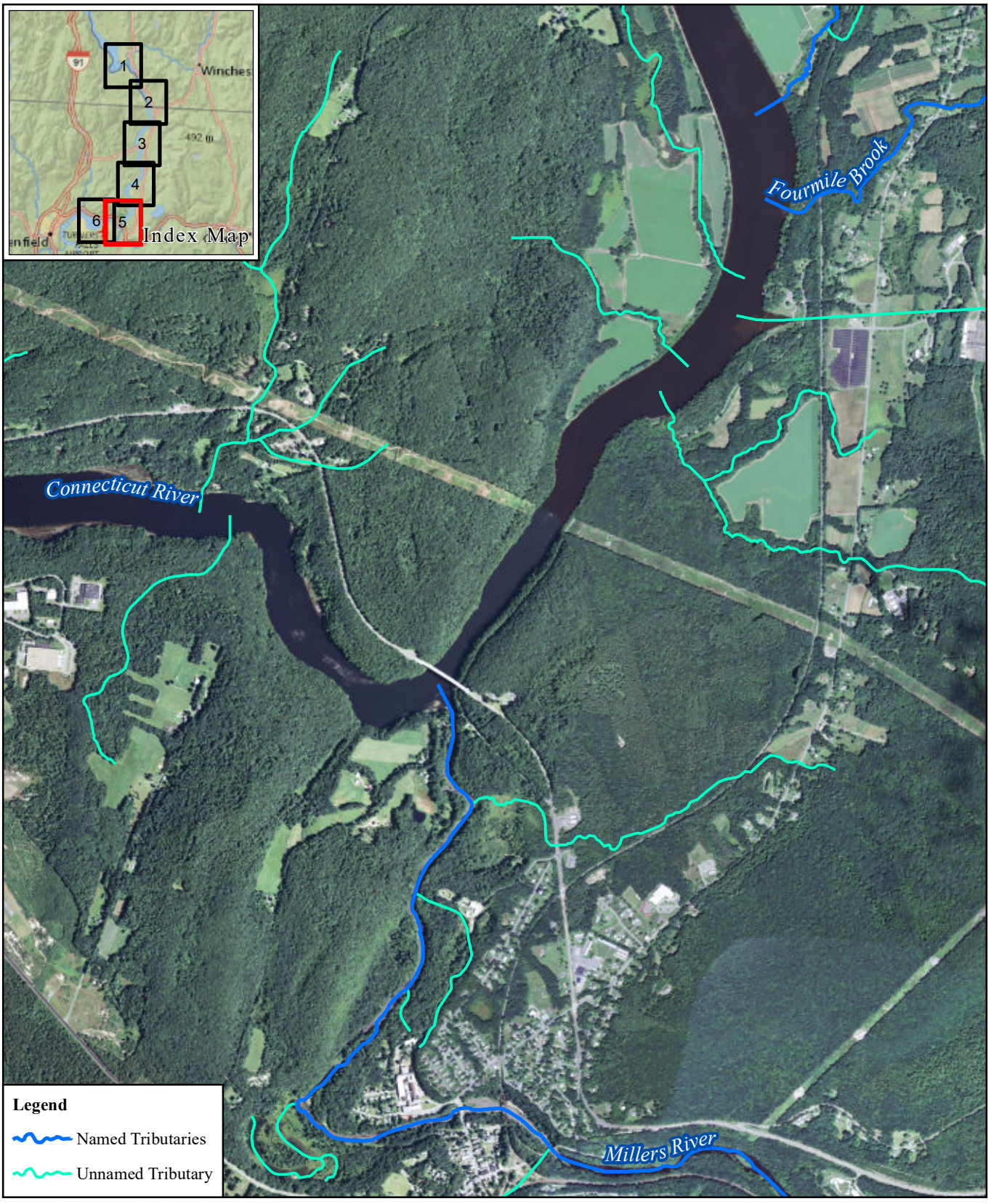

FIRSTLIGHT HYDRO GENERATING COMPANY
Northfield Mountain Pumped Storage Project No. 2485
Turners Falls Hydroelectric Project No. 1889

STUDY 3.1.2

FirstLight Power Resources

N

0 1,000 2,000 4,000 Feet

Figure 2.4-5: Turners Falls Impoundment Tributaries Map 5

Path: W:\gis\studies\3_1_2\maps\final_report\figure_2_4_5.mxd

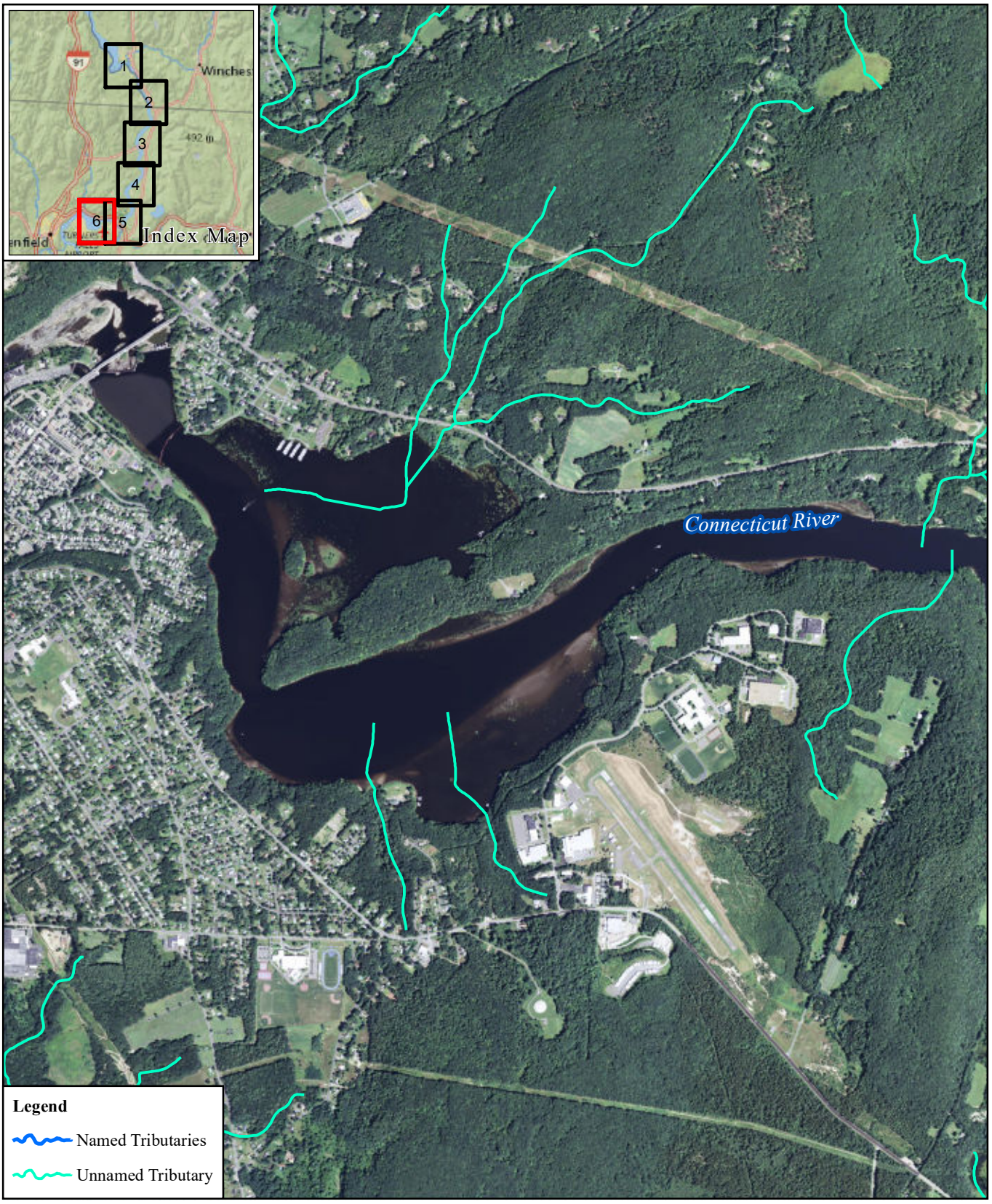

FIRSTLIGHT HYDRO GENERATING COMPANY
Northfield Mountain Pumped Storage Project No. 2485
Turners Falls Hydroelectric Project No. 1889

STUDY 3.1.2

FirstLight Power Resources

N

0 1,000 2,000 4,000 Feet

Figure 2.4-5: Turners Falls Impoundment Tributaries Map 6

Path: W:\gis\studies\3_1_2\maps\final_report\figure_2_4_5.mxd

2.5 Erosion comparison of the Turners Falls Impoundment and Connecticut River

S&A conducted a study which compared erosion along the extent of the Connecticut River from Holyoke Dam (Holyoke, MA), upstream through various hydropower impoundments (including Turners Falls, Vernon, Bellows Falls, and Wilder), and continuing to the un-impounded, free-flowing reach from Gilman Dam to Pittsburg, NH (S&A, 2012b). The study reach was approximately 240 miles long. The study was conducted partially in response to recommendations made in Field (2007) which presented a list of "highest priority recommendations." One of the priority recommendations identified by Field (2007) was to study the patterns of erosion in other reaches of the Connecticut River for comparative purposes.

The study found that riverbank features and characteristics vary considerably along the length of the river. While portions of the river consist of bedrock outcrops that are very stable, much of the riverbanks consist of hillsides or alluvial material that are formed primarily of silt to sand sized material. There are areas that consist of gravel to cobble sized material that are generally less erodible but still are alluvial or transportable by fluvial processes. Much of the riverbanks are quite well vegetated, which generally adds to riverbank stability, although there are segments where a range of erosion and mass-wasting processes remove or damage vegetation and associated riparian land. Riverbank erosion was compared among various reaches to the extent feasible with available data as well as through photographs taken over the years at erosion sites. Key conclusions from this report found that (S&A, 2012b):

- The segment of river with the greatest extent of eroding riverbanks is the un-impounded northern reach (Pittsburg, NH down to Gilman Dam). At the time of the available study, 48.4% of the riverbanks were experiencing moderate or more significant erosion (Field, 2004). Riverbanks that had been rip-rapped covered 17.1% of the length of the river.

- Several erosion sites were identified and photographed in the Bellows Falls, Vernon, Turners Falls, and Holyoke Impoundments in 1997, and again in 2008. All of the erosion sites in 1997 in the Bellows Falls and Holyoke Impoundments and all but one of the 1997 erosion sites in the Vernon Impoundment remained in essentially the same state of erosion when photographed in 2008. Many of these sites were significant in both size and severity. In contrast, most of the erosion sites identified in the TFI in 1998 have been stabilized and were no longer eroding as of 2008.

- In addition to direct stabilization of many of the erosion sites in the TFI that were identified in the 1998 ECP, there is evidence of some natural stabilization processes including increased upper bank vegetation and areas of dense low bank aquatic vegetation that are helping provide a degree of additional stability in some areas.

- Despite the fact that similar percentages of riverbank have been stabilized in the northern, free-flowing reach as in the TFI; the percentage of erosion in the TFI is only about one-third the extent of erosion that is occurring in the northern, free-flowing reach of the Connecticut River (16.7% compared to 48.4%).

- Because riverbank erosion in the TFI is significantly less than in the northern free-flowing reach, erosion sites in other impoundments (Bellows Falls, Vernon, and Holyoke) continued eroding from 1997 to 2008, and many erosion sites have been stabilized in the TFI (including evidence of natural stabilization processes) it can be concluded that the riverbanks in the TFI are in the best condition (more stable and less eroding) than in any other part of the Connecticut River that was examined as part of the 2012 study.

- The TFI, which experiences water level fluctuations due to a combination of run of river/peaking power and pumped-storage hydropower operations, has less riverbank erosion than the other

impoundments (Wilder, Bellows Falls, Vernon, and Holyoke) which only experience water level fluctuations resulting from run of river and peaking power operations and do not experience additional fluctuations due to pumped-storage operations. The TFI also experiences significantly less erosion than the northern, free-flowing reach which has no hydropower operations and associated water level fluctuations.

Significant erosion has been occurring and is ongoing in the un-impounded (free-flowing) reaches of the Connecticut River as well as in the impoundments other than the TFI as documented in the comparison report. Examples of erosion in these reaches of river are shown photographically in Figures 2.5-1 through 2.5-10. Figure 2.5-1 shows large-scale and severe erosion in a free-flowing reach of the river. An example of some of the erosion sites located in 1997 in the Bellows Falls Impoundment is shown in Figure 2.5-2, while other erosion examples in the Vernon and Holyoke Impoundments are shown in Figures 2.5-3 and 2.5-4.

The erosion sites identified in 1997 were revisited in 2008 to photographically document any changes that might have occurred since 1997. Sets of photographs showing 1997 and 2008 images at the same sites are presented in Figures 2.5-5 and 2.5-6 for the Bellows Falls Impoundment; Vernon – Figures 2.5-7 and 2.5-8; and Holyoke – Figures 2.5-9 and 2.5-10. For these three impoundments, erosion sites in 1997 were observed to be in the same eroding condition in 2008.

Figure 2.5-1: Erosion of Glacial Outwash Deposits in Un-impounded Reach of Connecticut River (Field, 2004)

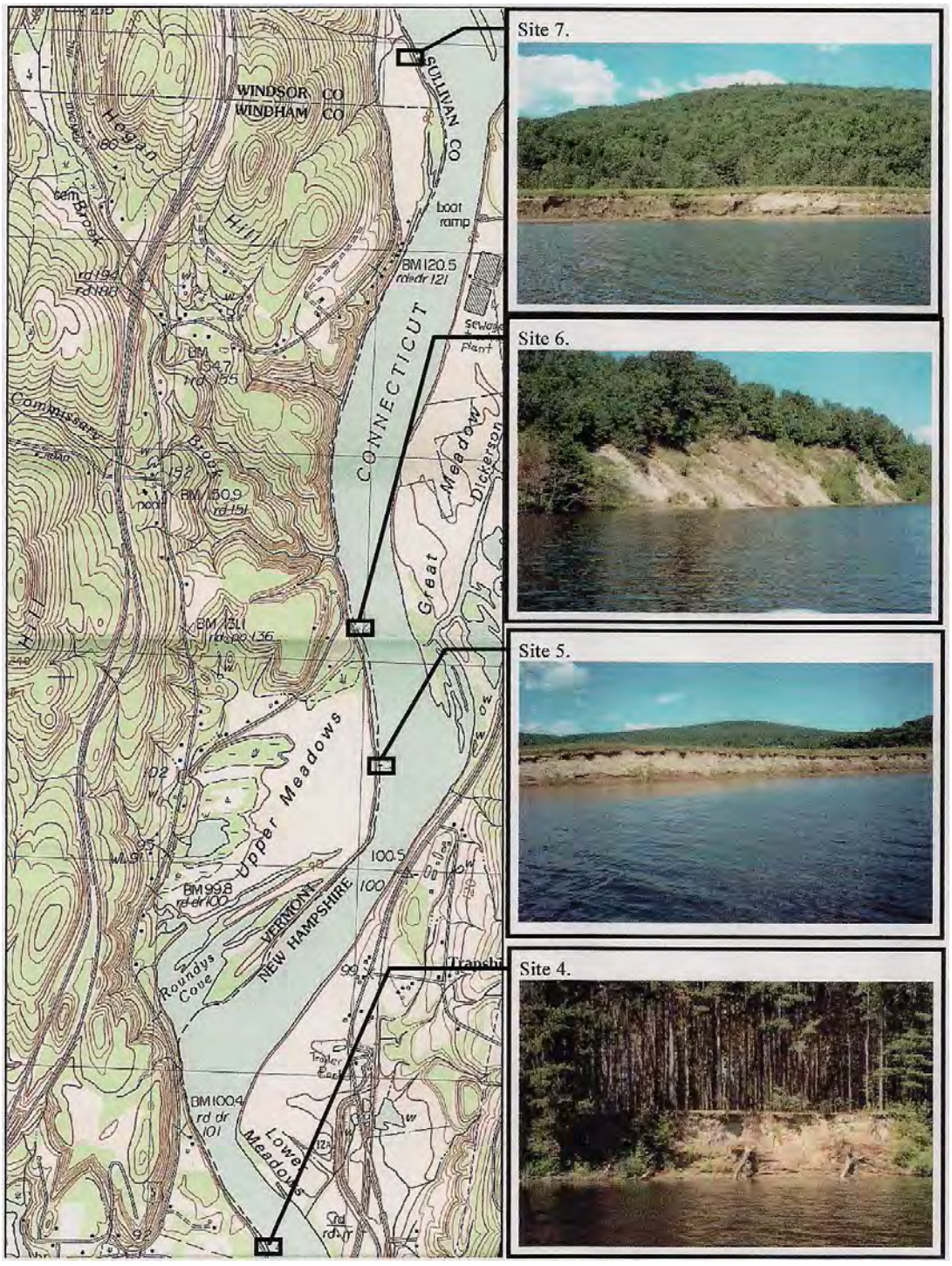

Figure 2.5-2: Erosion sites 4-7, Bellows Falls Impoundment (1997)

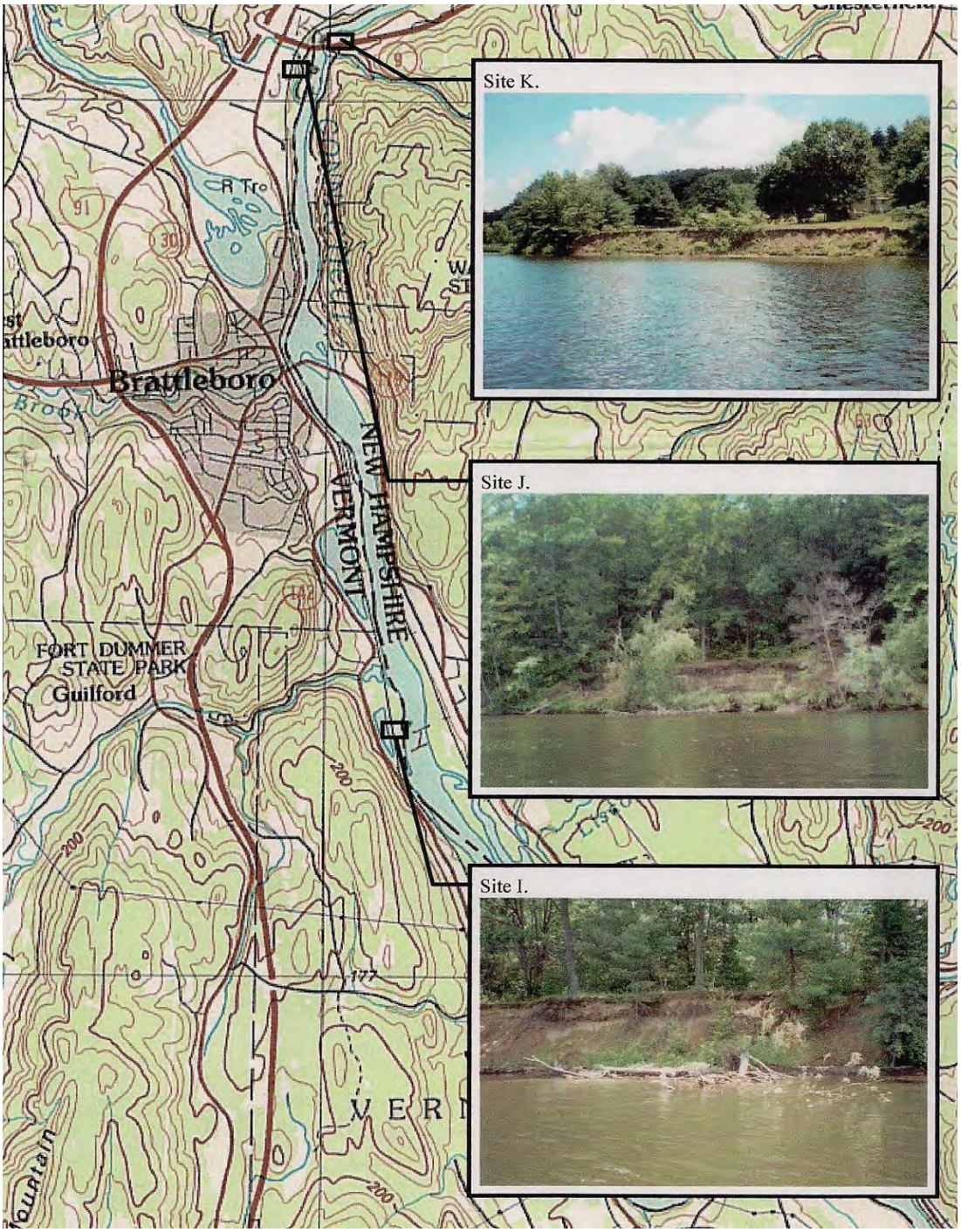

Figure 2.5-3: Erosion sites I-K, Vernon Impoundment (1997)

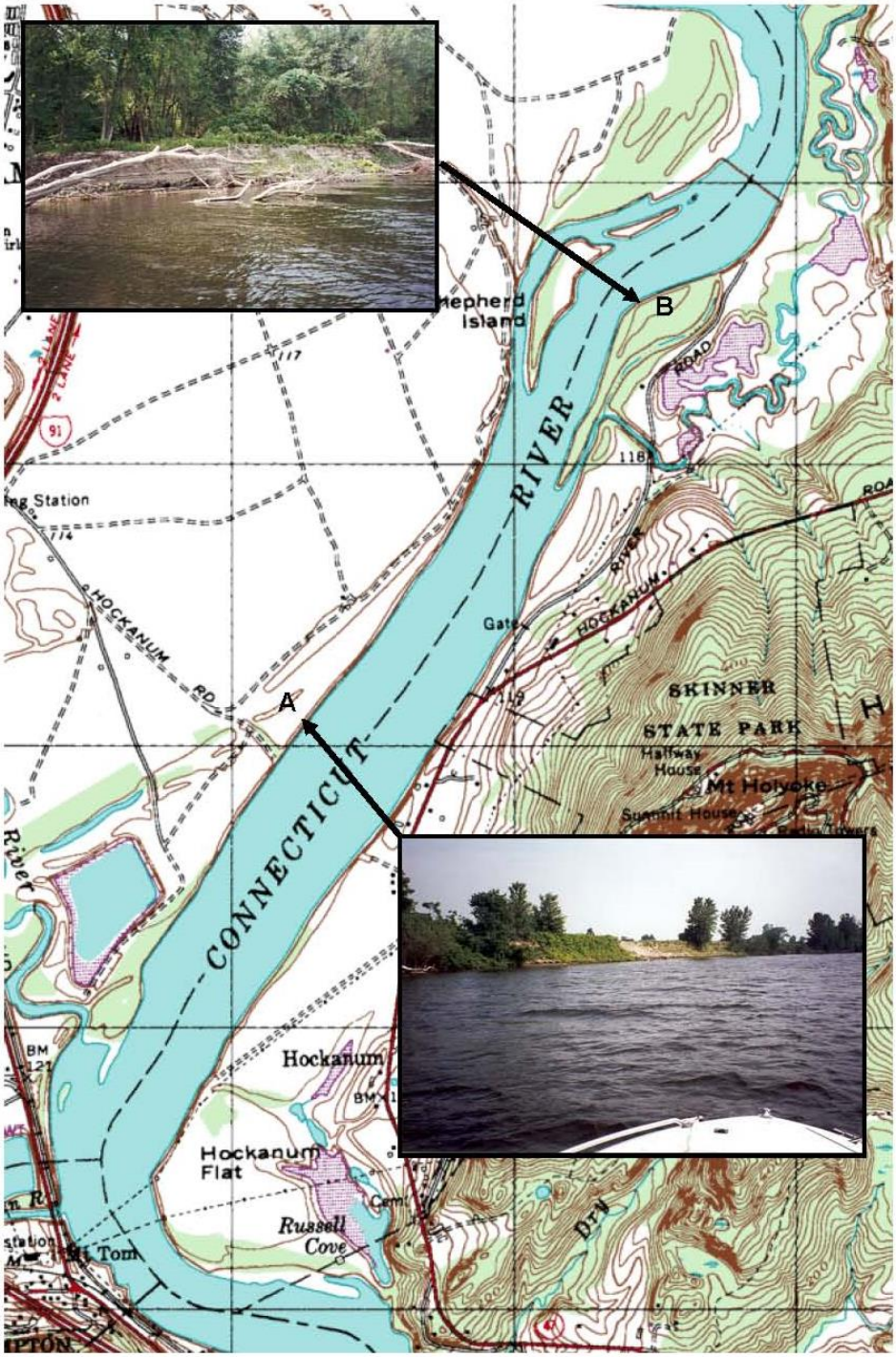

Figure 2.5-4 Erosion sites A and B, Holyoke Impoundment (1997)

Figure 2.5-5: Bellows Falls Impoundment – Location 8 (1997)

Figure 2.5-6: Bellows Falls Impoundment – Location 8 (2008)

Figure 2.5-7: Vernon Impoundment – Location I (1997)

Figure 2.5-8: Vernon Impoundment – Location I (2008)

Figure 2.5-9: Holyoke Impoundment – Location D (1997)

Figure 2.5-10: Holyoke Impoundment – Location D (2008)

2.6 Summary Discussion of the Geomorphology of the Connecticut River

Recent geomorphic history[9] suggests that the Connecticut River was formed by the retreat of a large glacial lake (Lake Hitchcock) following the last ice age. As the Connecticut River formed it cut down through sediment that had been deposited in Lake Hitchcock, changing from a depositional to erosional geomorphic feature. The Connecticut River, with the exception of rare bedrock lined sections such as the French King Gorge, is an alluvial river. Alluvial rivers by definition continue to adjust over time through processes of aggradation, degradation, scour, deposition, lateral migration, and bank erosion. Given this, although the river has reached a state of dynamic equilibrium over time, some degree of erosion is expected to continue. According to Leopold *et al*. (Leopold *et al*., 1964), an ideal natural channel in equilibrium essentially means that the channel size generally retains an overall unchanging average size, with erosion in one place balanced by deposition in another, resulting in a channel changing its position over time. That is, the form of the cross-section is stable, but the position of the channel is not.

Various groups have evaluated and analyzed erosion over time by examining historic maps, aerial photographs, and other datasets ranging from the 1700's to present day. Historic geomorphic comparisons and analyses, while limited by their accuracy, provide valuable context and insights into the modern geomorphology of the Connecticut River. Historic observations (prior to the 1940's) found that the Connecticut River, in some locations, changed hundreds of feet up to approximately 1,000 feet. In recent decades, comparisons of river change using aerial photographs found that measured riverbank changes were typically within the accuracy of the analysis. The observation that the Connecticut River changed more significantly prior to the 1940's than later is believed to be due to three main reasons: (1) historic floods which occurred prior to the 1940's have not occurred of the same magnitude since (e.g., the flood of 1936); (2) construction of flood control projects throughout the Connecticut River watershed following the flood of 1936 have resulted in reduced flood peaks; and (3) construction or raising of mainstem Connecticut River dams have reduced river velocities and shear stresses. Due to these factors, and others, the potential for erosion was higher prior to the 1940's than compared to recent decades.

In addition to the historic geomorphology of the Connecticut River it is also important to understand the modern geomorphology and topography when evaluating causes of erosion. Available USGS maps indicate that 36 named and un-named tributaries enter the TFI while analysis of available LiDAR derived contour information demonstrates that numerous upland erosion features have formed in the land surface in the vicinity of the river. These tributaries and upland erosion features were formed via erosion processes and result in additional inflow to the TFI. When evaluating the 20 most severely eroded sites identified in the ECP (S&A, 1999), as well as several sites recently recommended for stabilization, it was found that the majority of the sites were located at tributaries and upland erosion features. Additionally, through comparisons of historic aerial photographs from 1952 and 1961 it is observed that the majority of these sites were eroded prior to the raising of the Turners Falls Dam and operation of the Northfield Mountain Project.

The dynamic nature of the Connecticut River is evident by how riverbank erosion occurs to one degree or another throughout its length in both free-flowing and impounded reaches. Simons & Associates (2012b) conducted a comparison study to evaluate the varying erosion conditions throughout the Connecticut River from Holyoke Dam (Holyoke, MA) to Pittsburg, NH (240 mile long reach), which included both free flowing and impounded reaches. The study found that the segment of river with the greatest extent of eroding riverbanks was actually the un-impounded northern reach (Pittsburg, NH down to Gilman Dam), further illustrating the alluvial nature of the Connecticut River. This is consistent with the findings of the

[9] Recent geomorphic history is considered as beginning at the end of the last ice age when the Connecticut River formed as Lake Hitchcock drained. Modern or current geomorphology is considered as being the time period over the past few hundred years as development occurred in the watershed.

USACE who noted in their 1979 erosion study that: (1) erosion in free flowing, un-impounded reaches was 1.35 times more likely to occur than in impounded reaches, and (2) the presence of impoundments reduces bank erosion on the order of 34% (USACE, 1979).

3 POTENTIAL CAUSES OF EROSION

One of the main objectives of this study was to evaluate and identify the causes of erosion, and the forces associated with them, throughout the TFI. Erosion occurs when the forces that act on a riverbank exceed the forces that resist movement of riverbank material. Forces acting on a riverbank that may cause erosion range from flowing water against the riverbank to rapid water level fluctuations, ice, boat waves, or land-use, to a name a few. While there are multiple causes of erosion there are also multiple riverbank characteristics and phenomena that resist the forces that can lead to erosion. These could include, among others, the size or size distribution of soil particles that form the riverbank, the cohesion and frictional properties of the soil particles, vegetation, and bank geometry. Riverbank erosion or stability is the result of a complex interaction between riverbank features and characteristics, the forces that cause erosion, and the resistance to erosion that the riverbank provides.

While there are many different forces which can lead to erosion, actual riverbank erosion generally falls into two primary process categories: 1) particle by particle erosion of surficial materials, or 2) mass wasting. Mass wasting is defined as the process where riverbanks experience movement of blocks or other large pieces of bank material downslope under the influence of gravity. Further complicating the riverbank erosion process is that several processes of erosion may be occurring either simultaneously or in sequence at one or more positions vertically or laterally in a segment of riverbank. For example, the river current may gradually erode the lower portion or toe of the riverbank in a particle by particle process undercutting and removing support for the upper riverbank. The upper bank may then collapse, rotate, or slide in a mass-wasting event. The upper bank mass-wasting event could be caused by a number of factors, or combination of factors, including a high flow event, wave action, seepage and positive pore-water pressure.

This section presents discussion of the causes of erosion, and the forces associated with them, which are present throughout the TFI and which were the basis for this study.

3.1 Identification of Causes of Erosion

When initially developing the methodology for this study a list of potential causes of erosion present in the TFI was developed and included in the RSP. This list was developed based on the geomorphic history of the study area as well as past experience conducting FRR's and other geomorphic evaluations of the Connecticut River. The list of potential, contributing causes of erosion presented in the RSP included (in no particular order):

- Hydraulic shear stress due to flowing water;
- Water level fluctuations due to hydropower operations;
- Boat waves;
- Wind waves;
- Land management practices and anthropogenic influences to the riparian zone (e.g., removal of riparian vegetation, cattle grazing to the river's edge, heavily traveled recreation trails, etc.);
- Animals;
- Seepage and piping;
- Freeze-thaw; and

- Ice or debris

This potential list was then finalized and divided in the RSP into two classifications: 1) potential primary causes of erosion, and 2) potential secondary causes of erosion. Potential primary causes of erosion were those which were thought to be most prevalent throughout the TFI based on past experience conducting geomorphic assessments on the Connecticut River, and other alluvial rivers, as well as from a preliminary investigation of existing documentation. In accordance with the RSP, these causes were studied in great detail at a number of detailed study sites throughout the geographic extent of the TFI. In addition to encompassing the geographic extent of the TFI, the detailed study sites also exhibited the full range of riverbank features and characteristics as observed during the 2013 FRR. The results from the various field investigations which occurred at each site were then incorporated into BSTEM or were used for independent, supplemental analyses as described in Section 5. Potential primary causes of erosion included (in no particular order):

- Hydraulic shear stress due to flowing water;
- Water level fluctuations due to hydropower operations;
- Boat waves;
- Land management practices and anthropogenic influences to the riparian zone; and
- Ice

During study plan development it was anticipated that potential secondary causes of erosion such as animals, wind waves, seepage and piping, and freeze-thaw could be present at specific locations in the TFI. Based on the geomorphic understanding of the study area it was anticipated that these potential secondary causes of erosion were likely to have minimal to no influence on erosion in the TFI (other than in any specific locations where they may exist). Accordingly, these causes of erosion were analyzed sufficiently to determine their relative contribution to erosion but not to the level of detail and specificity as the potential primary causes of erosion mentioned above.

When the RSP was filed with FERC (August 14, 2013), ice was initially classified as a secondary cause of erosion. Following the announced closure of VY in 2014 it was anticipated that Connecticut River water temperatures would decrease which could potentially result in the increased presence of ice in the TFI during the winter months. As a result of this potential change to the baseline conditions of the study, ice was elevated from a potential secondary cause of erosion to a potential primary cause and studied in greater detail during the winter of 2015-2016 in accordance with the methodology laid out in the addendum to the RSP.

Each of the potential primary causes of erosion which were found to exist in the TFI, as well as the potential secondary causes of erosion which were observed, are discussed in more detail below.

3.2 Erosion Processes

This section presents a more detailed discussion of the potential primary and secondary causes of erosion, and the forces associated with them, which were found to be present in the TFI based on the results of the analyses conducted as part of this study. Information pertaining to the methods, field studies, and data collection pertaining to each cause can be found in Section 4 while details pertaining to the analysis of each cause, and the forces associated with them, can be found in Section 5. Maps and information classifying the cause(s) of erosion at each riverbank segment throughout the TFI can be found in Section 6.

3.2.1 Hydraulic Shear Stress due to Flowing Water

As water flows downstream along a riverbank it exerts a force, often referred to as shear stress or tractive force. Shear stress can be related to the velocity of flowing water. Shear stress increases with increasing velocity or water surface slope of the flowing water. This force tries to remove soil particles whenever the shear stress exceeds what is called the critical shear stress. For non-cohesive sediment particles (such as sand, gravel, cobbles, and boulders), the critical shear stress depends on the size or weight of the particle. Smaller, lighter particles are easier to move and transport than larger, heavier particles. As the velocity or shear stress increases, the sizes of sediment particles that may be removed and transported increases, as does the quantity of sediment that is transported. Thus, higher flows with higher velocities induce greater stresses on riverbanks causing greater erosion and sediment transport. For cohesive soils (clay and to some degree, silt) electro-chemical bonds cause sediment particles to be bound together such that erosion occurs when hydraulic forces exceed the strength of these bonds. A critical shear stress or permissible velocity may be used to describe the relationship between hydraulic forces (boundary shear stress) and whether or not erosion of cohesive sediments may occur.

In addition to the simple concept of hydraulic shear stress exerted by the flow on riverbanks, there are several natural tendencies of rivers that cause erosion. Irregularities in riverbank alignment and other non-uniform flow conditions may cause the formation of eddies. An eddy is a circular pattern of flow that separates or breaks away from the main direction of flow and is directed towards the riverbank, then upstream along the bank, before completing a circular pattern returning again to a downstream direction farther away from the bank. Eddies may cause riverbank erosion by increasing the velocity of flow adjacent to the bank which may then induce further mass-movement of riverbank material.

Rivers do not flow in a straight path, they meander. Meandering is evident along the Connecticut River as it bends and curves from side to side as it generally flows north to south. Meander bends tend to migrate slowly downstream over time. These bends also become over-extended or compressed resulting in the formation of cutoffs of bends and oxbow lakes. All of these processes result in migration of the river via the ongoing erosion and deposition process.

Geomorphic processes of meandering and hydraulic processes of eddy formation tend to cause riverbank erosion and movement of riverbanks through lateral migration and even avulsion. These processes were considered in the analysis of riverbank erosion in the TFI.

3.2.2 Water Level Fluctuations

The water level in the TFI varies over time as a result of a number of factors including seasonal and other hydrological flow variations and hydropower operations. Water level variations due to hydrological flow variations can include snowmelt and rainfall runoff from the watershed which can vary on a daily (or shorter) basis to seasonally. Water level variations due to hydrologic events take hours, days or weeks and range from a few feet up to as many as 10 feet or more in magnitude in major runoff events. Storm events or snow melt, from the upstream watershed or tributaries, drive these major flow variations.

Water levels in the TFI also vary due to hydropower operations from three projects that effect flow and water level, including the Vernon Hydroelectric Project at the upstream end of the TFI, Northfield Mountain (upstream of the French King Gorge), and Turners Falls Hydroelectric Project at the downstream end of the TFI at Turners Falls Dam. Fluctuations due to the various hydropower operations occur on an hourly basis with a magnitude on the order of 3 to 5 feet over a daily cycle; the FERC license permits a 9 foot fluctuation as measured as the Turners Falls Dam.

As water rises, it infiltrates into the riverbank and, if sustained over a sufficient period of time, the high water levels can saturate the soil to a certain depth. Water in the pore spaces within the riverbank material increases the weight of the soil resulting in increased gravitational forces. The added weight can, in some instances, overcome forces resisting movement of riverbank material to the point where pieces of material

break loose and fall or slide down the riverbank when the water level recedes. As the water level falls, water levels in the bank drop. Some may seep back out of the bank through processes of seepage and piping (see Section 3.2.7). Seepage and piping can induce hydraulic forces that by themselves may cause erosion.

3.2.3 Boat Waves

Boat or wind waves can result in water surface fluctuations of relatively small amplitude (on the order of a few inches up to about 1 foot) and short frequency (on the order of seconds or less).

Wind waves on the Connecticut River are relatively small and typically do not form breaking waves since the wind cannot act over a significant length of water (called fetch) because the river lies at the bottom of a valley protected on both sides by mountains. This is particularly true of winds that blow in the west to east direction, across the river that primarily flows north to south. Fetch is also relatively short for winds that blow in the north-south direction because the river flows around bends thereby limiting the length over which wind can build waves. Given this, wind waves were generally not found to be a factor in erosion processes throughout the TFI and are not discussed further in this report.

While boat and wind waves have some similarities, boat waves, particularly those that are formed close to the shore, can cause an impact and greater disturbance than just a simple fluctuation. Boat waves tend to be larger in amplitude than wind waves and were observed to travel across the water surface impacting the riverbanks in the TFI. Wave energy is converted to a shear stress acting as a vector sum with the shear stress due to flow. The repeated crashing of boat waves against the riverbank can result in repeated particle by particle erosion until, eventually, a mass wasting event occurs due to the undermined bank. This can be especially true when water levels are elevated and/or the boat waves are repeatedly crashing against the same elevation of the bank for extended periods of time. This is particularly true when the waves impact the toe of the upper bank (or higher) as opposed to the flat lower bank (beach).

3.2.4 Land Management Practices and Anthropogenic Influences to the Riparian Zone

Land-use or management practices may affect the stability of riverbanks. A healthy riparian zone including vegetation that dampens the velocity and effective stress acting on the bank material, and attenuates waves near the riverbank that can significantly reduce erosion. In addition, the fine-root structure helps bind the soil particles together; further increasing the resistance to hydraulic forces. Increased shear strength is also provided by root reinforcement within the upper bank. To the extent that riparian vegetation is impacted by land-use, land management practices, or anthropogenic influences the erosion resistance from vegetation may be likewise reduced. Vegetation may be cleared for agriculture, housing or other types of development. On the other hand, erosion protection or riverbank stabilization may prevent or minimize erosion in segments of the river. It is also recognized that erosion protection at a given location along a river may adversely affect adjacent riverbank areas in the vicinity of where erosion protection has been developed.

3.2.5 Ice

Ice may cause erosion or damage to riparian vegetation which can cause erosion. Sheet ice may increase the velocity or flow of water in the area below the ice and adjacent to the riverbank. With changing water levels, it may pull or scrape vegetation. If ice floes form during ice breakup, moving blocks of ice can again scrape, damage, or even shear off vegetation. Ice floes may also impact directly against the bank moving or breaking off blocks of soil. Through damage or removal of vegetation or direct displacement of the soil itself, ice has the capacity to erode riverbanks.

In addition, water is found in at least some of the pore spaces between soil particles in riverbanks. During sufficiently cold weather (in terms of temperature and duration), some of the water in riverbanks can freeze. As water freezes it expands thereby loosening soil particles or causing an expansion of the space between particles or causing cracks in the soil matrix. Additional water can find its way into larger spaces and with

additional freeze-thaw cycles more disruption of the soil matrix can occur. This freeze-thaw process is a common cause of damage to pavement on roads. In cold climates, freeze-thaw can adversely affect riverbank stability allowing flow-related forces or gravity to have an enhanced erosive effect on riverbanks.

3.2.6 Animals

As noted in the RSP, animals can be both a potential primary and/or secondary cause of erosion. Cattle grazing to the river's edge or the removal or trampling of vegetation resulting from animal trails leading to the river are potential land management or anthropogenic factors which were evaluated as potential primary causes of erosion. These activities can lead to runoff issues, gullying, and damage to the soil matrix which all contribute to bank instability. Wild animals and birds (potential secondary cause) can also contribute to bank instability and erosion; an example of which are animals that burrow into riverbanks which may lead to concentrated points of seepage or direct damage to the bank.

3.2.7 Seepage and Piping

When the flow and water level is higher than the water level in the ground, water can infiltrate laterally into the riverbank. Either when high water recedes or when the ground-water table is higher than the river, a hydraulic gradient drives water from the surrounding ground towards the river. Water moves through the soil but may not drain as quickly as the water level. The pressure gradient can weaken or act against the standing riverbanks causing blocks of sediment to loosen, drop, or slide. During periods of declining stage, seepage of water occurs towards the river and out of the riverbanks. This water may find a layer of coarser sediment, with greater hydraulic conductivity, where seepage flows with greater velocity through the riverbank. Seepage of water through the soil in general, or piping through confined layers or concentrated areas of flow, can move soil particles causing internal erosion or weakening. This can lead to the development of undercuts and to greater movement of blocks of soil acted on by gravity.

While a few limited areas of seepage were identified flowing over the lower bank or beach in the TFI, these areas did not exhibit significant erosion or sloughing due to seepage related erosion on the upper riverbank areas. As such, seepage and piping were not found to be a significant factor in erosion processes throughout the TFI at the detailed study sites and are not discussed further in this report. Groundwater data collected from monitoring wells adjacent to the river are discussed in Section 5.5.2.1 as it pertains to the impact of water level fluctuations in the TFI.

4 FIELD STUDIES, DATA COLLECTION, AND MODELING BACKGROUND

Various geomorphic, geotechnical, hydraulic, and hydrologic datasets were developed in the TFI during the 1990's and 2000's which provided a valuable foundation for this study. While the existing datasets proved useful, data gaps were identified during the data gathering and literature review conducted as part of RSP Task 1. Based on these data gaps, additional field studies and data collection efforts were identified and completed in order to satisfy the objectives established in the RSP. Additional field studies and data collection efforts were a combination of investigations associated with other relicensing studies (e.g., Study No. 3.1.1, 3.2.2, etc.) and those unique to this study (e.g., BSTEM input parameters). Field studies and data collection efforts which were conducted in accordance with RSP Task 4 included:

- Compilation of Project operations and USGS data (water surface elevation, flow, etc.) for the period 2000-2014;
- 2013 Full River Reconnaissance Survey (Study No. 3.1.1) which characterized the riverbank features, characteristics, and erosion conditions throughout the TFI;
- Bathymetric surveys of the TFI to support development of the hydraulic models (Study No. 3.2.2)
- Development of a HEC-RAS model of the TFI (Study No. 3.2.2);
- Development of a River2D model of the TFI;
- Compilation of annual historic cross-section surveys and development of new cross-section surveys for the long-term fixed riverbank transects (2000-2014)[10] and newly identified detailed study sites (2014 and 2015);
- Various input datasets for BSTEM;
- Suspended sediment monitoring and sampling (Study No. 3.1.3); and
- Investigation of ice and its potential impact on riverbank processes

Each of these field studies or data collection efforts are discussed in greater detail in the following sections. The data yielded from these efforts, combined with the considerable amount of existing information, provided the geomorphic, geotechnical, hydraulic, and hydrologic data needed to satisfy the goals and objectives of this study, including determining the impact of Project operations on erosion and bank instability. As discussed in Section 5, these datasets were used for a range of analyses as part of the three-level analysis approach previously discussed.

Field studies and data collection efforts conducted as part of this study occurred at a number of detailed study sites located throughout the geographic extent of the TFI.[11] Detailed study sites were identified in 2014 in consultation with stakeholders, FERC, and MADEP in accordance with FERC's SPDL. The

[10] While some long-term fixed riverbank transects have been surveyed as far back as the 1990's, only the survey data from 2000-2014 was utilized for this study as this was the period modeled in BSTEM.
[11] Due to accessibility issues, ice monitoring and boat wake data collection occurred at locations other than the detailed study sites.

detailed study site selection process was presented in the 2014 report titled *Study No. 3.1.2 Northfield Mountain/Turners Falls Operations Impact on Existing Erosion and Bank Instability – Selection of Detailed Study Sites – September 2014* (FirstLight, 2014b). A summary of this process is presented in the following section.

4.1 Selection of Detailed Study Sites

To gain a thorough understanding of the causes of erosion, the forces associated with them, and their relative importance at a particular location, FirstLight developed a methodology to identify and select a number of detailed study sites where investigation and analyses would occur as part of this study. Data collected at each of the detailed study sites were used as input parameters for BSTEM as well as other analyses associated with the three-level approach. In-depth investigation at the detailed study sites was typically limited to the potential primary causes of erosion, and the forces associated with them, although observations of any potential secondary causes of erosion were made if such causes were present. The final set of detailed study sites represented both existing permanent transects and newly identified sites. The study sites spanned the geographic extent of the TFI and encompassed the full range of riverbank features, characteristics, and erosion conditions observed during the 2013 FRR.

The final set of detailed study sites were selected based on a four step methodology:

1. Evaluate Existing, Permanent Transects and Identify Calibration and/or Representative Locations for Detailed Study;

2. Identify Supplemental Representative Locations for Detailed Study;

3. Evaluate the Range of Riverbank Features and Characteristics of the Representative Locations Selected for Detailed Study; and

4. Evaluate the Geographic Distribution of the Representative Locations Selected for Detailed Study

An existing, permanent transect is a permanently established cross-section that has been surveyed from one bank, across the river, to the other bank. These transects were established in areas where erosion had been known to occur dating back to the 1990's and have generally been surveyed annually. Typically a benchmark with a known vertical and horizontal datum is placed on the endpoints such that future surveys can be compared. Due to varying hydraulic and geomorphic conditions found along a river, riverbank features, characteristics, and erosion conditions can vary from one bank to the other at a given transect. As such, each transect represented two potential detailed study points. For the purposes of this study, a detailed study point was defined as the specific location (i.e. right or left bank) where detailed investigation, field data collection, and analysis occurred.

Existing permanent, transects were evaluated and compared against the results of the 2013 FRR at which time they were classified as: (1) calibration only sites; (2) both calibration and representative sites; or (3) eliminated from consideration. *Calibration sites* were defined as detailed study sites established at an existing, permanent transect location where data collection would be used to calibrate BSTEM. Establishing these sites at the existing, permanent transects provided the opportunity to calibrate BSTEM with actual erosion amounts or changes in bank geometry as it has occurred over a period of historic flows and water level data. *Representative sites* were defined as detailed study sites established throughout the TFI at locations that exhibit a range of representative features, characteristics, and erosion conditions. These sites did not have repetitive surveys for calibration of BSTEM. Calibration sites could only exist at existing, permanent transects while representative sites can exist anywhere in the TFI. The selected existing, permanent transects were then compared against a table of riverbank characteristics of interest to identify potential gaps.

Riverbank features and characteristics identified during this gap analysis were then supplemented with additional representative detailed study points. Supplemental representative detailed study points were proposed based on the results of the detailed geomorphic and geotechnical assessments conducted during the 2013 FRR land-based survey as well as the results of the 2013 FRR boat-based survey. The newly identified supplemental representative detailed study points were selected at only one bank, however, full cross-section surveys were collected at each location. The combination of representative existing, permanent transects and supplemental representative detailed study points resulted in a comprehensive set of locations which were representative of the riverbank features and characteristics of interest found throughout the TFI.

Once the list of representative locations selected for detailed study was selected the range of riverbank features and characteristics of those locations were evaluated to ensure they were representative of conditions found throughout the TFI. In order to be considered representative, the detailed study sites must have exhibited the range of riverbank characteristics of interest and met the following criteria:

- Locations where riverbanks are stable (including at least one site where bank stabilization has occurred as a result of the ECP and at least one site that is naturally stable with no bank stabilization work present);
- Locations where the potential for future erosion is low;
- Locations where the potential for future erosion is high; and
- Locations where active erosion is occurring

Following the completion of the representativeness assessment, the geographic distribution of the representative locations selected for detailed study was evaluated to ensure they were appropriately distributed throughout the TFI.

After completing this four step methodology FirstLight presented a list of proposed representative and calibration study sites to MADEP, CRWC, FRCOG, CRSEC, and the New Hampshire Department of Environmental Services (NHDES) for review and comment as per FERC's SPDL (FERC, 2013). After receiving written comments and meeting with the MADEP and Stakeholders, FirstLight updated and finalized the location of detailed study sites based on the feedback received.[12] After filing the final set of detailed study site locations with FERC, no further comments were received from MADEP or the Commission.

The final list of detailed study sites established for this study included 25 locations throughout the geographic extent of the TFI which encompassed a representative range of riverbank features, characteristics, and erosion conditions. Of the 25 detailed study sites, 16 were classified as representative (of which 7 are both calibration and representative), and 9 were classified as calibration sites. In other words, 16 detailed study sites are located at existing, permanent transects while 9 were established at new locations identified as a result of the 2013 FRR. Table 4.1-1 demonstrates the riverbank features and characteristics of interest and which detailed study site(s) exhibits those traits while Table 4.1-2 and 4.1-3 provide additional details about each site. The location of the detailed study sites is depicted in Figures 4.1-1 and 4.1-2.

[12] Meetings were held on June 4, 2014 at MADEP offices in Springfield, MA and June 24, 2014 and August 4, 2014 at the Northfield Mountain Visitors Center.

As illustrated in Table 4.1-1, the selected representative sites have a balanced distribution over the various Stages of Erosion and Extents of Current Erosion found throughout the TFI. In regard to the Stage of Erosion, of the 16 representative sites, two are located where Potential Future Erosion exists, five at Actively Eroding sites, four at Eroded sites, and five at Stable sites.[13] In regard to the Extent of Erosion, six representative sites are located where None/Little Erosion exists, five where Some Erosion exists, three where Some to Extensive Erosion exists, and two where Extensive Erosion exists. In addition, a broad range of significant upper and lower riverbank features including vegetation, slope, sediment, and bank height are well represented. Finally, as demonstrated in Figures 4.1-1 and 4.1-2 the final list of detailed study sites adequately covers the geographic extent of the TFI.

A discussion of how the detailed study sites were selected and the full results of this process are found in, *"Relicensing Study 3.1.2 Northfield Mountain/Turners Falls Operations Impact on Existing Erosion and Potential Bank Instability Selection of Detailed Study Sites – September 2014"* (FirstLight, 2014b). Field efforts associated with Study No. 3.1.2 began in July 2014 and continued through September 2014. Data collection was completed in the summer of 2015. Data collection efforts are discussed in detail in the ensuing sections. Detailed site sketches of each detailed study site developed by Kit Choi (geotechnical engineer) are found in Volume III (Appendix D).

[13] Sites classified as Stable represent locations that were Stable at the time of observation.

Table 4.1-1: Summary of Riverbank Features and Characteristics – Representative Locations for Detailed Study

FEATURES	CHARACTERISTICS[14]					
Upper Riverbank Slope	**Overhanging** 26, 87(B)	**Vertical** 2L, 21, 29, 75(B)	**Steep** 7L, 8B-L, 12(B), 21, 26, 29, 119(B)	**Moderate** 4L, 7R, 10R, 18, 303B, BC-1R	Flat	
Upper Riverbank Height	Low	**Medium** 4L, 303B	**High** 2L, 7L, 7R, 8B-L, 10R, 12(B), 18, 21, 26, 29, 75(B), 87(B), 119(B), BC-1R			
Upper Riverbank Sediment[15]	Clay	**Silt/Sand** 2L, 4L, 7L, 7R, 8B-L, 10R, 12(B), 18, 21, 26, 29, 75(B), 87(B), 119(B), 303B, BC-1R	Gravel	Cobbles	Boulders	Bedrock
Upper Riverbank Vegetation	**None to Very Sparse**	**Sparse** 12(B), 75(B), 87(B), 119(B)	**Moderate** 2L, 8B-L, 21	**Heavy** 4L, 7L, 7R, 10R, 18, 26, 29, 303B, BC-1R		
Lower Riverbank Slope[16]	Vertical	Steep	**Moderate** 7R, 10R	**Flat/Beach** 2L, 4L, 7L, 8B-L, 12(B), 18, 21, 26, 29, 75(B), 87(B), 119(B), 303B, BC-1R		

[14] Categories that are highlighted in yellow were identified as characteristics that are indicative of areas where active erosion is most likely to occur or the potential for future erosion is high. Highlighted categories were identified based on review of historic geomorphic data and the results of the 2013 FRR. Transects and detailed study points that will be used for investigation and analyses associated with Study No. 3.1.2 are based on the highlighted categories.
[15] While clay, gravel, cobble, boulder, and bedrock upper riverbank sediments may exist in some locations throughout the Impoundment, these locations are rare and therefore are not representative of riverbank features and characteristics found in the study area. As such, these characteristics are not of interest to the objectives of this study.
[16] Vertical and Steep lower riverbank slopes are typically indicative or areas where active erosion is occurring or the potential for future erosion is high and therefore would normally be highlighted in yellow. These categories are not highlighted, however, as these specific riverbank conditions do not exist in the Impoundment.

FEATURES	CHARACTERISTICS[14]					
Lower Riverbank Sediment	Clay	**Silt/Sand** 2L, 4L, 7L, 8B-L, 12(B), 18, 26, 29, 75(B), 87(B), 119(B), 303B, BC-1R	**Gravel** 21	**Cobbles** 10R	**Boulders** 7R	Bedrock
Lower Riverbank Vegetation	**None to Very Sparse** 2L, 4L, 7L, 7R, 8B-L, 12(B), 18, 21, 26, 29, 75(B), 87(B), 119(B), BC-1R	**Sparse** 10R	**Moderate**	**Heavy** 303B		
Stage of Erosion	**Potential Future Erosion** 7L, 8B-L	**Active Erosion** 12(B), 21, 26, 29, 75(B)	**Eroded** 18, 2L*, 87(B), 119(B)	Stable 4L, 7R, 10R, 303B, BC-1R		
Extent of Current Erosion	**None/Little** 4L, 7L, 7R, 10-R, 303B, BC-1R	**Some** 2L, 8B-L, 18, 26, 29	**Some to Extensive** 21, 87(B), 119(B)	**Extensive** 12(B), 75(B)		

Table 4.1-2: Overview of Representative and Calibration Locations for Detailed Study

Location ID	Source	Bank[17]	Representative or Calibration Site	Comments
BC-1R	Existing, Permanent Transect	Right Bank	Both	Surveyed transect at the entrance to Barton Cove
2L	Existing, Permanent Transect	Left Bank	Both	Surveyed transect just downstream of major tributary (Ashuelot River), erosion with recent stabilization using vegetation only.
3L	Existing, Permanent Transect	Left Bank	Calibration	Surveyed transect, right bank – stabilized (2007, Kendall site), left bank – located downstream of Kendall with multiple types of erosion and indicators of potential erosion. Both banks of the surveyed transect includes an area with erosion occurring prior to stabilization in 2007 and stabilization since then with the opposite bank experiencing several types of erosion and potential erosion indicators with concurrent survey data.
3R	Existing, Permanent Transect	Right Bank	Calibration	
4L	Existing, Permanent Transect	Left Bank	Both	Surveyed transect – cross-section shows some change and left bank exhibits potential erosion indicators and erosion (right bank stable with limited potential indicators of future erosion)
5CR	Existing, Permanent Transect	Right Bank	Calibration	Surveyed transect with right bank showing erosion and multiple types of potential erosion, left bank previously stabilized by COE experimental techniques (tires).
6AL	Existing, Permanent Transect	Left Bank	Calibration	Surveyed transect at a location of erosion and heavy boat use in the past with both banks stabilized (Flagg, 2000 and Skalski, 2004). An island bank that is not stabilized is also included to be studied.
6AR	Existing, Permanent Transect	Right Bank	Calibration	
7L	Existing, Permanent Transect	Left Bank	Both	Surveyed transect with one forested high bank and the other a farmed terrace with indicators of potential future erosion.
7R	Existing, Permanent Transect	Right Bank	Both	
8BL	Existing, Permanent Transect	Left Bank	Both	Surveyed transect with one bank with erosion and indicators of potential future erosion and other bank with erosion that is in the process of being stabilized with current techniques of large woody debris, built-up toe and vegetation (Wallace, Bathory/Gallagher, 2012). Detailed study will occur at both banks of the transect.
8BR	Existing, Permanent Transect	Right Bank	Calibration	
9R	Existing, Permanent Transect	Right Bank	Calibration	Surveyed transect with right bank that had eroded but stabilized with preventative maintenance measures (Campground Point, 2008)
10L	Existing, Permanent Transect	Left Bank	Calibration	Surveyed transect with erosion occurring before stabilization in 2001-2002 on right bank (Urgiel upstream), stable left bank. A recent vertical shift in the bank has developed both through the stabilized site and upstream which is of interest in understanding and monitoring.
10R	Existing, Permanent Transect	Right Bank	Both	
11L	Existing, Permanent Transect	Left Bank	Calibration	Surveyed transect through island, left bank and bank of island exhibits erosion and potential erosion indicators
18	FRR Land-based Survey	Left Bank	Representative	Land-based point located between surveyed Transects 2 and 3, multiple indicators of potential erosion
21	FRR Land-based Survey	Right Bank	Representative	The land-based point is experiencing more than one type of erosion and multiple indicators of potential erosion and may be considered for some type of future stabilization
26	FRR Land-based Survey	Right Bank	Representative	Land-based site exhibits various types of erosion and potential future erosion and may represent bank conditions prior to stabilization of transect 10 - right bank.
29	FRR Land-based Survey	Right Bank	Representative	Located between transects 4 and 5A, erosion and multiple indicators of potential erosion
12B	FRR Boat-based Survey	Left Bank	Representative	Boat-based segment with extensive, active erosion and limited vegetation; located downstream of French King Gorge and just upstream of Barton Cove
75B	FRR Boat-based Survey	Left Bank	Representative	Boat-based segment with extensive, active erosion just downstream of the Northfield Mountain Tailrace.

[17] Defined as looking downstream

Location ID	Source	Bank[17]	Representative or Calibration Site	Comments
87B	FRR Boat-based Survey	Left Bank	Representative	Boat-based segment exhibits eroded conditions and several indicators of potential future erosion; located upstream of Northfield Mountain Tailrace and a short distance downstream of Shearer stabilization site
119B	FRR Boat-based Survey	Left Bank	Representative	Boat-based segment exhibits eroded conditions and several indicators of potential future erosion; located near the downstream end of Kidds Island
303B	FRR Boat-based Survey	Left Bank	Representative	Boat-based segment located downstream of the Ashuelot River confluence. Segment exhibits Heavy lower riverbank vegetation and Medium upper riverbank height.
9	*Supplemental sites selected based on the results of the 2013 FRR*			
7	*Existing, permanent transect sites that will be used as both representative and calibration locations*			
9	*Existing, permanent transect sites that will be used as supplemental calibration locations*			
25				

Table 4.1-3: Summary of Riverbank Features and Characteristics – Representative and Calibration Locations for Detailed Study

Location ID	Bank	Source	Representative or Calibration	UPPER RIVERBANK				LOWER RIVERBANK			Type of Erosion	Indicator(s) of Potential Erosion	Stage of Erosion	Extent of Current Erosion
				Slope	Height	Sediment	Vegetation	Slope	Sediment	Vegetation				
BC-1R	Right Bank	Existing, Permanent Transect	Both	Moderate	High	Silt/Sand	Heavy	Flat/Beach	Silt/Sand	None/Very Sparse	Undercut	Creep/Leaning Trees	Stable	None/Little
2L	Left Bank	Existing, Permanent Transect	Both	Vertical	High	Silt/Sand	Moderate	Flat/Beach	Silt/Sand	None to Very Sparse	Rotational Slump	Creep/Leaning Trees, Overhanging	Eroded	Some
3L	Left Bank	Existing, Permanent Transect	Calibration	Moderate	Low	Silt/Sand	Heavy	Flat/Beach	Silt/Sand	None to Very Sparse	Undercut, Rotational Slump	Creep/Leaning Trees, Overhanging	Eroded	Some
3R	Right Bank	Existing, Permanent Transect	Calibration	Moderate	High	Silt/Sand	Heavy	Moderate	Gravel	None to Very Sparse	-	-	Stable	None/Little
4L	Left Bank	Existing, Permanent Transect	Both	Moderate	Medium	Silt/Sand	Heavy	Flat/Beach	Silt/Sand	None to Very Sparse	-	Creep/Leaning Trees	Stable	None/Little
5CR	Right Bank	Existing, Permanent Transect	Calibration	Steep	High	Silt/Sand	Moderate	Flat/Beach	Silt/Sand	None to Very Sparse	Slide or Flow	Overhanging Bank, Exposed Roots, Creep/Leaning Trees	Eroded	Some
6AL	Left Bank	Existing, Permanent Transect	Calibration	Moderate	High	Silt/Sand	Heavy	Moderate	Cobbles	None to Very Sparse	-	-	Stable	None/Little
6AR	Right Bank	Existing, Permanent Transect	Calibration	Steep	High	Silt/Sand	Heavy	Flat/Beach	Silt/Sand	Heavy	-	-	Stable	None/Little
7L	Left Bank	Existing, Permanent Transect	Both	Steep	High	Silt/Sand	Heavy	Flat/Beach	Silt/Sand	None to Very Sparse	Undercut	Creep/Leaning Trees	Potential Future Erosion	None/Little
7R	Right Bank	Existing, Permanent Transect	Both	Moderate	High	Silt/Sand	Heavy	Moderate	Boulders	None to Very Sparse	-	-	Stable	None/Little
8BL	Left Bank	Existing, Permanent Transect	Both	Steep	High	Silt/Sand	Moderate	Flat/Beach	Silt/Sand	None to Very Sparse	Undercut	Creep/Leaning Trees, Exposed Roots, Overhanging Bank	Potential Future Erosion	Some
8BR	Right Bank	Existing, Permanent Transect	Calibration	Steep/Overhanging	High	Silt/Sand	Heavy	Flat/Beach	Gravel	None to Very Sparse	-	Overhanging	In process of stabilization	None/Little
9R	Right Bank	Existing, Permanent Transect	Calibration	Moderate	High	Silt/Sand	Moderate	Flat/Beach	Silt/Sand	None to Very Sparse	-	Creep/Leaning Trees	Stable	None/Little
10L	Left Bank	Existing, Permanent Transect	Calibration	Moderate	High	Silt/Sand	Heavy	Flat/Beach	Silt/Sand	None to Very Sparse	-	-	Stable	None/Little
10R	Right Bank	Existing, Permanent Transect	Both	Moderate	High	Silt/Sand	Heavy	Moderate	Cobbles	Sparse	-	-	Stable	None/Little
11L	Left Bank	Existing, Permanent Transect	Calibration	Moderate	High	Silt/Sand	Heavy	Flat/Beach	Silt/Sand	None to Very Sparse	Undercut	Undercut, Creep/Leaning trees	Stable	None/Little

Location ID	Bank	Source	Representative or Calibration	UPPER RIVERBANK				LOWER RIVERBANK			Type of Erosion	Indicator(s) of Potential Erosion	Stage of Erosion	Extent of Current Erosion
				Slope	Height	Sediment	Vegetation	Slope	Sediment	Vegetation				
18	Left Bank	FRR Land-based Survey	Representative	Moderate	High	Silt/Sand	Heavy	Flat/Beach	Silt/Sand	None/Very Sparse	Undercut	Undercut, Exposed Roots, Creep/Leaning Trees	Eroded	Some
21	Right Bank	FRR Land-based Survey	Representative	Steep (some vertical)	High	Silt/Sand	Moderate	Flat/Beach	Gravel, Silt/Sand	None/Very Sparse	Rotational Slump, Undercut	Undercut, Exposed Roots, Creep/Leaning Trees	Active	Some to extensive
26	Right Bank	FRR Land-based Survey	Representative	Steep/Overhanging	High	Silt/Sand	Heavy	Flat/Beach	Silt/Sand	None/Very Sparse	Rotational Slump, Undercut	Undercut, Exposed Roots, Creep/Leaning Trees	Active	Some
29	Right Bank	FRR Land-based Survey	Representative	Steep (near vertical)	High	Silt/Sand	Heavy	Flat/Beach	Silt/Sand	None/Very Sparse	Rotational Slump, Undercut	Undercut, Exposed Roots, Creep/Leaning Trees	Active	Some
12B	Left Bank	FRR Boat-based Survey	Representative	Steep	High	Silt/Sand	Sparse	Flat/Beach	Silt/Sand	None to Very Sparse	Undercut	Exposed Roots, Overhanging Bank	Active	Extensive
75B	Left Bank	FRR Boat-based Survey	Representative	Vertical	High	Silt/Sand	Sparse	Flat/Beach	Silt/Sand	None to Very Sparse	Topple, Overhanging Bank	Creep/Leaning Trees, Overhanging Bank	Active	Extensive
87B	Left Bank	FRR Boat-based Survey	Representative	Overhanging	High	Silt/Sand	Sparse	Flat/Beach	Silt/Sand	None to Very Sparse	Undercut, Rotational Slump	Exposed Roots, Creep/Leaning Trees, Overhanging Bank	Eroded	Some to Extensive
119B	Left Bank	FRR Boat-based Survey	Representative	Steep	High	Silt/Sand	Sparse	Flat/Beach	Silt/Sand	None to Very Sparse	Slide or Flow	Exposed Roots, Creep/Leaning Trees, Overhanging Bank	Eroded	Some to Extensive
303B	Left Bank	FRR Boat-based Survey	Representative	Moderate	Medium	Silt/Sand	Heavy	Flat/Beach	Silt/Sand	Heavy	-	-	Stable	None/Little

Legend

- Boat-based Representative Location
- Land-based Representative Location
- Existing Transect Calibration Location
- Existing Transect Calibration & Representative Location

Existing, Permanent Transect Location

- Calibration Location
- Calibration and Representative Location

Vernon Dam
HINSDALE
WINCHESTER
11L
2L
303B
VERNON
18
3L
3R
21
VERMONT
MASSACHUSETTS
NEW HAMPSHIRE
MASSACHUSETTS
4L
29
BERNARDSTON
Route 10 Bridge
(Bennett's Meadow Bridge)
5C-R
NORTHFIELD
LEYDEN
26
10L
10R
6A
119(B)
6A
GILL
7R
7L
GREENFIELD
8B-R
8B-L
87(B)
Northfield Mountain
Upper Reservoir
Northfield Tailrace
Barton Cove
75(B)
ERVING
BC1R
9R
Turners Falls Dam
French King
Bridge (Route 2)
MONTAGUE
12(B)
WENDELL
French King Gorge

FirstLight Power Resources

N

FIRSTLIGHT HYDRO GENERATING COMPANY
Northfield Mountain Pumped Storage Project No. 2485
Turners Falls Hydroelectric Project No. 1889
STUDY 3.1.2

0 0.5 1 2
Miles

Figure 4.1-1 :
Detailed Study Sites
Turners Falls Impoundment

Service Layer Credits: Source: Esri, DigitalGlobe, GeoEye, Earthstar Geographics, CNES/Airbus DS, USDA, USGS, AEX, Getmapping, Aerogrid, IGN, IGP, swisstopo, and the GIS User Community

Path: W:\gis\studies\3_1_2\maps\final_report\figure_4_1-1.mxd

Legend

- 500' River Marker
- 1000' River Marker
- Boat-based Representative Location
- Land-based Representative Location
- Existing Transect Calibration Location
- Existing Transect Calibration & Representative Location
- Existing Transect Calibration Location
- Existing Transect Calibration & Representative Location

French King Gorge

French King Bridge (Route 2)

Millers River

Barton Cove

Barton Cove Island

Turners Falls Dam

230+00, 220+00, 210+00, 200+00, 190+00, 180+00, 170+00, 160+00, 150+00, 140+00, 130+00, 120+00, 110+00, 100+00, 90+00, 80+00, 70+00, 60+00, 50+00, 40+00, 30+00, 20+00, 10+00, 0

9R, BC1R, 12(B)

ERVING, MONTAGUE, GILL, GREENFIELD

MOHAWK TRAIL, RIVER ROAD, KING FRENCH HIGHWAY, MILLERS FALLS ROAD, MAIN ROAD, GUNN SQUARE BRIDGE, UNITY STREET, CANAL STREET

Map 5, Map 4, Map 3, Map 2, Map 1

FIRSTLIGHT HYDRO GENERATING COMPANY
Northfield Mountain Pumped Storage Project No. 2485
Turners Falls Hydroelectric Project No. 1889

STUDY 3.1.2

0 625 1,250 2,500 Feet

Figure 4.1-2:
Representative & Calibration Locations for Detailed Study
Map 1

Service Layer Credits: Sources: Esri, HERE, DeLorme, USGS, Intermap, increment P Corp., NRCAN, Esri Japan, METI, Esri China (Hong Kong), Esri (Thailand), MapmyIndia, © OpenStreetMap contributors, and the GIS User Community

Path: W:\gis\studies\3_1_2\maps\final_report\figure_4_1-2.mxd

Legend

- 500' River Marker
- 1000' River Marker
- Boat-based Representative Location
- Land-based Representative Location
- Existing Transect Calibration Location
- Existing Transect Calibration & Representative Location
- Existing Transect Calibration Location
- Existing Transect Calibration & Representative Location

6A
420+00
Kidds Island
410+00
6A
400+00
119(B)
390+00
NORTHFIELD
MILLERS FALLS ROAD
Ashuela Brook
7R
380+00
Dry Brook
7L
370+00
Pine Meadow Brook
360+00
350+00
340+00
330+00
8B-L
8B-R
GILL
320+00
Fourmile Brook
310+00
87(B)
300+00
290+00
280+00
Northfield Tailrace
270+00
75(B)
260+00
250+00
240+00
230+00
NORTHFIELD ROAD
FRENCH KING HIGHWAY
French King Gorge
220+00
French King Bridge (Route 2)
210+00
200+00
MONTAGUE
ERVIN

Map 5
Map 4
Map 3
Map 2
Map 1

FIRSTLIGHT HYDRO GENERATING COMPANY
Northfield Mountain Pumped Storage Project No. 2485
Turners Falls Hydroelectric Project No. 1889

STUDY 3.1.2

N

0 625 1,250 2,500 Feet

Figure 4.1-2:
Representative & Calibration Locations for Detailed Study
Map 2

Service Layer Credits: Sources: Esri, HERE, DeLorme, USGS, Intermap, increment P Corp., NRCAN, Esri Japan, METI, Esri China (Hong Kong), Esri (Thailand), MapmyIndia, © OpenStreetMap contributors, and the GIS User Community

Path: W:\gis\studies\3_1_2\maps\final_report\figure_4_1-2.mxd

Legend

- 500' River Marker
- 1000' River Marker
- Boat-based Representative Location
- Land-based Representative Location
- Existing Transect Calibration Location
- Existing Transect Calibration & Representative Location
- Existing Transect Calibration Location
- Existing Transect Calibration & Representative Location

620+00
610+00
600+00
590+00
580+00
570+00
560+00
550+00
540+00
530+00
520+00
510+00
500+00
490+00
480+00
470+00
460+00
450+00
440+00
430+00
420+00

Route 10 Bridge
(Bennett's Meadow Bridge)

5C-R
26
10L
10R
6A

Kidds Island

Bennett Brook
Millers Brook
Bailey Brook
Ashuela Brook
Otter Run
Roaring Brook
Connecticut River

MOUNT HERMON
ROUTE 10
GILL CENTER ROAD
MAIN ROAD
MAIN STREET
MAPLE STREET
WARWICK ROAD
MILLERS FALLS ROAD

BERNARDSTON
GILL
NORTHFIELD

Map 5
Map 4
Map 3
Map 2
Map 1

FIRSTLIGHT HYDRO GENERATING COMPANY
Northfield Mountain Pumped Storage Project No. 2485
Turners Falls Hydroelectric Project No. 1889

STUDY 3.1.2

N

0 625 1,250 2,500 Feet

Figure 4.1-2:
Representative & Calibration Locations for Detailed Study
Map 3

Service Layer Credits: Sources: Esri, HERE, DeLorme, USGS, Intermap, increment P Corp., NRCAN, Esri Japan, METI, Esri China (Hong Kong), Esri (Thailand), MapmyIndia, © OpenStreetMap contributors, and the GIS User Community

Path: W:\gis\studies\3_1_2\maps\final_report\figure_4_1-2.mxd

Legend

- 500' River Marker
- 1000' River Marker
- Boat-based Representative Location
- Land-based Representative Location
- Existing Transect Calibration Location
- Existing Transect Calibration & Representative Location
- Existing Transect Calibration Location
- Existing Transect Calibration & Representative Location

NEW HAMPSHIRE
VERMONT
VERMONT
MASSACHUSETTS
VERMONT
MASSACHUSETTS
NEW HAMPSHIRE
MASSACHUSETTS
HINSDALE
WINCHESTER
VERNON
NORTHFIELD
Connecticut River
Newton Brook
Bottom Brook
Mallory Brook
Mill Brook
Pauchaug Brook
Louisiana Brook
Bolton Woods
Bolton Rd
South Parish Rd
Staddle Hill Rd
Gosselin Rd
Mine Rd
Hinsdale Road
Wanamaker Road
Pauchaug Ramp Road
East Northfield Road
West Northfield Road
Mountain Station Road
Fort Bridgman Rd
Mothfield Rd
Avery Cir
Wake's Ln

830+00
800+00
790+00
780+00
770+00
760+00
750+00
740+00
730+00
720+00
710+00
700+00
690+00
680+00
670+00
660+00
650+00
640+00
630+00

3L
3R
21
4L
29

Map 5
Map 4
Map 3
Map 2
Map 1

FIRSTLIGHT HYDRO GENERATING COMPANY
Northfield Mountain Pumped Storage Project No. 2485
Turners Falls Hydroelectric Project No. 1889

STUDY 3.1.2

N

0 625 1,250 2,500 Feet

Figure 4.1-2:
Representative & Calibration Locations for Detailed Study
Map 4

Service Layer Credits: Sources: Esri, HERE, DeLorme, USGS, Intermap, increment P Corp., NRCAN, Esri Japan, METI, Esri China (Hong Kong), Esri (Thailand), MapmyIndia, © OpenStreetMap contributors, and the GIS User Community

Path: W:\gis\studies\3_1_2\maps\final_report\figure_4_1-2.mxd

Legend

- 500' River Marker
- 1000' River Marker
- Boat-based Representative Location
- Land-based Representative Location
- Existing Transect Calibration Location
- Existing Transect Calibration & Representative Location
- Existing Transect Calibration Location
- Existing Transect Calibration & Representative Location

Vernon Dam
1060+00
1050+00
11L
1040+00
1010+00
1000+00
990+00
980+00
1030+00
1020+00
Stebbins Island
970+00
960+00
950+00
2L
303B
940+00
930+00
Upper Island
920+00
910+00
900+00
890+00
880+00
870+00
18
860+00
850+00
840+00
830+00
Ashuelot River
No Name
VERNON
VERMONT
NEW HAMPSHIRE
Newton Brook
Northfield Rd
Map 5
Map 4
Map 3
Map 2
Map 1

FIRSTLIGHT HYDRO GENERATING COMPANY
Northfield Mountain Pumped Storage Project No. 2485
Turners Falls Hydroelectric Project No. 1889

STUDY 3.1.2

0 625 1,250 2,500 Feet

Figure 4.1-2:
Representative & Calibration Locations for Detailed Study
Map 5

Service Layer Credits: Sources: Esri, HERE, DeLorme, USGS, Intermap, increment P Corp., NRCAN, Esri Japan, METI, Esri China (Hong Kong), Esri (Thailand), MapmyIndia, © OpenStreetMap contributors, and the GIS User Community

Path: W:\gis\studies\3_1_2\maps\final_report\figure_4_1-2.mxd

4.2 Field Data Collection Methodology

Study No. 3.1.2 included the collection of a considerable amount of field data upon which a range of analyses and computer modeling were conducted. Field data collection efforts conducted in support of the analyses discussed in Section 5 are presented in-depth throughout this section, including:

- Project operations and water level data – Section 4.2.1
- 2013 Full River Reconnaissance Survey (Study No. 3.1.1) – Section 4.2.2
- Hydraulic modeling (HEC-RAS (Study No. 3.2.2) and River2D) – Section 4.2.3
- Cross-section surveys – Section 4.2.4
- Riverbank sediment particle size distribution, erodibility, geotechnical, and vegetation root density and strength data for BSTEM – Sections 4.2.5 – 4.2.7
- Boat wave data – Section 4.2.8
- Sediment transport (Study No. 3.1.3) – Section 4.2.9
- Groundwater data – Section 4.2.10
- Ice – Section 4.2.11

4.2.1 Project Operations and Water Level Data

At several key locations throughout the TFI, FirstLight has collected and recorded various data to support the operation and management of the Turners Falls and Northfield Mountain Projects. These data include such information as upstream flow released from Vernon Dam and water level, water level at the Northfield Mountain tailrace, water level and storage volume in the Northfield Mountain Upper Reservoir, water levels in the vicinity of Turners Falls Dam and power canal, and flow through the power canal to Cabot Station. These data, along with other information, are recorded on an hourly basis on Hydraulic Computation Data Sheets by FirstLight. Data from the handwritten sheets were digitized for the time period 2000-2014. The digitized data have been utilized in a variety of ways to show variations in water level and flow over time and to understand important relationships between flow and water level.

In support of various relicensing studies FirstLight also installed temporary water level loggers at various locations throughout the TFI from approximately August 1 to November 19, 2013 and from late March to November 7, 2014. The temporary water level loggers were typically deployed in the spring once flows receded and were left in place until late fall at which time they were removed for the winter. Data was typically collected on a 15 or 30 minute time step. The data collected via the seasonal water level loggers provided additional data coverage throughout the geographic extent of the TFI.

In addition to the data collected and recorded by FirstLight, tributary inflow data was obtained from USGS gages located on the Ashuelot (USGS Gage No. 01161000) and Millers Rivers (USGS Gage No. 01166500). Data recorded at these gages, and obtained for this study, included both flow and water level. The USGS also operates a gage on the Connecticut River downstream of the Turners Falls Project in Montague, MA[18] (USGS Gage No. 01170500) which provides flow and water level data.

[18] Note the Montague USGS Gage includes flow contribution from the Deerfield River.

Figure 4.2.1-1 provides the locations where permanent and temporary data collection occurs as well as the locations of the USGS gages previously mentioned.

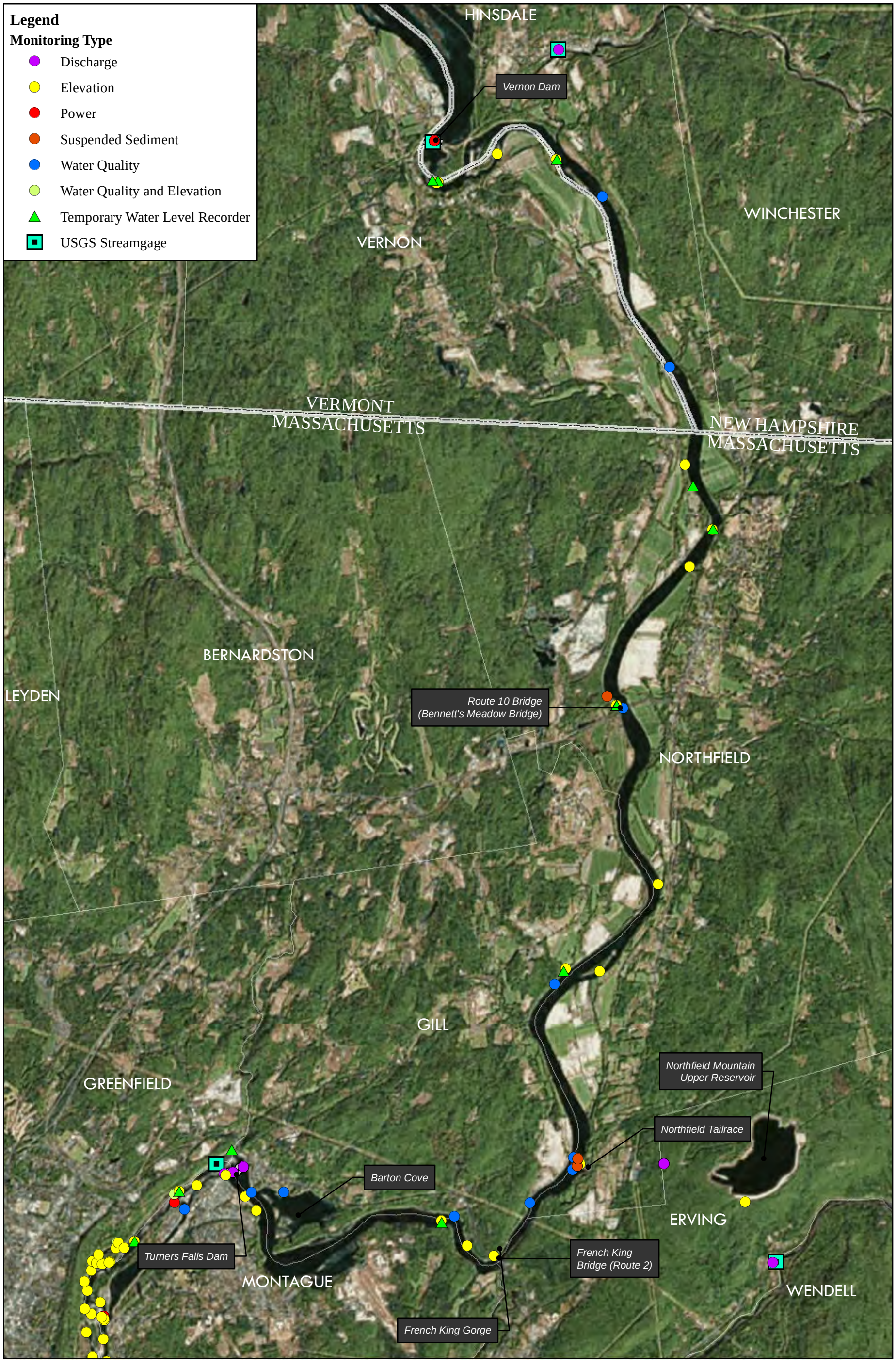

FIRSTLIGHT HYDRO GENERATING COMPANY
Northfield Mountain Pumped Storage Project No. 2485
Turners Falls Hydroelectric Project No. 1889

STUDY 3.1.2

FirstLight Power Resources

N

0 0.5 1 2 Miles

Figure 4.2.1-1:
TFI Water Level and
Flow Equipment Locations

Service Layer Credits: Source: Esri, DigitalGlobe, GeoEye, Earthstar Geographics, CNES/Airbus DS, USDA, USGS, AEX, Getmapping, Aerogrid, IGN, IGP, swisstopo, and the GIS User Community

Path: W:\gis\studies\3_1_2\maps\final_report\figure_4_2_1-1.mxd

4.2.2 2013 Full River Reconnaissance Survey

Relicensing Study No. 3.1.1 – *2013 Full River Reconnaissance* was conducted in 2013[19] with a goal of documenting riverbank features, characteristics, and erosion conditions throughout the TFI from Vernon to the Turners Falls Dam. The main field components of the FRR included: (1) land-use mapping; (2) sensitive receptor mapping; (3) evaluation of past bank stabilization projects; (4) land-based survey; and (5) boat-based survey. An evaluation of the existing, permanent transects located throughout the TFI was also conducted as part of the land- and boat-based surveys. Georeferenced video and geo-tagged photographs were captured at each riverbank segment in order to document riverbank conditions as they were in November 2013. In addition riverbank features and characteristics, land-use, sensitive receptors, and stabilization projects observed during the 2013 FRR were developed into maps in ArcGIS. A final report was filed with FERC on September 15, 2014[20] with an addendum to the report filed with FERC on February 24, 2015.

The boat-based survey identified and recorded the coordinates of the start and end points of riverbank segments based on common riverbank features, characteristics, and erosion conditions as defined in the RSP for Study No. 3.1.1 (FirstLight, 2014a). All riverbanks throughout the TFI, including islands, were assessed during the survey. The boat-based survey provided the best vantage point and perspective of the entire riverbank (i.e. upper and lower bank) the findings of the boat-based survey were used as the primary data source when establishing riverbank segments and developing summary statistics.

The 2013 boat-based survey resulted in delineation of 641 total riverbank segments, including islands. Of the 641 segments, 596 segments totaling 228,009 ft. were located on riverbanks with an additional 45 segments on islands. Segment lengths ranged from 13 ft. to 3,330 ft. with an average river segment length of 383 ft. The minimum and maximum segment lengths for previous FRR's ranged from 20 to over 4,000 ft. with segment lengths ranging from 480 to 1,267. The segment lengths for the 2013 FRR are shorter than all previous FRRs by a significant percentage in all statistical categories resulting in more detailed spatial data.

The land-based survey, conducted simultaneously with the boat-based survey as per MADEP request, identified and defined indicators of potential erosion and bank instability as well as erosion features that may not have been visible from a boat. Land-based segments were delineated and defined based on features and characteristics observed while traversing the top of the bank throughout the entire TFI, including islands. The land-based survey included all riverbanks and islands in the TFI except in areas where: (1) access was not possible or the area was deemed impassible; (2) access was unsafe; or (3) bank conditions did not warrant assessment (e.g. bedrock areas). Detailed geotechnical and geomorphic assessments, including field notes, sketches, and photographs, were also conducted at areas of interest as noted by the fluvial geomorphologist and geotechnical engineer. Overall a total of 38 detailed assessments were conducted. Observations made during the land-based survey were used to complement the findings of the boat-based survey and provide supplemental information and perspective to the overall assessment of TFI riverbanks.

The results of the 2013 FRR indicated that the majority of the upper riverbanks in the TFI were found to have moderate or steep slopes, heights greater than 12 ft., be comprised of silt/sand, and have heavy vegetation. The majority of the lower riverbanks were found to have flat/beach to moderate slopes, be comprised of silt/sand, and have none to very sparse vegetation. Erosion conditions in the TFI were found to be generally stable with None/Little current erosion occurring through much of this reach. As noted in the report, 84.8% of the total length of the TFI riverbanks were found to have None/Little erosion, 14.1%

[19] The majority of the field work associated with the FRR was conducted in the fall of 2013 with supplemental field work occurring in the spring and summer of 2014.
[20] *Relicensing Study No. 3.1.1 2013 Full River Reconnaissance Northfield Mountain Pumped Storage Project (No. 2485) and Turners Falls Hydroelectric Project (No. 1889)*

Some erosion, 0.5% Some to Extensive erosion, and 0.6% Extensive erosion. Furthermore, 5.5% of the total length of TFI riverbanks were found to have Potential Future Erosion, 0.6% Active Erosion, 9.1% Eroded, 83.5% Stable, and 1.3% in the Process of Stabilization. Table's 4.2.2-1 and 4.2.2-2 provide riverbank classification criteria and classification definitions which were used during the 2013 FRR. Table 4.2.2-3 includes summary statistics for TFI riverbank features and characteristics. Figure 4.2.2-1 depicts the extent of erosion throughout the TFI as observed during the 2013 FRR.

The findings of the 2013 FRR were used to inform the selection of detailed study sites and, combined with the annual cross-section surveys, in support of various analyses and modeling discussed in Section 5. A more in-depth discussion of the 2013 FRR, including all related figures and tables, can be found in the final study report issued in September 2014 (FirstLight, 2014a).

Table 4.2.2-1: Turners Falls Impoundment Riverbank Classifications for the 2013 FRR Boat-based survey (FirstLight, 2014a)

UPPER RIVERBANK CHARACTERISTICS[21]						
Upper Riverbank Slope	Overhanging *>90°*	Vertical *90°*	Steep *(>2:1)*	Moderate *(4:1-2:1)*	Flat *(<4:1)*	
Upper Riverbank Height *(total height above normal river level)*	Low *(<8 ft.)*	Medium *(8-12 ft.)*	High *(>12 ft.)*			
Upper Riverbank Sediment	Clay *(.001-.062mm)*	Silt/Sand *(.062-2 mm)*	Gravel *(2-64mm)*	Cobbles *(64-256mm)*	Boulders *(256-2048mm)*	Bedrock
Upper Riverbank Vegetation	None to Very Sparse *(<10%)*	Sparse *(10%-25%)*	Moderate *(25%-50%)*	Heavy *(>50%)*		
Sensitive Receptors	*Important wildlife habitat located at or near the riverbank*					
LOWER RIVERBANK CHARACTERISTICS						
Lower Riverbank Slope	Vertical *90°*	Steep *(>2:1)*	Moderate *(4:1-2:1)*	Flat / Beaches *(<4:1)*		
Lower Riverbank Sediment	Clay *(.001-.062mm)*	Silt/Sand *(.062-2 mm)*	Gravel *(2-64mm)*	Cobbles *(64-256mm)*	Boulders *(256-2048mm)*	Bedrock
Lower Riverbank Vegetation	None to Very Sparse *(<10%)*	Sparse *(10%-25%)*	Moderate *(25%-50%)*	Heavy *(>50%)*		
Sensitive Receptors	*Important wildlife habitat located at or near the riverbank*					
EROSION CLASSIFICATION						
Type(s) of Erosion	Falls – Undercut	Falls – Gullies	Topples	Slide or Flow	*Planar Slip* *Rotational Slump* *Flow*	
Indicators of Potential Erosion	Tension Cracks	Exposed Roots	Creep/ Leaning Trees	Overhanging bank	Notching	Other
Stage(s) of Erosion	Potential Future Erosion	Active Erosion	Eroded	Stable		
Extent of Current Erosion	None/Little *(<10%)*	Some *(10%-40%)*	Some to Extensive *(40%-70%)*	Extensive *(>70%)*		

[21] All quantitative classification criteria (e.g. slope, height, vegetation, extent, etc.) were based on approximate estimates made during field observations of riverbanks. The FRR was a reconnaissance level survey that did not include quantitative field measurements of characteristics.

Table 4.2.2-2: 2013 FRR Riverbank Classification Definitions (FirstLight, 2014a)

RIVERBANK CHARACTERISTICS *(Upper and Lower)*[22]	
Riverbank Slope	**Overhanging** – any slope greater than 90º
	Vertical – slopes that are approximately 90º
	Steep – exhibiting a slope ratio greater than 2 to 1
	Moderate – ranging between a slope ratio of 4 to 1 and 2 to 1
	Flat – exhibiting a slope ratio less than 4 to 1[23]
Riverbank Height	**Low –** height less than 8 ft above normal river level[24]
	Medium – height between 8 and 12 ft above normal river level
	High – height greater than 12 ft above normal river level
Riverbank Sediment	**Clay –** any sediment with a diameter between .001 mm and 2 mm
	Silt / Sand – any sediment with a diameter between .062 mm and 2 mm
	Gravel – any sediment with a diameter between 2 mm and 64 mm
	Cobbles – any sediment with a diameter between 64 mm and 256 mm
	Boulders – any sediment with a diameter between 256 mm and 2048 mm
	Bedrock – unbroken, solid rock
Riverbank Vegetation	**None to Very Sparse –** less than 10% of the total riverbank segment is composed of vegetative cover
	Sparse – 10-25% of the total riverbank segment is composed of vegetative cover
	Moderate – 25-50% of the total riverbank segment is composed of vegetative cover
	Heavy – 50 % or greater of the total riverbank segment is composed of vegetative cover
Sensitive Receptors	Important wildlife habitat located at or near the riverbank.
EROSION CLASSIFICATIONS	
Type(s) of Erosion[25]	**Falls –** Material mass detached from a steep slope and descends through the air to the base of the slope. Includes erosion resulting from transport of individual particles by water.
	Topples – Large blocks of the slope undergo a forward rotation about a pivot point due to the force of gravity. Large trees undermined at the base enhance formation.
	Slides – Sediments move downslope under the force of gravity along one or several discrete surfaces. Can include planar slips or rotational slumps.
	Flows – Sediment/water mixtures that are continuously deforming without distinct slip surfaces.
Indicators of Potential Erosion	**Tension Cracks –** a crack formed at the top edge of a bank potentially leading to topples or slides (FGS, 2007)
	Exposed Roots – trees located on riverbanks with root structures exposed, overhanging.
	Creep – defined as an extremely slow flow process (inches per year or less) indicated by the presence of tree trunks curved downslope near their base (FGS, 2007)
	Overhanging Bank – any slope greater than 90º
	Notching – similar to an undercut, defined as an area which leaves a vertical stepped face presumably after small undercut areas have failed.

[22] All quantitative classification criteria (e.g. slope, height, vegetation, extent, etc.) were based on approximate estimates made during field observations of riverbanks. The FRR was a reconnaissance level survey that does not include quantitative analysis.
[23] Beaches are defined as a lower riverbank segment with a flat slope
[24] For the purpose of this study, Normal Water Level was defined as water levels within typical pool fluctuation levels, but below 186 ft.
[25] FGS, 2007

	Other – Indicators of potential erosion that do not fit into one of the four categories listed above will be noted by the field crew.[26]
Stage(s) of Erosion	**Potential Future Erosion –** riverbank segment exhibits multiple or extensive indicators of potential erosion
	Active Erosion – riverbank segment exhibits one or more types of erosion as well as evidence of recent erosion activity
	Eroded – riverbank segment exhibits indicators that erosion has occurred (e.g. lack of vegetation, etc.), however, recent erosion activity is not observed. A segment classified as Eroded would typically be between Active Erosion and Stable on the temporal scale of erosion.
	Stable – riverbank segment does not exhibit types or indicators of erosion
Extent of Current Erosion	**None/Little[27] –** generally stable bank where the total surface area of the bank segment has approximately less than 10% active erosion present.
	Some – riverbank segment where the total surface area of the bank segment has approximately 10-40% active erosion present
	Some to Extensive – riverbank segment where the total surface area of the bank segment has approximately 40-70% active erosion present
	Extensive – riverbank segment where the total surface area of the bank segment has approximately more than 70% active erosion present

[26] Segments with features classified as "Other" exhibited various erosion processes that did not fit in one of the existing classification categories.

[27] Riverbanks consist of an irregular surface and include a range of natural materials (silt/sand, gravel, cobbles, boulders, rock, and clay), above ground vegetation (from grasses to trees), and below ground roots of different densities and sizes. Due to these characteristics, there are small areas of disturbance which often occur at interfaces between materials, particularly in the vicinity of the water surface. These small disturbed areas can be considered as erosion, or sometimes can result from deposition or even eroded deposition. No natural riverbank exists which does not have at least some relatively small degree of disturbance or erosion associated with the natural combination of sediment types/sizes and vegetation. As such, the extent of erosion for generally stable riverbanks that include these relatively small disturbed areas is characterized as little/none.

Table 4.2.2-3: Summary statistics of Turners Falls Impoundment riverbank features and characteristics – 2013 FRR (FirstLight, 2014a)

Riverbank Features	Characteristics					
Upper Riverbank Slope	Overhanging 1.8%	Vertical 1.6%	Steep 28.0%	Moderate 59.8%	Flat 8.8%	
Upper Riverbank Height	Low 15.5%	Medium 5.7%	High 78.8%			
Upper Riverbank Sediment	Clay -	Silt/Sand 95.6%	Gravel -	Cobbles -	Boulders 0.9%	Bedrock 3.5%
Upper Riverbank Vegetation	None to Very Sparse 1.9%	Sparse 1.3%	Moderate 17.1%	Heavy 79.7%		
Lower Riverbank Slope	Vertical 0.8%	Steep 2.3%	Moderate 27.5%	Flat/Beach 69.4%		
Lower Riverbank Sediment	Clay <0.1%[28]	Silt/Sand 59.6%	Gravel 7.9%	Cobbles 8.7%	Boulders 11.9%	Bedrock 11.9%
Lower Riverbank Vegetation	None to Very Sparse 88.3%	Sparse 3.5%	Moderate 3.2%	Heavy 5.0%		
Type of Erosion	Falls-Undercut 43.4%	Falls-Gullies 0.03%	Topples 1.1%	Slide or Flow 6.2%	Planar Slip 1.1%	Rotational Slump 1.5%
Potential Indicators of Erosion	Tension Cracks <0.10[29]%	Exposed Roots 38.1%	Creep/Leaning Trees 62.7%	Overhanging Bank 12.7%	Notch 5.0%	Other 1.1%

[28] Clay was found in few segments of the river but where some clay was found the sediment was dominated by another type of sediment either vertically or horizontally within a segment. When this occurred the segment was classified using the dominant sediment type. For example, some clay was observed in segment 342 (just downstream of Vernon Dam on the left bank) but the segment was classified using the dominant sediment type.

[29] Tension cracks can only be observed from land-based observations. Some tension cracks were observed during the land-based survey and are reported at those sites as indicated in the notes for the land-based work. Tension cracks were not observed to be significant in the more general top of bank observations when walking along the length of the TFI.

Riverbank Features	**Characteristics**					
Stage of Erosion	Potential Future Erosion 5.5%	Active Erosion 0.6%	Eroded 9.1%	Stable 83.5%	In Process of Stabilization 1.3%[30]	
Extent of Current Erosion	None/Little 84.8%	Some 14.1%	Some to Extensive 0.5%	Extensive 0.6%		

[30] While originally not one of the RSP erosion condition classifications, one riverbank segment was classified as being "In the Process of Stabilization" due to the fact that riverbank stabilization work was being constructed at this particular segment (421, Bathory/Gallagher 2013) during the 2013 FRR. A gravel beach at the top of the lower riverbank had been placed along with large woody debris. Vegetation is then being planted to provide additional stabilization on the gravel beach as well as extending other vegetation onto portions of the upper riverbank.

Legend

- 1000' River Marker
- 500' River Marker
- Extensive
- Some to Extensive
- Some
- None/Little

French King Gorge

French King Bridge (Route 2)

Barton Cove

Barton Cove Island

Turners Falls Dam

230+00
220+00
210+00
200+00
190+00
180+00
170+00
160+00
150+00
140+00
130+00
120+00
110+00
100+00
90+00
80+00
70+00
60+00
50+00
40+00
30+00
20+00
10+00
0

MOHAWK TRAIL
RIVER ROAD
ERVING
Millers River
MONTAGUE
GILL
GREENFIELD
MAIN ROAD
FRENCH KING HIGHWAY
Fall River
AVENUE A
THIRD STREET
UNITY STREET
CANAL STREET
MILLERS FALLS ROAD

Index Map
Map 5
Map 4
Map 3
Map 2
Map 1

FIRSTLIGHT HYDRO GENERATING COMPANY
Northfield Mountain Pumped Storage Project No. 2485
Turners Falls Hydroelectric Project No. 1889

STUDY 3.1.2

FirstLight Power Resources

N

0 650 1,300 2,600
Feet

Figure 4.2.2-1:
Extent of Current Erosion
Map 1

Path: W:\gis\studies\3_1_2\maps\final_report\figure_4_2_2-1.mxd

Legend

- 1000' River Marker
- 500' River Marker
- Extensive
- Some to Extensive
- Some
- None/Little

Ashuela Brook
Kidds Island
420+00
410+00
400+00
390+00
380+00
370+00
360+00
350+00
340+00
330+00
320+00
310+00
300+00
290+00
280+00
270+00
260+00
250+00
240+00
230+00
220+00
210+00
200+00
Dry Brook
NORTHFIELD
Pine Meadow Brook
GILL
MILLERS FALLS ROAD
Fourmile Brook
Northfield Tailrace
FRENCH KING HIGHWAY
NORTHFIELD ROAD
French King Gorge
French King Bridge (Route 2)
MONTAGUE
ERVI

Index Map
Map 5
Map 4
Map 3
Map 2
Map 1

FIRSTLIGHT HYDRO GENERATING COMPANY
Northfield Mountain Pumped Storage Project No. 2485
Turners Falls Hydroelectric Project No. 1889

STUDY 3.1.2

FirstLight Power Resources

N

0 650 1,300 2,600 Feet

Figure 4.2.2-1:
Extent of Current Erosion
Map 2

Path: W:\gis\studies\3_1_2\maps\final_report\figure_4_2_2-1.mxd

Legend

- 1000' River Marker
- 500' River Marker
- Extensive
- Some to Extensive
- Some
- None/Little

620+00
610+00
600+00
590+00
580+00
570+00
560+00
550+00
540+00
530+00
520+00
510+00
500+00
490+00
480+00
470+00
460+00
450+00
440+00
430+00
420+00

Route 10 Bridge
(Bennett's Meadow Bridge)

MOUNT HERMON STATION ROAD
ROUTE 10
GILL CENTER ROAD
MAIN ROAD
MAIN STREET
MAPLE STREET
WARWICK ROAD
MILLERS FALLS ROAD

Millers Brook
Bailey Brook
Bennett Brook
Ashuela Brook
Otter Run
Roaring Brook
Connecticut River

NORTHFIELD
BERNARDSTON
GILL

Kidds Island

Index Map
Map 5
Map 4
Map 3
Map 2
Map 1

FIRSTLIGHT HYDRO GENERATING COMPANY
Northfield Mountain Pumped Storage Project No. 2485
Turners Falls Hydroelectric Project No. 1889
STUDY 3.1.2

FirstLight Power Resources

N

0 650 1,300 2,600 Feet

Figure 4.2.2-1:
Extent of Current Erosion
Map 3

Service Layer Credits: Sources: Esri, HERE, DeLorme, USGS, Intermap, increment P Corp., NRCAN, Esri Japan, METI, Esri China (Hong Kong), Esri (Thailand), MapmyIndia, © OpenStreetMap contributors, and the GIS User Community
Source: Esri, DigitalGlobe, GeoEye, Earthstar Geographics, CNES/Airbus DS, USDA, USGS, AEX, Getmapping, Aerogrid, IGN, IGP, swisstopo, and the GIS User Community

Path: W:\gis\studies\3_1_2\maps\final_report\figure_4_2_2-1.mxd

Legend

- 1000' River Marker
- 500' River Marker
- Extensive
- Some to Extensive
- Some
- None/Little

830+00
820+00
810+00
800+00
790+00
780+00
770+00
760+00
750+00
740+00
730+00
720+00
710+00
700+00
690+00
680+00
670+00
660+00
650+00
640+00
630+00

WINCHESTER
HINSDALE
VERNON
NORTHFIELD

Newton Brook
Bottom Brook
Mallory Brook
Pauchaug Brook
Louisiana Brook
Connecticut River

POND RD
FORT BRIDGMAN RD
VALLEY VIEW DR
KY HOMESTEAD
South Schofield Mt Rd
Bolton Rd
Bolton Woods
Bolton Lights
South Parish Rd
Staddle Hill Rd
Saczawa Dr
Northfield Rd
McNamara Dr
Avery Cir
Walker's Ln
Gosselin Rd
Mine Rd
MOUNT HERMON STATION ROAD
WEST NORTHFIELD ROAD
HINSDALE ROAD
WANAMAKER ROAD
PAUCHAUG RAMP ROAD
EAST NORTHFIELD ROAD
MAIN ST REZ

Index Map
Map 5
Map 4
Map 3
Map 2
Map 1

FIRSTLIGHT HYDRO GENERATING COMPANY
Northfield Mountain Pumped Storage Project No. 2485
Turners Falls Hydroelectric Project No. 1889
STUDY 3.1.2

FirstLight Power Resources

N

0 650 1,300 2,600 Feet

Figure 4.2.2-1:
Extent of Current Erosion
Map 4

Path: W:\gis\studies\3_1_2\maps\final_report\figure_4_2_2-1.mxd

Legend

- 1000' River Marker
- 500' River Marker
- Extensive
- Some to Extensive
- Some
- None/Little

Vernon Dam

1060+00
1050+00
1040+00
1030+00
1020+00
1010+00
1000+00
990+00
980+00
970+00
960+00
950+00
940+00
930+00
920+00
910+00
900+00
890+00
880+00
870+00
860+00
850+00
840+00
830+00

Stebbins Island

Upper Island

Ashuelot River

Newton Brook

VERNON

HINSDALE

Index Map

Map 5
Map 4
Map 3
Map 2
Map 1

FIRSTLIGHT HYDRO GENERATING COMPANY
Northfield Mountain Pumped Storage Project No. 2485
Turners Falls Hydroelectric Project No. 1889

STUDY 3.1.2

0 650 1,300 2,600 Feet

Figure 4.2.2-1:
Extent of Current Erosion
Map 5

Path: W:\gis\studies\3_1_2\maps\final_report\figure_4_2_2-1.mxd

4.2.3 Hydraulic Modeling

Hydraulic modeling was conducted as an integral part of this study in support of the analysis of: (1) water levels and how they change over time, and (2) the hydraulic forces that flowing water impose on riverbanks. Two hydraulic models were utilized for this effort: HEC-RAS and River2D. The HEC-RAS model was developed as part of Study No. 3.2.2 *Hydraulic Study*, while the River2D model was created specifically for the Causation Study. Both models encompassed the geographic extent of the TFI from Vernon Dam to the Turners Falls Dam and relied on similar input and calibration datasets. Input datasets used for these models included historic and updated (2014) TFI bathymetric data, water level data derived from the permanent FirstLight monitoring equipment and seasonal water level loggers, and flow data derived from FirstLight and/or USGS data.

The HEC-RAS model was integral in support of the BSTEM runs and analyses discussed in Section 5. After the HEC-RAS model was calibrated, it was utilized to generate historic water levels and water surface slopes on an hourly basis through the TFI and at the 25 Detailed Study Sites utilizing historic upstream inflows at Vernon and tributaries (Ashuelot and Millers Rivers), Northfield Mountain operations (flows used for pumping and generating), and historic water levels at the Turners Falls Dam. Another scenario (Scenario 1 – Northfield Mountain idle) was then developed and run through HEC-RAS to provide hourly water levels for BSTEM at the 25 Detailed Study Sites to determine erosion associated with this modeling scenario.

The results of the two-dimensional River2D model were used to better understand velocities and shear stresses in the near bank environment. The model was calibrated and then verified with three separate flow events. The verification events represented the full range of available observed flows. Once verified, six production runs were performed in order to investigate changes in velocity and shear stress in the near bank area at the 25 detailed study sites and at areas where unique hydraulic conditions were observed (e.g., eddying).

The HEC-RAS and River2D models are discussed further in Section 5.2.

4.2.4 Cross-section Surveys

Following completion of the first FRR in 1998 and development of the subsequent ECP, 22 permanent transects were established in the TFI for continued monitoring. The 22 transects were selected for two primary reasons: (1) they were relatively evenly spaced throughout the geographic extent of the TFI, and (2) most were located at sites where erosion had been observed. The 22 transects have been surveyed annually since 1999 to monitor any changes in riverbank or channel geometry. Transect surveys typically entailed surveying the complete cross-section starting at one riverbank, across the channel bed, and up the other riverbank. Permanent markers are typically placed on both banks denoting the start/end points of the cross-section survey to allow for direct comparison of past and future surveys.

In addition to the 22 permanent transects established in 1998, FirstLight identified 9 supplemental transects during the detailed study site selection process discussed in Section 4.1. Although the supplemental detailed study sites were only located on one riverbank, full cross-section surveys have been conducted annually at each of these locations since 2014. Figure 4.2.4-1 shows the location of both the permanent and supplemental transects.

Cross-section survey data were used to calibrate BSTEM and for analysis of changes in cross-section geometry over time. Cross-section plots have been created comparing the results of each annual survey. These plots have also been updated to include the Ordinary High Water Mark (OHWM). Discussion pertaining to how the OHWM was identified can be found in Section 4.2.4-1.

Figure 4.2.4-2 provides an example of a cross-section plot. Cross-section plots for all transects are located in Volume III (Appendix E).

Legend

Permanent Cross Sections

Supplemental Cross Section

French King Bridge (Route 2)

French King Gorge

ERVING

RIVER ROAD

MOHAWK TRL

MONTAGUE

MILLERS FALLS ROAD

GILL

FRENCH KING HIGHWAY

BC-5

Barton Cove

9

12BL

BC-2

BC-1

BC-3

MAIN ROAD

MONTAGUE BRIDGE

Turners Falls Dam

UNITY STREET

FIRST STREET

CANAL STREET

GREENFIELD

Map 5

Map 4

Map 3

Map 2

Map 1

FIRSTLIGHT HYDRO GENERATING COMPANY
Northfield Mountain Pumped Storage Project No. 2485
Turners Falls Hydroelectric Project No. 1889

STUDY 3.1.2

FirstLight Power Resources

N

0 625 1,250 2,500 Feet

Figure 4.2.4-1:
Turners Falls Impoundment
Cross-section

Service Layer Credits: Sources: Esri, HERE, DeLorme, USGS, Intermap, increment P Corp., NRCAN, Esri Japan, METI, Esri China (Hong Kong), Esri (Thailand), MapmyIndia, © OpenStreetMap contributors, and the GIS User Community

Path: W:\gis\studies\3_1_2\maps\final_report\figure_4_2_4-1.mxd

Legend

Permanent Cross Sections

Supplemental Cross Section

6A

119BL

12

7

NORTHFIELD

MILLERS FALLS ROAD

8B

GILL

8A

87BL

Northfield Tailrace

75BL

French King Gorge

French King Bridge (Route 2)

FRENCH KING HIGHWAY

MOHAWK TRAIL

MONTAGUE

NORTHFIELD ROAD

ERVIN

Map 5

Map 4

Map 3

Map 2

Map 1

FirstLight Power Resources

N

0 625 1,250 2,500 Feet

FIRSTLIGHT HYDRO GENERATING COMPANY
Northfield Mountain Pumped Storage Project No. 2485
Turners Falls Hydroelectric Project No. 1889

STUDY 3.1.2

Figure 4.2.4-1:
Turners Falls Impoundment
Cross-section

Service Layer Credits: Sources: Esri, HERE, DeLorme, USGS, Intermap, increment P Corp., NRCAN, Esri Japan, METI, Esri China (Hong Kong), Esri (Thailand), MapmyIndia, © OpenStreetMap contributors, and the GIS User Community

Path: W:\gis\studies\3_1_2\maps\final_report\figure_4_2_4-1.mxd

Legend

Permanent Cross Sections

Supplemental Cross Section

5A

5E

5D

5C

26R

10

6A

6B

Route 10 Bridge
(Bennett's Meadow Bridge)

NORTHFIELD

BERNARDSTON

GILL

MOUNT HERMON STATION ROAD

ROUTE 10

GILL CENTER ROAD

MAIN ROAD

MAIN STREET

MAPLE STREET

MILLERS FALLS ROAD

WARWICK ROAD

Map 5

Map 4

Map 3

Map 2

Map 1

FIRSTLIGHT HYDRO GENERATING COMPANY
Northfield Mountain Pumped Storage Project No. 2485
Turners Falls Hydroelectric Project No. 1889

STUDY 3.1.2

N

0 625 1,250 2,500 Feet

Figure 4.2.4-1:
Turners Falls Impoundment
Cross-section

Service Layer Credits: Sources: Esri, HERE, DeLorme, USGS, Intermap, increment P Corp., NRCAN, Esri Japan, METI, Esri China (Hong Kong), Esri (Thailand), MapmyIndia, © OpenStreetMap contributors, and the GIS User Community

Path: W:\gis\studies\3_1_2\maps\final_report\figure_4_2_4-1.mxd

Legend

- Permanent Cross Sections
- Supplemental Cross Section

NEW HAMPSHIRE
VERMONT

VERNON

HINSDALE

WINCHESTER

3

21R

VERMONT
MASSACHUSETTS

VERMONT
MASSACHUSETTS

NEW HAMPSHIRE
MASSACHUSETTS

NORTHFIELD

4

29R

Map 5
Map 4
Map 3
Map 2
Map 1

FIRSTLIGHT HYDRO GENERATING COMPANY
Northfield Mountain Pumped Storage Project No. 2485
Turners Falls Hydroelectric Project No. 1889

STUDY 3.1.2

N

0 625 1,250 2,500
Feet

Figure 4.2.4-1:
Turners Falls Impoundment
Cross-section

Service Layer Credits: Sources: Esri, HERE, DeLorme, USGS, Intermap, increment P Corp., NRCAN, Esri Japan, METI, Esri China (Hong Kong), Esri (Thailand), MapmyIndia, © OpenStreetMap contributors, and the GIS User Community

Path: W:\gis\studies\3_1_2\maps\final_report\figure_4_2_4-1.mxd

Legend

- Permanent Cross Sections
- Supplemental Cross Section

Vernon Dam

1

11

2

303BL

18L

NEW HAMPSHIRE

VERMONT

VERNON

HINSDALE

Map 5

Map 4

Map 3

Map 2

Map 1

FIRSTLIGHT HYDRO GENERATING COMPANY
Northfield Mountain Pumped Storage Project No. 2485
Turners Falls Hydroelectric Project No. 1889

STUDY 3.1.2

0 625 1,250 2,500
Feet

Figure 4.2.4-1:
Turners Falls Impoundment
Cross-section

Service Layer Credits: Sources: Esri, HERE, DeLorme, USGS, Intermap, increment P Corp., NRCAN, Esri Japan, METI, Esri China (Hong Kong), Esri (Thailand), MapmyIndia, © OpenStreetMap contributors, and the GIS User Community

Path: W:\gis\studies\3_1_2\maps\final_report\figure_4_2_4-1.mxd

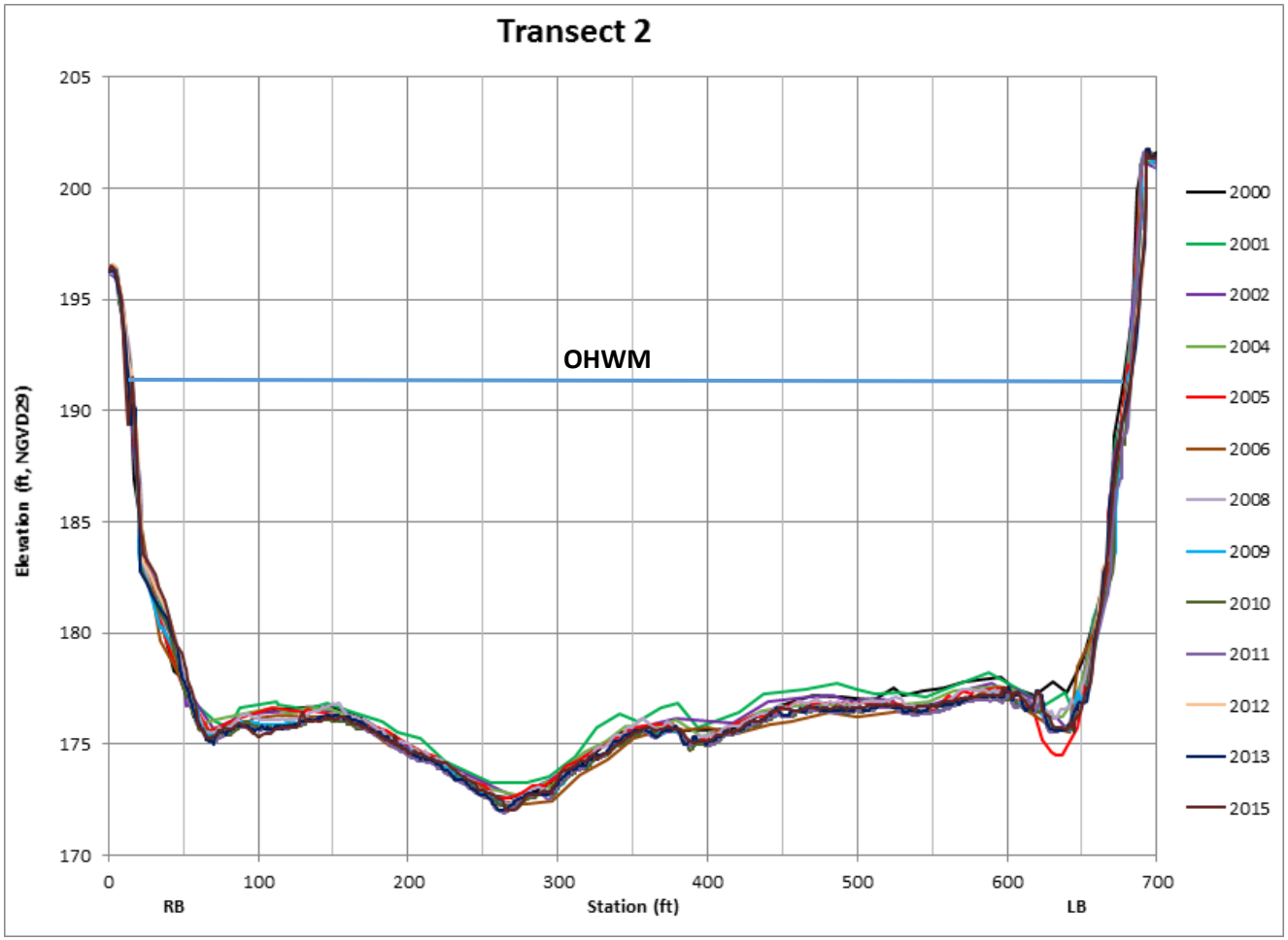

Figure 4.2.4-2 Example cross-section plot

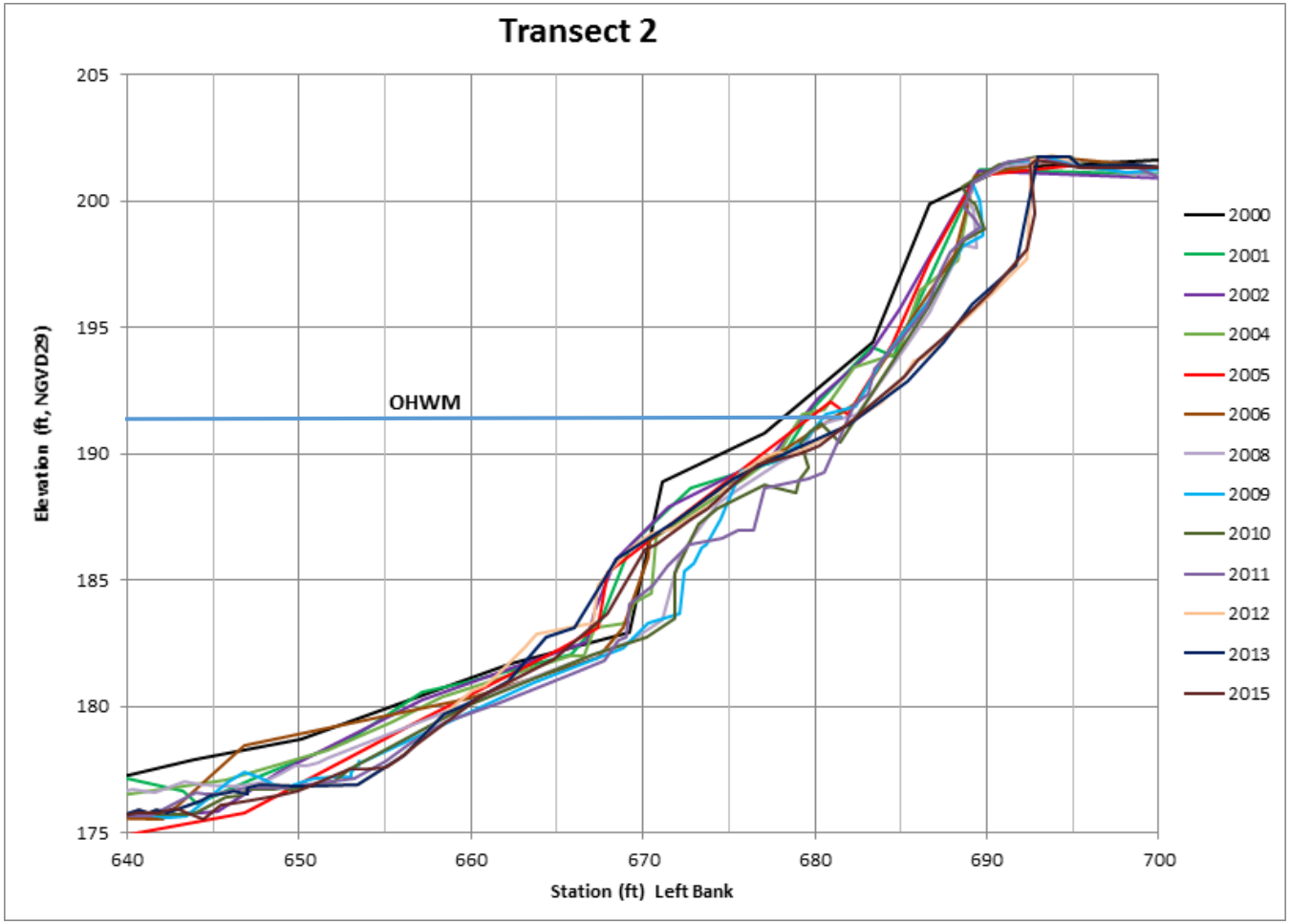

Figure 4.2.4-2 Example cross-section plot

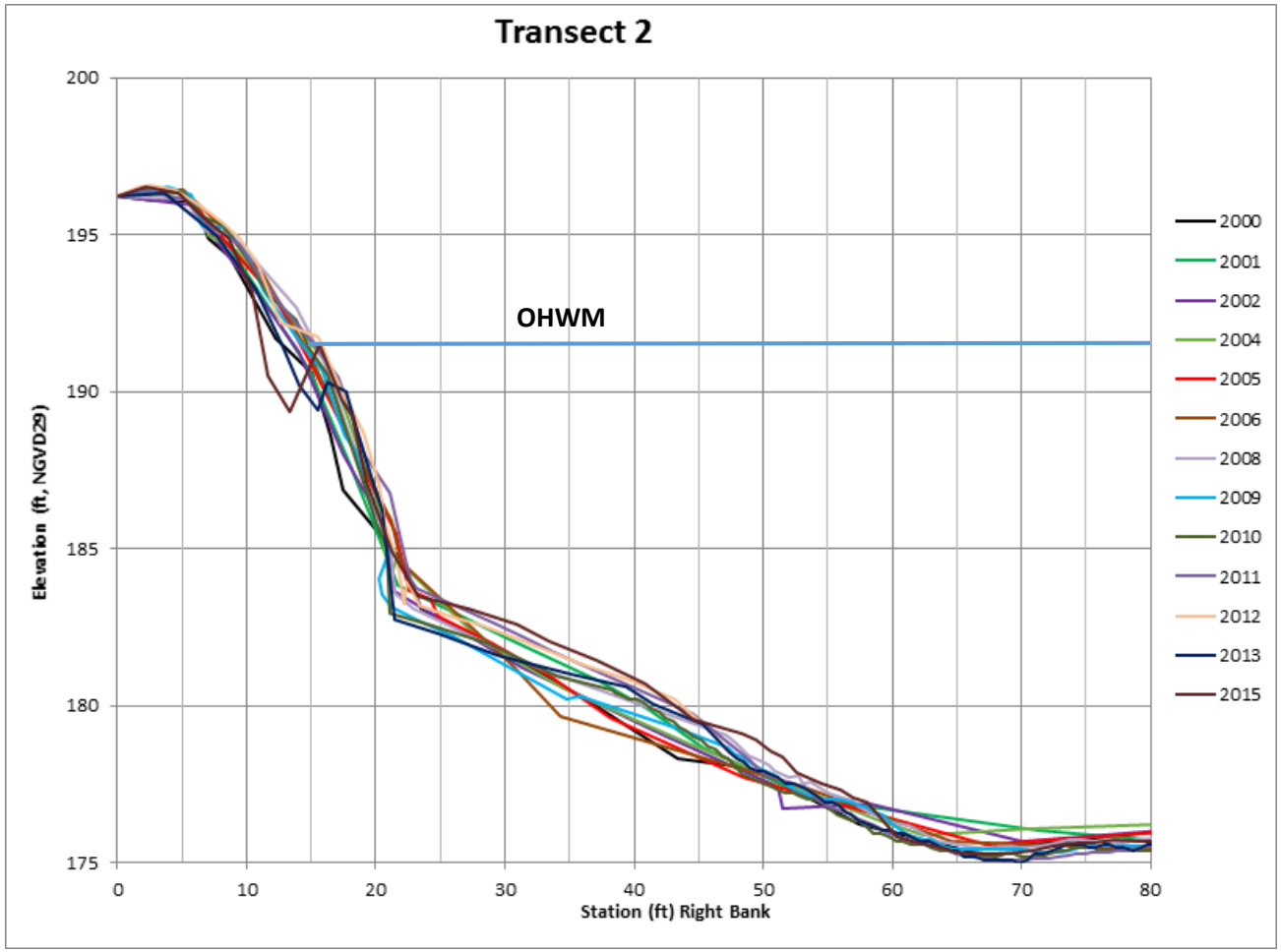

Figure 4.2.4-2 Example cross-section plot

4.2.4.1 Ordinary High Water Mark

On November 5, 2013, following the issuance of FERC's first SPDL, FirstLight met with representatives of MADEP to review the RSP and discuss, among other things, the methodology for Relicensing Study No. 3.1.2. During this meeting MADEP requested that FirstLight identify the OHWM in the TFI as part of the Causation Study. Based on this request, the attendees agreed that FirstLight would develop a methodology to determine the OHWM and, once developed, consult with MADEP for its approval. In the subsequent months following that meeting FirstLight developed a methodology to identify the OHWM in the TFI. FirstLight presented this approach to MADEP on May 27, 2016; receiving approval from the Department on June 1, 2016. The methodology, discussed in more detail below, combined statistical analysis using the available HEC-RAS model and field evaluation based on the USACE OHWM determination criteria.

OHWM Definition and Criteria

Ordinary High Water Mark is defined in Title 33: Navigation and Navigable Waters, CHAPTER II: CORPS OF ENGINEERS, DEPARTMENT OF THE ARMY, DEPARTMENT OF DEFENSE PART 328: DEFINITION OF WATERS OF THE UNITED STATES 328.3 – Definitions:

> *(e) The term ordinary high water mark means that line on the shore established by the fluctuations of water and indicated by physical characteristics such as clear, natural line impressed on the bank, shelving, changes in the character of soil, destruction of terrestrial vegetation, the presence of litter and debris, or other appropriate means that consider the characteristics of the surrounding areas.*

Physical characteristics to consider in determining the Ordinary High Water Line are described in REGULATORY GUIDANCE LETTER No. 05-05 Date: 7 December 2005 SUBJECT: Ordinary High Water Mark Identification

> *b. The following physical characteristics should be considered when making an OHWM determination, to the extent that they can be identified and are deemed reasonably reliable:*

- Natural line impressed on the bank
- Shelving
- Changes in the character of soil
- Destruction of terrestrial vegetation
- Presence of litter and debris
- Wracking
- Vegetation matted down, bent, or absent
- Sediment sorting
- Leaf litter disturbed or washed away
- Scour
- Deposition
- Multiple observed flow events
- Bed and banks
- Water staining
- Change in plant community

Further guidance regarding determination of OHWM was provided by the USACE when they noted that the: *"list of OHWM characteristics is not exhaustive. Physical characteristics that correspond to the line on the shore established by the fluctuations of water may vary depending on the type of water body and conditions of the area. There are no "required" physical characteristics that must be present to make an OHWM determination. However, if physical evidence alone will be used for the determination, districts*

should generally try to identify two or more characteristics, unless there is particularly strong evidence of one."

The USACE recognized the difficulties in determining OHWM by field investigation stating that *"where the physical characteristics are inconclusive, misleading, unreliable, or otherwise not evident, districts may determine the OHWM by using other appropriate means that consider the characteristics of the surrounding areas, provided those other means are reliable. Such other reliable methods that may be indicative of the OHWM include, but are not limited to, lake and stream gage data, elevation data, spillway height, flood predictions, historic records of water flow, and statistical evidence."*

Methodology

The determination of the elevation defining the OHWM combined field observations and statistical analysis at surveyed transects upstream of the French King Gorge.[31] A statistical analysis of the water level data from the calibrated HEC-RAS model for 2000-2014 was conducted to determine an appropriate, statistically-based OHWM elevation. The range of water levels examined during the statistical analysis were then field verified at a number of the permanent transects located upstream of the French King Gorge based on the physical characteristics described by the USACE. Based on the results of the field evaluation and the statistical analysis, the water surface elevation associated with the 2% exceedance was selected as the OHWM. This elevation was found to be reasonably conservative based on the results of the statistical analysis while also often being well above (i.e. at a higher elevation) the majority of the physical characteristics defined by the USACE. This approach follows guidance provided by the USACE in the available literature. The methodology used to determine the OHWM in the TFI is summarized below:

1. Conduct statistical analysis of water level data from the calibrated HEC-RAS model for 2000-2014, including: peak annual water levels and associated statistics (minimum, maximum, average, median), water level duration analysis, and average water level

2. Using a range of water level durations, mark and photograph, riverbanks at a number of detailed study sites so that assessments can be made of physical characteristics related to OHWM

3. Based on assessment of field data, select appropriate statistical definitions of OHWM

4. Develop cross-sections / maps of OHWM

Statistical Analysis

At the detailed study sites, water levels were computed on an hourly basis using the historic discharge at Vernon Dam as the upstream boundary condition, tributary inflow, the operation of the Northfield Mountain Pumped Storage Project, and historic water levels at Turners Falls Dam as the downstream boundary condition. This hydraulic modeling analysis produced hourly water levels for the time period from 2000 through 2014, consisting of a set of approximately 131,400 numbers. Two types of statistical analyses were conducted using these sets of data: peak annual water level, minimum peak annual water level, averages and medians of annual peak water levels, and a water level-duration analysis. The peak annual water level analysis results in a set of numbers at the detailed study sites while the water-level duration analysis results

[31] Sites located below French King Gorge were not evaluated in the field due to the fact that the water surface elevation differences between the modeled scenarios (i.e. 0.27%, 0.5%, 1%, and 2%) were minimal as a result of the relatively flat nature of this portion of the TFI and since the water level is largely determined by the operation of the Turners Falls Dam. Water surface elevation differences between the various exceedances were found to be greater upstream of the hydraulic constriction at the French King Gorge.

in a graph showing the percentage of time that given water levels are equaled or exceeded. Figure 4.2.4.1-1 provides an example of the water-level duration analysis conducted at Site 8BR.

To provide a range of water levels for comparison, water levels at several percentage durations were determined from the water level-duration curves (0.27%, 0.5%, 1%, 2%, 5%). These percentage durations represent the corresponding lengths of time in days (on an annualized basis): 1, 1.83, 3.65, 7.3 and 18.3. In other words, a 0.5% duration represents a water level which is exceeded the equivalent of 1.83 days per year over the 2000-2014 time period (or 27.4 days over 15 years). The results of these statistical analyses are condensed into Table 4.2.4.1-1 and compared against the average, median, maximum and minimum peak water levels achieved over that period.

Table 4.2.4.1-1: Statistical Summary of Peak Annual Water Levels and Water Level Duration Analysis (2000-2014)

Yearly Peaks	BC-1R*	9R*	12BL*	75BL	87BL	8BR	8BL	7R	7L	119BL	6AR	6AL	10L
Average	184.57	184.57	184.57	189.42	189.80	189.94	189.94	190.48	190.48	190.75	190.81	190.81	191.07
Median	184.40	184.41	184.41	189.5	189.88	190.03	190.03	190.61	190.61	190.90	190.97	190.97	191.24
Maximum	185.50	185.50	185.50	193.61	194.08	194.24	194.24	195.02	195.02	195.41	195.52	195.51	195.84
Minimum	184.07	184.07	184.07	186.59	186.89	187.05	187.05	187.54	187.54	187.74	187.79	187.79	187.99
Exceedances													
5%	183.31	183.32	183.32	184.84	185.06	185.22	185.22	185.62	185.62	185.83	185.89	185.89	186.14
2%	183.70	183.70	183.70	186.69	187.02	187.20	187.20	187.74	187.74	188.03	188.09	188.09	188.36
1%	183.90	183.89	183.89	187.81	188.17	188.36	188.36	188.94	188.94	189.23	189.30	189.30	189.59
0.50%	184.01	184.01	184.01	188.58	188.96	189.14	189.14	189.74	189.74	190.06	190.13	190.13	190.41
0.27%	184.20	184.20	184.21	189.15	189.53	189.72	189.72	190.36	190.36	190.68	190.75	190.75	191.05

Yearly Peaks	10R	26R	5CR	29R	4L	21R	3L	18L	303BL	2L	11R	11L
Average	191.10	191.13	191.52	191.95	192.59	192.94	193.03	193.76	194.48	194.42	195.52	195.54
Median	191.28	191.3	191.71	192.15	192.62	192.97	193.07	193.79	194.51	194.45	195.55	195.57
Maximum	195.88	195.91	196.43	197.03	200.17	200.49	200.58	201.15	201.80	201.69	202.57	202.59
Minimum	188.01	188.04	188.41	188.85	189.33	189.70	189.80	190.55	191.25	191.23	192.32	192.34
Exceedances												
5%	186.16	186.18	186.52	186.89	187.29	187.58	187.66	188.33	189.01	189.02	190.02	190.03
2%	188.39	188.41	188.80	189.23	189.70	190.04	190.12	190.85	191.58	191.55	192.63	192.65
1%	189.62	189.65	190.05	190.49	190.97	191.32	191.41	192.17	192.90	192.86	193.96	193.98
0.50%	190.44	190.47	190.91	191.38	191.86	192.23	192.33	193.10	193.85	193.8	194.92	194.94
0.27%	191.08	191.11	191.54	192.00	192.50	192.87	192.97	193.74	194.47	194.42	195.51	195.53

Notes:
* Denotes location below French King Gorge
Average peak = Average of the peak 1 hour annual water level in each year from 2000-2014
Median peak = Median of the peak 1 hour annual water levels in each year from 2000-2014
Maximum peak = Highest single 1 hour annual peak water level during period 2000-2014 (which was in 2011)
Minimum peak = Lowest single 1 hour annual peak water level during period 2000-2014

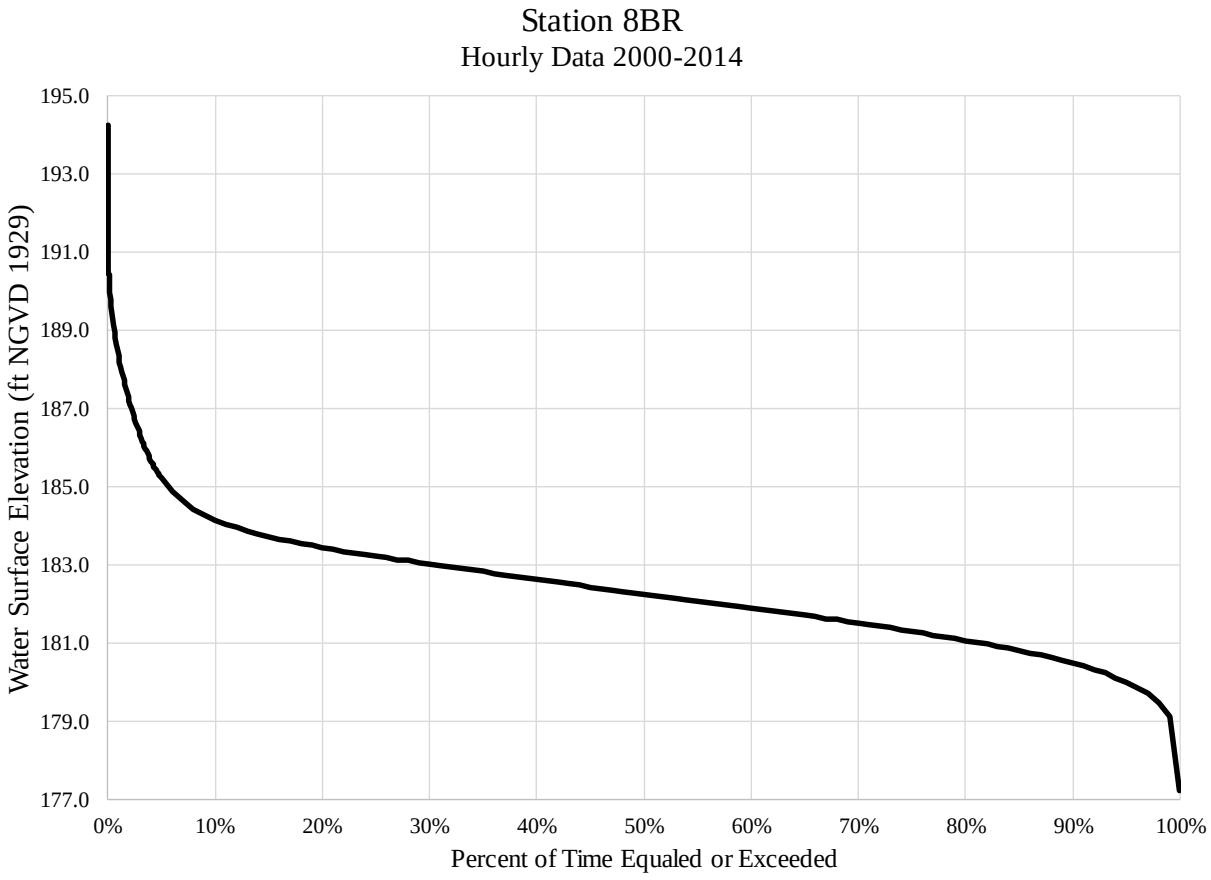

Figure 4.2.4.1-1. Water level-duration curve at Site 8BR

Field Analysis

The field analysis was conducted by surveying a range of water levels at eleven detailed study sites along the length of the TFI upstream of the French King Gorge. Water levels selected for survey during the field component included 0.27%, .5%, 1% and 2% which, as described previously, represent from 1 to 7.3 days per year. Figures were developed showing these water levels on a photograph of the riverbanks. The photographs were then analyzed in order to identify the various physical characteristics noted by the USACE, and discussed earlier in this section, which were present.

Photographs of the riverbanks at a number of sites along the TFI were then labeled with observed physical characteristics as well as a range of water levels from the water level-duration analysis to help determine which statistical measure should be used to define an appropriate water level to represent the ordinary high water mark (Figures 4.2.4.1-2 through 4.2.4.1-8). These figures show the OHWM which is marked as a horizontal yellow line, with physical characteristics labeled above and below the OHWM as observed at each site. At many of these sites there are multiple physical characteristics that identify the OHWM, while at some there are none visible since they are below water.

Figure 4.2.4.1-2. Physical characteristics of OHWM at Site 8BR

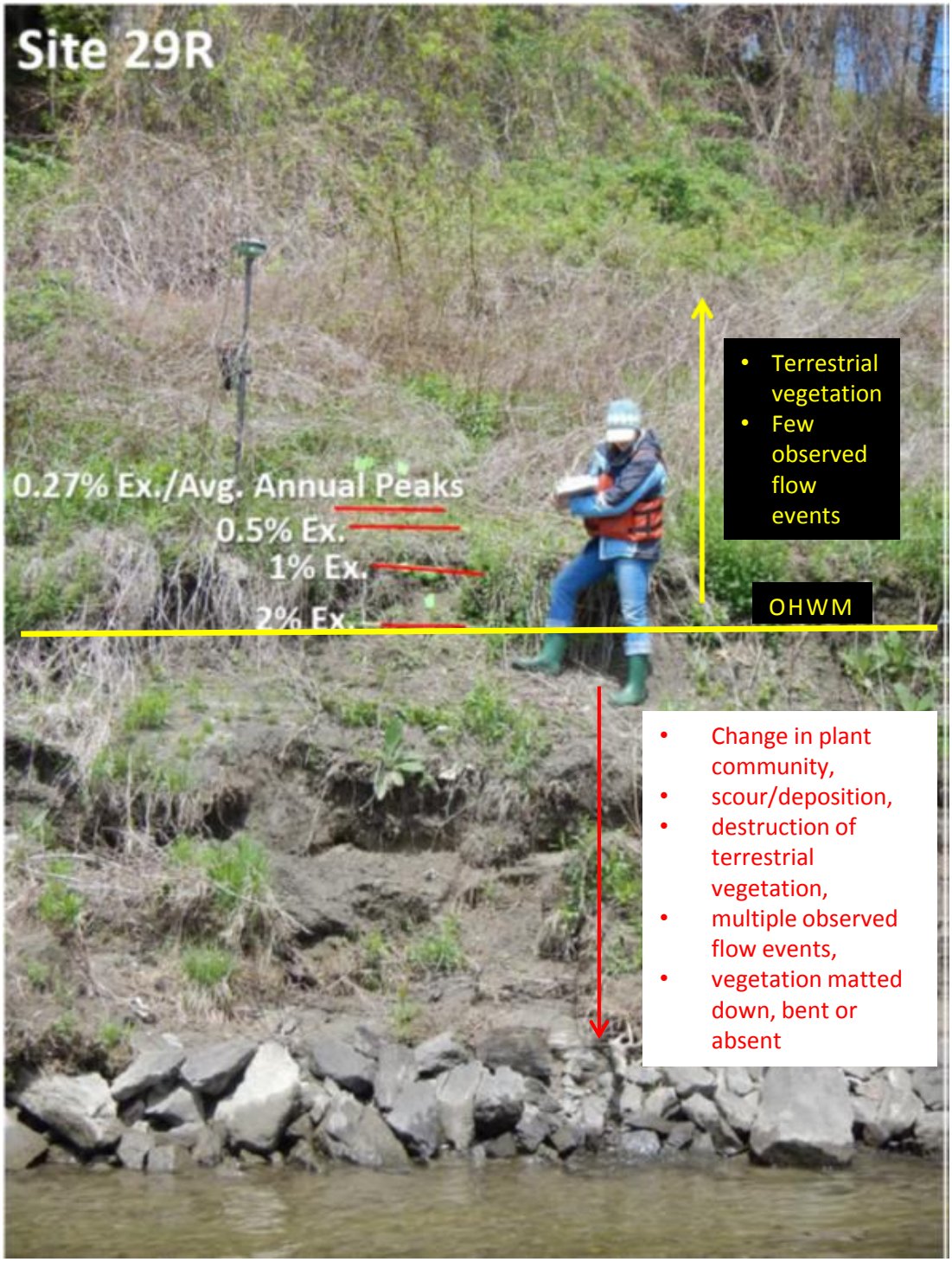

Figure 4.2.4.1-3. Physical characteristics of OHWM at Site 29R

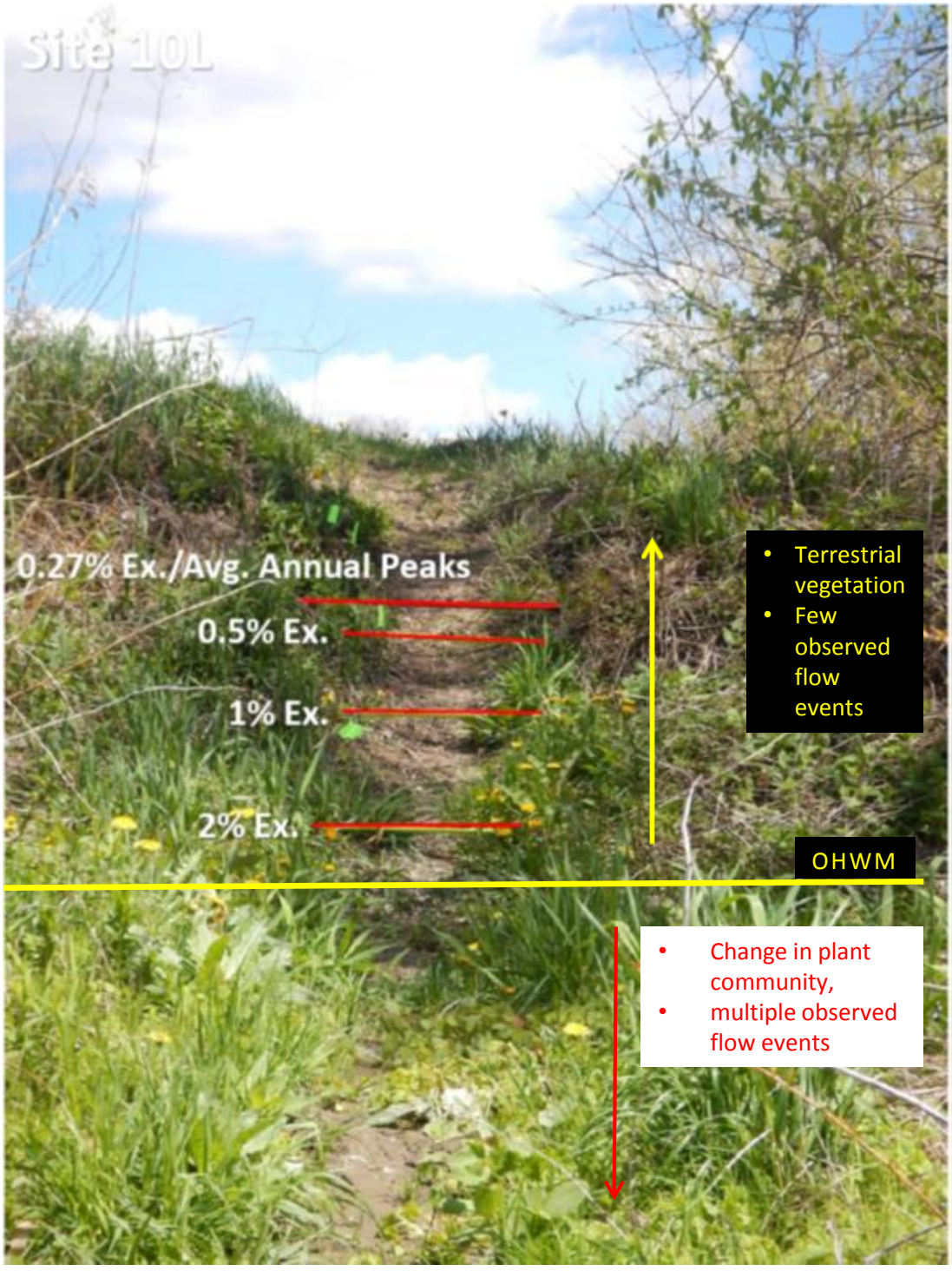

Figure 4.2.4.1-4. Physical characteristics of OHWM at Site 10L

Figure 4.2.4.1-5. Physical characteristics of OHWM at Site 6AR

Figure 4.2.4.1-6 Physical characteristics of OHWM at Site 10R

Figure 4.2.4.1-7 Physical characteristics of OHWM at Site 11L

Figure 4.2.4.1-8 Physical characteristics of OHWM at Site 2L

Determination of OHWM

The determination of OHWM consisted of a field survey/observation component and statistical analysis of water levels. At a number of sites, there were a number of physical characteristics that indicated the location of the OHWM. Where such physical characteristics were observed, they were linked to water level via the water level-duration analysis. At some locations there were no readily observed physical characteristics of the OHWM for the region of the bank below the OHWM due to the water level at the time of the field survey. Table 4.2.4.1-2 summarizes the results of the combination of field observations and statistical analysis of water level.

Some locations exhibited physical characteristics indicating the OHWM at a water level associated with the statitistical analysis, some locations below this level, and others where field observations were inconclusive (below OHWM characteristics not observed due to water level at the time of the survey), the guidelines from the USACE were followed. This approach considers physical characteristics used to characterize the OHWM and also follows the Regulatory Guidance Letter, No. 05-05, December 7, 2005 (USACE) regarding the concept where *"physical characteristics are inconclusive, misleading, unreliable, or otherwise not evident,"* in cases where *"water levels or flows may be manipulated by human intervention for power generation or water supply"* by applying *"elevation data," "historical records of water flow, and statistical evidence."*

In order to develop a conservatively high elevation for the OHWM in the TFI, the highest water level where numerous OHWM physical characteristics were observed was selected. At four locations, the 2% exceedance water level was the highest elevation of the OHWM observed at sites investigated. At five locations, observations indicate that the OHWM was lower than the 2% exceedance water level, and at two locations, physical characteristics indicative of conditions below the OHWM were submerged below the water level at the time of the field work meaning that the OHWM was below the elevation of the 2% exceedance. This approach results in an OHWM that is conservatively high in that at some locations, the actual OHWM could be lower, but at no locations is there indication of a higher OHWM. The 2% level represents an upper limit of what the OHWM is; and to be consistent, the 2% level was then applied at all locations through the TFI.

Based on the statistical analysis of water levels, the ordinary high water mark as indicated by the 2% level was plotted on cross-sections at detailed study sites upstream of the French King Gorge. Other water levels were also plotted to put the results of the OHWM into perspective, these included the 0.27% (which is close to the average and median 1 hour peak annual flow), 5%, and the overall average flow for 2000-2014. An example of a set of such graphs is provided below for Site 8B (Figures 4.2.4.1-9 through 4.2.4.1-11). Cross-section plots depicting the OHWM at each transect are included in Volume III (Appendix E).

Table 4.2.4.1-2: OHWM Elevation at Field Investigated Sites

Site	OHWM elevation
11L	Physical characteristics above OHWM observed above water level, <2%
2L	Physical characteristics above OHWM observed above water level, <2%
29R	2%
26R	2%
10L	<2%
10R	<2%
6AL	<2%
6AR	2%
7L	<2%
8BR	2%
75BL	<2%

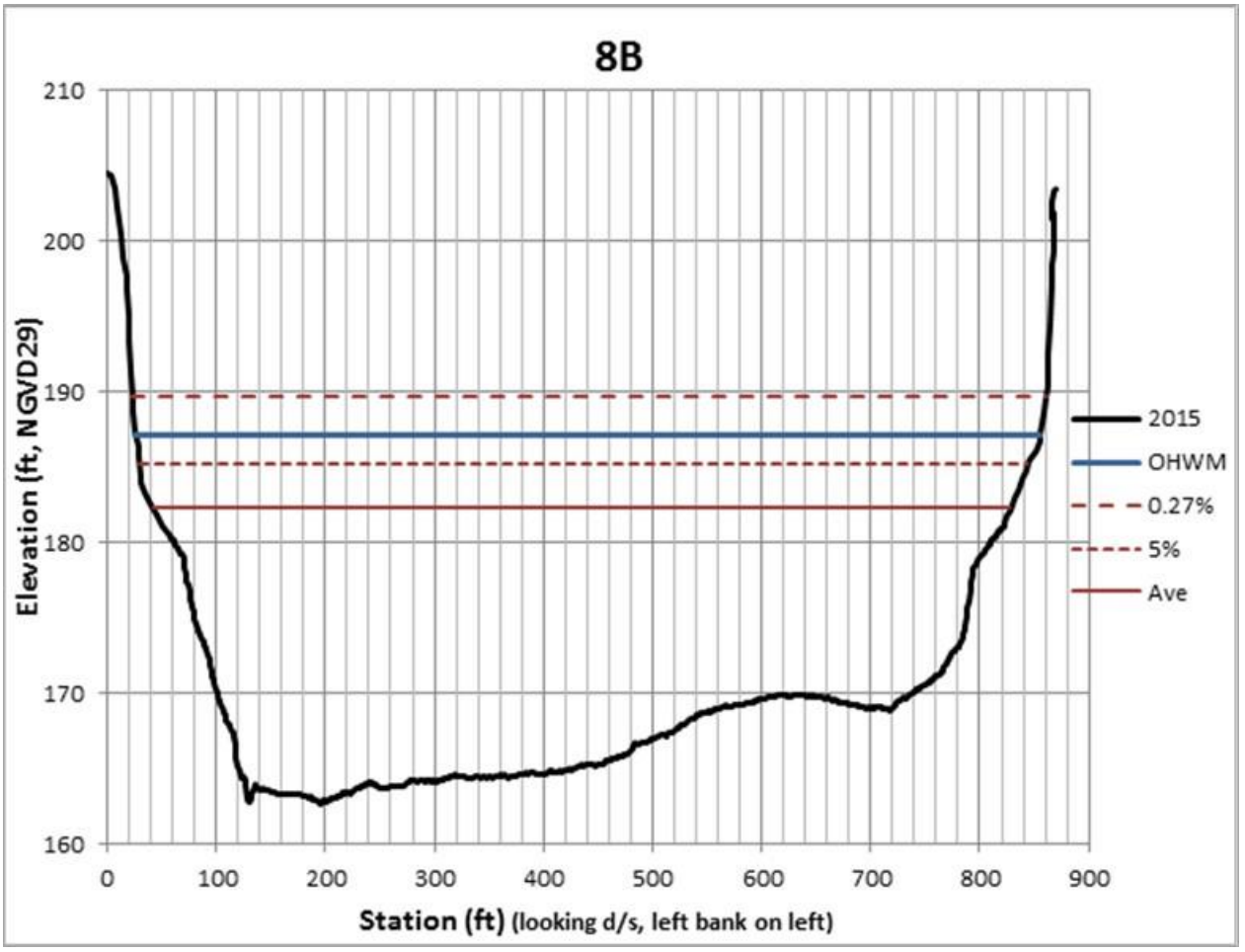

Figure 4.2.4.1-9. OHWM at Site 8B, complete cross-section

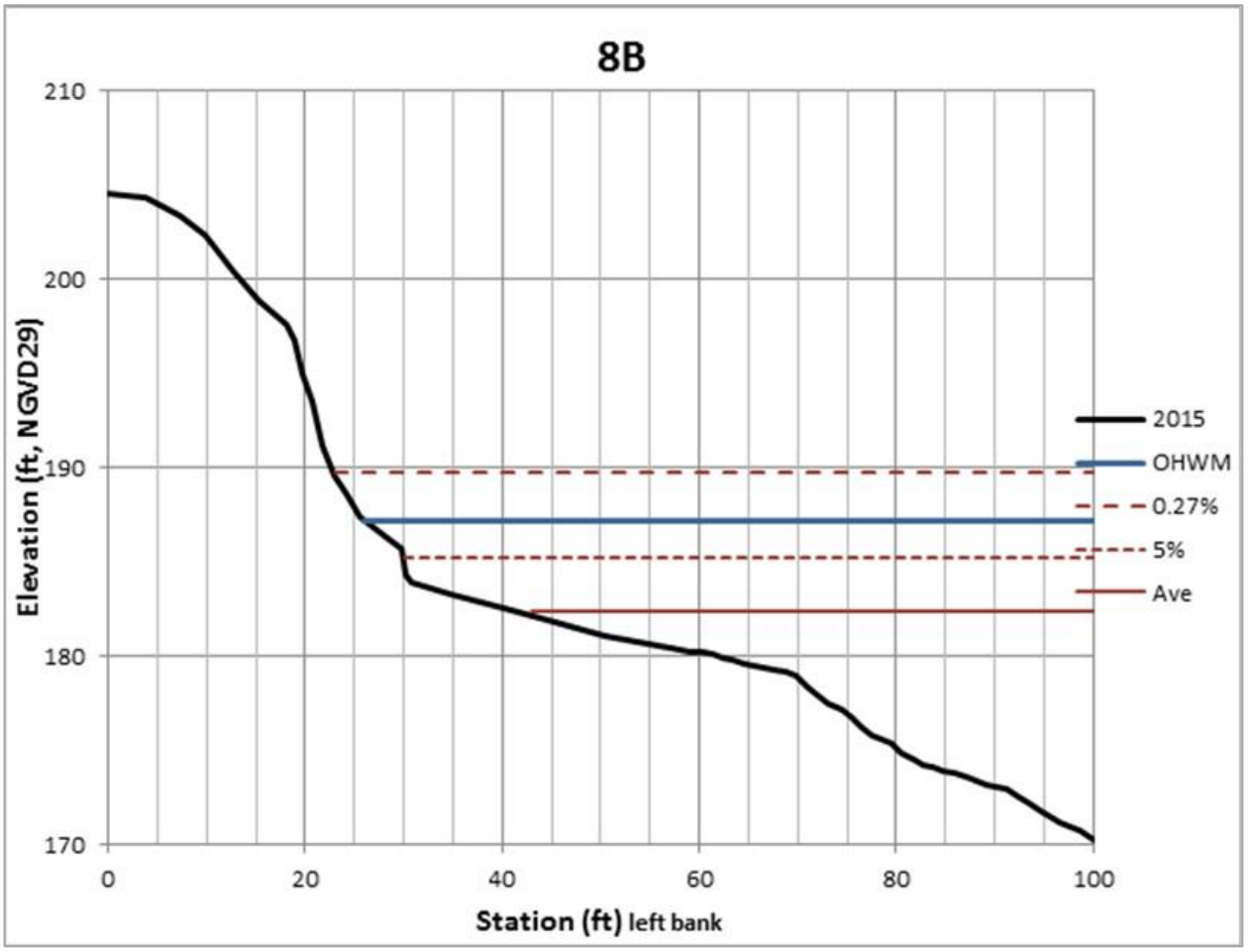

Figure 4.2.4.1-10. OHWM at Site 8B, left bank

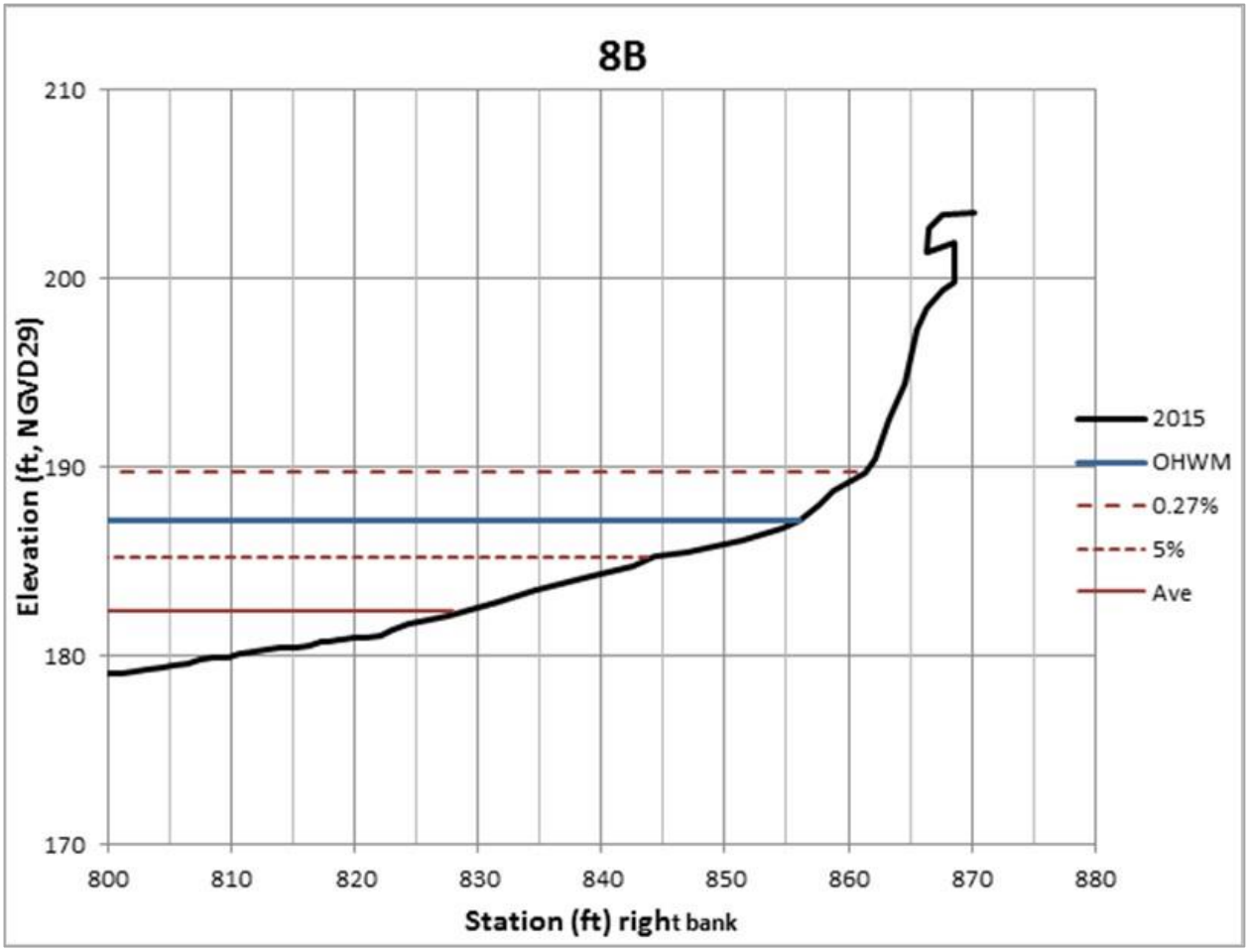

Figure 4.2.4.1-11. OHWM at Site 8B, right bank

4.2.5 Bank Stability and Toe Erosion Model (BSTEM)

BSTEM is a mechanistic bank-stability model specifically designed for alluvial channels. It is programmed in Visual Basic and exists in the Microsoft Excel environment as a simple spreadsheet tool. Data input, along with the various sub-routines are included in different worksheets. The user is able to move freely between worksheets according to their needs at various points of model application. The static version of BSTEM is available to the public free of charge at:

http://www.ars.usda.gov/Research/docs.htm?docid=5044

More details regarding the technical background of BSTEM, and its subroutines (streambank stability, toe erosion and RipRoot), are contained within Volume III (Appendix F). The technical background regarding the newly added wave algorithm is contained within Volume III (Appendix G).

4.2.5.1 General Model Capabilities

The original model, developed by Simon and Curini (Simon & Curini, 1998) Simon *et al.* (Simon, Curini, Darby, & Langendoen, 1999; 2000) is a Limit Equilibrium analysis in which the Mohr-Coulomb failure criterion is used for the saturated part of the streambank, and the Fredlund *et al.* (Fredlund, Morgenstern, Widger, 1978) criterion is used for the unsaturated part. The latter criterion indicates that apparent cohesion changes with matric suction (negative) pore-water pressure, while effective cohesion remains constant. In addition to accounting for positive and negative pore-water pressures, the model incorporates complex geometries, up to five user-definable layers, changes in soil unit weight based on water content, and external confining pressure from streamflow. Current versions combine three limit equilibrium-method models that calculate Factor of Safety (Fs) for multi-layer streambanks. The methods simulated are horizontal layers (Simon *et al.*, 1999; 2000), vertical slices with tension crack (Morgenstern & Price, 1965) and cantilever failures (Thorne & Tovey, 1981). The model can easily be adapted to incorporate the effects of vegetation, geotextiles or other bank-stabilization measures that affect soil strength.

The version of BSTEM described in Simon *et al.*, (Simon, Pollen-Bankhead & Thomas, 2011) and available (Ver. 5.4) includes a sub-model to predict bank-toe and bank-surface erosion, and undercutting by hydraulic shear. This is based on an excess shear-stress approach that is linked to the geotechnical algorithms. Complex geometries resulting from simulated bank-toe erosion are used as the new input geometry for the geotechnical part of the bank-stability model. The geometry of the potential failure plane can be determined automatically by an iterative search routine that locates the most critical failure-plane geometry. In the Static version, if a failure is simulated, the resulting bank geometry can be exported back into either sub-model to simulate conditions over time by running the sub-models iteratively with different flow and water-table conditions. In the Dynamic version, this is done automatically by the model.

The mechanical, reinforcing effects of riparian vegetation (Simon & Collison, 2002; Micheli & Kirchner, 2002) can be included in model simulations. This is accomplished with the RipRoot model (Pollen & Simon, 2005) that is based on fiber-bundle theory and included in the Bank Vegetation and Protection worksheet. The current static version of BSTEM (Ver. 5.4) also includes new features that can account for enhanced hydraulic stresses on the outside of meander bends as well as reduced, effective hydraulic stress operating on fine-grained materials in a reach characterized by a rougher boundary.

The bank-modeling work included in Simon and Curini (1998), Simon *et al.* (2000) and Simon and Collison (2002) utilized a research version of BSTEM that includes the same fundamental algorithms as the Static version but also allows for input of an unsteady flow series (i.e. stage can vary at each time step). This version was called BSTEM-Dynamic 1.0. To more accurately simulate bank-erosion processes, BSTEM-Dynamic Ver. 2.0 includes a near-bank groundwater sub-model that permits dynamic adjustment of pore-water pressures over extended hydrographs. This version has been used by scientists at the U.S. Department of Agriculture - Agricultural Research Service (USDA-ARS) National Sedimentation Laboratory and at Cardno to simulate bank-erosion processes and to predict bank-erosion rates over time periods of up to 100

years (Simon & Klimetz, 2012). BSTEM-Dynamic has been applied successfully in diverse environments across the globe including Australia, New Zealand, Taiwan, China, England, California, Mississippi, Vermont, South Dakota, Washington, and now along the Connecticut River. This dynamic version of BSTEM will be made available to the public in the future at the discretion of the USDA-ARS, National Sedimentation Laboratory.

In this study we used BSTEM Dynamic Ver. 2.3 which was further modified (from Ver. 2.0) to include variable roughness by layer, and the effect of boat waves in each modeled time step.

4.2.5.2 Bank Toe Erosion Sub-Model

The Bank-Toe Erosion sub-model is used to estimate erosion of bank and bank-toe materials by hydraulic shear stresses. The effects of toe protection are incorporated into the analysis by changing the characteristics of the toe material in the model. The model calculates an average boundary shear stress from channel geometry and flow parameters, defined by flow depth and the duration of the time step (steady, uniform flow). The assumption of steady, uniform flow is not critical insomuch as the model does not attempt to route flow and sediment and is used only to establish the boundary shear stress for a specified duration (the period of the time step) along the bank surface. The model also allows for different critical shear stress and erodibility of separate zones with potentially different materials at the bank and bank toe. The bed elevation is fixed because the model does not incorporate the simulation of bed sediment transport. Toe erosion by hydraulic shear is calculated using an excess shear approach. Modifications made to BSTEM Dynamic Ver. 2.0 for this study allow the toe erosion sub-model to account for variations in water-surface slope in each time step.

4.2.5.3 Bank Stability Sub-Model

The bank stability sub-model simulates planar failure types in steep banks, and shear failure in banks that have been undercut by preferential erosion of an erodible basal layer (Figure 4.2.5.3-1). These are shear-type failures that occur when the driving force (stress) exceeds the resisting force (strength). The model combines two limit-equilibrium methods that estimate the Factor of Safety (F_s) of multi-layer streambanks. F_s is the ratio between the resisting and driving forces acting on a potential failure block. A value of unity indicates that the driving forces are equal to the resisting forces and that failure is imminent ($F_s = 1$). Instability exists under any condition where the driving forces exceed the resisting forces ($F_s < 1$), conditional stability is indicated by F_s values between 1 and 1.3, with stable bank conditions having a $F_s > 1.3$.

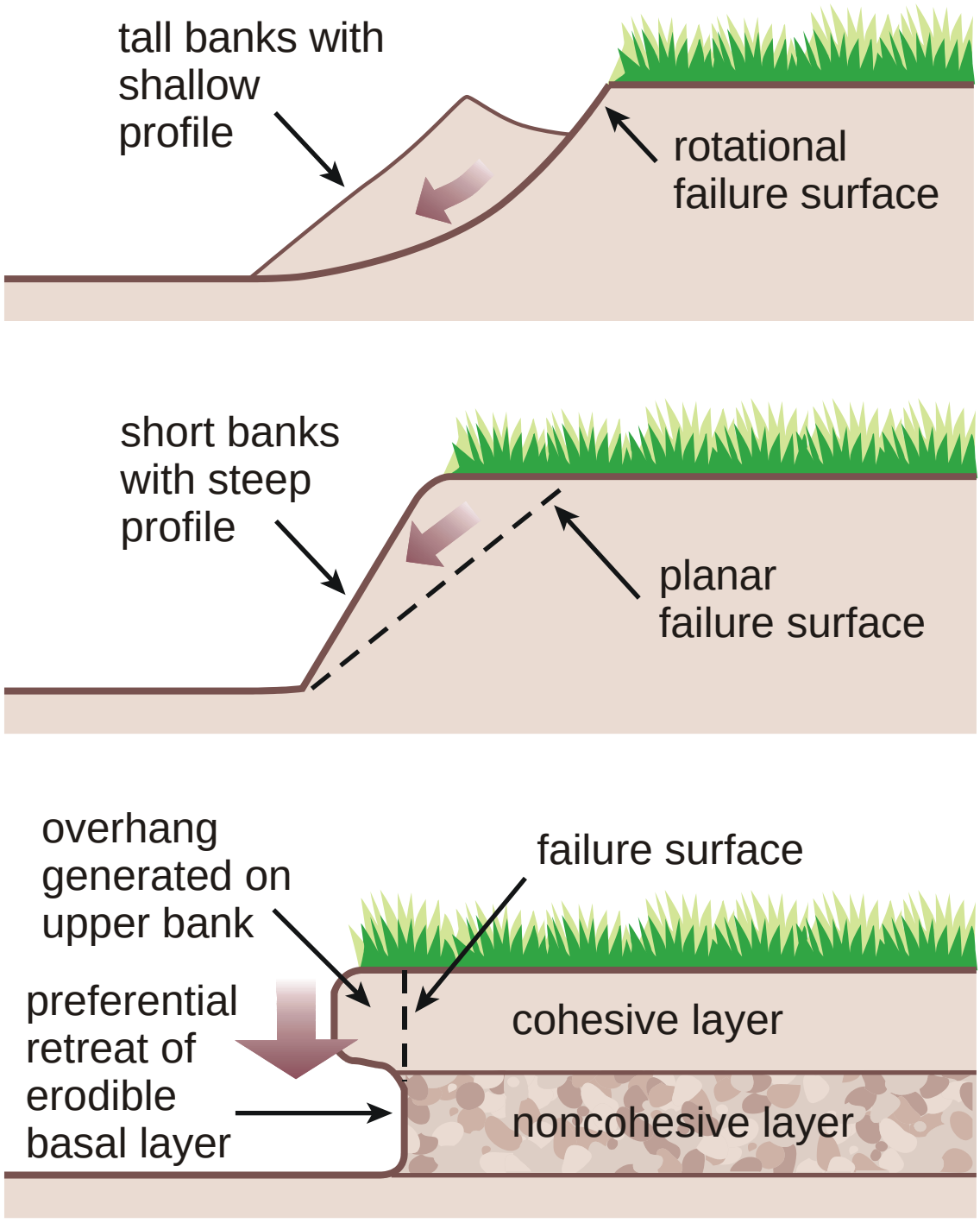

Figure 4.2.5.3-1: Streambank Failure Mechanisms

4.2.5.4 Root Reinforcement Sub-Model (RipRoot)

Vegetation can have a number of positive and negative effects on streambank stability. Of these effects, one of the most important to account for in stability calculations is the effect of root-reinforcement on soil shear strength. Soil is generally strong in compression, but weak in tension. The fibrous roots of trees and herbaceous species are strong in tension but weak in compression. Root-permeated soil, therefore, makes up a composite material that has enhanced strength (Thorne, 1990). Many studies have found an inverse power relationship between ultimate tensile strength, T_r, and root diameter, d (examples include but are not limited to: Waldron & Dakessian, 1981; Gray and Sotir, 1996; Abernethy and Rutherfurd, 2001; Simon & Collison, 2002; Pollen & Simon, 2005), and have shown that root-reinforcement can affect the shear-strength of the bank materials, and locations of shear failure surfaces within the banks.

In the RipRoot model currently embedded in BSTEM, a vegetation assemblage can be created by accessing the species database contained in the sub model; the user enters species, approximate vegetation ages, and approximate percent cover of each species at each site to estimate root density. Root-reinforcement values are then calculated automatically using RipRoot's progressive breaking algorithm. The database of species contained within RipRoot includes tests performed across the United States and has been expanded as part of this study to include five of the most common species found along the Turner Falls reach of the Connecticut River.

4.2.5.5 BSTEM Data Requirements

As BSTEM is a mechanistic model, the data required to operate the model are all related to quantifying the driving and resisting forces that control the hydraulic and geotechnical processes that operate on and along a streambank. Input-parameter values can all be obtained directly from field surveying and testing. If this is not possible, the model provides default values by material type for many parameters.

Data required for BSTEM fall into three broad categories: (1) bank geometry and stratigraphy, (2) hydraulic data, and (3) geotechnical data. A summary of the required input parameters is provided in Table 4.2.5.5-1. The default geotechnical values that are included in the model are provided in Table 4.2.5.5-2 (Simon *et al.*, 2011).

Table 4.2.5.5-1: Required User-Input Parameters for BSTEM

Hydraulic Processes: Bank Surface					
Driving Forces			**Resisting Forces**		
Parameter	**Purpose**	**Source**	**Parameter**	**Purpose**	**Source**
Channel Slope (*S*)	Boundary shear stress (τ_o)	Field survey or design plan	Particle diameter (*D*) (*cohesionless*)	Critical shear stress (τ_c)	Bulk sample particle size (*cohesionless*); Default values in model
			Critical shear stress (τ_c) (*cohesive*)	Critical shear stress (τ_c)	Jet test (*cohesive*); Default values in model
Flow depth (*h*)	Boundary shear stress (τ_o)	Field survey, gage information, design plan	Particle diameter (*D*) (*cohesionless*)	Erodibility coefficient (*k*)	Bulk sample particle size (*cohesionless*); Default values in model
			Critical shear stress (τ_c) (*cohesive*)	Erodibility coefficient (*k*)	Jet test (*cohesive*); Default values in model
Unit weight of water (γ_w)	Boundary shear stress (τ_o)	Considered constant, 9810 N/m^3			
Geotechnical Processes: Bank Mass					
Parameter	**Purpose**	**Source**	**Parameter**	**Purpose**	**Source**
Unit weight of sediment (γ_s)	Weight (*W*), Normal force (σ)	Core sample in bank unit; Default values in model	Unit weight of sediment (γ_s)	Weight (*W*), Normal force (σ)	Core sample in bank unit; Default values in model
Bank height (*H*)	Shear stress	Field survey or design plan	Effective cohesion (*c'*)	Shear strength (τ_f)	Borehole shear, direct shear, triaxial shear; Default values in model
Bank angle (α)	Shear stress	Field survey or design plan	Effective angle (φ')	Shear strength (τ_f)	
			Pore-water pressure (μ_w)	Shear strength (τ_f)	Interpolated from water table

Table 4.2.5.5-2: Default Values in BSTEM (bold) for Geotechnical Properties

Soil Type	Statistic	*c'* (kPa)	Φ' (degrees)	γ_{sat} (kN/m^3)
Gravel (uniform)*		0.0	36.0	20.0
Sand and Gravel*		0.0	47.0	21.0
Sand	75th percentile	1.0	32.3	19.1
	Median	**0.4**	**30.3**	**18.5**
	25th percentile	0.0	25.7	17.9
Loam	75th percentile	8.3	29.9	19.2
	Median	**4.3**	**26.6**	**18.0**
	25th percentile	2.2	16.7	17.4
Clay	75th percentile	12.6	26.4	18.3
	Median	**8.2**	**21.1**	**17.7**
	25th percentile	3.7	11.4	16.9

Data derived from more than 800 *in situ* direct-shear tests with the Iowa Borehole Shear Tester except where indicated (From Hoek and Bray (1977) as cited by Simon *et al.*, 2011).

4.2.5.6 General Model Limitations

BSTEM can simulate the most common types of bank failures that typically occur along alluvial channels. Once failure is simulated, the failed material is assumed to enter the flow. The model does not simulate rotational failures that generally occur in very high banks of homogeneous, fine-grained materials characterized by low bank angles. Although potentially damaging with regards to the amount of land loss, these failures are not common along the reach. Evidence of historical rotational failures was observed only on high-terrace surfaces, far removed from the active channel. Bank undercutting by seepage erosion is similarly not included in the version described herein. This is not considered a problem along the Turners Falls reach as evidence of seepage processes were observed at only a few sites by field crews. Finally, the hydrologic effects of riparian vegetation, including interception, evapo-transpiration and the accelerated delivery of water along roots and macro pores cannot be simulated at this time.

4.2.5.7 BSTEM Summary

BSTEM Dynamic contains both geotechnical-stability and hydraulic-erosion algorithms, thereby allowing for deterministic analysis of bank stability over time. As such, flow stage at each time step is read into the model, and the amount and location of hydraulic erosion is calculated. The resulting new bank geometry for that time step is then used in the geotechnical algorithm to determine the stability of the bank by calculating the bank's Factor of Safety (<1.0 = unstable) at that time step. If a geotechnical failure is predicted, the geometry is updated again to account for the failure before the next flow-stage value is read in at the next time step. In this way BSTEM Dynamic 2.3 can predict the retreat of a streambank for flow series ranging in length from hours to decades. In addition to being able to take into account both hydraulic and geotechnical processes, the model has a groundwater component that contributes to the geotechnical strength algorithm, and can account for the effects of root-reinforcement provided by riparian vegetation, through the RipRoot sub-model (Pollen & Simon, 2005; Pollen, 2007; Thomas & Bankhead, 2010).

4.2.6 BSTEM Input Data Collection

To determine the erosion resistance of the 25 detailed study sites throughout the TFI (as previously shown in Figure 4.1-1 and 4.1-2), Cardno staff, with assistance of staff from NEE, performed field tests to quantify the geotechnical and hydraulic resistance of the bank and bank-toe materials at each site. The locations of these sites were discussed in Section 4.1, are representative of the range of conditions present along the reach and are spaced relatively evenly. Rough surveys of the tested banks were also carried out at each site with a tape and Brunton compass to provide bank heights, angles, and stratigraphic layering for the tested bank. The data collected in the field were used by Cardno to populate BSTEM-Dynamic 2.3.

4.2.6.1 Geotechnical Data Collection: Borehole Shear Tests

To properly determine the resistance of bank materials to erosion by mass movement, data must be acquired on those characteristics that control shear strength; that is cohesion, angle of internal friction, pore-water pressure, and bulk unit weight. Cohesion and friction angle data can be obtained from standard laboratory testing (triaxial shear or unconfined compression tests), or by in-situ testing with a borehole shear-test (BST) device (Lohnes & Handy 1968; Thorne, Murphey & Little, 1981; Lutenegger & Hallberg, 1981; Little, Thorne & Murphy, 1982). To gather data on the internal shear-strength properties of the banks, in-situ tests with the Iowa Borehole Shear Tester (BST) were used (Figure 4.2.6.1-1 - Figure 4.2.6.1-2).

The BST provides direct, drained shear-strength tests on the walls of a borehole. To use the BST, a 0.069 m (2.75 in) diameter hole is bored using an auger, from the floodplain or other flat surface into a particular bank layer to be tested. Under a known initial pressure, the shear head is then placed in the borehole to the desired depth and expanded to the walls of the borehole, using CO_2 gas connected to the Normal Stress console. After initial consolidation, the pulling assembly is used to apply an axial stress to the shear head, measured on the shear gauge, until failure beyond the walls of the borehole occurs. The axial stress is

released, and the normal pressure is raised typically in increments of about 10-20 kPa, and an additional 5-30 minutes of consolidation is provided, depending on the soil type and moisture content.

The shearing process is repeated to generate a series of data points representing the material's shear stress at failure at each associated normal stress applied to the walls of the borehole. The data points are then plotted, with normal stress on the x-axis and shear stress on the y-axis (Figure 4.2.6.1-3). The gradient of the resulting linear relation represents the friction angle of the soil layer tested and the y-intercept represents the apparent cohesion (ca) of the soil layer. Effective cohesion (c') is then calculated by subtracting a measure of the soil suction (negative pore-water pressure; asymptote in Figure 4.2.6.1-4) from the value of apparent cohesion (y-intercept in Figure 4.2.6.1-3). This is done by solving for c', substituting the asymptotic suction value from Figure 4.2.6.1-4, and assuming a value of ϕ^b. We generally use a value of 10^o based on field tests in alluvial materials (Simon *et al*., 2000).

The friction angle can be thought of as being similar to the angle of repose; this is the steepest angle that a cohesionless slope can maintain without losing its stability. When a slope or streambank possesses this angle, its shear strength perfectly counterbalances the force of gravity acting upon it, and remains stable unless other driving forces are also present (for example water). Pore-water pressure at the time of sampling is obtained using a digital tensiometer inserted into a core that has been retrieved from the test depth.

Advantages of the BST include:

1. The test is performed *in situ* and testing is, therefore, performed on undisturbed material;

2. Cohesion and friction angle are evaluated separately. The cohesion value represents apparent cohesion (ca). Effective cohesion (c') is then obtained by adjusting ca according to measured pore-water pressure and ϕ^b (rate of increase in strength with increasing matric suction);

3. A number of separate trials are run at the same sample depth to produce single values of cohesion and friction angle based on a standard Mohr-Coulomb failure envelope;

4. Data and results obtained from the instrument are plotted and calculated on site, allowing for repetition if results are unreasonable; and

5. Tests can be carried out at various depths in the bank to locate weak strata (Thorne *et al*. 1981).

At each testing depth, a small core of known volume was removed and sealed to be returned to the laboratory. The samples were weighed, dried and weighed again to obtain values of moisture content and bulk density, the latter required for analysis of streambank stability. In addition, bulk samples were obtained at each testing depth for particle-size analysis.

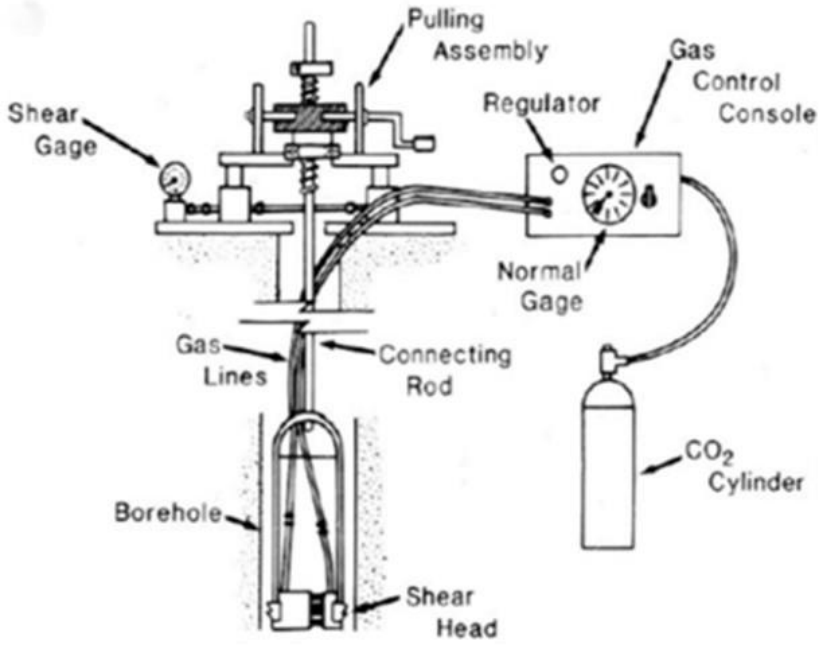

Figure 4.2.6.1-1: Schematic Representation of Borehole Shear Tester (BST)

Figure 4.2.6.1-2: Conducting a Borehole Shear Test (BST)

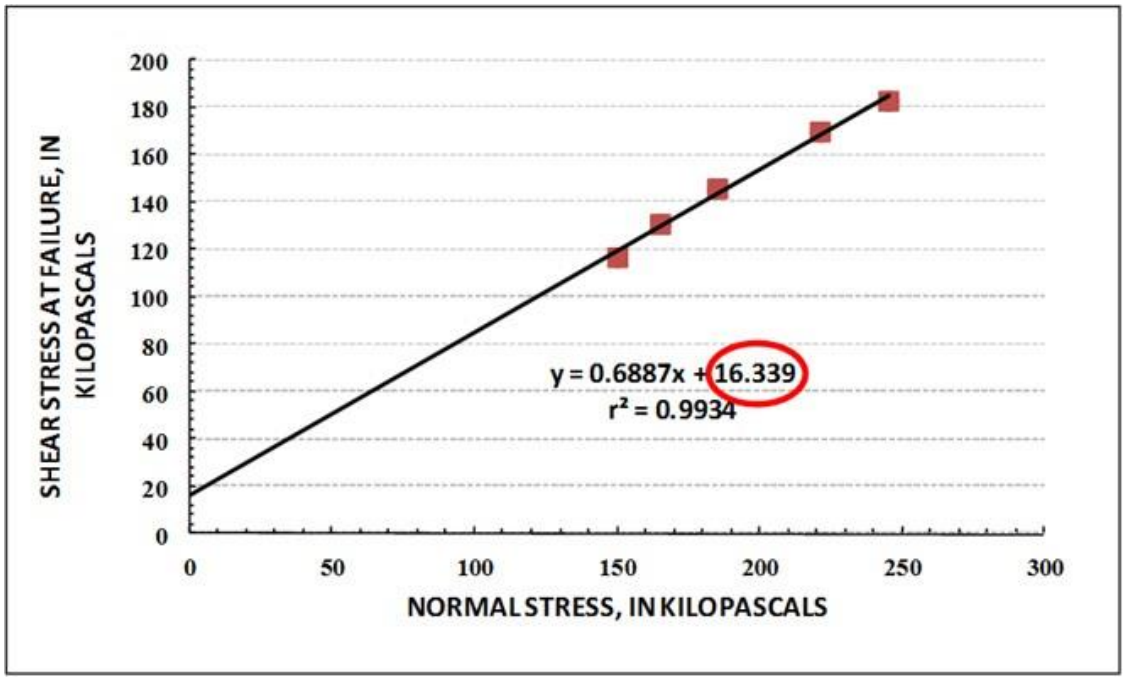

Figure 4.2.6.1-3: Example of a Borehole Shear Test (BST)

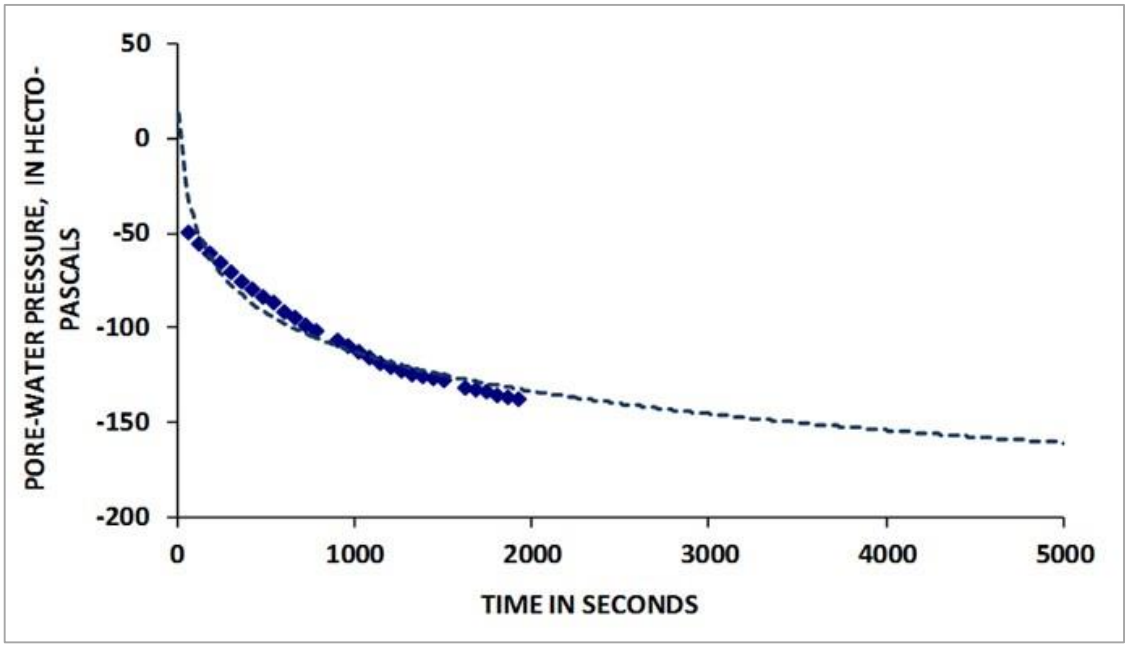

Figure 4.2.6.1-4: Typical Pore-Water Pressure Data Obtained from a Core using a Digital Tensiometer

4.2.6.2 Hydraulic-Resistance Data Collection: Submerged Jet Tests

Hydraulic-resistance of the bank-toe and bank face are important for predicting scour and undercutting of the channel banks within BSTEM. Where materials are non-cohesive, resistance is due to particle size and weight, therefore, a bulk particle-size or particle count is sufficient to describe resistance properties. However, cohesive materials are not entrained into the water column predictably due to particle size and weight but due to the electro-chemical bonds between particles. To test *in situ* erodibility of cohesive materials, a submerged jet test was developed by the USDA-ARS (Figure 4.2.6.2-1; Hanson, 1990; ASTM, 1995). This device was developed based on knowledge of the hydraulic characteristics of a submerged jet and the characteristics of soil-material erodibility.

The Mini-Jet used throughout this project is a scaled-down version of the original instrument. Side-by-side testing of the mini-jet and the standard submerged jet are reported in Simon *et al.*, (2010; 2011) and Al-Madhhachi *et al.*, 2013 (Figure 4.2.6.2-2). The method provided by Al-Madhhachi *et al.*, (2013) to scale mini-jet results to the full-size jet was adopted in this work.

Depth-of-scour is measured manually using a point gauge at known increments over time. As the scour depth increases with time, the applied shear stress decreases, due to increasing dissipation of jet energy within the plunge pool. Detachment rate is initially high and asymptotically approaches zero as applied shear stress approaches the critical shear stress of the material (Figure 4.2.6.2-3). A difficulty in determining equilibrium scour depth is that the length of time required to reach equilibrium can be large. Fitting time-series scour data to the logarithmic-hyperbolic method described in Hanson and Cook (Hanson & Cook, 1997), however, provides the critical shear stress, (τ_c) and the erodibility coefficient, (k). Essentially, k is the slope of the scour vs. time curve, expressing the volume of material eroded per unit force (Newtons) and per unit time (seconds) (Figure 4.2.6.2-3). Hence, k is expressed as cm^3/N-s. As part of the field program, bulk samples were also taken of the surficial bank sediments to be tested for particle-size distribution.

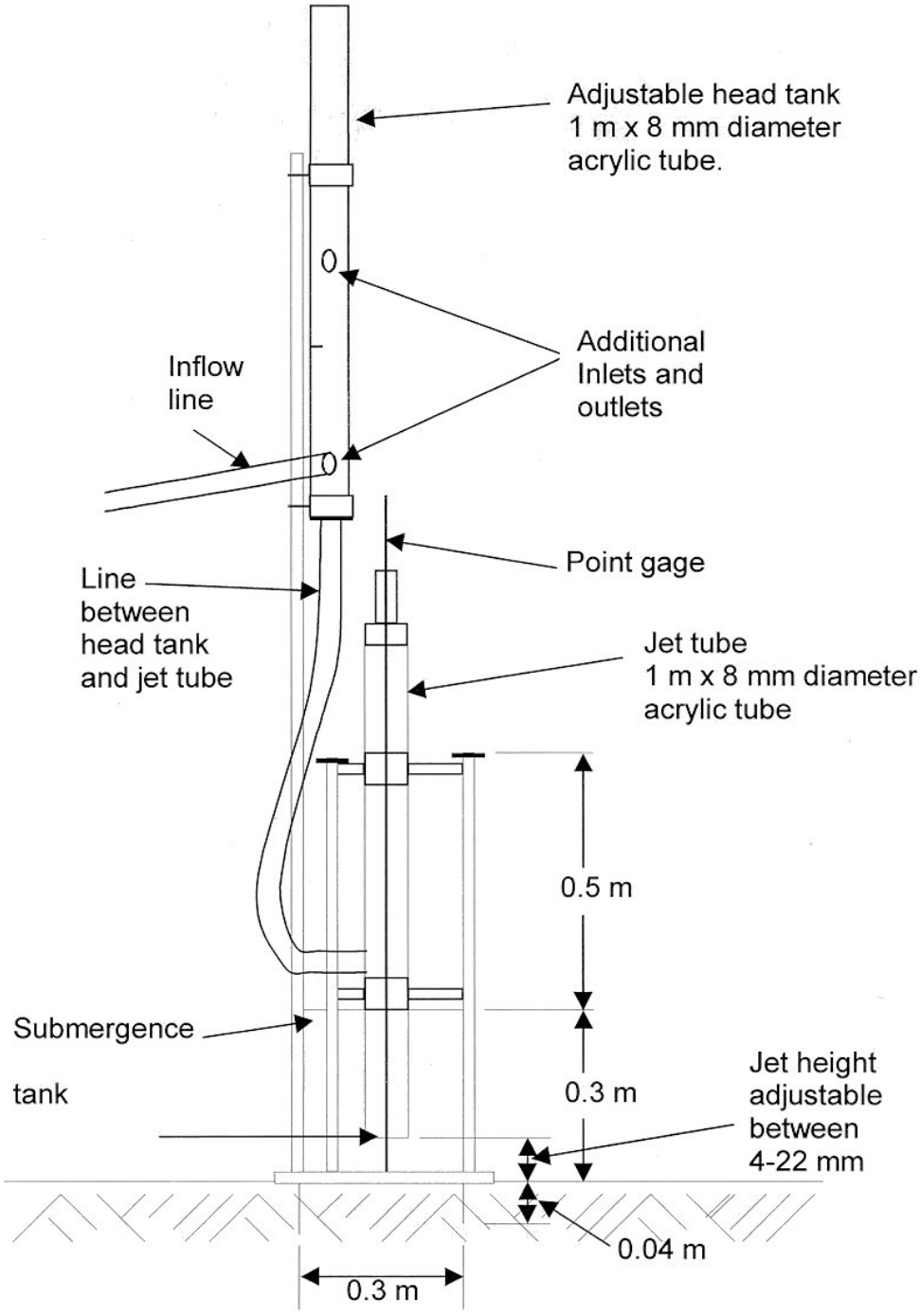

Figure 4.2.6.2-1: Schematic of Original Jet-Test Device

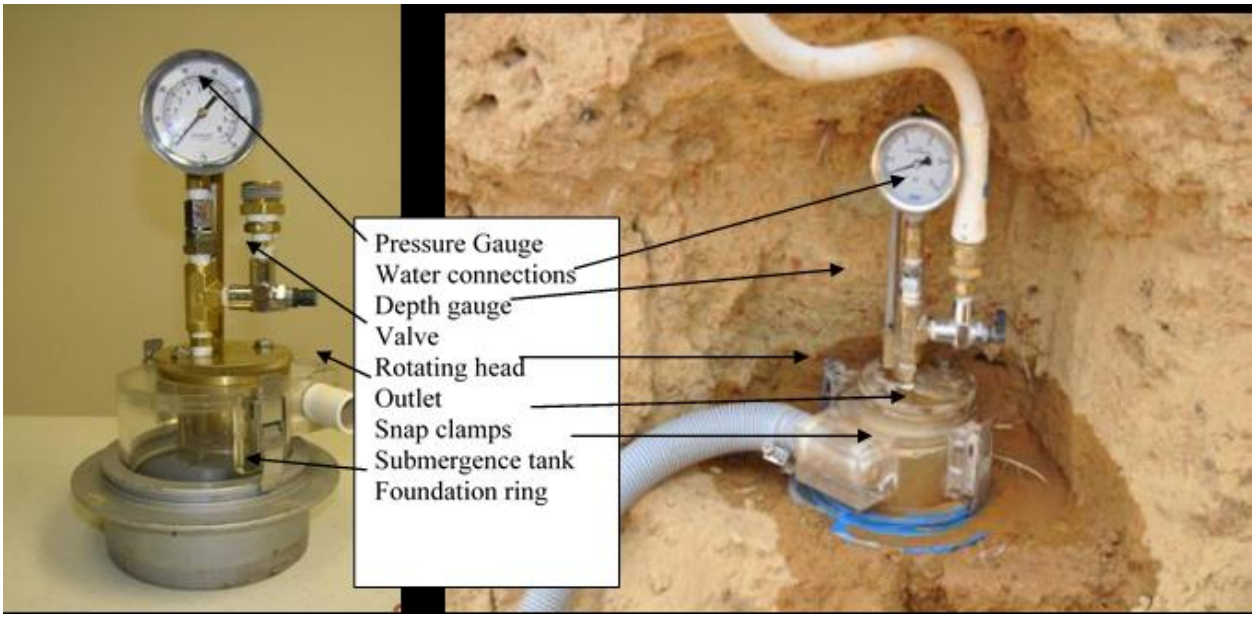

Figure 4.2.6.2-2: Photographs of Scaled-down "Mini-jet"

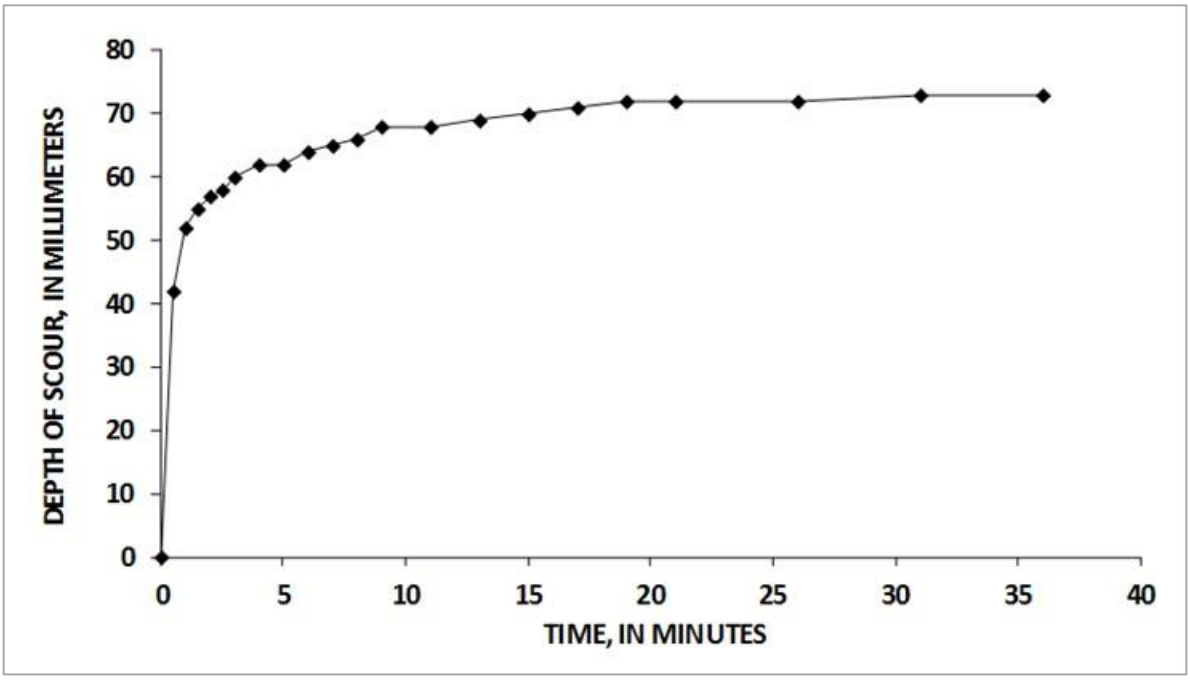

Figure 4.2.6.2-3: Example Scour Plot From Mini-jet Test

4.2.6.3 Particle Size of Bank Sediments

Bulk bank-material samples were taken at each location tested by the BST and the submerged jet test device. In addition, if coarse-grained materials were present (gravels and cobbles) measurements of 100 particles were conducted to determine the size distribution. These data were then combined with the bulk-sample particle-size analysis to determine an overall distribution of sizes. These data were collected to associate test results with general material types, and to provide information on entrainment thresholds for non-cohesive materials. The laboratory used a particle size of 0.063 mm as the break point between sand and silt. Thus, reference to fine-grained materials is defined as that proportion of the sample finer than 0.063 mm. A total of 126 bulk and particle-count samples of bank face, bank toe (beach) and internal bank materials were collected and analyzed. Results from an example analysis are shown in Figure 4.2.6.3-1.

Bank materials at the test locations are, for the most part, a combination of sands and silts in varying proportions (Table 4.2.6.3-1 and Figure 4.2.6.3-2). The median composition of the bank materials is 0% gravel, 51.5% sand, 41.8% silt and 3.8% clay. This is not to say that gravel is not present at some of the sites. Particle counts were conducted at 10 sites along the reach owing to the presence of some gravel and cobbles along the beach- bank toe regions. In some cases, their presence was due to placement as part of restoration works. Full distributions by particle-size class are shown in Figure 4.2.6.3-2.

The majority of the materials (72%) can be classified as either sandy or silt loams Table 4.2.6.3-2. This and the general lack of clays in the bank strata should limit the magnitude of permeability differences in the banks that would relate to issues with perched groundwater and seepage. Values used for saturated hydraulic conductivity (according to textural class) were obtained from the Natural Resources Conservation Service (NRCS) website (NRCS, 2015). These are also shown in Table 4.2.6.3-2.

Sorting the samples into distinct sampling locations of beach-toe, bank face, and internal bank materials provides further insights into the nature of the bank materials. The low-bank surfaces most susceptible to hydraulic erosion are those that are impacted most frequently by flows, the “beach” and “bank-toe” locations. The materials at these locations generally contain more sand (about 79%) than the bank face (43% sand) or internal bank materials (56% sand) (Table 4.2.6.3-3). Also note the general lack of fines (about 16% silts and clays) in the beach and bank-toe materials. The general lack of cohesive clays in the bank materials, particularly on the bank-toe and beach surfaces can make them relatively susceptible to erosion by hydraulic forces and wave action. Those sites with gravel along the beach and bank toe are, however, less susceptible to erosion by hydraulic forces because of the increased resistance provided by the larger clasts. The median diameter (d_{50}) of the gravel materials ranges from 7 mm at site 8B-L to 57.5 mm at site 10R. This latter size is characteristic of two other sites (57 mm at site 6A-L and 55.5 mm at site 3R) where restoration measures, including gravel toe protection have been implemented

Some of the distinct similarities and differences in the composition of the three types of sampling locations become evident in comparing the longitudinal distribution of the materials (Figure 4.2.6.3-3). Equal ranges of sand and silt, with zero gravel mark the bank face and internal-bank sediment distributions. This is not surprising given that they both represent in situ bank materials. The striking difference in the beach-toe distributions along with the locations of the predominantly gravel sites can be clearly seen in Figure 4.2.6.3-3 (Bottom). It is those sites containing gravel at the beach-toe locations that are much less susceptible to hydraulic erosion because of shear stresses that are generally less than critical shear stress required for entrainment.

A list of the results for all sites and locations, along with the average values by site are summarized in Table 4.2.6.3-4. Those sites that show some gravel proportion are indicative of gravels along the beach-bank toe region as none were observed within the bank mass.

Table 4.2.6.3-1: Textural Classes of Bank-material Sediments along the Study Reach

Percentile	% Gravel	% Sand	% Silt	% Clay	% Fines
75th	0.0	69.5	57.2	6.0	64.2
50th	0.0	51.5	41.8	3.8	46.9
25th	0.0	33.0	23.7	1.9	25.2

Table 4.2.6.3-2: Classification of Bank Materials in the Study Reach and Associated Saturated Hydraulic Conductivity (K_{sat}) Obtained from NRCS (2015)

Material Type	Number	Percent of total	K_{sat} (m/s)
Loam	2	1.7	9.15E-06
Loamy sand	16	13.2	9.17E-05
Sand	15	12.4	1.41E-04
Sandy loam	45	37.2	2.82E-05
Silt loam	42	34.7	9.15E-06
Silty clay loam	1	0.8	2.82E-06

Table 4.2.6.3-3: Median Composition of Bank-material Sediments from Different Sampling Locations

Location	Number	% Gravel	% Sand	% Silt	% Clay	% ML+CL
Internal	62	0.0	56.2	40.0	3.6	43.8
Beach-Toe	25	0.0/77.5	69.5	13.7	1.6	16.3
Bank Face	39	0.0	42.0	52.4	5.7	58.0

Table 4.2.6.3-4: Particle-size Data of the Bank Materials along the Turners Falls Impoundment

Site	Type	Station	% Gravel	% Sand	% Silt	% Clay	% ML+CL	d_{50}	Texture	Site Average				
										% Gravel	% Sand	% Silt	% Clay	% ML+CL
10L	Bank Face	49000	0	16.9	72.8	10.3	83.1		silt loam	0.0	54.6	39.7	5.7	45.4
10L	Bank Face	49000	0	20.9	67.1	12.0	79.1		silt loam					
10L	Beach-Toe	49000	0	64.3	32.3	3.5	35.7		sandy loam					
10L	Internal	49000	0	89.9	9.3	0.8	10.1		sand					
10L	Internal	49000	0	66.0	30.1	3.9	34.0		sandy loam					
10L	Internal	49000	0	69.7	26.6	3.6	30.3		sandy loam					
10R	Bank Face	49000	0	31.6	62.4	6.0	68.4		silt loam	25.0	36.9	35.8	2.3	38.1
10R	Beach-Toe	49000	100	0.0	0.0	0.0	0.0	57.5	gravel					
10R	Internal	49000	0	51.3	47.1	1.6	48.7		sandy loam					
10R	Internal	49000	0	64.8	33.6	1.6	35.2		sandy loam					
119BL	Bank Face	41000	0	25.1	68.9	6.0	74.9		silt loam	0.0	38.1	59.0	3.8	61.9
119BL	Bank Face	41000	0	42.0	54.4	3.7	58.0		silt loam					
119BL	Beach-Toe	41000	0	53.4	45.0	1.6	46.6		sandy loam					
119BL	Internal	41000	0	49.8	46.7	3.5	50.2		sandy loam					
119BL	Internal	41000	0	35.3	59.0	5.7	64.7		silt loam					
119BL	Internal	41000	0	40.6	56.6	2.8	59.4		silt loam					
119BL	Internal	41000	0	20.8	75.7	3.5	79.2		silt loam					
11L	Bank Face	100000	0	54.7	38.7	6.6	45.3		sandy loam	0.0	25.4	63.7	10.9	74.6
11L	Internal	100000	0	13.7	73.4	12.9	86.3		silt loam					
11L	Internal	100000	0	7.8	79.1	13.1	92.2		silt loam					
12BL	Bank Face	6750	0	78.7	21.6	0.3	21.9		loamy sand	0.0	89.4	10.3	0.4	10.7
12BL	Beach-Toe	6750	0	89.1	10.2	0.8	10.9		sand					

Site	Type	Station	% Gravel	% Sand	% Silt	% Clay	% ML+CL	d_{50}	Texture	Site Average				
										% Gravel	% Sand	% Silt	% Clay	% ML+CL
12BL	Internal	6750	0	84.9	15.1	0.0	15.1		loamy sand					
12BL	Internal	6750	0	96.1	3.1	0.8	3.9		sand					
12BL	Internal	6750	0	98.4	1.6	0.0	1.6		sand					
18L	Bank Face	87000	0	62.4	64.0	3.6	37.6		sandy loam	0.0	62.6	33.2	4.2	37.4
18L	Bank-Face	87000	0	25.0	66.4	8.6	75.0		silt loam					
18L	Beach-Toe	87000	0	94.6	4.9	0.5	5.4		sand					
18L	Internal	87000	0	68.4	27.6	3.9	31.6		sandy loam					
21R	Bank Face	79250	0	46.7	48.9	4.5	53.3		sandy loam	0.0	55.6	40.3	4.1	44.4
21R	Bank Face	79250	0	66.0	30.5	3.5	34.0		sandy loam					
21R	Beach-Toe	79250	0	74.7	24.4	0.8	25.3		loamy sand					
21R	Internal	79250	0	56.7	38.7	4.6	43.3		sandy loam					
21R	Internal	79250	0	49.1	45.6	5.3	50.9		sandy loam					
21R	Internal	79250	0	40.4	53.9	5.8	59.6		silt loam					
26R	Bank Face	79250	0	16.8	72.9	10.3	83.2		silt loam	7.6	43.0	44.8	4.6	49.4
26R	Bank Face	50000	0	20.8	81.0	8.2	79.2		silt loam					
26R	Beach-Toe	50000	38	51.9	9.6	0.6	10.2		gravelly sand					
26R	Internal	50000	0	82.2	16.2	1.6	17.8		loamy sand					
26R	Internal	50000	0	43.5	54.5	2.0	56.5		silt loam					
29R	Bank Face	66000	0	51.9	44.2	3.9	48.1		sandy loam	0.0	56.5	39.6	3.9	43.5
29R	Back Face	66000	0	31.2	61.9	6.9	68.8		silt loam					
29R	Beach-Toe	66000	0	78.2	20.2	1.7	21.8		loamy sand					
29R	Internal	66000	0	71.2	26.3	2.5	28.8		sandy loam					
29R	Internal	66000	0	50.0	45.5	4.5	50.0		sandy loam					

Site	Type	Station	% Gravel	% Sand	% Silt	% Clay	% ML+CL	d_{50}	Texture	Site Average				
										% Gravel	% Sand	% Silt	% Clay	% ML+CL
2L	Bank Face	94500	0	52.8	41.8	5.4	47.2		sandy loam	0.0	47.5	48.5	4.0	52.5
2L	Bank Face	94500	0	23.7	70.6	5.6	76.3		silt loam					
2L	Beach-Toe	94500	0	74.1	24.0	1.9	25.9		loamy sand					
2L	Internal	94500	0	48.9	47.7	3.4	51.1		sandy loam					
2L	Internal	94500	0	38.2	58.1	3.7	61.8		silt loam					
303BL	Bank Face	94000	0	66.0	30.1	3.8	34.0		sandy loam	0.0	49.2	45.9	4.9	50.8
303BL	Bank Face	94000	0	32.3	62.6	5.1	67.7		silt loam					
303BL	Beach-Toe	94000	0	83.7	13.7	2.6	16.3		loamy sand					
303BL	Internal	94000	0	25.7	66.4	7.9	74.3		silt loam					
303BL	Internal	94000	0	38.5	56.6	5.0	61.5		silt loam					
3L	Bank Face	79500	0	46.4	47.9	5.7	53.6		sandy loam	0.0	59.5	36.7	3.8	40.5
3L	Bank Face	79500	0	54.6	40.9	4.5	45.4		sandy loam					
3L	Beach-Toe	79500	0	79.3	18.0	2.7	20.7		loamy sand					
3L	Internal	79500	0	59.0	37.5	3.5	41.0		sandy loam					
3L	Internal	79500	0	58.2	38.9	2.9	41.8		sandy loam					
3R	Bank Face	79500	0	66.3	29.9	3.8	33.7		sandy loam	20.0	52.6	24.7	2.8	27.4
3R	Bank Face	79500	0	52.7	41.8	5.5	47.3		sandy loam					
3R	Beach-Toe	79500	100	0.0	0.0	0.0	0.0	55.5	gravel					
3R	Internal	79500	0	76.0	22.4	1.6	24.0		loamy sand					
3R	Internal	79500	0	67.9	29.2	2.9	32.1		sandy loam					
4L	Bank Face	74000	0	44.8	49.6	5.6	55.2		sandy loam	0.0	55.6	39.9	4.5	44.4
4L	Bank Face	74000	0	47.0	47.0	6.0	53.0		sandy loam					
4L	Beach-Toe	74000	0	69.5	28.8	1.7	30.5		sandy loam					

Site	Type	Station	% Gravel	% Sand	% Silt	% Clay	% ML+CL	d_{50}	Texture	Site Average				
										% Gravel	% Sand	% Silt	% Clay	% ML+CL
4L	Internal	74000	0	58.2	37.4	4.4	41.8		sandy loam					
4L	Internal	74000	0	58.4	36.9	4.8	41.6		sandy loam					
5CR	Bank Face	57250	0	48.4	45.6	6.0	51.6		sandy loam					
5CR	Bank Face	57250	0	56.4	39.8	3.8	43.6		sandy loam					
5CR	Bank Face	57250	0	43.2	51.0	5.7	56.8		silt loam					
5CR	Beach-Toe	57250	0	85.6	12.5	1.9	14.4		loamy sand	0.0	52.7	42.3	5.0	47.3
5CR	Internal	57250	0	55.8	40.5	3.7	44.2		sandy loam					
5CR	Internal	57250	0	39.1	51.4	8.5	60.9		silt loam					
5CR	Internal	57250	0	40.4	54.3	5.3	59.6		silt loam					
6AL	Bank Face	41750	0	41.6	51.4	6.1	58.4		silt loam					
6AL	Bank Face	41750	0	34.3	58.5	7.2	65.7		silt loam					
6AL	Beach-Toe	41750	0	0.0	0.0	0.0	0.0	57.0	gravel	20.0	50.7	25.7	3.6	29.3
6AL	Internal	41750	0	90.0	6.9	3.1	10.0		sand					
6AL	Internal	41750	0	87.8	10.8	1.4	12.2		sand					
6AR	Beach-Toe	41750	0	44.7	48.3	7.0	55.3		loam					
6AR	Beach-Toe	41750	0	56.9	38.1	5.1	43.1		sandy loam	0.0	38.0	54.0	8.0	62.0
6AR	Internal	41750	0	20.3	69.2	10.5	79.7		silt loam					
6AR	Internal	41750	0	30.1	60.6	9.3	69.9							
75BL	Bank Face	27000	0	63.3	34.3	2.3	36.7							
75BL	Beach-Toe	27000	78	17.7	4.1	0.2	4.3	28.5	gravel					
75BL	Internal	27000	0	90.0	8.1	1.9	10.0		sand	13.0	52.2	31.4	3.5	34.8
75BL	Internal	27000	0	75.1	22.1	2.8	24.9		loamy sand					
75BL	Internal	27000	0	51.6	43.6	4.7	48.4		sandy loam					

Site	Type	Station	% Gravel	% Sand	% Silt	% Clay	% ML+CL	d_{50}	Texture	Site Average				
										% Gravel	% Sand	% Silt	% Clay	% ML+CL
75BL	Internal	27000	0	15.1	76.1	8.8	84.9		silt loam					
7L	Bank Face	37500	0	27.5	64.5	8.0	72.5		silt loam	0.0	59.7	36.4	3.9	40.3
7L	Beach-Toe	37500	0	95.8	4.2	0.0	4.2		sand					
7L	Internal	37500	0	32.6	59.0	8.4	67.4		silt loam					
7L	Internal	37500	0	73.1	25.2	1.7	26.9		loamy sand					
7L	Internal	37500	0	69.4	28.9	1.7	30.6		sandy loam					
7R	Bank Face	37500	0	51.0	44.2	4.9	49.0		sandy loam	0.0	63.3	32.3	4.4	36.7
7R	Bank Face	37500	0	34.7	57.4	7.9	65.3		silt loam					
7R	Beach-Toe	37500	0	75.1	22.8	2.0	24.9		loamy sand					
7R	Internal	37500	0	98.4	1.6	0.0	1.6		sand					
7R	Internal	37500	0	92.8	5.3	1.9	7.2		sand					
7R	Internal	37500	0	27.6	62.6	9.8	72.4		silt loam					
87BL	Bank Face	30750	0	34.3	59.0	6.7	65.7		silt loam	0.0	37.4	56.3	6.4	62.6
87BL	Bank Face	30750	0	19.5	71.0	9.5	80.5		silt loam					
87BL	Beach-Toe	30750	0	42.4	50.6	7.0	57.6		silt loam					
87BL	Internal	30750	0	56.8	39.5	3.8	73.2		sandy loam					
87BL	Internal	30750	0	52.5	45.0	2.5	27.5		sandy loam					
87BL	Internal	30750	0	18.8	72.5	8.7	81.2		silt loam					
8BL	Bank Face	32750	0	36.0	57.1	6.9	64.0		silt loam	18.0	35.5	55.8	6.2	62.1
8BL	Beach-Toe	32750	72.0	28.0	--	--	--	7.0	gravel					
8BL	Internal	32750		45.3	48.5	6.2	54.7		sandy loam					
8BL	Internal	32750		32.6	61.9	5.5	67.4		silt loam					
8BR	Bank Face	32750		35.2	59.8	5.0	64.8		silt loam	19.3	46.1	42.1	4.0	46.2

Site	Type	Station	% Gravel	% Sand	% Silt	% Clay	% ML+CL	d_{50}	Texture	Site Average				
										% Gravel	% Sand	% Silt	% Clay	% ML+CL
8BR	Beach-Toe	32750		23.0	--	--	--	13.0	gravel					
8BR	Internal	32750		66.4	30.1	3.5	33.6		sandy loam					
8BR	Internal	32750		59.9	36.5	3.6	40.1		sandy loam					
9R	Bank Face	6500		8.9	77.9	13.2	91.1		silt loam					
9R	Beach-Toe	6500		89.4	9.1	1.5	10.6		sand					
9R	Internal	6500		76.2	21.9	1.9	23.8		loamy sand	0.0	53.9	39.5	6.6	46.1
9R	Internal	6500		86.0	12.4	1.6	14.0		sand					
9R	Internal	6500		8.9	76.4	14.7	91.1		silt loam					
BC-1R	Beach-Toe	4750	23.0	75.8	1.2	0.0	1.2		gravelly sand					
BC-1R	Internal	4750		95.2	1.5	3.3	4.8		sand					
BC-1R	Internal	4750		45.3	46.4	8.3	54.7		loam	5.8	58.8	25.6	9.9	35.5
BC-1R	Internal	4750		18.9	53.4	27.8	81.1		silty clay loam					

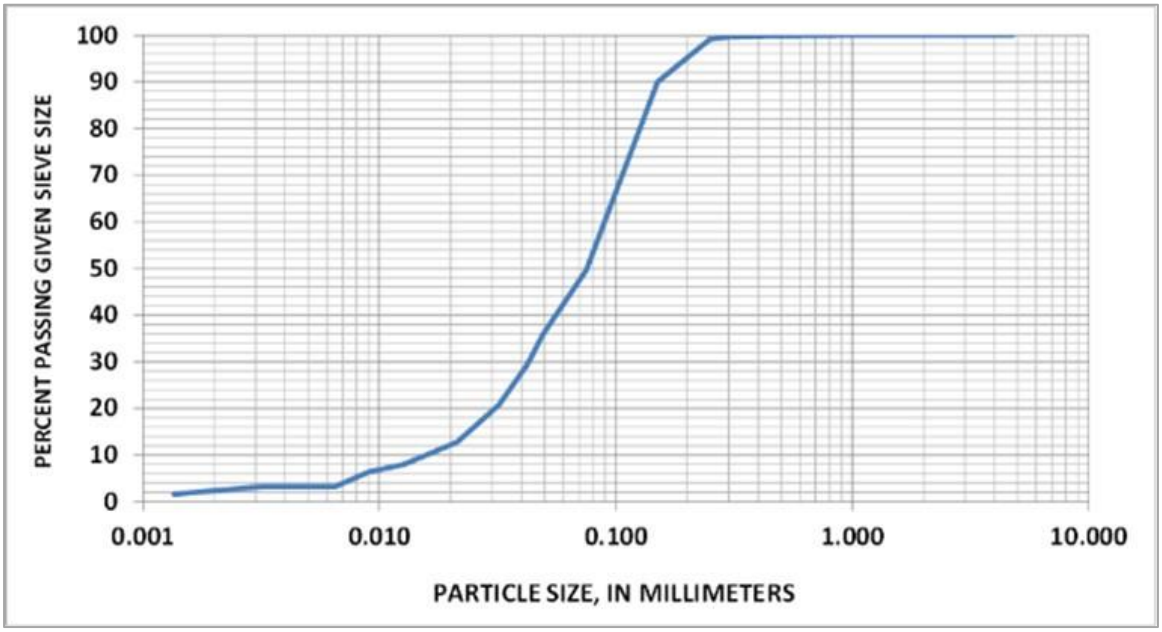

Figure 4.2.6.3-1: Example Results of Particle-size Analysis Showing Composition of Bank

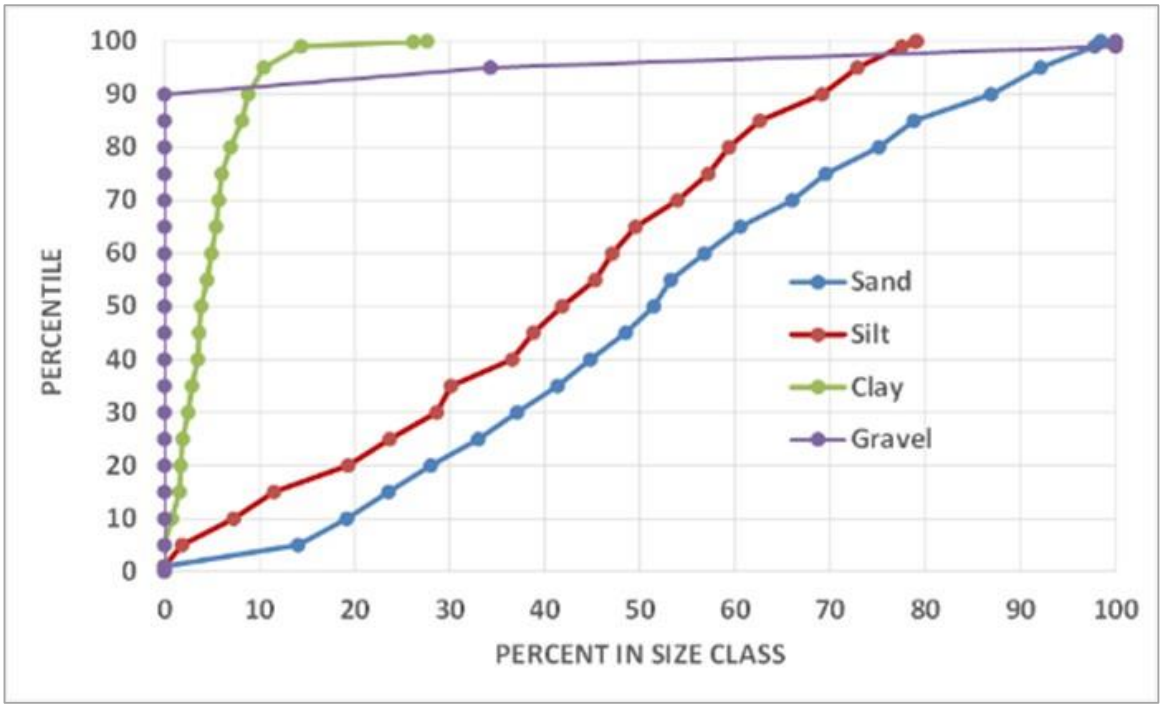

Figure 4.2.6.3-2: Frequency Distribution of the Composition of the Bank Material Sediments for the 25 Study Sites

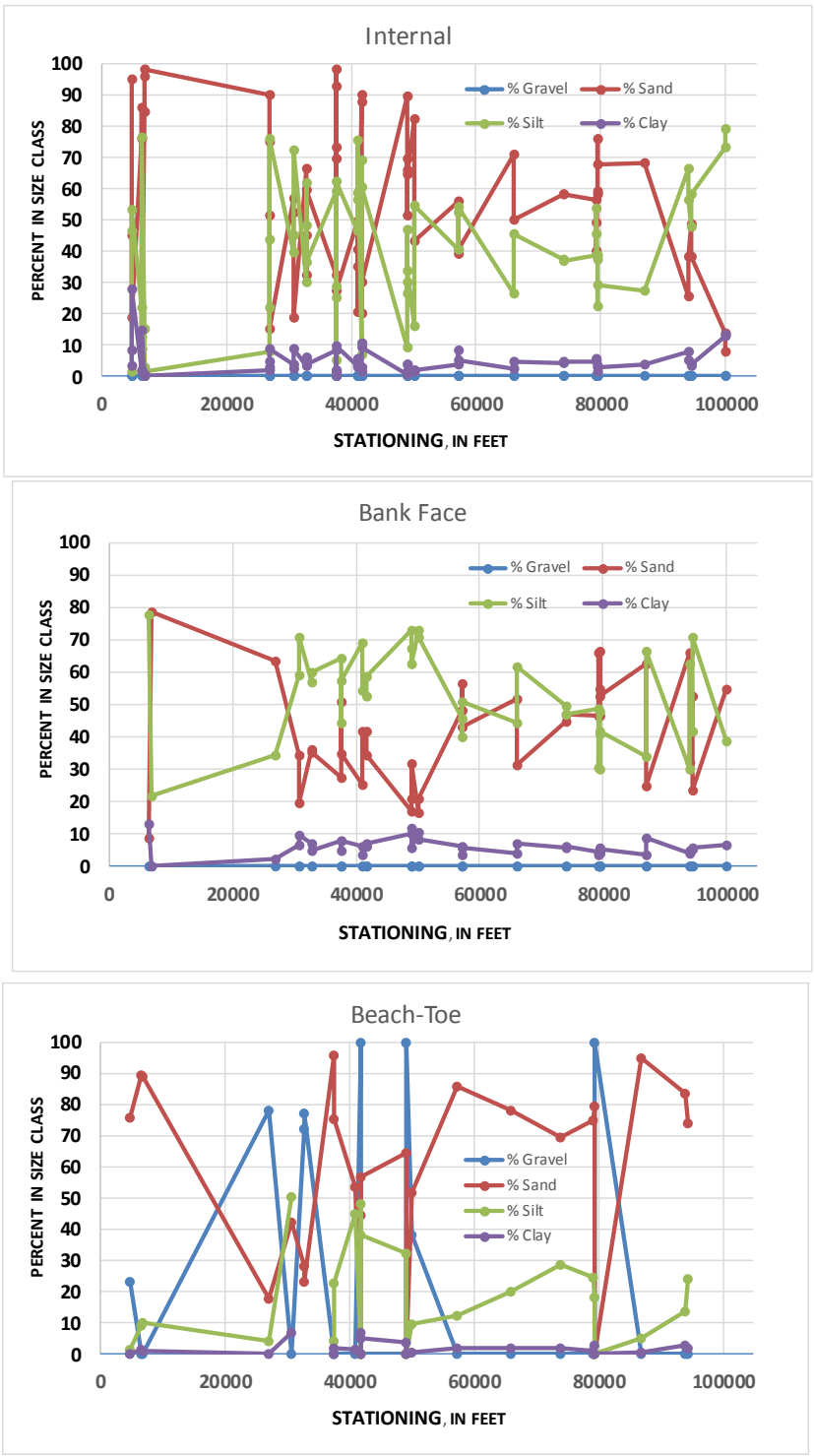

Figure 4.2.6.3-3: Longitudinal Distribution of Bank-material Composition for the Three Types of Sampling Locations – Internal (Top), Bank face (Middle), and Beach-Toe (Bottom)

4.2.6.4 Bulk Density of *In Situ* Bank Sediments

Bulk density is one of the required parameters within BSTEM to calculate both the driving and resisting forces responsible for bank stability. As such, a 2-inch by 2-inch diameter core was extracted from each borehole at the depth of geotechnical testing with the BST. Bulk density tends not to be highly variable, particularly in alluvial settings.

A total of 57 bulk-density samples were obtained at the study sites (Table 4.2.6.4-1). The median value under ambient conditions was 91.9 lbs/ft^3 (1.47 g/cm^3). Table 4.2.6.4-1 also shows values for dry bulk density and moisture content (at the time of testing) with the latter in the range of 8-18% range for most samples. Values of bulk density are adjusted within BSTEM as the water table raises and falls during a simulation.

Table 4.2.6.4-1: Summary of Bulk Density Data Collected at Sites in the Turners Falls Impoundment

Site	Location	Test #	Depth	Dry Bulk Density		Ambient Bulk Density		Ambient moisture content
			(ft)	g/cm^3	lbs/ft^3	g/cm^3	lbs/ft^3	(%)
10L	Left Bank	BST-2	2.6	1.27	79.2	1.55	97.1	18.4
10L	Left Bank	BST-1	3.9	1.29	80.7	1.40	87.6	7.9
10L	Left Bank	BST-3	8.2	1.26	78.7	1.46	91.0	13.5
10R	Right Bank	BST-1	2.6	1.39	86.8	1.66	103.9	16.4
10R	Right Bank	BST-2	4.9	1.33	82.9	1.58	98.4	15.8
119BL	Left Bank	BST-1	2.0	1.49	93.1	1.83	114.1	18.4
119BL	Left Bank	BST-2	3.3	1.22	76.2	1.36	85.1	10.5
119BL	Left Bank	BST-5	4.9	1.31	81.7	1.52	94.8	13.9
119BL	Left Bank	BST-4	9.8	1.36	84.6	1.64	102.5	17.5
11L	Left Bank	BST-1	5.6	1.21	75.7	1.58	98.4	23.1
11L	Left Bank	BST-2	8.9	1.22	76.2	1.55	96.6	21.1
12BL	Left Bank	BST-1	3.3	1.39	87.0	1.47	91.9	5.3
12BL	Left Bank	BST-4	3.3	1.38	86.2	1.44	90.1	4.3
12BL	Left Bank	BST-1	5.6	1.40	87.2	1.47	91.5	4.7
18L	Left Bank	BST-1	2.3	1.32	82.7	1.43	89.4	7.5
21L	Left Bank	BST-3	3.3	1.28	80.1	1.47	92.0	12.9
21L	Left Bank	BST-1	3.6	1.17	73.1	1.45	90.6	19.3
21L	Left Bank	BST-2	9.5	1.33	82.9	1.67	104.4	20.6
26R	Right Bank	BST-1	3.3	1.22	76.3	1.41	88.2	13.5
26R	Right Bank	BST-2	7.2	1.66	103.7	1.75	109.1	5.0
29R	Right Bank	BST-1	4.6	1.39	86.8	1.62	101.4	14.3
29R	Right Bank	BST-2	9.8	1.33	82.9	1.47	91.9	9.7
2L	Left Bank	BST-1	3.3	1.26	78.5	1.44	90.1	12.8

Site	Location	Test #	Depth	Dry Bulk Density		Ambient Bulk Density		Ambient moisture content
			(ft)	g/cm^3	lbs/ft^3	g/cm^3	lbs/ft^3	(%)
2L	Left Bank	BST-2	4.9	1.31	81.9	1.48	92.5	11.5
303BL	Left Bank	BST-1	3.6	1.22	75.9	1.41	88.2	13.9
303BL	Left Bank	BST-2	4.9	1.28	80.1	1.44	89.7	10.6
3L	Left Bank	BST-1	3.6	1.17	73.3	1.33	83.3	12.0
3L	Left Bank	BST-2	5.2	1.34	83.8	1.57	98.3	14.8
3R	Right Bank	BST-2	4.9	1.31	81.9	1.44	89.6	8.6
3R	Right Bank	BST-1	5.2	1.38	86.3	1.55	97.0	11.0
4L	Left Bank	BST-1	3.3	1.19	74.1	1.42	88.9	16.6
4L	Left Bank	BST-2	4.9	1.22	76.0	1.39	86.8	12.5
5CR	Right Bank	BST-1	3.9	1.10	68.9	1.24	77.1	10.7
5CR	Right Bank	BST-3	4.9	1.25	77.7	1.54	96.2	19.2
5CR	Right Bank	BST-2	7.5	1.34	83.9	1.66	103.7	19.1
6AL	Left Bank	BST-1	2.3	1.80	112.2	1.92	119.7	6.2
6AL	Left Bank	BST-2	4.6	1.43	89.5	1.56	97.7	8.4
6AR	Right Bank	BST-1	4.9	1.20	75.0	1.54	95.9	21.8
6AR	Right Bank	BST-2	Low bank	1.25	77.9	1.68	104.9	25.8
75BL	Left Bank	BST-2	2.3	1.39	86.6	1.44	89.6	3.3
75BL	Left Bank	BST-2	3.3	1.22	76.1	1.38	85.9	11.4
75BL	Left Bank	BST-1	4.3	1.31	82.0	1.60	99.9	17.9
7L	Left Bank	BST-1	5.2	1.38	86.0	1.45	90.6	5.1
7L	Left Bank	BST-2	9.8	1.34	83.5	1.46	91.4	8.7
7R	Right Bank	BST-1	4.9	1.41	87.9	1.46	91.1	3.5
7R	Right Bank	BST-2	9.2	1.61	100.7	1.67	104.3	3.4
87BL	Left Bank	BST-2	3.0	1.15	71.8	1.46	91.4	21.4
87BL	Left Bank	BST-1	5.0	1.24	77.2	1.34	83.6	7.7
87BL	Left Bank	BST-3	9.8	1.25	77.8	1.35	84.5	8.0
8BL	Left Bank	BST-1	5.2	1.09	67.9	1.20	74.7	9.1
8BR	Right Bank	BST-1	4.9	1.39	86.5	1.62	101.1	14.5
8BR	Right Bank	BST-2	10.2	1.35	84.4	1.52	94.7	10.9
9R	Right Bank	BST-2	1.3	1.37	85.3	1.79	111.9	23.8
9R	Right Bank	BST-1	3.9	1.51	94.1	1.56	97.2	3.2
9R	Right Bank	BST-3	4.6	1.35	84.0	1.46	91.0	7.7

Site	Location	Test #	Depth	Dry Bulk Density		Ambient Bulk Density		Ambient moisture content
			(ft)	g/cm^3	lbs/ft^3	g/cm^3	lbs/ft^3	(%)
BC-1R	Right Bank	TOB	1.0	1.32	82.6	1.38	86.1	4.1
BC-1R	Right bank	BST-2	1.6	1.25	78.3	1.58	98.4	20.5
75th Percentile				**1.38**	**86.21**	**1.58**	**98.40**	**17.5**
Median				**1.31**	**82.02**	**1.47**	**91.92**	**12.0**
25thPercentile				**1.24**	**77.23**	**1.44**	**89.60**	**7.9**

4.2.6.5 Geotechnical Parameters: Effective Cohesion and Friction Angle

Geotechnical data (cohesion and friction angle) obtained *in situ* with the BST are the fundamental measures of bank strength used to simulate and predict bank stability under a range of moisture conditions. Results of the 61 BST tests show that the cohesive strengths of banks along the TFI are quite variable but generally low (Table 4.2.6.5-1). Average values of effective cohesion and friction angle are 5.2 kPa and 30.5º, respectively. A more reliable measure of the central tendency of the distributions is the median values because outliers have less of an affect. As such, the median values for c' and ϕ' are 1.9 kPa and 31.6º, respectively, indicating that many banks are generally without much cohesive strength. Given the lack of clay-sized materials, this was expected. The frequency distribution for effective cohesion (Figure 4.2.6.5-1) shows that about 30% of the tests were in cohesionless materials while 35% were < 0.5 kPa and 50% were < 2.0kPa. Materials with greater cohesive strengths are evenly distributed across the range. Less than 20% of the tested materials had cohesive strengths greater than 10 kPa. Friction angles show the typical narrow range of values with the central 50% of the distribution ranging from 29.2 to 33.3º (Figure 4.2.6.5-1; Bottom).

The longitudinal distribution of average, effective-cohesion (c') values along the TFI also shows considerable variability (Figure 4.2.6.5-2). Average values are often not a good index of the strength of the bank as these values could be made up of different layers of widely varying strengths. They are shown here along with the individual test results to provide a visual presentation of the range of values over the study reach. Even at sites with some cohesive layers, there are often materials of low to zero cohesion making up the remainder of the bank. A notable exception is site BC-1R at station 4,900 where the tested bank materials displayed significant cohesive strengths.

Table 4.2.6.5-1: Summary of Geotechnical Data Collected in 2014 with the Borehole Shear Tester and a Digital Tensiometer for Sites along the Turners Falls Impoundment

Site	Station (feet)	Test #	Location	Depth	c_a	Suction	c'	ϕ'
				(m)	(kPa)	(kPa)	(kPa)	(degrees)
2L	94700	1	L	1.0	18.3	7.5	**5.4**	**21.8**
2L	94700	2	L	1.6	4.6	17.2	**1.6**	**33.7**
3L	79600	1	L	1.1	20.1	13.6	**17.7**	**26.0**
3L	79600	2	L	1.6	2.3	15.1	**0.0**	**34.4**
3R	79600	1	R	1.6	3.8	9.9	**2.1**	**31.0**
3R	79600	2	R	1.5	3.7	11.1	**1.7**	**30.9**
4L	74000	2	L	1.2	0.0	19.1	**0.0**	**32.3**
4L	74000	combined	L	1.5	0.0	19.1	**0.0**	**33.2**
5CR	57300	1	R	1.5	9.6	21.5	**5.9**	**32.4**
5CR	57300	2	R	1.2	6.3	19.8	**2.9**	**31.0**
5CR	57300	3	R	2.8	6.7	14.1	**4.2**	**31.4**
6AR	41800	1	R	1.2	9.0	27.0	**4.3**	**33.7**
6AR	41800	2	R	0.6	12.2	35.0	**6.1**	**29.5**
6AR	41800	3	R	1.1	4.7	27.0	**0.0**	**32.9**
6AR	41800	5	R	2.9	4.5	50.0	**0.0**	**33.7**
6L	41800	1	L	0.6	10.1	50.0	**8.0**	**29.5**
6L	41800	2	L	1.0	0.4	70.0	**0.0**	**33.2**
7L	37600	1	L	1.6	20.1	25.1	**15.7**	**26.6**
7L	37600	2	L	3.0	0.0	21.0	**0.0**	**35.3**
7R	37600	1	R	1.5	0.0	6.3	**0.0**	**29.7**
7R	37600	2	R	2.8	2.5	4.8	**1.7**	**29.0**
7R	37600	5	R	3.8	6.5	5.0	**5.6**	**31.3**
8BL	32800	1	L	1.6	0.0	19.5	**0.0**	**33.2**
8BR	32800	1	R	1.0	8.7	15.0	**6.1**	**28.1**
8BR	32800	2	R	2.0	7.0	22.0	**3.2**	**33.7**
8BR	32800	3	R	2.8	16.2	16.2	**12.7**	**20.0**
9R	65100	2	R	0.4	15.6	5.1	**14.7**	**28.2**
9R	65100	3	R	1.5	1.3	9.4	**0.0**	**33.1**
10L	49100	1	L	1.2	1.5	9.6	**0.0**	**30.3**
10L	49100	2	L	0.8	0.0	10.6	**0.0**	**33.4**
10L	49100	3	L	2.5	2.8	11.6	**0.8**	**33.3**

Site	Station (feet)	Test #	Location	Depth	c_a	Suction	c'	ϕ'
				(m)	(kPa)	(kPa)	(kPa)	(degrees)
10R	49100	1	R	0.8	15.6	1.8	**15.0**	**25.6**
10R	49100	2	R	1.5	3.3	12.4	**1.2**	**31.0**
11L	100000	1	L	1.0	2.1	10.0	**0.4**	**33.2**
11L	100000	3	L	0.9	3.2	19.0	**0.0**	**31.8**
12BL	6700	2	L	1.0	5.6	4.9	**4.7**	**31.4**
12BL	6700	3	L	1.5	7.7	13.8	**5.3**	**29.2**
12BL	6700	4	L	1.0	5.0	2.9	**4.5**	**25.4**
18L	87000	1	L	0.9	2.0	16.7	**0.0**	**31.0**
21R	79100	1	R	1.1	25.0	23.4	**20.9**	**19.8**
21R	79100	2	R	2.9	3.7	8.7	**2.2**	**32.8**
21R	79100	3	R	1.0	21.5	17.7	**18.4**	**24.2**
21R	79100	4	R	1.0	5.9	23.4	**1.8**	**31.6**
26R	49800	1	R	1.0	0.0	14.8	**0.0**	**31.3**
26R	49800	2	R	2.2	5.6	7.0	**4.4**	**35.4**
26R	49800	3	R	0.9	0.5	14.8	**0.0**	**31.4**
29R	66000	1	R	1.4	11.9	16.1	**9.1**	**31.8**
29R	66000	2	R	3.0	0.0	14.3	**0.0**	**34.1**
75BL	27000	1	L	1.3	0.3	6.4	**0.0**	**33.8**
75BL	27000	4	L	1.0	8.6	38.1	**1.9**	**36.7**
87BL	30700	1	L	1.6	18.7	25.7	**14.2**	**27.3**
87BL	30700	2	L	0.9	13.1	20.9	**9.5**	**32.3**
87BL	30700	3	L	3.0	21.5	19.1	**18.2**	**27.7**
87BL	30700	4	L	0.8	4.7	20.9	**1.1**	**33.9**
119BL	40600	2	L	1.0	5.6	34.9	**0.0**	**35.3**
119BL	40600	4	L	3.0	5.0	12.9	**2.8**	**33.0**
119BL	40600	5	L	1.5	3.1	30.2	**0.0**	**36.2**
303L	94000	1	L	1.1	9.0	41.7	**1.7**	**32.8**
303L	94000	2	L	1.5	2.7	22.8	**0.0**	**36.2**
BC-1R	4900	1	R	0.8	30.0	7.9	**28.6**	**11.3**
BC-1R	4900	2	R	0.5	34.0	7.9	**32.6**	**16.7**

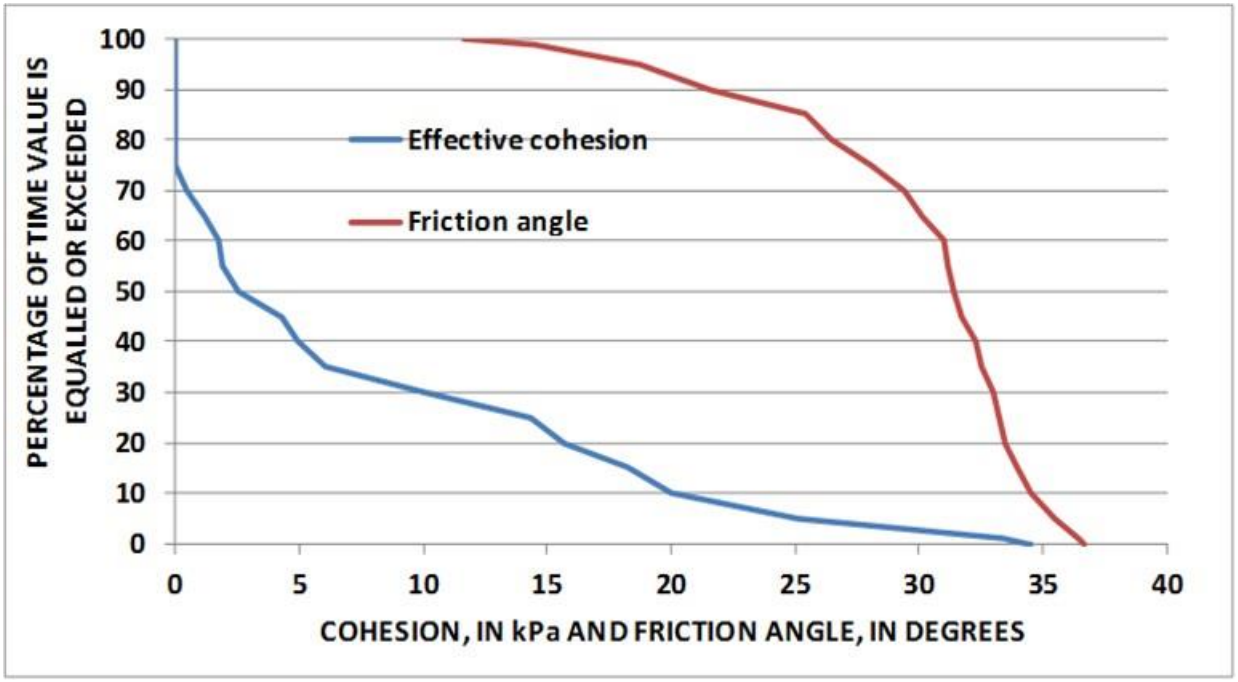

Figure 4.2.6.5-1: Frequency Distribution of Effective Cohesion and Friction Angle for the 60 Geotechnical Tests taken with the BST at the 25 Study Sites along the TFI

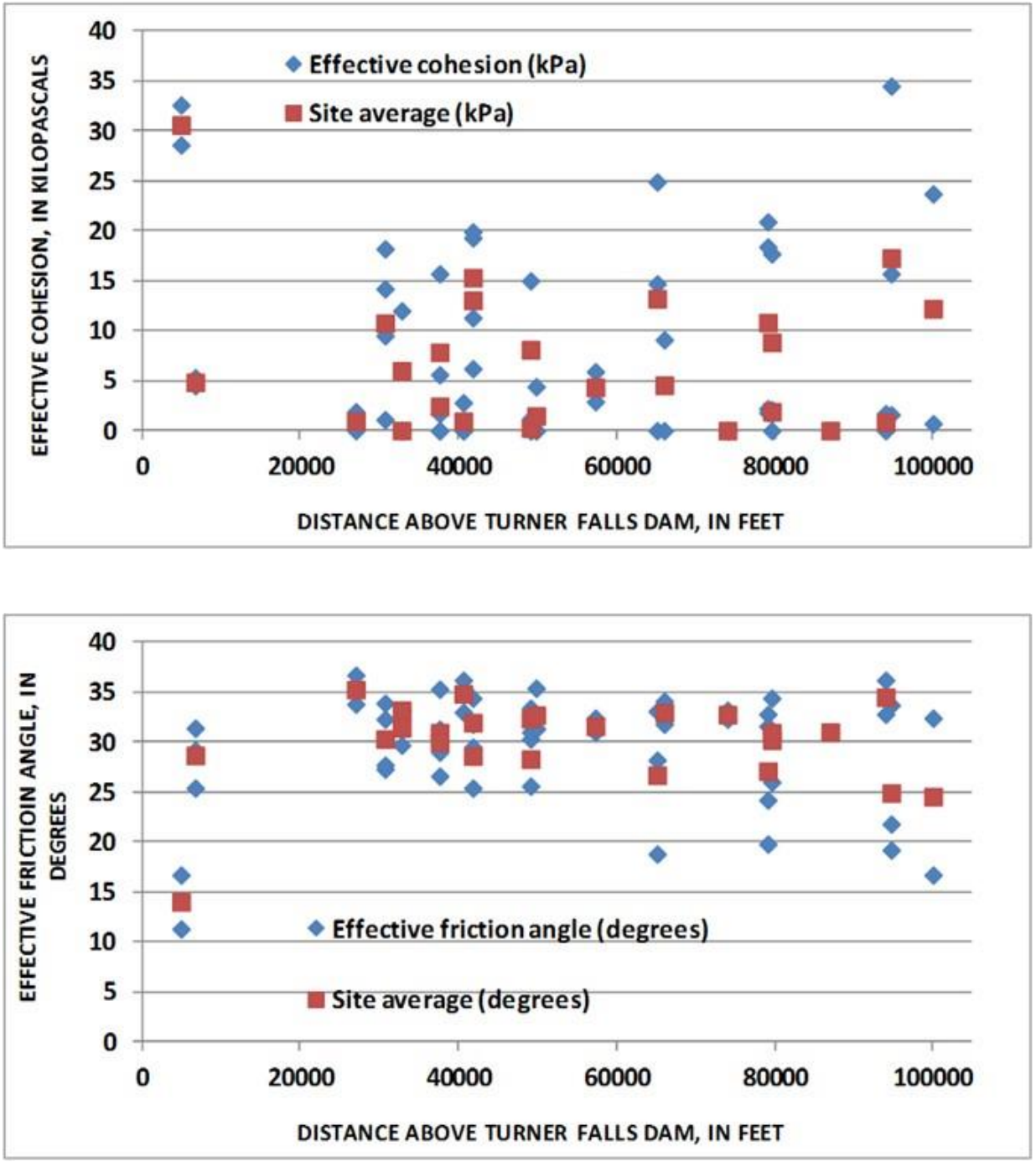

Figure 4.2.6.5-2: Effective Cohesion (Top) and Friction Angle (Bottom) for Sites along the TFI

4.2.6.6 Hydraulic Resistance: Critical Shear Stress and Erodibility

The susceptibility of surficial-bank and bank-toe materials to erosion by hydraulic forces is important to modeling and predicting bank-erosion rates because it is the hydraulic processes (during peak flows and/or from wave action) that can cause undercutting of the bank making it more susceptible to collapse. Results from *in situ* testing with the submerged jet test device and by conducting particle counts of cohesionless sediment show relatively erodible sediment.

Jet tests were carried out at 23 of the 25 sites. Results of these 71 tests are shown in Table 4.2.6.6-1. The exceptions were site BC-1R where a dense matting of moss and roots prevented successful tests, and at 12BL where the surficial materials were composed of sand and could be characterized by bulk particle size. Values of critical shear stress for surficial materials at these two sites were determined from calculations using the Shields criteria and the median particle diameter (d_{50}) as the representative size. Recall that hydraulic resistance of other, larger cohesionless materials was also determined this way based on particle-count data.

Using the rule of thumb that the hydraulic resistance of surficial sediments measured in Pa is generally equivalent to the resistance of cohesionless materials in mm, we can state that in general, the resistance of the surficial materials in the reach is representative of sand-sized materials. The inter-quartile range of critical shear stresses range from about 0.14 Pa to about 2.3 Pa with a median value of 0.54 Pa (Table 4.2.6.6-2). More resistant materials were tested at several sites. Only 5% of the tests had materials with critical shear-stress values greater than 12.2 Pa; 1% with values greater than 18.3 Pa. Some beach/toe locations that contain placed rock such as sites 3R, 6AL, and 10R have the greatest critical shear stresses because of the size and weight of the clasts at these three sites (d_{50} ranges from 55.0 mm to 57.5 mm). The full distribution of jet test values can be seen in Table 4.2.6.6-2 as well as in Figure 4.2.6.6-1. Values of the erodibility coefficient (k) were calculated from the equation published by Hanson and Simon, (Hanson & Simon, 2001):

$$k = 0.2\ \tau_c^{-0.5} \qquad (1)$$

where τ_c = critical shear stress, in Pa; and k = erodibility coefficient, in $cm^3/N\text{-}s$.

Their frequency distribution is shown in Figure 4.2.6.6-2. The spatial variation in critical shear stress for individual tests and for site medians are shown in Figure 4.2.6.6-3.

Table 4.2.6.6-1: Jet Test Data for Bank Materials of the Turners Falls Impoundment

Site	Test	τ_c (Pa)	Median τ_c (Pa)	Calculated *k* Cm^3/N-s)	Location
2L	1	12.0	0.137	0.58	BF
2L	2	0.271		0.384	BF
2L	3	0.0022		4.23	BF
2L	4	0.0003		11.7	BF
3L	1	2.73	0.777	0.121	BF
3L	2	0.777		0.227	BF
3L	4	0.328		0.349	BF
3R	1	0.261	0.639	0.391	BF
3R	3	0.639		0.250	BF
3R	4	0.685		0.242	BF
4L	1	0.0511	0.106	0.885	BF
4L	2	0.200		0.447	BF
4L	3	0.16		0.500	BF
4L	4	0.0051		2.80	BF
5CR	1	1.03	1.03	0.197	BF
5CR	6	0.66		0.246	BF
5CR	7	1.08		0.192	BF
6AL	2	2.900	0.64	0.117	BT
6AL	3	0.236		0.412	BF
6AL	4	0.640		0.250	BF
6AR	1	0.428	0.475	0.306	BF
6AR	6	0.475		0.290	BF
6AR	3	0.669		0.245	BT
7L	1	1.17	0.748	0.185	BF
7L	2	0.326		0.350	BF
7R	1	0.54	7.14	0.272	BT
7R	2	2.37		0.130	BT
7R	3	11.9		0.058	BF
7R	4	17.4		0.048	BF
8BL	1	2.77	3.33	0.120	BF
8BL	2	3.88		0.102	BF
8BR	1	0.336	0.627	0.345	BT
8BR	2	0.918		0.209	BT
9R	1	20.5	10.3	0.044	BF
9R	2	0.0003		11.5	BF
10L	1	0.190	0.585	0.459	BF
10L	2	0.629		0.252	BF
10L	3	0.541		0.272	BF
10L	4	2.23		0.134	BF
10R	1	0.836	3.47	0.219	BF
10R	2	6.1		0.081	BF
11L	1	8.29	2.91	0.069	BT
11L	2	0.181		0.470	BT
11L	3	2.91		0.117	BF
18L	1	3.27	3.27	0.111	BT
18L	2	17.2		0.048	BT
18L	4	2.13		0.137	BF
75BL	2	6.71	3.41	0.077	BF
75BL	3	0.11		0.603	BF

Site	Test	τ_c (Pa)	Median τ_c (Pa)	Calculated *k* $Cm^3/N\text{-}s$	Location
87BL	1	0.0514	0.082	0.882	BF
87BL	2	0.0917		0.660	BF
87BL	3	0.314		0.357	BF
87BL	4	0.0726		0.742	BF
21R	1	0.00164	0.1945	4.94	BF
21R	2	0.177		0.475	BF
21R	3	1.7		0.153	BF
21R	4	0.212		0.434	BF
26R	1	0.00158	0.024	5.03	BF
26R	3	0.0243		1.28	BF
26R	4	0.0302		1.15	BF
29R	1	2.94	1.51	0.117	BF
29R	2	1.47		0.165	BF
29R	3	0.0795		0.709	BF
29R	4	1.549		0.161	BF
119BL	1	0.00081	0.0025	7.03	BF
119BL	3	0.00246		4.03	BF
119BL	4	0.1015		0.628	BF
303BL	1	4.78	2.49	0.091	BT
303BL	2	12.3		0.057	BT
303BL	3	0.0708		0.752	BF
303BL	4	0.205		0.442	BF

Table 4.2.6.6-2: Frequency Distribution for the 71 Jet Tests Conducted Along the Turners Falls Impoundment

Percentile	Critical shear stress: τ_c		Calculated *k*
	(Pa)	(lbs/ft^2)	(**cm^3/N-s**)
99.99	205	0.43	11.74
99.9	203	0.42	11.73
99	18.3	0.38	11.6
95	12.2	0.254	4.99
90	6.71	0.140	2.80
85	3.58	0.0747	0.883
80	2.90	0.0606	0.709
75	2.30	0.0480	0.552
70	1.55	0.0324	0.459
65	1.06	0.0220	0.423
60	0.777	0.0162	0.357
55	0.650	0.0136	0.325
50	0.541	0.0113	0.272
45	0.382	0.0080	0.248
40	0.314	0.0066	0.227
35	0.224	0.0047	0.195
30	0.190	0.0040	0.161
25	0.135	0.0028	0.132
20	0.0795	0.0017	0.117
15	0.0513	0.0011	0.106
10	0.0051	0.0001	0.077
5	0.0016	0.00003	0.057
1	0.00030	0.00001	0.047
0.1	0.00029	0.00001	0.0444
0.01	0.0029	0.00001	0.0442

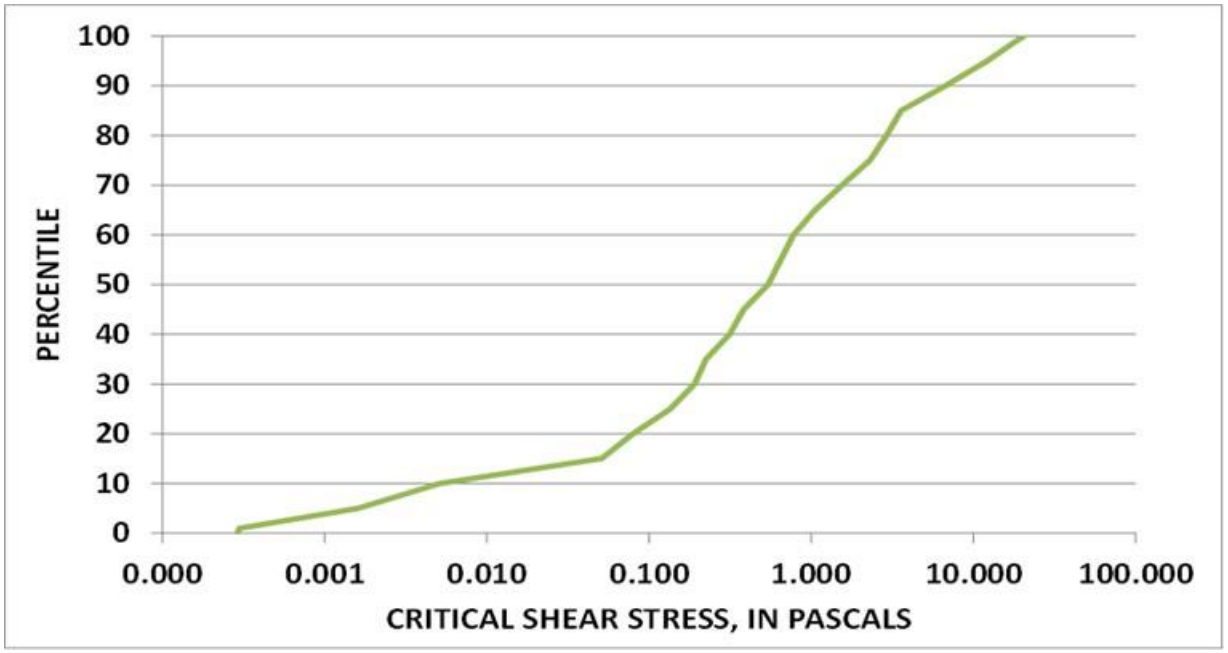

Figure 4.2.6.6-1: Plot of Frequency Distribution of Critical Shear Stress (t_c) from the 71 Jet Tests Conducted along the TFI

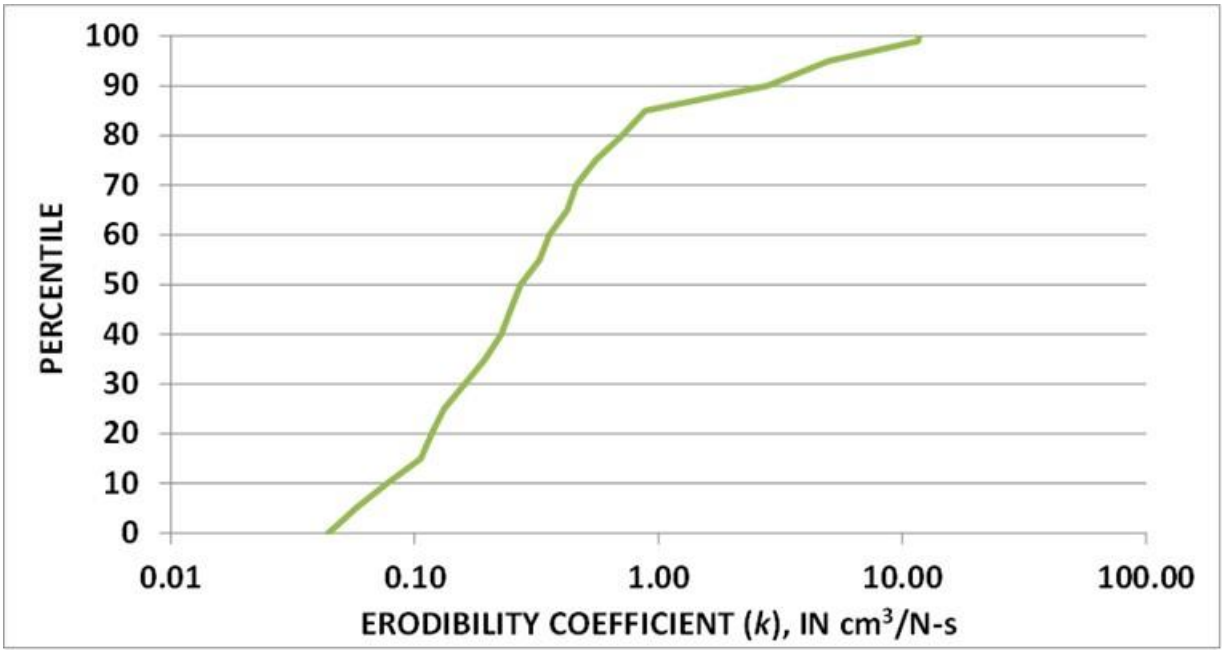

Figure 4.2.6.6-2: Plot of Frequency Distribution of the Erodibility Coefficient (k) for the 71 Jet Tests Conducted along the TFI

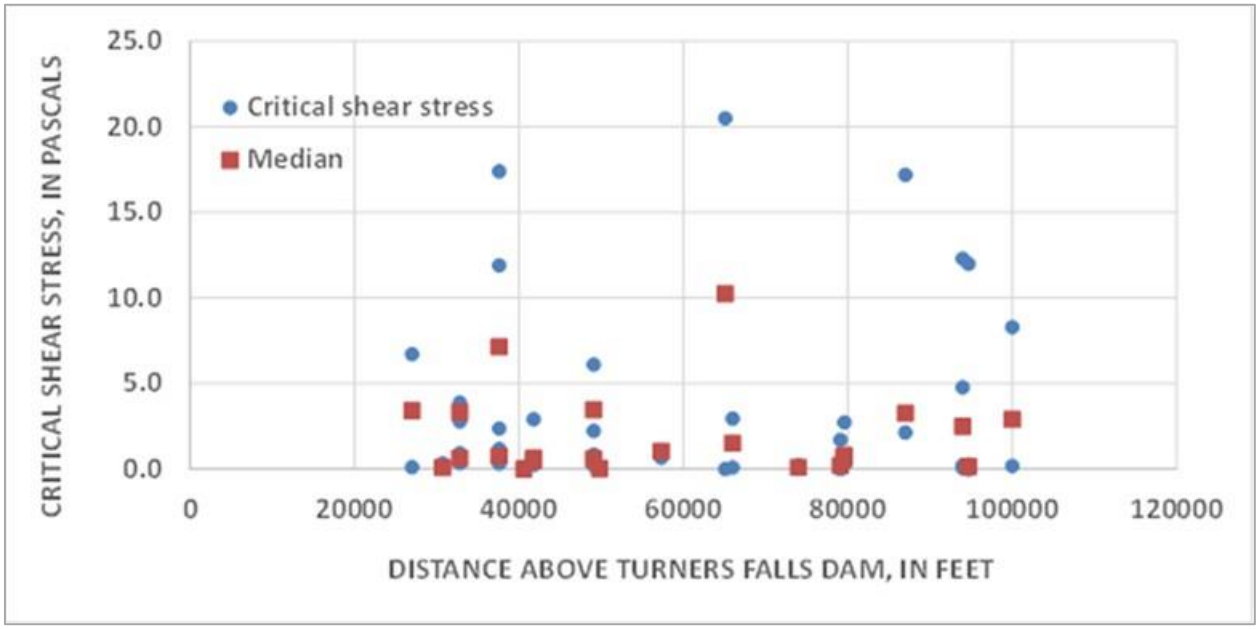

Figure 4.2.6.6-3: Longitudinal Distribution of Measured Critical Shear Stress of Surficial Bank Materials at the Study Sites

4.2.7 Methodology for Quantifying Root-Reinforcement

Vegetation has a number of effects on the geotechnical and hydraulic processes occurring within and at channel margins. Of particular importance is the reinforcement that can be provided to a bank by the roots growing within it. This reinforcement of soil by roots is akin to the reinforcement of concrete by rebar; the soil matrix is strong in compression, and the roots are strong in tension. The combination of the two materials provides a reinforced matrix, the strength of which can be quantified through knowledge of the soil strength alone, and the number, diameters, and tensile strengths of the roots present within the banks. Therefore, to quantify root-reinforcement in the context of bank stability two types of data collection are necessary: 1) root tensile strength data (which varies by species), and 2) the rooting density with associated root diameter distributions at varying depths throughout the banks (which is species and site specific), also known as the root architecture. The latter is obtained through a combination of root mapping of representative species in the reach and applied to specific sites with data on canopy cover of species assemblages.

BSTEM contains a root-reinforcement algorithm, RipRoot that currently contains a database of 25 species, for which root tensile strength and root architecture have previously been collected. The data collection has focused largely on Southeastern, and Western USA riparian species. As part of this study, five species commonly found along the study reach were investigated, to be added to the RipRoot database, and used in BSTEM model simulations of the TFI.

Collection and analysis of root architecture data is time consuming and laborious. To be efficient with this data collection, root architecture data was collected for a range of tree ages for each of the species, and the average distribution of root densities and diameters was calculated for the range of ages. Plant assemblage data (percent cover, species and age) was recorded at each of the BSTEM modeling sites, so that these average root-architecture parameters and species specific root tensile-strength relations could be applied to give a specific root-reinforcement value at each BSTEM modeling site.

4.2.7.1 Testing for Tensile Strength

The five species selected for study along the TFI were: Red oak, Silver maple, American elm, Green ash and Basswood. These species were selected through consultation with the FirstLight study team and were selected because of their dominance throughout the TFI. Root tensile strength measurements for each of the five species were collected at exposed bank faces using a root-puller device (Figure 4.2.7.1-1). This device is comprised of a metal frame and winch, connected to a load cell. Each root was winched until it broke and the peak load before breaking recorded, along with the root diameter at the breaking point, so that each root's tensile strength could be calculated.

For each species at least 48 roots of various diameters (ranging from 0.5 mm to 5 mm) were tested, to allow for the development of species-specific tensile strength–diameter relations that can be used in the RipRoot model, and associated BSTEM simulations. 30 roots is the minimum number of roots necessary to develop a relation where statistics do not have to be adjusted for a low number of trials. Where possible, more roots were tested to strengthen the confidence in the relationship. Roots larger than 5mm were not tested since the tensile strength-diameter relation for roots is a power function that flattens out around this threshold. For each species, locations were selected where exposed roots were visible, attached to living trees, and easily identifiable as being from a tree of known species. The number of trees tested for each species varied according to the number of roots available at the sites located, and the range of root diameters present. The GPS locations and the number of trees and roots tested for each species are shown in Table 4.2.7.1-1.

Table 4.2.7.1-1: List of GPS Locations for Root Tensile Strength Testing and the Number of Trees Tested

	GPS locations			Number of trees tested	Total number of roots tested
Green ash	N 42.69222	N42.69222	-	3	56
	W 72.47222	W72.47222	-		
Red oak	N42.62244	N42.67754	-	2	48
	W72.48399	W72.46957	-		
Silver maple	N42.72319	-	-	15	59
	W72.45639	-	-		
American elm	N42.62756	N42.70070	N42.69539	4	77
	W72.48412	W72.46786	W72.47020		
Basswood	N42.677931	-	-	6	48
	W72.469924	-	-		

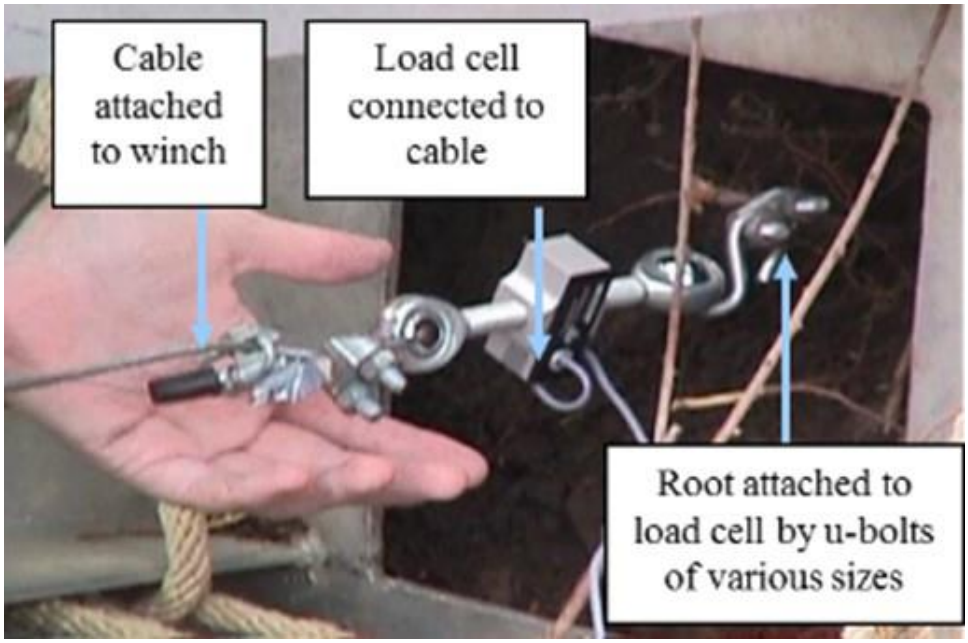

Figure 4.2.7.1-1: Photo Showing a Close-up of the Way that the Load Cell and Roots/Rhizomes are Connected to the Winching Cable of the Root-puller

4.2.7.2 Measurements of Root Densities and Root Diameter Distributions

The RipRoot model also requires knowledge of typical rooting densities, and root diameter distributions throughout the bank (Figure 4.2.7.2-1). Data were collected in the field to provide the typical ranges of these parameters for each of the five selected species so that the RipRoot and BSTEM models can accurately account for vegetation under existing conditions. For each of the five species under investigation, trees of various ages growing at the bank edge were selected. Trees sampled ranged in age from approximately 8 years to over 100 years (sample sizes and ages are shown in Table 4.2.7.2-1). The age of each tree was estimated by developing a diameter at breast height (DBH) to age relation for each species, from tree-ring cores taken in the field. Once a relation had been established for each species, only a DBH measurement was required to estimate the age of subsequent trees.

The collection of root architecture data is laborious. To collect the most data as possible in an efficient manner, a combination of field and photo analysis techniques were used to quantify root density and root diameter distributions. Initially, several trees were measured using both techniques, to verify the number of roots counted using each method, and test that the photo analysis method provided comparable results to the field method. To measure root architecture in the field, a 0.5m x 0.5m grid, marked off into 0.1m x 0.1m squares was attached to the bank face over the exposed roots of each study tree (Figure 4.2.7.2-2). A digital caliper was used to measure the number and diameter of roots in each square and the results recorded so that lateral and vertical patterns and extent could be determined.

In addition, each tree and its roots were photographed using a high resolution camera. In each image a tape measure was made visible, so that each photo could be calibrated with the imaging software SigmaScan. In addition, five roots in each photograph were measured in the field, and then measured in the photo using the image-analysis software to check the calibration for each image. Once the field data and photo-analysis data had been compared in detail for 3 trees, the field crews switched to just taking the digital photos of each tree to be sampled, thus allowing for faster field-data collection, and a larger sample size in the time available. To analyze each image, the field photos were merged so that one image existed for each tree to be investigated (e.g. Figure 4.2.7.2-3).

Next, the tape measure in each image was used to calibrate the “measure” tool in SigmaScan, and the five flagged roots in each image were measured and compared to the field measurements as a check, before starting detailed image analysis. Once the distance calibration had been confirmed, a 0.1m x 0.1m grid was superimposed onto the image (Figure 4.2.7.2-4), and the area of the image to be studied was isolated.

Then, just as was done in the field, the number and diameters of roots in each cell was recorded. The SigmaScan software puts each root measurement into a spreadsheet automatically, which makes this process easier than measuring and recording in the field, and having to enter this data manually later. In both methods, each root is only counted once, at the location where it first emerges from the bank. Thus, a root that is hanging down the face of the bank is not counted in every cell it can be seen in. This is because the object is to quantify the number of roots cutting across the potential failure plane of the bank, in this case, assumed to be the bank face itself. This makes both field measurement, and analysis of the digital photos time consuming, as it is easy to count roots several times if care is not taken.

Root data for each tree was then analyzed according to the standard root diameter size classes used in the RipRoot Model (<1mm, 1-2mm, 2-3mm, 3-5mm, 5-10mm, 10-20mm, and >20mm). Variations between species were investigated, as well as variations within species, over the age ranges tested.

At three locations, measurements were taken in the field, and were then compared to the results of the digital photo analysis, to insure that the results were within acceptable limits of error. An example of the results of one of these comparisons is presented in Figure 4.2.7.2-5 for an American elm tree. The results of this comparison show that for the smallest root classes (<1mm and 1-2mm), the number of roots identified was slightly higher in the field, but in the 2 to 3mm diameter range and above the photo analysis

method identified more roots. These results make sense in that the finer roots were easier to see up close, in person.

Data collection pertaining to the larger roots can get confusing to count in the field as each should only be counted once, where it emerges from the bank. It can be hard to keep track of this in the field, and due to the proximity to the river it can be hard to physically step back and take a broader view of the root system. Using the photo analysis method each root can be labeled and counted more easily, and the software can be used to zoom in and out as necessary. For the example presented below, the total number of roots counted in the field was 70, and the number of roots counted using the photo analysis method was 79, a difference of 12.9%, but considering the variability in rooting density even between specimens of the same species and age, this is within an acceptable range of variation. The other two comparisons of the two methods showed similar results, in each case with slightly more roots being recorded in the image analysis compared to in the field. This is likely a result that when performing the image analysis it is easier to zoom in and out, to label the roots you've already counted, and to get a better overview of the root system as a whole. The percent difference between the two methods ranged from 8.5% to the example shown here of 12.9%. The use of the photo analysis method allowed for analysis of a much larger dataset for this project than would have been possible using the field method alone.

In total, the root architecture of 33 trees was recorded and measured. The species, ages, and GIS locations of the trees sampled are shown in Table 4.2.7.2-1. Trees ages ranged from 6 years to approximately 100 years, with the distribution of ages sampled varying between species, as per the prevalence and resulting availability of trees to test at the bank edge.

Table 4.2.7.2-1: Summary of Trees Tested for Root Architecture

SPECIES	Number of trees tested	Tree Age from average field growth rates	GPS location	
			N	W
Red oak	6	9	42.62244	-72.48399
		16	42.62775	-72.48412
		35	42.67754	-72.46957
		102	42.62244	-72.48399
		30	42.62046	-72.48283
		59	42.63864	-72.48854
		88	42.7745	-72.49963
Silver maple	7	17	42.69222	-72.47222
		28	42.71873	-72.45532
		31	42.71873	-72.45532
		33	42.71873	-72.45532
		56	42.71873	-72.45532
		58	42.67169	-72.46969
		67	42.64347	-72.47790
American elm	8	6	42.69539	-72.47020
		26	42.62756	-72.48412
		31	42.66364	-72.46963
		57	42.62756	-72.48412
		49	42.7007	-72.46786
		64	42.70476	-72.46219
		71	42.64381	-72.47780
Green ash	6	8	42.69222	-72.47222
		19	42.62756	-72.48412
		23	42.69222	-72.47222
		35	42.6527	-72.46745
		45	42.66467	-72.47023
		53	42.64966	-72.47131
Basswood	6	7	42.67782	-72.46983
		11	42.64624	-72.47168
		13	42.67782	-72.46983
		13	42.64624	-72.47168
		14	42.63525	-72.48743
		15	42.67782	-72.46983
		18	42.63525	-72.48743
		30	42.64437	-72.47628

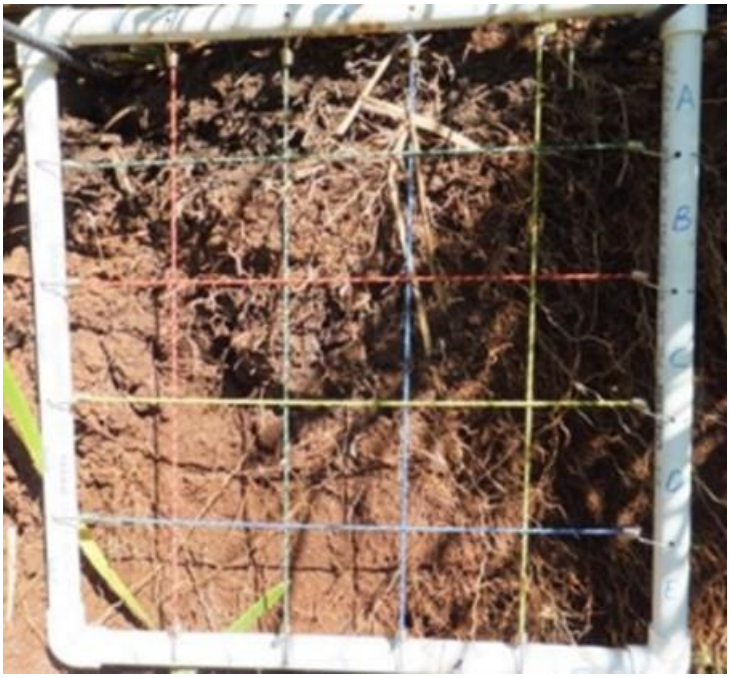

Figure 4.2.7.2-1: Example of Grid Used for Root Diameter and Density Measurements in the Field

Figure 4.2.7.2-2: Merged Image Ready for Analysis in SigmaScan

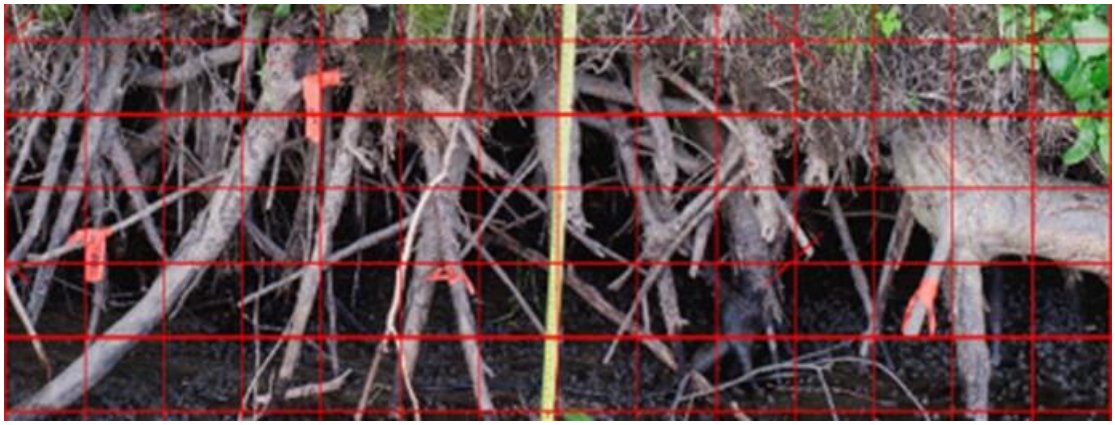

Figure 4.2.7.2-3: Image with 0.1m x 0.1m Grid Superimposed, Ready for Analysis in SigmaScan

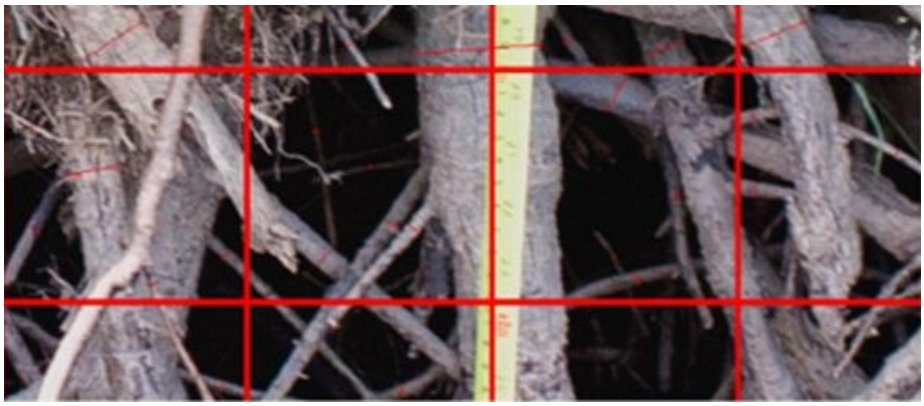

Figure 4.2.7.2-4: Zoomed Image with 0.1m x 0.1m Grid Superimposed, Showing Individual Root Diameter Measurements Made in SigmaScan

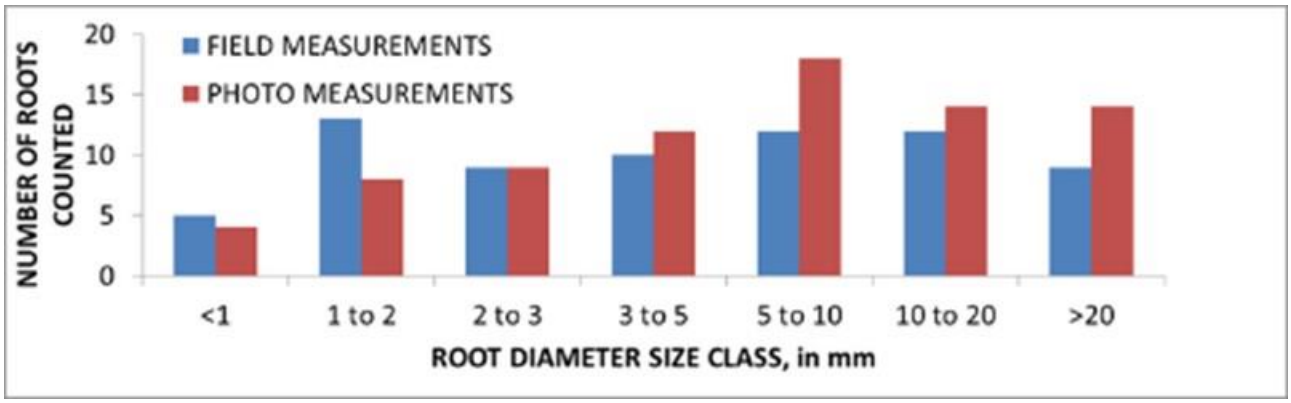

Figure 4.2.7.2-5: Comparison of the Number of Roots Measured for an American Elm Tree – Field vs. Photo Measured

4.2.7.3 Tensile-Strength Relationships

The tensile strength relations for each of the five species are best represented using a non-linear power function that is typical of other species (Simon & Collison, 2002; Pollen-Bankhead & Simon, 2013):

$$T_r = a\, D^{-b} \quad (2)$$

where T_r = root tensile strength in Megapascals (MPa) and D is root diameter, in mm.

The regression parameter a (representing the strength at 1 mm) varied from 28.7 for Red oak to 53.2 for Silver maple. As can be seen from Figure 4.2.7.3-1, however, there is a great deal of overlap between the data sets of the five species, which is a typical finding when comparing data sets between species (Pollen-Bankhead & Simon, 2013). In addition, r^2 values ranged from 0.291 for Silver maple, to 0.613 for American elm, reflecting the natural inherent variability, not only between species, but also within species. The literature around this topic reports that although difference between species does exist, several different factors can add to the scatter in the data. Of these factors, variations in root moisture, and cellulose content (Hales *et al.*, 2009) are the biggest reasons for variations within and between species, as these vary temporally and spatially according to local soils and topography, which are independent of the species tested. The species-specific relations shown below have been added to the BSTEM RipRoot database, so that site specific root-reinforcement values could be calculated for each site modeled with BSTEM.

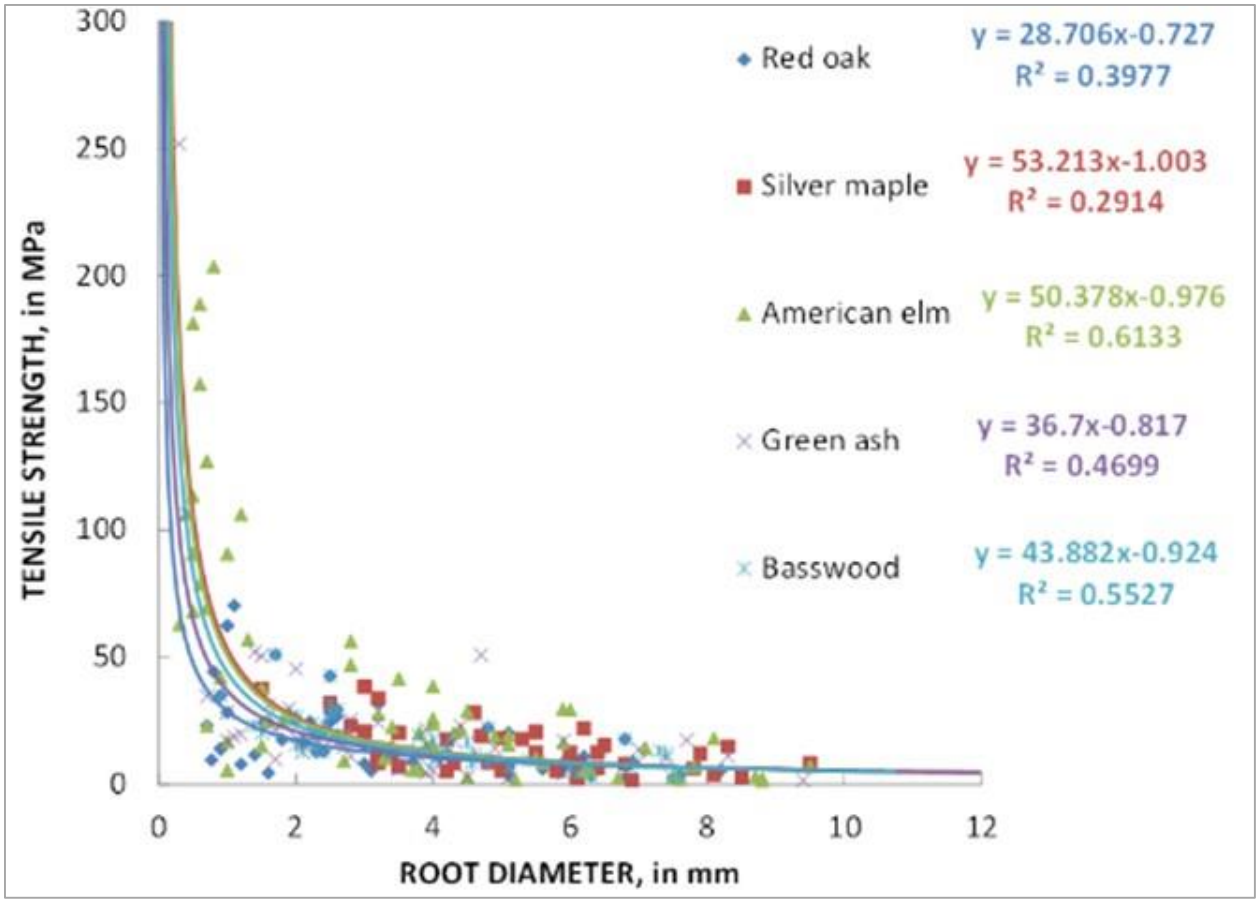

Figure 4.2.7.3-1: Root-diameter Tensile Strength Relations for Each of the Five Species Studied along the TFI

4.2.7.4 Diameter-Age Relations

Diameter–age relations were developed for each species so that the root-architecture data collected here could be applied to each of the 25 modeling sites by simply noting on each field form the dominant species at each site and typical values for DBH. Tree cores were taken for all of the trees sampled for root density and root diameter distribution so that average annual growth rates could be calculated and compared to values found in the literature (Table 4.2.7.4-1). The annual growth rates (mm/y) calculated from the field data matched literature values well, except in the case of Basswood, where the field data suggested a faster annual growth rate than reported in the literature (Burns *et al.*, 1990). The reference cited provides the silvic characteristics of about 200 forest tree species, including the five species from this study. The growth rates reported in this citation are, therefore, based on a broad geographic area encompassing the limits of growth for each species, which could explain the local variation seen here for Basswood trees. The field data suggest that the Basswood trees sampled had the fastest growth rate (13 mm/y) with the other four species ranging from 7-9 mm/y.

Table 4.2.7.4-1: Field Data for Diameter-age Relations and Calculated Average-annual Growth Rates for Each Species based on Field Data and Literature Values

	Diameter (cm)	Rings	Calculated annual growth (mm/y)	Average growth rate from field data (mm/y)	Growth rate reported in literature (mm/y)	
AE1	10	20	5	7	7	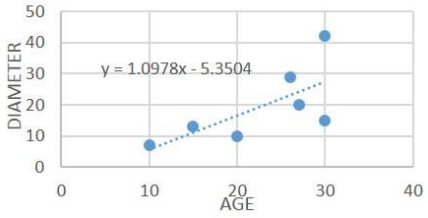
AE2	15	30	5			
AE3	20	27	7			
AE4-1	42	30	Core did not get center			
AE4-2	13	15	9			
AE5	29	26	11			
AE6	7	10	7			
BA1-1	18	-	No core taken	13	4	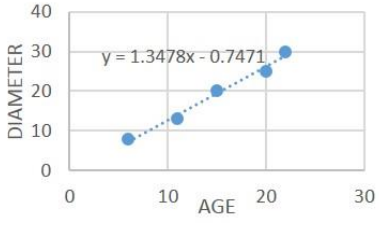
BA1-2	20	15	13			
BA1-3	30	22	14			
BA2-1	13	11	12			
BA2-2	8	6	13			
BA2-3	25	20	13			
GA1	45	41	11	8	7	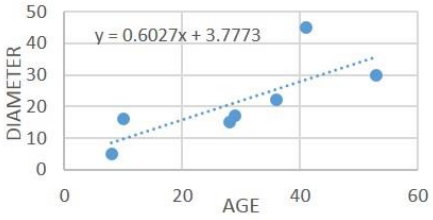
GA2	15	25	5			
GA3	5	8	6			
GA4	17	29	6			
GA5	22	36	6			
GA7	16	10	16			
GA8	30	53	6			
RO-1-1	20	22	9	8	5	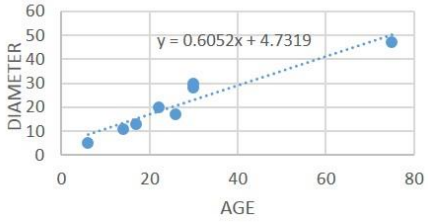
RO-1-2	28	30	9			
RO2	30	30	10			
RO3	11	14	8			
RO4	17	26	7			
RO5	5	6	8			
RO6	47	75	Core did not get center			
RO7	13	17	8			
SIM1-1	11	15	7	9	7 to 25	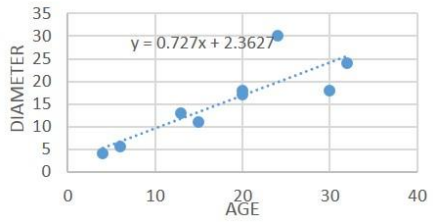
SIM1-2	17	20	9			
SIM1-3	18	30	6			
SIM4-1	30	24	13			
SIM4-2	5.5	6	9			
SIM5-1	13	13	10			
SIM5-2	4	4	10			
SIM6-1	18	20	9			
SIM7	24	32	8			

4.2.7.5 Root-Architecture Data

The root-architecture data collected in the field and processed during the digital photo analysis were collated and summarized by tree age species to look at variations in numbers of roots in each diameter size class. Maximum rooting densities along the TFI recorded as part of this study ranged from 246 roots per m^2 of bank face for Northern red oak to 790 roots per m^2 of bank face for Basswood trees. These densities are within the range of maximum rooting densities for species already coded into RipRoot, which range from 240 roots per m^2 of bank face for Black willow trees to 890 roots per m^2 of bank face for Cottonwood trees.

The data for the five study species show that in terms of the total number of roots present at the bank face there was an increase in rooting density up to the 20-50 year old category for three of the five species studied (Red oak, Silver maple and American elm; Table 4.2.7.5-1). For these three species, trees in the oldest category (>50 years) had less roots overall. It is interesting to note, however, that although the total number of roots recorded decreased beyond the 20-50 year old age group, the size of the roots present tended to increase, showing a coarsening of the root mass in the banks (Figure 4.2.7.5-1 shows an example for Red oak). In the case of the Green ash trees investigated along the study reach, the rooting density continued to increase across all of the age classes covered by the data collected, and similar to the previous three species, there was also a coarsening of the root diameters (Table 4.2.7.5-1). The Basswood trees showed the opposite trend to the Green ash, with rooting density declining as trees matured, but again the percent of roots in each size class shifted towards coarser roots in the oldest age class (Table 4.2.7.5-1).

The variations in rooting densities and the diameter distributions that make up that density for each species and age class have implications for the amount of root-reinforcement that is calculated by the RipRoot model (Table 4.2.7.5-1; Figure 4.2.7.5-2). The root-reinforcement values in Table 4.2.7.5-1 assume a 100% cover of that individual species and age category. Fine roots are stronger per unit area than larger diameter roots, but it takes hundreds if not thousands of these smaller roots to make up the area of one large root. In the case of the rooting densities measured along the study reach, the presence of coarser roots in the >10 mm diameter size class has more effect on the root-reinforcement calculations in RipRoot than the rooting density of the finer roots. This can be seen in the results in Figure 4.2.7.5-2 and Table 4.2.7.5-1 showing how estimated root-reinforcement for each species varies for each age class of trees.

For example, even though the total number of Red Oak roots is lower in the >50 year old category, the estimated root-reinforcement is higher than in the 20-50 year old category. This is because although the total number of roots decreased in the >50 year old category, the number of larger diameter roots increased (Table 4.2.7.5-1; Figure 4.2.7.5-1). The increased area of the larger roots outweighed the decrease in the area of the smaller roots in the 20-50 year category. The same pattern can be seen in the American elm data.

In the case of Basswood where the overall rooting density declined from the youngest to oldest age category, root-reinforcement correspondingly declined from the 0-10 year category to the 10-20 year tree category as root numbers declined. In the oldest category for this species, however, the root-reinforcement then increased again, because although the overall number of roots declined further in this category there was a shift to larger root diameters, the effect of which outweighed the decrease in root numbers when root-reinforcement was calculated.

The previous paragraphs discussed variations in root-reinforcement for varying ages of each species. Variations in root-reinforcement *between* species occur as a result of not only the rooting densities and diameter distributions discussed above, but also the species specific tensile-strength curve parameters. In addition, the vegetation present at each site is an assemblage of several species usually with a range of tree ages present. The way that these species specific rooting densities and tensile strength curve parameters were applied to each site is discussed in the next section.

Rooting depths in the root architecture analyses of the bank top trees, were noted to range from approximately 0.3 to 1.5 m below the top of the bank. Rooting densities generally decline exponentially from the soil surface downwards, with roots being concentrated in the top meter of soil (Pollen-Bankhead

& Simon, 2009). The data collected in this study also showed this to be the case, with the 0.5 to 1.0 meter layers showing the highest density of roots >1mm in diameter. Fine roots were concentrated near the soil surface, some of which may have been tree roots, and some of which may have been associated with understory shrubs and grasses.

Table 4.2.7.5-1: Distribution of Roots within Each Diameter Size Class, Broken Down by Species and Averaged for Each Tree-age Class

Red Oak	**Root Diameter in mm**								**Calculated Root-reinforcement from RipRoot (kPa)**
Age	<1	1 to 2	2 to 3	3 to 5	5 to 10	10 to 20	>20	Total	
0 to 10	3	11	11	6	5	2	1	37	1.78
10 to 20	20	16	16	9	15	4	1	81	2.27
20 to 50	27	66	53	42	33	17	8	246	9.70
50+	19	32	23	25	32	18	12	157	13.2
Silver Maple	**Root Diameter in mm**								**Calculated Root-reinforcement from RipRoot (kPa)**
Age	<1	1 to 2	2 to 3	3 to 5	5 to 10	10 to 20	>20	Total	
0 to 10	-	-	-	-	-	-	-	-	-
10 to 20	0	0	0	0	3	11	24	37	21.7
20 to 50	23	72	50	106	93	45	23	412	26.2
50+	9	18	15	16	22	11	6	97	6.84
American Elm	**Root Diameter in mm**								**Calculated Root-reinforcement from RipRoot (kPa)**
Age	<1	1 to 2	2 to 3	3 to 5	5 to 10	10 to 20	>20	Total	
0 to 10	72	40	8	8	12	8	0	148	2.8
10 to 20	78	112	39	36	26	14	6	311	7.66
20 to 50	84	183	69	65	40	20	13	475	13.6
50+	12	90	46	57	21	16	17	260	15.9
Green Ash	**Root Diameter in mm**								**Calculated Root-reinforcement from RipRoot (kPa)**
Age	<1	1 to 2	2 to 3	3 to 5	5 to 10	10 to 20	>20	Total	
0 to 10	64	32	4	24	8	12	8	152	9.11
10 to 20	75	127	24	35	26	23	22	332	23.3
20 to 50	35	149	62	37	31	26	28	367	29.4
50+	20	103	67	80	130	53	53	507	54.8
Basswood	**Root Diameter in mm**								**Calculated Root-reinforcement from RipRoot (kPa)**
Age	<1	1 to 2	2 to 3	3 to 5	5 to 10	10 to 20	>20	Total	
0 to 10	148	396	96	74	40	28	8	790	12.8
10 to 20	27	42	36	25	21	11	5	467	6.24
20 to 50	2	1	2	2	7	12	15	40	14.4
50+	-	-	-	-	-	-	-	-	-

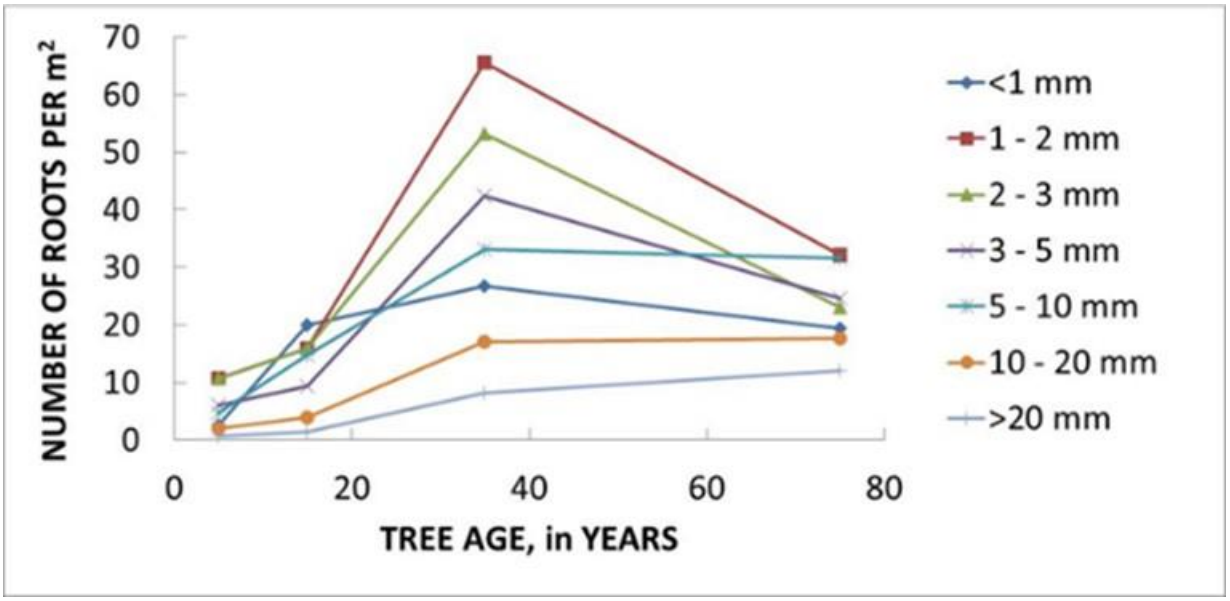

Figure 4.2.7.5-1: Frequency of Red Oak Roots of Different Diameters for Different Age Categories

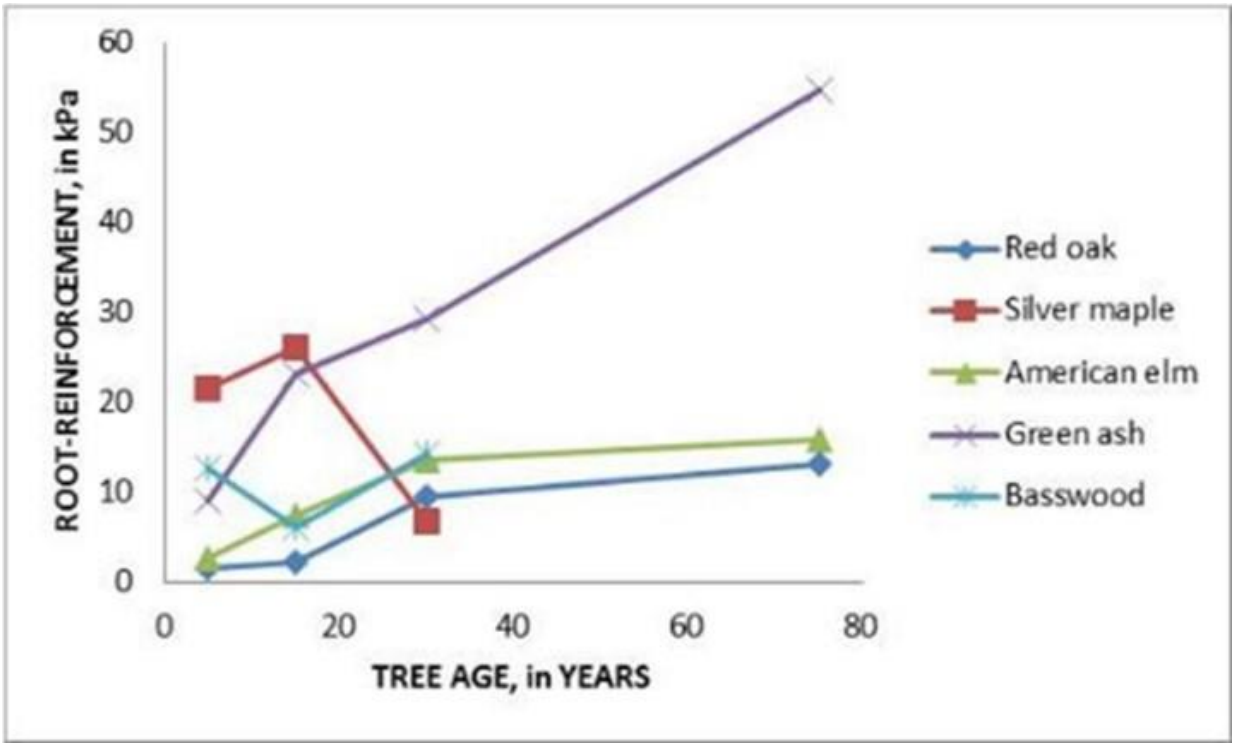

Figure 4.2.7.5-2: RipRoot Root-reinforcement Estimates for Each of the Five Study Species, Assuming 100% Coverage of that Species and Age

4.2.7.6 Calculating Root-Reinforcement at Each Study Site

Vegetation surveys were completed at each of the 25 detailed study sites so that vegetation could be correctly accounted for in the RipRoot algorithm within BSTEM using the species specific rooting densities and tensile strength curve parameters previously discussed. At each site the composition of the vegetation assemblage present was recorded, separating the vegetative cover into bank top, bank face and bank toe. For each part of the bank the percent contribution to vegetative cover from each species and the approximate age of that species was noted. Data were separated into tree cover and understorey cover so that both could be accounted for in root-reinforcement calculations in RipRoot. The percent tree cover and understorey data are summarized in Figures 4.2.7.6-1 – 4.2.7.6-3.

On the bank top, the percent cover of trees varies from 0 to 100% (Figure 4.2.7.6-1), but at all but four of the intensive sites tree cover is 20% or greater. At those sites where few or no trees are present, crops are the dominant land-use at one (Site 3R), and grasses at two others (Sites 119L and 6AR), with a mixture of bare soil, grasses, and herbaceous cover dominating the bank top at Site BC-1R. Where the percent cover of trees is higher, this obviously positively impacts the amount of root-reinforcement that is provided to the upper part of any potential failure surfaces within the streambanks.

On the bank face, the percent tree cover is consistently higher along the study reach than on the bank top, exceeding 40% cover at all but 5 sites. Where trees are more sparse (Figure 4.2.7.6-2; e.g. Site 3R, 6AR) there is still a good cover of shrubs and herbaceous species so there is still some vegetation cover present. This impacts both root-reinforcement of the bank and also bank roughness and the erodibility of the bank to hydraulic shear stresses. It should be noted that although the tree cover is 95% and 70% at sites 75BL and BC-1R respectively, the understorey data at these locations indicates a high percentage (80%) of the soil under the trees is bare. In these cases, although the trees are contributing to root-reinforcement within the banks themselves, there is less surface protection from hydraulic forces.

The percent tree cover at the bank toe (Figure 4.2.7.6-3) is generally lower than both on the bank top and on the bank face. This is unsurprising given the increased magnitude and duration of shear stresses acting at this point on each bank which results in lower occurrences of seedling germination and survival. Trees are still present on many of the bank toes throughout the study reach, but the percent cover did not exceed 65%. The understorey data also shows that even where trees are present there is a very little understorey vegetation, with >80% bare soil being recorded at 15 of the sites at the bank toe. At this point on the bank, tree roots that are present have little to no impact on reinforcement of potential shear surfaces through the bank, but any roots or vegetation present will impact channel roughness and susceptibility of the bank toe region to hydraulic shear stresses.

Figure 4.2.7.6-4 shows the percent cover of each of the five study tree species at each site along the reach, from upstream to downstream (left to right), which was used as input to BSTEM. As can be seen in the figure, at most sites at least one of the five study species was present either on the bank top, face or toe of the banks. Silver maple trees were more commonly found in the upstream half of the reach, whereas Red oaks, while present throughout the study reach, tended to dominate the assemblages in the downstream half of the reach. Green ash trees were found in higher frequencies between sites 21R and 5CR, although they were also found throughout the study reach.

The bank top and bank-face vegetation data were used as input to the RipRoot algorithm as these trees are the ones whose roots are most likely to be growing through potential failure planes within the bank. The percent cover for the bank face and bank toe were taken into consideration when applying roughness (n) values to those corresponding layers. In addition to the five tree species included in this study, any understorey vegetation was noted and included in the RipRoot run for each site. Where tree species other than the five species studied were present at a study site their percent composition was substituted by the most similar tree species from the RipRoot database. Table 4.2.7.6-1 shows an example of the input for Site 8R. RipRoot outputs for the bank top and bank face at the remaining sites are shown in Table 4.2.7.6-2.

The root-reinforcement values derived from RipRoot and utilized in BSTEM ranged from 0.3 to 14.1 kPa, with a median value of 3.75 kPa (Figure 4.2.7.6-5). If we consider these values in the context of the strength of the soil matrix (bank materials) we gain a better perspective of the importance of the root networks for bank stability. The effective cohesion values along the study reach tended to be quite low, which is characteristic of the sandy loam soils that dominate these banks. The median effective cohesion (*c'*) value for the bank materials along the study reach was 1.9 kPa (mean = 5.2 kPa), which is within the effective cohesion range for a loamy sand. BST tests also showed that 30% of the tested bank materials were cohesionless, 35% were less than 0.5 kPa, and only 20% were greater than 10 kPa. A median root-reinforcement value of 3.75 kPa is 97% greater than the median strength of the soil samples tested, meaning that on average, the reinforced soil-root matrix along the reach is 200% stronger than the soil alone. Where roots reinforce a weaker, sandier soil, this percentage increase in strength could be even higher. Conversely, at sites such as BC-1R where effective soil cohesion is very high (28.6 and 32.6 kPa) or where bank slopes are high in the absence of bank-face vegetation, the contribution from roots can be limited.

Table 4.2.7.6-1: Example of RipRoot Input Data for Site 8R

Species	Percent of Assemblage	Approximate Age (years)
Grasses	10	-
Am. basswood	5	7.5
Green ash	10	12.5
Northern red oak	7.5	7.5
Northern red oak	7.5	50

Table 4.2.7.6-2: RipRoot Outputs for Root-reinforcement to be added to the Bank Top and Bank Face Where Applicable in the BSTEM Simulations

Site	RipRoot Output (kPa)		Notes
	Top Bank	Bank Face	
11L	3.43		
2L	2.53	6.22	
303L	3.90		
18L	3.44		
3L	9.40		
3R	0.30		
21R	4.00	3.60	Layer 2 only. From 1.0m depth to 3.6m depth
4L	2.10	5.20	
29R	6.90		
5CR	14.1		
26R	4.54		
10L	4.90	3.5	Layers 2 and 3. All but Toe.
10 R	3.18		
6AL	3.20		
6AR	0.47		
119L	2.17		
7L	11.4		
7R	2.30	10.5	Layers 2 and 3. All but Toe.
8BL	1.94	6.1	Layers 2 and 3. All but Toe.
8BR	4.62	1.7	Layers 2 and 3. All but Toe.
87L	13.9		
75BL	5.90		
9R	3.89	3.6	Layers 2 and 3. All but Toe.
12L	4.59		
BC-1R	3.56	2.5	Layers 2 and 3. All but Toe.

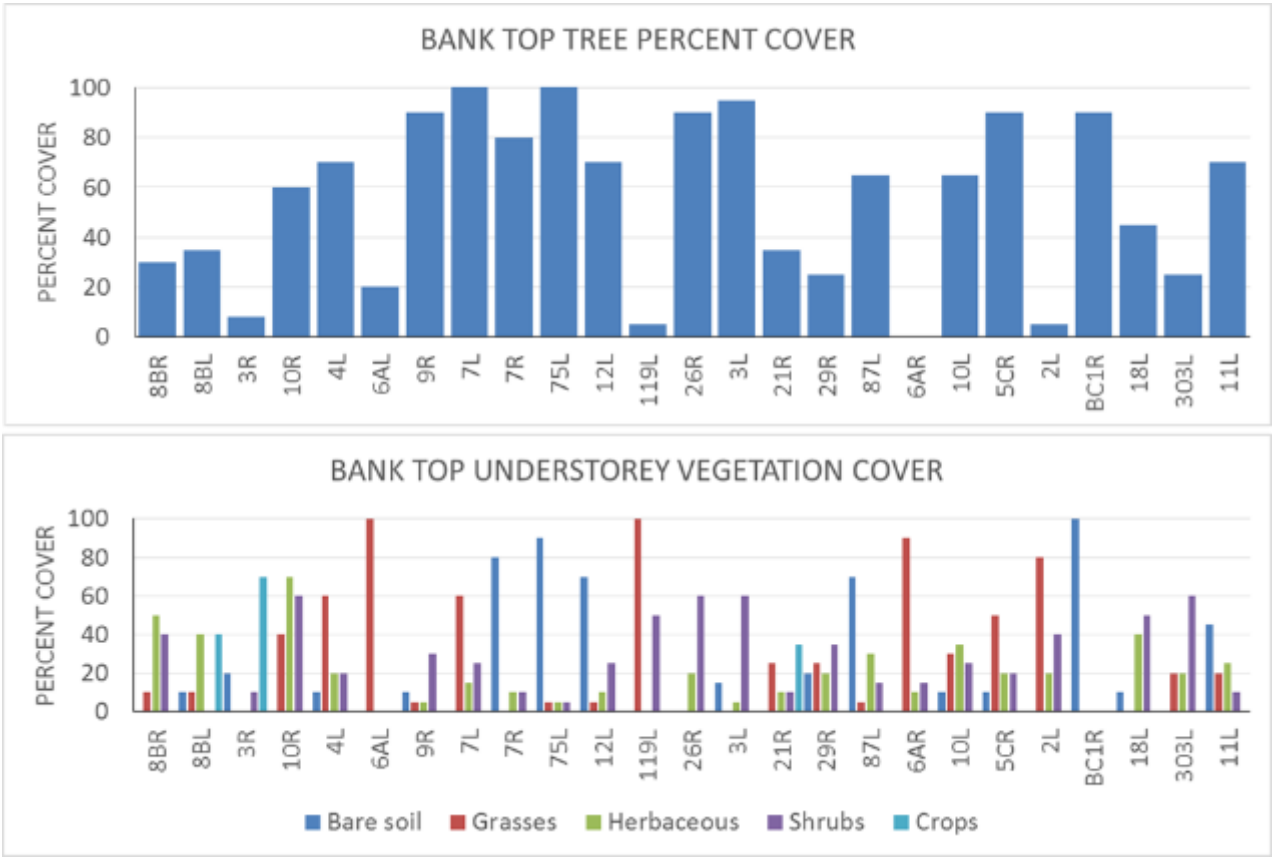

Figure 4.2.7.6-1 Percent cover for tree and understory vegetation categories on the bank top, at each site

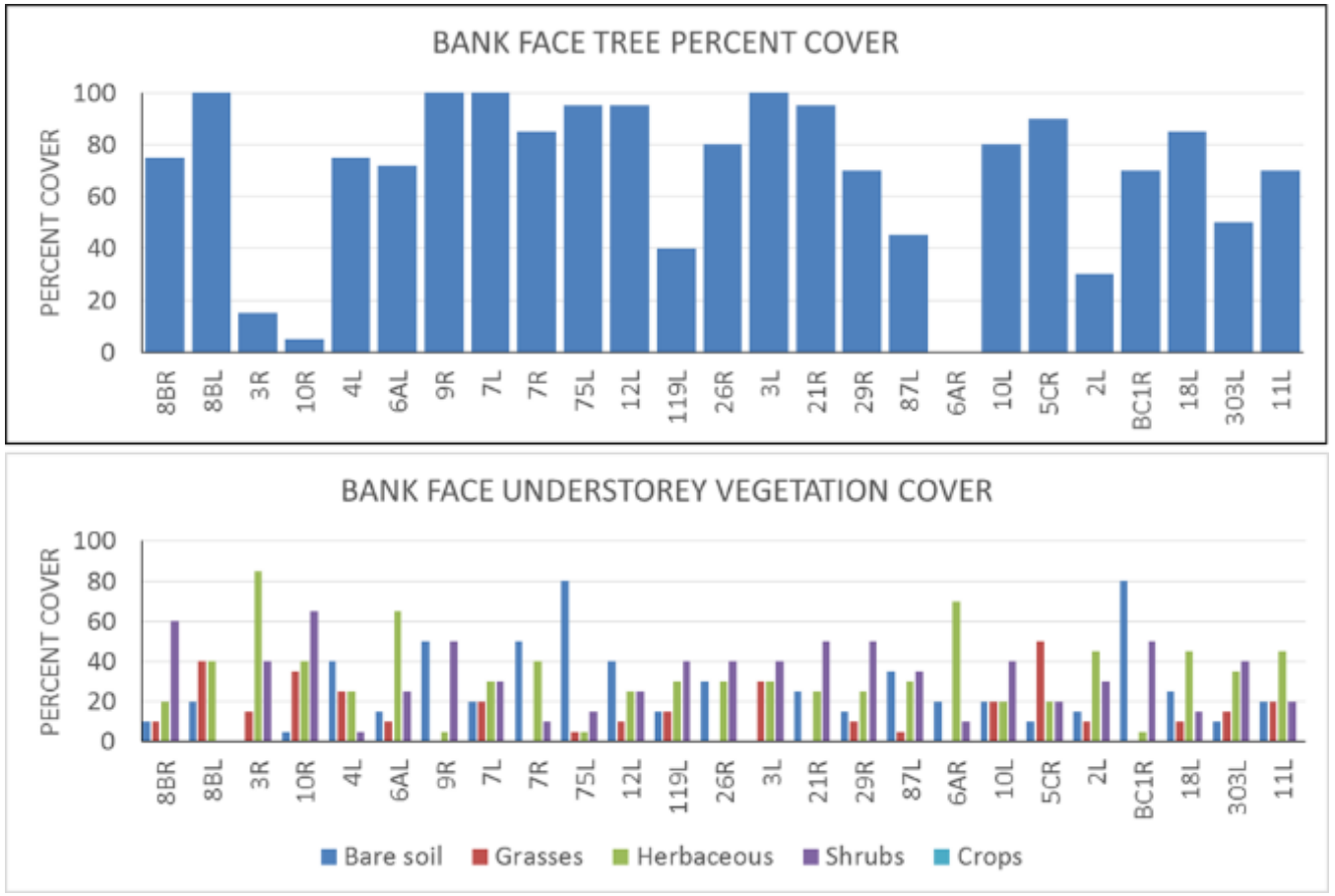

Figure 4.2.7.6-2: Percent Cover for Tree- (Top) and Understory-vegetation (Bottom) Categories on the Bank Face at Each Site

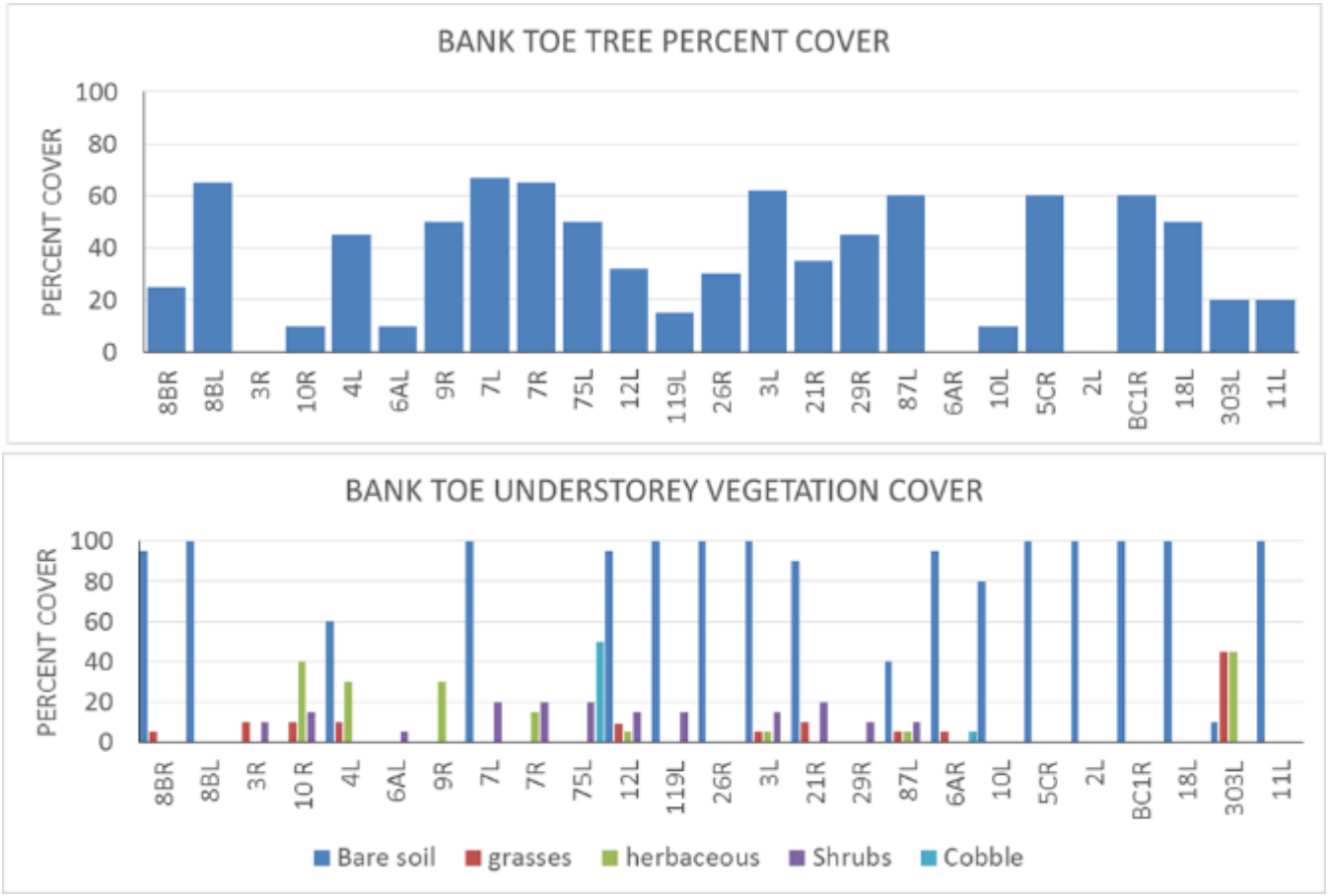

Figure 4.2.7.6-3 Percent cover for tree and understorey vegetation categories at the bank toe, at each site

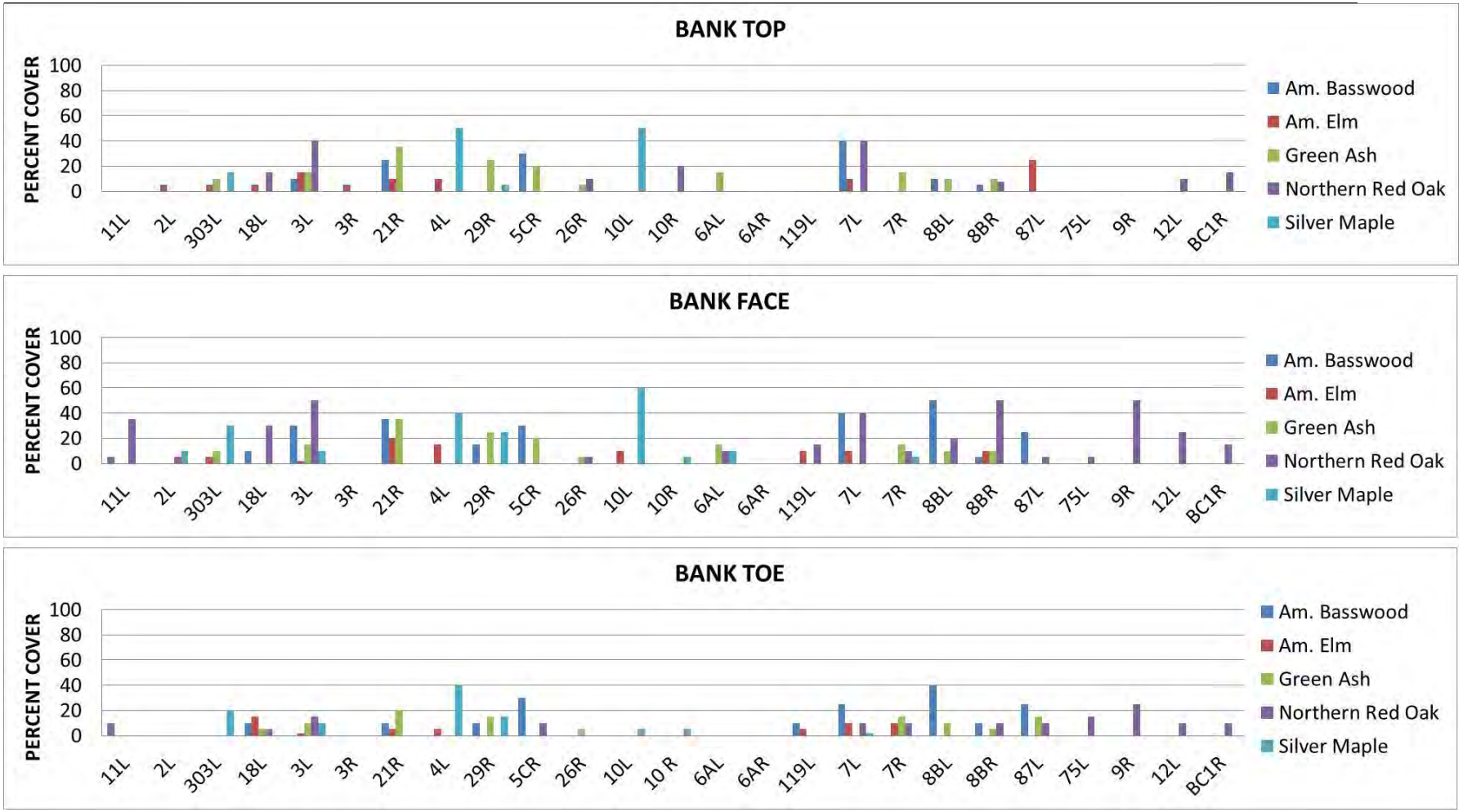

Figure 4.2.7.6-4 Longitudinal distribution of percent cover for the five tree species investigated for root-reinforcement along the study reach

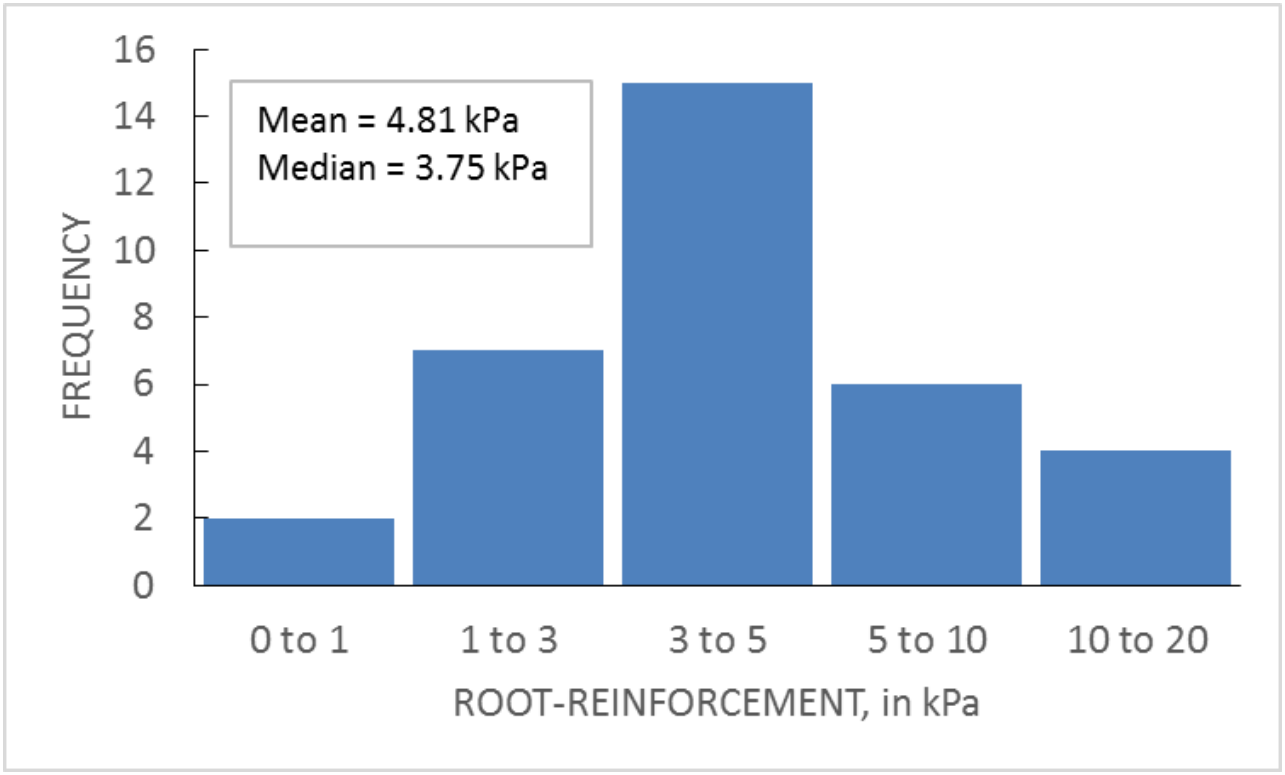

Figure 4.2.7.6-5 Distribution of root-reinforcement values along the Turners Falls Impoundment

4.2.8 Boat-Generated Wave Management on the Connecticut River - BSTEM

Basic relations describing the wave pattern around a moving boat are presented in Volume III (Appendix G). The generated wave system can simply be defined by the wave period (or wavelength), wave height and direction of wave propagation. The total energy carried by the wave train is a function of the wave height, and the wave height depends on many different factors including the velocity of the boat, dimension (length, width, draft) and the shape of the boat and the hull design, total displacement volume, distance of the shoreline from the sailing line, channel width, water depth, and the cross-sectional area. Wave height estimations necessitate more sophisticated methods due to the number of variables involved. Simple empirical methods can provide reasonable approximations of boat-generated wave prediction but the validity of these models are limited by the range of data used in their derivation.

Boat-wave data were collected during several time periods from the late 1990's up through the summer of 2015. The initial data consisted of placing a staff gage in the water near the riverbank and videotaping boat waves. From this, the frequency and magnitude of the wave amplitude as they approached and broke on the riverbank was developed from the video information. Some near-bank suspended sediment samples were also collected when boat waves were breaking. Boat-wave data, as described above, were collected on the following dates: May 8, 1997, July 12-13, 1997, July 26-27, 2008, and during September 2008. Appendix H provides boat wave data collected during these time periods.

A set of boat wave data was specifically collected in 2015 in support of the Causation Study for use in BSTEM. The hydrodynamics of boat waves and the approach to collect detailed boat wave data in 2015 is described below. This section concerns field measurement of boat traffic and boat-generated wave properties at three monitoring locations throughout the TFI. Each measurement station consisted of one or more wave loggers to measure the water-surface displacement and a time-lapse camera to capture the boats as they pass. Wave-logger data analysis procedures, boat statistics and wave properties during the measurement period are presented in the following sections.

4.2.8.1 Boat Wave Monitoring Sites

Boat-monitoring sites were established at three locations throughout the geographic extent of the TFI. Figure 4.2.8.1-1 shows the relative distances between the sites. Figure 4.2.8.1-2 depicts the locations of the wave logger sites and camera installation sites as well as the location of the detailed study sites examined in BSTEM.

The monitoring sites were selected based on the availability of camera installation sites suitable for boat monitoring (i.e. bridges). In order to have the field of view covering an area large enough to resolve the boat activity, the cameras had to be installed sufficiently high and far from the river, yet close enough to have enough spatial resolution. The relations between spatial and temporal resolution, and the target distance for the selected cameras are explained in the following section. Both banks of the river are covered with shrubs and trees, which limited the field of view of the cameras. Moving closer to the river to avoid vegetation limited the field of view and camera height, which made the banks impractical for boat monitoring. The cameras also require frequent maintenance for download and battery replacement; therefore, installing the cameras on the existing bridges along the river was the most viable option due to the ease of access and a sufficiently wide field of view. Six cameras were installed on three bridges, Schell Bridge (Cam-1), Route 10 Bridge (Rt. 10) (Cam-2), and the French King Bridge (Cam-3).

A wave-logger station was constructed near each camera site. The first wave logger (WLOG-1) was located upstream of the Schell Bridge, close to left bank of the river, near site 4L. The second wave logger (WLOG-2) was located downstream of the Rt. 10 Bridge, on the right bank near site 5CR. The remaining two wave loggers (WLOG-3 and WLOG-4) were located upstream of French King Bridge and downstream of site 75BL, on the left bank. These locations were selected based on the site conditions and camera field of view. The objective was to measure the boat-generated waves close to the shore before they shoal and break. Each

wave logger was attached to a T-post, which was driven with a sledge hammer into the riverbed near the bank. The length of the T-posts also limited workable water depth and constrained the wave logger site locations. Given these limitations, only a narrow section along the river cross-section was suitable for the placement of wave loggers.

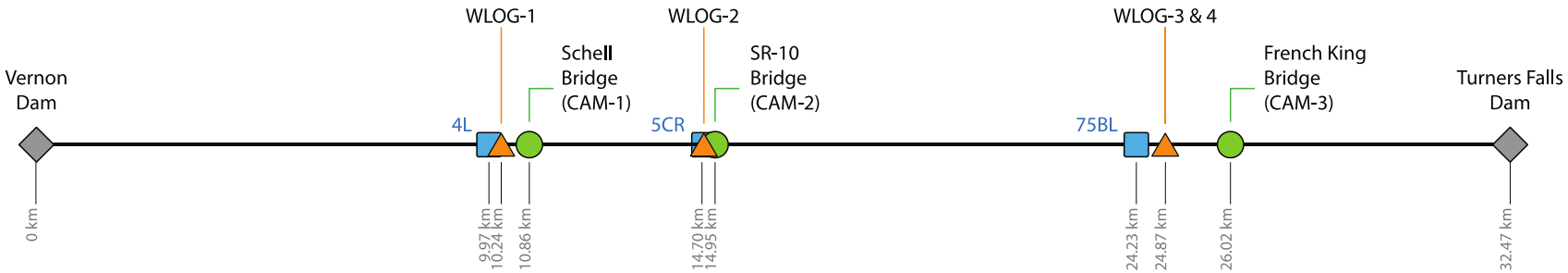

Figure 4.2.8.1-1: Relative Distance between Boat-monitoring Sites

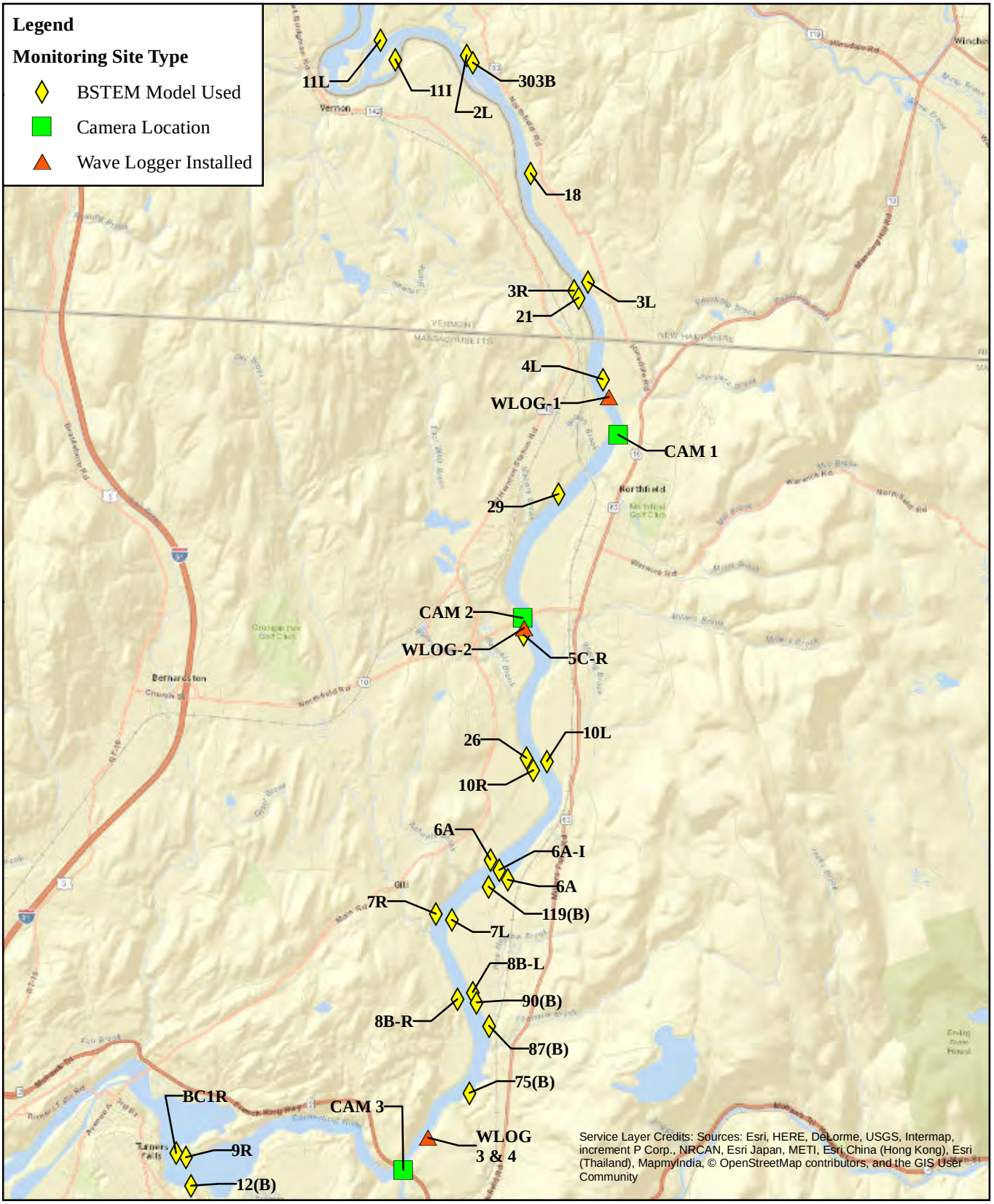

FIRSTLIGHT HYDRO GENERATING COMPANY
Northfield Mountain Pumped Storage Project No. 2485
Turners Falls Hydroelectric Project No. 1889

STUDY 3.1.2

Figure 4.2.8.1-2:
Locations of Boat-monitoring Sites

N

0 0.75 1.5 3 Miles

Path: W:\gis\studies\3_1_2\maps\final_report\figure_4_2_8_1-2.mxd

4.2.8.2 Instrumentation and Data Collection

Two types of equipment were utilized for the collection of data related to boat-waves – cameras and wave loggers. In-depth discussion pertaining to each type of equipment is presented below.

Cameras

Two different types of consumer-grade cameras were used during the measurements. The specifications of these cameras are listed in Table 4.2.8.2-1. Both cameras were configured to take pictures at 10-second intervals at a pixel resolution of 1280 by 720 during daylight. Each field site was equipped with one of each type of camera. The wide-angle camera (Brinno) served as the primary camera while the other one was used as the backup. Both cameras are rated to run over two weeks with this configuration without replacing the batteries and the memory card.

The primary difference between the two types of cameras was the area each picture covers, described by the Field of View concept (FOV). FOV is the area that is visible to the camera sensor through its optical component. For the same sensor resolution (or pixel resolution) the camera with the wider FOV will provide a larger portion of the outside word at a smaller resolution. This is explained in Figure 4.2.8.2-1. The wide-angle camera (Brinno) (illustrated with the orange line in Figure 4.2.8.2-1) has 115° FOV while the narrow-angle camera (Moutrie) (illustrated with the green line) has 50° FOV. The wide-angle camera covers a relatively larger area but it won't detect smaller objects due to the lowered resolution. A boat will appear smaller on the wider FOV camera and resolved with fewer pixels compared to the one with narrower FOV. However, the boat will stay longer in the wide-angle FOV; therefore, for a given time lapse interval, faster boats can be detected.

The frame interval (time interval between two frames) and the maximum operation time of the cameras with both types of lenses (50° and 115° FOV) based on a boat moving at 20 m/s are shown in Figure 4.2.8.2-1. The boat sailing line is assumed to be perpendicular to the camera direction. The frame interval is reduced when the boats are closer to the camera, increasing the frame rate, which also increases the energy and memory requirements. Pulling the camera back from the target is one solution to this problem, but not practical for this field setup. When the camera is oriented in the streamwise direction, which was adapted in the current study, the vertical FOV becomes more important than the horizontal FOV in terms of positioning the cameras. This is illustrated in Figure 4.2.8.2-2 where the two plots show how pixel resolution changes with distance for various camera heights.

The illustrated geometry on top is plotted for x vs s_h, and x/h_c vs s_h/x_c, where x is the distance from the camera, s_h is the spatial dimension of each pixel and h_c is the height of the camera. The pixel resolution reduces asymptotically in the vertical direction and the rate depends on the height of the camera. In order to have a wider vertical FOV, the camera has to be raised. When the camera is lowered, the vertical resolution is reduced considerably. Streamwise camera orientation is advantageous for capturing high-speed boats, but the camera height limits the precision of the measurements. Figure 4.2.8.2-3 shows example shots from the two types of cameras at the three sites. Each pair of pictures refers to the same time for comparison.

The cameras were held in place on the bridge hardware by hose clamps and zip ties. Data from the cameras were downloaded every two weeks at which time the batteries were also replaced. The Rt. 10 Bridge and French King Bridge cameras were mounted in the middle of the bridge rail, whereas the Schell Bridge camera was close to the left bank to provide a better view angle of the river upstream.

Table 4.2.8.2-1: Comparison of Camera Specifications

	Brinno HDR	Moultrie-1100i
		
Resolution	1280x720 (1.3 MP) HDR	1280 x 720 (1.3 MP) 2304 x 1296 (3 MP) 2688 x 1512 (4MP) 4608 x 2592 (12 MP)
Aperture	F2.0, 19mm (35mm eqv.)	
Time lapse	1s – 24hrs	10s, 30s, 1min – 1day
Field of view (FOV)	112˚	50˚
Memory	32 GB	32 GB
Batteries	4 x AA	8 x AA
Video resolution	720p	720p
No of photos with 32GB memory	77,280 photos	77,280 photos
No of photos with 4AA batteries	80,000 photos	80,000 photos
Other		80 ft infrared Temperature gauge

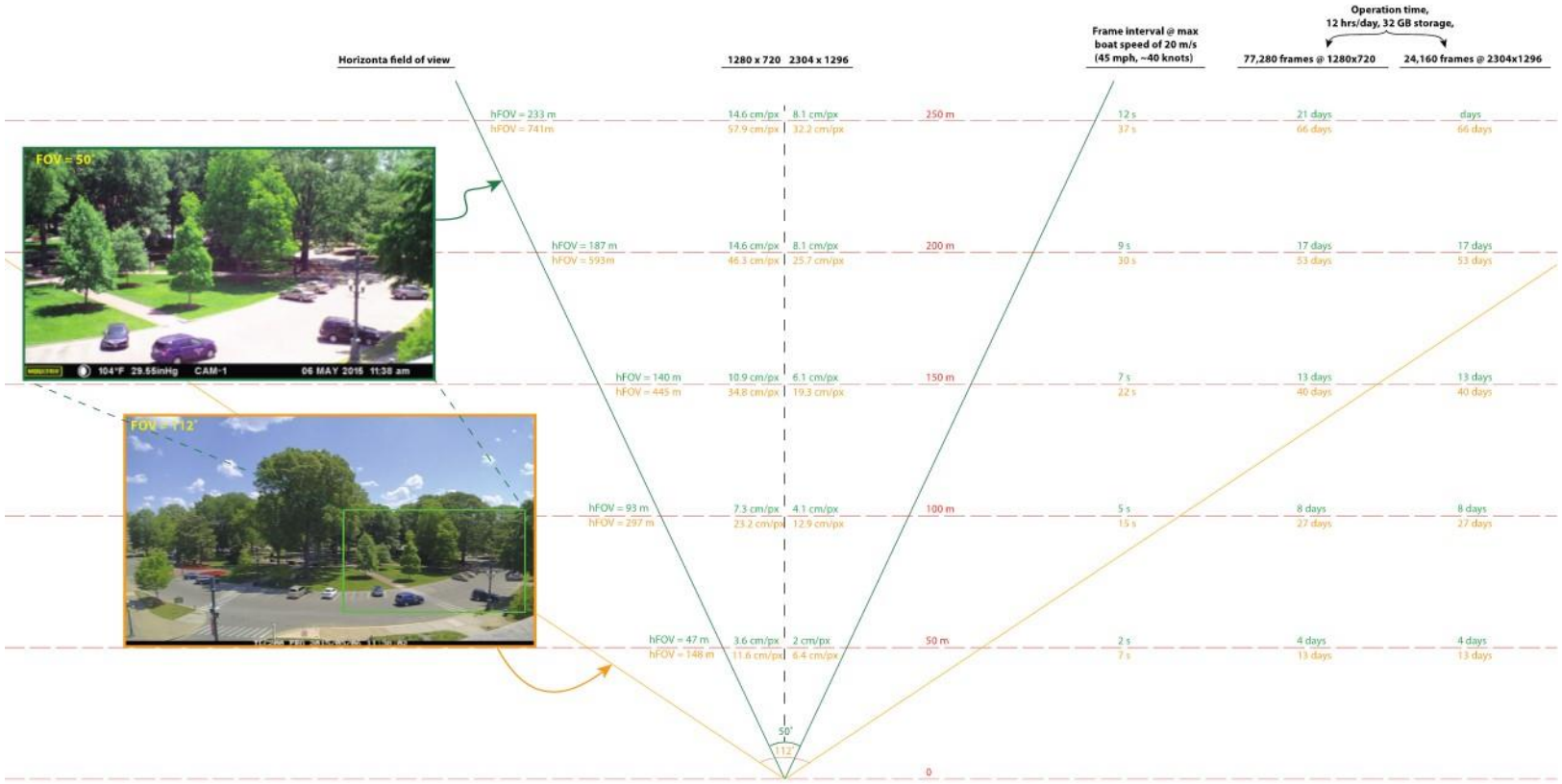

Figure 4.2.8.2-1: Camera Field of View (FOV) Comparison

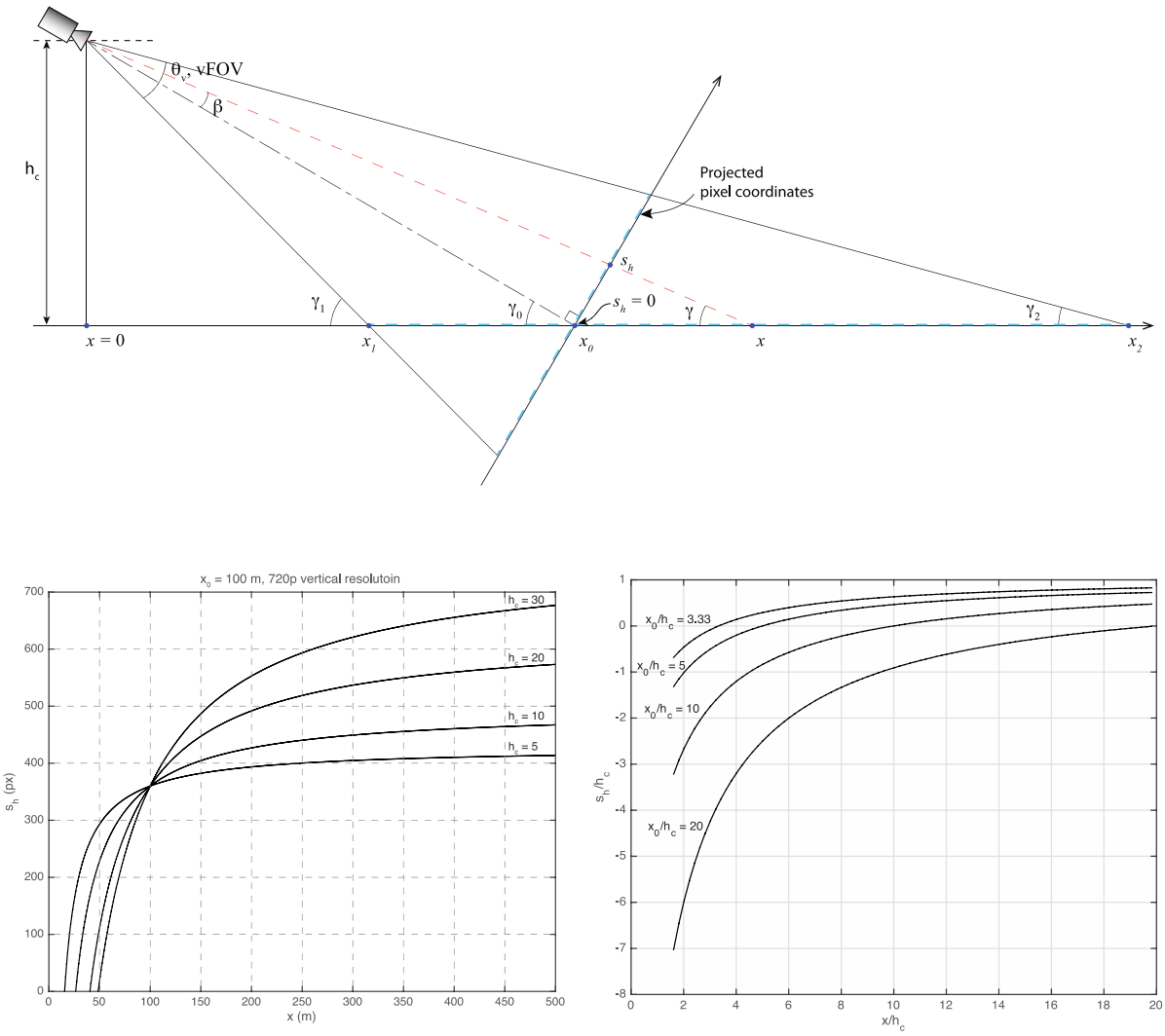

Figure 4.2.8.2-2 Pixel resolution and camera height relations

Schell/M1

Schell/B1

Rt. 10/M2

Rt. 10/B2

French King/M3

French King/B3

Figure 4.2.8.2-3: Example Photographs Recorded at the Monitoring Sites

Wave Loggers

Four wave loggers were used to measure water-surface displacement at three sites in the study area. The wave loggers include a capacitance type wave staff and a battery powered microprocessor that stores the water level. The specifications of the wave loggers are given in Figure 4.2.8.2-4. The loggers were operated continuously (100% burst time/interval time) at 30Hz frequency. Equipped with 2GB flash cards, the expected uninterrupted recording time of the loggers was on the order of months at 30Hz frequency. Nonetheless, the recorded data was downloaded at two-week intervals to avoid unexpected data loss.

The loggers recorded the water-surface displacement at 30Hz frequency and the ambient air temperate at 2.5Hz. Boat- and wind-generated waves in the study area are mostly in a frequency range of 0.2Hz – 2Hz. The 30Hz measurement frequency provided a fairly good temporal resolution, which is 15-readings-per-wave at the high frequency end of this range. Each logger had a 2-m-long staff producing an integer count between 0-4095 depending on the wave level relative to the staff, which is equivalent to a spatial resolution of approximately 0.5 mm.

For the wave loggers to measure the water level, the wave staffs had to be in contact with the water surface at all times. The optimum elevation of the wave loggers that maximized its contact with the water was calculated knowing the stage history. Stage histograms were generated for each site using HEC-RAS simulations of the 15-year long period between 2000 and 2014. The simulation results closest to the wave-logger sites were used for this analysis. Figure 4.2.8.2-5 shows the exceedance probability of the entire water-level dataset, and for the summer months from May through September (MJJAS) at site 4L (near WLOG-1), 5CR (near WLOG-2) and site 75BL (near WLOG 3 & 4). Mean elevations for 12 months and MJJAS, and the minimum and maximum elevations are also shown in these plots. Red lines indicate the stage when the discharge is 20,000 cfs and 40,000 cfs. The mid-height of the wave staffs were determined using the calculated mean values.

Figures 4.2.8.2-6 through 4.2.8.2-8 illustrate the installed elevations of the wave loggers compared to the probability distribution of the stage. Red marks on the staffs indicate the midpoint of the staffs. A maximum measurable water-surface elevation is reached when 90% of the staff is submerged in the water. The stage is above this elevation less the 10% of the time during summer mouths (MJJAS).

Galvanized steel T-posts were installed to support the wave loggers. 8-ft (2.44 m) long T-posts were vertically driven into the riverbed using a sledge hammer (Figure 4.2.8.2-9). Additional sections were bolted on top of the post as it was driven into the bed until 4-5 ft. (1.2 -1.5 m) was under the riverbed. The loggers were bolted to these T-posts and plumbed. Reflectors and flags were attached to increase visibility. Staffs were secured to the T-posts at 2/3 their height to limit its motion. T-posts were then anchored to the bank with flagged nylon ropes.

Table 4.2.8.2-2 summarizes the camera and wave-logger settings used during the field monitoring. Beginning dates of the data recording for each instrument are also listed in this table. Figure 4.2.8.2-10 shows pictures of the cameras and wave loggers after the installation.

Table 4.2.8.2-2: Camera and Wave Logger Configurations

Camera location	Schell Bridge	Rt. 10 Bridge	French King Bridge
Camera type	Moultrie	Moultrie	Moultrie
Frame rate	0.1 fps	0.1 fps	0.1 fps
Interval	7am - 8pm	7am - 7pm	6am - 9pm
Start date	20-May	15-May	15-May
Camera type	Brinno	Brinno	Brinno
Frame rate	0.1 fps	0.1 fps	0.1 fps
Interval	6am - 9pm	6am - 9pm	6am - 9pm
Start date	21-May	15-May	15-May
Logger location	Upstream of 4L	Downstream of 5CR	Upstream of 75BL
Frequency	30Hz	30Hz	30Hz
Start date	20-May	13-May	21-May

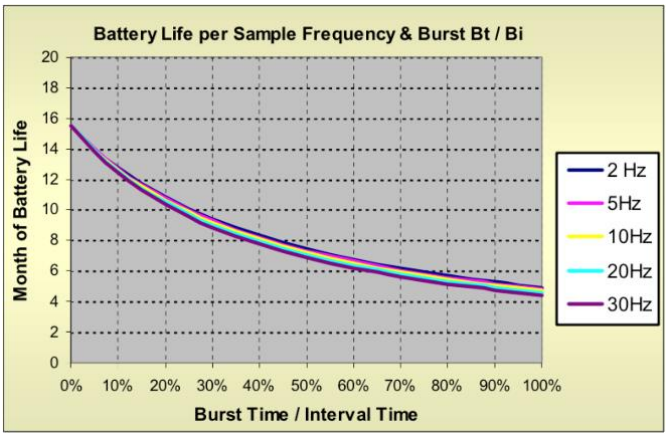

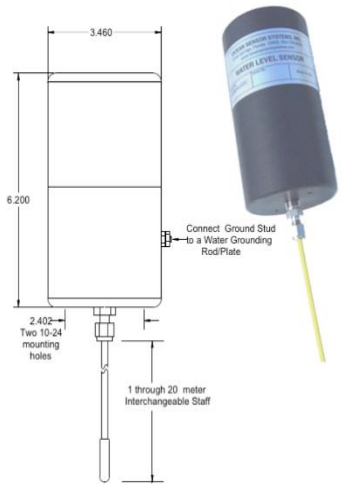

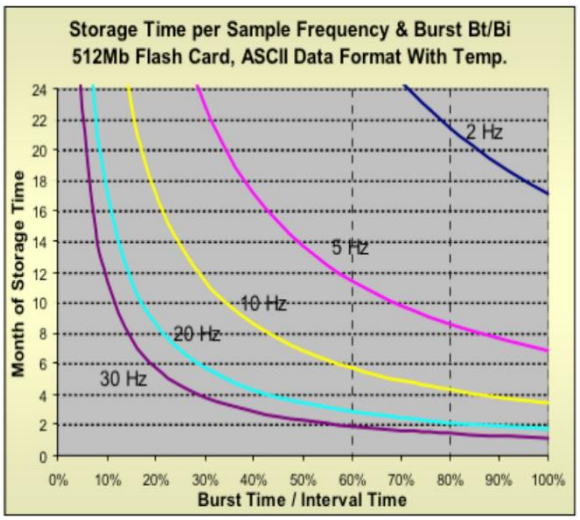

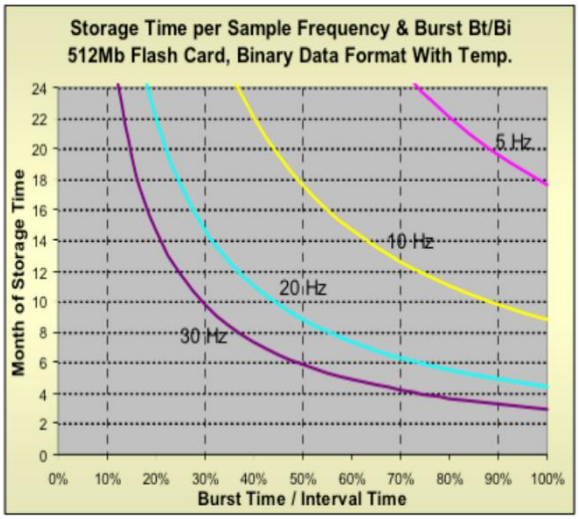

Figure 4.2.8.2-4: Wave Logger Specifications

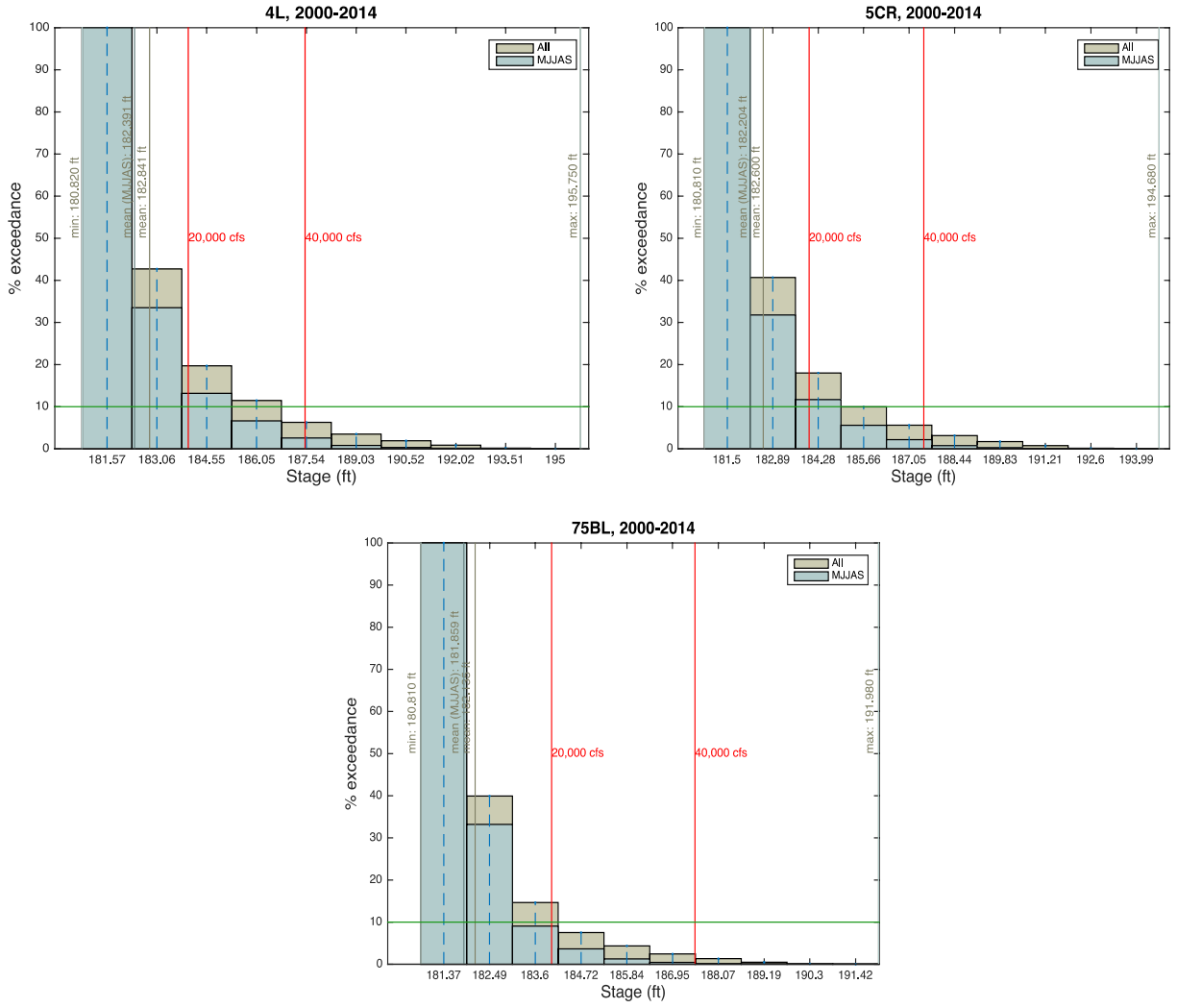

Figure 4.2.8.2-5: Exceedance Probability of the Stage at Sites 4L, 5CR, and 75BL

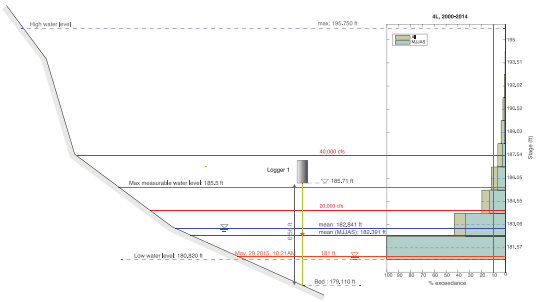

Figure 4.2.8.2-6: WLOG-1 Installation Elevation

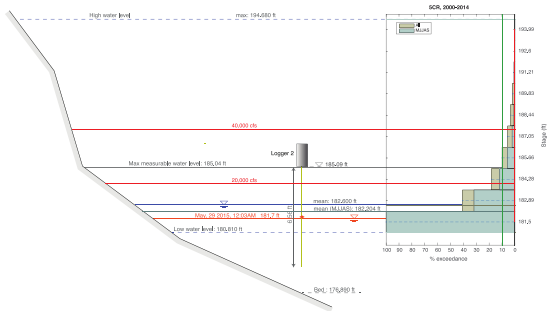

Figure 4.2.8.2-7: WLOG-2 Installation Elevation

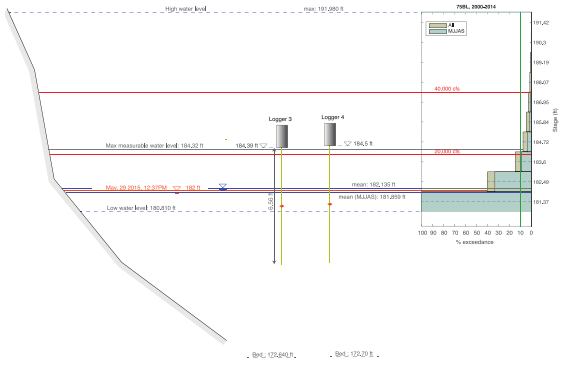

Figure 4.2.8.2-8: WLOG-3 Installation Elevation

Figure 4.2.8.2-9: Installation of the T-posts

Figure 4.2.8.2-10: Cameras and Wave Loggers at the Three Installation Sites

4.2.8.3 Data Analysis

Boat waves were recorded continuously at four loggers between May 22, 2015 and September 14, 2015. Quantitative boat-traffic statistical data and boat-generated wave data were obtained mainly from the wave logger data analysis. The time-lapse recordings supported the wave analysis by providing visual information. For instance, the boat signatures in the wave data are validated using the video recordings. Figure 4.2.8.3-1 shows an example time series of the water-surface displacement and its spectrum after two boats passing by WLOG-2. The pictures of the two boats are recorded on CAM-2 as shown in the figure. Pictures clearly indicate that the boat in the top frame (at 2:15 pm) was traveling at supercritical speed (see Volume III - Appendix G) in the downstream direction, and the one in the bottom frame (at 2:17 pm) was traveling at subcritical speed in the upstream direction. Subcritical and supercritical speeds are identical to displacement and planing speeds respectively. This information was used to separate the individual wave envelopes of different boats in the time series data. Rain event information was also acquired from the video recordings.

Raw wave-logger data includes elevation counts (integer between 0 - 4095), which represents the water level relative to the staff length, recorded at 30Hz data rate. Each logger generates a separate file every 24 hours with 2.592 million data points. Counts were converted to actual elevations using a linear calibration, and transformed to a reference datum (NAVD88, US feet) through Real Time Kinematics (RTK) GPS survey of the water-surface elevations at the wave-logger sites (Table 4.2.8.3-1) (obtained from Gomez and Sullivan Engineers). Each measurement was repeated three times to reduce uncertainty (~2-3 cm accuracy).

The time series at the four-wave loggers were analyzed to obtain mean-water level and water-surface displacements during the monitoring period. Daily signals were filtered using a low-pass IRR (internal impulse response) filter of order 10 and with a 10 s cut-off length to remove high frequency components. This process removed the high frequency noise in the data as well as the boat wave, leaving only the gradual changes in the water level throughout the day. The original signal was normalized with the filtered signal to obtain water-surface fluctuations, including the boat waves. The high frequency components were removed using another low-pass filter, of order 10 and cut-off length. A sample of collected wave data can be seen in Figure 4.2.8.3-2. Boat waves at a fixed location appear as short low- to high-frequency “chirps” superimposed into the random wind waves. Boat waves are magnified in Figure 4.2.8.3-2 to show their distinctive shapes.

Boat waves have distinct characteristics that can be used to identify them in the recorded signal. Waves with different frequencies travel with different speeds in water. At a stationary point, the recorded wave signal shows a wave group gradually shifting from low to high frequency, due to frequency dispersion. This transient wave group has a unique oscillatory pattern, and usually much more energetic then irregular wind-generated waves. The amplitude of the wave’s increases as the frequencies increase until maximum wave amplitude is reached.

The frequency content and steady oscillatory signal can be found using Fourier transform. Fourier transform converts the time series signal into a spectrum in the frequency domain; hence the resulting spectrum is not time dependent. The time history of the frequencies of a transient signal, similar to boat waves can be found using local time-frequency analysis (i.e. wavelet transform or windowed Fourier transform). Wavelet transform uses inner products to measure the similarity between the time series signal and a wavelet function. The resulting transformation is visually represented by a scalogram. Figure 4.2.8.3-3 shows an example boat-wave group and its scalogram using Morlet wavelet. The vertical axis of the scalogram is frequency and the color indicates the correlation of the signal with the scale for a given frequency. Windowed Fourier transform divides the signal into segments, and each segment is transformed into Fourier space using a window function. The time-series signal is decomposed into its time-frequency-spectral density components, which is visually represented by the spectrogram. The spectrogram is a function of both the frequency and time since the decomposition is local.

Both methods produced similar results in the current study to detect boat waves in the recorded signal. Windowed Fourier transform was faster than the wavelet transform and, therefore, adopted in this study. Figure 4.2.8.3-4 illustrates a typical signal and its spectrogram, which is obtained using windowed Fourier transform. Figure 4.2.8.3-5 shows a 14-hour long signal recoded at WLOG-2 on May 24, 2015, and the spectrogram of the same signal. Horizontal axis is time, vertical axis is frequency and the contours represent the energy level. The spectrogram is obtained using a Hamming windowed Fourier transform, of 512 (number of data points in the 30Hz signal) with 75% overlapping. Each segment of the signal and the spectrogram indicated by a rectangle is magnified to show details. The low frequency to high-frequency "chirp" pattern can be easily identified. The photo in the figure shows the boat that generated the recorded wave group in the final plot.

Using the spectrogram, individual boat passes were identified in the frequency domain. The locations of the maximum wave heights and the wave frequencies associated with those waves were obtained in each boat-wave signal using zero-crossing analysis. The waves are defined between two successive zero down crossings in the normalized signal. The wave height is the difference between the maximum and minimum water-surface displacement in each wave and the wave period is the time length of each wave.

Wind-generated waves are irregular and narrow banded in waters with limited fetch. Neither period nor the heights of the wind-generated waves are constant. The waves are represented in terms of statistical quantities. They are described by spectral quantities rather than individual wave properties. Irregular waves from water-surface recordings can be considered as a combination of a series of regular waves with different periods that are superimposed with a random phase, and a certain amount of energy is transmitted by each component. The distribution of the energy for each wave frequency can be determined by transforming the wave record from the time domain to the frequency domain. The distribution of wave heights closely follows the Rayleigh distribution for wind-generated waves, assuming the random water surface elevation follows a Gaussian distribution. Significant wave height can be approximated by the standard deviation (square root of the variance of the signal) (Longuet-Higgins 1952).

$$H_{mo} = 4.004\sqrt{m_o} \tag{1}$$

where m_o is the zero-th moment of the spectrum. The *i*-th moment of the continuous spectrum is obtained by,

$$m_i = \int_0^\infty f^i S(f)\,df \tag{2}$$

where *S(f)* is the wave energy spectral density and designates the distribution of variance with frequency, *f*, assuming that the function is continuous in the frequency domain. The spectral definition of the significant wave height, H_{m0} is approximately equal to the average of the highest one-third of the waves in a wave record.

Table 4.2.8.3-1: Water-surface Elevations at the Wave-logger Sites

Point Id	Location	Northing[1]	Easting[1]	Orth. height[2]	Quality pos.	Quality hgt.	Quality pos. + hgt.	Quality pos. + hgt.
BW.US.PAUCH.2	U/S Schell Br. / Pauchaug	3087969.294	399610.9674	181.044	0.0221	0.0389	0.0448	0.0448
BW.US.PAUCH.3	U/S Schell Br. / Pauchaug	3087969.35	399610.9731	181.0357	0.0235	0.0411	0.0474	0.0474
BW.US.PAUCH.4	U/S Schell Br. / Pauchaug	3087969.373	399610.8988	181.0248	0.0343	0.0613	0.0702	0.0702
BW.RT10.1	D/S Rt. 10 Bridge	3074722.91	394885.5408	181.6438	0.0939	0.1505	0.1774	0.1774
BW.RT10.2	D/S Rt. 10 Bridge	3074724.397	394887.1386	181.6687	0.0852	0.1464	0.1694	0.1694
BW.RT10.3	D/S Rt. 10 Bridge	3074726.058	394888.6429	181.7639	0.0712	0.1276	0.1461	0.1461
BW.FK.1	U/S French King Bridge	3047261.858	389916.4445	181.9623	0.0995	0.1821	0.2075	0.2075
BW.FK.2	U/S French King Bridge	3047258.927	389915.7756	182.0804	0.0851	0.1474	0.1702	0.1702
BW.FK.3	U/S French King Bridge	3047255.204	389915.2834	182.0352	0.0781	0.138	0.1586	0.1586

[1] NAD83 Massachusetts State Plane (US Feet) Coordinate System
[2] NAVD88 (US Feet)

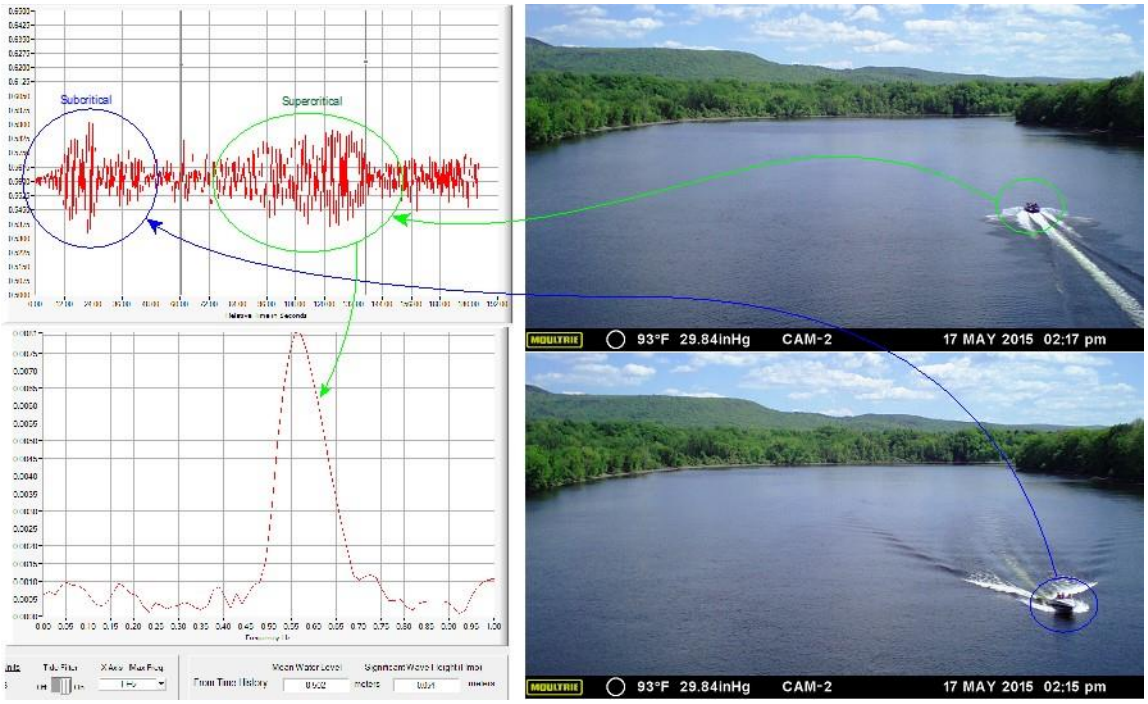

Figure 4.2.8.3-1 An example of collected boat-wave data

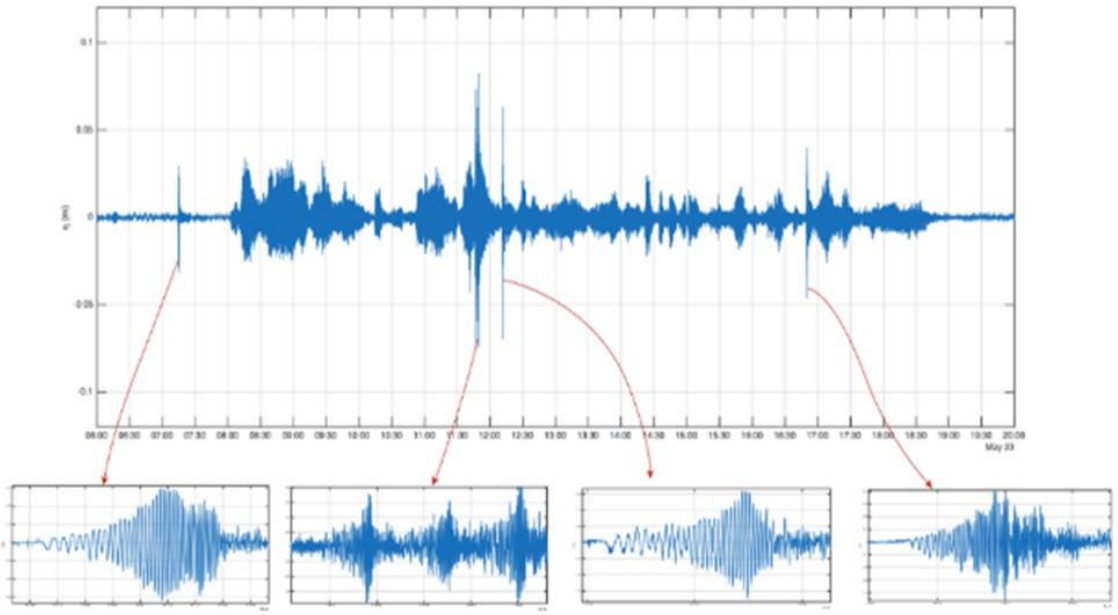

Figure 4.2.8.3-2 An example of water-surface displacement data showing boat waves

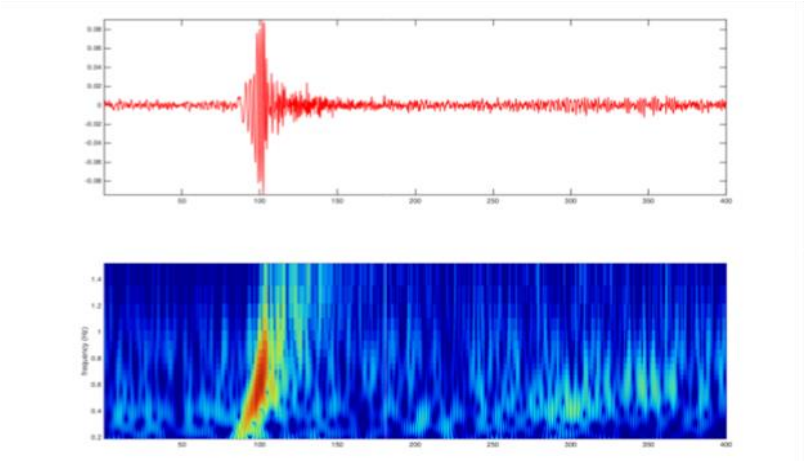

Figure 4.2.8.3-3 A typical boat wave group and its scalogram

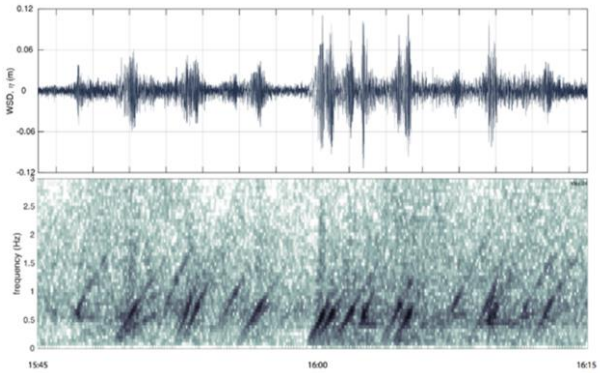

Figure 4.2.8.3-4 Example spectrogram

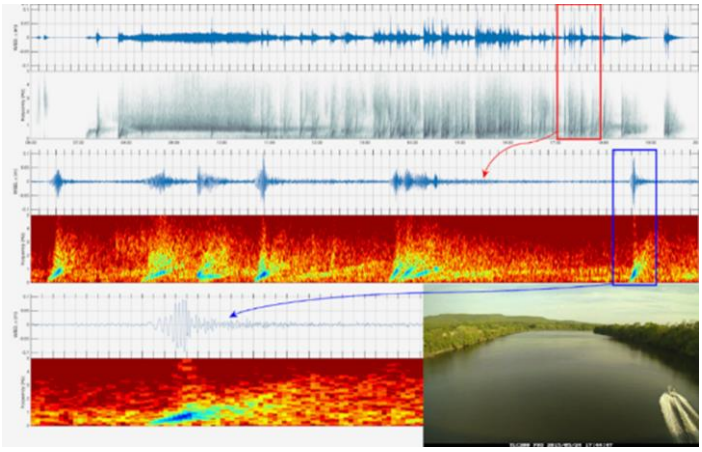

Figure 4.2.8.3-5: A Day-long Recording of the Wave Signal at WLOG-2 and its Spectrogram

4.2.8.4 Summary of Analysis Procedures for the Wave-Logger Data

Important steps of the boat-detection algorithm are summarized below:

- Separate the water-surface fluctuations, $h(t)$, and mean water level, z(t), from the water-level row signal with a low pass IRR filter.
- Apply windowed Fourier transform to find the spectrogram $S(t, f)$ using Hamming window of size 512 and 75% overlap. The windows are 17s long and 4.3s apart, center-to-center.
- Find the mean spectral density, $\bar{S}(t)$, in the low frequency band 0.05Hz-0.8Hz. Most of the wind-generated waves are left on the high-frequency side of this range.
- Remove low-frequency modulations $\bar{S}(t)$ in using a third-order Savitzky-Golay filter.
- Find the peaks and their locations (tpeak) in the filtered $\bar{S}(t)$ time-series. The locations are defined as the window centers.
- Filter the high frequency components in the water-surface fluctuations $h(t)$ with a low pass IRR filter and isolate waves in the frequency range of 0.1Hz - 2.5 Hz,
- Apply zero-crossing analysis and calculate the wave height H(t) and wave period T(t) time series,
- Calculate the spectral estimate for the significant wave height Hm0 using the equations 1 and 2.
- Find the peak zero-crossing wave heights H_{max} and wave periods T_{max}, nearest to tpeak.
- Compare the results with the time-lapse videos and remove the falsely detected boats.

The analysis with the steps summarized above was automated except for the final step in which the detected boat waves were compared with the time-lapse videos. The procedure was applied to the collected data to calculate boat-traffic statistics and the wave properties at each logger. In Figures 4.2.8.4-1 through 4.2.8.4-3, the analytic results are plotted for each site for selected days. Each figure consists of three plots: the one on top is the mean-water depth and water-surface elevation (NAVD88, US Feet) on the secondary axis, the middle plot is the water-surface displacement, significant wave height, the zero-crossing wave amplitude, and the temperature (secondary axis), and the bottom plot is the spectrogram, which shows the spectral energy, frequency and time relationship.

The 24-hour long data in Figure 4.2.8.4-1a was recorded at WLOG1 on June 13, 2015. The identified boats are marked with red on both the water-surface displacement plot and the spectrogram. 56 boat passes were recorded throughout that day. The temperature recorded inside the wave logger housing was usually overestimated during daylight hours, however, it is still included in the figures to show relative change. Darker areas in the spectrogram for frequency >~1.5Hz indicate low-energy, wind-generated waves, smoothly distributed in time and in the high-frequency area of the frequency axis. Figure 4.2.8.4-1b shows the results on June 14, 2015. 50 boats were detected on this day, but no wind waves are visible in the spectrogram. High-energy boat waves are discontinuous and spread across a wide range of frequencies. Wave height for the boat waves were mostly 3-4 times higher than that of the wind generated waves, which translates to an order of magnitude difference in their energies.

Wave data on June 8th (Monday) between 6 am and 9 pm, at WLOG2 is plotted in Figure 4.2.8.4-2a. No boats were recorded throughout the day. The source of waves was the wind, which can be seen in the spectrogram. Due to the sustained wind, the wave spectrogram peaked around 0.5Hz frequency. This was one of the few days that wind waves reach the energy level in the figure, yet the wave height was still around 5 cm - 6 cm. Near the Rt. 10 Bridge, where the WLOG2 site was located, the river widens as much as 300 m and the fetch length can be as long as 800 m depending on the wind direction. Both sides of the river are nearly flat and lack woody vegetation (Figure 4.2.8.4-4). Therefore, among all three wave-monitoring locations, the WLOG2 site is expected to have the highest wind-generated waves. Wave data for another windy day, July 15th (Saturday) near the Rt. 10 Bridge is shown in Figure 4.2.8.4-2b. Boat waves are separated from the wind waves with their relatively high energy content and leading low-frequency wave in the wave group.

Two examples for WLOG3 data near the French King Bridge are plotted in Figure 4.2.8.4-3. The first set of plots (Figure 4.2.8.4-3a) corresponds to June 28th, the second set (Figure 4.2.8.4-3b) corresponds to June 14th. Inspecting the spectrogram for these two days, the number of boats on June 28th was far less than the number of boats on June 14th, and June 28th was relatively windy. Even though both days were Sundays, time-lapse video data reveals that June 28th was a rainy day, which can be seen in Figure 4.2.8.4-5. The significance of rainy days in the analysis of boat-traffic statistics is explained in the following sections.

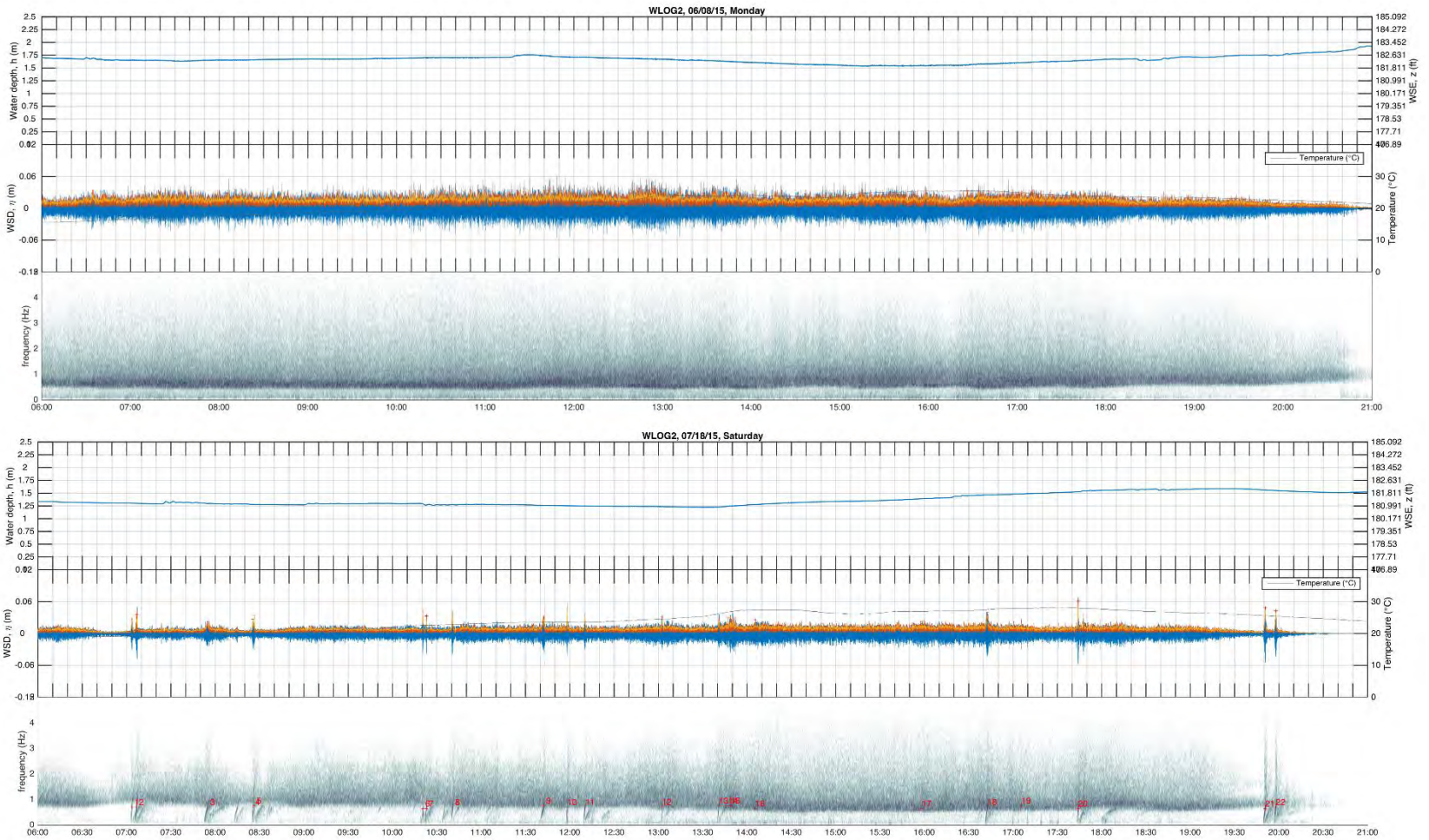

Figure 4.2.8.4-1 Wave data analysis summary for WLOG-1

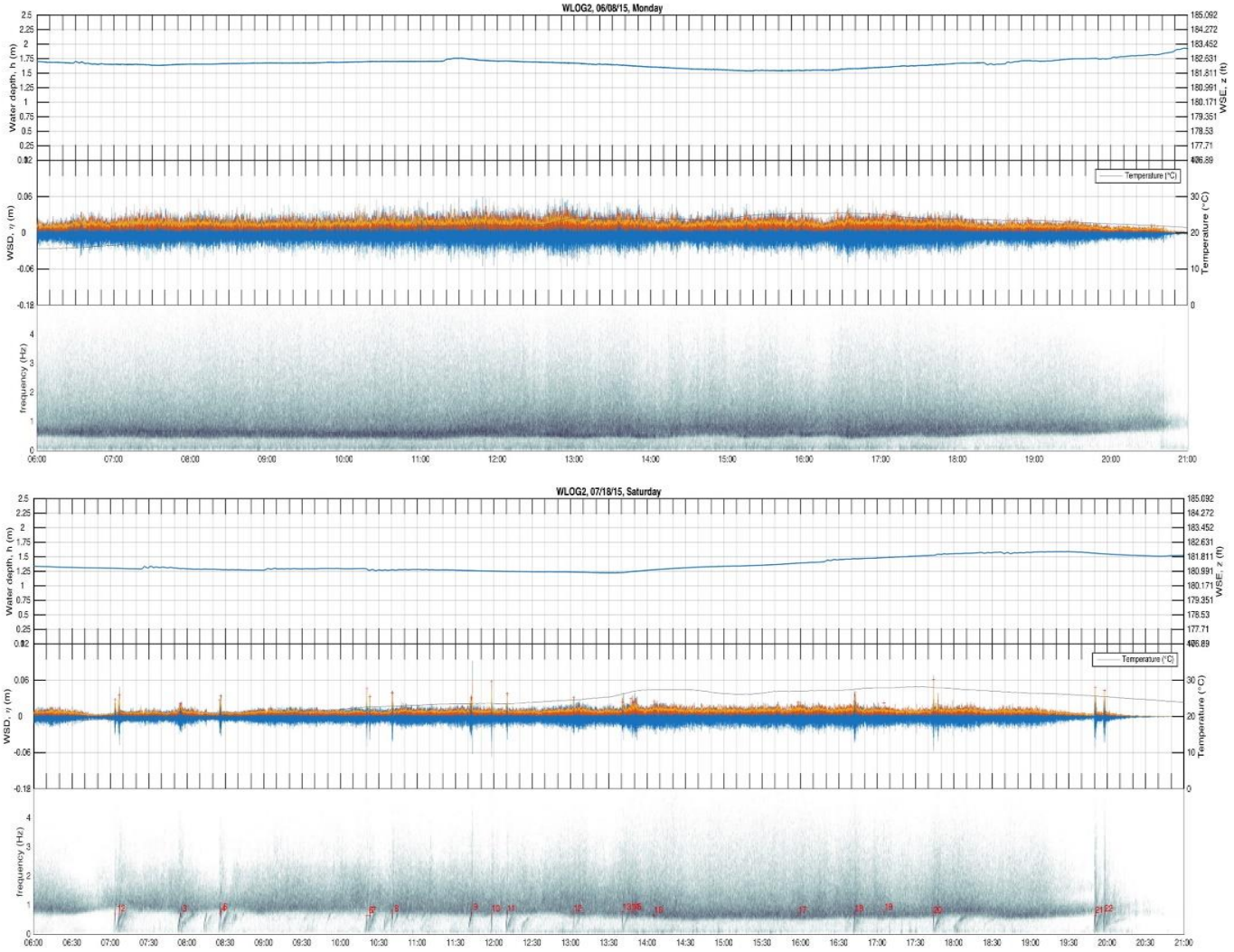

Figure 4.2.8.4-2 Wave Data Analysis Summary for WLOG-2 (a – top group, b – bottom group)

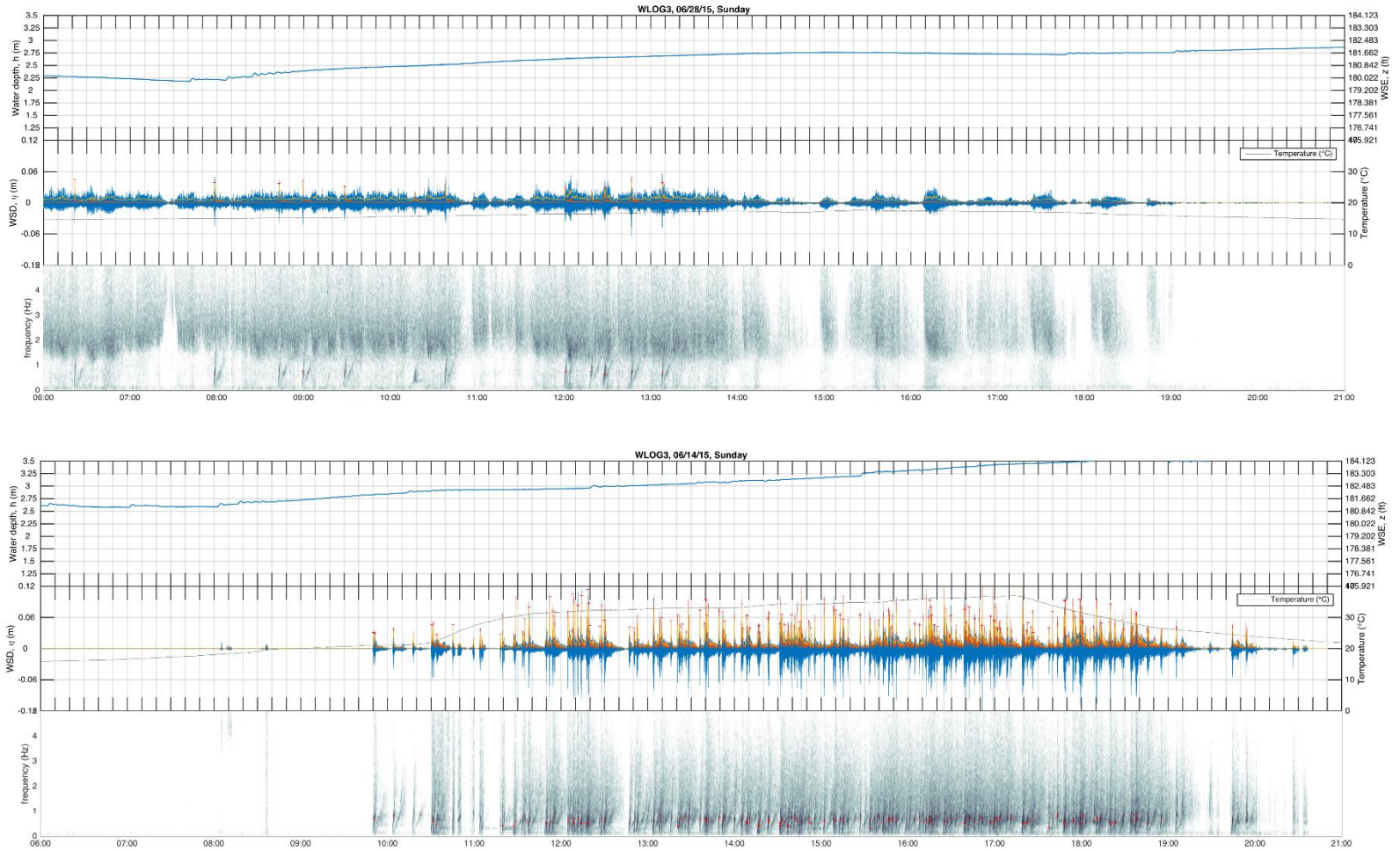

Figure 4.2.8.4-3 Wave data analysis summary for WLOG3 (a – top group, b – bottom group)

Figure 4.2.8.4-4: Rt. 10 Bridge Site CAM2 View and Aerial View (Google)

Figure 4.2.8.4-5: Comparison of Dry and Rainy Sundays: a View from the French King Bridge

4.2.8.5 Results of Boat and Wave Statistics

The total number of boats estimated from the wave-logger data analysis is listed in Table 4.2.8.5-1. 12,148 boating events were recorded at three sites during the 117-days of data collection (WLOG3 and WLOG4 data is averaged). The WLOG3 and WLOG4 site near the French King Bridge had the busiest boat traffic compared to the other two locations. This is possibly because the site is closer to the boat ramps and small marinas around the Turner Falls, MA area. It's also attractive to tourism and recreation for its scenic views.

The daily number of boats (daily traffic) at each wave logger site along with the rainy days (obtained from the recorded videos) are listed in Table 4.2.8.5-2. Figure 4.2.8.5-1 illustrates the daily distribution of the boat traffic during data-collection period. Green bars indicate dry days and blue bars indicate rainy days. Sundays and holidays are highlighted with dark green or blue. Daily- maximum and daily-minimum temperatures are also plotted in the same figures. The analysis results show that the weekend traffic can exceed 200 boats for some days. Weekends, especially Sundays, have significantly higher daily traffic then that of the weekdays. Boat traffic drops drastically during rainy days regardless of the day of the week. There is no noticeable trend between the months; nevertheless, the traffic is relatively low in June, which may be due to relatively frequent rainy days. In summary, the results show that the daily traffic depends primarily on the day of the week, precipitation or weather conditions, and location along the river.

Mean-daily traffic for each day of the week is listed for the entire dataset in Table 4.2.8.5-3, and for only dry days in Table 4.2.8.5-4. Figure 4.2.8.5-2 shows the bar charts for the same data. The highest traffic is on Sunday at all of the sites. The lowest mean traffic flow rate is during the weekdays, Monday to Thursday (MTWT). The traffic flow rate begins increasing on Friday and peaks on Saturday on dry days. The French King Bridge site has the highest mean-daily traffic with up to 180 boats per day on dry Sundays.

Rain dramatically affects the boat traffic flow, regardless of the location. In Figure 4.2.8.5-3 rainy days and dry days are compared for Sunday and weekdays (MTWT). Error bars are the standard deviations. The mean traffic flow can drop as low as 10% if it rains on Sundays and 20% on a weekday. The uncertainty of the average traffic flow is higher on weekdays because of the limited number of boating events. These ratios are similar at all three sites.

Figure 4.2.8.5-4 shows the hour-of-the-day distribution of the average boat traffic. The traffic. The chart is based on the entire dataset. The highest frequency of boats was observed between noon and 8 pm, peaking around 2 pm. Hourly peak-traffic flow rate ranged between 2.5 and 8. The WLOG3 and WLOG4 site shows double peaks, which is because the traffic peaked at different times for each direction of traffic flow. Upstream traffic peaked around 2 pm while downstream traffic peaked around 5 pm.

The distribution of the wave parameters H_{max} and T_{max}, and the water depth, h is shown in Figures 4.2.8.5-5 through 4.2.8.5-7. Various probability-distribution models are fitted to these histograms. The average maximum wave height was around 7 to 8 cm and the average wave period was approximately 1.4 s. Both wave-height and wave-period histograms are skewed to the left. Mean wave height and time-lapse video analysis revealed that the majority of the boat traffic consists of 6 m to 9 m-long high-speed recreational vessels moving at supercritical speeds.

Table 4.2.8.5-1: Total Measured Number of Boats

Wave Logger	Location	Dates	Number of Boats
WLOG-1	Schell Bridge	May 21 – Aug 28	2,133
WLOG-2	Rt. 10 Bridge	May 21 – Sep 14	2,650
WLOG-3	French King Bridge	May 21 – Sep 14	7,365
WLOG-4	French King Bridge	May 21 – Sep 14	7,263

Table 4.2.8.5-2: Number of Boats Recorded for Each Day of the Sampling Period at the Four Wave Loggers

Date	WLOG-1		WLOG-2		WLOG-3		WLOG-4	
	N	Rain	N	Rain	N	Rain	N	Rain
21-May-15	2		3		5		4	
22-May-15	15		12		23		21	
23-May-15	19		7		39		39	
24-May-15	91		77		173		173	
25-May-15	32		26		50		51	
26-May-15	5		6		13		13	
27-May-15	9		3		15		15	
28-May-15	4		3		9		10	
29-May-15	24		24		72		69	
30-May-15	67		41		141		142	
31-May-15	7	1	6	1	17	1	17	1
1-Jun-15	2	1	0	1	2	1	2	1
2-Jun-15	0	1	2	1	6	1	6	1
3-Jun-15	1		1		8		8	
4-Jun-15	6		4		10		10	
5-Jun-15	8		15		37		37	
6-Jun-15	12		16		48		49	
7-Jun-15	38		46		139		142	
8-Jun-15	7		0		1		1	
9-Jun-15	5		4		12		12	
10-Jun-15	30		12		29		29	
11-Jun-15	14		13		29		30	
12-Jun-15	15		17		43		39	
13-Jun-15	56		19		97		100	
14-Jun-15	50		98		190		201	
15-Jun-15	2	1	0	1	0	1	0	1
16-Jun-15	2		1		3		3	
17-Jun-15	22		14		20		20	
18-Jun-15	9		6		17		17	
19-Jun-15	15		18		75		74	
20-Jun-15	30		39		115		113	

Date	WLOG-1		WLOG-2		WLOG-3		WLOG-4	
	N	Rain	N	Rain	N	Rain	N	Rain
21-Jun-15	10	1	6	1	34	1	36	1
22-Jun-15	14		12		45		46	
23-Jun-15	3		0		5		6	
24-Jun-15	0		1		20		15	
25-Jun-15	18		19		32		32	
26-Jun-15	23	1	21	1	48	1	43	1
27-Jun-15	32		36		87		87	
28-Jun-15	0	1	14	1	12	1	13	1
29-Jun-15	5		2		10		10	
30-Jun-15	9	1	4	1	14	1	14	1
1-Jul-15	2	1	0	1	5	1	5	1
2-Jul-15	11		13		37		39	
3-Jul-15	59		46		152		147	
4-Jul-15	12	1	11	1	35	1	34	1
5-Jul-15	80		107		239		235	
6-Jul-15	22		22		72		66	
7-Jul-15	5		6		10		10	
8-Jul-15	1		4		21		23	
9-Jul-15	16		18		37		37	
10-Jul-15	37		37		83		82	
11-Jul-15	59		62		161		165	
12-Jul-15	79		93		226		222	
13-Jul-15	5		9		27		23	
14-Jul-15	7		1		2		2	
15-Jul-15	7		3		23		24	
16-Jul-15	28		13		51		52	
17-Jul-15	29		28		85		84	
18-Jul-15	30		18		51		53	
19-Jul-15	76		94		205		206	
20-Jul-15	24		19		55		50	
21-Jul-15	20		18		42		43	
22-Jul-15	27		23		44		44	

Date	WLOG-1		WLOG-2		WLOG-3		WLOG-4	
	N	Rain	N	Rain	N	Rain	N	Rain
23-Jul-15	22		22		36		40	
24-Jul-15	29		11		56		56	
25-Jul-15	66		56		214		201	
26-Jul-15	69		42		77		72	
27-Jul-15	9		3		13		13	
28-Jul-15	11		17		30		26	
29-Jul-15	32		24		87		84	
30-Jul-15	0	1	3	1	12	1	12	1
31-Jul-15	36		36		96		98	
1-Aug-15	49		78		151		162	
2-Aug-15	94		71		180		181	
3-Aug-15	15		12		54		57	
4-Aug-15	3		4		22		22	
5-Aug-15	13		8		45		44	
6-Aug-15	16		16		46		42	
7-Aug-15	34		14		76		71	
8-Aug-15	25		41		172		170	
9-Aug-15	63		73		185		183	
10-Aug-15	17		15		42		42	
11-Aug-15	1	1	0	1	0	1	0	1
12-Aug-15	1		7		16		17	
13-Aug-15	13	1	14	1	61	1	51	1
14-Aug-15	10		21		76		61	
15-Aug-15	40		49		143		100	
16-Aug-15	67		116		212		207	
17-Aug-15	10		14		65		58	
18-Aug-15	1		13		54		50	
19-Aug-15	4		19		43		44	
20-Aug-15	1		2		21		24	
21-Aug-15	0	1	4	1	18	1	14	1
22-Aug-15	20		31		139		133	
23-Aug-15	1	1	7	1	38	1	35	1

Date	WLOG-1		WLOG-2		WLOG-3		WLOG-4	
	N	Rain	N	Rain	N	Rain	N	Rain
24-Aug-15	4		13		36		36	
25-Aug-15	0	1	0	1	2	1	1	1
26-Aug-15	1		4		25		24	
27-Aug-15	5		6		26		17	
28-Aug-15	2		16		62		64	
29-Aug-15			72		147		143	
30-Aug-15			53		198		204	
31-Aug-15			15		42		45	
1-Sep-15			12		42		47	
2-Sep-15			15		44		43	
3-Sep-15			6		21		21	
4-Sep-15			14		41		51	
5-Sep-15			67		191		192	
6-Sep-15			65		209		203	
7-Sep-15			75		196		202	
8-Sep-15			12		35		36	
9-Sep-15			15		41		46	
10-Sep-15			5		5		5	
11-Sep-15			11		22		21	
12-Sep-15			36		83		86	
13-Sep-15		1	2	1	7	1	8	1
14-Sep-15			0		2		3	
TOTAL	**2,133**		**2,175**		**6,039**		**5,907**	

Table 4.2.8.5-3: Daily Average Number of Boats: Rainy and Dry Days

	Monday	Tuesday	Wednesday	Thursday	Friday	Saturday	Sunday
WLOG-1	12.0	5.1	10.7	11.0	22.4	36.9	51.8
WLOG-2	13.9	6.3	9.6	9.8	20.3	39.9	57.1
WLOG-3	41.9	18.3	30.4	26.8	62.6	118.5	137.7
WLOG-4	41.5	18.2	30.3	26.1	60.7	115.8	137.5

Table 4.2.8.5-4: Daily Average Number of Boats: Dry Days Only

	Monday	Tuesday	Wednesday	Thursday	Friday	Saturday	Sunday
WLOG-1	13.7	6.3	11.4	11.7	24.1	38.8	70.7
WLOG-2	11.6	8.0	10.2	9.9	21.3	41.8	77.9
WLOG-3	36.7	23.4	32.1	25.5	66.6	123.7	186.1
WLOG-4	35.8	23.4	32.0	25.3	65.0	120.9	185.8

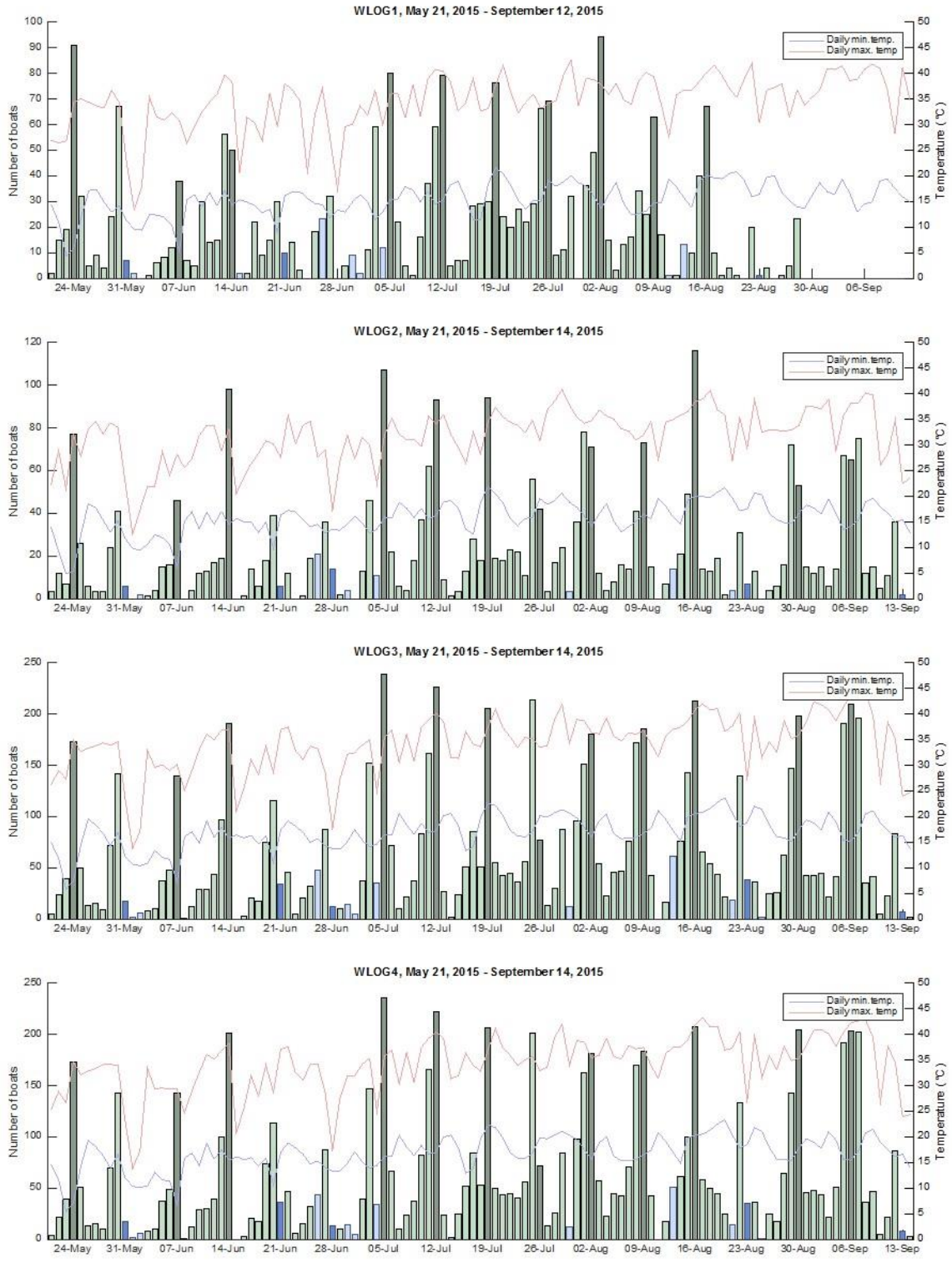

Figure 4.2.8.5-1: Boat Traffic Statistics Between May 21st and Sep 14th

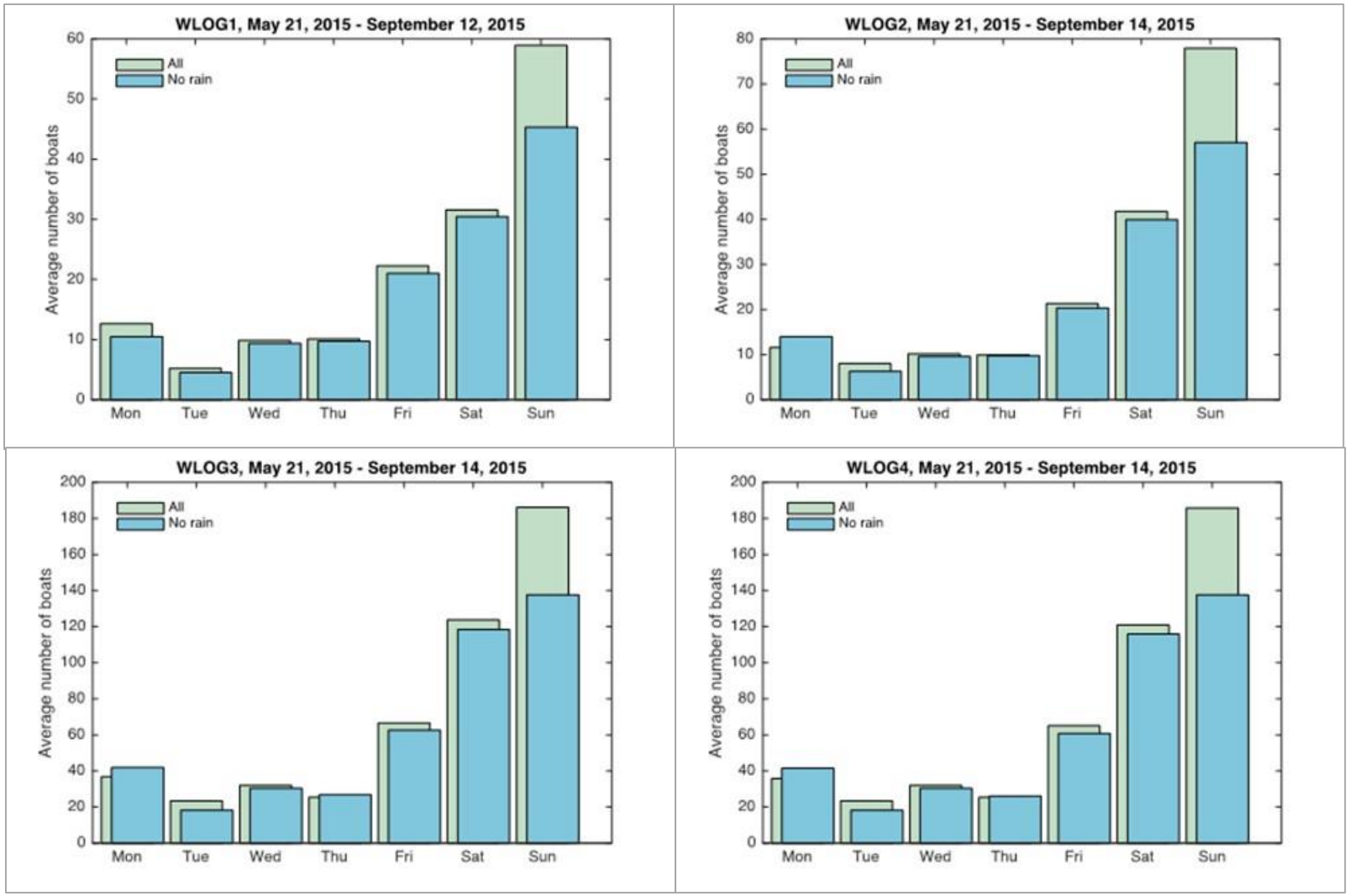

Figure 4.2.8.5-2: Day-of-the-week Boat Traffic Mean Flow: Dry and Rainy Days

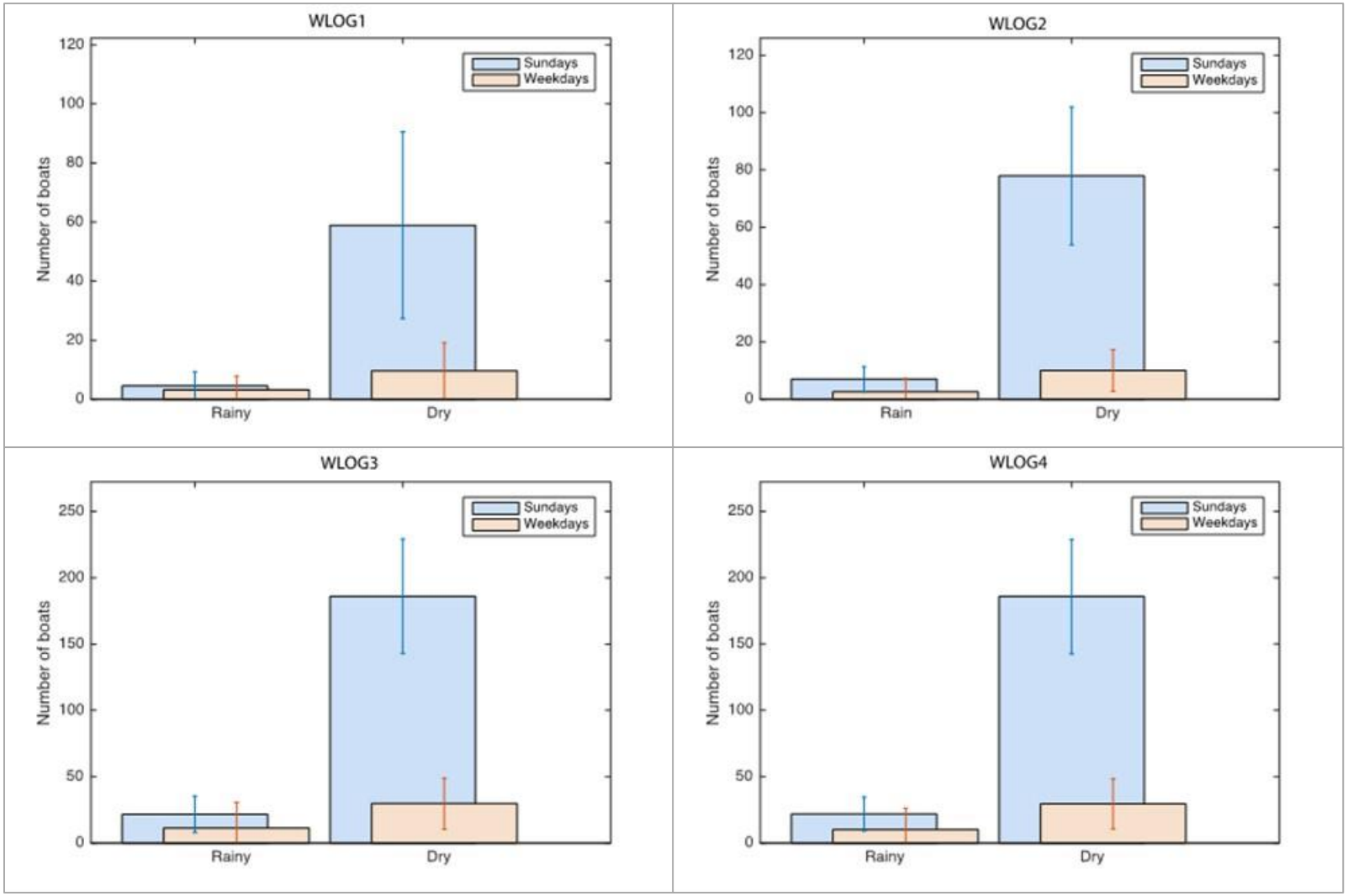

Figure 4.2.8.5-3: Average Rainy and Dry Day Boat Traffic Flow: Sundays and Weekdays

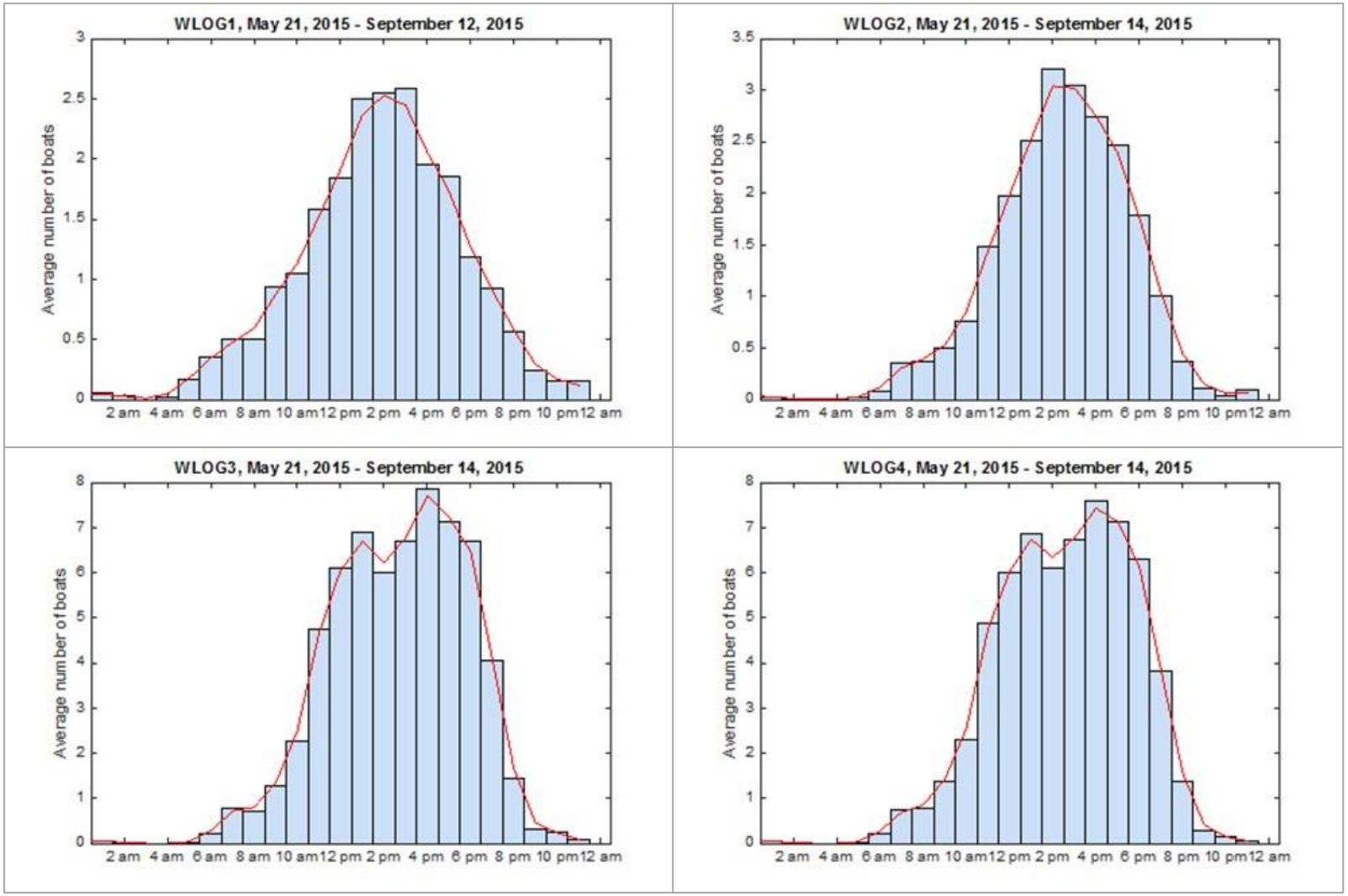

Figure 4.2.8.5-4: Hourly Distribution of the Boat Traffic Flow

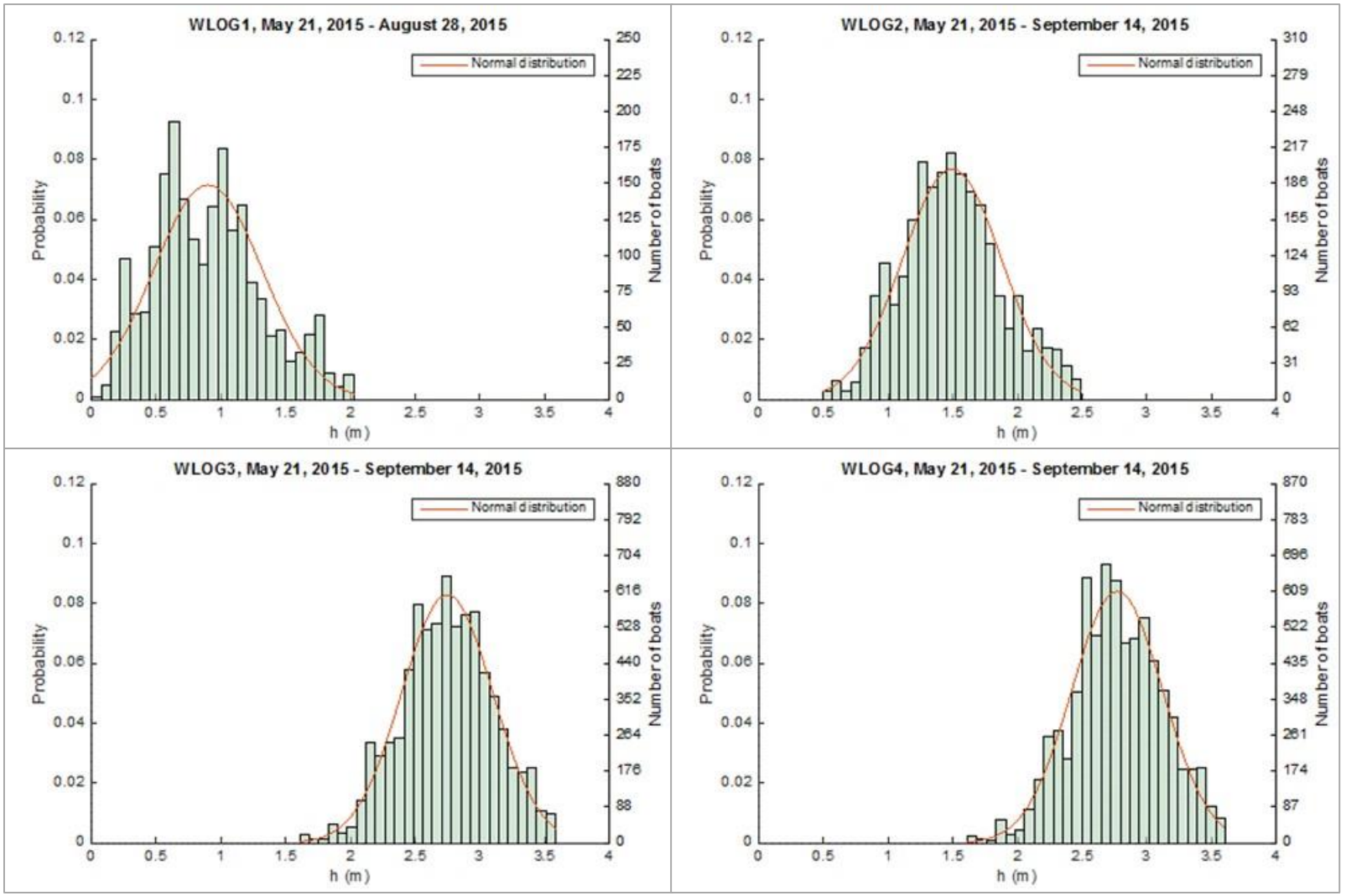

Figure 4.2.8.5-5: Water Depth Distribution

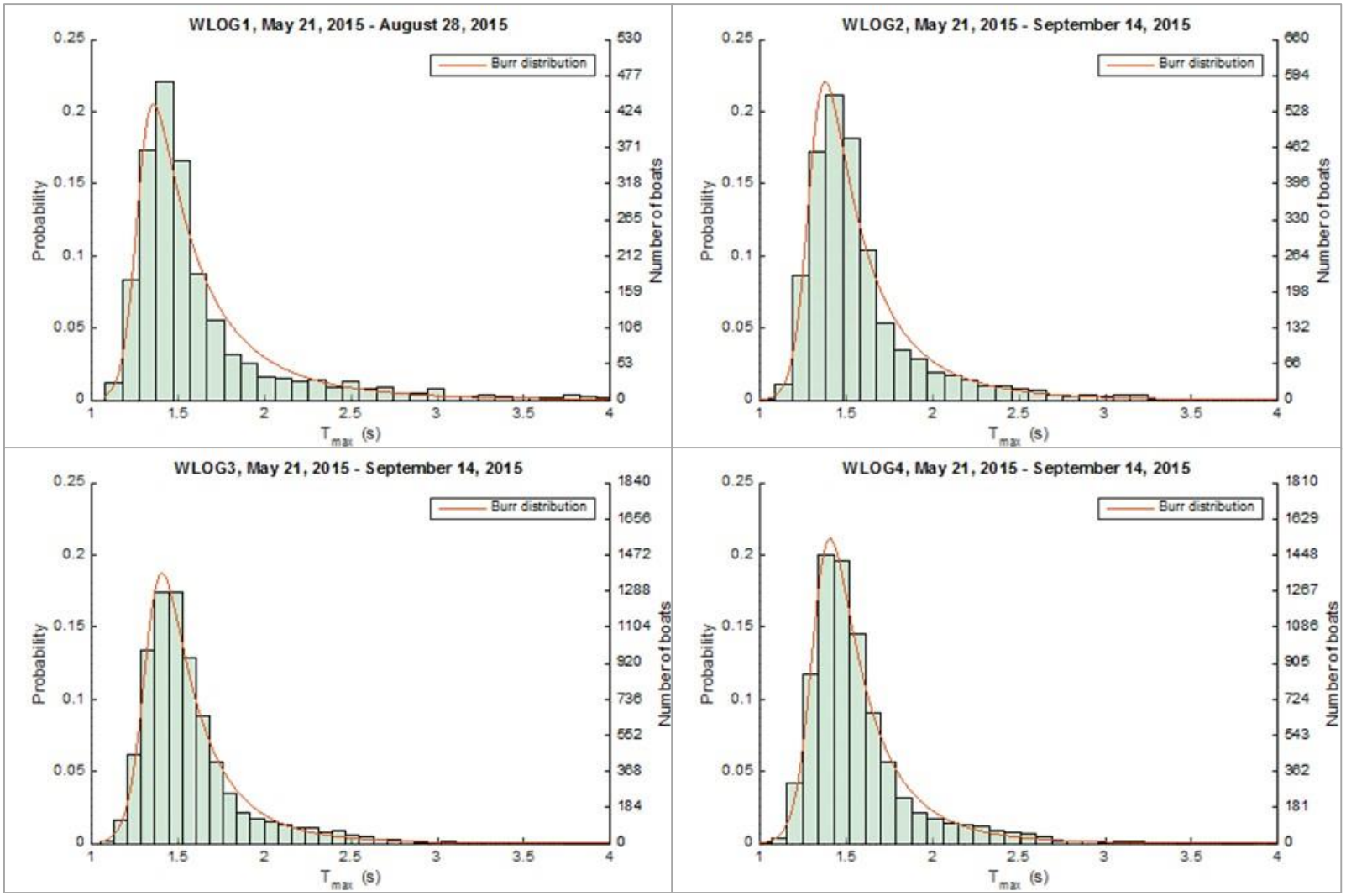

Figure 4.2.8.5-6: Maximum Wave Period Distribution

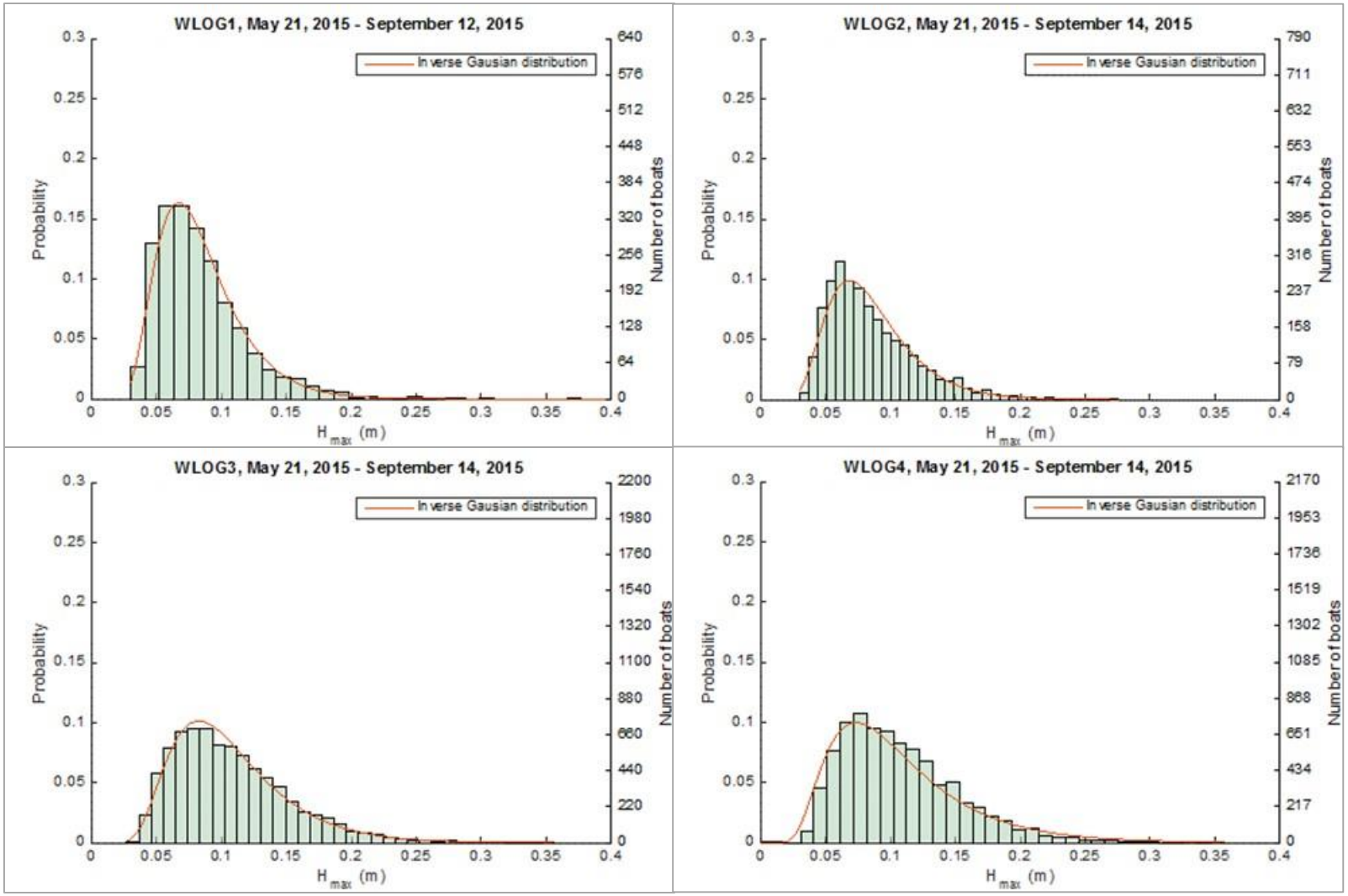

Figure 4.2.8.5-7: Wave Height Distribution

4.2.8.6 Temporal and Spatial Extrapolation of Boat-Traffic Data

Estimation of the relative contribution of boat waves to streambank erosion requires knowledge of the spatial and temporal distribution of instances of boat passage and the properties of the generated waves during each passage. Despite their substantial impact, the availability of historic boat-wave data was extremely limited for hydraulic and bank-erosion modeling. Currently, the BSTEM wave model uses maximum wave height, H_{max} and the wave period, Tmax associated with H_{max} to estimate the hydraulic erosion due to waves. Long-term BSTEM simulations required prediction of wave-traffic statistics and boat-generated wave properties by spatial and temporal extrapolations. The analysis described here includes development of methods to estimate the wave parameters, H_{max} and T_{max} at 20 locations (25 sites – five locations have right and left banks) longitudinally along the river over the 15-year period, and generation of input datasets for BSTEM using these distributions. A 15-year, hourly dataset was developed by combining measured daily and weekly variations of boat traffic, together with information on seasonal variations, boat ownership statistics and historic rainfall data obtained from various sources.

Methods and Results

As part of boat-generated, wave-measurement study, four wave loggers recorded wave data at three sites along the TFI. Boat traffic and boat-generated waves were continuously recorded at 30Hz between May 22, 2015 and September 14, 2015 (sample period). Analysis of the recorded data revealed boat-induced waves and their properties at each site. The generated data was used to extract boat-wave statistics including daily and hourly distribution of the number of boat passes, as well as water level, wave height (H_{max}) and wave period (T_{max}) histograms which can be used as input into the BSTEM boat wave model for boat-generated wave erosion prediction. The available data were used to predict historical boat traffic during the 15-year period between January 1st, 2000 and December 31st 2014.

Temporal Extrapolation

The majority of the boats observed during the field monitoring were recreational boats. Time lapse videos at the three sites indicated that over 90% of the recorded boat passes were recreational boats of sizes less then 25ft long. Consequently, the boat traffic in the area strongly depends on the day of the week as well as the weather conditions. Analysis of the collected data and personal communications with local boat owners in the area supports this conclusion. The results presented in the previous section show that the number of boats per day (daily traffic flow, or daily traffic) observed during a weekday was 10%-20% of the daily flow on a Sunday. Daily flow was reduced to as low as 20% during rainy days. Recreational traffic also varies seasonally mainly due to the weather conditions and restrictions during off-season. Even though the measurement period wasn't long enough to see the long-term trends in the boat traffic, it's still possible to estimate yearly and decadal trends from other sources. The measured boat-wave statistics data were supplemented by historic climate and boat-ownership data to generate a 15-year boat-generated wave data for BSTEM-Dynamic 2.3.

Here, a simple partially deterministic model is used to calculate daily traffic (N) by introducing a series of coefficients that modifies an ideal value for daily traffic (N_0).

$$N = c_1 c_2 c_3 c_4 N_0 \tag{3}$$

Or

$$N = C N_0 \tag{4}$$

where

$$C = c_1 c_2 c_3 c_4 \quad (5)$$

In this model N_0 is the number of boats per day during an ideal day, which is defined as a dry Sunday during high season. The N_0 value is calculated by averaging the number of boats observed on the 'sunny' Sundays between Memorial Day (May 25th, 2015) and Labor Day (September 7th, 2015). Since each wave logger produced a separate traffic dataset, a unique N_0 value is calculated for each wave logger site. N_0 values for the wave logger sites are listed in Table 4.2.8.6-1.

The coefficients c_1, c_2, c_3 and c_4 are assumed to be independent and their product C for each site is the ratio of the daily boat traffic flow on a given day relative to that of the ideal day. The coefficients are defined as follows:

c_1: Rainy-day coefficient ($0 < c_1 < 1$). Reduces the number of boats by a factor if it is a rainy day. If most of the daytime hours were cloudy and noticeable precipitation was observed during this period, then the day was considered as a "rainy day". Rainy days were manually identified using the time-lapse recording. Each day in the sample period was identified as rainy or dry to assign a value for c_1 of unity (1.0) for dry days whereas it takes different values for weekdays and weekends and for each wave logger (Table 4.2.8.6-2). Daily- rainfall data for Amherst, MA was used to calculate c_1 for the simulation period (source: NOAA National Climatic Data Center Asheville NC).

c_2: Day of the week coefficient ($0 < c_2 < 1$). This coefficient reduces the number of boats for each day of the week based of the weekday distribution during the sample period. Only dry days were used during averaging (Table 4.2.8.6-3).

$$c_2 = N_{day} / N_{Sunday,dry} \quad (6)$$

c_2 coefficient for holidays (Labor Day, Independence Day etc.) is changed to unity regardless of the day of the week they fall on.

c_3: Month of the year coefficient ($0 < c_3 < 1$). Reduces the number of boats based on the month of the year. Monthly distribution of total boating hours in the United States in 2001-2002 was used to calculate this coefficient (Note – while this is a distribution for the United States it is only being used to determine the coefficient that is being applied to the measured data. The data collected from the TFI is actual use from Memorial Day to Labor Day and it correlates closely with the distribution being applied). Figure 4.2.8.6-1 shows the number of people boating and number of hours in the water in the United States. Rearranging the months, a normal distribution can be obtained in Figure 4.2.8.6-2. c_3 was assumed to be unity (1.0) around the peak, for the months June, July, and August and the remaining moths were calculated based on this distribution.

$$c_3 = \frac{P_{month}}{(P_{June} + P_{July} + P_{August})/3} \quad \text{(P is persons boating)} \quad (7)$$

c_4: Year coefficient ($c4 > 0$). The coefficient is calculated for each year between 2000 and 2014 using historic variations in the boat ownership in the United States. It was assumed that the variation in the boat traffic follows the same trend with the boat ownership variations. Based on the trend depicted in Figure 4.2.8.6-3, a linear decline in the boat ownership was used to calculate c_4 for the year between 2000 and 2008. c_4 was assumed to be unity (1.0) for the years 2009 to 2014 (Table 4.2.8.6-4).

Table 4.2.8.6-5 shows a sample list of coefficients and the bar chart in Figure 4.2.8.6-4 shows the complete list of *C* values for the simulation period. Each day between 1/1/2000 and 12/31/2014 has a *C* coefficient,

which is multiplied by N_0 (for each site) to determine the number of boat passes for a given day (k) and at a given site (j). The procedure described above is deterministic; hence, the N values will be identical for the same C coefficients. In reality, daily traffic flow can vary due to various reasons that are not considered in the simulation. These uncertainties are introduced by adding a Gaussian noise in the daily traffic flow of the ideal day.

$$N_{0j}^{*} = N_{0j} + \frac{1}{4}\sigma_s \eta^k \tag{8}$$

where N_{0j}^{*k} is the number of boats on an ideal day for site j and σ_s is the standard deviation of the observed ideal days during the sampling period. Time series η^k is Gaussian random noise with zero mean and unit standard deviation (unit normal distribution). After adding the uncertainty, N_{0j}^{*k} varies in time and specific for each wave logger site.

Table 4.2.8.6-1: N_0 Values for Each Wave Logger

	Dates	Number of boats	N_0
WLOG-1	May 21 – Aug 28	2,133	70.7
WLOG-2	May 21 – Sep 14	2,650	81.7
WLOG-3	May 21 – Sep 14	7,365	182.6
WLOG-4	May 21 – Sep 14	7,263	182.2

Table 4.2.8.6-2: Rainy Day Coefficients

c_1	WLOG-1	WLOG-2	WLOG-3	WLOG-4
Weekday	0.210	0.130	0.186	0.192
Weekend	0.064	0.101	0.138	0.139

Table 4.2.8.6-3: Weekday Coefficients

c_2	WLOG-1	WLOG-2	WLOG-3	WLOG-4
Monday	0.19	0.15	0.21	0.21
Tuesday	0.08	0.08	0.10	0.10
Wednesday	0.16	0.12	0.17	0.17
Thursday	0.17	0.13	0.16	0.16
Friday	0.32	0.25	0.35	0.34
Saturday	0.55	0.46	0.66	0.64
Sunday	1.00	1.00	1.00	1.00

Table 4.2.8.6-4: Month Coefficient (c_3) and Year Coefficient (c_4)

Month	c_3
January	0.2
February	0.16
March	0.19
April	0.38
May	0.61
June	1.00
July	1.00
August	1.00
September	0.75
October	0.51
November	0.30
December	0.22

Year	c_4
2000	1.183
2001	1.167
2002	1.151
2003	1.135
2004	1.118
2005	1.102
2006	1.086
2007	1.070
2008	1.054
2009	1.000
2010	1.000
2011	1.000
2012	1.000
2013	1.000
2014	1.000

Table 4.2.8.6-5: A Sample Coefficients List

WLOG-4	c_1	c_2	c_3	c_4	C
08/24/06	1.000	0.159	1	1.086	0.172
08/25/06	0.139	0.336	1	1.086	0.051
08/26/06	0.139	0.639	1	1.086	0.096
08/27/06	1.000	1.000	1	1.086	1.086
08/28/06	0.192	0.207	1	1.086	0.043
08/29/06	1.000	0.096	1	1.086	0.104
08/30/06	0.192	0.165	1	1.086	0.034
08/31/06	1.000	0.159	1	1.086	0.172
09/01/06	1.000	0.336	0.75	1.086	0.273
09/02/06	1.000	0.639	0.75	1.086	0.521
09/03/06	0.139	1.000	0.75	1.086	0.113
09/04/06	0.139	1.000	0.75	1.086	0.113

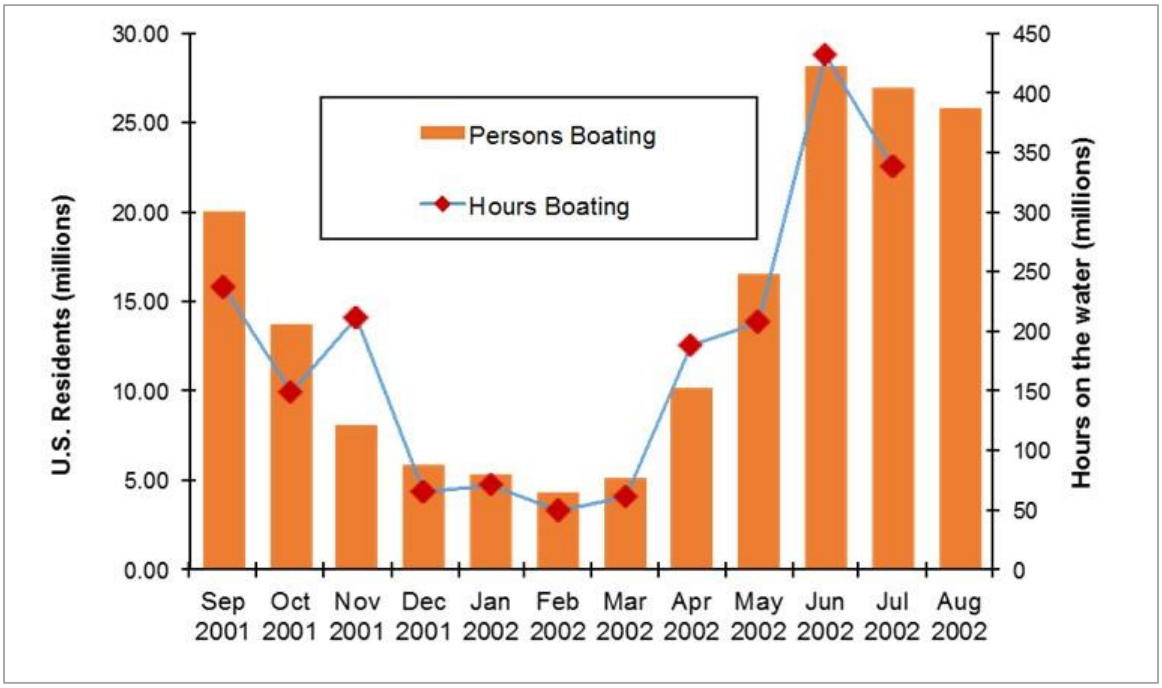

Figure 4.2.8.6-1: Monthly Distribution of Persons Boating and Hours of Boating in the United States

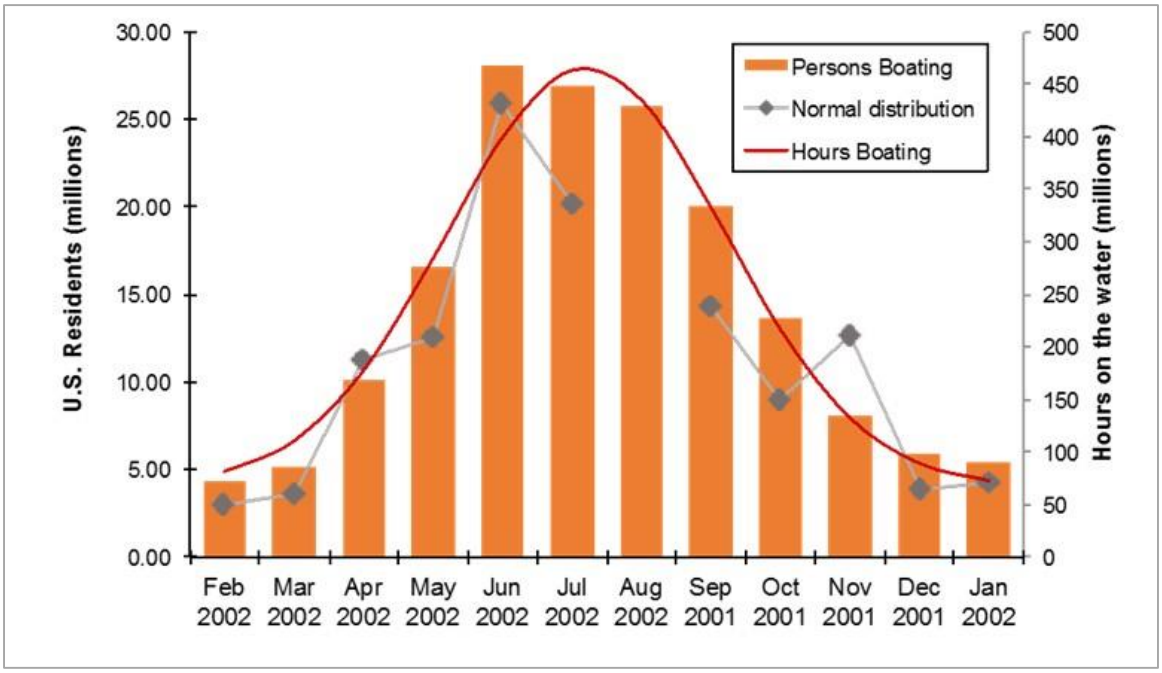

Figure 4.2.8.6-2: Monthly Distribution of Persons Boating and Hours of Boating in the United States; Rearranged

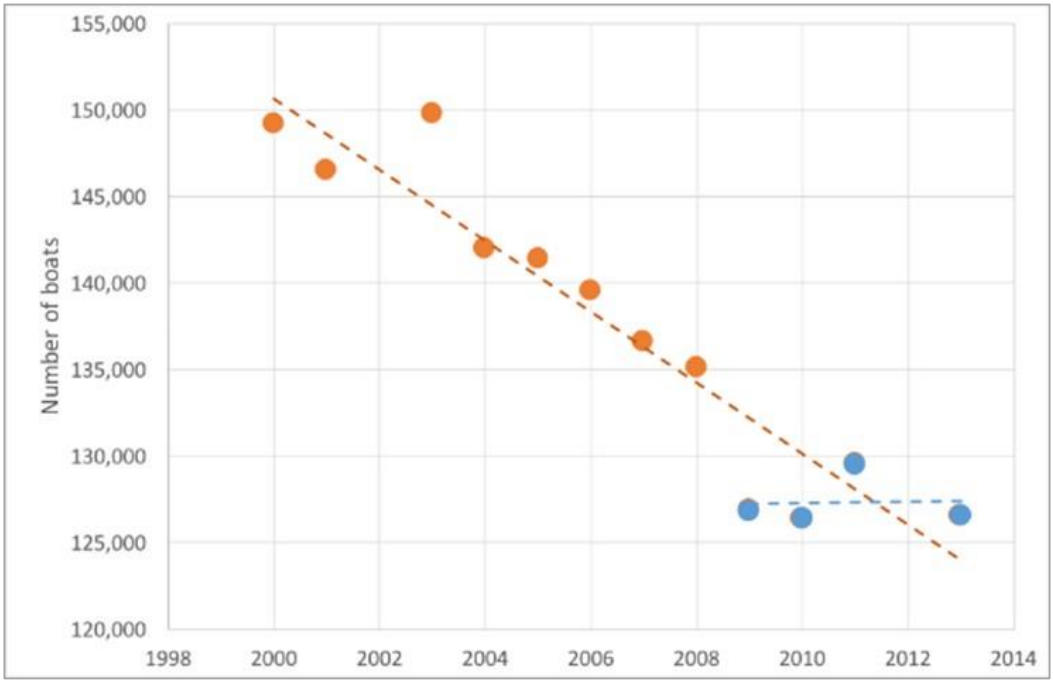

Figure 4.2.8.6-3: Historic Variations in Boat Ownership

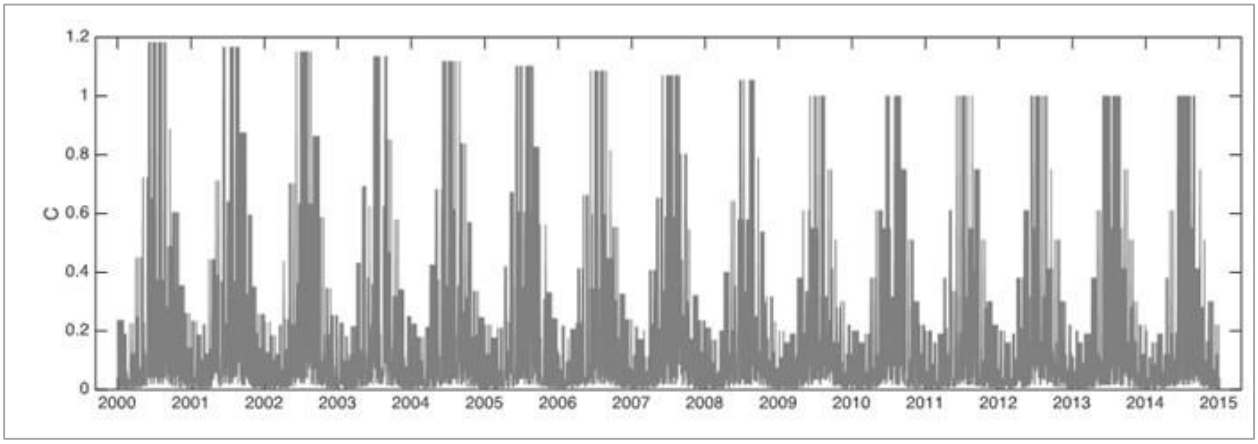

Figure 4.2.8.6-4: WLOG-4, Coefficient "C"

Spatial Interpolation

Boat traffic along the river varied as a function of boat-ramp access, site conditions etc. These differences were observed at the three wave-logger sites during data collection. Ideal-day boat counts (*N*) at 20 intermediate sites between WLOG-1 and WLOG-3 were interpolated by inverse distance weighting using the two nearest wave-logger sites. Upstream of WLOG-1 and downstream of WLOG-3, *N* is equal to the nearest wave logger measurement. With this procedure, seven sites upstream of WLOG-1 used the N_{WLOG1} and the three sites downstream of WLOG-3 used N_{WLOG4}. *N* for the remaining 10 sites was interpolated using the closest two wave-logger measurements. With the two-point interpolation, equation 8 is modified as:

$$N_j^k = round\left(W_A C_A^k N_{0A}^{*k} + W_B C_B^k N_{0B}^{*k}\right) \tag{9}$$

where *k* is the day index, *j* is the site index, W_A and W_B are the weights, C_A and C_B are the correction coefficients, and N_{0A} and N_{0B} are the ideal day daily traffic flow. *A* and *B* refer to the two wave-logger sites closes to site *j*. The weights W_A and W_B, and the wave- logger sites *A* and *B* for the interpolated sites, are listed in Table 4.2.8.6-6. The 20 locations (25 sites – five locations have right and left banks) where the 15-year daily simulated boat traffic was interpolated are shown in Figure 4.2.8.6-5 while the actual simulated results are shown in Figure 4.2.8.6-6.

Table 4.2.8.6-6: Inverse Distance Weights for the Simulation Sites

Site	$WLOG_A$	W_A	$WLOG_B$	W_B
11L	1	1	1	0
2L	1	1	1	0
303BL	1	1	1	0
18L	1	1	1	0
3L	1	1	1	0
21R	1	1	1	0
4L	1	0.951	2	0.049
29R	2	0.503	1	0.497
5CR	2	1	2	0
26R	2	0.779	3	0.221
10L	2	0.748	3	0.252
6AL	2	0.527	3	0.473
119BL	2	0.504	3	0.496
7L	3	0.603	2	0.397
8BL	3	0.748	2	0.252
87BL	3	0.809	2	0.191
75BL	3	0.924	2	0.076
12BL	3	1	3	0
9R	3	1	3	0
BC-1R	3	1	3	0

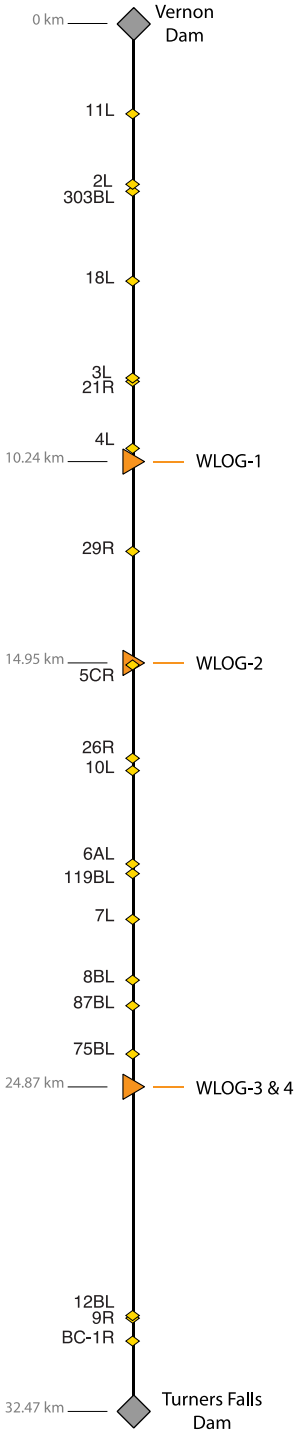

Figure 4.2.8.6-5: Simulation Sites Along the Study Reach

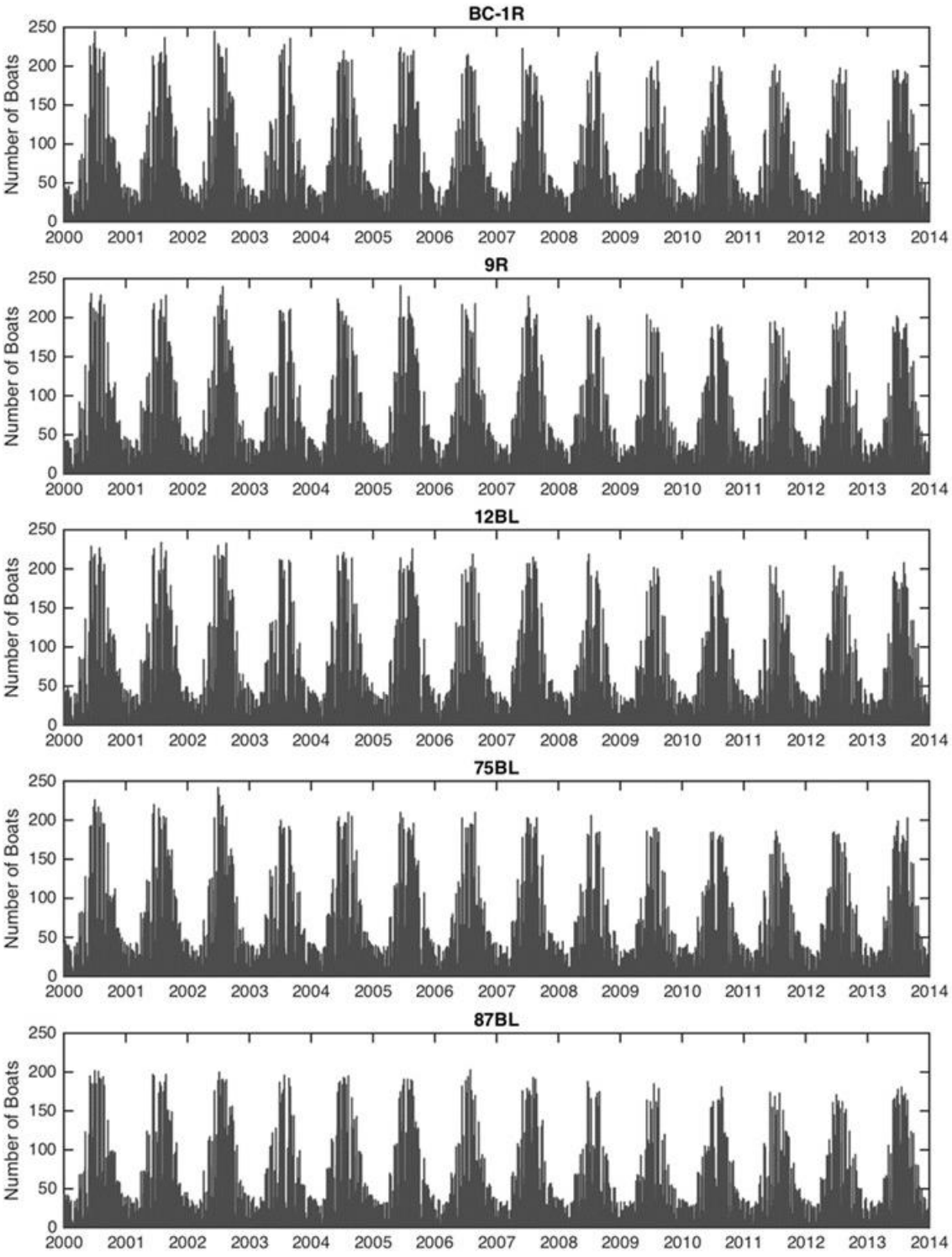

Figure 4.2.8.6-6: Simulated 15-year Daily Boat Traffic

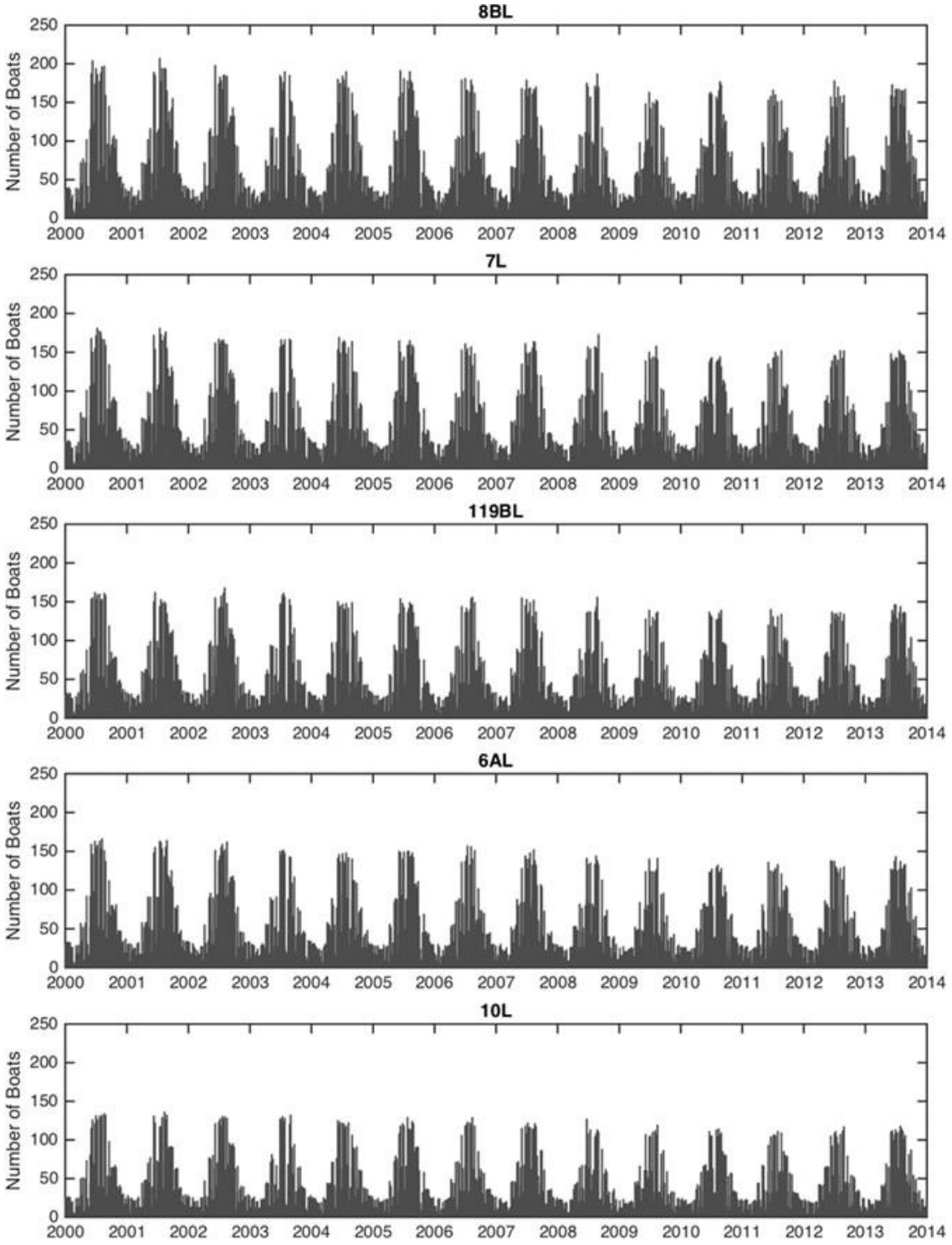

Figure 4.2.8.6-6: Simulated 15-year Daily Boat Traffic (cont.)

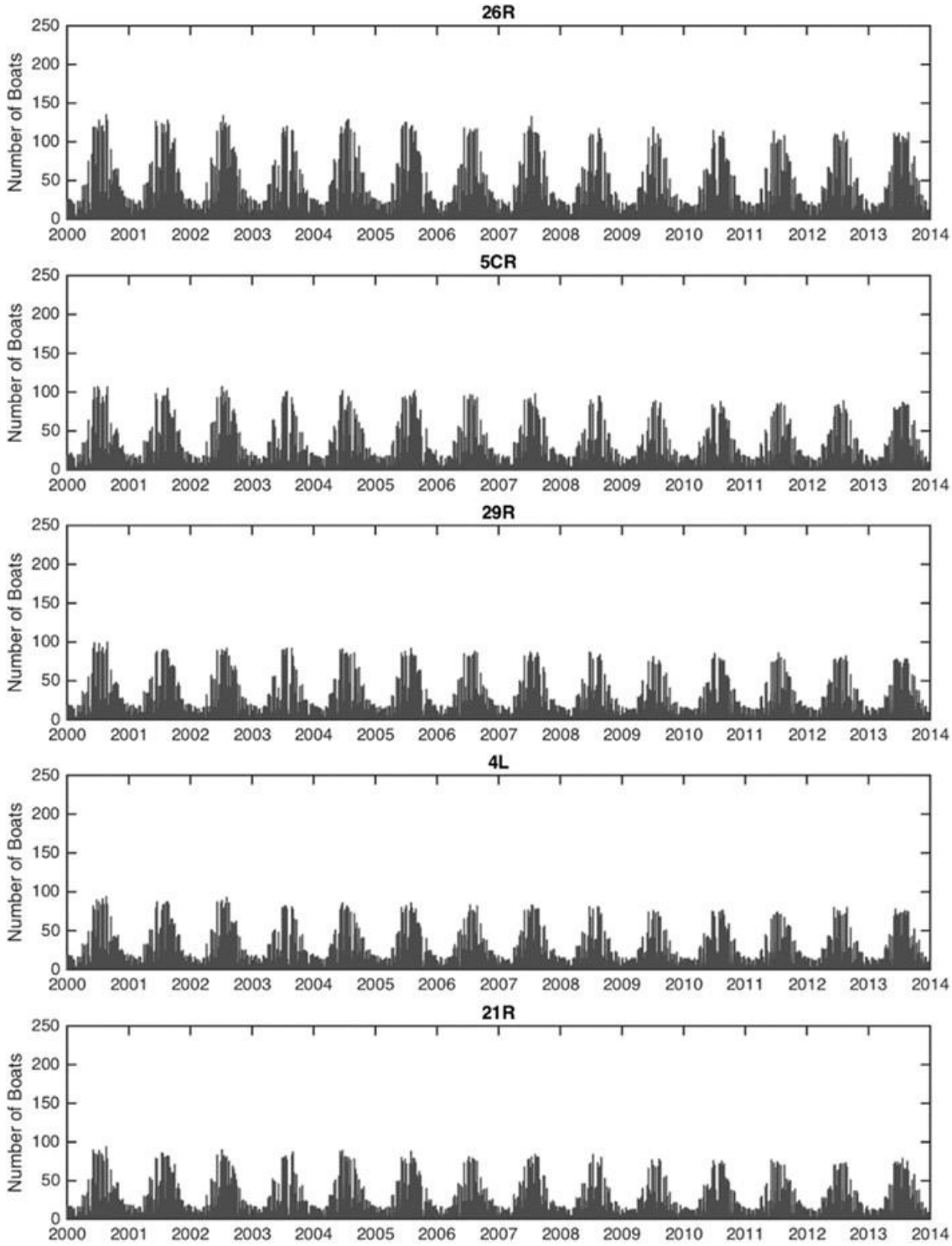

Figure 4.2.8.6-6: Simulated 15-year Daily Boat Traffic (cont.)

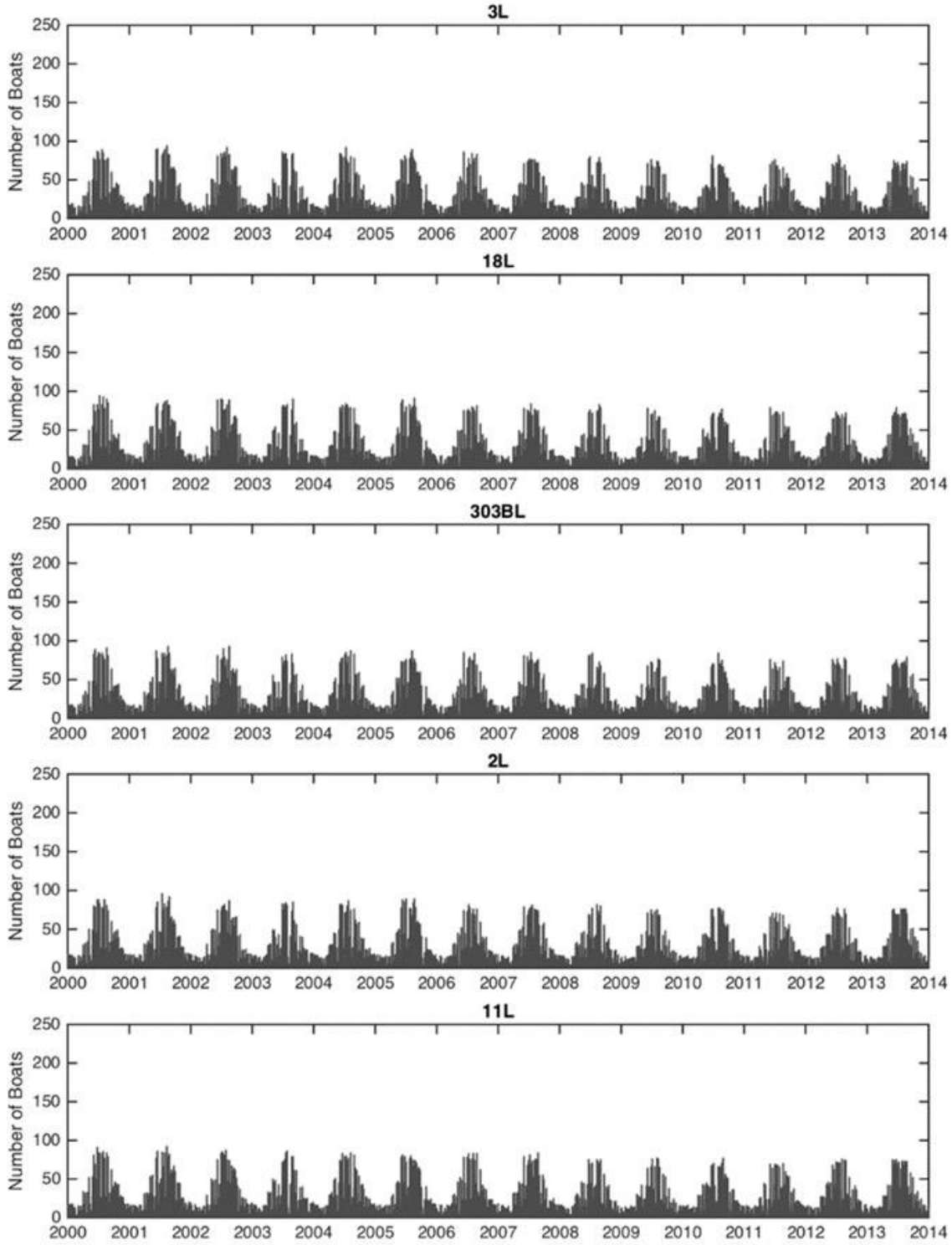

Figure 4.2.8.6-6: Simulated 15-year Daily Boat Traffic (cont.)

4.2.8.7 Distribution of the Daily Traffic

The previous section describes the temporal extrapolation and spatial interpolation methods used to calculate daily boat traffic at 20 locations (25 sites – five locations have right and left banks) for the 15-year simulation period. A table that includes the number of boats per day was obtained for 5,479 days at each site. The next step was to distribute the daily traffic throughout the day, using the measured, hourly volume of boat traffic (boats-per-hour, bph).

First, the hourly volumes of boat traffic at the wave-logger sites were normalized to calculate the average probability-density function (boat traffic hourly probability density function, *bPDF*) of the measured boat traffic. bPDF of the remaining 20 sites ($bPDF_j$) was interpolated using the measured *bPDF*'s ($bPMF_{WLOG}$). The interpolation was carried out using the same inverse distance weights, W_A and W_B, given in the previous section:

$$bPDF_j(t_h) = W_A \times bPDF_A(t_h) + W_B \times bPDF_B(t_h) \quad (10)$$

where, t_h indicates the hour of the day. This procedure is illustrated in Figure 4.2.8.7-1 $bPDF_j$s of the 20 sites are shown in Figure 4.2.8.7-1.

$bPDF_j$ was used as a kernel to distribute the traffic flow, N_j^k (Eq. 9) for each day of the simulation. Hourly volume can be defined simply by:

$$bhv_j(t_h) = round(N_j^k \times bPDF_j(t_h)) \quad (11)$$

However, this relation results in significant leak due to the round-off error in the hourly volume, $bhv_j(t_h)$ Especially for weekdays when daily traffic flow is small (on the order of 10-20 boats/day), Equation 11 can give hourly volume in the order 0.1 to 1 boats/hour, which will lead to a round-off in the order of 50%-100%:

$$\sum_{t_h=12am}^{12pm} bhv_j(t_h) \neq N_j^k \quad (12)$$

Therefore, a conservative approach that preserves the daily total number of boats (N_j^k) is used to calculate the hourly volume. In this approach, N_j^k is distributed starting from the hour slot with the highest probability. The number of boats for this hour slot is calculated by:

$$bhv_j(t_{h\max}) = ceil\left(bPDF_j(t_{h\max}) \times N_j^k\right) \quad (13)$$

In Eq. 13, t_{hmax} refers to the hour slot with the highest probability and function *ceil* calculates the nearest integer in the direction of +infinity. If the remaining number of boats $Nr_j^k = N_j^k - bhv_j(t_{h\max})$ is greater than zero, the same procedure was repeated with the second highest probability hour-slot, except the number of boats is truncated to the nearest integer instead of *ceil*. This process is repeated until all of the boats are distributed throughout the day.

Since all of the boats are assigned to a time slot, the total number of boats for a given day is preserved. Figure 4.2.8.7-2 shows an example application of this procedure for site 7L. The histogram on the left is the sorted bPDF for site 7L and the table on the right shows how 20 boats are distributed starting from the highest-ranking hour slot down to the lowest.

Finally, the boats in the hour slots were randomly assigned to the minutes of the hour by a non-overlapping uniform distribution. It was assumed that each boat event in an hour slot had an equal chance of being in one of the 60 minutes of the hour, and that no boats can share the same minute slot. Thus, each boat record in the simulated dataset has a unique time stamp down to the resolution of minutes.

Figure 4.2.8.7-3 is a bar chart showing the number of boating events for each site during the 15 year-long simulations. The number of sites with the same kernel distribution (e.g. BC-1R, 9R and 12BL) slightly varies due to the added uncertainty. The distribution of the total number or boating events over the river reach is shown in Figure 4.2.8.7-4.

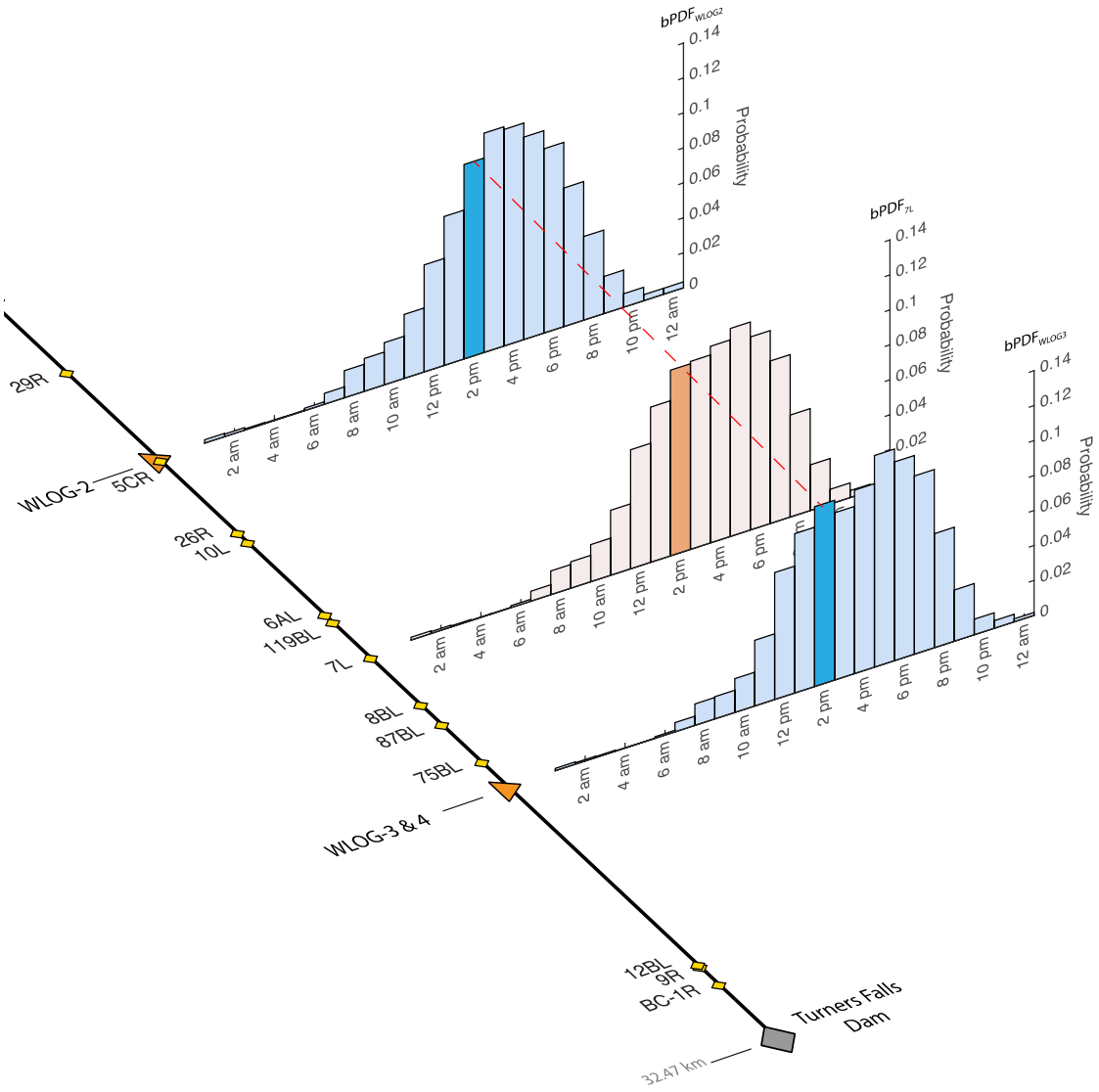

Figure 4.2.8.7-1: Illustration of the bPDFj Interpolations

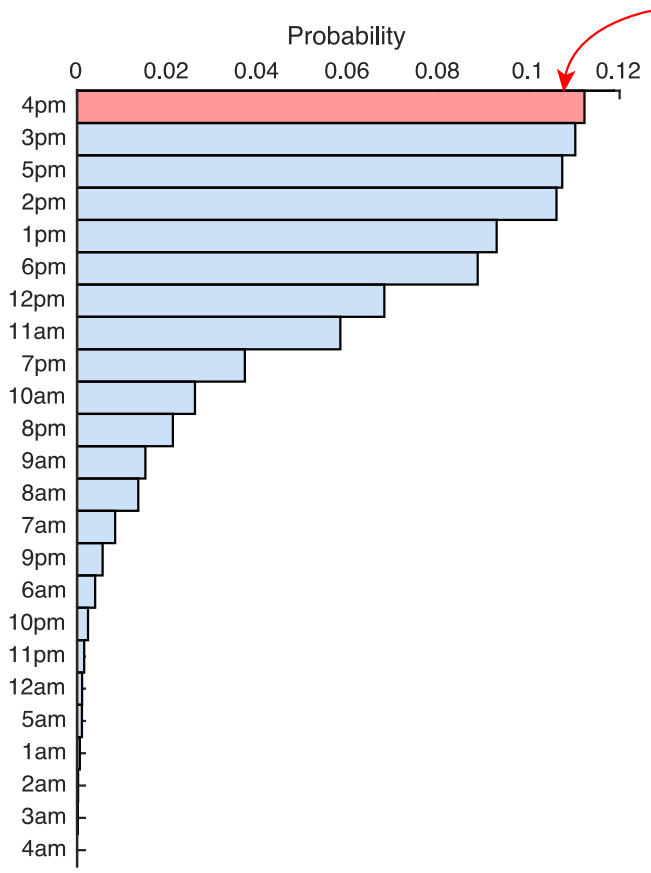

Hour	bPDF	bhv	round(bPDF)	Nr
4 pm	0.1190	2.3798	3	17
3 pm	0.1125	2.2493	2	15
5 pm	0.1104	2.2079	2	13
2 pm	0.1075	2.1503	2	11
1 pm	0.1062	2.1246	2	9
6 pm	0.0930	1.8594	2	7
12 pm	0.0888	1.7758	2	5
11 am	0.0681	1.3619	1	4
7 pm	0.0583	1.1664	1	3
10 am	0.0372	0.7437	1	2
8 pm	0.0261	0.5220	1	1
9 am	0.0212	0.4247	0	0
8 am	0.0151	0.3023	0	0
7 am	0.0136	0.2711	0	0
9 pm	0.0084	0.1686	0	0
6 am	0.0057	0.1131	0	0
10 pm	0.0040	0.0798	0	0
11 pm	0.0024	0.0479	0	0
12 am	0.0015	0.0309	0	0
5 am	0.0011	0.0220	0	0
1 am	0.0011	0.0214	0	0
2 am	0.0006	0.0122	0	0
3 am	0.0002	0.0042	0	0
4 am	0.0002	0.0031	0	0

Figure 4.2.8.7-2: Hourly Distribution for a Day with 20 Boats Passes at Site 7L

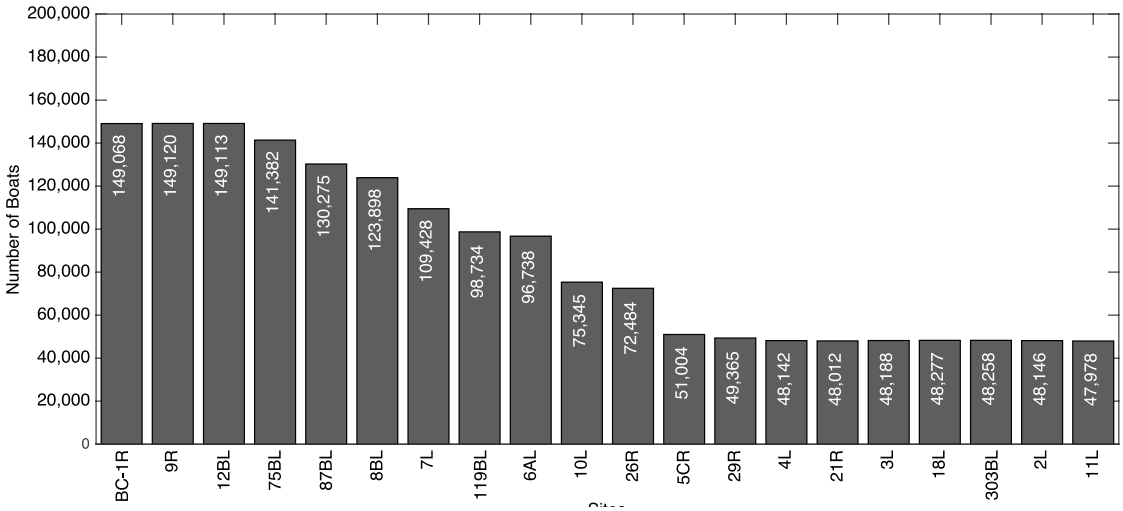

Figure 4.2.8.7-3: Total Number of Boats over the 15-year Period for the 20 Unique Locations (Sites)

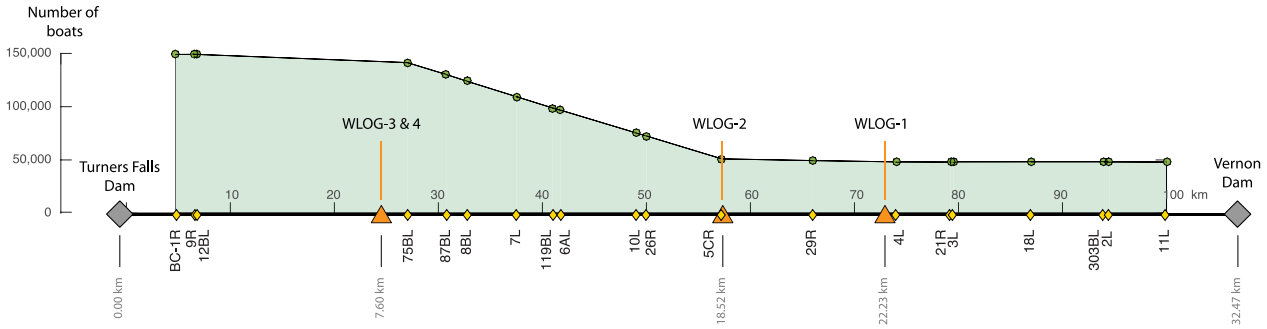

Figure 4.2.8.7-4: The Simulated Number of Boats on an Ideal Day, Distributed Along the Simulation Sites

4.2.8.8 Simulation of Wave Properties

Boat-generated waves were characterized by their maximum height, H_{max} and the wave period (for H_{max}), T_{max}. The manual wave-data input option in the BSTEM Dynamic v2.3, wave model requires a pair of H_{max} and T_{max} for each boating activity. The wave properties, H_{max} and T_{max} mainly depend on the boat speed, size and shape, and water depth. For the simulated boats, these properties were assumed to be similar for the last 15 years, and temporal variations are neglected. However, collected data shows that boat wave properties depend also on the measurement location. Even for the same type of boat, generated wave properties may vary between sites due to river geometry and boat operating conditions. For instance, at wider river sections distance between the sailing line and the shoreline will most likely be longer than that of a narrower section of the river. Because the travel distance of the waves is increased, they will attenuate and spread more due to frequency dispersion and friction. These effects are included in the data generation as uncertainties by using a weighted random-pick procedure. According to this procedure, the likelihood of observing a boat and waves similar to those observed at the measurement sites is inversely proportional to the distance from those measurement sites.

For each of the simulated boating events to be used for BSTEM simulations, a pair of H_{max} and T_{max} was randomly picked from the 12,148 boating events recorded during fieldwork. If the total number of boats simulated for 15 years for a given site j is M_j then $W_A M_j$ of those boats are picked from the measured boating events at wave logger A and $W_B M_j$ of them are picked from wave logger site B. The resulting set of H_{max} and T_{max} pairs are then permuted randomly and assigned to a simulated boating event.

4.2.8.9 Wind Generated Waves

Wave heights of boat-generated waves were 3-4 times higher than the wind-generated waves. This translates to an order of magnitude difference in their energy content since wave energy is a function of wave height squared. Moreover, due to the limited fetch length and sheltering, wind-generated waves are confined in the high frequency band. The energy of the high-frequency waves (or short waves) are concentrated close to the water surface which further limits their contribution in wave erosion.

4.2.9 Sediment Transport

Along with water flowing through river systems, rivers typically transport sediment that has been eroded from the upstream watershed, riverbanks, or the riverbed in response to flow or rainfall events and other processes that erode sediment. Sediment is transported in two modes, in suspension with the water column as it flows downstream (suspended sediment load) and sediment that flows at or near the bed of the river (bedload). Part of the reason for breaking sediment transport into these two components is due to the two methods of traditionally sampling sediment transport: suspended sediment sampling and bedload sampling. For this study emphasis was placed on investigating and evaluating available suspended sediment data collected throughout the TFI. Analysis of suspended sediment data was conducted in order to identify any correlations between flow, suspended sediment concentration, and erosion processes and to independently verify the BSTEM results, to the extent possible.

As part of Study No. 3.1.3 *Sediment Management Plan* (Study No. 3.1.3), FirstLight operated continuous suspended sediment monitors at three locations in the TFI from 2012 to 2015, except during the winter period (due to freezing temperatures). Continuous suspended sediment monitoring equipment which was used included two Laser In-situ Scattering Transmissometry (LISST) HYDRO units (HYDROs) and one LISST-StreamSide (StreamSide) unit. Continuous data was collected on an hourly, or less, basis during the monitoring period. The LISST-HYDROs were installed at the Northfield Mountain Project (initially in the powerhouse and then relocated to the tailrace in 2013) while the StreamSide was installed just upstream of the Rt. 10 Bridge. Additional LISST equipment utilized during Study No. 3.1.3 included the LISST-100X which was used to collect cross-sectional data at the Rt. 10 Bridge and Northfield Mountain tailrace boat barrier line in 2013.

In addition to the LISST instruments, grab samples were taken from the drain hoses of the HYDROs and StreamSide (2012-2015), from the edge-of-water at each LISST instrument (2015), and across the Rt. 10 Bridge over a range of flows (2015). Figures 4.2.9-1 through 4.2.9-4 depict the locations of the various suspended sediment monitoring which occurred as part of Study No. 3.1.3. In-depth discussion and analyses pertaining to this study can be found in the report titled, *Relicensing Study 3.1.3 Northfield Mountain Pumped Storage Project Sediment Management Plan 2015 Summary of Annual Monitoring* filed with FERC in December 2015 (FirstLight, 2015a).

For the purposes of the Causation Study, emphasis was placed on evaluating and analyzing the continuous suspended sediment and grab sample data collected in the vicinity of the Rt. 10 Bridge, more specifically the StreamSide data (2013-2015) and the Rt. 10 Bridge cross-section grab samples (2015). The data collected in the vicinity of the Rt. 10 Bridge allowed for a direct analysis of suspended sediment dynamics in the mainstem Connecticut River (as opposed to the data collected in the Northfield Mountain tailrace which was set back from the mainstem). In-depth discussion pertaining to the analysis of the suspended sediment dataset can be found in Section 5.3.

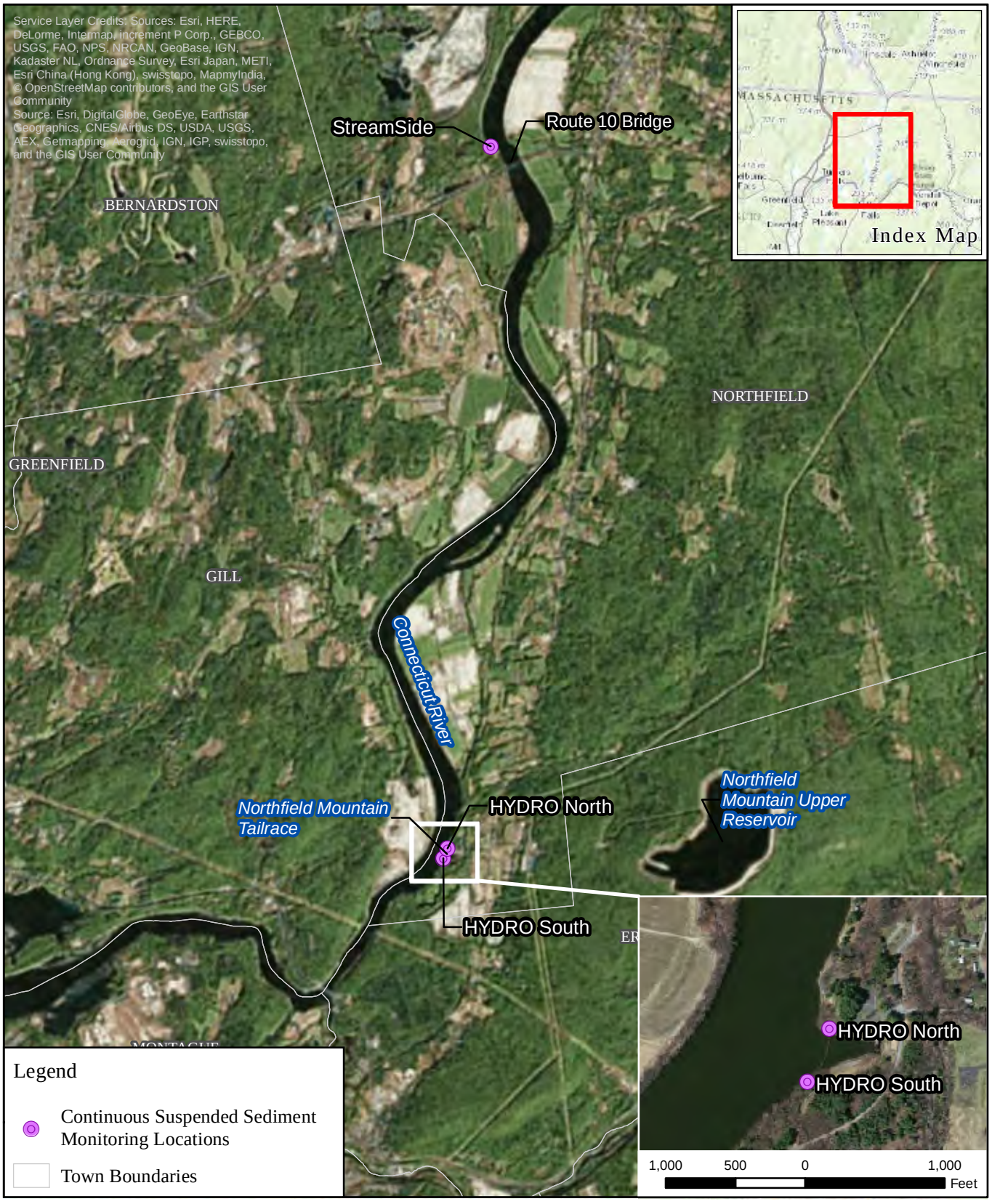

FIRSTLIGHT HYDRO GENERATING COMPANY
Northfield Mountain Pumped Storage Project No. 2485
Turners Falls Hydroelectric Project No. 1889

STUDY 3.1.2

Figure 4.2.9-1:
Locations of LISST Continuous Suspended Sediment Monitors

Path: W:\gis\studies\3_1_2\maps\final_report\figure_4_2_9-1.mxd

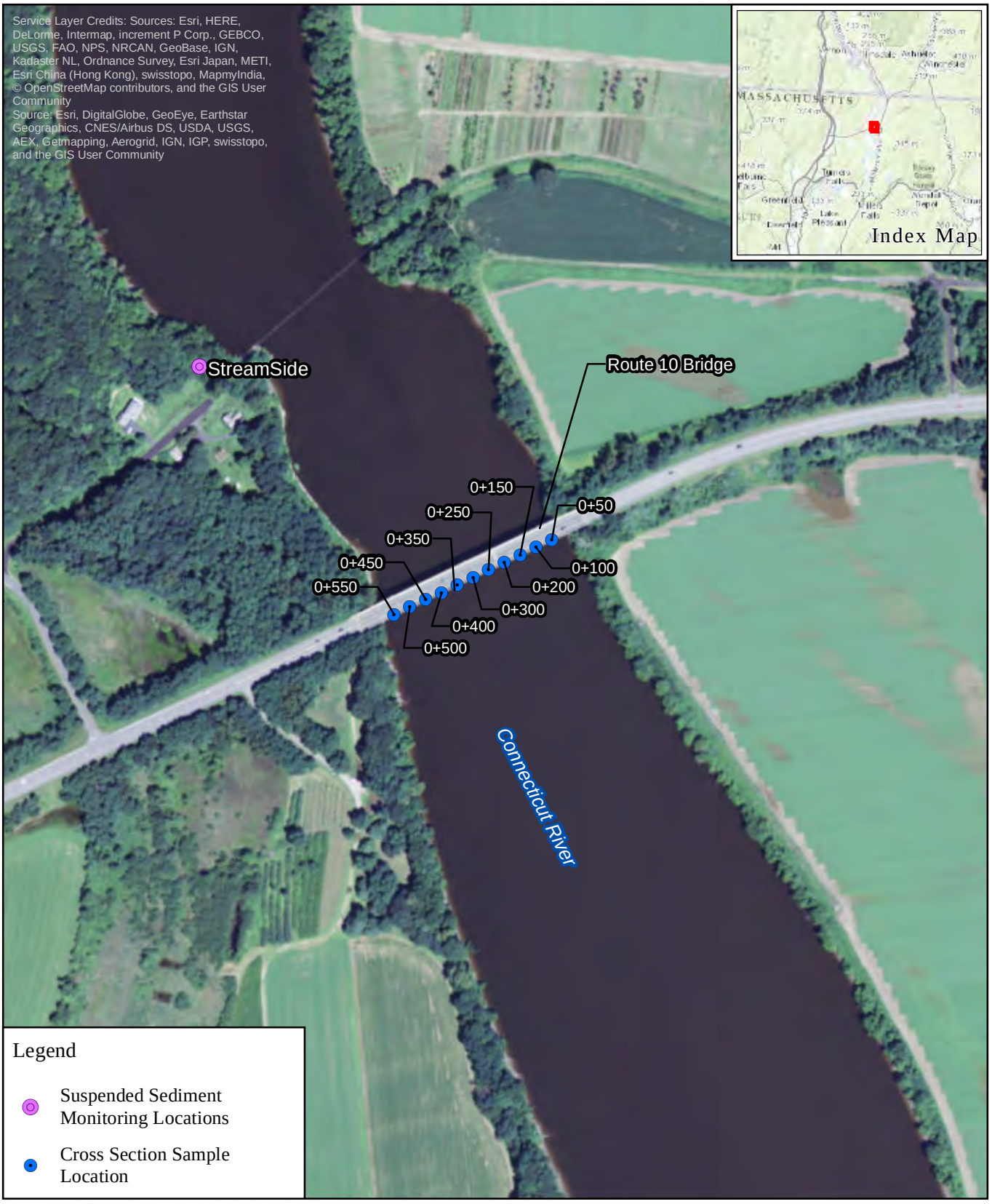

FIRSTLIGHT HYDRO GENERATING COMPANY
Northfield Mountain Pumped Storage Project No. 2485
Turners Falls Hydroelectric Project No. 1889

STUDY 3.1.2

N

0 200 400 800 Feet

Figure 4.2.9-2:
Location of LISST-StreamSide and LISST-100X Cross-section

Path: W:\gis\studies\3_1_2\maps\final_report\figure_4_2_9-2.mxd

FIRSTLIGHT HYDRO GENERATING COMPANY
Northfield Mountain Pumped Storage Project No. 2485
Turners Falls Hydroelectric Project No. 1889

STUDY 3.1.2

N

0 100 200 400 Feet

Figure 4.2.9-3:
Location of LISST HYDROs and LISST-100X Cross-section

Path: W:\gis\studies\3_1_2\maps\final_report\figure_4_2_9-3.mxd

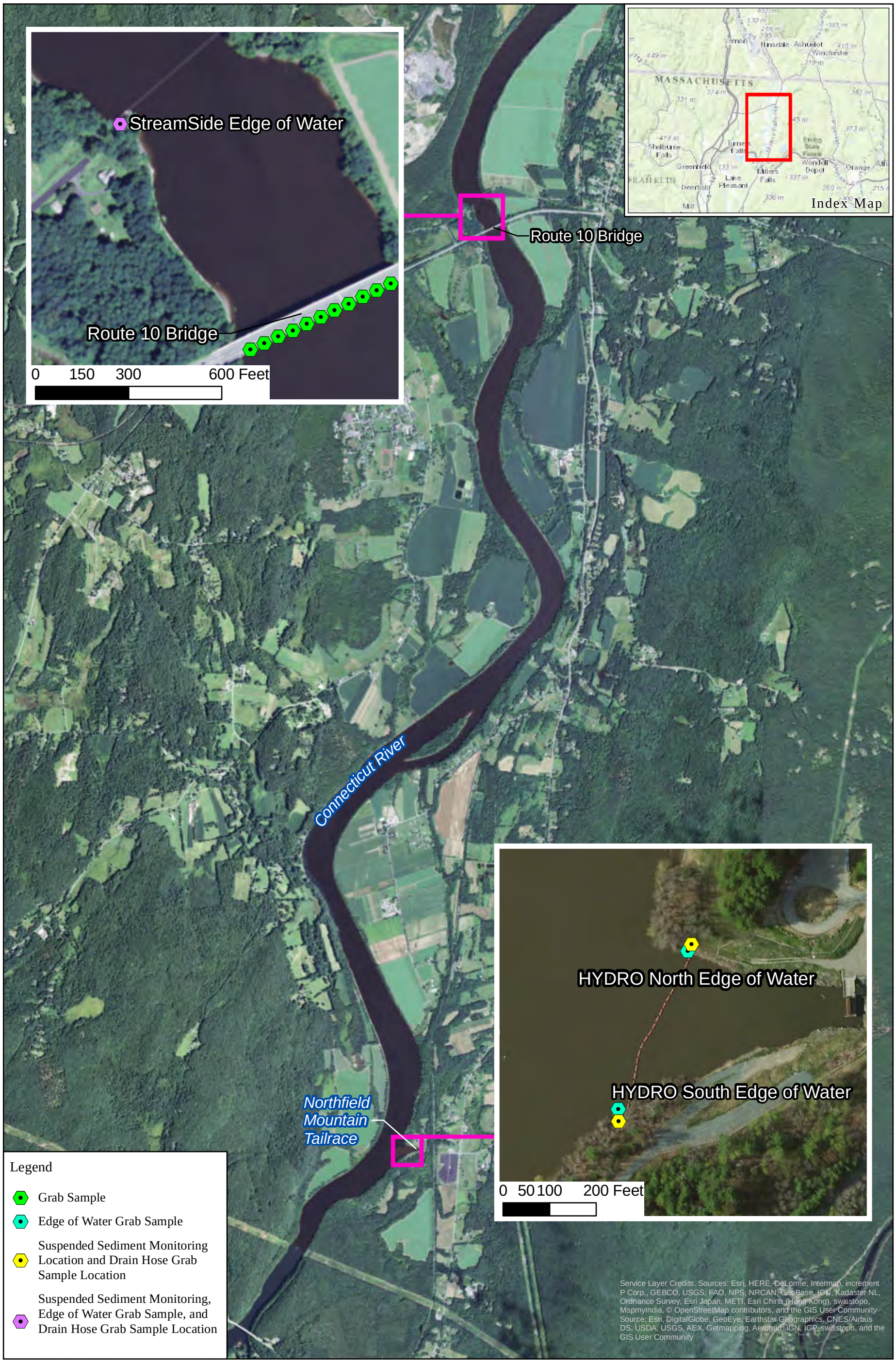

Figure 4.2.9-4:
Grab Sampling Locations

Path: W:\gis\studies\3_1_2\maps\final_report\figure_4_2_9-4.mxd

4.2.10 Groundwater Data

Groundwater data was collected in the 1990's to investigate the impact of water level fluctuations on the potential movement of water into and out of riverbanks in the TFI. Pressure transducers to measure water level fluctuations were placed in the river and in three monitoring wells adjacent to the river in the Bennett Meadow area on the west bank of the river a short distance downstream of the Route 10 Bridge. One transducer was placed in the river itself to monitor impoundment fluctuations and the three monitoring wells were placed in a line perpendicular to the riverbank at various distances away from the river (52, 65, and 210 feet back from the edge). Monitoring of these transducers was conducted from mid-July 1997 through February 1998 (see Figure 4.2.10-1). Figures 4.2.10-2 and 4.2.10-3 show these data plotted over time. These groundwater data are provided in Volume III (Appendix I). The findings of this analysis are discussed further in Section 5.5.2.1.

Figure 4.2.10-1: Groundwater Monitoring

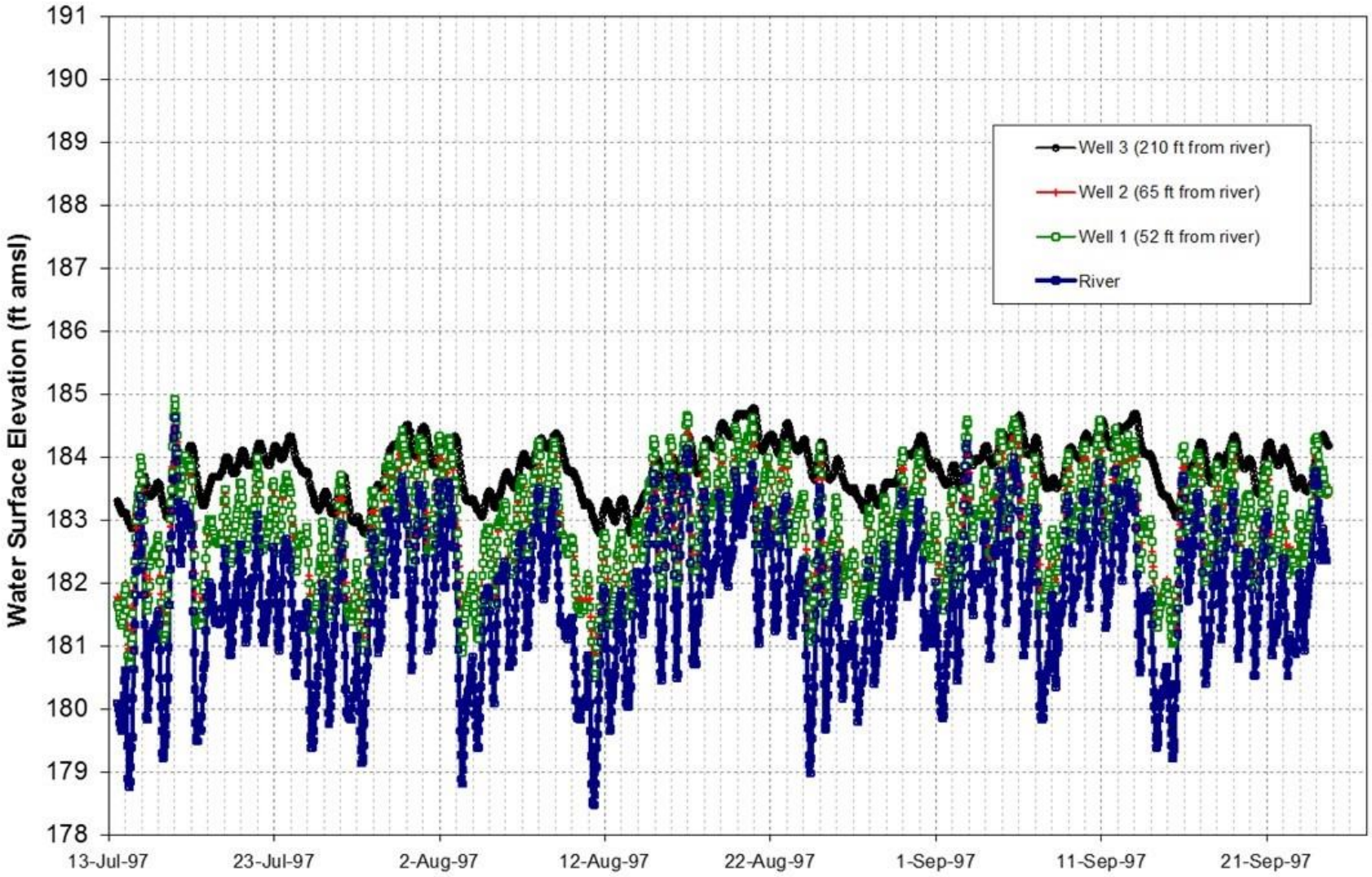

Figure 4.2.10-2: Groundwater Data (July 13, 1997 – September 21, 1997)

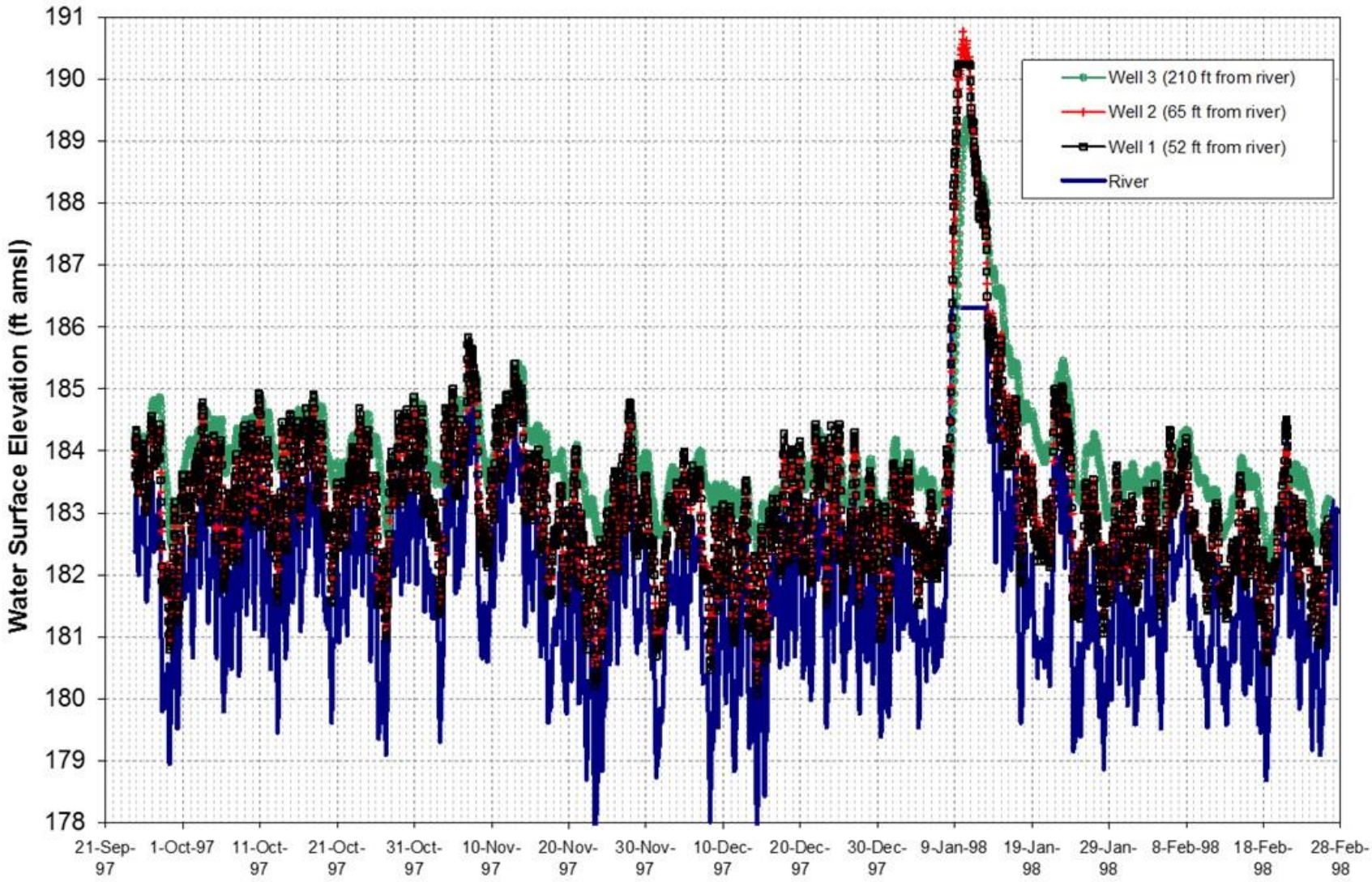

Figure 4.2.10-3: Groundwater Data (September 21, 1997 – February 28, 1998)

4.2.11 Ice

When initially developing the potential causes of erosion discussed in Section 3, ice was listed as a potential secondary cause of erosion. For decades ice had not been a significant factor affecting erosion in the TFI due potentially to the operation of VY located immediately upstream in the Vernon Impoundment. When in operation, VY used water from the Connecticut River for cooling after which heated water was discharged back to the river. The operation of VY may have been the reason why the TFI would rarely ice over completely during the winter months.

In 2013, when Entergy announced the closing of VY by December 29, 2014, FERC issued an Interim ILP schedule for Study Plan Determination. During this period, FirstLight elevated ice from a potential secondary cause of erosion to a potential primary cause of erosion to account for the fact that ice may play a more significant role in riverbank erosion processes in the future. FirstLight filed an addendum to the RSP for Study No. 3.1.2 with FERC in September 2014[32] which highlighted the methodology to be used to more thoroughly examine ice as a potential primary cause of erosion.

In accordance with the RSP addendum, FirstLight completed the following ice related tasks:

- A review was conducted of the USACE, Cold Regions Research and Engineering Laboratory (CRREL) database to document known ice jams recorded on the Connecticut River in the area between Wilder Dam and Turners Falls Dam. CRREL maintains an ice jam database and clearing house. The database was inventoried to determine historic ice jams along the Connecticut River. Similarly, contact was made with the USGS to identify any recorded ice jams or ice floes on the Connecticut River at their gaging stations.

- TransCanada was contacted to determine if it had any historic and/or current information on the timing, extent and duration of sheet ice development and ice-break up in the Wilder and Bellows Falls Impoundments. In addition, information on the thickness of the sheet ice and whether any ice floes have been documented in these impoundments, below the dams, or at the mouths of major tributaries emptying into the impoundments was requested.

- Historic daily air temperature data were obtained to determine any correlation between air temperature and the timing of ice sheet development and break-up for any historic ice formation data collected by TransCanada. Historic air temperature data were also obtained near the TFI. Specific sites from which air temperature data were obtained include:

    - Amherst, MA;
    - Vernon, VT;
    - Keene, NH; and
    - Hanover, NH

  Temperature data obtained at each of these sites is included in Volume III (Appendix J).

- Photographs of ice conditions were taken at a number of predetermined locations throughout the TFI during the winter of 2015/2016, including:

    - Vernon Dam;
    - Confluence of Ashuelot River;

[32] The RSP Addendum addressing the evaluation of ice as a potential primary cause of erosion was filed with FERC as part of the Relicensing Study No. 3.1.2 Initial Study Report Summary.

- Pauchaug Boat Launch;
- Route 10 Bridge;
- Northfield Tailrace;
- French King Bridge;
- Confluence of Millers River; and
- Turners Falls Dam

These sites were selected for two primary reasons: 1) they were easily and safely accessible during winter conditions, and 2) they covered the geographic extent of the TFI. Figure 4.2.11-1 depicts these locations. Photos were taken on:

- December 15, 2015;
- January 5, 2016;
- January 14, 2016;
- January 21, 2016;
- January 28, 2016;
- February 11, 2016;
- February 19, 2016; and
- March 8, 2016

The original intent of the timing of the photographs was to observe: (1) when sheet ice developed; (2) during formation of sheet ice; (3) during ice break-up; and (4) after ice break-up occurred. While ice development was observed during the monitoring period, due to an unseasonably mild winter the TFI never completely iced over. Although the RSP Addendum called for photographs to be taken from December 1 through March 31, ice was not observed at the monitoring sites during the March 8, 2016 site visits. As such, the decision was made to curtail any future site visits.

In addition to the winter 2015/2016 photos, supplemental photos were taken on four occasions during the winter of 2014/2015 to document ice conditions during what was a relatively cold winter.[33] A full set of photographs at all locations is presented in Volume III (Appendix J).

Using the ice and temperature data, correlations between air temperature and ice were developed following a similar approach to that which had been utilized to evaluate ice formation, breakup and subsequent erosion on the Platte River (*Analysis of Ice Formation on the Platte River* (S&A, 1990a), *Physical Process Computer Model of Channel Width and Woodland Changes on the North Platte, South Platte and Platte Rivers* (S&A, 1990b), *Calibration of SEDVEG Model Based on Specific Events from Demography Data* (S&A, 2002)). Additional analysis conducted as part of this study included examining the forces that ice transmits to riverbanks and the type of damages that may potentially occur. These analyses are discussed further in Section 5.5.5.

[33] Supplemental photographs taken during the winter of 2014/2015 were captured on: January 5, January 29, February 25, and March 3, 2015.

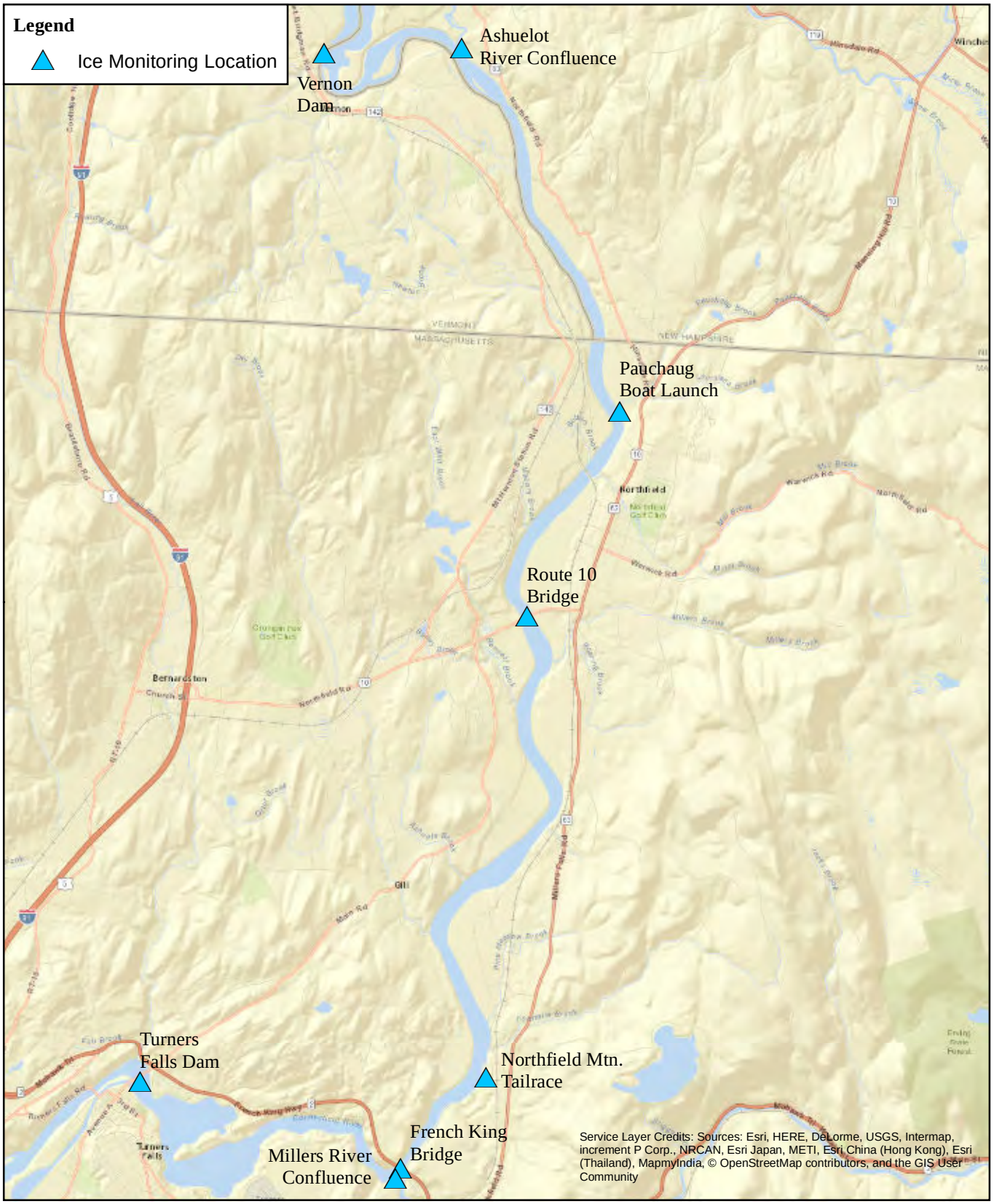

FIRSTLIGHT HYDRO GENERATING COMPANY
Northfield Mountain Pumped Storage Project No. 2485
Turners Falls Hydroelectric Project No. 1889

STUDY 3.1.2

Figure 4.2.11-1:
Ice Monitoring Locations
Winter 2015/2016

N

0 0.75 1.5 3
Miles

Path: W:\gis\studies\3_1_2\maps\final_report\figure_4_2_11-1.mxd

5 DATA ANALYSES & EVALUATION OF THE CAUSES OF EROSION

In order to identify, quantify and rank the causes of erosion in the TFI, a thorough understanding of the forces associated with each primary cause of erosion must be developed. The results of the data analyses presented in this section provides an understanding of: (1) the magnitude of those forces; (2) the vertical location those forces impact the riverbank; (3) the longitudinal location; (4) the duration of the forces; (5) the various types of riverbank materials; and (6) the physical properties of the bank materials that resist hydraulic and geotechnical erosion. The results of the various analyses and modeling described in this section were further used to quantify the relative percentages of the primary causes of erosion at each detailed study site as well as throughout the TFI. While discussion pertaining to the evaluation of the causes of erosion is presented in this section, a summary discussion is also presented in Section 6. All analyses was conducted in accordance with the requirements of the RSP.

BSTEM, including its field collected and hydraulic model input data, was the primary tool used to analyze and evaluate primary causes of erosion in the TFI. BSTEM is a state-of-the-science model which allowed for the analysis of potential primary causes of erosion, including: hydraulic shear stress due to flowing water, water level fluctuations, and boat waves.

In addition to the modeling conducted with BSTEM, supplemental data analyses were conducted as a means of comparison with the BSTEM results. These analyses were used to: (1) investigate the potential primary causes of erosion not included in the BSTEM analysis (i.e. land-use and ice); (2) provide additional analyses of the causes of erosion examined by BSTEM; and (3) to examine secondary causes of erosion present in the TFI (i.e. animals and unique hydraulic and/or geomorphic conditions). Land-use and land management practices were analyzed via geospatial analysis (GIS) and observations made during the 2013 FRR land-based survey. Analysis of the effects of ice was conducted in accordance with the methodology laid out in Section 4.2.11 and the RSP Addendum.

The Hydrology, Hydraulics, and Sediment Transport discussions presented in Sections 5.1, 5.2, and 5.3 respectively, provide the foundation for the BSTEM and supplemental analyses discussed later. BSTEM analyses, including discussion pertaining to input data and results, is presented in Section 5.4. Supplemental analyses are found in Section 5.5, including:

- Hydraulic shear stress (Section 5.5.1);
- Water level fluctuations (Section 5.5.2);
- Boat Waves (Section 5.5.3);
- Land-use and management practices (Section 5.5.4);
- Ice (Section 5.5.5); and
- Animals (Section 5.5.6)

The BSTEM and supplemental analyses discussed in this section, combined with the geomorphic understanding of the Connecticut River discussed in Section 2, represent all components of the three-level approach as discussed in Section 1 and are consistent with the requirements of the RSP.

5.1 Hydrology

In order to understand the erosion processes of the TFI, it is necessary to first understand the hydrology and hydraulics of the study area. As such, this section focuses on the hydrologic characteristics of the TFI in terms of daily flow variations and hourly flow and water level fluctuations. Discussion pertaining to the tools used to evaluate the hydraulics of the TFI can be found in Section 5.2. Evaluation of the hydrologic and hydraulic characteristics of the TFI provides additional information and longer term perspective that is useful in developing an understanding of the patterns and interaction that flow and associated hydropower operations may have on erosion processes.

5.1.1 Hydrologic Setting

While there is no USGS gaging station measuring flow within the TFI, there is a USGS gage on the Connecticut River at Montague, MA (USGS gage no. 01170500), which is located a short distance downstream of Turners Falls Dam. The drainage areas at the Turners Falls Dam and at the Montague gage are 7,163 mi^2 and 7,860 mi^2, respectively; a difference of 697 mi^2. The major tributary between the dam and Montague gage is the Deerfield River with a drainage area of 665 mi^2. Flow on the Deerfield River is regulated from peaking hydroelectric facilities and by two seasonal storage reservoirs located in Vermont. For purposes of this section, the summary of the Montague gage is included to provide a general understanding of the long term average flow regime of the Connecticut River. In addition, FirstLight has maintained an hourly database of flows within the Project area over the past 16 years. This database includes discharges from Vernon Dam, Northfield Mountain Operations, flows over the Turners Falls Dam, and flows to the power canal.

The Connecticut River follows a fairly typical seasonal hydrograph as shown by the mean daily flow from 1904 to 2014 (Figure 5.1.1-1). As shown in this figure, flow at the Montague gage in January through most of February averages just over 10,000 cfs. In late February to early March, the mean flow rises due to spring runoff or freshet peaking in April to about 40,000 cfs. The lowest flow (slightly over 5,000 cfs) occurs during the late summer to early fall.

Another important flow statistic is the annual peak flow as this can be related to flooding and flood related damages. Figure 5.1.1-2 shows the variation in annual peak streamflow for the Connecticut River at Montague from 1904 to 2015. As observed from the Montague gage data, several large floods occurred on the Connecticut River prior to 1940. The largest three floods within the period of record had peak flows of 236,000 cfs (1936), 195,000 cfs (1938), and 179,000 cfs (1928).

The flood of 1936 caused substantial damage and provided the impetus for the construction of flood control reservoirs in the Connecticut River Watershed. In response to the 1936 flood, the USACE completed 9 flood control reservoirs on tributaries to the Connecticut River upstream of Turners Falls Dam between 1941 and 1961 (Table 5.1.1-1). Note that this table does not include mainstem projects such as Moore Dam (completed in 1956) which provides a limited amount of flood storage, or other much smaller local flood mitigation projects. The flood control projects have likely been at least partially responsible for the lower peak flows on the Connecticut River since 1961. Since 1938, no flood peak has exceeded 150,000 cfs with the three highest peaks being: 143,000 cfs (1984), 126,000 cfs (1987), and 127,000 cfs (2011, associated with Tropical Storm Irene).

Most of the analyses used in this study, including BSTEM, were based on hourly hydrologic data from January 1, 2000 to December 31, 2014. This 15-year time period was used for two primary reasons: (1) it was representative of post flood control Connecticut River conditions, and (2) it marked the period of time when the most data was available (i.e. digital FirstLight operations data). In order to determine if the 2000-2014 analysis period was representative of longer term conditions, FirstLight investigated changes in the shape of the flow duration curves and average flows for four time periods:

- 1904-2014 (representing the entire period of record other than 2015);
- 1904-1960 (pre-flood control through flood control development period);
- 1961-2014 (post-flood control period); and
- 2000-2014 (BSTEM modeling period)

As shown in Figure 5.1.1-3, the average yearly peak flow for the 1961-2014 period is 83,600 cfs, 14,000 cfs less than the average yearly peak flow for the 1904-1960 period (97,600 cfs). Table 5.1.1-2 provides the mean daily flows for the four periods. While the average yearly peak flow for the 1961-2014 and 2000-2014 time periods are approximately 7,000 cfs less compared to the 1904-2014 period, and 13,000 to 14,000 cfs less than the 1904-1960 time period; the mean daily flow is higher during these same periods compared to the overall and earlier time periods. This shows that peak flows have been reduced by approximately 8% compared to the overall time period. This is likely due to the previously mentioned flood control projects; contrasted to the time period (2000-2014) for which the mean daily flows are approximately 16% higher.

Flow duration curves based on the mean daily flows for these same periods are plotted in Figures 5.1.1-4 and 5.1.1-5. Figure 5.1.1-4 presents the full range of flows from approximately 1,000 to 240,000 cfs and exceedance percentages from 0 to 100%; while Figure 5.1.1-5 focuses on the upper 2% of the flow range. The slight shift observed for the different time periods can at least be partially explained by the effects of the flood control projects as previously discussed.

The flow duration curve for the 2000-2014 time period is quite similar to the recent, longer post flood control time period (1961-2014) indicating that the 2000-2014 flow regime is representative of the longer time period and reflects the effect that flood control projects now have in the Connecticut River Basin. Using the 2000-2014 time period for flow statistics and for analysis of erosion is supported by this comparison of flows in other time periods in the historic record.

Table 5.1.1-1: Flood Control Dams – Connecticut River

Flood Control Dam	Tributary Watershed	Date Completed	Flood Control Volume (acre-ft)
Union Village	Ompompanoosuc	1950	38,054
North Hartland	Ottauquechee	1961	71,198
North Springfield	Black	1960	51,250
Ball Mountain	West	1961	54,626
Townshend	West	1961	33,758
Surry Mountain	Ashuelot	1941	32,530
Otter Brook	Ashuelot	1958	17,493
Birch Hill	Millers	1942	50,023
Tully	Millers	1949	22,004

Table 5.1.1-2: Average Flows – Connecticut River at Montague

Time Period	Mean Daily Flow (cfs)
1904-2014	14,300
1904-1960	13,800
1961-2014	14,900
2000-2014	16,600

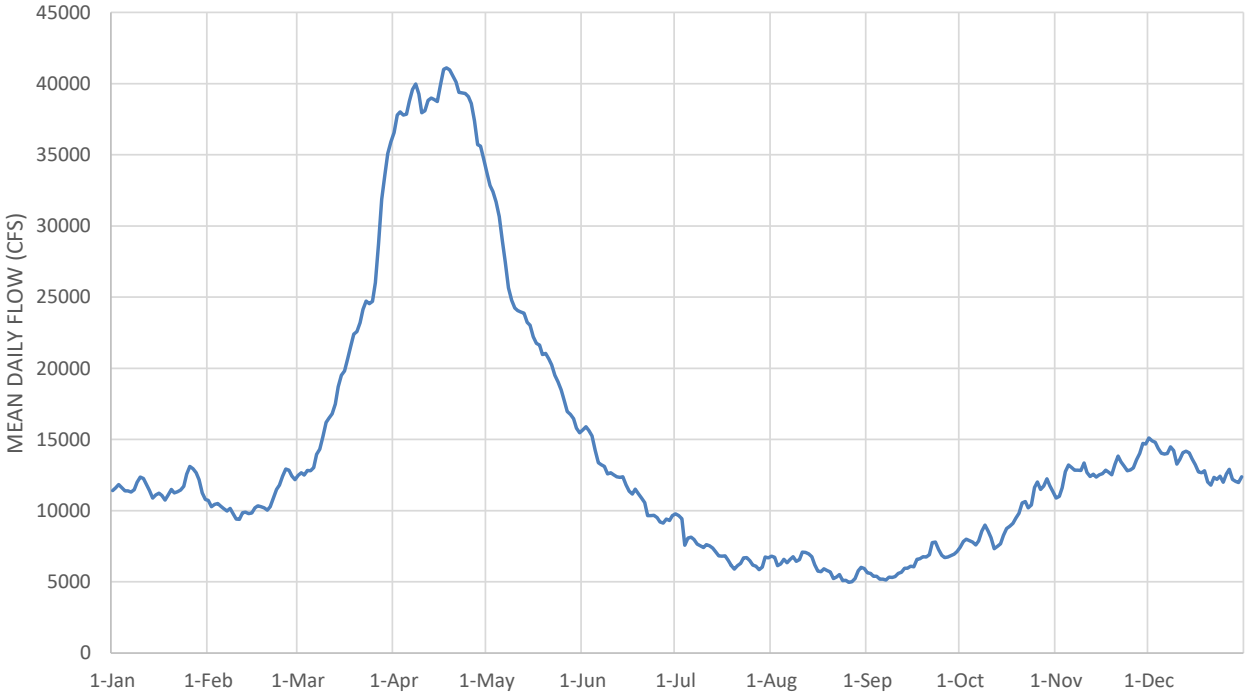

Figure 5.1.1-1: Average Annual Hydrograph – Connecticut River at Montague

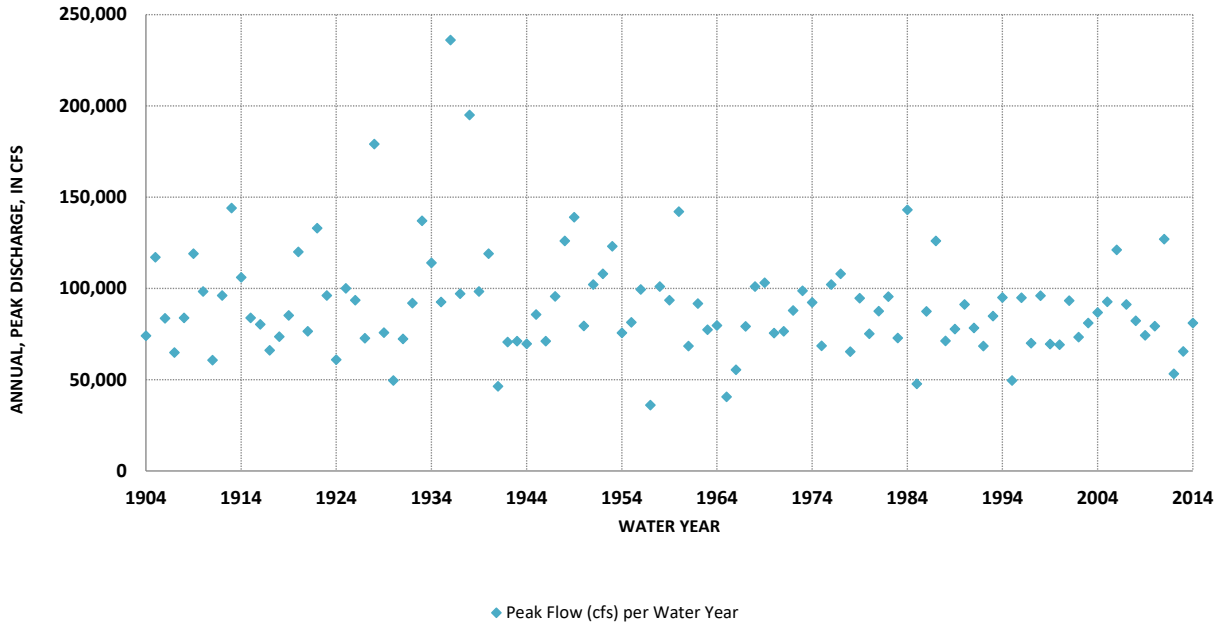

Figure 5.1.1-2: Annual Peak Streamflow on the Connecticut River at Montague, MA (USGS)

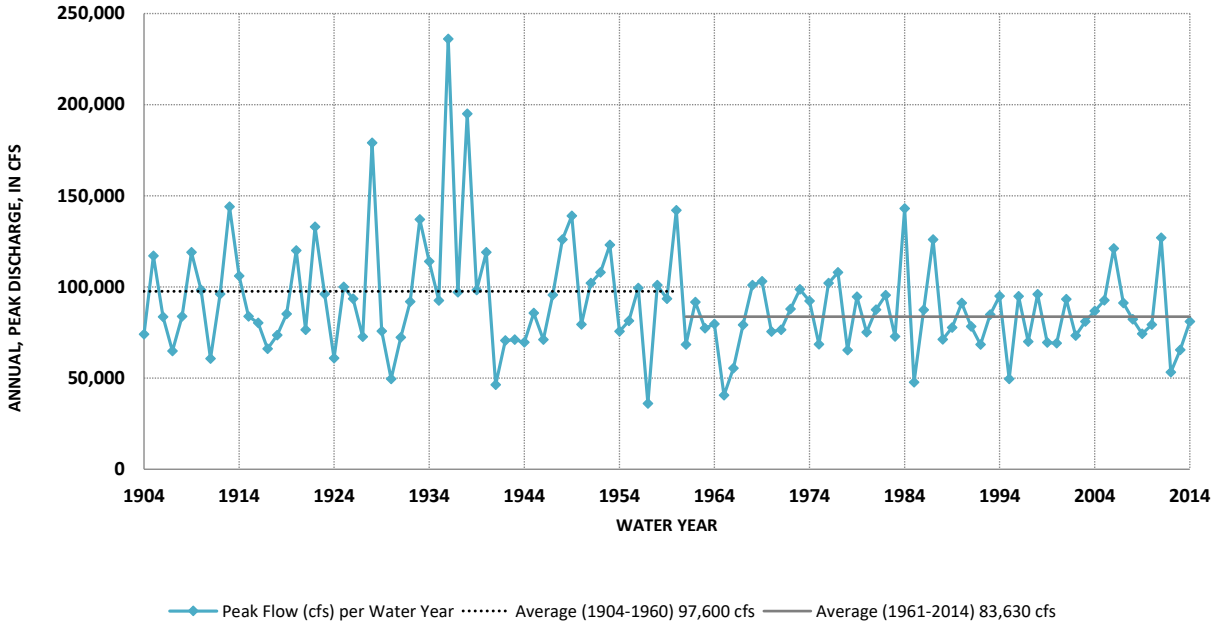

Figure 5.1.1-3: Connecticut River Peak and Average Peak Flows at Montague, MA (USGS)

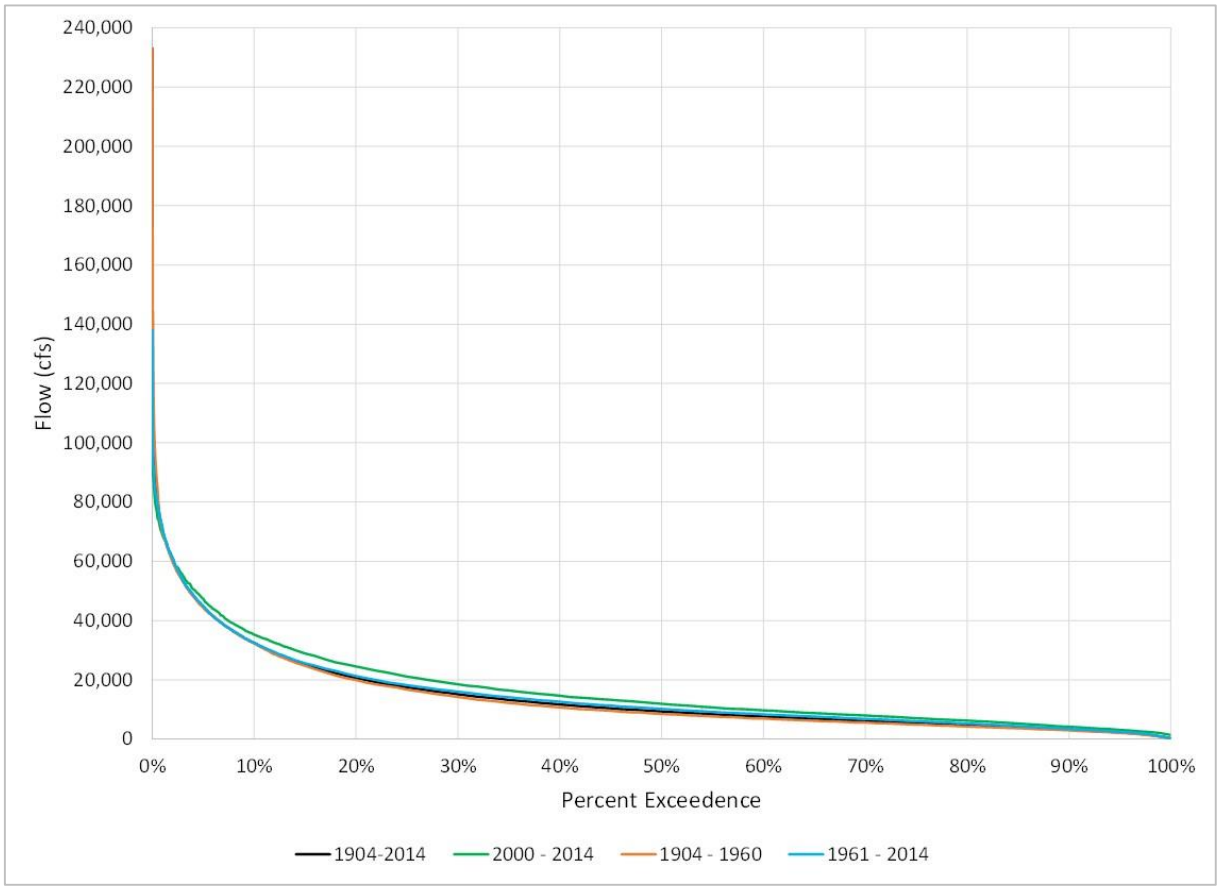

Figure 5.1.1-4: Flow-Duration Curves: Connecticut River at Montague, MA (USGS)

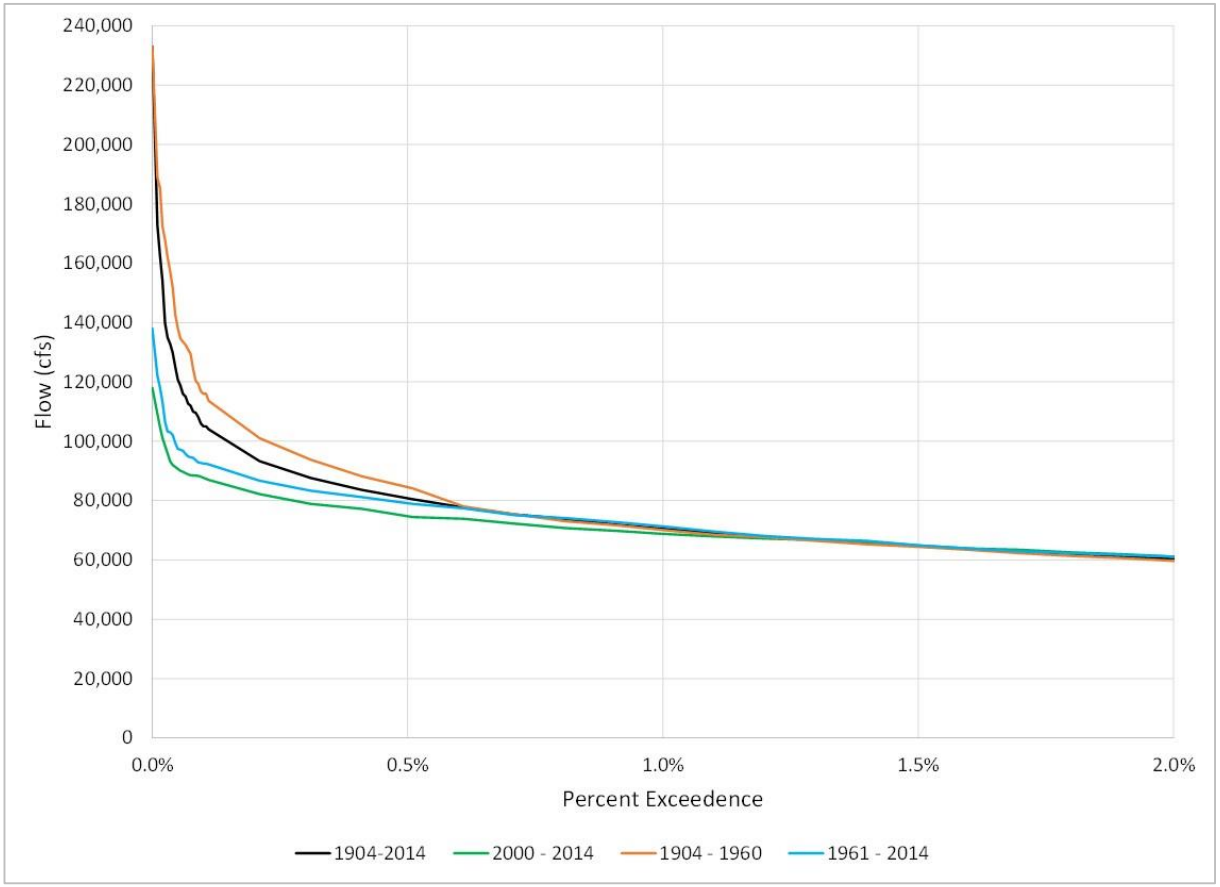

Figure 5.1.1-5: Flow-Duration Curves: Connecticut River at Montague, MA (USGS). 0 to 2 percent exceedance

5.1.2 Daily Flow Variations

The flow on the Connecticut River on a mean daily basis over an annual cycle is unsteady and highly variable. To further understand the variability of flow in the Connecticut River, an annual hydrograph based on the mean daily flow at the Montague USGS gage was developed for 2014 (Figure 5.1.2-1). In addition to the mean daily flow for 2014, the figure also shows the mean daily flow for the 2000-2014 period (note that for the 2000-2014 period all Jan 1, Jan 2, and Dec 31 mean daily flows were averaged to create a long term hydrograph). This hydrograph demonstrates the significant variability in flow over time with changes in flow ranging from a few thousand cfs to several tens of thousands of cfs occurring over relatively short periods of time (days to several days). The mean daily flow peaked at about 80,000 cfs in mid-April 2014. Many other peaks also occurred during 2014 including during late December at about 50,000 cfs and other flow events over 25,000 cfs at numerous other times through the year. During the summer and fall, the flow generally averaged less than 10,000 cfs. The 2014 hydrograph shows considerable variability in flow especially on a weekly basis due mostly to the variability of natural flows, which is typical for the Connecticut River.

Volume III (Appendix K) presents the annual hydrographs for the Connecticut River at Montague, MA from 2000 through 2014; Table 5.1.2-1 summarizes peak flow and variability of these annual hydrographs. The hydrographs from 2000 through 2014, as presented in Volume III and Table 5.1.2-1, typically show a primary peak along with multiple secondary peak flow events occurring each year. Over the period from 2000 through 2014 there were 88 peak flows exceeding 40,000 cfs. On average there were approximately 6 peak flow events greater than 40,000 cfs per year during this period but the number of peaks per year over 40,000 ranged from one in 2012 to 11 in 2006.

Table 5.1.2-1: Summary Mean Daily Annual Hydrographs of the Connecticut River at Montague, MA 2000-2014

Calendar Year	Mean Daily Peak Flow	Summer Maximum (June-Sept)	Comments
2000	66,600 cfs 12/18	Multiple summer peaks (2 > 30,000 cfs, 2 > 20,000 cfs)	Multiple secondary peaks in the spring (3 peaking at about 60,000 cfs, 1 > 50,000 cfs)
2001	88,300 cfs 4/24	One significant peak > 40,000 cfs in early June then primarily less than 10,000 cfs the rest of the summer	Other than the primary spring peak and one early summer peak, flow most of the rest of the year was less than 10,000 cfs
2002	68,200 cfs 4/16	One summer peak in early June > 45,000 cfs	A primary spring peak with two secondary spring peaks in the 40,000 to 50,000 cfs range
2003	80,500 cfs 10/30	One summer peak reaching about 30,000 cfs	Four secondary peaks over 50,000 cfs, one in the spring and three in the fall and early winter
2004	82,700 cfs 4/2	Only three peaks over 20,000 cfs, all in September	Three peaks over 40,000 cfs, two in the spring and one in December
2005	102,000 cfs 10/9	One peak in June just under 40,000 cfs	Multiple peaks in the spring and fall ranging from 50,000 to 90,000 cfs range
2006	81,600 cfs 1/19	Three early summer peaks over 30,000 cfs with one over 50,000 cfs	Numerous winter, spring, and late fall peaks over 40,000 cfs
2007	88,600 4/17	One summer peak in early June over 20,000 cfs	Two peaks over 50,000 cfs, one in January, one late March
2008	78,700 cfs 4/14	Two summer peaks > 50,000 cfs	Multiple spring and winter peaks over 40,000 cfs
2009	66,500 cfs 4/5	One summer peak over 50,000 cfs in early August	Two peaks over50,000 cfs, one in October and one in December
2010	74,300 cfs 3/31	No summer peaks over 20,000 cfs	An additional peak over 70,000 cfs in March and five peaks over 40,000 cfs in the fall and winter.
2011	118,000 cfs 8/29	Other than on 8/29, only one peak over 30,000 cfs, about 75,000 cfs on 9/8	One peak slightly over 80,000 cfs in April and numerous other peaks over 40,000 cfs in the fall, winter and spring
2012	42,100 cfs 4/24	Over than a peak slightly over 30,000 cfs in early June, no other peaks above 20,000 cfs	Several peaks over 30,000 cfs in the late fall, winter and spring.
2013	56,300 cfs 7/4	An additional peak over 50,000 cfs in mid-June	Five peaks over 40,000 cfs in the winter and spring
2014	79,200 cfs 4/17	Four peaks over 20,000 cfs, none over 30,000 cfs	Four peaks over 40,000 cfs in the winter and spring

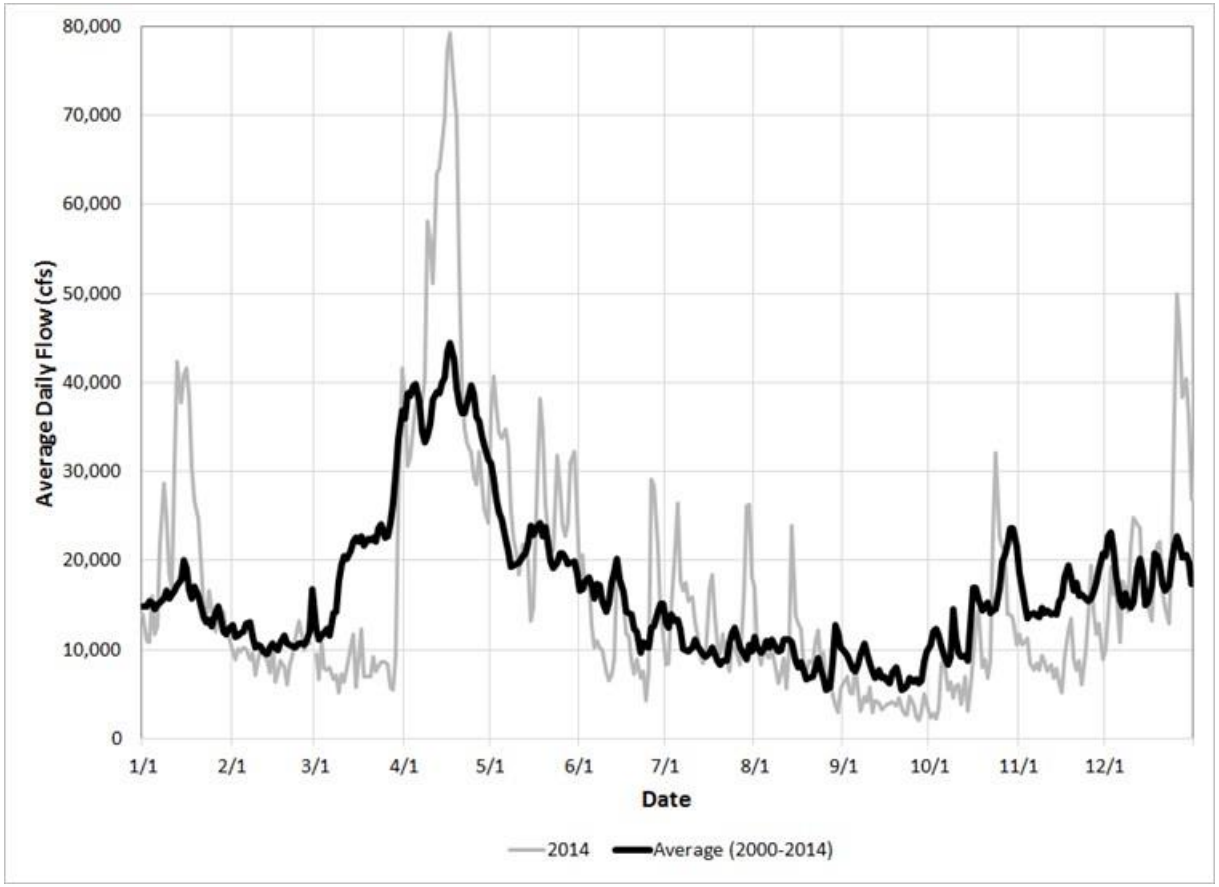

Figure 5.1.2-1: Annual Hydrograph 2014, Connecticut River at Montague, MA (USGS)

5.1.3 Hourly Flow and Water Level Fluctuations

Examination of mean daily flows reported by the USGS at the Montague Gage does not describe the intraday variability of flow on the Connecticut River, especially in the TFI. In order to more fully understand flow and water level variations examination of these data on an hourly time basis is required. Most dams on the Connecticut River having hydropower facilities operate as peaking generation facilities. Under inflow conditions below their generating hydraulic capacities, these facilities often store water in their impoundments on a daily cycle to allow them to generate additional electricity during portions of the day when the power demand and market prices increase. Table 5.1.3-1 provides an overview of the hydraulic capacity of the Vernon, Northfield Mountain, and Turners Falls Hydroelectric Projects.

The main source of inflow into the TFI is TransCanada's Vernon Hydroelectric Project, which normally operates as a peaking facility when inflows are low. The drainage area of the Connecticut River at Vernon Dam is 6,266 mi^2, the station has a total hydraulic capacity[34] of 17,130 cfs, and a minimum flow requirement of 1,250 cfs. The drainage area at Turners Falls Dam is 7,163 mi^2, 897 mi^2 larger than at Vernon Dam. Two main tributaries flow into the TFI, the Ashuelot River about 2 miles below Vernon Dam, and the Millers River, about 4 miles above Turners Falls Dam. Table 5.1.3-2 summarizes the two USGS gages on these tributaries. These gages capture most of the drainage area of the tributaries and 88% of the incremental drainage area between Vernon Dam and Turners Falls Dam.

Northfield Mountain uses the TFI as its lower reservoir and its tailrace, which is located about 5.2 miles upstream of the Turners Falls Dam. Northfield Mountain has 4 reversible pump/turbines that at maximum, can pump at 15,200 cfs or can discharge 20,000 cfs. The Upper Reservoir currently has a FERC maximum usable storage capacity of 12,318 acre-ft. Given this, the Project can pump at maximum capacity for 9.8 hours and generate at maximum capacity for 7.5 hours; however, in reality, the Project rarely pumps or generates at its maximum capacity or utilizes all of the Upper Reservoir volume in a single day.

FirstLight's current FERC license allows the TFI water level to be fluctuated within a 9-foot band between a minimum water surface elevation of 176 and a maximum of 185 ft. NGVD 1929[35], as measured at the Turners Falls Dam. This 9-foot water level fluctuation provides about 16,150 acre-ft. of storage, if fully utilized; however, FirstLight rarely fluctuates the TFI by more than 4 feet in a day even though the TFI acts as the lower reservoir for Northfield Mountain and the headpond for the power canal (which leads to the generation facilities at Station No. 1 and Cabot Station). During normal operations when inflow to the TFI is less than about 17,000 cfs, FirstLight manages the water surface elevation and storage in the TFI to limit spillage at the Turners Falls Dam while allowing efficient generation and pumping cycles at Northfield Mountain and generation at the Turners Falls Project. The combined hydraulic generation capacity of Vernon and Northfield Mountain is 37,130 cfs, much greater than the Cabot and Station No. 1 combined hydraulic generation capacity of 15,938 cfs. Therefore, FirstLight normally operates the TFI water surface elevation such that by early to mid-morning the water surface elevation is at a low for the day after pumping associated with Northfield Mountain. Based on hourly data, the median water surface elevation at the Turners Falls Dam is 181.3, but the normal daily variations in the water level in the TFI downstream of French King Gorge is between 1 and 3 feet. During times when the naturally routed inflow to the TFI is above 30,000 cfs, an agreement between the USACE and FirstLight requires that the water surface elevation at the dam be lowered (but not below an elevation of 176 ft.) to limit flooding upstream of the dam.

As discussed in the March 2015 report for Relicensing Study No. 3.2.2 *Hydraulic Study of Turners Falls Impoundment, Bypass Reach, and Below Cabot* (the Hydraulic Study), at higher flows (i.e., above 30,000 cfs) the natural constriction at the French King Gorge becomes a hydraulic control affecting water levels in

[34] Hydraulic capacity is the maximum flow that can be run through the turbines to generate electricity. Flow greater than this magnitude is discharged over the spillway.
[35] All elevations mentioned in Section 5.1 reference the vertical datum NGVD 1929 (US Feet)

the mid and upper sections of the TFI. Therefore at higher flows, the effects of water level management at the Turners Falls Dam by FirstLight becomes much less of a controlling influence of the water surface elevations in the middle and upper parts of the TFI (FirstLight, 2015b).

As part of the hydraulic modeling associated with this study, FirstLight modeled 15 years (January 1, 2000 to December 31, 2014) of inflow and operational data to develop historical water levels throughout the TFI. Figure 5.1.3-1 provides the elevation duration curves for five key locations within the TFI. This figure does not show the extreme highest water levels reached during this time period such as a peak elevation at the Vernon Tailrace of 204.58 ft during Tropical Storm Irene in August of 2011 or the water levels during the shutdown of Northfield Mountain from May to November 2010.

Flow fluctuations on a fifteen minute basis are shown in Figure 5.1.3-2 from the Vernon Hydroelectric Project, Northfield Mountain Project, prorated inflow from the Ashuelot and Millers Rivers, and the corresponding water level at the Turners Falls Dam during a 10 day period from August 24, 2014 to September 3, 2014. This period represents a low flow period, typical Vernon peaking operations, and typical Northfield Mountain operations. At Vernon, peaking power flow releases of normally 6,000 to 10,000 cfs typically started in the early afternoon and continued into the early evening before dropping down to slightly below 2,000 cfs. During this time period inflow from the Ashuelot and Millers Rivers was low and stable and normally in the 200 to 300 cfs range. Northfield Mountain was active with pumping starting normally around midnight and continuing until about 8 am at rates between 10,000 and 15,000 cfs. Generation at Northfield Mountain normally started at about 11 am and continued until early evening. The water level at the Turners Falls Dam showed the effects of the inflow from Vernon, with a travel time delay and a quicker response to pumping or generation at Northfield Mountain. Not shown on this graph is the varying water releases to the power canal which ranged from a minimum flow of about 3,000 cfs to maximum peaking releases often over 10,000 cfs, generally in a similar timeframe as Vernon.

From 2012 to 2015, FirstLight had 10 or more water level recorders throughout the TFI for use in numerous relicensing studies. Figure 5.1.3-3 provides a plot of 10 water level recorders for the same time period as shown in Figure 5.1.3-2 (August 24 to September 3, 2014). The water level data show the variations in water level associated with peaking power operation flow releases from the Vernon Hydroelectric Project combined with the peaking power operations at the Turners Falls Dam and Northfield Mountain. As seen in Figure 5.1.3-3, there is a hydraulic control upstream of Stebbins Island which prevents the water level near Vernon Dam from falling below an elevation of about 181.3 even under low flow conditions from Vernon and low TFI levels. The magnitude of water level fluctuations at all 10 locations shown on Figure 5.1-3-3 is about 3.5 feet on most of the days.

During moderate to high flow events hydroelectric generation operations shift from a peaking power operation mode to a run-of-river mode as the flow exceeds the hydraulic capacity of the power plants at Vernon Dam and Turners Falls (17,130 cfs at Vernon and 15,938 cfs at Turners Falls). Flows in excess of the generating capacity are discharged at the dams. During high flow periods in excess of 30,000 cfs, per an agreement with the USACE, FirstLight lowers the water level at the Turners Falls Dam (but not below El. 176) to limit high water in the Barton Cove area and to a lesser extent, the middle section of the TFI. If we consider the hydraulic capacity of Vernon Dam as approximately 17,000 cfs at the upstream end of the TFI and that Northfield Mountain can provide an additional 20,000 cfs, flows in excess of 37,000 cfs can be considered “natural” high-flow events in the lower impoundment. At flows above 65,000 cfs as per an agreement with the USACE, if Northfield Mountain is operating, the combined usable volume of the Upper Reservoir and the TFI is required to be kept constant in order to limit discharges from Northfield Mountain adding to the outflow from Turners Falls Dam. As a result of this agreement, if Northfield Mountain is operating during such high flows the hydrologic effect in the TFI is minor.

An example of a recent moderate to high flow event occurred during April 2014 when flow in the Connecticut River exceeded the hydraulic capacity at both Vernon and Turners Falls Dams and peak

discharge from Vernon reached almost 70,000 cfs. As shown in Figure 5.1.3-4, the discharge at Vernon on April 18 was about 65,000 cfs, falling to about 25,000 cfs by April 27. Figure 5.1.3-4 provides the water surface elevations during this time period at 6 locations within the TFI. As demonstrated in the figure, at higher flows the hydraulic constriction at French King Gorge, about 3 miles upstream of the Turners Falls Dam, limits the effect of the water level at the dam on the water level at the middle and upper portions of the TFI. For example, at a Vernon discharge of 62,000 cfs, the water surface elevation at Vernon Tailrace was about 198.5 ft, about 192.0 ft at the Rt. 10 Bridge, and about 190.0 ft at the Northfield Tailrace, while the water elevation at the Turners Falls Dam was about 181.0 ft.

Table 5.1.3-1: Hydraulic Capacities of the Vernon, Northfield Mountain, and Turners Falls Hydroelectric Projects

Project Name	Hydraulic Capacity (cfs)
Vernon	17,130
Northfield Mountain (Pumping)	15,200
Northfield Mountain (Generating)	20,000
Turners Falls	15,938

Table 5.1.3-2: USGS Gage Information of the Ashuelot and Millers Rivers

Gage No.	Gage Name	Period of Record	Gage Drainage Area	Total River Drainage Area
01161000	Ashuelot River at Hinsdale, NH	1907-current	420 mi^2	420 mi^2
01166500	Millers River at Erving, MA	1915-current	372 mi^2	390 mi^2

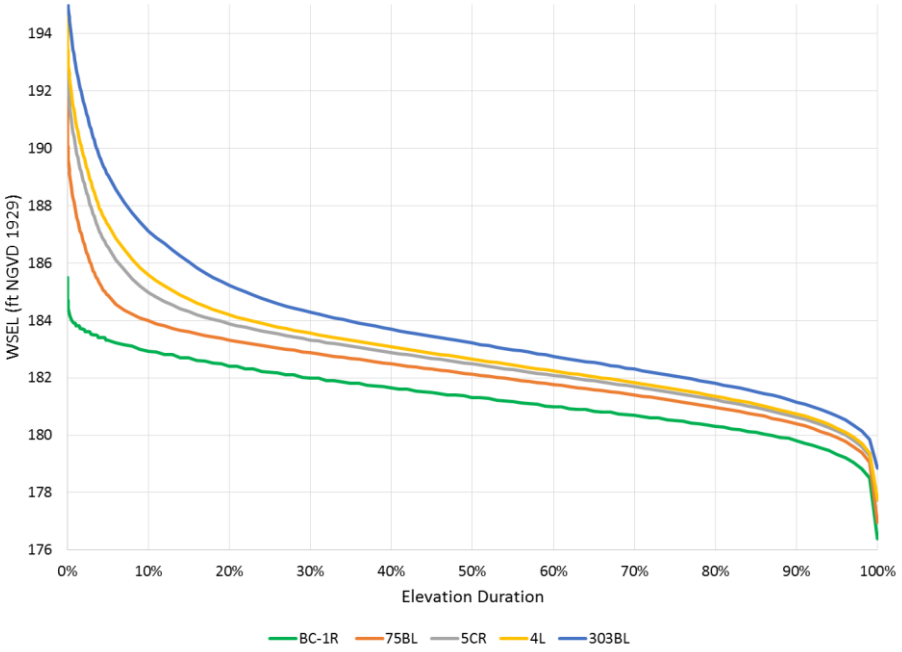

Figure 5.1.3-1: Elevation Duration Curves within the Turners Falls Impoundment (2000-2014)

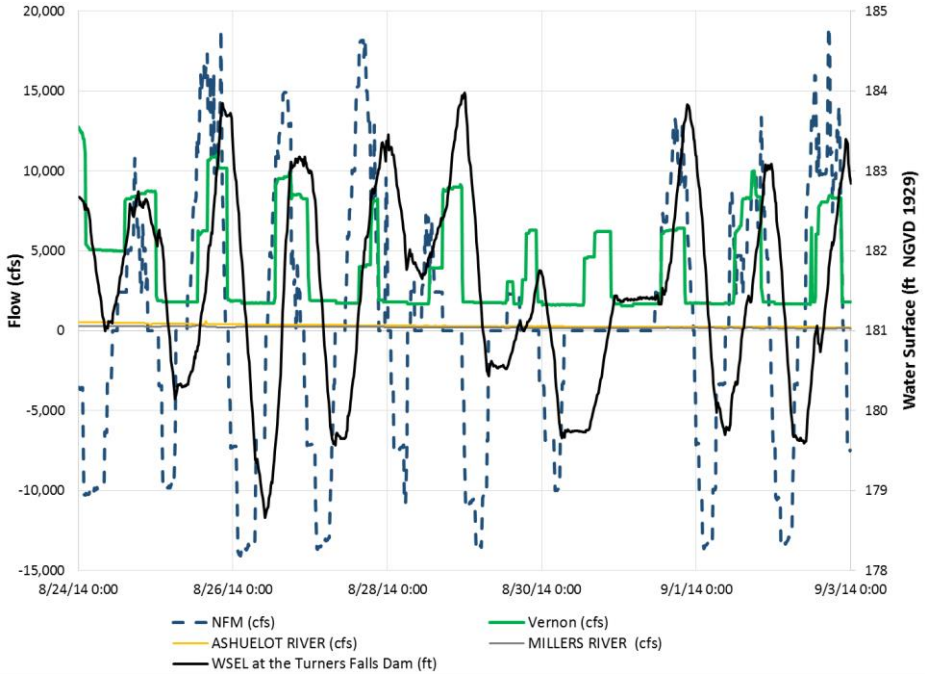

Figure 5.1.3-2: Turners Falls Impoundment Conditions for August 24 – September 3, 2014

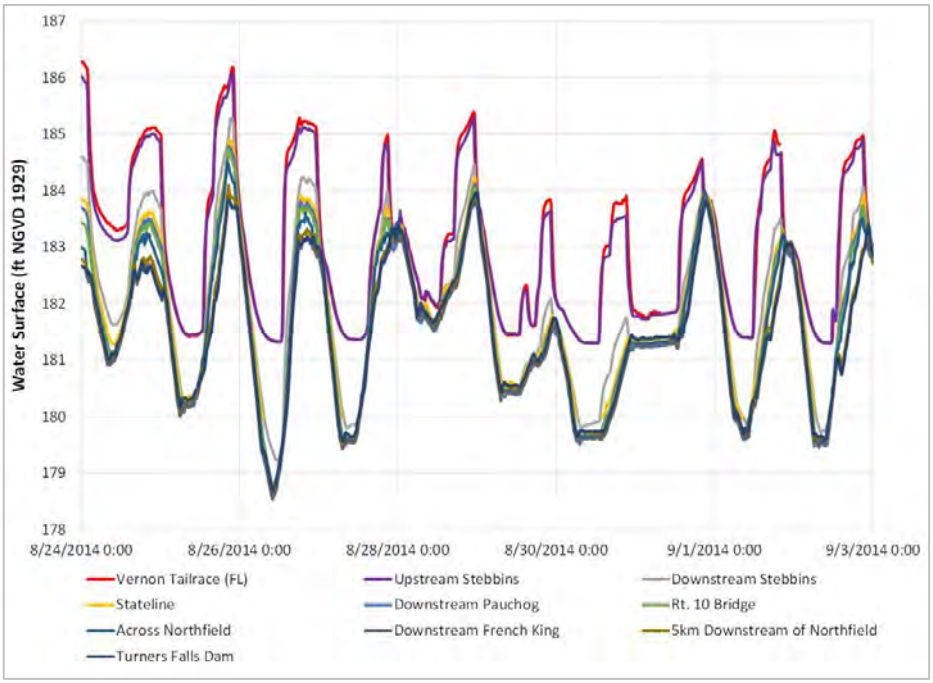

Figure 5.1.3-3: Turners Falls Impoundment Water Surface Elevations for August 24 – September 3, 2014

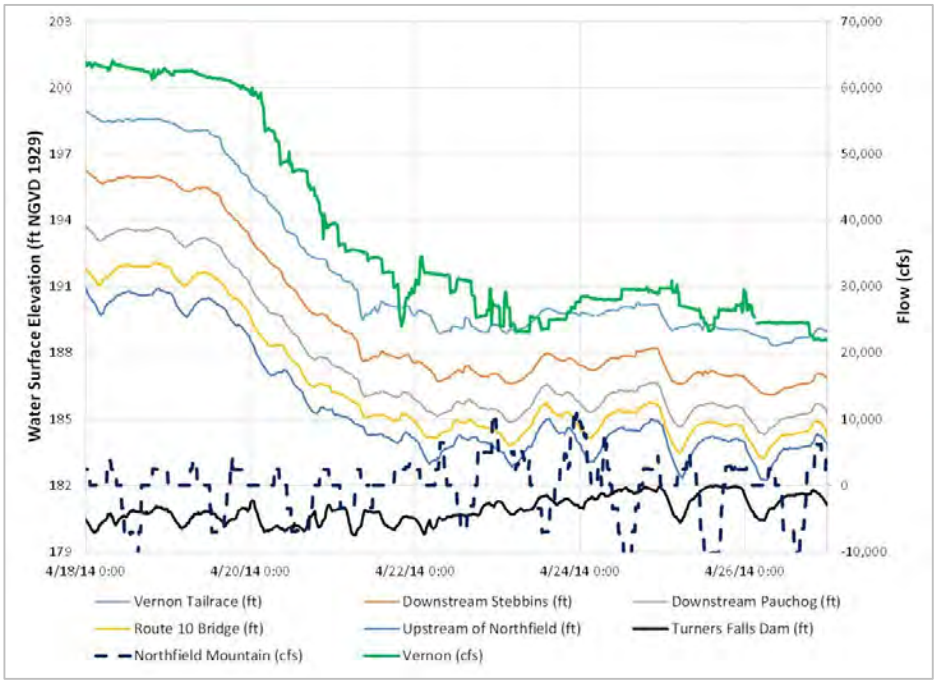

Figure 5.1.3-4: Turners Falls Impoundment Water Surface Elevations for April 18-27, 2014

Location and Duration of Hydraulic Forces

Discussion in this section focuses on the location and duration of hydraulic forces, or more specifically, on the duration at which various water surface elevations are equaled or exceeded and the corresponding location of the water surface relative to bank position.

As noted in USACE (1979), the forces acting on the bank can be broken into two categories: (1) those acting near the surface of the flow, and (2) those acting with the greatest intensity nearer the bottom of the submerged banks. Figures 5.1.3-5 through 5.1.3-7 present examples of this dynamic. Given that erosion processes associated with (1) hydraulic shear stress due to flowing; (2) water level fluctuations due to hydropower operations; (3) boat waves; and (4) ice occur at and below the water surface it is vital to understand where on the riverbank the water surface rests and for what duration.

TFI riverbanks are typically characterized by a lower and upper riverbank. The lower bank is typically a flat, beach-like feature that is submerged or experiences daily water level fluctuations during low to moderate flows as a result of hydropower peaking operations. Depending on its location in the TFI, the lower bank may or may not be vegetated. As one moves away from the normal edge-of-water, the lower bank transitions to an upper bank; the toe of which is clearly identifiable on most cross-section plots. The upper bank is typically steep, has some degree of vegetation, and is usually above the water surface except during high flows. Figure 5.1.3-8 provides an example of a typical TFI lower and upper bank configuration.

The distinction between the lower and upper bank is an important one given that the BSTEM modeling results and the results of the supplemental analyses found that forces acting at the water surface and along the submerged banks typically do not cause erosion at lower flows and minimal erosion at moderate flows when the water surface rests on the lower bank (i.e., below the toe of the upper bank). It is not until the water surface rises and rests on the upper bank during high flow events that riverbank erosion potentially commences; even then the flow threshold to initiate erosion was found to be greater than 37,000 cfs at the majority of detailed study sites.

Although peaking hydropower operations can result in water level fluctuations up to 4 feet over the course of a day, during low to moderate flow periods the water surface typically rests on the lower bank. To determine the amount of time the TFI water surface rests on the lower bank vs. the upper bank a water level duration analysis was conducted at a subset of the 25 detailed study sites. The 5 sites chosen spanned the geographic extent of the TFI, were located in areas with varying hydraulic characteristics, and were found to be representative of the other sites in proximity to them. The results of this analysis found the following:

- At Site BC-1R (at HEC-RAS transect 3518), the water surface rests on the lower bank (defined as that portion of the bank below El. 184.0) 99% of the time;
- At Site 75BL (at HEC-RAS transect 25845), the water surface rests on the lower bank (defined as that portion of the bank below El. 184.0) 90% of the time;
- At Site 5CR (at HEC-RAS transect 56235), the water surface rests on the lower bank (defined as that portion of the bank below El. 184.0) 82% of the time;
- At Site 4L (at HEC-RAS transect 72416), the water surface rests on the lower bank (defined as that portion of the bank below El. 184.0) 78% of the time; and
- At Site 303BL (at HEC-RAS transect 93012), the water surface rests on the lower bank (defined as that portion of the bank below El. 185.0) 79% of the time

As observed above, the water level rests on the lower bank the vast majority of the time at all locations, however, as one moves upstream the water level rests on the lower bank less than in the downstream reaches.

The relationship between location in the TFI and the duration of which the water level rests on the lower bank is a result of the TFI becoming more riverine as you move in the upstream direction. Figure 5.1.3-1 demonstrated the results of the water-level duration analysis at each location previously mentioned.

To further understand the location and duration of hydraulic forces on the bank, stage-discharge relationships were developed at the same sites where the water level duration analyses were conducted to determine at what flow the water surface reaches the upper bank. TFI flow duration curves for the individual locations based on hourly data for the period 2000-2014 were then analyzed to determine the percent of time flows of that magnitude occur in the TFI. The results of this analysis found:

- At Site BC-1R, the water surface is largely a function of the water level as controlled by FirstLight at the Turners Falls Dam, so there is not a distinct stage vs discharge relationship in this part of the TFI;

- At Site 75BL, where the water level can still be a function of the Turners Falls Dam water surface elevation, the water surface generally reaches the upper bank at flows of about 32,000 cfs or greater. This flow is equaled or exceeded about 10% of the time;

- At Site 5CR, the water surface reaches the upper bank at flows of about 23,000 cfs or greater. This flow is equaled or exceeded about 18% of the time;

- At Site 4L, the water surface reaches the upper bank at flows of about 17,000 cfs or greater. This flow is equaled or exceeded about 22% of the time; and

- At Site 303BL, the water surface reaches the upper bank at flows of about 17,500 cfs or greater. This flow is equaled or exceeded about 21% of the time

Figure 5.1.3-9 demonstrates the generalized stage-discharge relationships developed at each site other than BC-1R. At lower elevations at these four sites, the observed and modeled stage storage graph is a scatter plot due to the influence of the water surface elevation at Turners Falls Dam. Figures 5.1.3-10 and 5.1.3-11 depict the flow duration curve for the four sites for the period 2000-2014. These figures show that the high flow regime is very similar at all four sites; however, at flows below about 20,000 cfs there is more of a variation in the flow regime at 75BL (near Northfield Mountain) due to the effects of pumping and generation cycles.

The final step in this analysis was to compare the upper bank flow and water level analysis against the 95% erosion flow threshold (i.e., the flow above which 95% of all erosion occurs at a given site) derived from the BSTEM modeling results at each site (discussed later in the report). The 95% erosion flow threshold for each site was then compared against the flow duration curve to determine the amount of time that flow may be equaled or exceeded. To provide context, the corresponding water surface elevation for the erosion threshold was compared against the elevation of the toe of the upper bank. This analysis found:

- At sites 75BL, 5CR, and 303BL the 95% erosion flow threshold is near or exceeds the natural high flow threshold (37,000 cfs for Sites 75BL and 5CR, 17,130 cfs for Site 303BL), the water surface elevation rests at, or several feet above, the toe of the upper bank, and the percent of time the 95% erosion flow threshold is exceeded is less than 10% (7%, 4%, and 3%, respectively);

- While the 95% erosion flow threshold is noticeably lower at site 4L (~7,000 cfs), the 50% erosion flow threshold (i.e., the flow above which the majority of erosion occurs at a given site) is about 83,500 cfs which equates to a water surface elevation of 195 and is exceeded <1% of the time, however at this site the calculated erosion is very low (0.017 $ft^3/ft/y$); and

- Analysis of BC1-R was not possible given that a reliable stage-discharge relationship could not be developed for this location.

The results of the analyses discussed above are summarized in Table 5.1.3-3. As observed in the table, and to summarize, the water level rests on the lower bank the vast majority of the time. The period of time in which the water surface rests on the lower bank also coincides with the periods when Vernon, Northfield Mountain, and/or Turners Falls are typically operating in a peaking mode (i.e. low and moderate flow periods). This is significant given that the majority of erosion in the TFI only occurs once the water level reaches the upper bank. Furthermore, the 95% erosion flow threshold is near or exceeds the natural high flow threshold at three of the five sites and only occurs 3-7% of the time at those sites.[36] This finding is consistent at the majority of sites throughout the TFI. The results from this analysis clearly indicate: (1) the importance of the water surface elevation and its corresponding location on the bank; (2) the importance of the duration of those water surface elevations; and (3) that the window for the majority of erosion to occur is quite small and well beyond the flows at which hydropower operations have an impact on flow or water level.

Table 5.1.3-3: Detailed Study Site Hydrologic Analysis

Detailed Study Site	Toe of Upper Bank – El.*	Water Level Duration		Flow to Reach Upper Bank (cfs)	% Time Flow is Exceeded	95% Erosion Flow Threshold (cfs, from BSTEM)	% Time Threshold Flow is Exceeded	Corresponding Threshold WSEL
		% Time on Lower Bank	% Time on Upper Bank					
BC-1R	184	99	1	NA	NA	I	NA	NA
75 BL	184	90	10	32,000	10	33,800	7%	184
5CR	184	82	18	23,000	18	47,900	4%	188
4L	184	78	22	17,000	22	7,000	60%	181
303BL	185	79	21	17,500	21	53,200	3%	192

*NGVD29, Feet I = Indeterminate

[36] The exception to this is Site 4L where the 95% flow threshold is 6,991 cfs. Further examination of this site indicates that the average rate of annual erosion is 0.017 $ft^3/ft/yr.$, making it the third lowest rate of erosion of all sites in the TFI. Although the 95% flow threshold at this site is very low, it is a product of how little erosion is actually occurring. By contrast, the 50% erosion flow threshold at this site was found to be 83,527 cfs which equates to a water surface elevation of El. 195, exceeded <1% of the time. It should also be noted that the erosion flow threshold at site BC-1R could not be established given that a reliable relationship between stage and discharge could not be developed in the Barton Cove area.

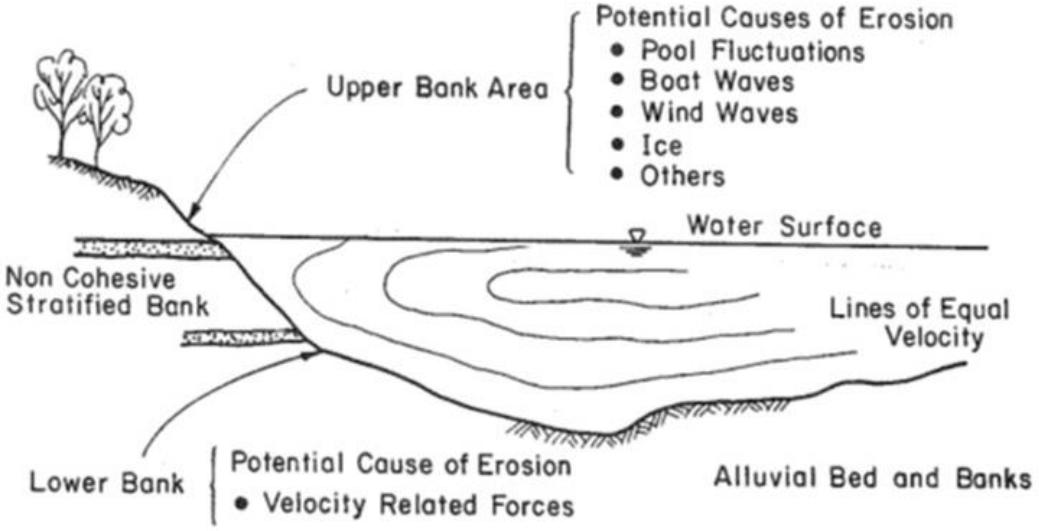

Figure 5.1.3-5: Assumed Initial Channel Conditions (USACE, 1979)

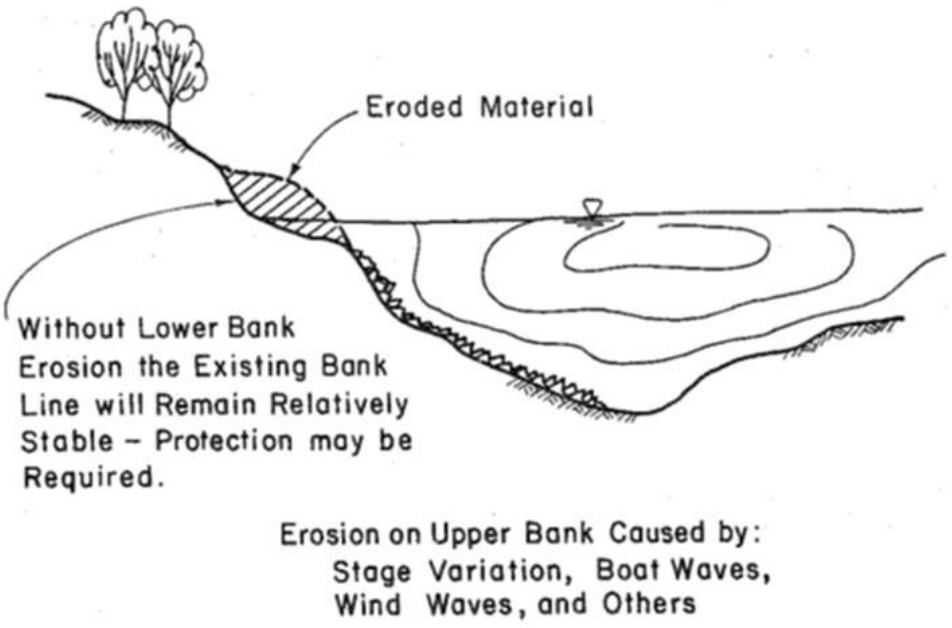

Figure 5.1.3-6: Potential Bank Line Geometry by Erosive Force Acting on the Bank near the Water Surface (USACE, 1979)

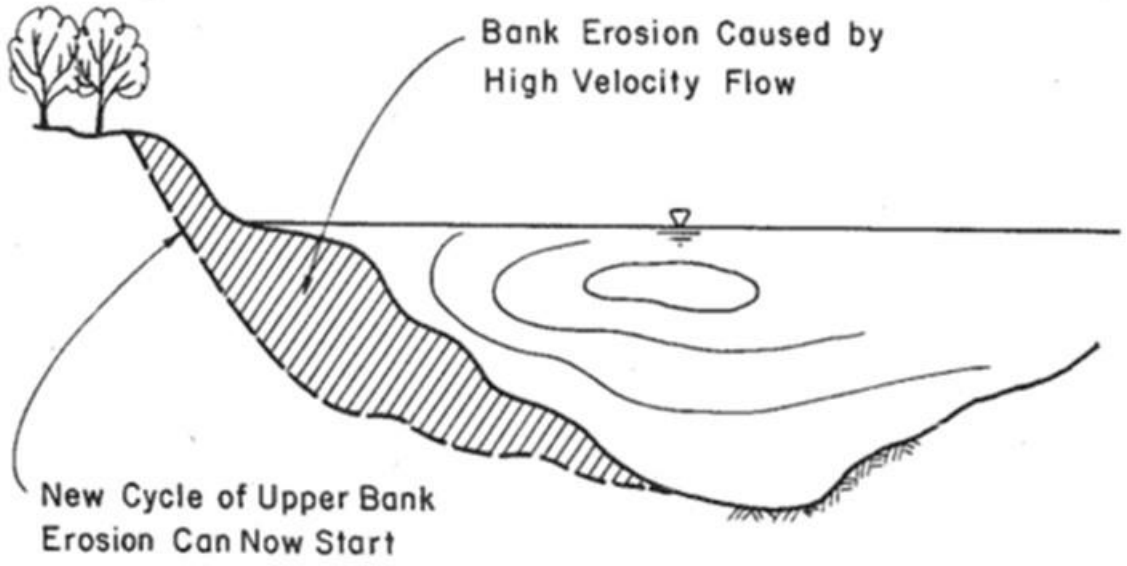

Figure 5.1.3-7: Bank Erosion Caused by Flood Stage High Velocity Flow (USACE, 1979)

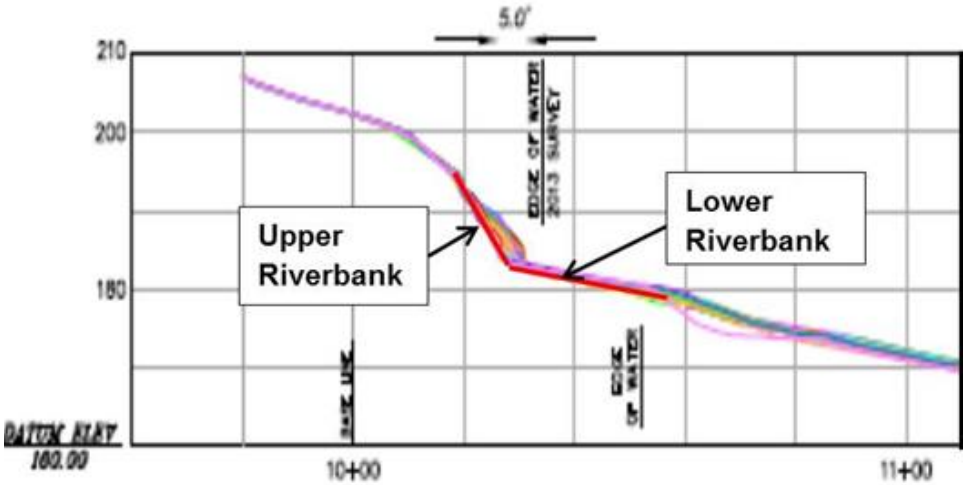

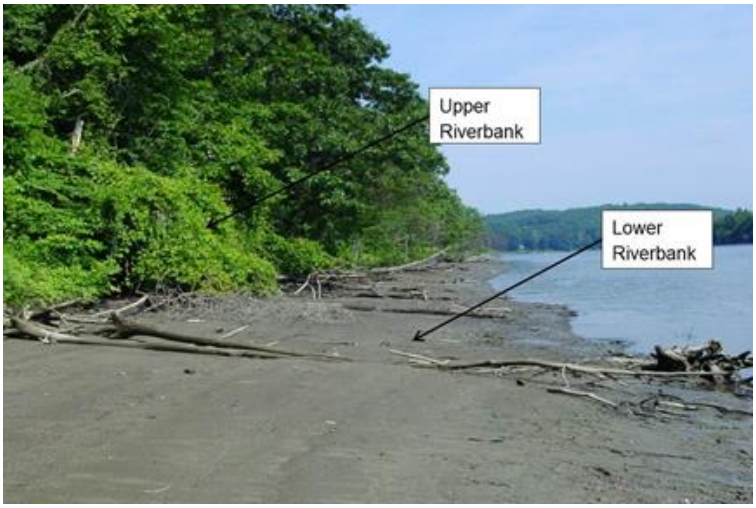

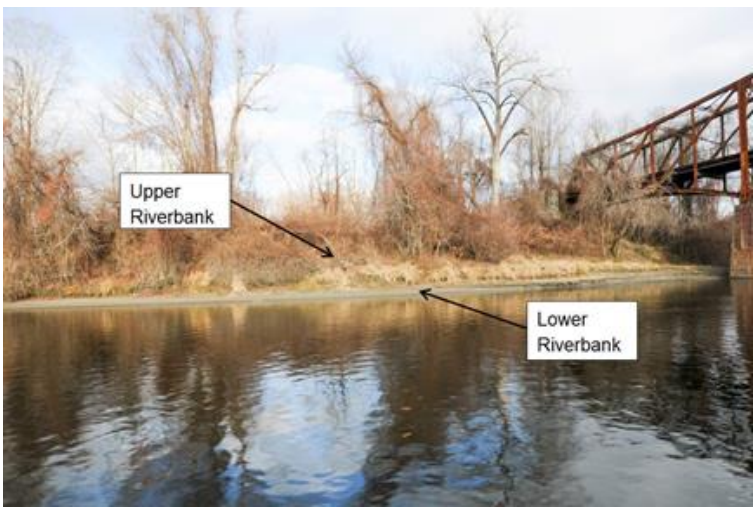

Figure 5.1.3-8: TFI Lower and Upper Riverbank Example

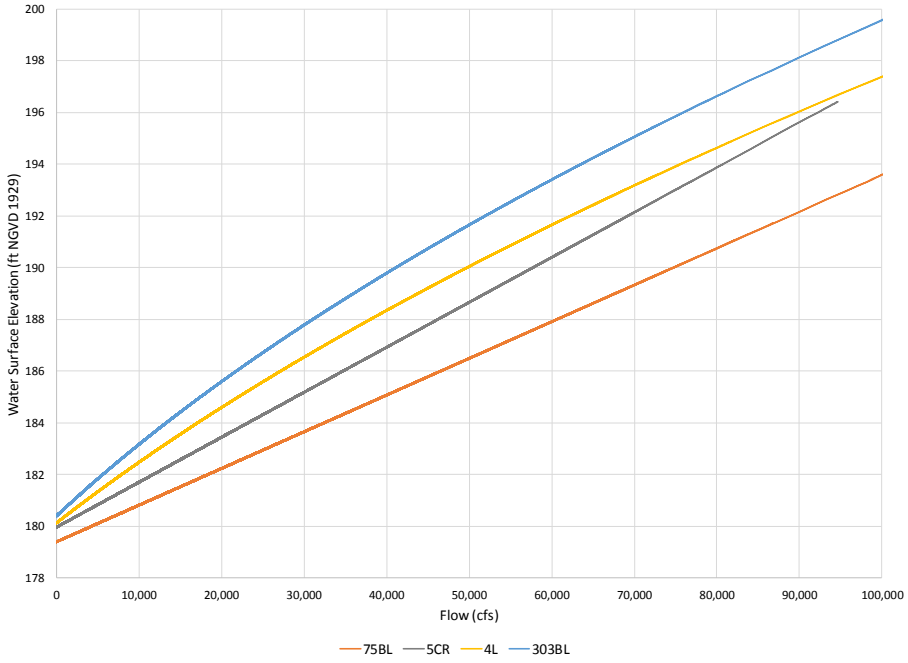

Figure 5.1.3-9 Generalized Stage vs Discharge Trendlines for 75BL, 5CR, 4L, and 303BL

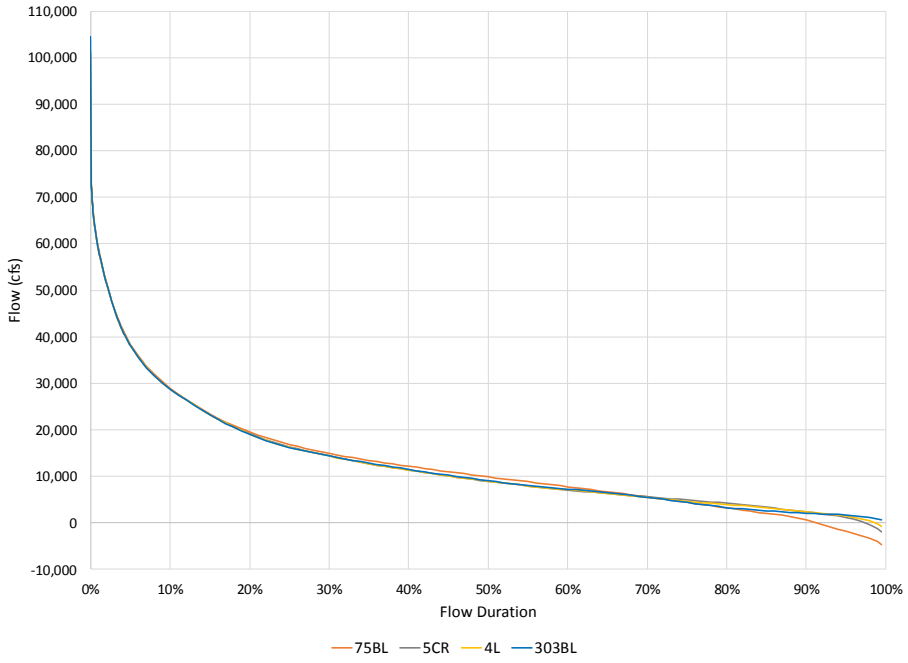

Figure 5.1.3-10 Flow Duration Curves for 75BL, 5CR, 4L, and 303BL

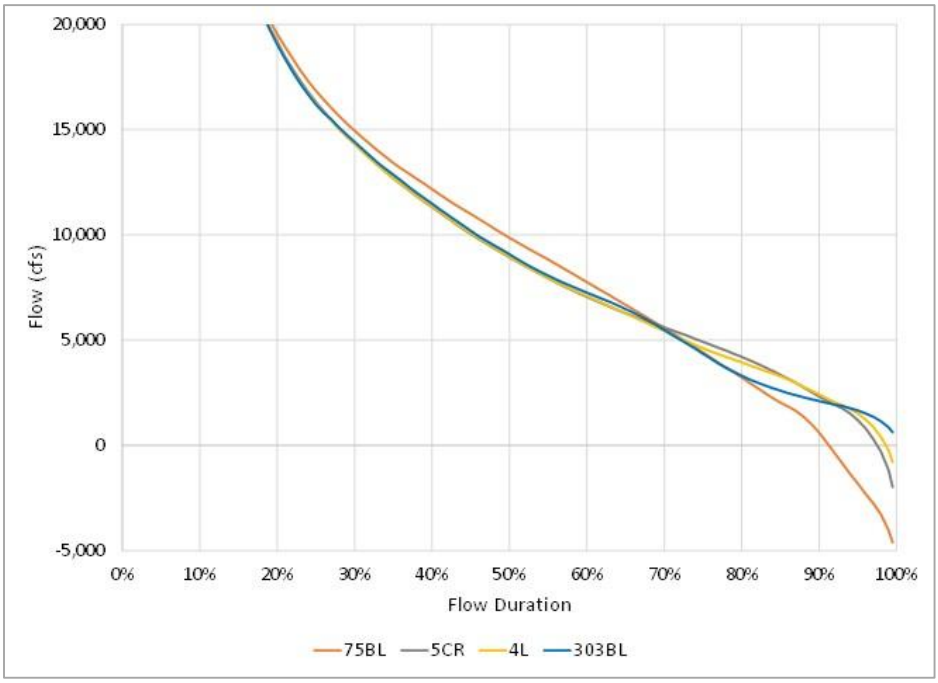

Figure 5.1.3-11 Zoomed in Flow Duration Curves for 75BL, 5CR, 4L, and 303BL

5.1.3.1 Hydrologic Effect of Northfield Mountain Operations

In order to understand the effect Northfield Mountain operations have on flow and water level fluctuations in the TFI, a number of historic time periods and modeled operational scenarios were analyzed. As presented below, analysis focused on two flow thresholds, (1) when the daily average inflow from Vernon Dam was below 18,000 cfs, and (2) when the daily average inflow from Vernon Dam exceeded 18,000 cfs. During these time periods the corresponding Project operations were investigated and the hydrologic effect at a number of detailed study sites was determined.

The low to moderate flow threshold (i.e., <18,000 cfs) was chosen as it represented a flow value just above the hydraulic capacities of Vernon (17,130 cfs) and Turners Falls (15,938 cfs) that would also take into consideration typical inflow from the Ashuelot and Millers Rivers. The moderate to high flow threshold (i.e., >18,000 cfs) was chosen as it represents conditions when Vernon operates in run-of-river mode (i.e., inflow equals outflow) and, as flow increases, the French King Gorge becomes the hydraulic control for the mid and upper TFI, as opposed to water level management at the Turners Falls Dam.

Flow and water level fluctuations during these flow periods were analyzed at the same subset of detailed study sites previously discussed, including:

- BC-1R: entrance to Barton Cove – low to moderate flow analysis only
- 75BL: just downstream of the Northfield Mountain tailrace
- 5CR: just downstream of the Rt. 10 Bridge
- 4L: downstream of the Pauchaug Boat Launch
- 303BL: between Upper Island and Stebbins Island

The transects associated with these detailed study sites were chosen as they covered the geographic extent of the TFI and were each located near one of the three hydropower projects on the TFI. Given that the results of the hydraulic model indicate that the French King Gorge becomes the hydraulic control for the mid and upper portion of the TFI at flows greater than 30,000 cfs (and potentially as low as 20,000 cfs), this analysis was not conducted at Site BC-1R for the moderate to high flow analysis.

Finally, it is important to reiterate that the flow thresholds used for this analysis refer to the inflow from Vernon and not the total TFI flow (i.e., without flow associated with Northfield Mountain operations). Depending on Northfield Mountain operations and the location in the TFI, the total flow can vary by as much as -15,200 cfs during pumping operations or +20,000 cfs during generation. For example, the inflow from Vernon at a given time could be 18,000 cfs, however, if Northfield Mountain is generating with 4 units the flow at site 75BL at that same time could be 38,000 cfs. This distinction will be important to remember when reviewing the BSTEM results found in Section 5.4.

Low to Moderate Flow Analysis (<18,000 cfs)

Northfield Mountain was not operational from May to November 2010 to allow for sediment removal in the Upper Reservoir. Examination of the modeled TFI water surface elevations during this time allows FirstLight to estimate the effects of water level variation within the TFI without Northfield Mountain's pumping and generation cycles. Although this analysis provides an idea of the effects of Northfield Mountain operations on flow and water level fluctuations during low flow conditions, it should be noted that also during this time FirstLight was not managing the water level at Turners Falls Dam as they typically would. That is, typical water level management at the Turners Falls Dam is based partially on Northfield Mountain's likely operational schedule. Figure 5.1.3.1-1 provides a representative time period (late June to

early August) in 2010 with Vernon's inflow and modeled water surfaces at 5 detailed study sites in the TFI. This graph shows that Vernon's base flow was about 2,000 cfs, peaking flow normally about 8,000 cfs with water level variation in the TFI normally about a foot per day.

In order to compare the May through November 2010 period when Northfield Mountain was not operational, the Vernon hydrologic and generation records were reviewed to find a similar May through November period. Upon review of the available information, the May to November 2012 period appeared to be similar to the 2010 period in terms Vernon generation and flow average. Table 5.1.3.1-1 provides a comparison of the monthly generation and flow values from Vernon for the May-November period for 2010 and 2012. While the correlation shown in Table 5.1.3.1-1 is not exact it is as close as was possible for recent years that are representative of current operations at Northfield Mountain. In addition to the monthly average generation and flows from Vernon, FirstLight also investigated if the mean daily flow, as measured at the Montague gage was similar for 2012 as it was for 2010 during the May-November time period. Figure 5.1.3.1-2 shows that similar to 2010, the daily flow at Montague was generally lower than average and other than in May and October, the 2010 and 2012 periods lacked the peak flows in the summer and higher than average flow periods that were common in 2008, 2009, 2011, 2013, and 2014. Based on these factors the 2012 period was used as a comparison.

Figure 5.1.3.1-3 provides an example of the flows from Vernon and Northfield Mountain and modeled water surface elevations at the 5 transects for July 20 – August 8, 2012, a low inflow period. This figure shows that daily water surface elevation fluctuations were about 3 feet on most days.

The hourly TFI water surface elevations from HEC-RAS were then used to analyze the maximum daily water surface elevation variation in the TFI at the five detailed study sites for the May to November 2010 and 2012 periods. In addition, two other periods were analyzed: (1) the entire period of record (2000-2014) other than May 1 – October 31, 2010, and (2) the entire period of record (2000-2014) other than May 1 – October 31, 2010 when the mean daily flow was less than 18,000 cfs from Vernon. The additional analysis using the full period of record were conducted to provide context. Given this, four datasets were analyzed for this analysis:

- The entire period of record (2000-2014) other than May1-Oct 31, 2010;
- The entire period of record (2000-2014) other than May 1-October 31, 2010 but only when the mean daily flow was less than 18,000 cfs from Vernon;
- The May 1 – October 31, 2010 period when the mean daily flow was less than 18,000 cfs from Vernon; and
- The May 1 – October 31, 2012 period when the mean daily flow was less than 18,000 cfs from Vernon.

18,000 cfs was chosen as the divider since it is slightly over the maximum generation capacity at Vernon (thus accounting for some inflow from the Ashuelot and Millers Rivers) and at those levels both the Vernon and Turners Falls Projects would be operating as a run of river. Only 18 days in the May 1 – October 31, 2010 period had a mean daily Vernon discharge above 18,000 cfs and 15 days in the same period in 2012. Figures 5.1.3.1-4 through 5.1.3.1-8 provide plots of how common the range of daily water surface elevation variations (at 0.4' intervals) are at the five transects. These plots show a similar general relationship for the daily extent of water surface elevation fluctuation at all 5 locations. For example, at 75BL near Northfield Mountain when the Vernon daily average flow is less than 18,000 cfs Figure 5.1.3.1-5 shows:

- For the May – November 2010 period: 60% of the daily WSEL variations were less than 0.8 feet, and 95% were less than 1.6 feet;

- For the May – November 2012 period: 20% of the daily WSEL variations were less than 1.6 feet and about 95% were less than 3.6 feet; and

- For all of the days (other than May – November 2010) that were modeled: 15% of the daily WSEL variations were less than 1.6 feet and about 95% were less than 4.0 feet.

As shown on the figures, when comparing the 95% value at each location for the 2010 and 2012 periods the combined effect of Northfield Mountain operations and Turners Falls Dam water level management accounts for approximately a 2 ft. fluctuation in water levels at the 5 detailed study sites.

Figure 5.1.3.1-9 provides a frequency curve for daily water surface elevation variation at 75BL near Northfield Mountain for days when Vernon had a mean daily flow of less than 18,000 cfs and over 18,000 cfs. This figure shows that, as expected, during days when Vernon flows are less than 18,000 cfs the daily water surface elevation variation is larger than during days with higher flows from Vernon.

Analysis of the May-November 2010 period combined with the modeled historical fluctuation analysis indicate that during low to moderate flows all three hydroelectric projects (Vernon, Northfield Mountain, and Turners Falls) affect flow and water levels in the TFI. During these periods, Vernon can discharge up to 17,130 cfs when peaking which, when combined with outflow from Northfield Mountain and water level management at Turners Falls Dam, can effect flow and water level fluctuations throughout the entire TFI. Vernon discharges were observed to affect water level fluctuations by up to a foot during the analysis period. The combined influences of Northfield Mountain operational cycles and management of the water level at the Turners Falls Dam for releases to the power canal are likely to have an effect on water level fluctuations of larger than one foot and generally in the two foot range, during low to moderate flow periods.

As previously noted, the flow thresholds established for this analysis were based on a mean daily flow from Vernon of 18,000 cfs. Depending on the location in the TFI, the total flow can reach as high as 37,000 cfs if Vernon (17,130 cfs) and Northfield Mountain (20,000 cfs) are generating at maximum capacity. In other words, even though the outflow from Vernon may only be 17,130 cfs, cumulative Vernon and Northfield Mountain operations can effect TFI hydrology up to 37,000 cfs at a given location.

Moderate to High Flow Analysis (>18,000 cfs)

When Vernon outflow exceeds 17,130 cfs both Vernon and Turners Falls operate in run-of-river mode (i.e., inflow is equal to outflow, no peaking). As the flow from Vernon (and the Ashuelot and Millers Rivers) increases, the effect of Turners Falls Dam operations on water surface elevation fluctuations decreases until the French King Gorge constriction become the dominant influence on water surface elevations in the mid and upper TFI. Based on the results of the hydraulic modeling, this typically occurs at flows equal to or greater than 30,000 cfs (but potentially as low as 20,000 cfs). At flows greater than 37,000 cfs, even though Northfield Mountain may still operate, the dominant hydrologic drivers are high inflows and hydraulic constrictions.

In order to determine the hydrologic effect of Northfield Mountain operations during high flow events historic time periods and modeled operational scenarios were analyzed. The period October 1-3, 2011 provides a historic example using actual data when inflow from Vernon exceeded 30,000 cfs and Northfield Mountain operated with a peak generation flow of 12,000 cfs and pumping flow of -10,000 cfs (Figure 5.1.3.1-10). As shown in the figure, historic (i.e., baseline) conditions were plotted against conditions from a HEC-RAS model run when Northfield Mountain was “turned off” (modeling Scenario 1, discussed later in this report in Section 5.2.1). The difference in water surface elevation of the historic condition and Scenario 1 indicate the effect of Northfield Mountain operations on water level at four of the detailed study sites during a high flow period. The results of this analysis found that during the October 1, 2011 generation period, the greatest difference in water surface elevations were observed at, or near, the Northfield Mountain

tailrace with progressively smaller differences observed in the upstream direction. Specifically, the analysis demonstrated (from downstream to upstream):

- **Site 75BL**: Observed difference in water surface elevation = 1.2 feet;
- **Site 5CR**: Observed difference in water surface elevation = 0.9 feet;
- **Site 4L**: Observed difference in water surface elevation = 0.7 feet; and
- **Site 303BL**: Observed difference in water surface elevation = 0.5 feet.

Examination of the October 2, 2011 pumping cycle exhibited similar differences in water surface elevation.

For the purpose of this study, a flow of 37,000 cfs at a given location (i.e. not Vernon inflow or naturally routed flow but instead the combined flow of all hydrologic influences) was determined to be the flow threshold at which natural high flows become the dominant driver of hydrologic conditions in the TFI for hydraulic reaches 1, 2, and 3 (hydraulic reaches are discussed in Section 5.4.1.1). For hydraulic reach 4 (upper most portion of the TFI near Vernon) 17,130 cfs was determined to be the natural high flow threshold as this represents the hydraulic capacity of the Vernon Project. 37,000 cfs was chosen as the natural high flow threshold for the majority of the TFI for a number of reasons, including: (1) it exceeds the flows at which the French King Gorge becomes the hydraulic control for the mid and upper portion of the TFI; (2) it exceeds the hydraulic capacity of Vernon; (3) it exceeds the maximum combined hydraulic capacity for Vernon and Northfield Mountain at a given location; and (4) although Northfield Mountain may still operate at flows greater than 37,000 cfs, historical operating records indicate this is less frequent than at lower flows.

In order to determine if 37,000 cfs was an appropriate flow threshold above which could be considered naturally occurring high flows, FirstLight reviewed the available Project operating data for the period 2000-2014 to determine the amount of time the Project operated at flows greater than 30,000 and 37,000 cfs (Table 5.1.3.1-2). As demonstrated in the table, the Project operated from 2000-2014 when flows exceeded 37,000 cfs as follows:

- Generation with 1 or more units occurred 2.6% of the time;
- Generation with 2 or more units occurred 0.82% of the time;
- Generation with 3 or more units occurred 0.14% of the time; and
- Generation with 4 units occurred 0.025% of the time;

This equates to about 9, 3, 0.5, and 0.1 days per year, respectively. Pumping operations when flows exceeded 37,000 cfs were found to follow a similar pattern.

Although FirstLight rarely operates Northfield Mountain when flows are greater than 37,000 cfs, they do still operate it at times and therefore can still have an effect on flows and water levels. In order to understand these potential effects, FirstLight executed four unsteady HEC-RAS model runs at flows of (1) 30,000 cfs; (2) 40,000 cfs; (3) 50,000 cfs; and (4) 60,000 cfs. 30,000 cfs was chosen as the low end of this analysis as it represents the flow at which the French King Gorge becomes the hydraulic control for the mid and upper portions of the TFI; whereas, 60,000 cfs was chosen as the high end of the analysis as it represents flows just below the point at which Northfield Mountain operations are determined by the USACE agreement (65,000 cfs). As a result of the requirements of the USACE agreement Northfield Mountain operations have

minimal to no effect on flow or water level fluctuations at flows greater than 65,000 cfs, if the Project operates at all.

During each of the model runs Northfield Mountain operations were modeled as follows:

- **1 & 2 Unit Generation ("typical" gen)**:8 hours at 10,000 cfs (2 generators); and

  8 hours at 5,000 cfs (1 generator)

- **1 & 2 Unit Pumping ("typical" pump)**:8 hours at 7,600 cfs (2 pumps); and

  8 hours at 3,800 cfs (1 pump)

The model runs were used to determine the effects that Northfield Mountain can have on water levels in the TFI by examining the results at the same four detailed study sites previously discussed in this section. The mean daily pumping and generation volume from the Upper Reservoir is about 4,200 acre-feet (about 1/3 of the total storage in the upper reservoir) for the 2000 to 2014 period. The average volume is equivalent to about 5 hours of generation with 2 units and slightly less than 7 hours of pumping with 2 units. However, Northfield Mountain operations often vary in the duration of the pumping and generation and the number of active units due largely to market cost of electricity. Therefore to analyze the effects of more typical pumping and generation cycles, FirstLight analyzed 1 and 2 unit operations at 8 hours a day which are more similar to the operations at Northfield Mountain and 'bounds' the long term daily operational average.

Figures 5.1.3.1-11 through 5.1.3.1-14 show the effects on the modeled water surface elevation at the four locations for the typical modeled scenarios summarized above. As shown on the figures, during more typical Northfield Mountain operations the water surface elevation near the Northfield Mountain tailrace (Site 75BL) could raise by about 1.4 ft or lower by about 1.0 ft. The effects are observed to progressively decrease in the upstream direction with water surface elevation increases on the order of about 0.6 feet and a decrease of about 0.3 ft. near Site 303BL.

Table 5.1.3.1-1: Monthly Generation and Flows at Vernon for 2010 and 2012

Year	Monthly Vernon Generation (MWH)						
	May	Jun	Jul	Aug	Sep	Oct	Average
2010	17,297	9,345	7,265	6,489	3,912	17,200	10,251
2012	20,322	13,912	6,900	4,566	5,709	11,832	10,540
Year	**Monthly Vernon Discharge (cfs)**						
2010	10,965	7,147	4,225	4,204	2,570	20,934	8,341
2012	16,563	9,915	3,625	2,674	3,320	7,400	7,250

Table 5.1.3.1-2: Analysis of Northfield Mountain Operations during High Flows

% of Time	NFM Operations - Gen				NFM Operations – Pump			
	Inflow <30,000 cfs	Inflow <37,000 cfs	Inflow >30,000 cfs	Inflow >37,000 cfs	Inflow <30,000 cfs	Inflow <37,000 cfs	Inflow >30,000 cfs	Inflow >37,000 cfs
4 Units	0.3%	0.3%	<0.05%	<0.05%	3.8%	3.8%	0.2%	0.2%
3 or more units	3.1%	3.2%	0.2%	0.1%	11%	11%	1.1%	0.7%
2 or more units	14%	15%	1.2%	0.8%	18%	19%	2.2%	1.3%
1 or more units	36%	37%	4.3%	2.6%	26%	27%	3.0%	1.9%

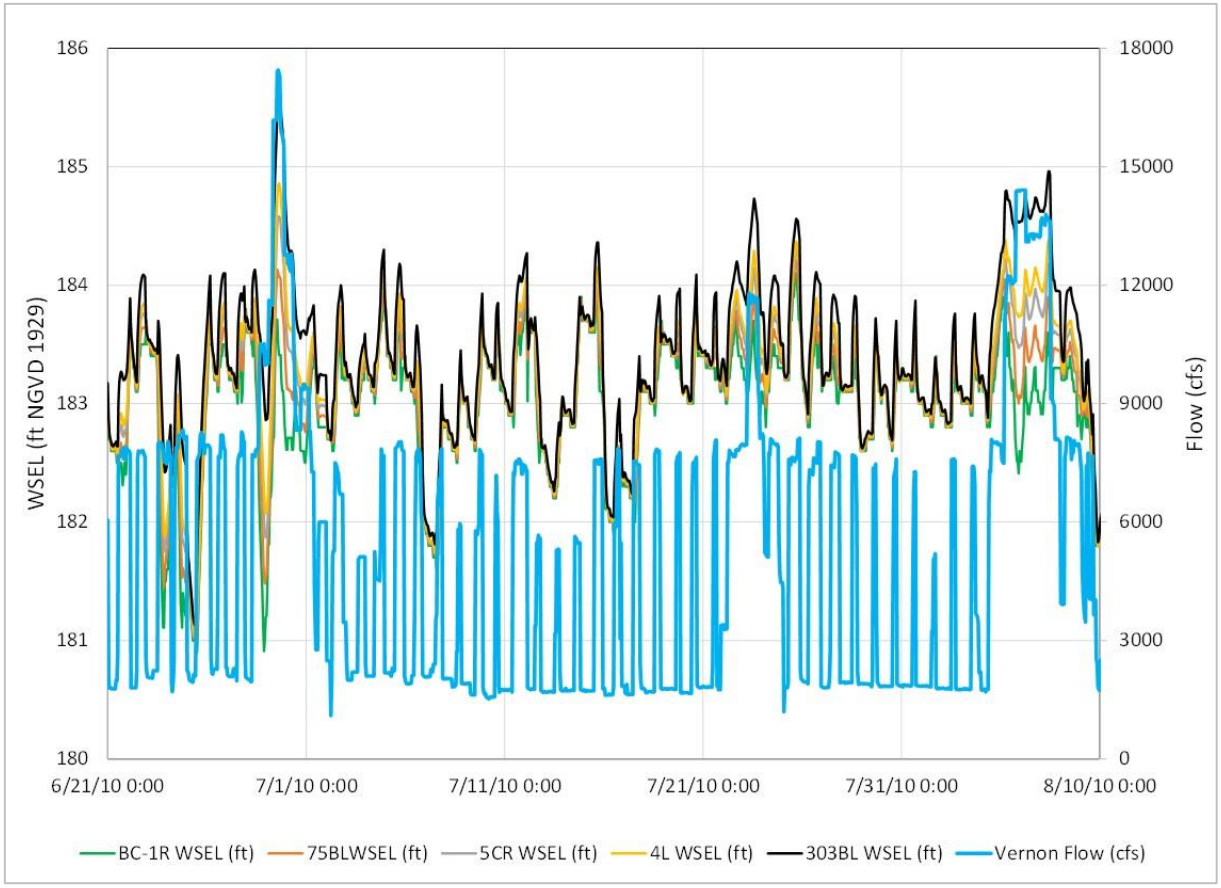

Figure 5.1.3.1-1: Turners Falls Impoundment Modeled Water Surface Elevations for June 21 – August 10, 2010

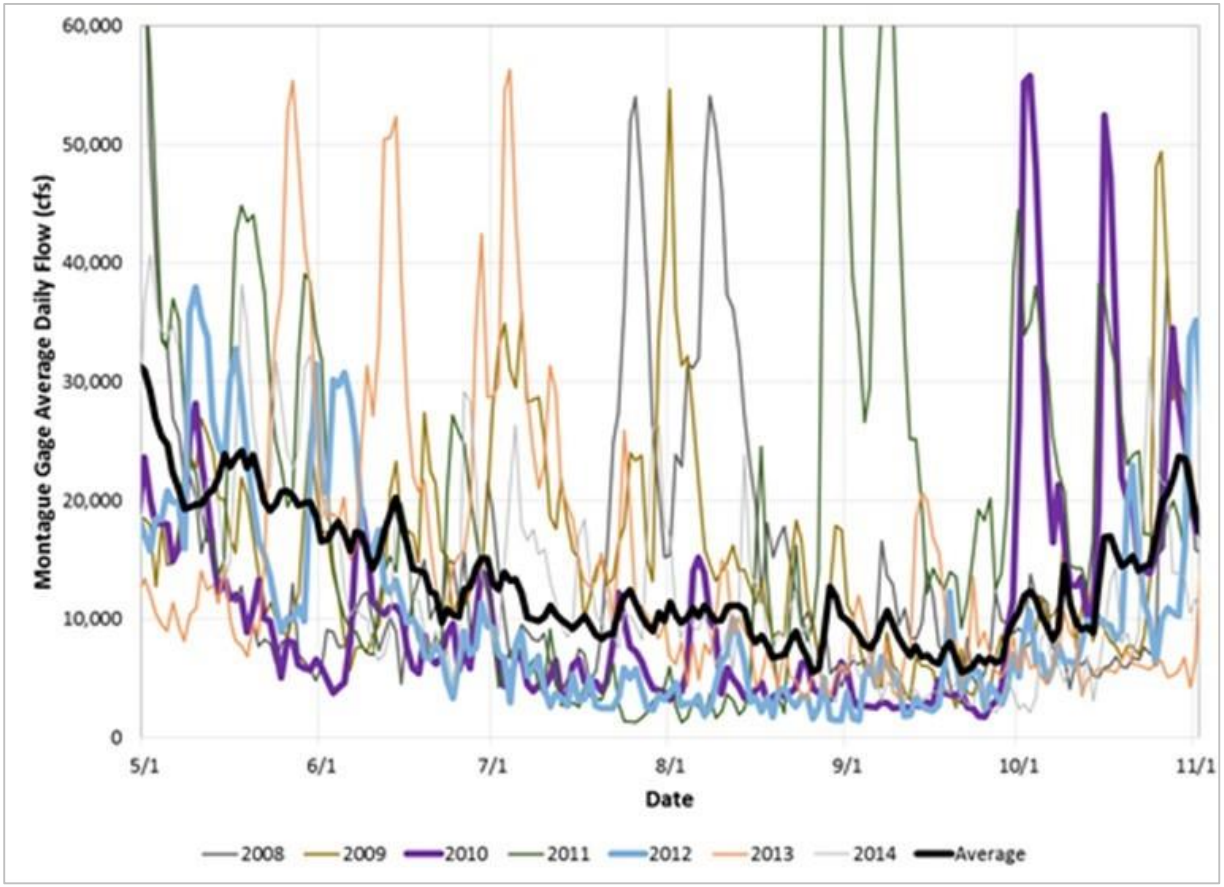

Figure 5.1.3.1-2: Mean Daily Flows at the Montague Gage - May 1 – November 1 for 2008-2014

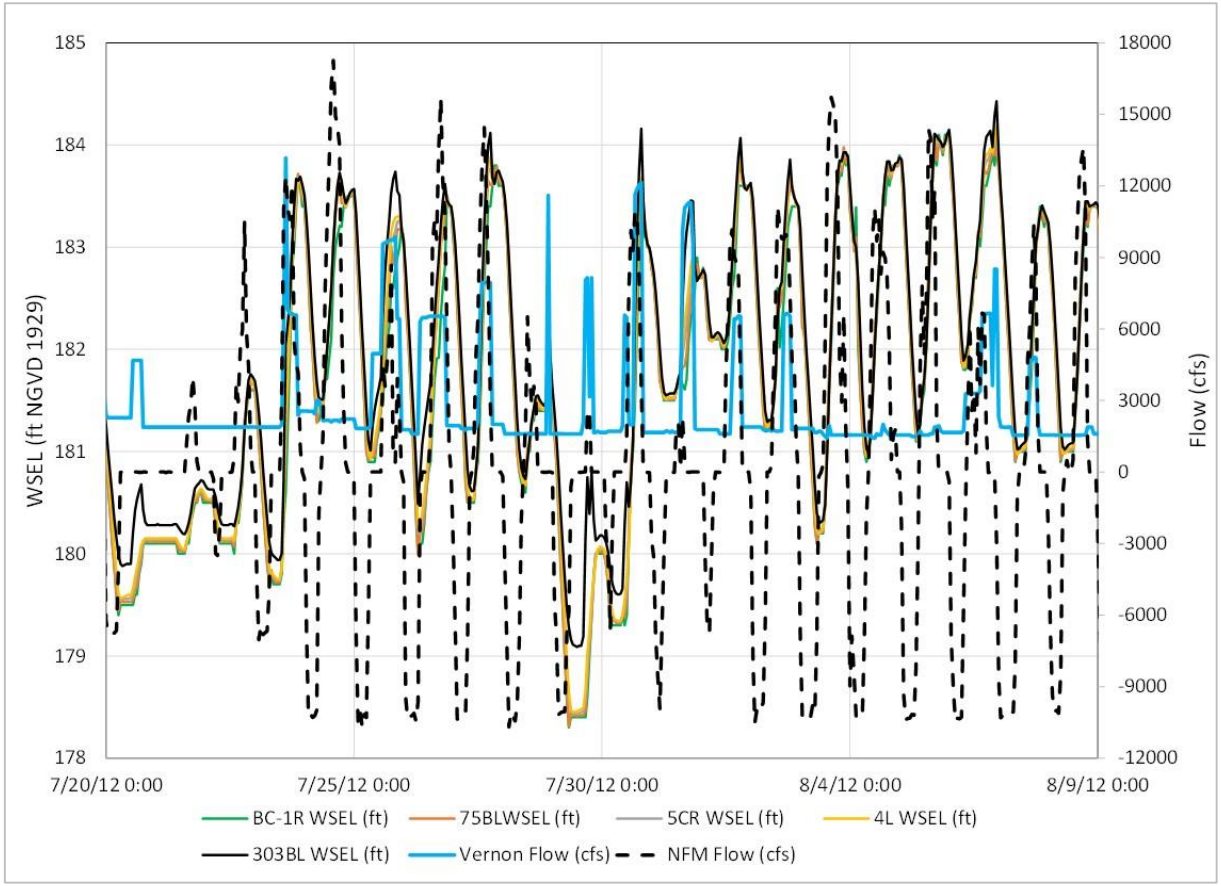

Figure 5.1.3.1-3: Turners Falls Impoundment Modeled Water Surface Elevations – July 20 – August 8, 2012

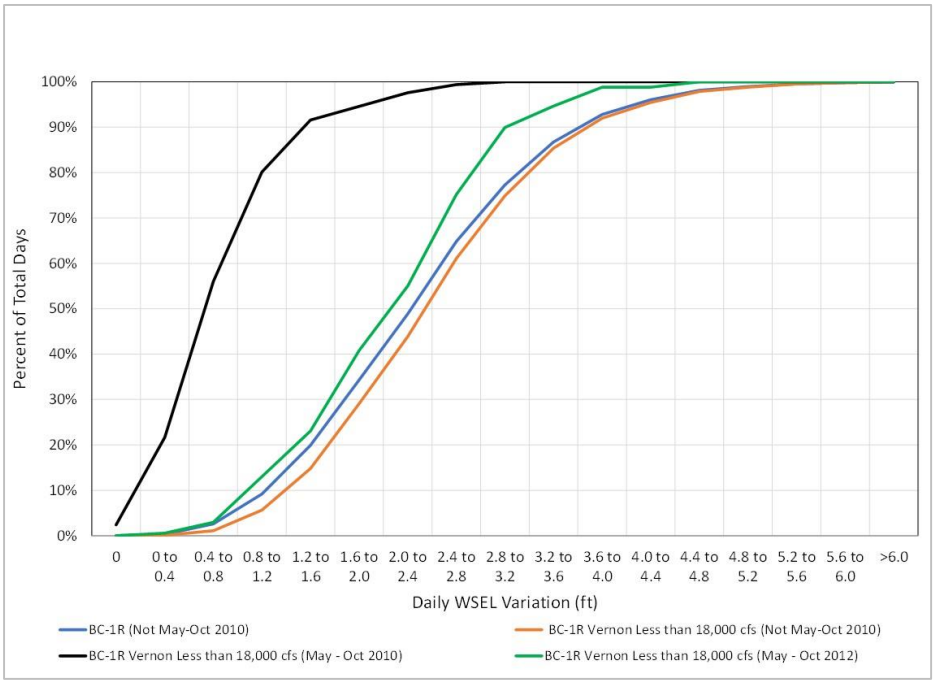

Figure 5.1.3.1-4: Modeled Historical Fluctuations at Transect BC-1R

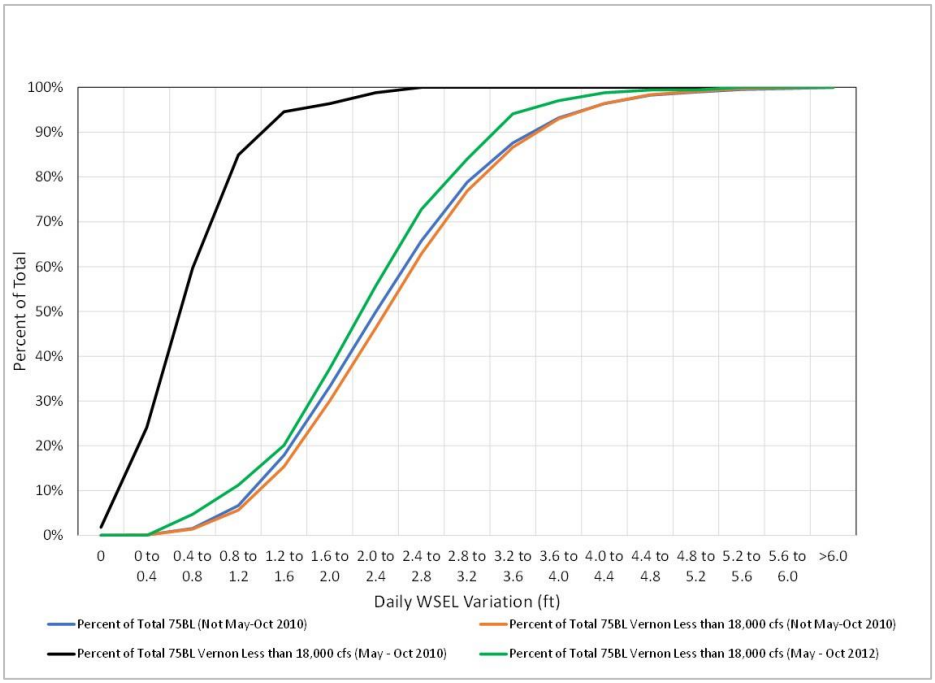

Figure 5.1.3.1-5: Modeled Historical Fluctuations at Transect 75BL

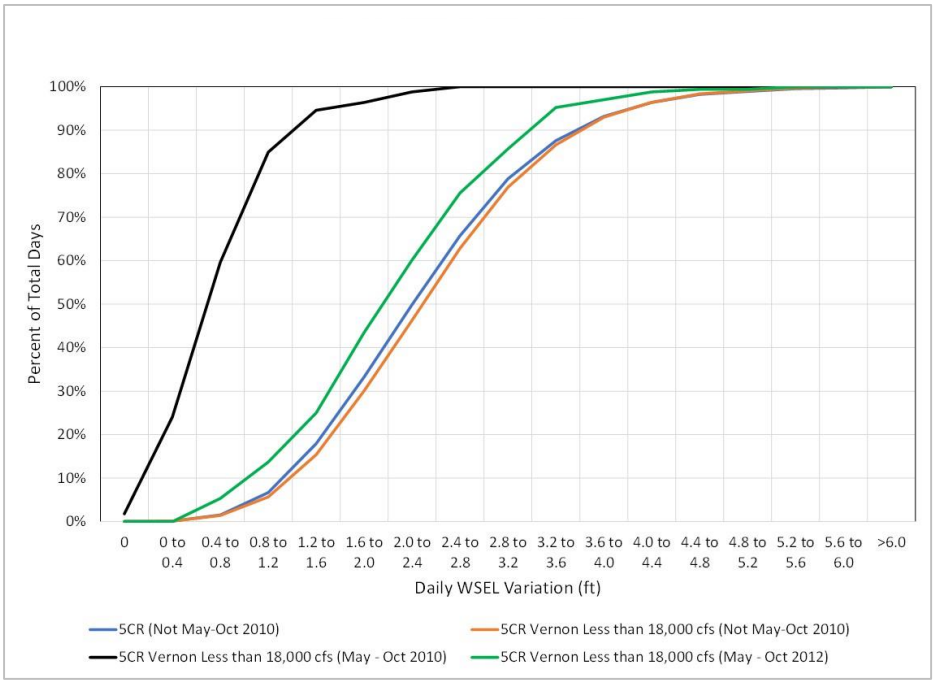

Figure 5.1.3.1-6: Modeled Historical Fluctuations at Transect 5CR

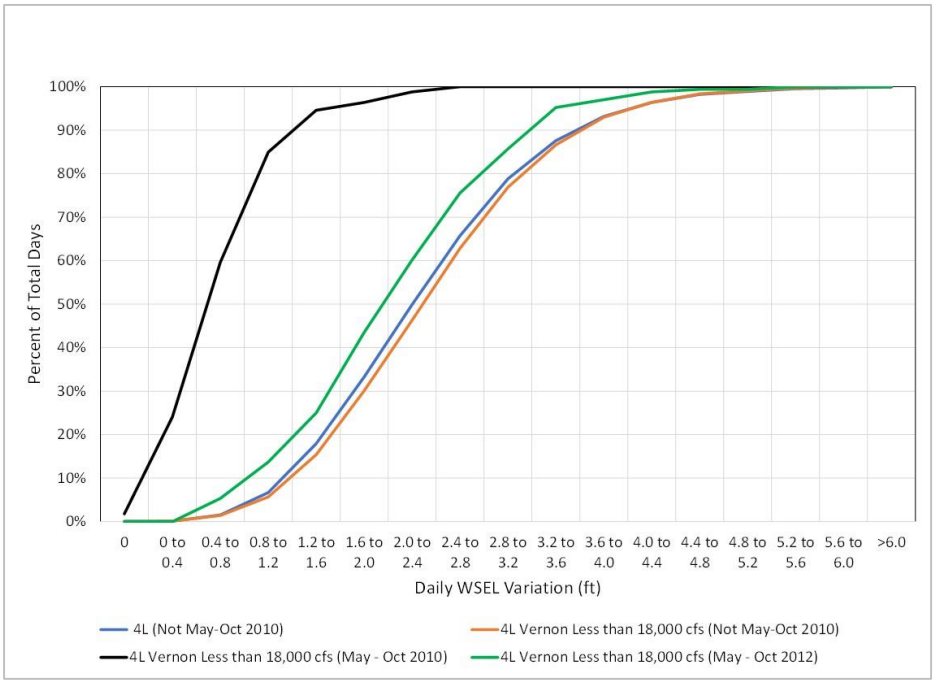

Figure 5.1.3.1-7: Modeled Historical Fluctuations at Transect 4L

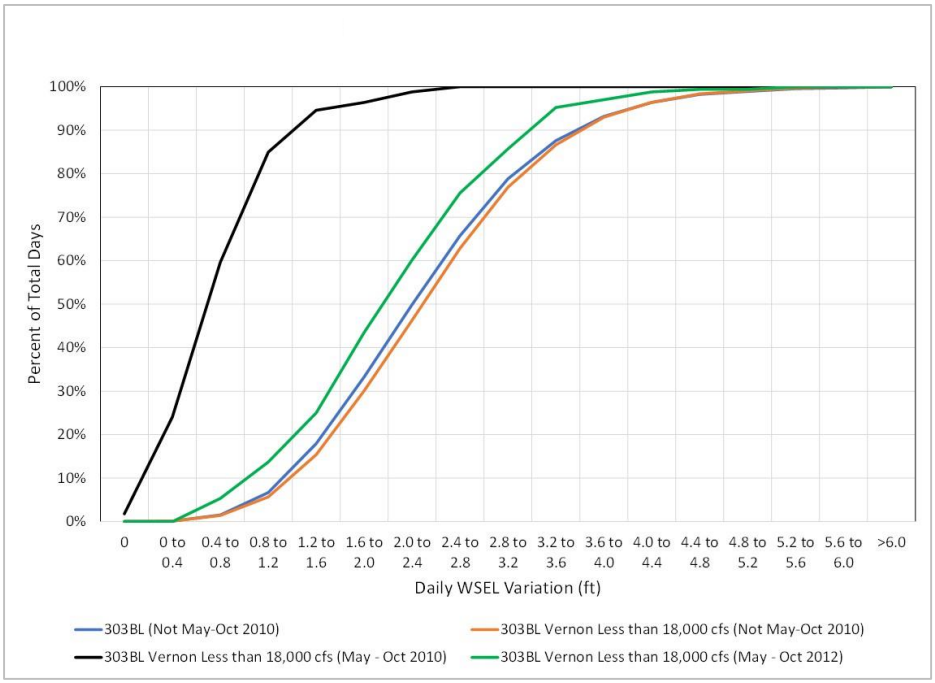

Figure 5.1.3.1-8: Modeled Historical Fluctuations at Transect 303BL

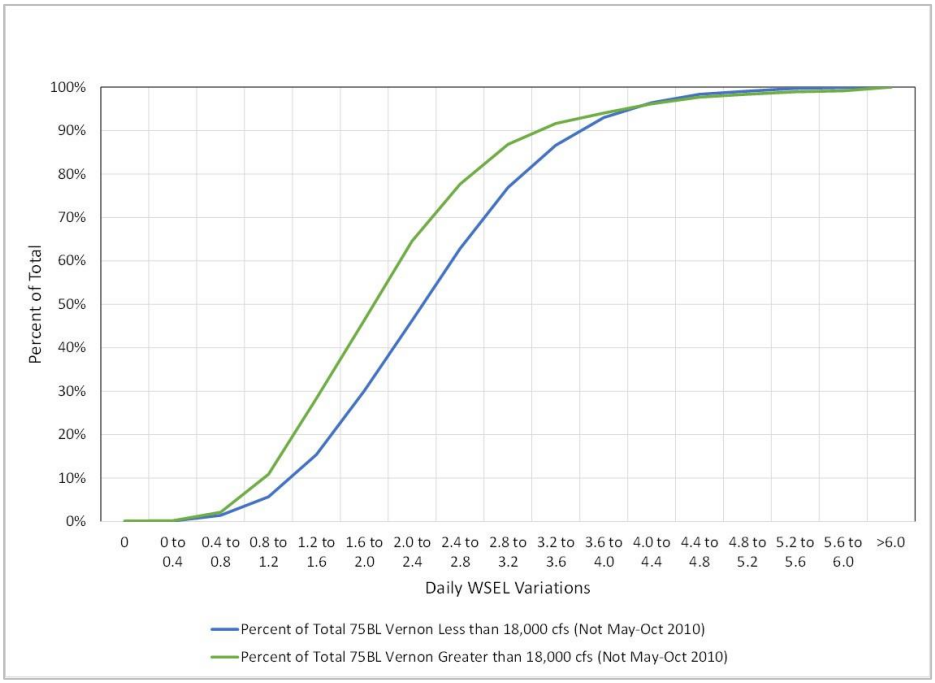

Figure 5.1.3.1-9: Frequency of Daily Water Surface Elevation Variations at Transect 75BL

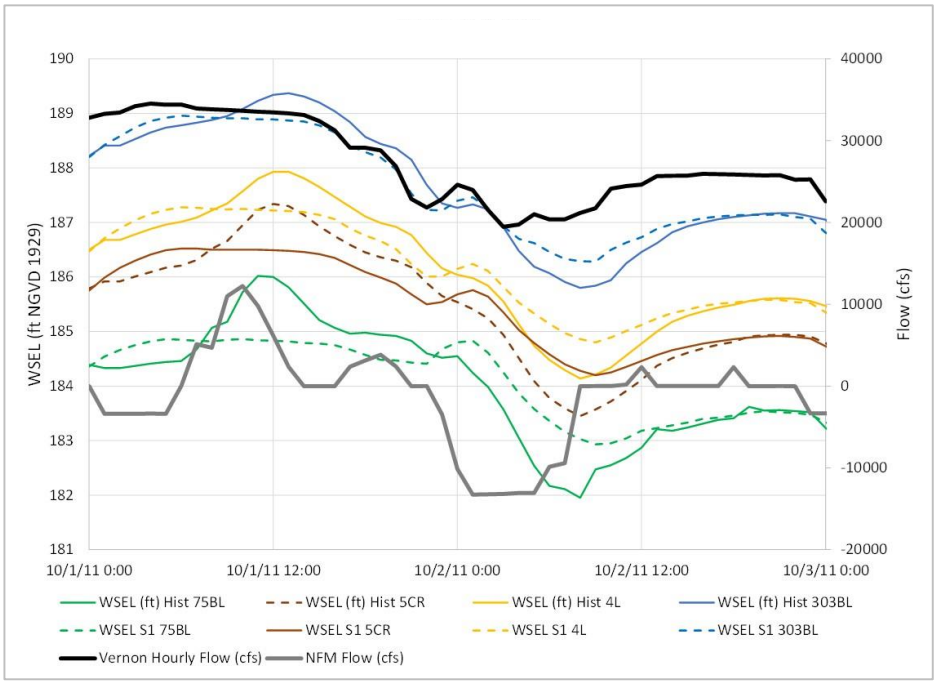

Figure 5.1.3.1-10: Effects of Northfield Mountain Generation during October 1-3, 2011

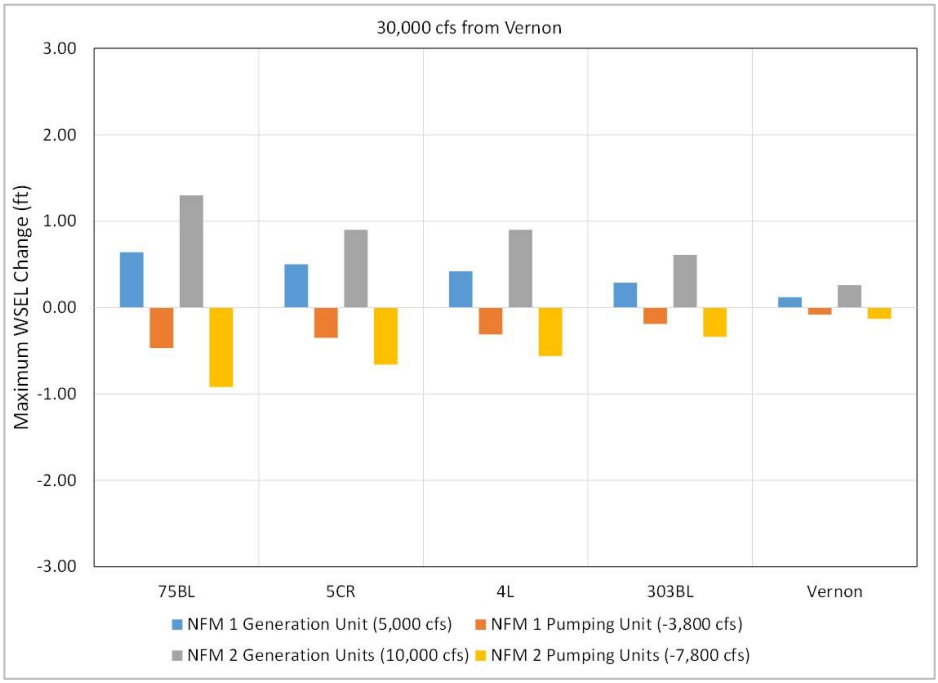

Figure 5.1.3.1-11: Modeled Typical Effects of Northfield Mountain Generation and Pumping during a Vernon inflow of 30,000 cfs

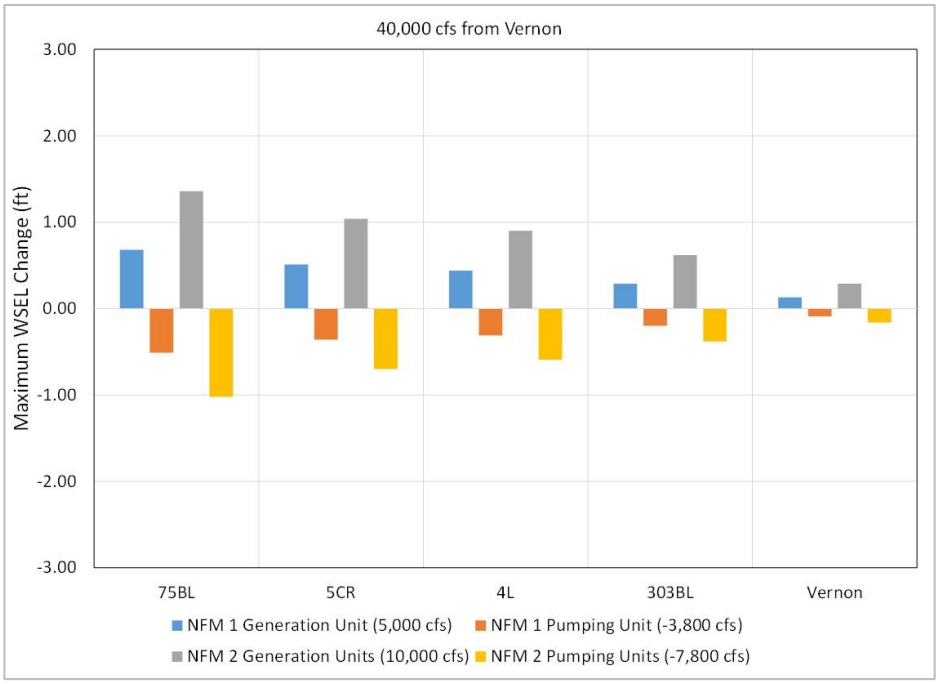

Figure 5.1.3.1-12: Modeled Typical Effects of Northfield Mountain Generation and Pumping during a Vernon inflow of 40,000 cfs

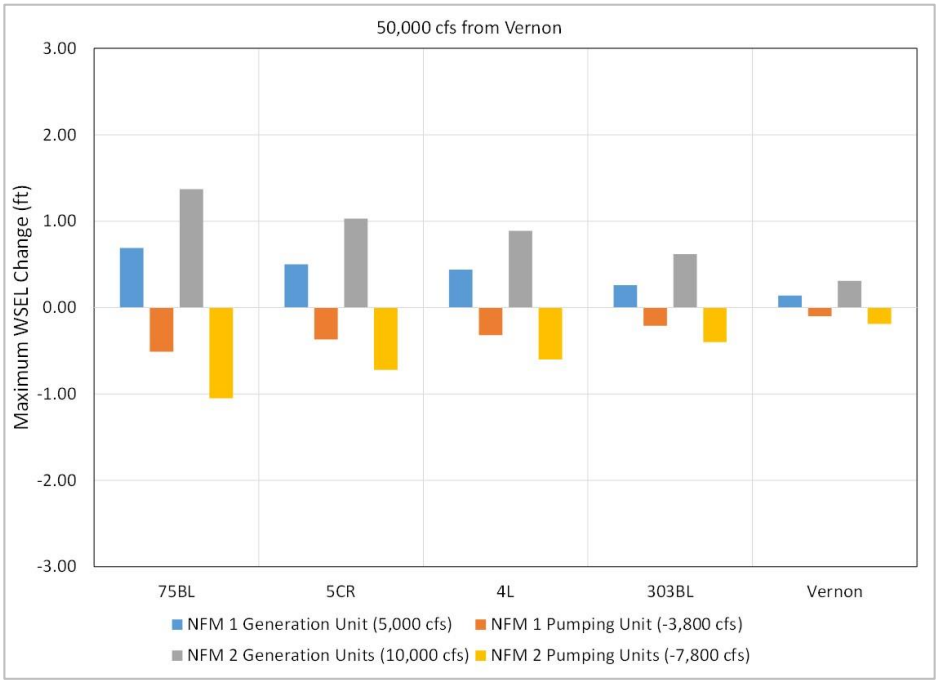

Figure 5.1.3.1-13: Modeled Typical Effects of Northfield Mountain Generation and Pumping during a Vernon inflow of 50,000 cfs

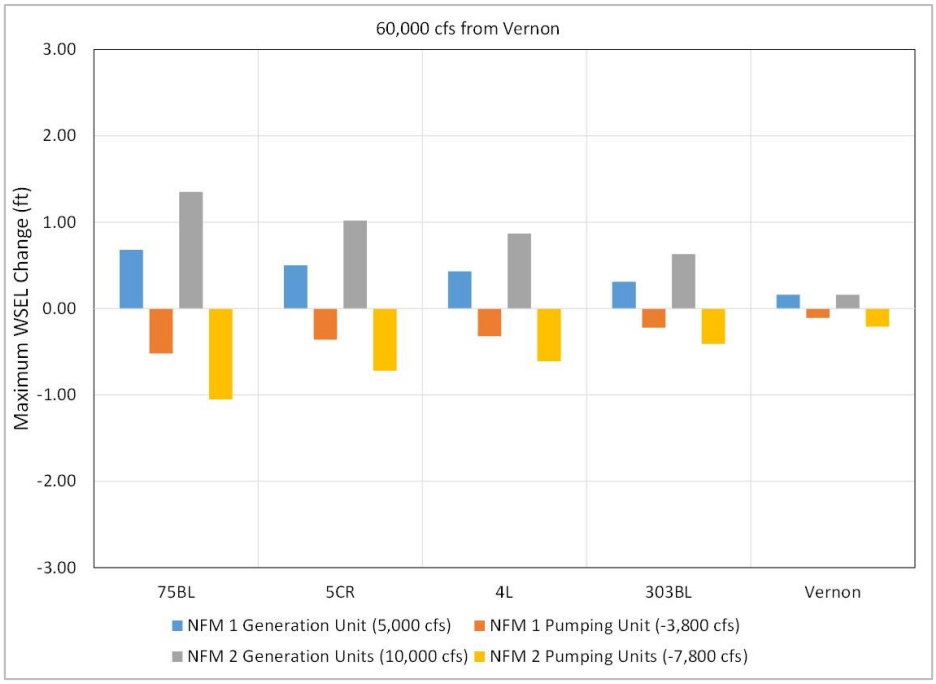

Figure 5.1.3.1-14: Modeled Typical Effects of Northfield Mountain Generation and Pumping during a Vernon inflow of 60,000 cfs

5.2 Hydraulics

Hydraulic modeling using HEC-RAS[37] and River2D [38] were conducted as an integral part of various studies associated with the Turners Falls / Northfield Mountain relicensing, including to provide data for this study. These models determined the water level fluctuations within the TFI that are affected by inflow from the TransCanada's Vernon Project, FirstLight Project operations, and inflows from tributaries. Both models require similar types of input data which included riverbed and bank geometry, flows, and water level data.

Full details of the HEC-RAS model, including the collection of the field data, model setup, model calibration, and analyses were provided in the study report for Study No. 3.2.2 *Hydraulic Study of Turners Falls Impoundment, Bypass Reach and Below Cabot* dated March 2015 (FirstLight, 2015b). The 2-dimensional River2D model was developed for the entire TFI from Vernon to Turners Falls Dam specifically for this study. Once calibrated, a number of production runs were executed to evaluate velocities and shear stresses in the near-bank area at each of the detailed study sites and other areas of interest.

Results from both of these modeling efforts were utilized to determine the water level variation throughout the TFI and shear stresses in the near bank environment. Both the HEC-RAS and River2D models are discussed in more detail in the ensuing sections.

5.2.1 HEC-RAS Modeling

The HEC-RAS model was initially calibrated to the water surface elevations (WSEL) measured at eight water level loggers during two periods when WSEL and flow fluctuations were minor (quasi steady-state conditions). The initial calibration, by adjusting the Manning's n value and the expansion and contraction coefficients, was completed during the following periods:

- May 4-5, 2014: Vernon average flow= 25,785 cfs (high flow event)
- May 8, 2014: Vernon average flow= 17,141 cfs (near Vernon's hydraulic capacity of 17,130 cfs)

Further fine-tuning of the Manning's n values occurred during unsteady-state conditions within the range of accurate flow measurement (turbine operations instead of spillage operations at Vernon) since this is the more common condition in the TFI and is more realistic than the quasi steady-state conditions used for the initial calibration. The flow and WSEL data for the period the water level loggers operated in the TFI were reviewed to identify periods where maximum peaking operations at Vernon and Northfield Mountain cycling occurred. Typically, these conditions occur during low flow, high energy demand periods in the mid-to-late summer. The period selected for further model calibration was August 24 to September 3, 2014, which exemplified peak electrical demand and low flow during non-generation periods.

Section 4 of the March 2015 Study No. 3.2.2 report contains figures of the comparisons of the observed to modeled WSELs for each of the water level logger locations. However, as an example, Figure 5.2.1-1 provides a comparison between the observed and modeled conditions at the Rt. 10 Bridge, near the middle of the TFI. As this figure (and the figures in the March 2015 Study No. 3.2.2 report) indicates, there is an excellent match relative to the magnitude and timing of the observed versus modeled WSELs at the water level loggers. Given the closeness of fit between observed and modeled conditions, the hydraulic model was deemed fully calibrated. Because the hydraulic model is well-calibrated to observed conditions, it was

[37] HEC-RAS Hydrologic Engineering Center River Analysis System is a one-dimensional hydraulic model developed by the USACE.
[38] River2D was developed at the University of Alberta and is a two-dimensional finite element depth averaged hydrodynamic and fish habitat model.

used to predict WSEL's at different locations in the TFI as long as the following data were available: Vernon discharge, USGS gage flows for the Ashuelot and Millers Rivers, Northfield Mountain operational data (pumping or generating flows), and elevation data at the Turners Falls Dam.

In support of the BSTEM modeling efforts associated with this study and the various supplemental analyses which were conducted (including those discussed in Section 5.1), the HEC-RAS model was utilized to generate historic (baseline) water levels and energy grade-line slopes on an hourly basis at the 25 detailed study sites. The Baseline Condition modeling scenario utilized historic upstream inflows at Vernon and tributaries (Ashuelot and Millers Rivers), Northfield Mountain operations, and historic water levels at the Turners Falls Dam. In addition to the Baseline Condition, an additional scenario was developed to provide water level and energy grade-line slope data for the BSTEM modeling at the 25 detailed study sites. The HEC-RAS scenarios used the January 1, 2000 to December 31, 2014 period and historic tributary inflows. The two HEC-RAS modeling scenarios had the following input variables:

- **Baseline Condition**: an hourly model mimicking historic conditions in the TFI.
- **Scenario 1**: an hourly model with Northfield Mountain idle but historic operation at both Vernon and the water level at TFI.

A more in-depth discussion of the scenarios used for the BSTEM modeling are provided in Section 5.4.1.

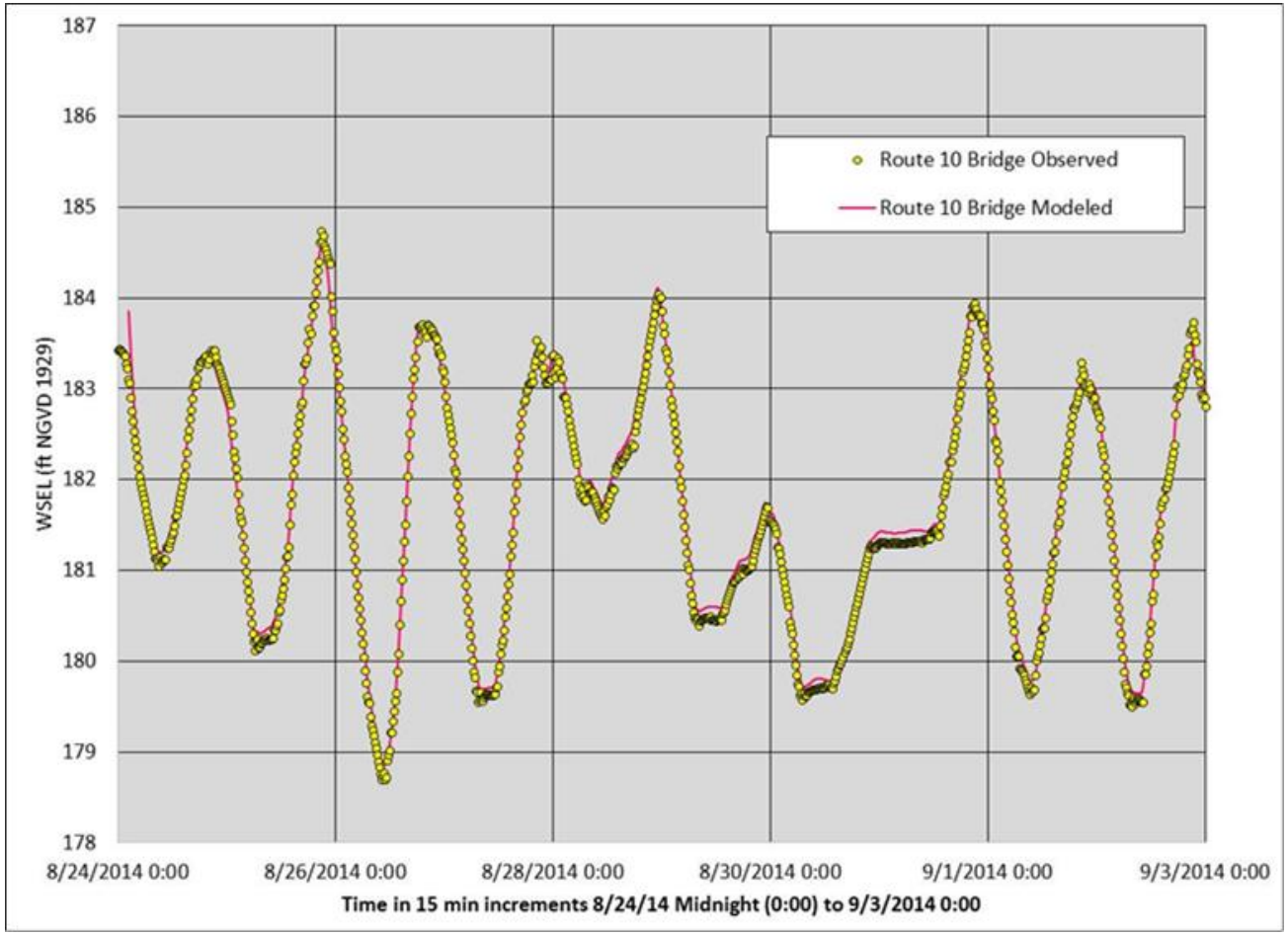

Figure 5.2.1-1 Comparison of Observed and Modeled WSELs at the Route 10 Bridge for the period August 24-September 3, 2014

5.2.2 River2D Modeling

The modeling program River2D was utilized to develop a two-dimensional model of the TFI to evaluate velocities and shear stresses over a range of flows. Due to the size of the TFI, the study area was split into two separate models with approximately 1.25 miles of overlap. This overlap allows for results from the downstream model to be used to define the downstream boundary condition of the upstream model while decreasing the possibility of boundary effects from the upstream boundary of the downstream model. The bed and mesh geometry were built with a finer resolution in the areas immediately surrounding the detailed study sites, while the remainder of the model has a courser resolution adequate for flow conveyance.

The model is intended for steady state evaluations, therefore calibration and verification of the roughness coefficients for each model was performed using observed conditions which were approximated to be steady state. The models were calibrated to an event with a discharge of approximately 31,200 cfs at the Turners Falls Dam, and then verified with three events with discharges at the Turners Falls Dam of approximately 2,500 cfs, 18,600 cfs, and 31,200 cfs. These events represent the full range of available observed flows for which steady state assumptions could be assumed. Calibration and verification at the observed stations was within 0.5 feet throughout the TFI, and generally within 0.25 feet. It should be noted that calibration of hydraulic models to within 0.5 feet is a common industry standard, and that the potential measurement error of the observation stations is approximately 0.2 feet.

Six production runs were performed for a range of conditions, including normal operating conditions, commonly occurring flows that might occur every few years, and more extreme events including the 100-year flood. None of these production runs assumed operation at Northfield Mountain. The primary impact of Northfield Mountain operations on model results at the detailed study sites would be to the range of flows evaluated at particular sites. With the wide range of flows that were analyzed, the exclusion of Northfield Mountain operations in the productions runs is not expected to impact the overall results of the analysis. Further, inclusion of Northfield Mountain operations is not expected to have a significant impact on near bank velocities at any of the detailed study sites for the range of flow conditions analyzed. Existing operations at Turners Falls Dam, and the Federal Emergency Management Agency's (FEMA) Flood Insurance Study (FIS) for Montague in Franklin County, Massachusetts were used to develop the production runs. Table 5.2.2-1 provides an overview of the boundary conditions used for the six production runs. The River2D model does not include bridge decks, but this is not expected to impact the results as water surface elevations remained lower than the bridge low chords reported in the FEMA FIS at all locations along the TFI for all production runs.

The results of the River2D model were used to evaluate velocity and shear stress in the near-bank area at each of the detailed study sites as well as other areas of interest. Discussion related to this analysis can be found in Section 5.5.1.

Table 5.2.2-1: River2D Production Run Boundary Conditions

Production Run	Flow from Vernon Dam (cfs)	Flow from Ashuelot River (cfs)	Flow from Millers River (cfs)	Flow at Turners Falls Dam (cfs)	Water Surface Elevation at Turners Falls Dam (ft)
Generating Capacity at Turners Falls Dam	14,365[1]	840[2]	735[2]	15,940	181.3[3]
Operation Rule Threshold A[4]	27,130[5]	1,495[6]	1,375[7]	30,000[4]	180[4]
Operation Rule Threshold B[4]	58,780[5]	3,245[6]	2,975[7]	65,000[4]	179[4]
10-Year Return Period	87,795[1]	5,845[6]	5,360[8]	99,000[8]	179[9]
50-Year Return Period	119,400[1]	9,860[6]	9,040[8]	138,300[8]	180[10]
100-Year Return Period	134,120[1]	12,300[6]	11,280[8]	157,700[8]	180[10]

Notes:

[1] Vernon flow was calculated as difference between flow at Turners Falls Dam and the combined flow from the Ashuelot and Millers Rivers as follows: $Q_{Ver} = Q_{TF} – (Q_{Ash}+Q_{Mil})$

[2] Mean flow: Ashuelot 1908-2014, Millers 1916-2014

[3] Operating rules state a range of 180.5 to 184.5, 181.3 is the median water level at the dam in the recent decade (Gomez & Sullivan)

[4] Operating rules differ for flows at Turners Falls Dam between 30,000 cfs (Operation Rule Threshold A) and 65,000 cfs (Operation Rule Threshold B). When flows are in this range, the USACE requires that FirstLight drawn the Turners Falls Impoundment elevation down as far as possible, but not below elevation 176 ft. Flows in this range likely have between 1 to 3 year return periods and occur on a relatively frequent basis. Note: during tropical storm Irene the water level at the dam was approximately 179 for flows of approximately 100,000 cfs. Water levels were selected for the various flows depending on flow.

[5] Vernon flow was calculated using the drainage area ratio method presented in the FEMA FIS based on flow at the Turners Falls Dam as follows: $Q_{Ver} = Q_{TF}*(6266/7165)^{\wedge}.75$

[6] Flows for the Ashuelot River were calculated using the drainage area method presented in the FEMA FIS based on flow from the Millers River as follows: $Q_{Ash} = Q_{Mil}*(440/392)^{\wedge}.75$.

[7] Flows for the Millers River were calculated using the drainage area ratio presented in the FEMA FIS based on the difference in flow between the Turners Falls and Vernon Dams as follows: $Q_{Mil} = (Q_{TF}-Q_{Ver})/[1+(440/392)^{\wedge}.75]$.

[8] Flows obtained directly from the FEMA FIS.

[9] If the Northfield Mountain Project is not operating and flows at Turners Falls Dam are between 65,000 cfs and 126,000 cfs, the Turners Falls Impoundment should be kept at a constant elevation. Note: during tropical storm Irene the water level at the dam was approximately 179 for flows of approximately 100,000 cfs.

[11] All flows presented in this table were rounded to the nearest 5 cfs.

5.3 Sediment Transport

As discussed in Section 4.2.9, rivers transport sediment that has been eroded from the upstream watershed or riverbanks and river bed in response to flow or rainfall events, as well as other processes that erode sediment. As part of Study No. 3.1.3, FirstLight collected continuous suspended sediment data and grab samples at two locations in the TFI – just upstream of the Rt. 10 Bridge and at the Northfield Mountain tailrace in order to better understand suspended sediment transport dynamics in the TFI.[39] For the purpose of this study, emphasis was placed on evaluating and analyzing the continuous suspended sediment and grab sample data collected in the vicinity of the Rt. 10 Bridge, or more specifically the StreamSide data (2013-2015) and Rt. 10 Bridge cross-section grab samples (2015). The data collected in the vicinity of the Rt. 10 Bridge allowed for a direct analysis of suspended sediment dynamics in the mainstem Connecticut River (as opposed to the data collected in the Northfield Mountain tailrace which was set back from the mainstem).

For the purposes of this study, the data collected and analyzed as part of Study No. 3.1.3 was evaluated to determine any potential relationships between flow, suspended sediment concentration (SSC), and potential erosion and to independently verify the findings of the hydraulic and BSTEM modeling, to the extent possible. Originally, the RSP called for using these data to analyze particle size distribution (PSD) as related to critical shear analysis using Shield's criteria; however, as discussed in the Study No. 3.1.3 December 2015 filing with FERC, the PSD data was not usable and therefore the analysis discussed in the RSP was not possible.

As expected, Study No. 3.1.3 found that suspended sediment measurements collected by the StreamSide and from grab samples collected in the vicinity of the StreamSide pump demonstrate strong correlations between flow and SSC. Over the course of the monitoring period (2013-2015) it was observed that as Connecticut River flows increase so too did SSC (Figure 5.3-1). That is, the highest SSC values were observed during the highest periods of flow while the lowest SSC values were observed during the lowest period of flows. This was a consistent observation for each year data were collected.

As shown in Figure 5.3-1, SSC values were relatively low and without an apparent trend when flows from Vernon Dam were below 12,000 cfs. 95% of SSC measurements observed when flows were below 12,000 cfs were below 14.5 mg/L with a median of 3 mg/L. From 12,000 to 35,000 cfs, SSC values exhibited an increasing trend with a median of 12 mg/L. Finally, SSC values associated with flows greater than 35,000 cfs increased more quickly with flow and were significantly higher with a median of 145 mg/L. The results of this analysis demonstrate that three flow thresholds generally exist in the TFI in regard to SSC values (as measured at the Rt. 10 Bridge): <12,000 cfs (low flow), 12,000-35,000 cfs (moderate flow), and >35,000 cfs (high flow).

As discussed in Section 5.1.3, for the purpose of this study, the flow threshold for natural high flows was determined to be 37,000 cfs for the middle, Northfield Mountain, and lower reaches of the TFI. This value represents the combined maximum hydraulic capacity of Vernon and Northfield Mountain at a given location and also represents flows at which Northfield Mountain operates on a very limited basis, if at all (i.e., less than 3% of the time). Given this, the suspended sediment flow thresholds identified as part of Study No. 3.1.3 are of particular interest as it is observed that significant levels of suspended sediment are not transported until flows reach or exceed the threshold for high flows. While the data collected at the Rt. 10 Bridge represents one location in a ~22 mile long impoundment, BSTEM results discussed in Section

[39] Details pertaining to the data collection efforts at each site were discussed in Section 4.2.9, in-depth discussion and details can further be found in the report titled, *Relicensing Study 3.1.3 Northfield Mountain Pumped Storage Project Sediment Management Plan 2015 Summary of Annual Monitoring* filed with FERC in December 2015.

5.4 observed similar behavior at most detailed study sites. That is, the majority of erosion in the TFI does not occur until flows at a given location exceed 35,000 cfs or higher.

The results of the supplemental cross-section grab samples collected across the Rt. 10 Bridge during the 2015 spring freshet further demonstrate the strong correlation between flow and SSC. Grab samples were collected over four days during the rising limb, on either side of the peak, and across the falling limb of the hydrograph. As shown in Table 5.3-1, as flow increased so too did SSC values with the highest concentrations observed at flows >40,000 cfs and the lowest concentrations at flows <20,000 cfs.

As part of Study No. 3.1.3 investigation then occurred to determine how often these flow thresholds occurred during the study period. Figure 5.3-2 depicts the flow duration curve for Vernon discharge from April through November for the years 2013-2015. As shown on the flow duration curve, flows of 12,000 cfs or less were equaled or exceeded 63% of the time, flows between 12,000-35,000 cfs were equaled or exceeded 32% of the time, while flows greater than 35,000 cfs were equaled or exceeded 5% of the time during the course of the study. In other words, flows of a magnitude when high concentrations were observed occurred only 5% of the time during the study period.

Historic suspended sediment samples and photographs collected during Tropical Storm Irene further demonstrate the strong relationship between flow and SSC values. Figure 5.3-3 demonstrates the contrast between the Millers River and the Connecticut River as affected by Tropical Storm Irene in August 2011. As observed in the figure, the relatively clear water from the Millers River flowed into the sediment laden Connecticut River in a classic, swirling mixing zone. SSC values taken from the Millers River ranged from non-detect (ND, <5 mg/L) to 6.5 mg/L while SSC values measured in the Connecticut River during the same period ranged from 140 to 1,900 mg/L.[40] As a point of comparison, the median SSC value observed during Study No. 3.1.3 for flows greater than 35,000 cfs was 145 mg/L.

Table 5.3-1: Summary of Rt. 10 Bridge Cross-section Grab Samples (2015)

Date	Vernon Discharge (cfs)	Max SSC (mg/L)	Min SSC (mg/L)	Median SSC (mg/L)	StreamSide SSC (mg/L)
4/14/2015	50,536 - 59,700	159	79	108	152
4/17/2015	47,970 - 52,591	106	80	89	82
4/20/2015	41,282 - 42,172	90	30	42	70
4/28/2015	19,112 - 20,437	14	6	12	13

[40] SSC samples collected during Tropical Storm Irene in the Connecticut River were collected as grab samples collected by boat while samples collected from the Millers River were collected as surface grab samples collected at the edge-of-water.

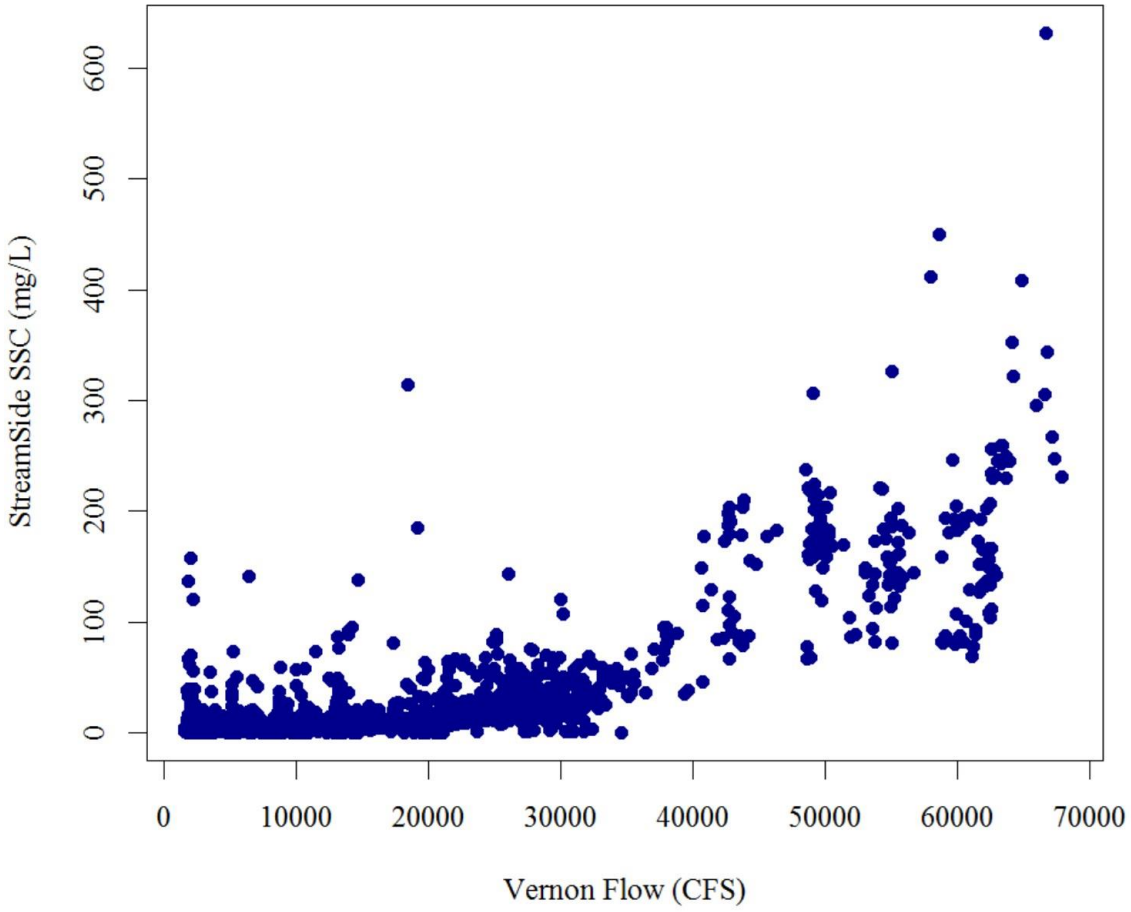

Figure 5.3-1 TFI Impoundment SSC vs. Vernon Discharge (2013-2015)

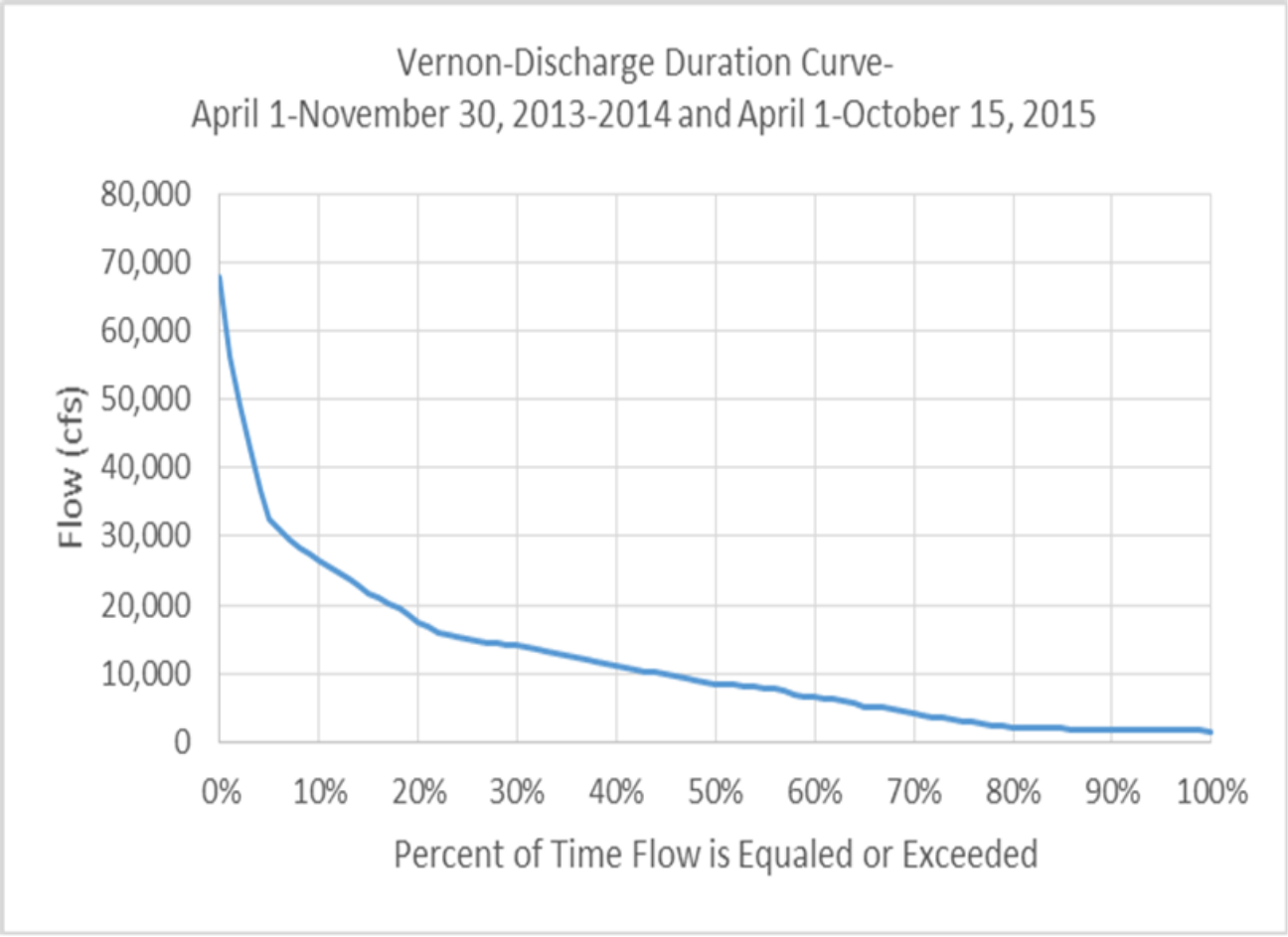

Figure 5.3-2 Flow Duration Curve for the Turners Falls Impoundment

Figure 5.3-3 Millers River Confluence with the Connecticut River (TFI), August 2011

5.4 Analysis of the Causes of Erosion - BSTEM

BSTEM is a state-of-the-science deterministic model that simulates the hydraulic and geotechnical processes responsible for bank erosion, including the effects of vegetation, pore-water pressure, and the confining forces due to flow in the channel. BSTEM was the principal tool used to evaluate the potential primary causes of erosion including hydraulic shear stress due to flowing water, water level fluctuations, and boat waves. Analysis pertaining to the other potential primary causes of erosion (land management practice and ice) are discussed in Section 5.5.

Both the static and dynamic versions of BSTEM have been used worldwide to predict and address issues involving bank erosion. The version used in this study represents the latest version of BSTEM-Dynamic (Ver. 2.3). By dynamic, we mean that instead of relying on a single ”burst” of discharge (a rectangular hydrograph) for a single flow event of given stage and duration, the user is able to input a complete flow series at the time step of their choosing. For this study, a 15-year flow series (2000-2014) was used with both of the modeled scenarios using hourly time steps.

Discussion in this section focuses on BSTEM input data and modeling results. Input data for BSTEM relied on three primary sources: field collected data (as discussed in Section 4); results from both HEC-RAS modeling scenarios; and cross-section surveys which have been conducted annually since 1999. Simulations using the input data discussed below provided the foundation for the BSTEM results and for determining the causes of bank erosion at each detailed study site.

BSTEM results are presented in two ways, (1) as general observations and findings throughout the TFI, and (2) as site-specific results for each detailed study site. BSTEM modeling results are discussed in the context of both hydraulic and geotechnical erosion processes. For the purpose of this study, hydraulic erosion is defined as erosion caused by hydraulic processes. That is, the particle-by-particle entrainment and erosion of surficial sediments when and where the boundary shear stress exerted by the flow exceeds the critical shear stress that characterizes the surficial bank sediments. Hydraulic erosion from river flow or by waves can steepen and undercut bank surfaces leading to a loss of support for the upper part of the bank and making them susceptible to collapse (geotechnical erosion). These processes are most important when shear stresses are highest as during high flows.

Geotechnical erosion is defined as erosion caused directly by gravitational forces as in the collapse of a hillslope or bank. Here, erosion occurs when the downslope, gravitational forces exceed the shearing resistance of the *in situ* materials. Any factors that increase the downslope gravitational forces (such as steepness and weight) or decrease the shearing resistance of the materials (such as generation of positive pore-water pressure) contribute to geotechnical erosion. Pore-water pressure can be generated within the bank by lateral infiltration (depending on the duration the water is at a certain elevation) during rises in stage. This can reduce the frictional component of shear strength (See Volume III - Appendix F). The confining pressure provided by the flow pressing against the bank surface, however, tends to offset this affect. An important point are the relative rates of decreasing stage and groundwater levels during water-level fluctuations because the loss of shear strength combined with a loss of confining pressure (known as the *drawdown* condition) is particularly critical for streambank stability. BSTEM handles these processes by calculating pore-water and confining pressures along potential failure surfaces during each time step of a simulation (See Volume III – Appendix F).

5.4.1 BSTEM Input Data

The required field data that was collected to support BSTEM were discussed in Sections 4.2.5 through 4.2.8. This section focuses on how those data were used and analyzed in support of the model.

5.4.1.1 Hydraulic Input Data

The purpose of the bank-stability modeling was to simulate bank-erosion rates under a range of operational conditions. For example, the Baseline Condition included "normal" peaking operations at Vernon and Northfield Mountain using hourly historical flows and historical water-surface elevations at Turners Falls Dam. Hourly values of water-surface elevations were derived for each of the 25 model locations from 1-D hydraulic modeling using HEC-RAS (Section 5.2.1). Previous versions of BSTEM-Dynamic relied on a single (constant) bed slope to internally calculate shear stress for each time step. To accommodate the more rapidly varying slopes typical during peaking operations, BSTEM-Dynamic was enhanced to allow for input of a unique slope for each time step. Thus, hourly energy slopes calculated in the HEC-RAS model were used for input into BSTEM. Because shear stress is the product of the hydraulic radius, energy slope and unit weight of water, this provided for more accurate evaluations and better temporal resolution of the shear stress calculations along the bank toe and bank face within BSTEM.

Hydraulic inputs provided to BSTEM, including flow elevation and energy slope for each site, provide important information on the forces that can cause particle-by-particle (hydraulic) erosion of the bank materials. As such, the distributions of energy slope along the reach for the Baseline Condition provide a picture of the absolute and relative magnitudes of how these hydraulic forces vary longitudinally along the TFI (Figure 5.4.1.1-1). The median (50^{th} percentile) energy slope for each site is represented by the gray line with 50% of the slopes over the modeling period greater than this value and 50% less. The blue and orange lines represent the 95^{th} and 75^{th} percentiles for each site, respectively. One cannot equate the 95^{th} percentile energy slopes with the greatest boundary shear stresses, however, as these slopes may occur at lower flows where flow depths (and hydraulic radius) are less.

Based on the distribution of the energy grade slope shown in the figure, four hydraulic reaches were identified. These hydraulic reaches included the Upper (Reach 4), Middle (Reach 3), Northfield Mountain (Reach 2), and Lower (Reach 1) reaches.[41] The steepest slopes occur in the "upper" part of the reach (Reach 4) just downstream from Vernon Dam and extending downstream to about station 80,000. That the steepest slopes are in the "upstream reach" is also shown by overlaying the energy slopes for each site in Figure 5.4.1.1-2, with the palest blue color for the most upstream site (11L) and slightly darker shades used for each site progressing downstream. Slopes for the "middle" reach, denoted as Reach 3 (downstream to station 42,000) are generally about an order of magnitude lower. Energy slopes for the Northfield Mountain Reach (Reach 2) are somewhat greater than for both Reaches 3 and the "lower" reach (Reach 1), the latter being the section just above Turners Falls Dam. The effects of operations at both Vernon Dam and Northfield Mountain on energy slopes can be seen (Figure 5.4.1.1-1), keeping in mind that flows above 17,130 cfs are in excess of the hydraulic capacity of Vernon Dam and, therefore, represent run of the river conditions. Figure 5.4.1.1-3 depicts the geographic distribution of the four study reaches in the TFI.

The hydraulic inputs represent only one of the factors determining bank-erosion rates. Quantifying bank-erosion is a matter of quantifying the driving and resisting forces that control the hydraulic and gravitational (geotechnical) processes acting on a bank. The *in situ* field measurements of bank-material properties described in Section 4.2.6 were used to quantify how the bank resists the hydraulic forces provided by the flow and by waves, and the gravitational forces which manifest as bank height and angle. Knowing the resisting forces, including vegetative factors, therefore, allows us to determine the response of each stream bank to a different suite of hydraulic conditions that are generated by different operational scenarios. Understanding the derivation and implications of the hydraulic flow series for each operational scenario is critical to interpretation of BSTEM-derived erosion rates and the causes of bank erosion throughout the reach.

[41] It should be noted that the delineation of the hydraulic reaches using the Energy Grade Line Slope was based on the model results at the 25 detailed study sites.

To better understand the impact various factors have on riverbank erosion processes (i.e. hydropower operations, naturally occurring high flows, etc.) two modeling scenarios were developed from which the results could be compared to tease out causes of erosion. As described above, the Baseline Condition, which includes peaking operations at both Vernon and Northfield Mountain, as well as boat waves, represents the first of two operational scenarios that were simulated to determine the causes of bank erosion throughout the TFI. The non-baseline scenario include various combinations of operations at Vernon and Northfield Mountain (Table 5.4.1.1-1) to help elucidate the roles of upstream flows and peaking operations.

- The **Baseline Condition** (All operating) utilizes measured, historical hourly flows. The resulting hydraulics reflect the combination of natural flows and the peaking operations at both Vernon and Northfield Mountain. Because this flow series represents "existing" conditions over the 2000-2014 period (including waves), it was used for model calibration;

- **Scenario 1** (Vernon operating plus natural flows) also uses historical, hourly data including water levels at the Turners Falls Dam, but in this case, Northfield Mountain is idle. Hydraulics derived from this scenario are the result of natural flows, Vernon operations and water levels at Turners Falls Dam;

It is important to note that the hydraulic time series for the modeled scenarios include all "natural flows" entering the reach between 2000-2014 at its upstream boundary and from tributaries. Simulated erosion rates at each of the 25 sites, therefore, include the effects of these natural hydrologic events during both scenarios. In addition, the simulations included boat waves unless otherwise specified.

Examples of the resulting flow series derived from the HEC-RAS runs are given in Figures 5.4.1.1-4 and 5.4.1.1-5. These examples show the range of flow elevations for the two operational scenarios relative to representative bank sections. Obviously, hydraulic erosion can only occur at locations where the flow can reach and has sufficient shear stress to overcome the resistance of the surficial bank sediments.

Ranges of water-surface elevations for the model scenarios are all comprised of hourly data and are quite similar. Slight variations in these ranges occur due to operational factors (i.e. Northfield Mountain idle) but are not significant, generally 2 feet or less (Figures 5.4.1.1-4 and 5.4.1.1-5). One can also see an extended period during 2010 when Northfield Mountain was not operating. A close up of the water-surface elevations for this year are shown in the vicinity of Northfield Mountain (site 87BL) and the upper reach (site 3R) for the modeled scenarios in Figure 5.4.1.1-6.

In the lower part of the TFI, represented by site 12BL about 6,500 feet upstream of the Turners Falls Dam, flows are restricted to a narrow band near the intersection of the beach/bank toe and the upper bank. This provides opportunity for boat waves to have an effect on undercutting of the bank because their effects are always focused within this narrow range of elevations. Moving upstream we see that the range of flow elevations increases to about 10 feet in Reach 2, 12 feet in Reach 3 to about 15 feet in Reach 4. These ranges do not include the peak flow for the period (102,600 cfs) which occurred as a result of Tropical Storm Irene at 2PM on August 29, 2011. Flow elevations associated with this event increase the range of flow elevations an additional 2 to 5 feet (Figures 5.4.1.1-4 and 5.4.1.1-5).

The band of water level fluctuations generally occurs near the upper portion of the lower bank with peak water surface elevations extending up onto the upper bank. A water surface elevation-duration analysis at a subset of the detailed study sites shows the extent of time that the water surface elevation is above and below the lower to upper bank transition (Section 5.1.3).

Hydraulic data as discussed in this section were input into BSTEM-Dynamic at all 25 sites along the study reach. In those cases where bank-stabilization and/or restoration measures were undertaken, the hydraulic dataset was split in two for model runs to represent pre- and post-restoration bank conditions and geometry. A summary of the range of dates used for each simulation, whether they represent pre- or post-restoration

conditions (for those sites that have been modified), and their location along the study reach is shown in Table 5.4.1.1-2.

Table 5.4.1.1-1: Operational Conditions and Associated Hydraulic Data for Each of the Modeled Scenarios

Model Scenario	Time step	Vernon Operations (flow)	NFM Operations (flow)	TFD Operations (elevation)
Baseline	Hourly	Historic	Historic	Historic
S 1	Hourly	Historic	Idle	Historic

Table 5.4.1.1-2: Summary of the Period Encompassing Each of the Hydraulic Datasets used for BSTEM

Site / Condition	Station (ft.)	Dates	
		Start	End
11L	100000	07/15/05	09/10/14
2L-Pre	94500	06/20/00	06/30/12
2L-Post	94500	07/01/12	08/28/14
303BL	94000	01/01/11	08/27/14
18L	87000	01/01/00	08/27/14
3L	79500	01/01/00	08/28/14
3R-Pre	79500	01/01/00	06/30/06
3R-Post	79500	07/01/06	08/28/14
21R	79250	01/01/00	08/27/14
4L	74000	01/01/00	08/28/14
29R	66000	01/01/00	08/27/14
5CR	57250	07/08/02	09/03/14
26R	50000	01/01/00	08/27/14
10L	49000	01/01/00	08/27/14
10R-Post	49000	07/01/01	08/27/14
6AL-Pre	41750	01/01/00	06/30/04
6AL-Post	41750	07/01/04	08/27/14
6AR-Post	41750	06/21/00	08/27/14
119BL	41000	01/01/00	08/27/14
7L	37500	01/01/00	08/26/14
7R	37500	01/01/00	08/26/14
8BL	32750	06/02/00	08/26/14
8BR-Pre	32750	06/02/00	06/30/12
8BR-Post	32750	07/01/12	08/26/14
87BL	30750	01/01/00	08/27/14
75BL	27000	01/01/00	08/27/14
9R-Pre	6750	06/02/00	06/30/08
9R-Post	6750	07/01/08	8/26/14
12BL	6500	01/01/00	08/27/14
BC-1R	4750	06/05/00	08/26/14

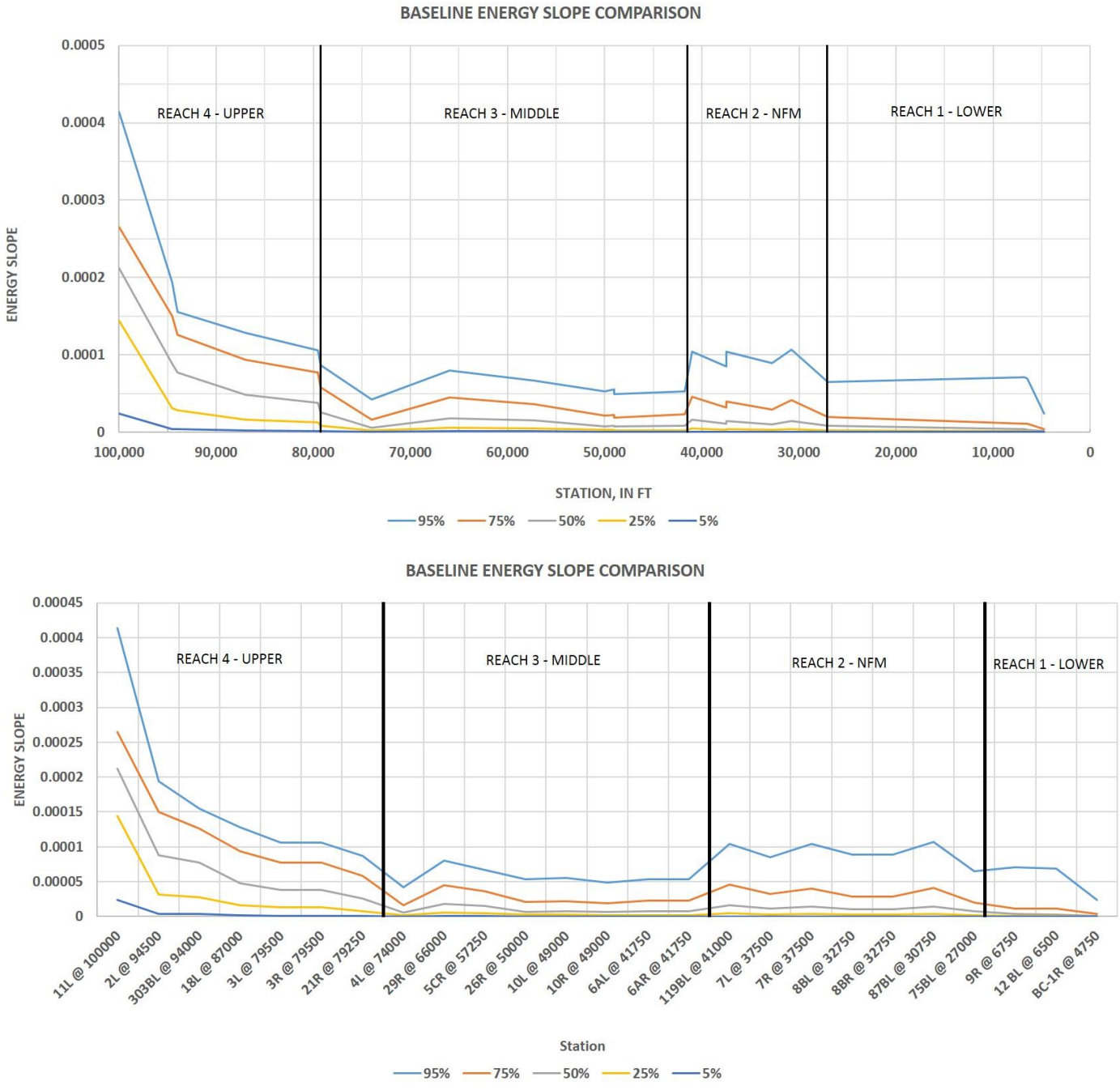

Figure 5.4.1.1-1 Longitudinal variation of energy slopes along the study reach for the Baseline Condition plotted by stationing (Top) and by site number (Bottom)

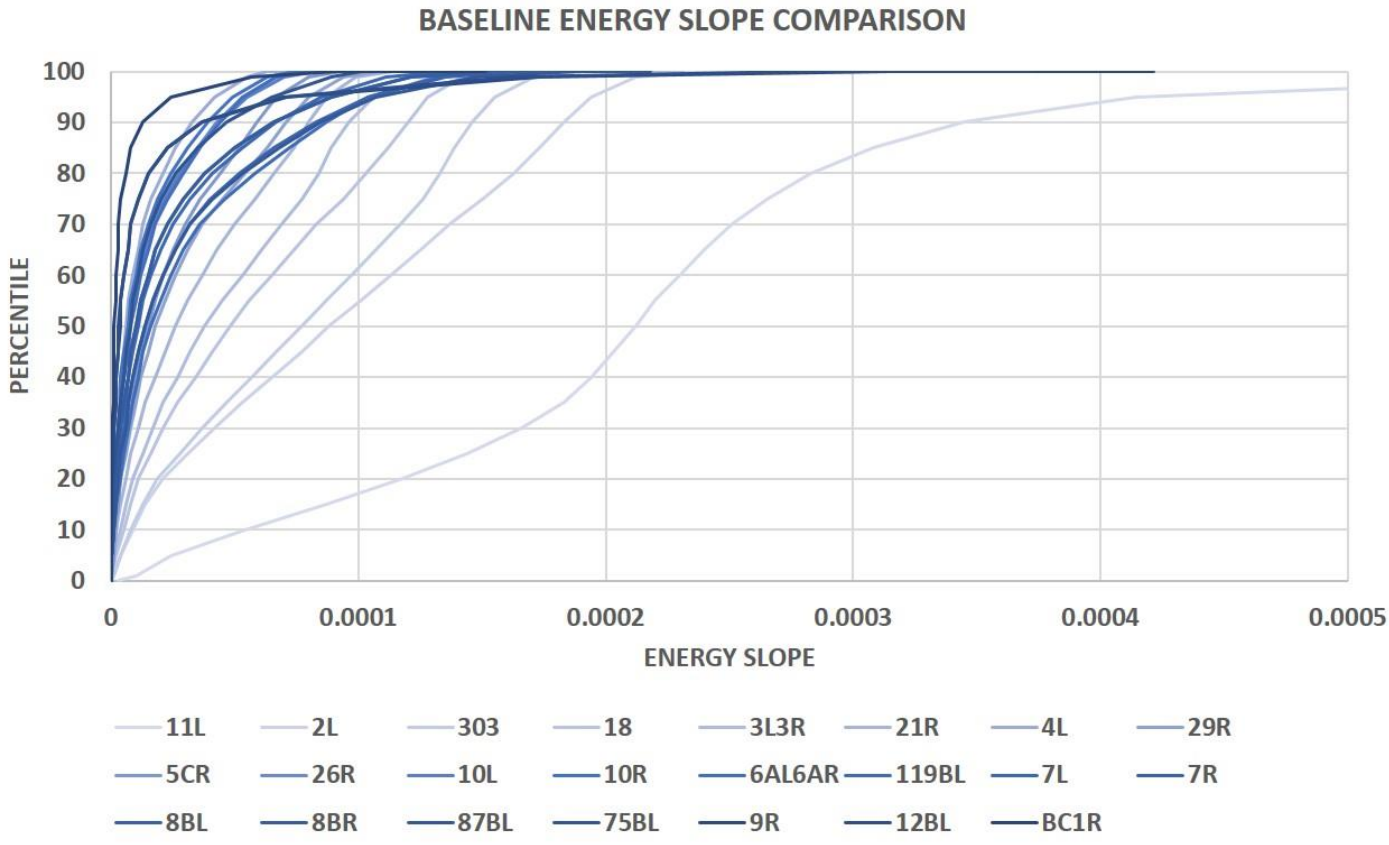

Figure 5.4.1.1-2: Comparison of the Range of Energy Slopes for Each Modeled Site along the Study Reach Showing Steepest Slopes in the "Upstream" Reach

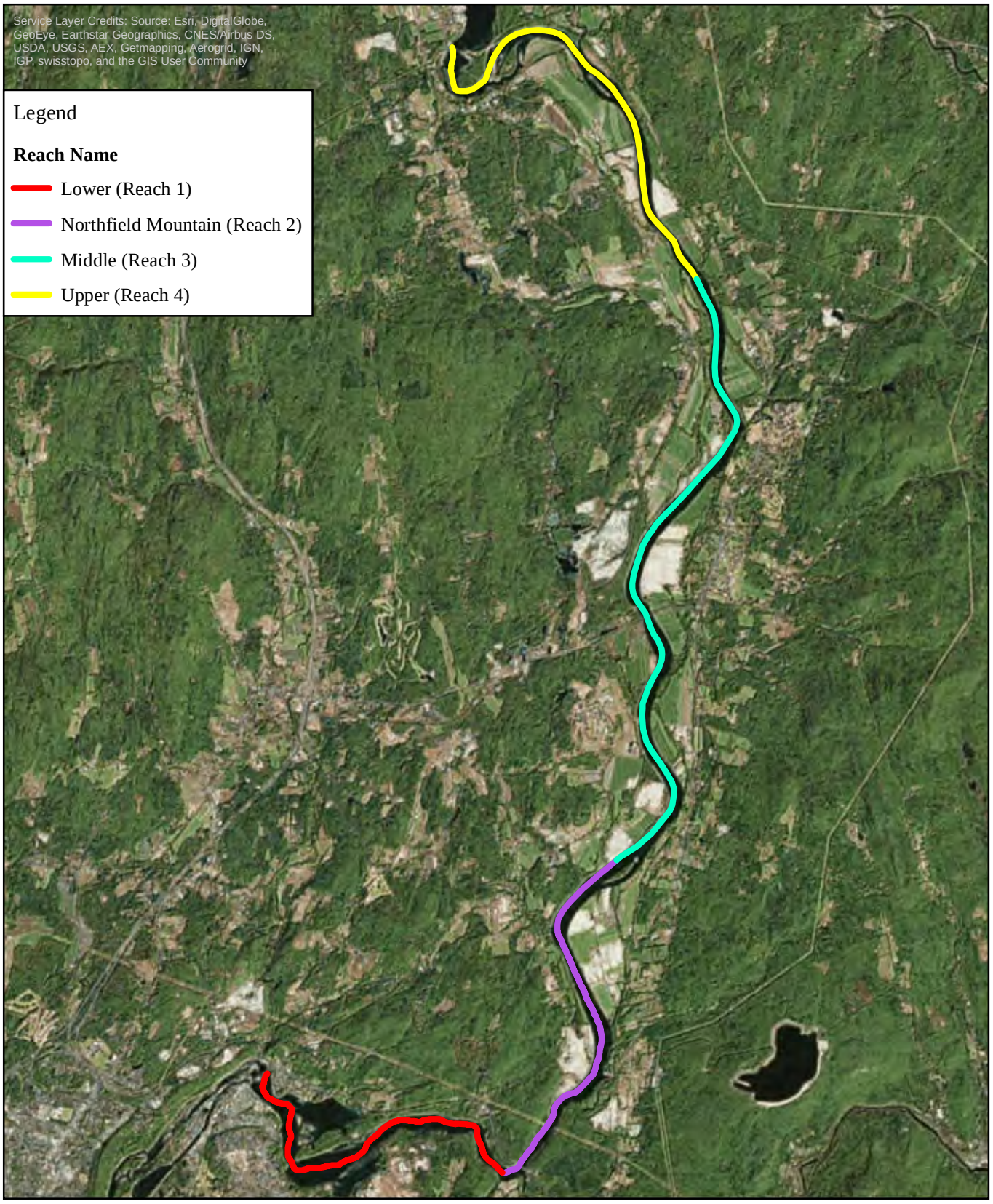

FIRSTLIGHT HYDRO GENERATING COMPANY
Northfield Mountain Pumped Storage Project No. 2485
Turners Falls Hydroelectric Project No. 1889

STUDY 3.1.2

N

0 0.75 1.5 3 Miles

Figure 5.4.1.1-3:
Study reaches within the TFI

Path: W:\gis\studies\3_1_2\maps\final_report\figure_5_4_1_1-3.mxd

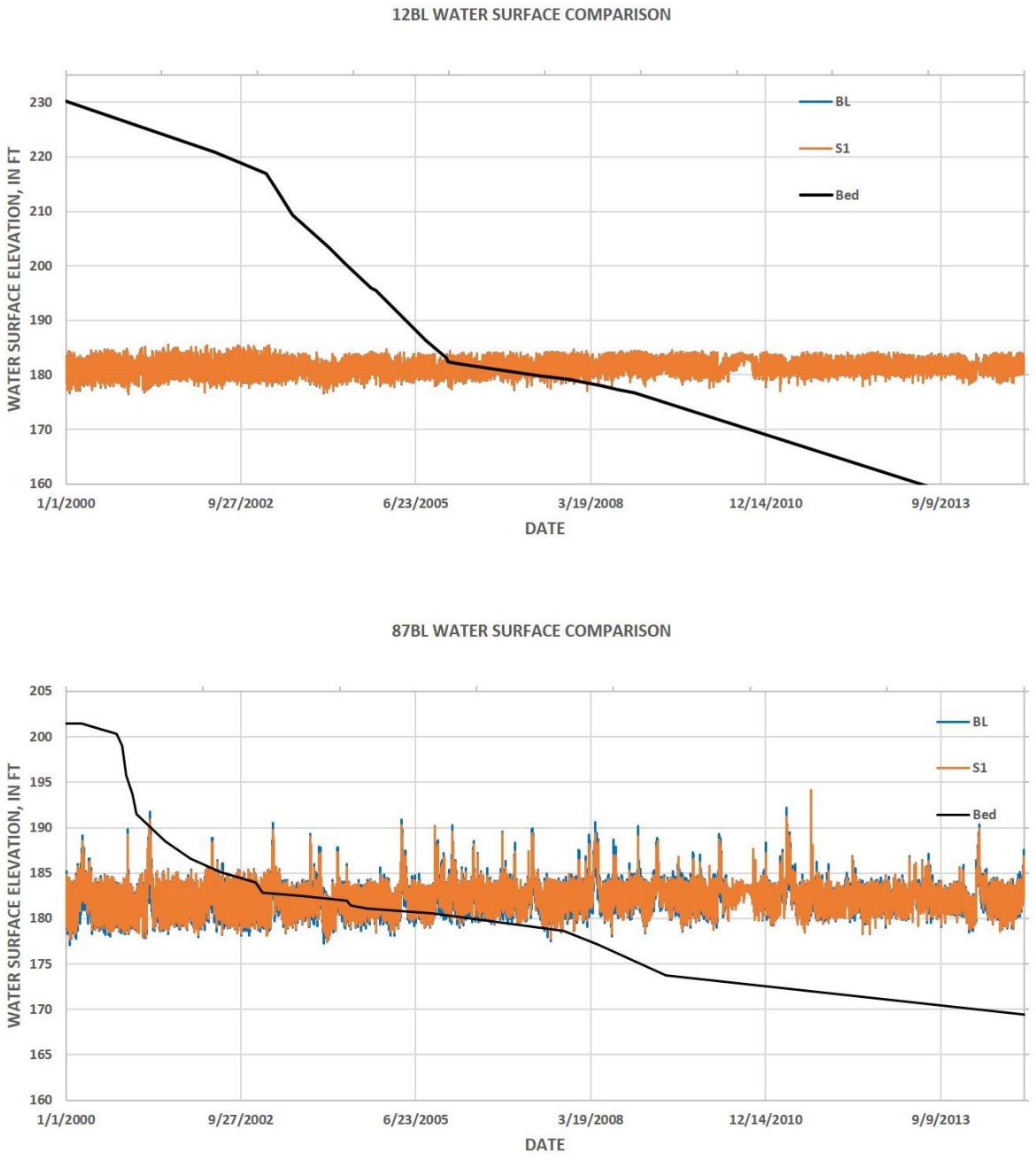

Figure 5.4.1.1-4: Water-surface elevations for representative sites within the Lower Reach (#1; site 12BL), and Northfield Mountain Reach (#2; site 87BL)

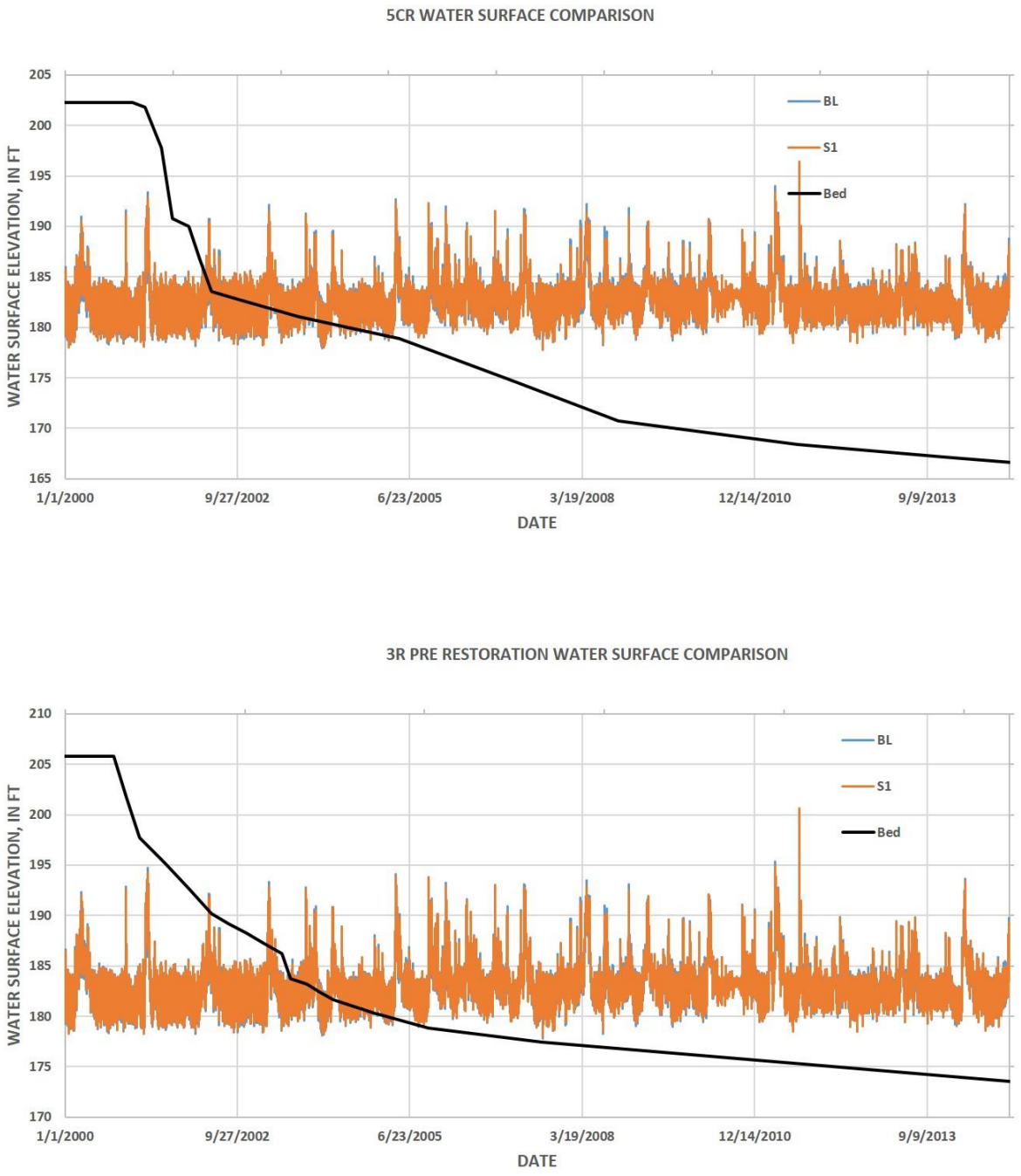

Figure 5.4.1.1-5 Water-surface elevations for representative sites within the Middle Reach (#3; site 5CR) and Upper Reach (#4; site 3R Pre-restoration)

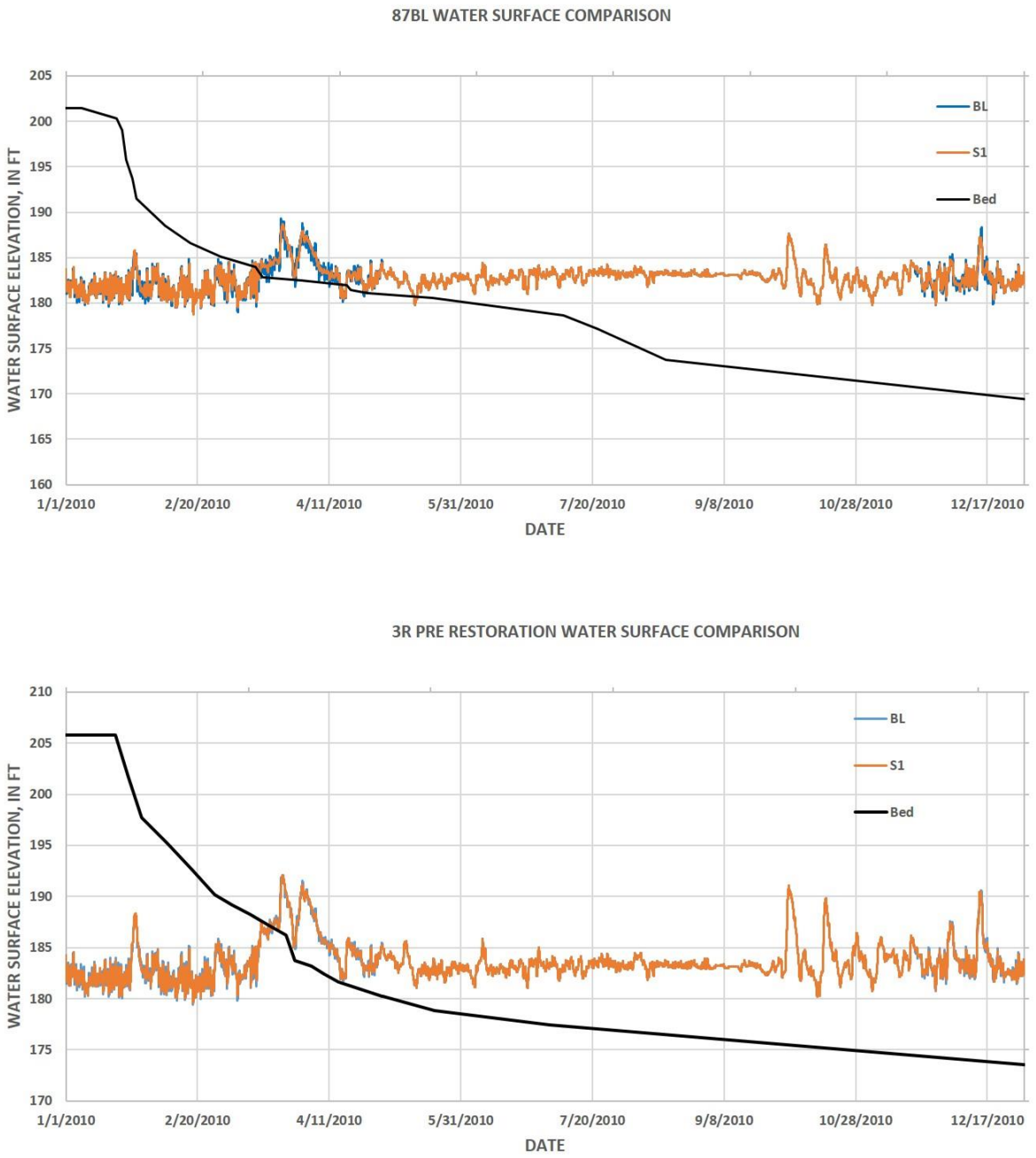

Figure 5.4.1.1-6: Representative 2010 water-surface elevations for Reach 2 (Top) and Reach 4 (Bottom) showing range of stages relative to channel-bank geometry

5.4.1.2 Site Conditions and Bank-Resistance Inputs

Site conditions relevant to bank-stability modeling include aspects of bank geometry (height and steepness), hydraulic and geotechnical resistance, and vegetative conditions. Seven of the sites had stabilization measures applied to the bank at some time during the modeling period (2000-2014) (Table 5.4.1.2-1). As alluded to in the previous section, modeling of these sites included a pre-and post–restoration period, with the output of bank geometry from the pre-restoration run halted and used as input for post-restoration conditions. If bank re-shaping was involved in the stabilization works, that new geometry was used as the starting geometry for the post-restoration simulations. In addition, modifications to other aspects of the bank surface were parameterized for the post-restoration run if needed.

Data on bank-material and vegetation properties for each of the 25 detailed study sites were determined from the *in situ* field investigations described in Section 4. An example of the bank-materials and roughness data are provided for a few sites in Table 5.4.1.2-2 and for the remainder of the sites in Volume III (Appendix L). Layer 5 which is below the minimum water-surface elevation was designated as the "channel bed" and set to be non-erodible because BSTEM is not a sediment-routing model. Data listed under "Toe-Model Data" refer to resistance data for the hydraulic erosion sub model along the entire bank face and not just the bank toe region. Friction angle and cohesion data are derived from the borehole shear tests conducted at each site. Groundwater-flow parameters are estimated according to soil texture, the associated values published by the NRCS (NRCS, 2015) and were discussed in Section 4. Critical shear stress of the surface sediments were obtained from either the Shields criteria for non-cohesive materials using d_{50}, or from jet-test data in the case of fine-grained materials. Summaries of these data and the data-collection methods are also provided in Section 4.

The version of BSTEM-Dynamic used in this study (Ver. 2.3) allowed the user to input a different value of Manning's roughness coefficient (n) for each bank layer. Estimates of n were developed from field observations and from current and historical photographs of each site. Photographs taken during the 2013 FRR and during field data collection associated with this study (2014-2015) represented current conditions while photos taken during the 1998 FRR were used to represent conditions in 2000.

For those sites with historical survey data, the initial bank geometry was obtained directly from the survey data and generally started on 1/1/2000. These sites, shown in bold in Table 5.4.1.2-3 provided an excellent opportunity to calibrate BSTEM by comparing the change in bank geometry at the end of the simulation with the measured change in geometry over the same period. In the general case, the end of the period was 2014 unless otherwise specified. As is customary in hydraulic modeling, Manning's n was the primary calibration parameter, serving to either increase or decrease the effective stress acting on the bank surface. A given calibration run was considered acceptable if the difference between the simulated and measured erosion (in ft^2) over the period was less than the potential survey error.

The potential survey error was termed "total survey variance" (TSV) and was calculated as the product of the slope length times the potential vertical error (Table 5.4.1.2-3). This vertical error was deemed to be about 0.5 feet for all surveys between 2000 and 2006 and about 0.4 feet for all surveys conducted in 2007 and later (R. Howard, written comm., 2015). The approach taken to determine TSV was to:

1. Take the unit survey variance of 0.5 ft^2/ft of slope length (for pre 2001 surveys) and multiply by the sum of the slope lengths undergoing erosion (as determined by the starting and ending surveys) to obtain total survey variance in ft^2.

2. Compare TSV with difference between simulated and "measured" erosion. If that difference is equal to or less than the calculated TSV, the calibration is successful.

For those sites that did not have historical surveys (non-bold in Table 5.4.1.2-3), the bank geometry used for the initial condition was the 2014 surveyed geometry. Hydraulic inputs (water-surface elevation and energy slope) were the same as for the calibration sites and roughness coefficients were estimated as before.

Table 5.4.1.2-1: Bank-stabilization Measures Conducted at the Detailed Study Sites during the Modeling Period

Site #	Project Name	Date Stabilized	Technique
9(R)	Campground	2008	Coir logs or other logs anchored at toe of upper bank, plant vegetation on upper bank
8B(R)	Bathory/Gallagher	2012	Gravel on lower bank along with large woody debris (anchored), planting of vegetation on lower bank
6A(R)	Flagg	2000	Re-shape upper bank to flatter slope, plant vegetation on upper bank, submerged rock toe with aquatic vegetation (which has subsequently accumulated sediment deposits)
6A(L)	Skalski	2004	Re-shape upper bank to flatter slope, plant vegetation on upper bank, coir logs, rock toe below coir logs
10(R)	Urgiel U/S	2001	Re-shape upper bank to flatter slope, plant vegetation on upper bank, coir logs, rock toe below coir logs
3(R)	Kendall	2008	Re-shape upper bank to flatter slope, plant vegetation on upper bank, coir logs, rock toe below coir logs
2(L)	Bonnette Farm	2012	Plant vegetation on upper bank

5CR												
	Bank Model Input Data					Groundwater Model Input Data			Toe Model Input Data		Roughness	
Layer Number	Friction angle f' (degrees)	Cohesion c' (kPa)	Saturated unit weight (kN/m^3)	ϕ^b (degrees)	Chemical concentration (kg/kg)	Hydraulic Conductivity k_{sat} (m/s)	van Genuchten a (1/m)	van Genuchten n	t_c (Pa)	k (cm^3/Ns)	Manning n ($s/m^{1/3}$)	Comments
Layer 1	31.0	2.9	18.0	10.0	-	2.823E-05	1.5073	1.8413	8.70	0.068	0.030	avg MJ 6&7 τc*10 for exposed roots
Layer 2	31.0	2.9	18.0	10.0	-	9.150E-06	0.6577	1.6788	0.87	0.195	0.018	avg MJ 6&7
Layer 3	32.4	5.9	18.0	10.0	-	9.150E-06	0.6577	1.6788	1.03	0.197	0.020	MJ 1
Layer 4	31.4	4.2	18.0	10.0	-	9.150E-06	0.6577	1.6788	0.13	0.555	0.050	beach-toe sample (.18 mm)

3R Post Restoration												
	Bank Model Input Data					Groundwater Model Input Data			Toe Model Input Data		Roughness	
Layer Number	Friction angle f' (degrees)	Cohesion c' (kPa)	Saturated unit weight (kN/m^3)	ϕ^b (degrees)	Chemical concentration (kg/kg)	Hydraulic Conductivity k_{sat} (m/s)	van Genuchten a (1/m)	van Genuchten n	t_c (Pa)	k (cm^3/Ns)	Manning n ($s/m^{1/3}$)	Comments
Layer 1	30.9	1.7	18.0	10.0	-	3.097E-06	2.3570	2.0037	0.66	0.246	0.025	
Layer 2	30.9	1.7	18.0	10.0	-	3.097E-06	2.3570	2.0037	0.66	0.246	0.025	
Layer 3	31.0	2.1	18.0	10.0	-	3.097E-06	2.3570	2.0037	0.66	0.246	0.040	
Layer 4	42.0	0.0	20.0	10.0	-	1.745E-03	3.5237	2.3286	53.46	0.027	0.060	d_{50} RipRap

9R Pre Restoration												
	Bank Model Input Data					Groundwater Model Input Data			Toe Model Input Data		Roughness	
Layer Number	Friction angle f' (degrees)	Cohesion c' (kPa)	Saturated unit weight (kN/m^3)	ϕ^b (degrees)	Chemical concentration (kg/kg)	Hydraulic Conductivity k_{sat} (m/s)	van Genuchten a (1/m)	van Genuchten n	t_c (Pa)	k (cm^3/Ns)	Manning n ($s/m^{1/3}$)	Comments
Layer 1	32.3	3.9	18.0	10.0	-	9.174E-05	3.2066	2.1662	0.09	0.667	0.020	from PS sample (.12 mm) + Rip Root value of 3.9 for c'
Layer 2	33.1	3.6	18.0	10.0	-	9.174E-05	3.2066	2.1662	0.29	11.782	0.016	d50 = 0.41 mm + Rip Root value of 3.6 for c'
Layer 3	28.2	18.3	18.0	10.0	-	9.150E-06	1.6788	2.0037	10.30	5.500	0.016	MJ average (new) + Rip Root value of 3.6 for c'
Layer 4	28.2	14.7	18.0	10.0	-	9.150E-06	1.6788	2.0037	0.21	3.500	0.020	d_{50} = 0.30 mm

Table 5.4.1.2-2: Examples of input bank-material, roughness and additional vegetation data used or BSTEM modeling at sites 5CR, 3R-post-restoration, and 9R pre-restoration

Table 5.4.1.2-3: Summary of BSTEM simulations showing total survey variance (TSV) for calibration runs conducted for the Baseline Condition

Site/Condition	Station (ft.)	Dates		Total Survey Variance (ft^2)
		Start	End	
11L	100000	07/15/05	09/10/14	13.7
2L-Pre	94500	06/20/00	06/30/12	19.13
2L-Post	94500	07/01/12	08/28/14	13.71
303BL	94000	01/01/00	08/27/14	-
18L	87000	01/01/00	08/27/14	-
3L	79500	01/01/00	08/28/14	17.6
3R-Pre	79500	01/01/00	6/30/06	20.3
3R-Post	79500	07/01/06	08/28/14	8.60
21R	79250	01/01/00	08/27/14	-
4L	74000	01/01/00	08/28/14	4.80
29R	66000	01/01/00	08/27/14	-
5CR	57250	07/08/02	09/03/14	23.2
26R	50000	01/01/00	08/27/14	-
10L	49000	01/01/00	08/27/14	2.81
10R-Post	49000	07/01/01	08/27/14	17.2
6AL-Pre	41750	01/01/00	06/30/04	13.2
6AL-Post	41750	07/01/04	08/27/14	6.60
6AR-Post	41750	06/21/00	08/27/14	4.94
119BL	41000	01/01/00	08/27/14	-
7L	37500	01/01/00	08/26/14	23.6
7R	37500	01/01/00	08/26/14	16.5
8BL	32750	06/02/00	08/26/14	18.5
8BR-Pre	32750	06/02/00	06/30/12	26.0
8BR-Post	32750	07/01/12	08/26/14	1.37
87BL	30750	01/01/00	08/27/14	-
75BL	27000	01/01/00	08/27/14	-
9R-Pre	6750	06/02/00	06/30/08	15.7
9R-Post	6750	07/01/08	08/26/14	14.0
12BL	6500	01/01/00	08/27/14	-
BC-1R	4750	06/05/00	08/26/14	4.74

5.4.2 BSTEM Simulation Results: General

This section brings together the results of the BSTEM simulations at the 25 detailed study sites within the TFI. The locations and stationing of these sites along the TFI are shown in Section 4 along with the flow, geometry and bank-resistance input data used to populate BSTEM for the different scenarios. The flow scenarios represent different operational conditions aimed at determining the role of water-level fluctuations, high flows and boat waves on bank-erosion rates. BSTEM calculates boundary shear stress caused by water-level fluctuations at each time step and at each node along the bank face. To address any issues related to drawdown conditions and effects as a result of hydro-power operations, BSTEM addresses these processes by calculating pore-water and confining pressures along potential failure surfaces during each time step of a simulation.

5.4.2.1 Baseline Conditions

The first set of BSTEM simulations were those for the Baseline Condition so that the calibration parameters could then be used for subsequent model scenarios. As a reminder, the Baseline Condition was designed to represent "existing" conditions, including Vernon and Northfield Mountain operations, natural flows and boat waves. These are the flow conditions that the sites had been subjected to over the 2000 to 2014 period and would serve as a means of comparison with the other flow scenario. Results of the baseline simulations (with waves on) are listed along with the measured erosion for that site (Table 5.4.2.1-1). Note that results from all of the sites have been normalized by dividing the total erosion over the period (in ft^3/ft of channel length) by the number of years of simulation because not all simulation periods were of equal duration. These values are then readily comparable to interpret relative degrees of bank instability along the reach.

For the Baseline Condition, simulated rates of bank erosion along the reach range from very close to zero $ft^3/ft/y$ to 15.4 $ft^3/ft/y$ at site 3R under pre-restoration conditions. Other sites with bank-erosion rates higher than the 75th percentile for the non-restored sites include 5CR (8.6 $ft^3/ft/y$), 2L pre-restoration (7.48 $ft^3/ft/y$), 8BR-pre-restoration (7.4 $ft^3/ft/y$), 3L (6.1 $ft^3/ft/y$), 119 BL (5.9 $ft^3/ft/y$) and 9R pre-restoration (5.4 $ft^3/ft/y$). Of these seven highest rates, four of the sites have been restored. Specific information regarding the erosion rates at these and the other sites will be provided in the following section. The spatial distribution of erosion rates along the reach are shown schematically in Figure 5.4.2.1-1.

The median value for all sites and conditions (including restored conditions) along the reach is about 1.9 $ft^3/ft/y$ compared to 2.4 $ft^3/ft/y$ including just the non-restored sites. The difference in the distributions for the Baseline Condition can be clearly seen in the Figure 5.4.2.1-2 showing the greater erosion rates when the restored sites are not included in the data set. Restoration measures have been very effective in reducing bank-erosion rates by about an order of magnitude throughout the reach (Figure 5.4.2.1-2; Middle and Bottom), with an average reduction of 83%. Median bank-erosion rates for the non-restored and restored sites are 7.42 and 0.28 $ft^3/ft/y$, respectively.

Table 5.4.2.1-1: Results of BSTEM Simulations for the Baseline Condition

Site/Condition[1]	Station	Dates		Total Survey Variance	Measured Erosion[2]	Baseline (Waves on)
	(ft)	Start	End	(ft^2/y)	(ft^2/y)	(ft^2/y)
11L	100000	07/15/05	09/10/14	1.49	0.576	0.297
2L-Pre	94500	06/20/00	06/30/12	1.59	7.64	7.48
2L-Post	94500	07/01/12	08/28/14	6.34	6.56	5.42
303BL	94000	01/01/00	08/27/14	-	N/A	0.647
18L	87000	01/01/00	08/27/14	-	N/A	1.09
3L	79500	01/01/00	08/28/14	1.20	6.40	6.09
3R-Pre	79500	01/01/00	06/30/06	3.13	16.7	15.4
3R-Post	79500	07/01/06	08/28/14	1.40	0.824	0.285
21R	79250	01/01/00	08/27/14	-	N/A	2.36
4L	74000	01/01/00	08/28/14	0.33	0.154	0.017
29R	66000	01/01/00	08/27/14	-	N/A	1.72
5CR	57250	07/08/02	09/03/14	1.91	7.04	8.61
26R	50000	01/01/00	08/27/14	-	N/A	1.19
10L	49000	01/01/00	08/27/14	0.19	0.140	0.160
10R-Post	49000	07/01/01	08/27/14	1.31	0.115	0.00
6AL-Pre	41750	01/01/00	06/30/04	2.92	2.73	2.67
6AL-Post	41750	07/01/04	08/27/14	0.65	0.456	0.00
6AR-Post	41750	01/01/00	08/27/14	0.35	0.243	0.21
119BL	41000	01/01/00	08/27/14	-	N/A	5.88
7L	37500	01/01/00	08/26/14	1.61	4.48	4.29
7R	37500	01/01/00	08/26/14	1.12	2.28	2.06
8BL	32750	06/02/00	08/26/14	1.30	0.522	0.427
8BR-Pre	32750	06/02/00	06/30/12	2.15	5.93	7.41
8BR-Post	32750	07/01/12	08/26/14	0.64	0.456	0.312
87BL	30750	01/01/00	08/27/14	-	N/A	3.57
75BL	27000	01/01/00	08/27/14	-	N/A	3.76
9R-Pre	6750	06/02/00	06/30/08	1.94	6.26	5.43
9R-Post	6750	07/01/08	08/26/14	2.27	0.472	0.227
12BL	6500	01/01/00	08/27/14	-	N/A	2.22
BC-1R	4750	06/05/00	08/26/14	0.333	0.478	0.168

[1] *Sites shown in bold have been calibrated*
[2] *Measured rates of erosion as determined from field surveys are included for comparison*

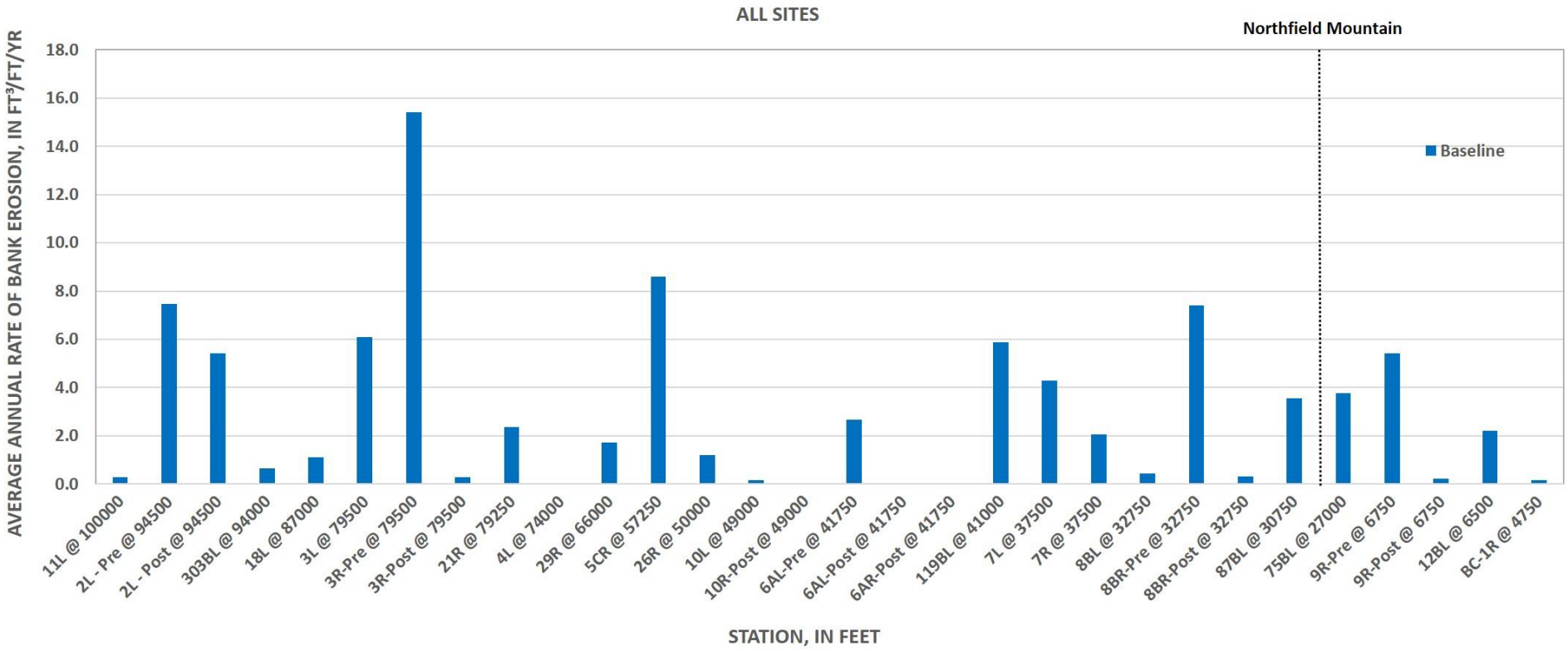

Figure 5.4.2.1-1: Spatial Distribution of Bank-erosion Rates for all Sites under Baseline Conditions

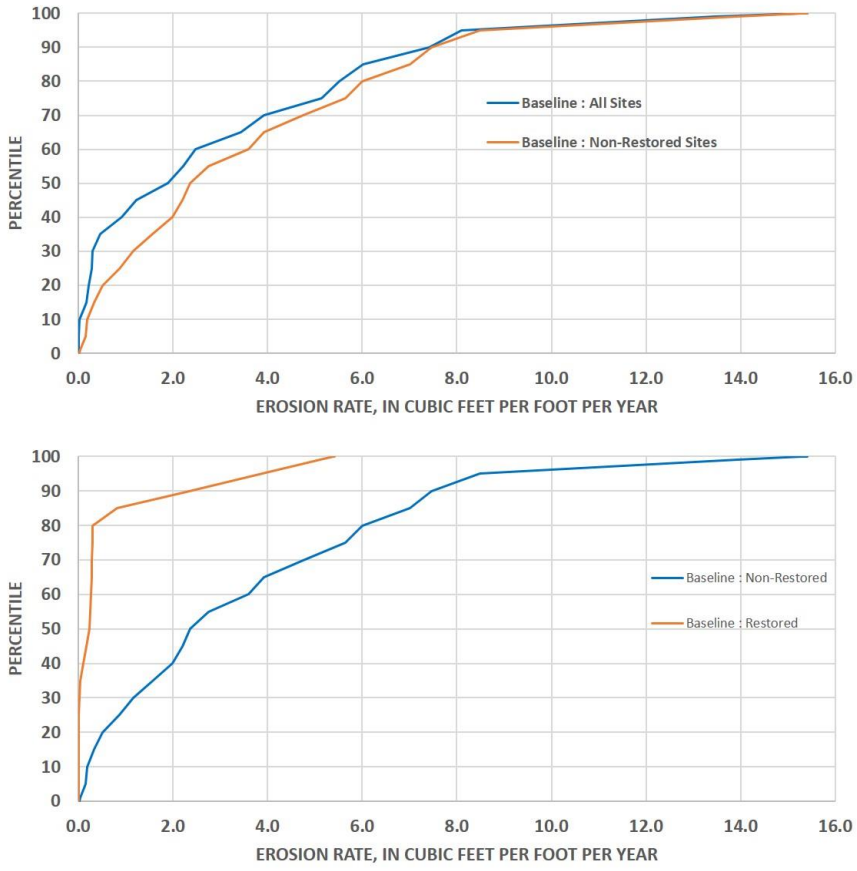

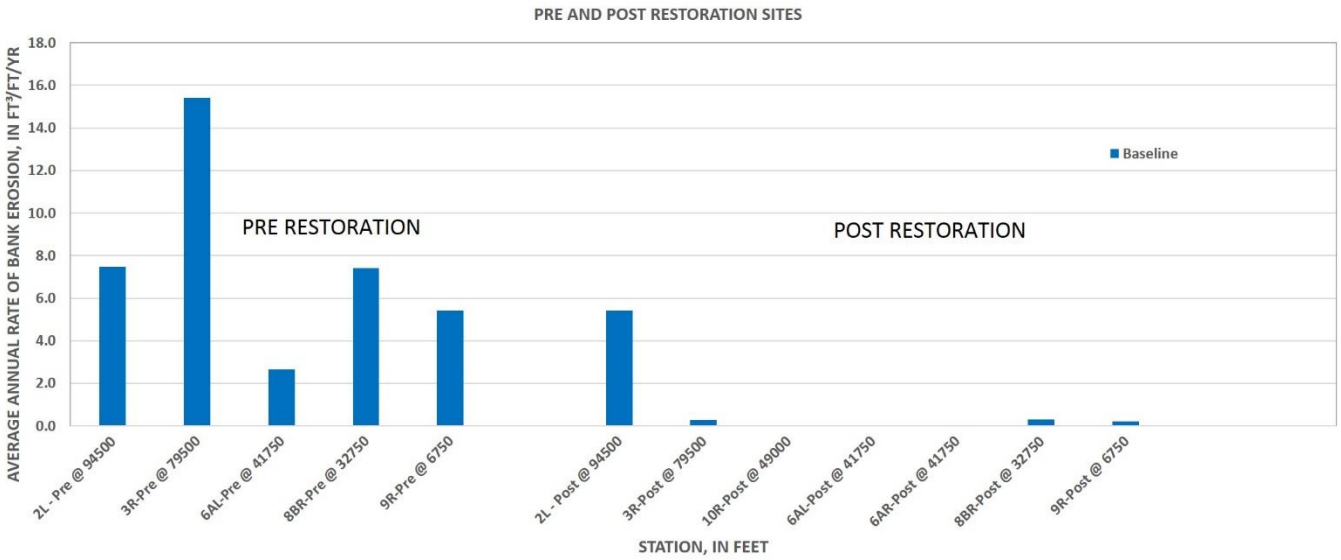

Figure 5.4.2.1-2: Distribution of Bank-erosion Rates for the Baseline Condition for All Sites/conditions versus Non-restored (Top), and for Restored versus Non-restored Simulations (Middle) and Direct Comparison (Bottom)

5.4.2.2 Comparisons with Other Modeling Scenarios

The other bank-erosion scenario modeled with BSTEM (S1) is based on hydraulic inputs representing a range of operational conditions along the TFI. This scenario is described in previous sections with the hydraulic assumptions summarized in Table 5.4.1.1-1. In addition to the basic operational and hydraulic scenarios, an additional Baseline Condition was run for each site with the wave sub-model turned off. Differences between the Baseline Condition with and without waves provided a convenient way to determine the role of boat-generated waves on bank erosion. Perhaps the easiest way to view and interpret the multitude of BSTEM simulations is to view the results in graphical form sorted schematically by station. Figure 5.4.2.2-1 shows the simulated bank-erosion rates (in $ft^3/ft/y$) along the entire study reach for ease of comparison of simulations of different lengths. Vernon Dam would be located at the far left of the plot with Turners Falls Dam at the far right. A numerical summary of these results is provided in Table 5.4.2.2-1.

Several interpretations about bank-erosion rates can be gleaned from Figure 5.4.2.2-1.

- First, is that there are no apparent longitudinal trends as one moves upstream or downstream from either Vernon Dam or Northfield Mountain, or along the reach as a whole.

- Second, erosion rates for the Baseline Condition (with waves) represent the maximum erosion rate at each of the sites. The slightly greater values (by about 1%) for S1 at sites 3R pre-restoration and 87BL should be considered the same as the Baseline as they are within the range of differences in failure geometries over the course of a 15-year simulation.

- Third, the role of boat waves has a small impact starting in the lower TFI (Reach 1) in the vicinity of station 27,000 (site 75BL) and generally increases downstream. This is related to the general lake-like conditions in the lower TFI where water-surface elevations vary across a narrow range (See Figure 5.4.1.1-4; Top from previous section), focusing wave impacts in the zone where the beach/toe intersect the lower-most part of the upper bank. A close up of the erosion at site 12BL (station 6,500) shows the increase in basal undercutting that took place with the "waves on" version of the Baseline Condition in comparison to the simulation without waves (Figure 5.4.2.2-2).

Role of Northfield Mountain Project Operations

One of the ways to determine the role of Northfield Mountain Project operations on bank-erosion rates is to attempt to isolate the effects of the peaking operations from Northfield Mountain at the exclusion of high flows (represented by the hourly data) and boat-generated waves. To accomplish this we subtract the bank-erosion rates predicted for S1 (Vernon operating, hourly peaks, boat waves and Northfield Mountain idle) from the erosion rates predicted for the Baseline Condition. The operational difference between the two scenarios would be manifest as altered hydraulic conditions (and assumedly erosion rates) resulting from operations at Northfield Mountain. As can be seen in Figure 5.4.2.2-3, Project operations as denoted by the orange bars (BL-S1) generally show very small effects. The apparent negative values for the Baseline – S1 Case are the result of slight differences in failure geometries caused by differences in the geometry of hydraulic erosion at several sites (i.e. slightly larger when NFM is idle in these cases).

The exception appears to be at site 8BR pre-restoration (station 32,750) where a large geotechnical failure occurred at a high flow of about 99,000 cfs but only under Baseline Conditions. The other model scenario for the site does not show this failure. Given that mass wasting are not a linear, continuous process such as entrainment of bed sediments under excess stress, it is reasonable that slightly more hydraulic erosion occurred during the Baseline Condition causing the failure. In comparison to site 8L which does not show a dominant impact from Northfield Mountain, 8BR is much steeper and less vegetated. Current and future erosion rates at this site, however, reflect the effect of restoration activities in 2012 that greatly reduced bank-erosion rates from about 7.4 $ft^3/ft/y$ to about 0.3 $ft^3/ft/y$ (Figure 5.4.2.1-2; Bottom).

The only other locations/conditions that show even a minor impact (> 0.1 $ft^3/ft/y$) from Northfield Mountain Project operations are sites 7L at station 37,500 (0.17 $ft^3/ft/y$) and perhaps 119BL at station 41,000 (0.09 $ft^3/ft/y$). These are all very low erosion rates and if considered in the context of average, annual-erosion rates for non-restoration sites under the Baseline Condition, these contributions fall at or below the 10^{th} percentile of erosion rates. At site 7L bank erosion due to Northfield Mountain Project operations (Baseline minus S1) accounts for about 4% of the erosion under Baseline Conditions while 95% of the erosion occurs at flows greater than 47,700 cfs. At site 119BL the contribution from Project operations is about 1.5%.

Overall contributions of Northfield Mountain Project operations on bank-erosion rates can be seen by comparing the BL-S1 erosion rate with the total erosion rate under Baseline Conditions. The contribution in percent (%) is plotted schematically (in orange) by site/station along with the bank-erosion rate (in blue) under the Baseline Condition (Figure 5.4.2.2-3). If looking at just the contributions from Northfield Mountain Project operations (BL-S1), values are generally low (less than 5%) with a few exceptions; sites 10R post-restoration (station 49,000), 6AL post-restoration (station 41,750), 8BR pre- and post-restoration (station 32,750) and 8BL (station 32,750). When including the information on erosion rates as well, we see that aside from 8BR pre-restoration, the remaining sites just mentioned are experiencing very low rates of erosion, with most representing restored conditions (Table 5.4.2.2-2).

Role of Naturally Occurring High Flows

The role of high flows on bank-erosion rates was investigated by analyzing the hourly outputs from each time step in BSTEM. The output data were sorted by the amount of bank erosion during each time step to determine what stages (flow elevations) and discharges were responsible for bank erosion along the reach. The stage data was converted to discharge by developing polynomial regression relations using data from HEC-RAS. An example plot is shown in Figure 5.4.2.2-4 that was used for sites 10R, 10L and 26R; all equations are listed in Table 5.4.2.2-3. Erosion data for each site were thus sorted into 10,000 discharge classes to determine how much erosion had occurred in each discharge class without biasing the classes because of different sizes. Data from each class were then summed to develop a cumulative frequency distribution for each model run.

The resulting database of erosion totals provides us with an opportunity to investigate the relative amounts of erosion that occur at different discharges. A metric that denotes the flows at which the vast majority of the erosion occurs is informative in determining causes. For example, Figure 5.4.2.2-5 shows the discharge at which 95% and 75% of the erosion occurs at flows greater than indicated. Conversely, only 5% of the erosion occurs at flows less than those shown in the top figure. The combined hydraulic capacity of Vernon Dam (17,130 cfs) and Northfield Mountain (20,000 cfs) of roughly 37,000 cfs is shown as the solid black line for the middle, Northfield Mountain, and lower impoundment. A threshold of 17,130 cfs is used to show the hydraulic capacity for the upper impoundment as a result of Vernon Dam only. The figure clearly shows that 95% of the bank-erosion for just about all of the sites, conditions and scenarios occurs at flows much greater than the hydraulic capacity of Vernon Dam. Again, these results need to be taken in the context of the actual amount of erosion that occurs at each site/condition. For example, of the sites where 95% of the erosion occurs at about 10,000 cfs or less including sites 4L, 29R, 10R post-restoration and 6AR post-restoration, only site 29R (station 66,000) had measureable amounts of erosion (about 1.7 $ft^3/ft/y$). Here, the initial condition (2014) of the bank showed a pronounced undercut at the start of the simulation (Figure 5.4.2.2-6). Mass wasting of the cantilever section of the bank occurred soon thereafter, regardless of the magnitude of the flow.

As further evidence of the critical role of high flows on bank-erosion rates, a number of examples of the discharges where bank-erosion occurs are provided in Figure 5.4.2.2-7. In this case we are looking at both the contribution of discharges to cumulative erosion at a particular site as well the individual discharge classes where the erosion occurred. The examples provided are for the following stations:

- Site 3L at station 79,500 where about 6.1 $ft^3/ft/y$ of erosion occurred
- Site 5CR at station 57,250 where 8.6 $ft^3/ft/y$ of erosion occurred;
- Site 6AL pre-restoration at station 41,750 where 2.6 $ft^3/ft/y$ occurred; and
- Site 6AR post-restoration also at 41,750 where only 0.02 $ft^3/ft/y$).

Vertical sections in the cumulative plots (sold traces) and peaks in the dotted traces generally indicate the occurrence of a mass wasting. These are most likely the result of bank steepening and undercutting during high-flow events. The most significant message to be taken for these plots, similar plots in the section on individual site write-ups (Section 5.4.3), and the results shown in Figure 5.4.2.2-5, is that measureable erosion processes do not begin at the vast majority of sites until flows exceed 25,000 to 30,000 cfs, with many occurring at flows above 60,000 cfs. In the examples shown in Figure 5.4.2.2-7, erosion throughout the range of flows occurred only at the site representing very low erosion rates (6AR post-restoration), indicating that some small amount of particle-by-particle erosion has occurred across the range of flows.

To obtain a clearer understanding of the flows that are responsible for bank erosion in the TFI under Baseline Conditions and to provide further evidence of the importance of high flows on bank-erosion rates data that describes the distribution of responsible flows for each site are shown in Table 5.4.2.2-4. With the exception of site 11L just downstream from Vernon Dam and effected by dam releases, and site 29R where a severe undercut in the existing bank geometry led to a sizeable failure at a relatively low discharge, one can see the bank-erosion was dominated by the high-flow discharges.

Table 5.4.2.2-1: Summary of BSTEM Results for the Various Operational Scenarios

Site/Condition	Station	Dates		Baseline (Waves On)	Baseline (Waves off)	S1
	(ft)	Start	End	($ft^3/ft/y$)	($ft^3/ft/y$)	($ft^3/ft/y$)
11L	100000	7/15/2005	9/10/2014	0.297	0.296	0.303
2L-Pre	94500	6/20/2000	6/30/2012	7.48	7.473	7.461
2L-Post	94500	7/1/2012	8/28/2014	5.416	5.411	5.396
303BL	94000	1/1/2000	8/27/2014	0.647	0.645	0.674
18L	87000	1/1/2000	8/27/2014	1.092	1.092	1.080
3L	79500	1/1/2000	8/28/2014	6.086	6.090	6.042
3R-Pre	79500	1/1/2000	6/30/2006	15.425	15.407	15.458
3R-Post	79500	7/1/2006	8/28/2014	0.285	0.281	0.282
21R	79250	1/1/2000	8/27/2014	2.359	2.291	2.355
4L	74000	1/1/2000	8/28/2014	0.017	0.014	0.017
29R	66000	1/1/2000	8/27/2014	1.718	1.709	1.718
5CR	57250	7/8/2002	9/3/2014	8.606	8.500	8.566
26R	50000	1/1/2000	8/27/2014	1.194	1.145	1.196
10L	49000	1/1/2000	8/27/2014	0.160	0.158	0.158
10R-Post	49000	7/1/2001	8/27/2014	0.000	0.000	0.000
6AL-Pre	41750	1/1/2000	6/30/2004	2.668	2.635	2.736
6AL-Post	41750	7/1/2004	8/27/2014	0.000	0.000	0.000
6AR-Post	41750	6/21/2000	8/27/2014	0.021	0.000	0.020
119BL	41000	1/1/2000	8/27/2014	5.876	5.722	5.789
7L	37500	1/1/2000	8/26/2014	4.291	4.242	4.125
7R	37500	1/1/2000	8/26/2014	2.058	2.037	2.047
8BL	32750	6/2/2000	8/26/2014	0.427	0.427	0.399
8BR-Pre	32750	6/2/2000	6/30/2012	7.415	7.394	1.954
8BR-Post	32750	7/1/2012	8/26/2014	0.312	0.312	0.248
87BL	30750	1/1/2000	8/27/2014	3.568	3.607	3.595
75BL	27000	1/1/2000	8/27/2014	3.755	3.475	3.927
9R-Pre	6750	6/2/2000	6/30/2008	5.426	0.967	5.192
9R-Post	6750	7/1/2008	8/26/2014	0.227	0.002	0.224
12BL	6500	1/1/2000	8/27/2014	2.221	0.239	2.150
BC-1R	4750	6/5/2000	8/26/2014	0.168	0.000	0.167

* Hydraulic assumptions for Scenario 1 (S1) are provided in *Table 5.4.1.1-1*

Table 5.4.2.2-2: Baseline Erosion Rates and Contribution to That Erosion by Project Operations as Determined by Subtracting Erosion Rates For S1 from those of the Baseline Condition

Site/Condition	Station	Total Erosion	Northfield Mtn. Erosion
		Baseline (waves on)	Baseline – S1
		(ft^3/ft)	% Contribution to Baseline
11L	100000	0.297	-2.2%
2L-Pre	94500	7.48	0.3%
2L-Post	94500	5.416	0.4%
303BL	94000	0.647	-4.2%
18L	87000	1.092	1.1%
3L	79500	6.09	0.7%
3R-Pre	79500	15.42	-0.2%
3R-Post	79500	0.285	1.1%
21R	79250	2.36	0.2%
4L	74000	0.017	0.6%
29R	66000	1.72	0.0%
5CR	57250	8.61	0.5%
26R	50000	1.19	-0.1%
10L	49000	0.160	1.1%
10R-Post	49000	0.0003	99.9%[1]
6AL-Pre	41750	2.67	-2.6%
6AL-Post	41750	0.00001	18.9%[1]
6AR-Post	41750	0.021	2.0%
119BL	41000	5.88	1.5%
7L	37500	4.29	3.9%
7R	37500	2.06	0.5%
8BL	32750	0.427	6.6%
8BR-Pre	32750	7.41	73.6%
8BR-Post	32750	0.312	20.4%
87BL	30750	3.57	-0.8%
75BL	27000	3.76	-4.6%
9R-Pre	6750	5.43	4.3%[2]
9R-Post	6750	0.227	1.4%[2]
12BL	6500	2.22	3.2%[2]
BC-1R	4750	0.168	0.4%[2]

1- Even though % Contribution shows a NFM influence the total erosion is almost zero

2 - % in this reach also includes a wave influence

Table 5.4.2.2-3: Stage-discharge Relations Developed from HEC-RAS Data for the Detailed Study Sites

HEC-RAS File	Station	Equation	Type	r^2
98769	11L	$Q = -188.1532x^3 + 33{,}742.6670x^2 - 1{,}998{,}2785x + 39{,}159{,}171.6988$	3-parameter	0.98
93245	2L	$Q = -325.1597x^3 + 57{,}051.4539x^2 - 3{,}317{,}743.6127x + 63{,}995{,}507.4672$	3-parameter	0.97
93245	303BL	$Q = -325.1597x^3 + 57{,}051.4539x^2 - 3{,}317{,}743.6127x + 63{,}995{,}507.4672$	3-parameter	0.97
85957	18L	$Q = -444.5923x^3 + 77477.8485x^2 - 4480900.9989x + 86050961.3259$	3-parameter	0.96
78453	3L	$Q = -602.1374x^3 + 401{,}357.5191x^2 - 6{,}007{,}824.1090x + 114{,}932{,}875.9390$	3-parameter	0.94
78453	#R	$Q = -602.1374x^3 + 401{,}357.5191x^2 - 6{,}007{,}824.1090x + 114{,}932{,}875.9390$	3-parameter	0.94
78453	21R	$Q = -602.1374x^3 + 401{,}357.5191x^2 - 6{,}007{,}824.1090x + 114{,}932{,}875.9390$	3-parameter	0.94
72416	4L	$Q = -707.4104x^3 + 122{,}336{,}1119x^2 - 7{,}030{,}226.6244x + 134{,}294{,}867.1744$	3-parameter	0.94
64708	29L	$Q = -907.9605x^3 + 156501.7740x^2 - 8968894.6763x + 170937379.1121$	3-parameter	0.92
56235	5CR	$Q = -1{,}098.8039x^3 + 188{,}972.1623x^2 - 10{,}809{,}028.2672x + 205{,}673{,}698.1172$	3-parameter	0.91
47938	26R	$Q = -205.59471389x^6 + 70387.15430583x^5 - 10038404.69817680x^4 + 763370519.39162800x^3 - 32645915306.65530000x^2 + 744424922625.25800000x - 7071331681422.40000000$	6-parameter	0.90
47938	10L	$Q = -205.59471389x^6 + 70387.15430583x^5 - 10038404.69817680x^4 + 763370519.39162800x^3 - 32645915306.65530000x^2 + 744424922625.25800000x - 7071331681422.40000000$	6-parameter	0.90
47938	10L	$Q = -205.59471389x^6 + 70387.15430583x^5 - 10038404.69817680x^4 + 763370519.39162800x^3 - 32645915306.65530000x^2 + 744424922625.25800000x - 7071331681422.40000000$	6-parameter	0.90
39952	6AL	$Q = -245.51028346x^6 + 83995.45306679x^5 - 11971140.24890380x^4 + 909742504.71487900x^3 - 38880163616.77810000x^2 + 886013079166.84800000x - 8410935562085.17000000$	6-parameter	0.88
39952	6AR	$Q = -245.51028346x^6 + 83995.45306679x^5 - 11971140.24890380x^4 + 909742504.71487900x^3 - 38880163616.77810000x^2 + 886013079166.84800000x - 8410935562085.17000000$	6-parameter	0.88
39952	119BL	$Q = -245.51028346x^6 + 83995.45306679x^5 - 11971140.24890380x^4 + 909742504.71487900x^3 - 38880163616.77810000x^2 + 886013079166.84800000x - 8410935562085.17000000$	6-parameter	0.88
36653	7L	$Q = -281.71574298x^6 + 96325.50879321x^5 - 13720463.52509040x^4 + 1042084875.6568000x^3 - 44511028775.98300000x^2 + 1013767141883.29000000x - 9618436642314.27000000$	6-parameter	0.87
36653	7R	$Q = -281.71574298x^6 + 96325.50879321x^5 - 13720463.52509040x^4 + 1042084875.6568000x^3 - 44511028775.98300000x^2 + 1013767141883.29000000x - 9618436642314.27000000$	6-parameter	0.87
30404	8BL	$Q = -314.92075666x^6 + 107664.35596156x^5 - 15333485.42641640x^4 + 1164441334.34417000x^3 - 49730804176.63400000x^2 + 1132505344005.5800000x - 10743643009686.7000000$	6-parameter	0.83
30404	8BR	$Q = -314.92075666x^6 + 107664.35596156x^5 - 15333485.42641640x^4 + 1164441334.34417000x^3 - 49730804176.63400000x^2 + 1132505344005.5800000x - 10743643009686.7000000$	6-parameter	0.83
30404	87BL	$Q = -314.92075666x^6 + 107664.35596156x^5 - 15333485.42641640x^4 + 1164441334.34417000x^3 - 49730804176.63400000x^2 + 1132505344005.5800000x - 10743643009686.7000000$	6-parameter	0.83
25845	75BL	$Q = -453.53388331x^6 - 154738.13119984x^5 - 21993407.72848850x^4 + 1666881999.57544000x^3 - 71048965952.00670000x^2 + 1614830996923.93000000x - 15289824117576.90000000$	6-parameter	0.83
4830	12BL	N/A	N/A	N/A
4830	9R	N/A	N/A	N/A
4830	BC-1R	N/A	N/A	N/A

Note that stage is in meters (units for BSTEM input) and discharge is in cfs (units for HEC-RAS). Regressions could not be developed for three sites in the lower impoundment due to lack of a relation.

Table 5.4.2.2-4 - Distribution of discharges responsible for 5%, 50% and 95% of the bank erosion at the 25 detailed study sites

Site	Station	Total Erosion Under Baseline, $ft^3/ft/yr$	Baseline Scenario Discharge, cfs		
			95% of Erosion: 5% of erosion occurs at flows greater than	50% of Erosion: 50% of erosion occurs at flows greater than	5 % of Erosion: 95% of erosion occurs at flows greater than
11L	100000	0.297	56869	4985	500
2L - Pre	94500	7.48	86993	66778	56081
2L - Post	94500	5.416	66947	32196	19537
303BL	94000	0.647	79881	64684	53194
18L	87000	1.092	73352	54485	17824
3L	79500	6.086	98234	78682	37098
3R-Pre	79500	15.425	73365	61470	39229
3R-Post	79500	0.285	87760	54420	36411
21R	79250	2.359	63852	46345	22928
4L	74000	0.017	95042	83527	6991
29R*	66000	1.718	11968	11968	11923
5CR	57250	8.606	76391	76391	47867
26R	50000	1.194	80503	60282	43294
10L	49000	0.160	98882	79003	58922
10R-Post	49000	0.000	49015	48156	46944
6AL-Pre	41750	2.668	77664	65442	56264
6AL-Post	41750	0.000	65167	63310	62287
6AR-Post	41750	0.021	29662	11191	7051
119BL	41000	5.876	70557	53969	24796
7L	37500	4.291	98753	65338	47731
7R	37500	2.058	98463	65880	53614
8BL	32750	0.427	84451	84138	77997
8BR-Pre	32750	7.415	99458	99458	64443
8BR-Post	32750	0.312	72009	69312	66504
87BL	30750	3.568	63968	42875	17849
75BL	27000	3.755	71586	48054	33822
9R-Pre	6750	5.426	I	I	I
9R-Post	6750	0.227	I	I	I
12BL	6500	2.221	I	I	I
BC-1R	4750	0.168	I	I	I

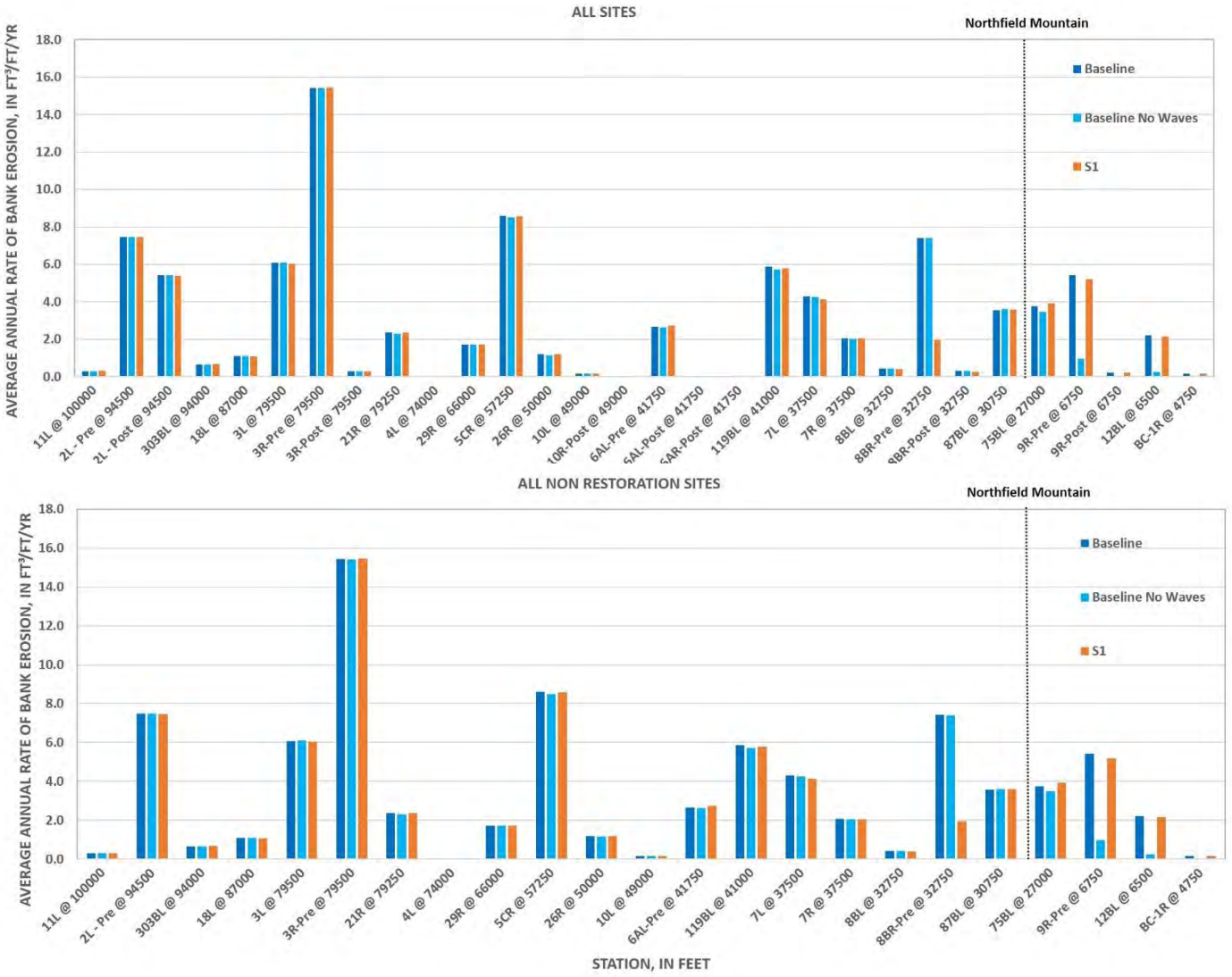

Figure 5.4.2.2-1: Summary of Bank-erosion Rates for All Sites (including restored conditions) and Modeling Scenarios along the Study Reach (Top) and for only the Non-restored Sites/Conditions (Bottom)

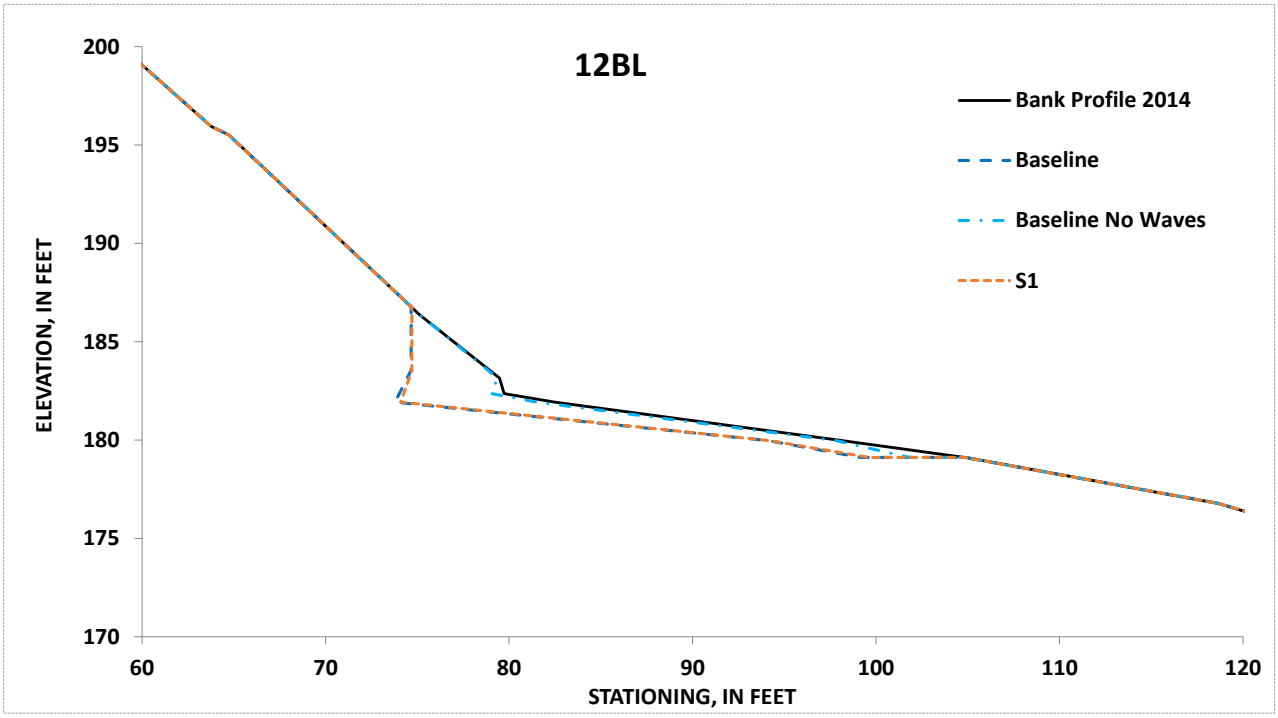

Figure 5.4.2.2-2: Example of the Important Effect of Boat Waves in the Lower TFI (Reach 1) showing the Greater amount of Hydraulic Erosion (Undercutting) between the Baseline Condition with Waves as Compared to the Baseline Condition Without Waves at Site 12BL

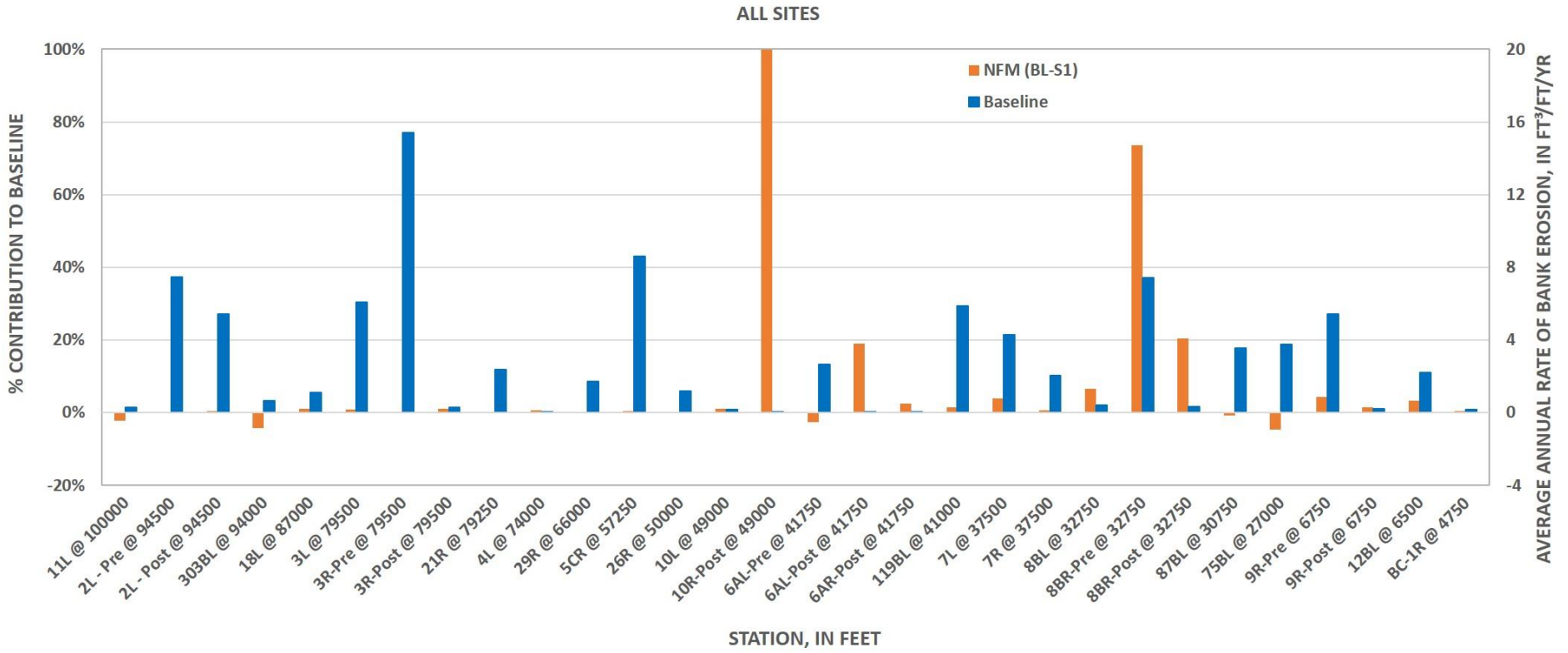

Figure 5.4.2.2-3: Contribution of Erosion Rates Due to Project Operations Compared to Erosion Rates for the Baseline Condition

Results need to be taken in context of the total amount of erosion at a particular site to interpret relative impact of the Project

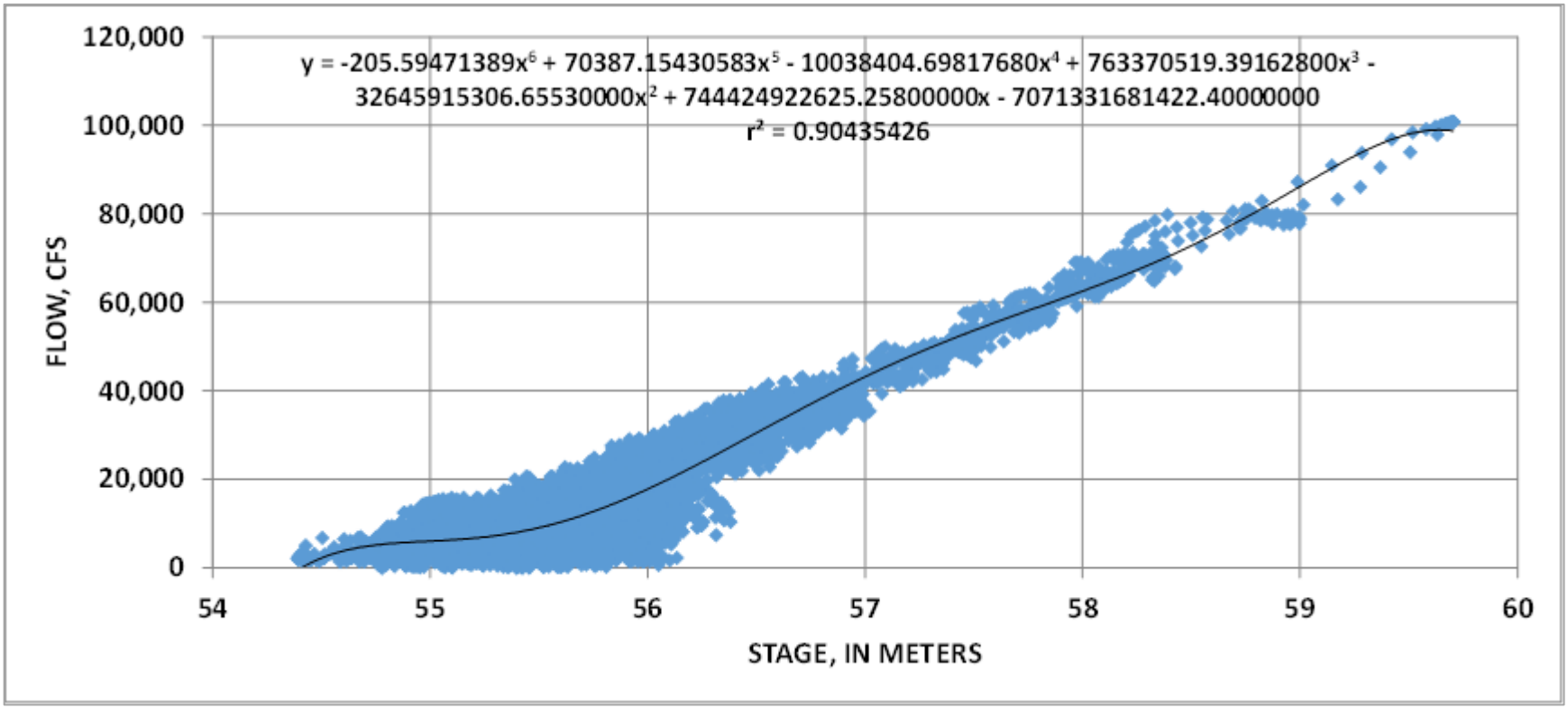

Figure 5.4.2.2-4: Example Stage-discharge Relationship Developed for Sites 10L, 10R and 26R from Hourly HEC-RAS Data

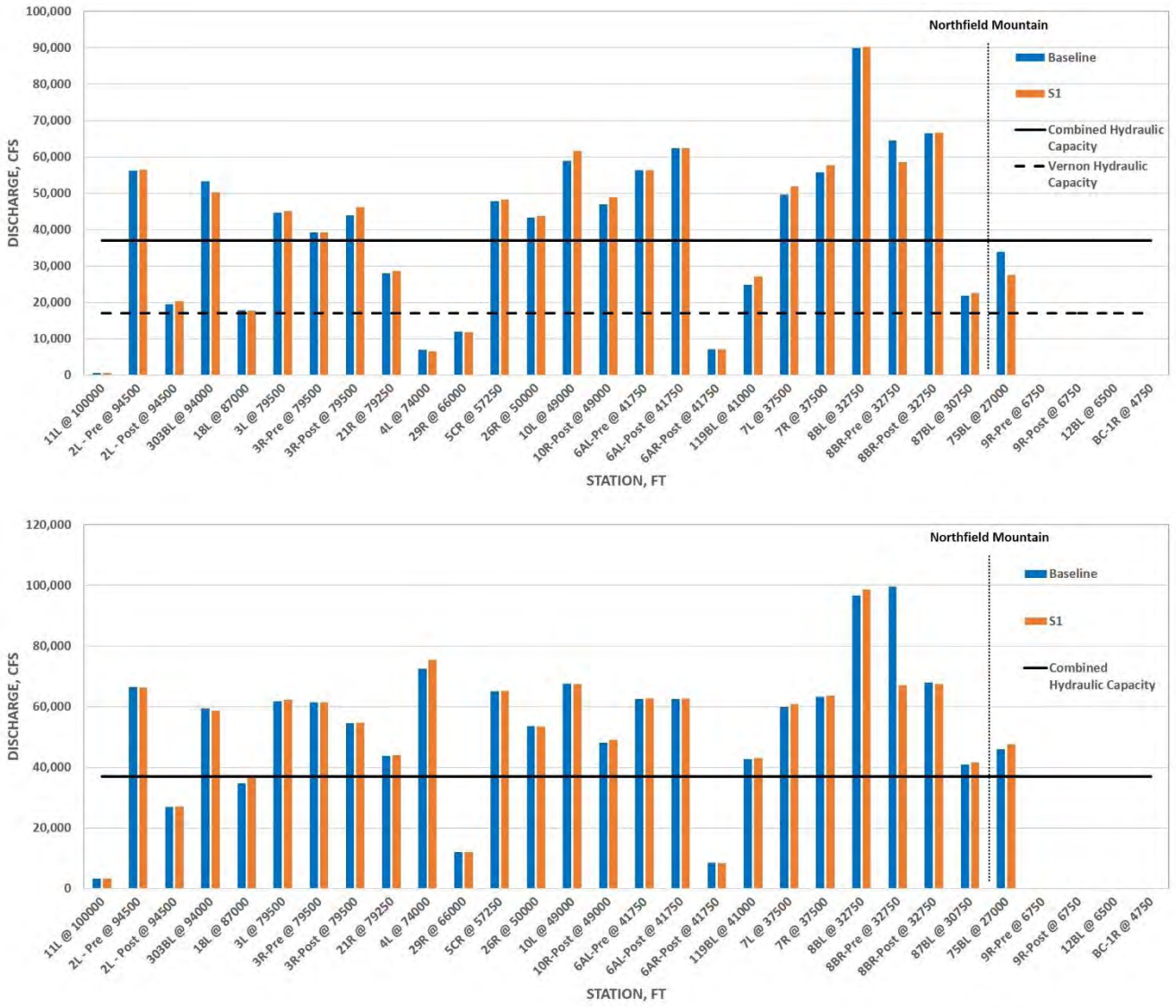

Figure 5.4.2.2-5: Discharge at which 95% of the erosion occurs at flows higher than indicated (Top) and where 75% of the erosion occurs at higher discharges (Bottom)

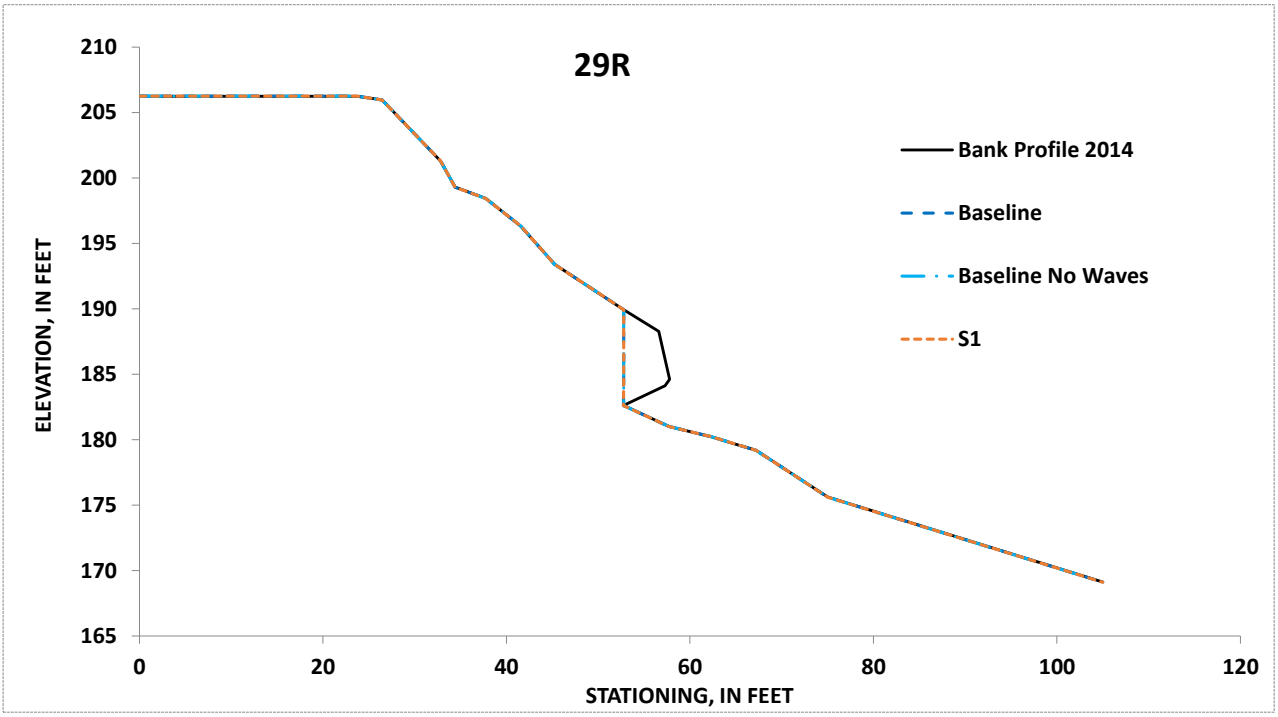

Figure 5.4.2.2-6: Bank profile for site 29R at Station 66,000 Showing Pronounced Undercut at the Start of the Simulations

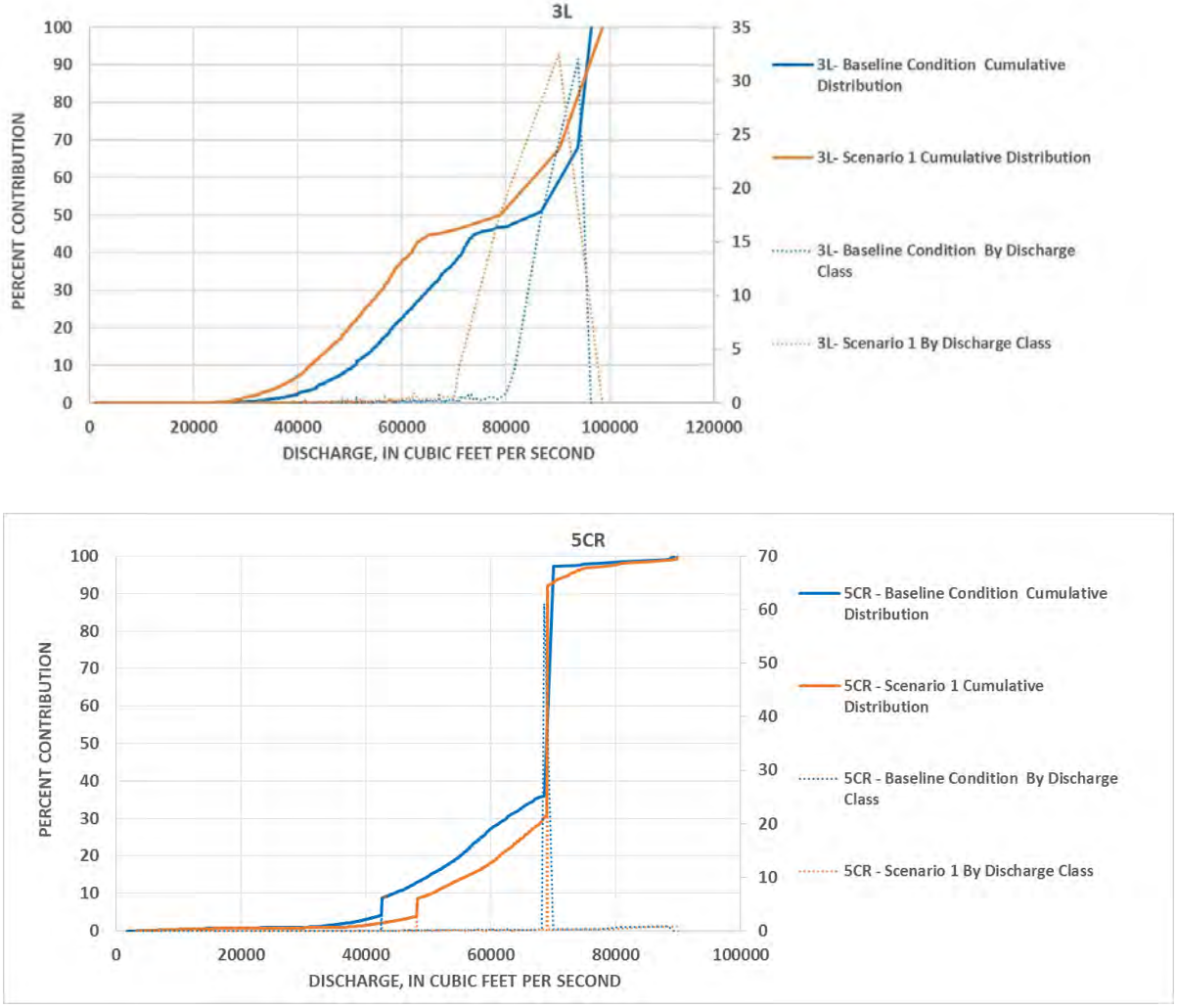

Figure 5.4.2.2-7 (Part 1 of 2): Distribution of Total Erosion at Four Sites According to Discharge Classes

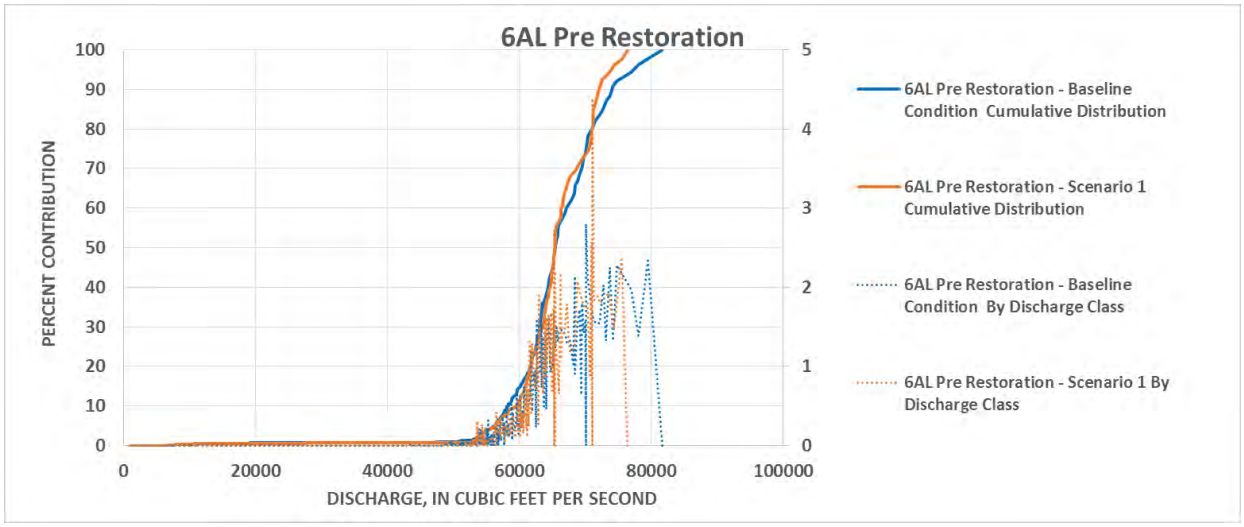

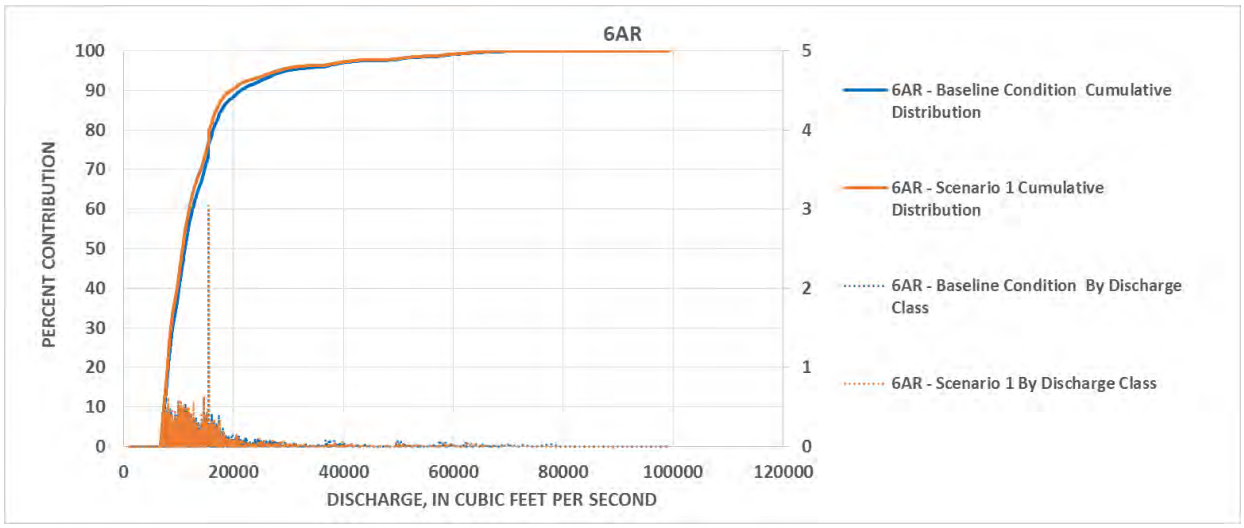

Figure 5.4.2.2-7 (Part 2 of 2): Distribution of Total Erosion at Four Sites According to Discharge Classes

5.4.2.3 Role of Boat-Generated Waves

The role of boat-generated waves for the Baseline Condition was briefly discussed in an earlier section. A plot from site 12BL (Figure 5.4.2.2-2, previous section) was used as an example of the much greater amounts of basal undercutting that can occur in the lower TFI as a result of boat-generated waves. This is related to the fact that water-surface elevations do not vary significantly in the lower TFI, thereby focusing all of the wave energy along a narrow band of elevations along the bank. Because the resulting basal erosion rate is the product of the magnitude of the excess shear stress and the duration of that excess stress at a given bank node, the greater durations provided along this narrow band makes boat-generated waves an important factor in bank erosion at these locations. This helps to explain why boat-generated wave action is not as important a factor in bank erosion rates in other parts of the TFI. As described in a previous chapter on wave characteristics, wind-generated waves in the study reach do not have sufficient energy to cause basal erosion, likely due to short fetches.

Acknowledging the importance of boat-generated waves for the Baseline Condition in the lower TFI led to re-running the other Operational scenarios without waves as well. A comparison of erosion rates with and without boat-generated waves for the four sites in the lower TFI is shown in Figure 5.4.2.3-1. Clearly, erosion rates drop significantly for all scenarios when the effects of waves are removed. As one moves upstream in the TFI, however, the effect is reduced to the point that at site 75BL (station 27,000), there is enough vertical flow variability that differences in erosion rates with and without waves become small (Figure 5.4.2.3-1). A summary of the bank-erosion rates in the lower TFI with and without waves for all Operational scenarios is provided in Table 5.4.2.3-1.

Table 5.4.2.3-1: Summary of bank-erosion rates for sites in the lower impoundment showing differences with and without boat-generated waves

Site/Condition	Station	Dates		Baseline (Waves on)	Baseline (Waves off)	S1 (Waves on)	S1 (Waves off)
	ft	Start	End	$ft^3/ft/y$	$ft^3/ft/y$	$ft^3/ft/y$	$ft^3/ft/y$
75BL	27000	01/01/00	08/27/14	3.76	3.47	3.93	3.72
9R-Pre	6750	06/02/00	06/30/08	5.43	0.97	5.19	0.77
9R-Post	6750	07/01/08	08/26/14	0.23	0.00	0.22	0.00
12BL	6500	01/01/00	08/27/14	2.22	0.24	2.15	0.19
BC-1R	4750	06/05/00	08/26/14	0.168	0.00	0.167	0.00

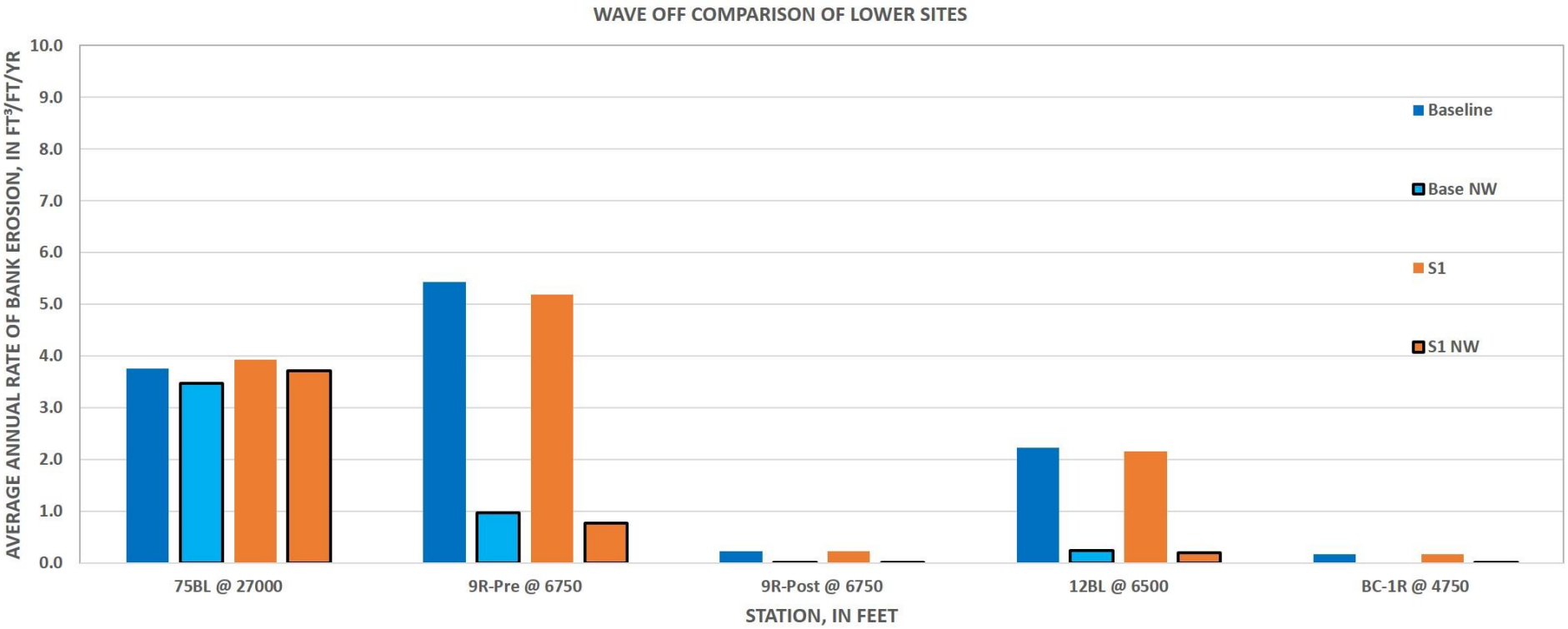

Figure 5.4.2.3-1 Comparison of Bank-erosion Rates with and without Boat-generated Waves for Sites in the Lower Turners Falls Impoundment

5.4.3 BSTEM Simulation Results: Site-Specific Results

The following section provides the results from BSTEM modeling conducted at each of the 25 detailed study sites to investigate the causes of bank erosion along the TFI. Descriptions start with the most upstream site 11L, just below Vernon Dam and continue downstream to BC-1R, just upstream of Turners Falls Dam. The locations and stationing of these sites are shown in Section 4 along with the flow, geometry and bank-resistance input data used to populate BSTEM for the different scenarios. This section discusses general site characteristics and the BSTEM results at each site.

The magnitude and distribution of bank erosion along the study reach is a combination of many factors that control the hydraulic and geotechnical processes that cause erosion. For each site, a comparison of the modeling results for each modeled scenario is presented including a discussion of the controlling factors and processes. The flow scenarios represent different operational conditions aimed at determining the role of water-level fluctuations, high flows and boat waves on bank-erosion rates. BSTEM calculates boundary shear stress caused by water-level fluctuations at each time step and at each node along the bank face. To address any issues related to drawdown conditions and effects as a result of hydro-power operations, BSTEM addresses these processes by calculating pore-water and confining pressures along potential failure surfaces during each time step of a simulation.

As a reminder, BSTEM modeling results are discussed in the context of both hydraulic and geotechnical erosion processes. For the purpose of this study, hydraulic erosion is defined as erosion caused by hydraulic processes. That is, the particle-by-particle entrainment and erosion of surficial sediments when and where the boundary shear stress exerted by the flow exceeds the critical shear stress that characterizes the surficial bank sediments. Hydraulic erosion from river flow or by waves can steepen and undercut bank surfaces leading to a loss of support for the upper part of the bank and making them susceptible to collapse (geotechnical erosion). These processes are most important when shear stresses are highest as during high flows.

Again to reiterate, geotechnical erosion is defined as erosion caused directly by gravitational forces as in the collapse of a hillslope or bank. Here, erosion occurs when the downslope, gravitational forces exceed the shearing resistance of the *in situ* materials. Any factors that increase the downslope gravitational forces (such as steepness and weight) or decrease the shearing resistance of the materials (such as generation of positive pore-water pressure) contribute to geotechnical erosion. Pore-water pressure can be generated within the bank by lateral infiltration (depending on the duration the water is at a certain elevation) during rises in stage. This can reduce the frictional component of shear strength (See Volume III – Appendix F). The confining pressure provided by the flow pressing against the bank surface, however, tends to offset this affect. An important point are the relative rates of decreasing stage and groundwater levels during water-level fluctuations because the loss of shear strength combined with a loss of confining pressure (known as the *drawdown* condition) is particularly critical for streambank stability. BSTEM handles these processes by calculating pore-water and confining pressures along potential failure surfaces during each time step of a simulation (See Volume IIII - Appendix F).

Geotechnical erosion (bank failure) generally does not occur unless there is a change to the equilibrium condition that the bank slope exists in. This change can be an increase in the downslope gravitational forces and/or the resistance of the materials. With streambanks, this change towards disequilibrium and instability is often related to a steepening of the bank by hydraulic action. Whether this steepening or undercutting is related to water-level fluctuations due to hydropower operations or to the shear stress imposed by high flows has been the subject of the analysis in the previous section. Results showed that in almost all cases that the bulk of the erosion occurred during high flows and not during periods of water-level fluctuations due to Project operations.

Model results, along with the measured erosion over the period (normalized by the number of years for each simulation) are shown in Table 5.4.3-1. Hydraulic erosion either from flows or boat-waves that cause

undercutting can be a contributing factor in erosion rates by instigating mass failure of the upper bank. Figure 5.4.3-1 shows the relative contributions of hydraulic and geotechnical erosion for all sites and operational scenarios along the study reach. Both the aforementioned Table and Figure provide the backdrop to the individual site write ups that follow.

Table 5.4.3-1: Summary of BSTEM Results for All Detailed Study Sites

Site/Condition	Station	Dates		Baseline (Waves On)	Baseline (Waves off)	S1
	(ft)	Start	End	(ft^3/ft/y)	(ft^3/ft/y)	(ft^3/ft/y)
11L	100000	7/15/2005	9/10/2014	0.297	0.296	0.303
2L-Pre	94500	6/20/2000	6/30/2012	7.480	7.473	7.461
2L-Post	94500	7/1/2012	8/28/2014	5.416	5.411	5.396
303BL	94000	1/1/2000	8/27/2014	0.647	0.645	0.674
18L	87000	1/1/2000	8/27/2014	1.092	1.092	1.080
3L	79500	1/1/2000	8/28/2014	6.086	6.090	6.042
3R-Pre	79500	1/1/2000	6/30/2006	15.425	15.407	15.458
3R-Post	79500	7/1/2006	8/28/2014	0.285	0.281	0.282
21R	79250	1/1/2000	8/27/2014	2.359	2.291	2.355
4L	74000	1/1/2000	8/28/2014	0.017	0.014	0.017
29R	66000	1/1/2000	8/27/2014	1.718	1.709	1.718
5CR	57250	7/8/2002	9/3/2014	8.606	8.500	8.566
26R	50000	1/1/2000	8/27/2014	1.194	1.145	1.196
10L	49000	1/1/2000	8/27/2014	0.160	0.158	0.158
10R-Post	49000	7/1/2001	8/27/2014	0.000	0.000	0.000
6AL-Pre	41750	1/1/2000	6/30/2004	2.668	2.635	2.736
6AL-Post	41750	7/1/2004	8/27/2014	0.000	0.000	0.000
6AR-Post	41750	6/21/2000	8/27/2014	0.021	0.000	0.020
119BL	41000	1/1/2000	8/27/2014	5.876	5.722	5.789
7L	37500	1/1/2000	8/26/2014	4.291	4.242	4.125
7R	37500	1/1/2000	8/26/2014	2.058	2.037	2.047
8BL	32750	6/2/2000	8/26/2014	0.427	0.427	0.399
8BR-Pre	32750	6/2/2000	6/30/2012	7.415	7.394	1.954
8BR-Post	32750	7/1/2012	8/26/2014	0.312	0.312	0.248
87BL	30750	1/1/2000	8/27/2014	3.568	3.607	3.595
75BL	27000	1/1/2000	8/27/2014	3.755	3.475	3.927
9R-Pre	6750	6/2/2000	6/30/2008	5.426	0.967	5.192
9R-Post	6750	7/1/2008	8/26/2014	0.227	0.002	0.224
12BL	6500	1/1/2000	8/27/2014	2.221	0.239	2.150
BC-1R	4750	6/5/2000	8/26/2014	0.168	0.000	0.167

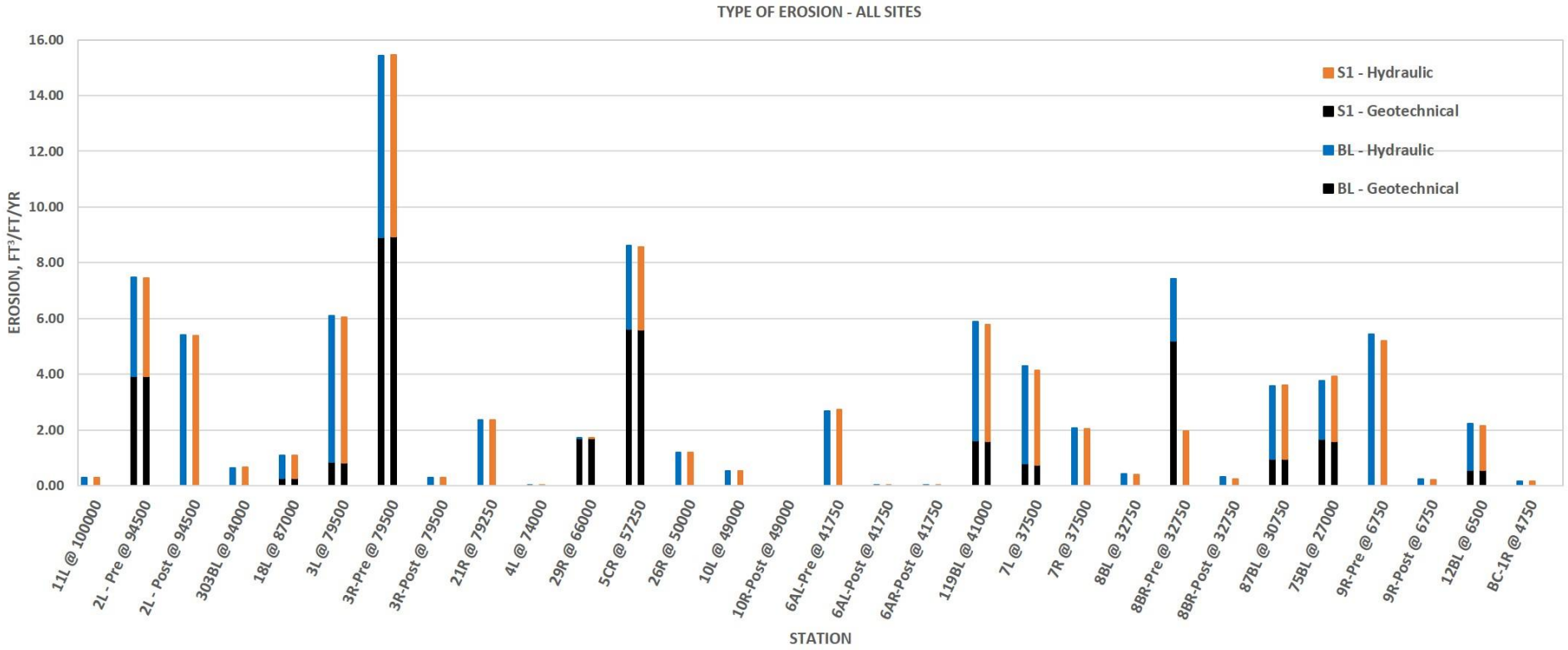

Figure 5.4.3-1: Bank-erosion Rates for all Sites, Conditions and Modeling Scenarios shown schematically from Upstream to Downstream along the Study Reach.

5.4.3.1 Site 11L

The river at site 11L has steep, heavily vegetated banks, located at station 100,000, at Stebbins Island, roughly 7,000 ft downstream of Vernon Dam (Figure 5.4.3.1-1). The bank is roughly 27 feet tall with a silt loam toe and upper bank. The bank is vegetated with grasses, shrubs, Black and Yellow Birch, Eastern Hemlock, and Red Maple trees. The first surveyed cross section for site 11L was taken on 7/15/2005, and was therefore used as the starting point for the model.

BSTEM runs at this site show that under the Baseline Condition, 2.72 ft^3 of erosion occurred per foot of bank, during the 2005-2014 flow period, averaging 0.297 $ft^3/ft/y$ (Table 5.4.3-1). This results in the 9th lowest erosion rate for the Baseline Condition, placing it between the 10th and 15th percentiles of erosion rates along the reach. The modeling also indicates that all 100% (0.297 $ft^3/ft/y$) of the erosion is due directly to hydraulic processes, and none of the bank erosion is the result of larger geotechnical failures.

The Baseline Condition (Waves off) resulted in 0.296 $ft^3/ft/y$, with 0.303 $ft^3/ft/y$ for Scenario 1. This resulted in the percent reductions in erosion rates of -2.2% for Scenario 1 (Figure 5.4.3.1-2). Baseline simulations with waves off showed virtually no reduction in erosion indicating that boat waves have little effect on erosion processes at this site. Because of this, all of the remaining scenarios were simulated with boat waves on.

For the Baseline Condition, 89.4% of the total erosion at site 11L occurs at flows below 17,130 cfs (Figure 5.4.3.1-3). These flows are well within the range of the hydraulic capacity of Vernon Dam. The remaining contributions to erosion are 10.4% due to high flows over the 17,130 cfs threshold and a very small 0.2% due to waves. Table 5.4.3.1-1 denotes the flows above which 95%, 50%, and 5% of all erosion occurs at the site as well as the amount of time those flows were exceeded for each year in the modeling period.

Table 5.4.3.1-1: Flow Exceedance Calculations for Site 11L

Site 11L	Percent of Erosion		
	95%	50%	5%
	Flow (cfs)		
Year	56,869	4,985	500
2000	0.90%	63.90%	100.00%
2001	2.50%	45.30%	99.99%
2002	0.30%	63.10%	99.95%
2003	1.10%	71.40%	100.00%
2004	0.10%	73.00%	99.99%
2005	1.60%	79.50%	99.99%
2006	1.10%	89.80%	100.00%
2007	2.60%	70.00%	100.00%
2008	2.40%	89.30%	100.00%
2009	0.50%	82.90%	100.00%
2010	0.60%	72.60%	100.00%
2011	3.80%	79.40%	100.00%
2012	NA	61.90%	99.99%
2013	0.10%	72.20%	100.00%
2014	1.80%	71.90%	100.00%

NA: Not Applicable since flows did not reach this value

Figure 5.4.3.1-1: Photos at Site 11L

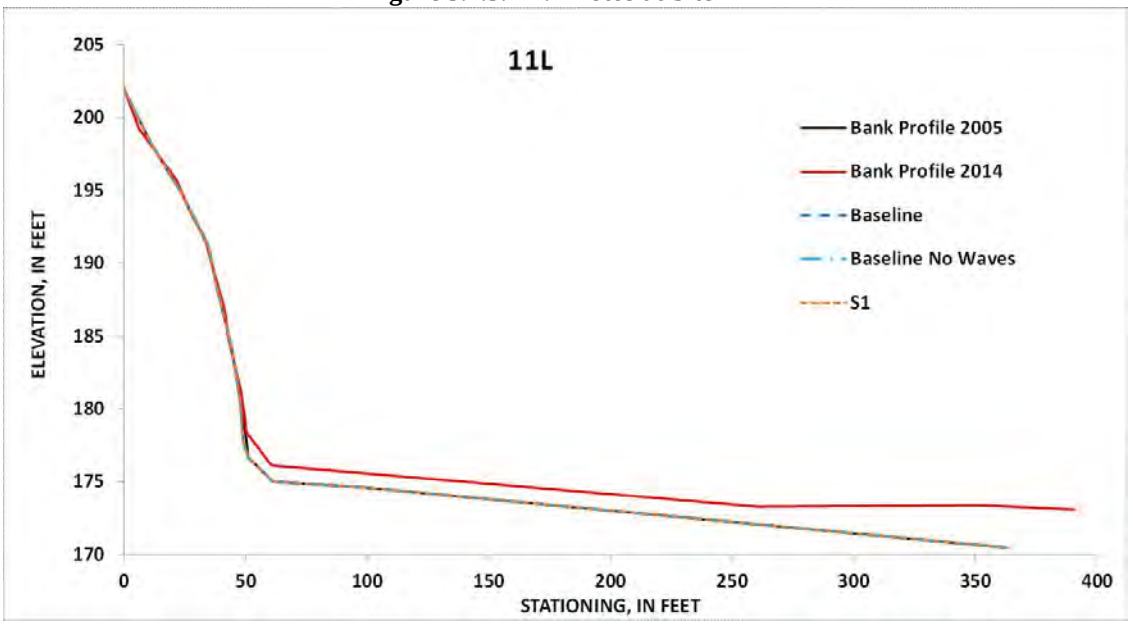

Figure 5.4.3.1-2: Simulated, future unit-erosion for the Baseline Condition (with boat waves on and off) and Scenario 1 at site 11L for the period 2005-2014

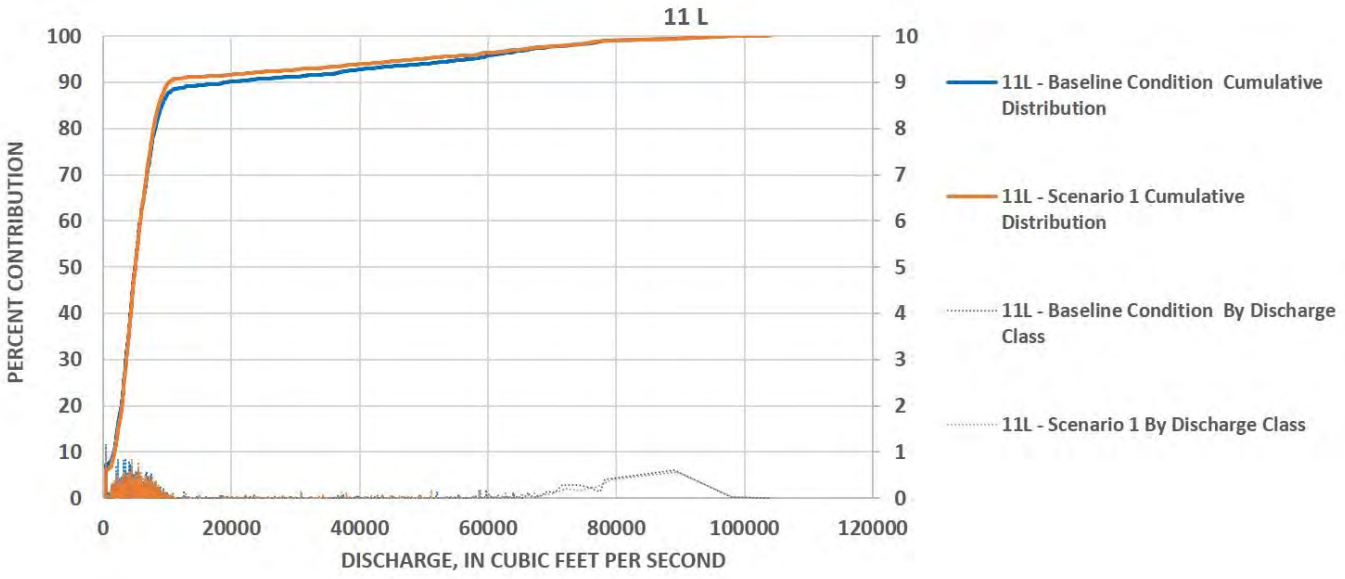

Figure 5.4.3.1-3: Simulated, percent contribution of total erosion by discharge for the Baseline Condition and Scenario 1 at site 11L for the period 2005-2014

5.4.3.2 Site 2L Pre-Restoration

The river at site 2L Pre-restoration (at station 94,500) has steep to vertical, very sparsely vegetated, moderately-high banks. The site is located, at the Bonnette Farm, just below the mouth of the Ashuelot River, south of Stebbins Island. The bank is roughly 18 feet tall, with a silty-sand bank and beach. Moderate vegetation was noted in the 2013 FRR for the Upper Riverbank slope, with very sparse to no vegetation on the lower riverbank slope (Figure 5.4.3.2-1).

BSTEM runs at this site show that under the Baseline Condition, 90 ft^3 of erosion occurred per foot of bank, during the 2000 to 2012 flow period prior to restoration, averaging 7.48 $ft^3/ft/y$ (Table 5.4.3-1). This results in the 3rd highest erosion rate for the Baseline Condition, placing it between the 90th and 95th percentiles of erosion rates along the reach. The modeling also indicates that 48% (3.56 $ft^3/ft/y$) of the erosion is due directly to hydraulic processes, whereas the other 52% (3.92 $ft^3/ft/y$) is the result of geotechnical processes and associated mass failures.

The Baseline Condition (with waves off) resulted in 7.47 $ft^3/ft/y$, 0.01 $ft^3/ft/y$ less than with waves on erosion. For Scenario 1, results showed similar erosion rates; 7.46 $ft^3/ft/y$ (Note – that while this site did show a small reduction in erosion between the BL and S1 Scenarios (0.02 $ft^3/ft/y$) the total reduction in erosion is well below the measureable/significant rate of 0.161 $ft^3/ft/y$). This resulted in the following percent reductions in erosion rates compared to the Baseline Condition: 0.10 % under the Baseline Waves off Condition and 0.26% for Scenario 1 (Figure 5.4.3.2-2 and Figure 5.4.3.2-3). Baseline simulations with waves off showed virtually no reduction in erosion, indicating that boat-generated waves had little effect on erosion processes at this site. Because of this Scenario 1 was simulated with boat waves on.

For the Baseline Condition, 99.9% of the total erosion occurs at flows of 17,130 cfs or greater (Figure 5.4.3.2-4). The amount of hydraulic erosion gradually builds across the range of flows between 50,000 cfs and 67,000 cfs, at which point a significant geotechnical failure occurs at the extreme high flows and a second failure occurs at about 70,000 cfs. Through this analysis we can conclude that those flows greater than the hydraulic capacity at Vernon are accounting for most of the total erosion. This is supported by the minimal reductions in erosion rates for the various scenarios (compared to Baseline). Table 5.4.3.2-1 denotes the flows above which 95%, 50%, and 5% of all erosion occurs at the site as well as the amount of time those flows were exceeded for each year in the modeling period.

Table 5.4.3.2-1: Flow Exceedance Calculations for Site 2L

Site 2L	Percent of Erosion		
	95%	50%	5%
	Flow (cfs)		
Year	**86,993**	**66,778**	**56,081**
2000	NA	NA	0.46%
2001	NA	1.10%	2.27%
2002	NA	NA	0.11%
2003	NA	0.04%	0.95%
2004	NA	NA	NA
2005	NA	0.53%	1.22%
2006	NA	0.02%	0.88%
2007	NA	0.02%	2.47%
2008	NA	0.05%	1.90%
2009	NA	NA	0.37%
2010	NA	NA	0.45%
2011	0.23%	1.48%	3.65%
2012	NA	NA	NA
2013	-	-	-
2014	-	-	-

NA: Not Applicable since flows did not reach this value

Figure 5.4.3.2-1: Photo at Site 2L Pre Restoration

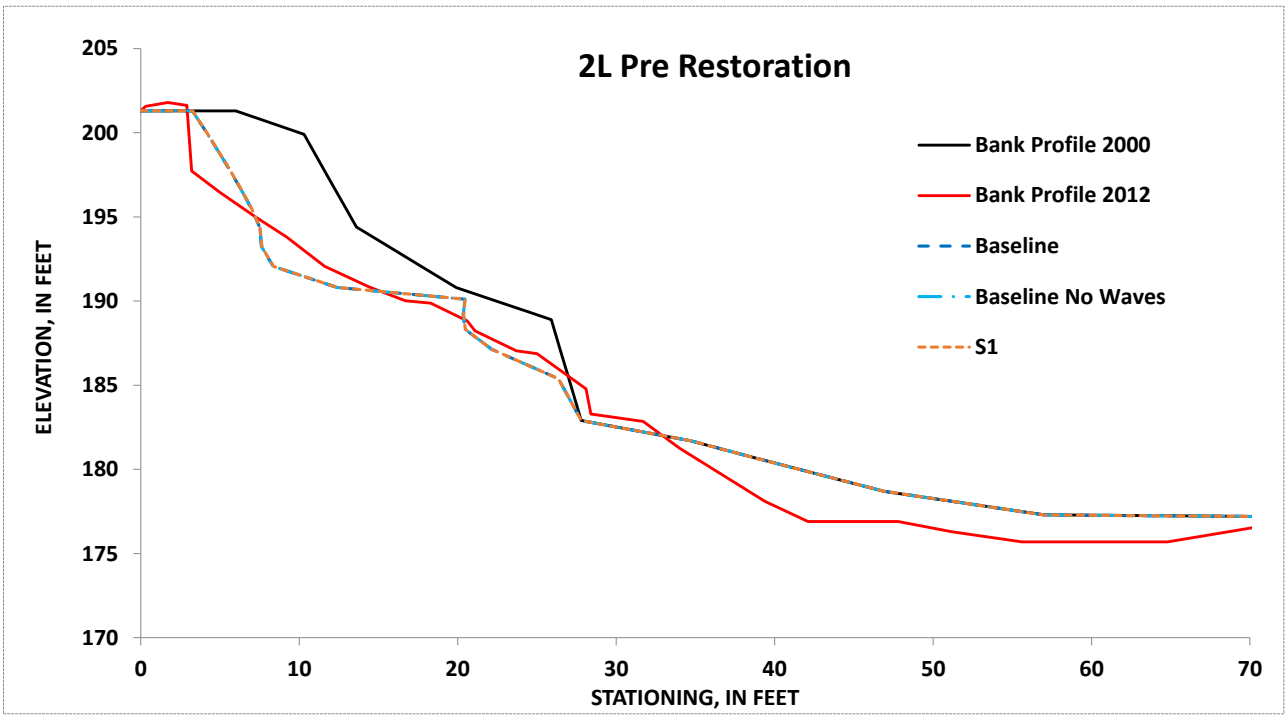

Figure 5.4.3.2-2: Simulated, future unit-erosion for the Baseline Condition (with boat waves on and off) and Scenario 1 at site 2L Pre Restoration for the period 2000-2012

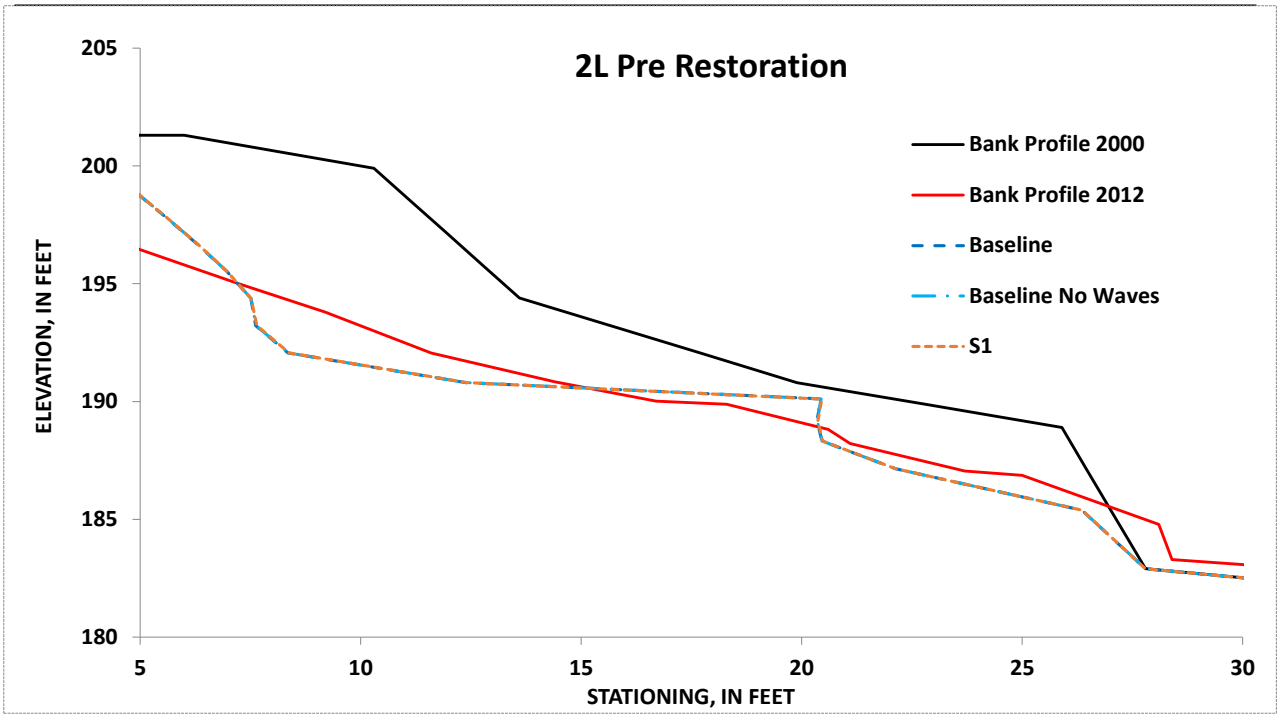

Figure 5.4.3.2-3: Simulated, future erosion for the Baseline Condition (with boat waves on and off) and Scenario 1 at site 2L Pre Restoration for the period 2000-2012. Zoomed in at area of erosion for illustrative purposes.

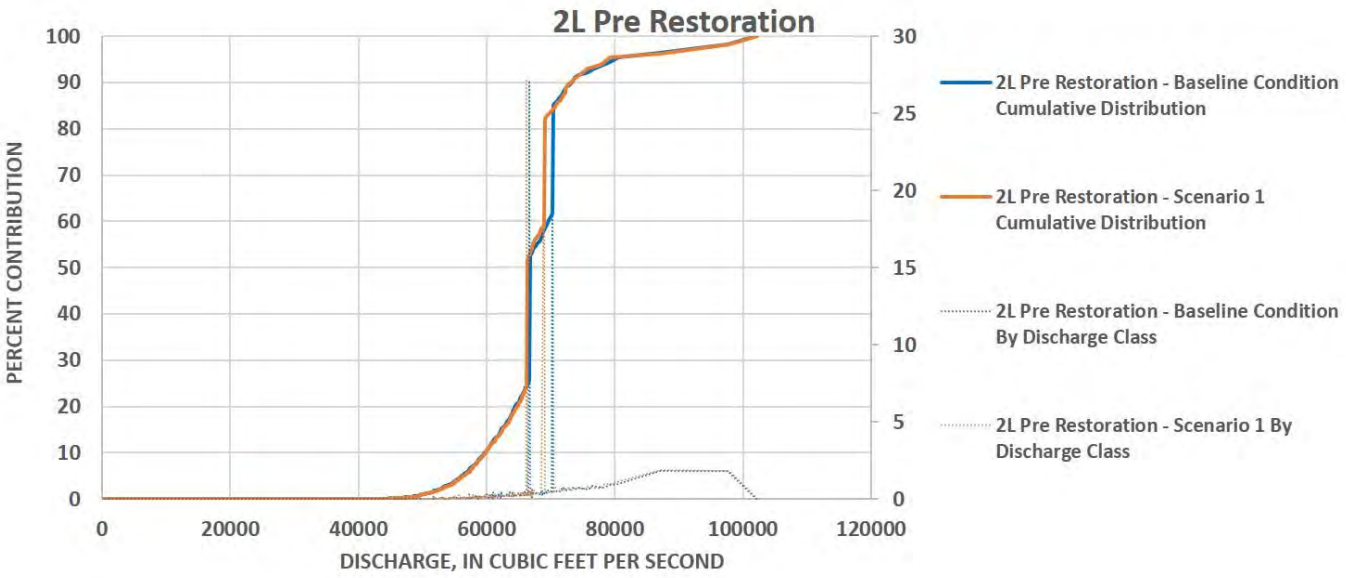

Figure 5.4.3.2-4: Simulated, percent contribution of total erosion by discharge for the Baseline Condition and Scenario 1 at site 2L for the period 2000-2012

5.4.3.3 Site 2L Post Restoration

The river at site 2L (station 94,500) Post Restoration has steep to vertical, heavily vegetated, moderately high banks. It is of course at the same location as for the Pre Restoration analysis. The bank is roughly 18 feet tall, with a silty sand bank and beach. The upper bank was re-planted with heavy vegetation including grasses and large shrubs (Figure 5.4.3.3-1).

BSTEM runs at this site show that under the Baseline Condition, 11.7 ft^3 of erosion occurred per foot of bank during the 2012 to 2014 flow period after restoration activities, averaging 5.42 $ft^3/ft/y$ (Table 5.4.3-1). This results in the 8th largest erosion rate for the Baseline Condition, placing it between the 70th and 75th percentiles of erosion rates along the reach. The modeling also indicates that all of the erosion is due directly to hydraulic processes, and none of the bank erosion is the result of geotechnical failures.

The Baseline Condition (Waves off) resulted in 5.41 $ft^3/ft/y$ of erosion, with 5.4 $ft^3/ft/y$ for Scenario 1. Note, that while this site did show a small reduction in erosion between the BL and S1 Scenarios (0.02 $ft^3/ft/y$) the total reduction in erosion is well below the measureable/significant rate of 0.161 $ft^3/ft/y$. This resulted in the following percent reductions in erosion rates: 0.09% for Baseline Wave off and 0.37% for Scenario 1 (Figure 5.4.3.3-2). Baseline simulations with waves off showed very little reduction in erosion (0.01 $ft^3/ft/y$).

For the Baseline Condition, 97.5% of the total erosion occurs at flows equal to or greater than 17,130 cfs (Figure 5.4.3.3-3). All of the erosion was hydraulic and occurs between 19,500 cfs and 70,000 cfs, above the hydraulic capacity of Vernon Dam, and can therefore be attributed to high flows. Table 5.4.3.3-1 denotes the flows above which 95%, 50%, and 5% of all erosion occurs at the site as well as the amount of time those flows were exceeded for each year in the modeling period.

The reduction from Pre-Restoration to Post-Restoration was strictly at elevations above where the restoration occurred. The bulk of the hydraulic erosion at Site 2L Post-Restoration occurs at flows above the high flow threshold and at an elevation below where the restoration occurred.

Table 5.4.3.3-1: Flow Exceedance Calculations for Site 2L

Site 2L	Percent of Erosion		
	95%	50%	5%
	Flow (cfs)		
Year	66,947	32,196	19,537
2000	-	-	-
2001	-	-	-
2002	-	-	-
2003	-	-	-
2004	-	-	-
2005	-	-	-
2006	-	-	-
2007	-	-	-
2008	-	-	-
2009	-	-	-
2010	-	-	-
2011	-	-	-
2012	NA	0.57%	9.50%
2013	NA	3.09%	14.10%
2014	0.30%	5.26%	17.80%

NA: Not Applicable since flows did not reach this value

Figure 5.4.3.3-1: Photos at Site 2L Post Restoration

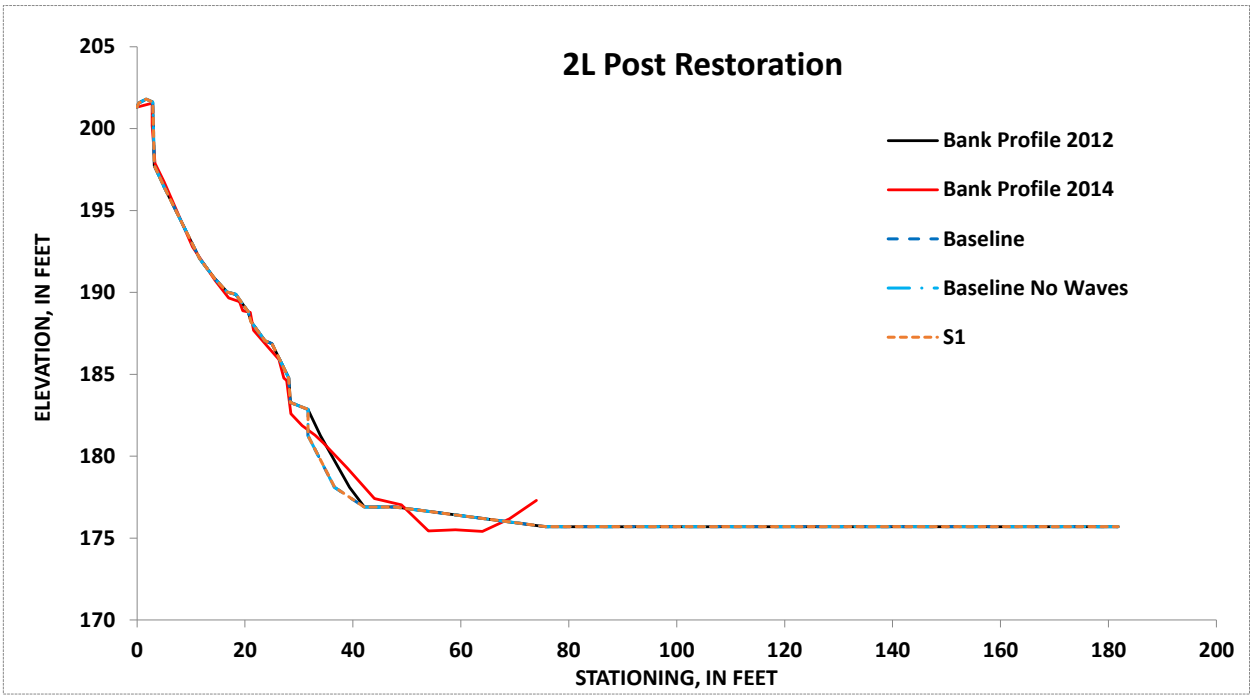

Figure 5.4.3.3-2: Simulated, future unit-erosion for the Baseline Condition (with boat waves on and off) and Scenario 1 at Site 2L Post Restoration for the period 2005-2014

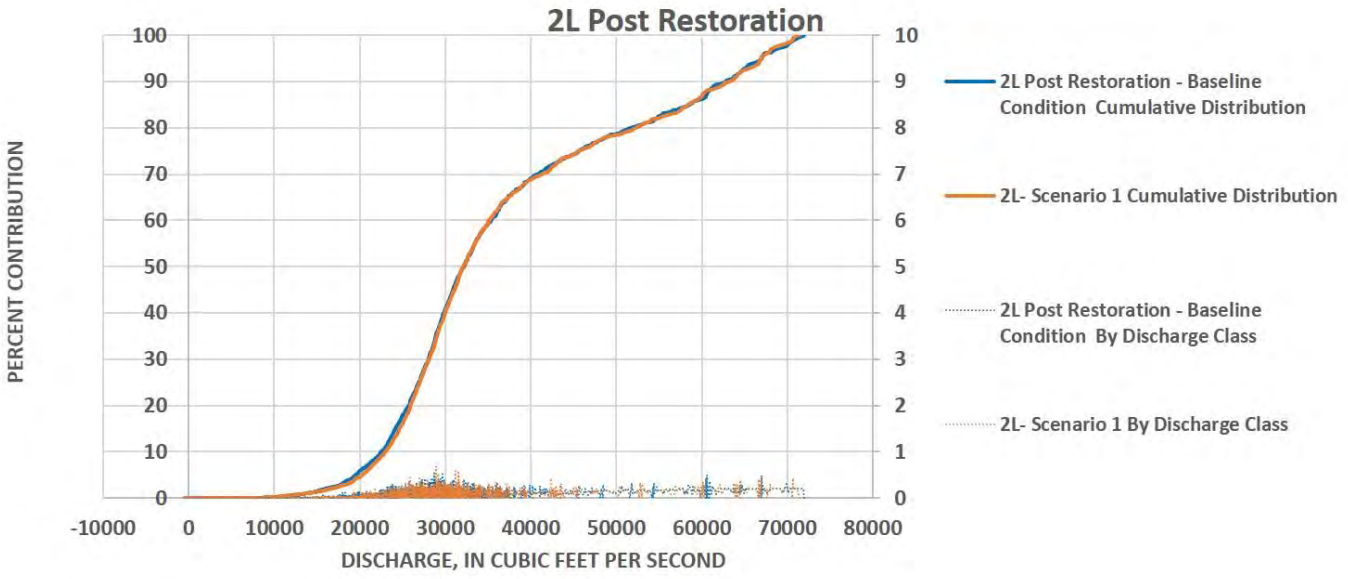

Figure 5.4.3.3-3: Simulated, percent contribution of total erosion by discharge for the Baseline Condition and Scenario 1 at site 2L for the period 2012-2014

5.4.3.4 Site 303BL

The river at site 303BL has steep to vertical, sparsely vegetated banks, located at station 94,000, downstream of Stebbins Island, immediately downstream of site 2L. The bank is roughly 16 feet tall with a sandy toe (d_{50}=0.11mm) and a silty bank face. The bank is vegetated mostly with grasses and small shrubs, but contains a few American elm, Green ash, and Silver maple trees. A significant amount of bare soil and exposed roots were noted on the bank face, and undercutting was present. No historical cross sections exist for this site. The site was surveyed in 2014 and this geometry was used as a starting point for the model runs (Figure 5.4.3.4-1).

BSTEM runs at this site show that under the Baseline Condition, 9.48 ft^3 of erosion occurred per foot of bank, during the 2000-2014 flow period, averaging 0.647 $ft^3/ft/y$ (Table 5.4.3-1). This results in the 12th lowest erosion rate for the Baseline Condition, placing it between the 20th and 25th percentiles of erosion rates along the reach. The modeling also indicates that 96% (0.622 $ft^3/ft/y$) of the erosion is due directly to hydraulic processes, whereas only 4% (0.025 $ft^3/ft/y$) is the result of geotechnical processes and associated mass failures. Bank undercutting and a large number of exposed roots were noted during fieldwork, supporting the predicted high percentage of hydraulic erosion compared to geotechnical erosion.

The Baseline Condition (Waves off) resulted in 0.645 $ft^3/ft/y$, with 0.674 $ft^3/ft/y$ for Scenario 1. This resulted in the following percent reductions (compared to the Baseline Condition) in erosion rates: 0.34% and -4.23% for Baseline Wave off and Scenario 1, respectively (Figure 5.4.3.4-2 and Figure 5.4.3.4-3). Baseline simulations with waves off showed virtually no reduction in erosion indicating that boat waves have little effect on erosion processes at this site. Because of this, all of the remaining scenario was simulated with boat waves on.

For the Baseline Condition, 95% of the total erosion occurs at flows of about 53,000 cfs or greater (Figure 5.4.3.4-4). Hydraulic erosion and small failures occurred between 53,000 and 80,000, at which point a larger (though still relatively small) failure occurred, resulting in the remaining 10% of total erosion at those extreme high flows. Through this analysis we can conclude that the high flows greater than the hydraulic capacity at Vernon Dam, Northfield Mountain, and Turners Falls are accounting for most of the total erosion at this site. Table 5.4.3.4-1 denotes the flows above which 95%, 50%, and 5% of all erosion occurs at the site as well as the amount of time those flows were exceeded for each year in the modeling period.

It should be noted that at this site, Scenario 1 showed greater erosion than the Baseline Condition. One possible cause for this is the variation in flows from peaking operations for Scenario 1. These flows created a geotechnical failure (4.2% of the total) at a flow of about 45,000 cfs, still above the hydraulic capacity of the dam. This failure did not occur for the Baseline Condition. The failure is likely due to the rapid decrease in water surface elevation after extreme high flows at a stage of 196.33 ft (79,000 cfs) (Figure 5.4.3.4-5). If we only look at the hydraulic erosion both scenarios produce the same amount (Figure 5.4.3-1), it was the one geotechnical failure under the Scenario 1 conditions that resulted in the increase in erosion. This failure may have occurred due to the lack of fluctuation of water surface leading up to the high flow event. The shear velocities are focused on a narrower range of the bank under the Scenario 1 conditions, it is possible that this caused a weakening in the bank that did not occur under the Baseline Conditions.

Table 5.4.3.4-1: Flow Exceedance Calculations for Site 303BL

Site 303BL	Percent of Erosion		
	95%	50%	5%
	Flow (cfs)		
Year	79,881	64,684	53,194
2000	NA	0.20%	1.30%
2001	NA	1.70%	2.90%
2002	NA	0.10%	0.50%
2003	NA	0.40%	1.90%
2004	NA	NA	0.30%
2005	NA	0.70%	2.40%
2006	NA	0.40%	1.80%
2007	NA	0.50%	2.70%
2008	NA	0.50%	3.60%
2009	NA	NA	1.10%
2010	NA	NA	1.30%
2011	0.40%	2.30%	4.70%
2012	NA	NA	NA
2013	NA	NA	0.10%
2014	NA	0.80%	2.20%

NA: Not Applicable since flows did not reach this value

Figure 5.4.3.4-1 Photos at site 303BL

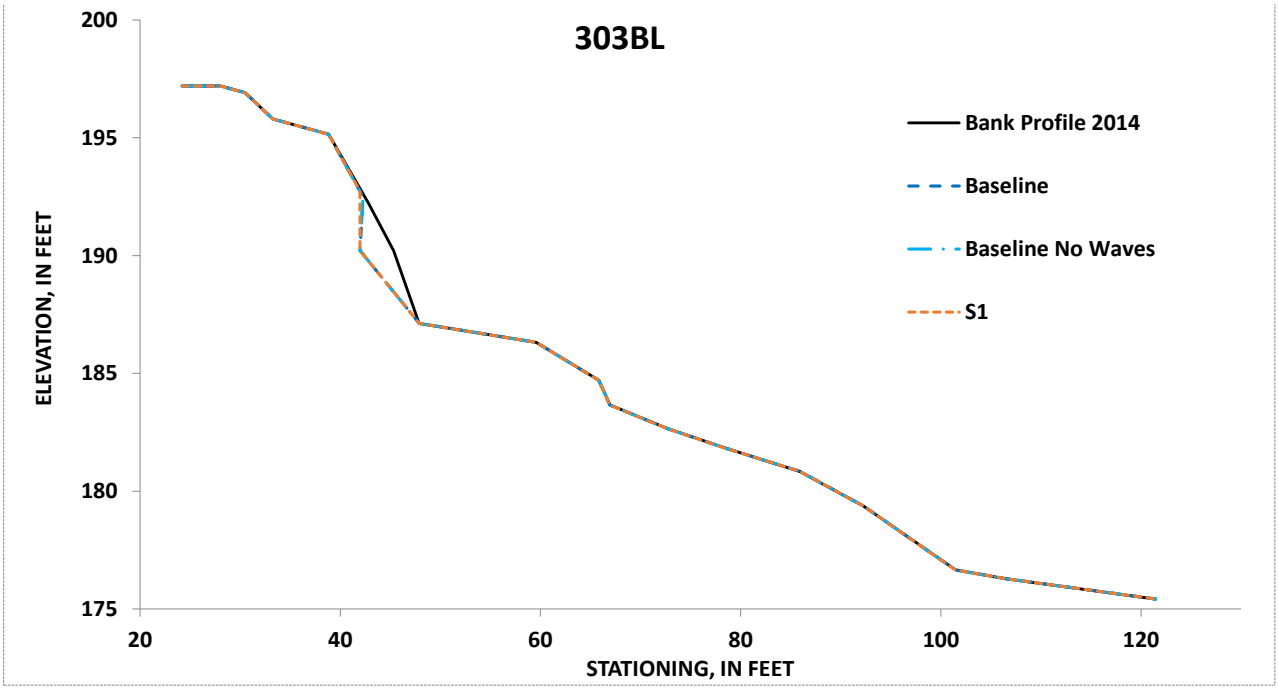

Figure 5.4.3.4-2: Simulated, future unit-erosion for the Baseline Condition (with boat waves on and off) and Scenarios 1 at site 303BL for the period 2000-2014

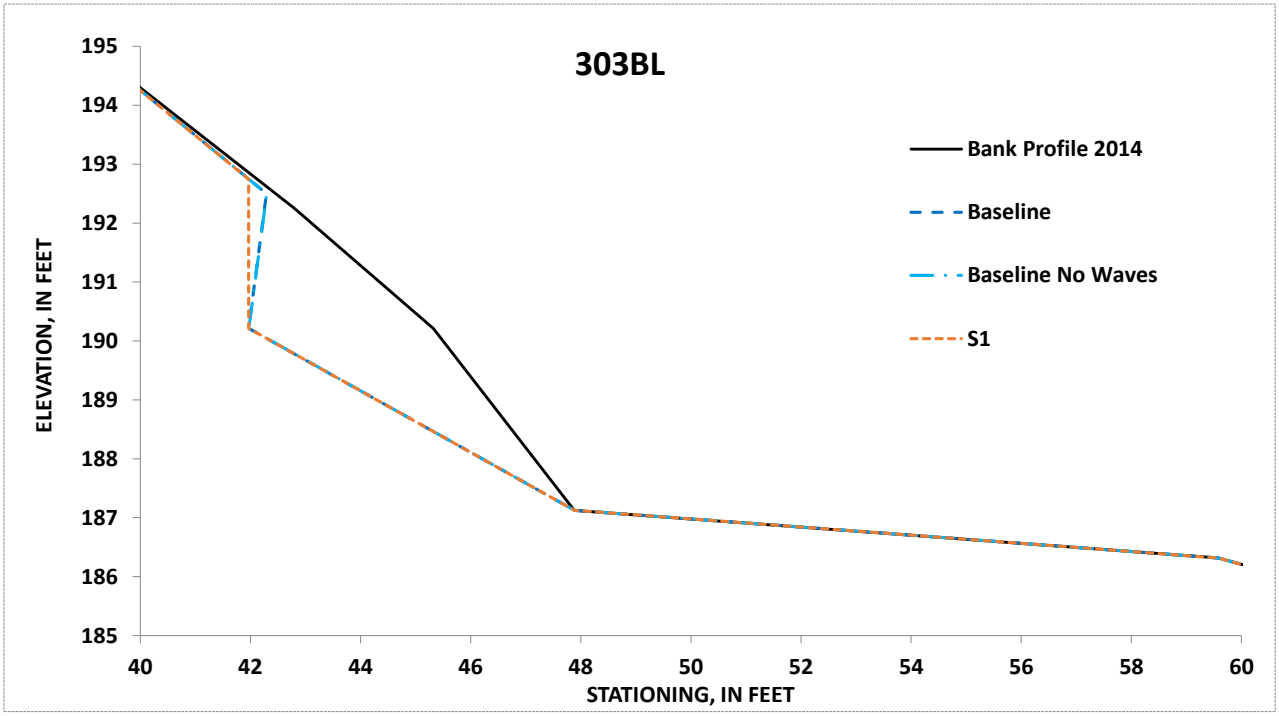

Figure 5.4.3.4-3: Simulated, future erosion for the Baseline Condition (with boat waves on and off) and Scenarios 1 at site 303BLfor the period 2000-2014. Zoomed in at area of erosion for illustrative purposes.

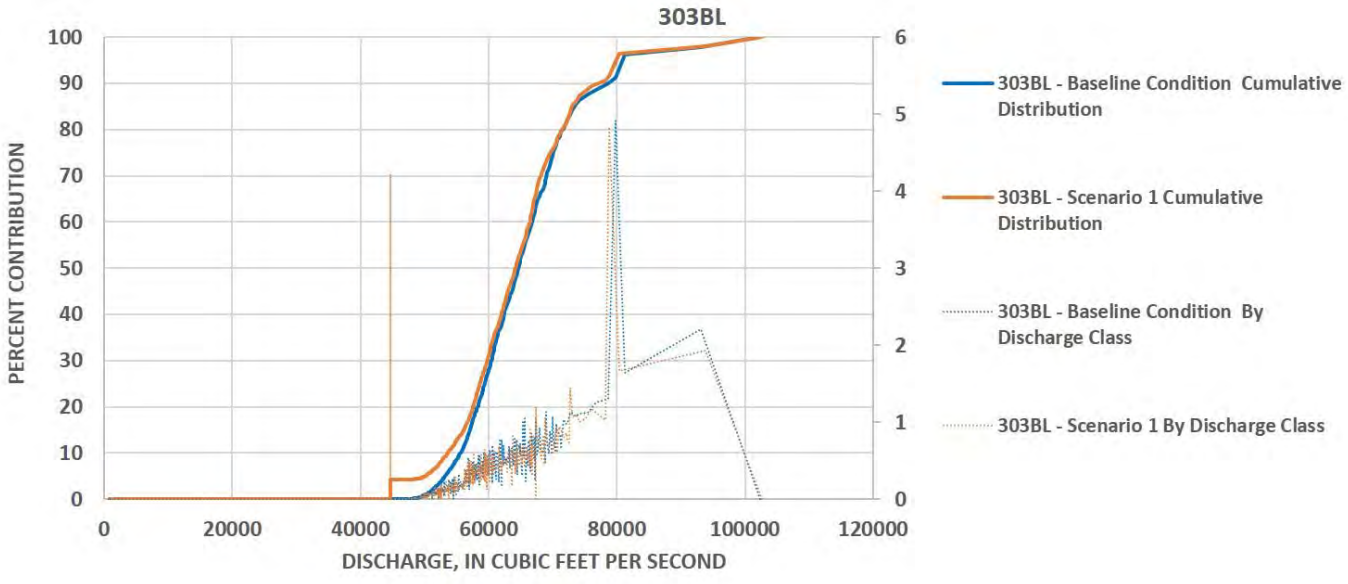

Figure 5.4.3.4-4: Simulated, percent contribution of total erosion by discharge for the Baseline Condition and Scenarios 1 at site 303BL for the period 2000-2014

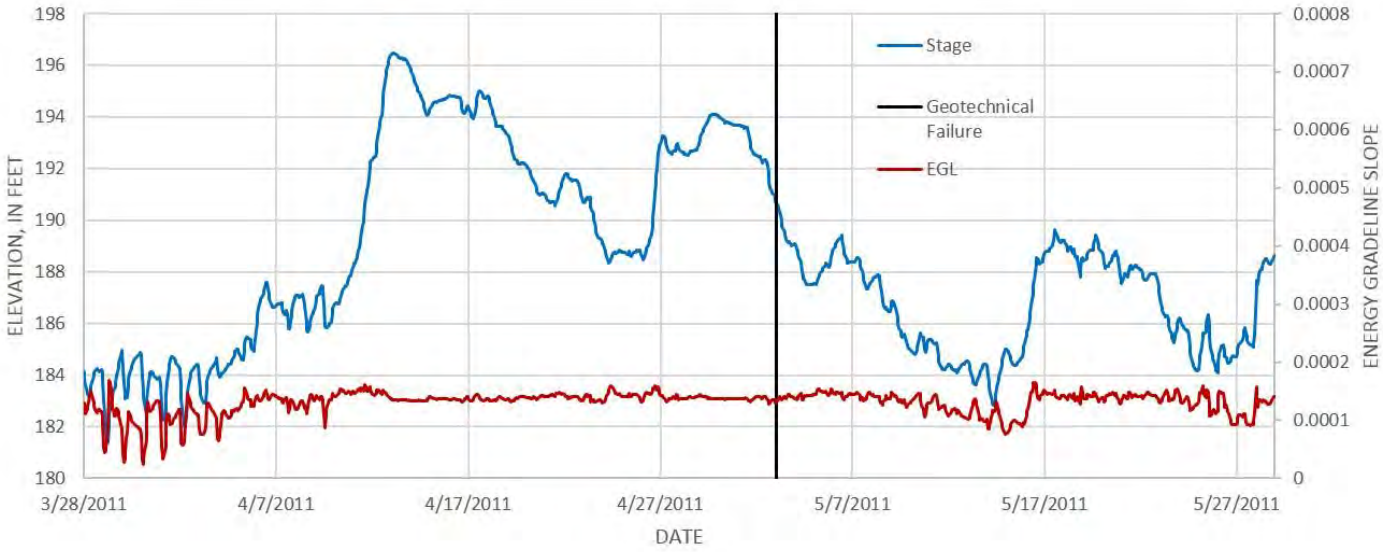

Figure 5.4.3.4-5: Stage and Energy Grade Line (EGL) of flows at Site 303BL under Scenario 1 around the time of the geotechnical failure on 05/03/2011 at 1:00AM (denoted by vertical black line).

5.4.3.5 Site 18BL

The river at site 18BL has steep to vertical, sparsely vegetated banks. It is located at station 87,000, roughly 5,000 ft downstream of Upper Island. The bank is roughly 23 feet tall, with a sandy-loam bank toe and bank face. The bank is vegetated mostly with grasses and small shrubs, but contains a few American elm, American sycamore, Green ash, and Red oak trees. A significant amount of bare soil and exposed roots were noted on the bank face, and undercutting was present. No historical cross sections existed for this site. A 2014 survey was used as the starting geometry for the model runs (Figure 5.4.3.5-1).

BSTEM runs at this site show that under the Baseline Condition, 16.0 ft^3 of erosion occurred per foot of bank during the 2000-2014 flow period, averaging 1.09 $ft^3/ft/y$ (Table 5.4.3-1). This results in the 13th lowest erosion rate for the Baseline Condition, placing it between the 25th and 30th percentiles of erosion rates along the reach. The modeling also indicates that 76% (0.83 $ft^3/ft/y$) of the erosion is due directly to hydraulic processes, whereas remaining 24% (0.26 $ft^3/ft/y$) is the result of geotechnical processes and associated mass failures. This is also shown in (Figure 5.4.3.5-4), as a very gradual smooth shape, with few large spikes that would indicate the prevalence of mass wasting.

The Baseline Condition (Waves off) resulted in 1.09 $ft^3/ft/y$, with 1.08 $ft^3/ft/y$ for Scenario 1 (Figure 5.4.3.5-2 and Figure 5.4.3.5-3). This resulted in a 1.1% reduction in erosion rates for Scenario 1 (Note- while this site did show a small reduction in erosion between the BL and S1 Scenarios the total reduction in erosion is well below the measureable/significant rate of 0.161 $ft^3/ft/yr$). As Baseline Condition (Waves off) scenario illustrated a zero reduction in erosion, it was concluded that boat waves had no impact on bank stability, and the remaining scenarios were not conducted with boat-waves off.

For the Baseline Condition, 98% of the total erosion occurs at flows of about 17,130 cfs or greater (Figure 5.4.3.5-4). There are two significant geotechnical failures that occur at 18,000 cfs and 27,000 cfs which account for the majority of the geotechnical erosion at site 18BL. The distribution of hydraulic erosion gradually builds between 27,000 and 80,000 cfs, where they begin to taper off at the extreme high flows. Through this analysis we can conclude that those flows greater than the hydraulic capacity at Vernon Dam are accounting for most of the total erosion. Table 5.4.3.5-1 denotes the flows above which 95, 50, and 5% of all erosion occurs at the site as well as the amount of time those flows were exceeded for each year.

Table 5.4.3.5-1: Flow Exceedance Calculations for Site 18BL

Site 18BL	Percent of Erosion		
	95%	50%	5%
	Flow (cfs)		
Year	73,352	54,485	17,824
2000	NA	1.20%	22.60%
2001	0.40%	2.70%	9.30%
2002	NA	0.40%	15.90%
2003	NA	1.60%	26.50%
2004	NA	0.20%	15.30%
2005	0.20%	2.20%	30.70%
2006	0.10%	1.50%	33.10%
2007	NA	2.70%	19.10%
2008	NA	3.30%	30.40%
2009	NA	0.80%	23.50%
2010	NA	1.00%	21.80%
2011	0.90%	4.50%	31.00%
2012	NA	NA	12.30%
2013	NA	0.10%	16.80%
2014	NA	2.10%	20.70%

NA: Not Applicable since flows did not reach this value

Figure 5.4.3.5-1 Photos at site 18BL

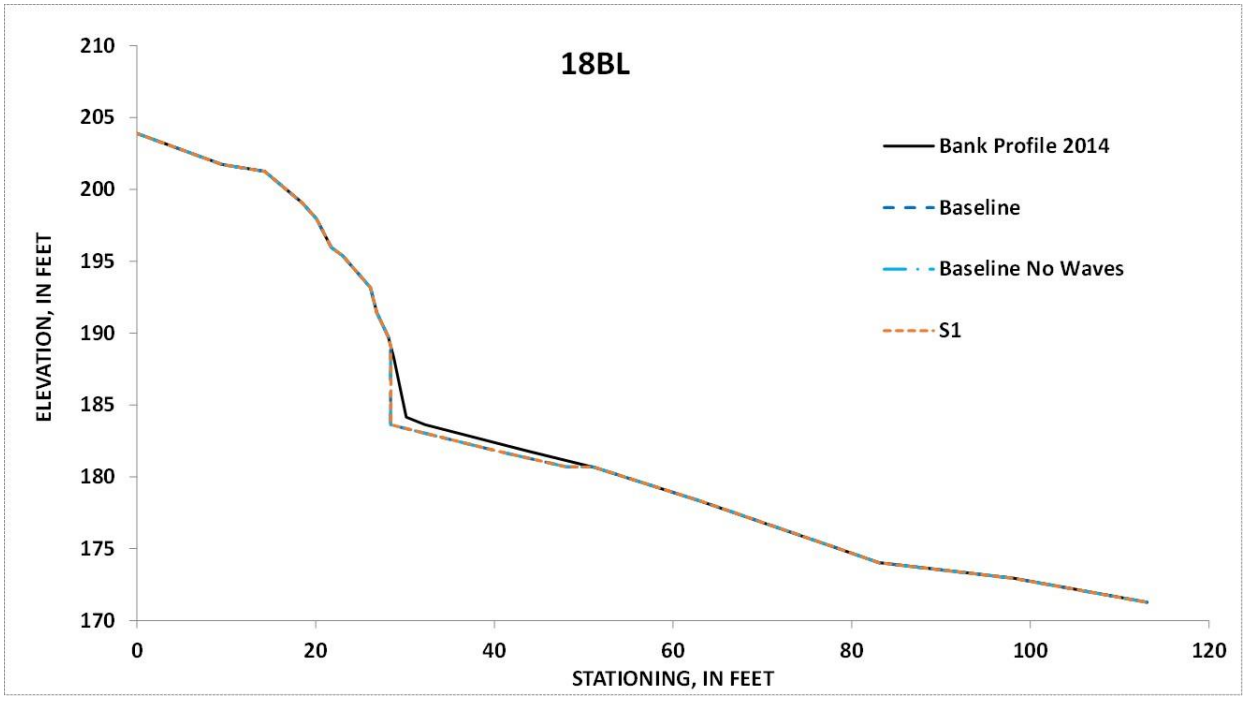

Figure 5.4.3.5-2: Simulated, future unit-erosion for the Baseline Condition (with boat waves on and off) and Scenarios 1 at site 18BL for the period 2000-2014

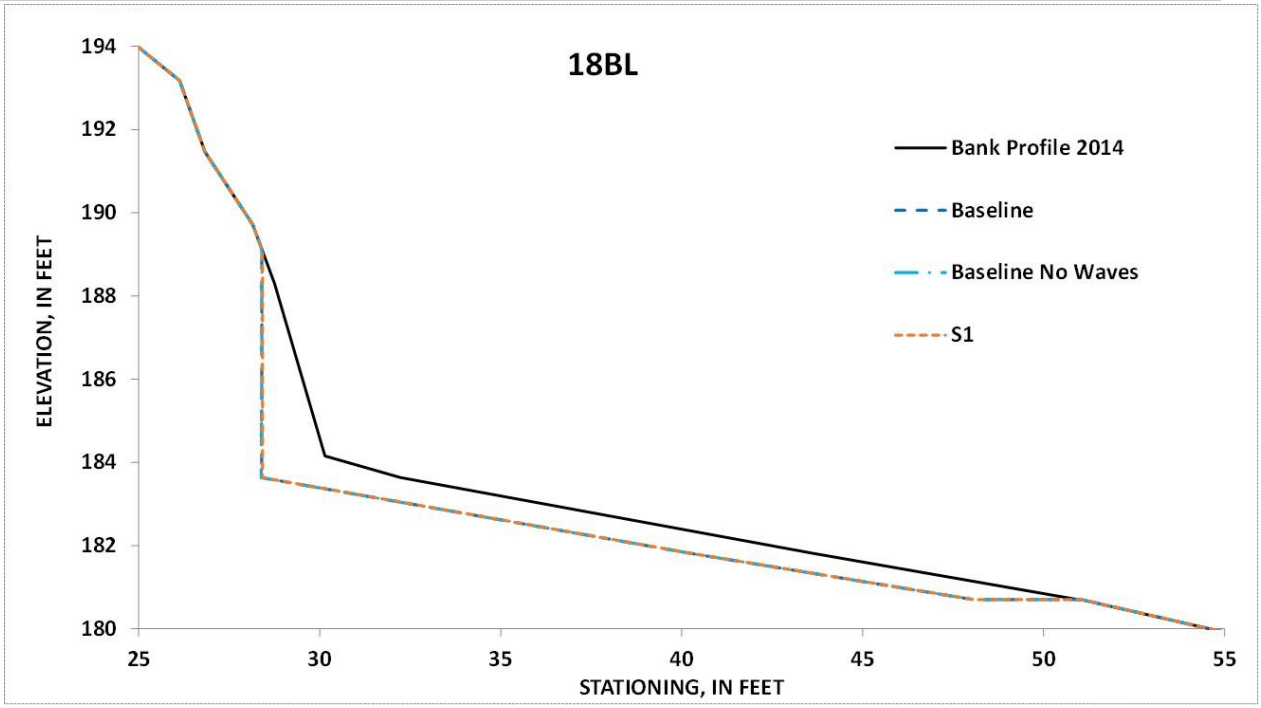

Figure 5.4.3.5-3: Simulated, future erosion for the Baseline Condition (with boat waves on and off) and Scenarios 1 at site 18BL for the period 2000-2014. Zoomed in at area of erosion for illustrative purposes.

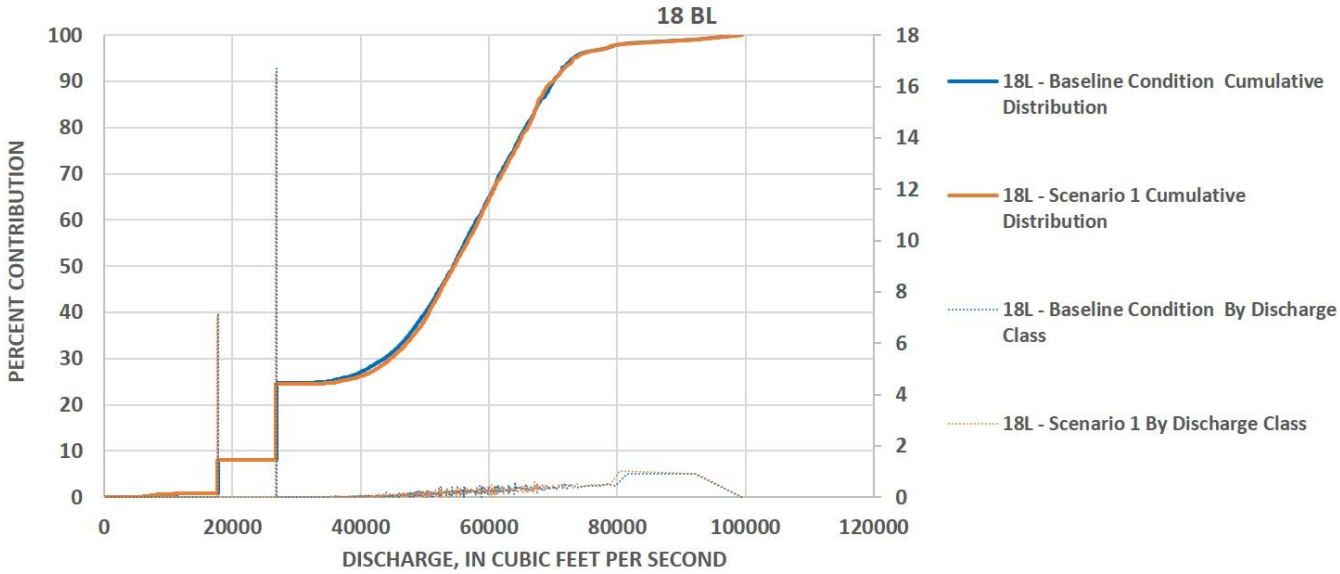

Figure 5.4.3.5-4: Simulated, percent contribution of total erosion by discharge for the Baseline Condition and Scenarios 1 at site 18BL for the period 2000-2014

5.4.3.6 Site 3L

The river at site 3L (station 79,500) has slightly more gradual, heavily vegetated banks, and is located north of the Massachusetts-Vermont border, just north of site 21R. The bank is roughly 20 feet tall, with a sandy-loam bank toe and upper bank. The bank is vegetated with grasses, shrubs, and large American elms, Green ash, Hickory and Northern red oak trees (Figure 5.4.3.6-1).

BSTEM runs at this site show that under the Baseline Condition, 89.2 ft^3 of erosion occurred per foot of bank during the 2000-2014 flow period, averaging 6.09 $ft^3/ft/y$ (Table 5.4.3-1). This results in the 5^{th} highest erosion rate for the Baseline Condition, placing it between the 80^{th} and 85^{th} percentiles of erosion rates along the reach. The modeling also indicates that 86% (5.25 $ft^3/ft/y$) of the erosion is due directly to hydraulic processes, whereas the remaining 14% (0.84 $ft^3/ft/y$) is the result of geotechnical processes and associated mass failures.

The Baseline Condition (Waves off) resulted in 6.09 $ft^3/ft/y$, with 6.04 $ft^3/ft/y$ for Scenario 1 (Note- while this site did show a small reduction in erosion between the BL and S1 Scenarios the total reduction in erosion is well below the measureable/significant rate of 0.161 $ft^3/ft/yr$). This resulted in a percent reduction in erosion rates for Scenario 1 of 0.7% (Figure 5.4.3.6-2). As Baseline Condition (Waves off) scenario showed a zero reduction in erosion, it was concluded that boat waves are not having a significant impact on bank stability, and the remaining scenario was not considered with boat waves off. For the Baseline Condition, 95% of the total erosion occurs at flows of about 37,000 cfs or greater (Figure 5.4.3.6-3). There is some hydraulic erosion and small failures between 35,000 and 78,000, at which point significant failures occur, resulting in 50% of the total erosion at site 3L. Through this analysis we can conclude that those flows greater than the hydraulic capacity at Vernon are accounting for most of the total erosion.

Table 5.4.3.6-1 denotes the flows above which 95%, 50%, and 5% of all erosion occurs at the site as well as the amount of time those flows were exceeded for each year in the modeling period.

Table 5.4.3.6-1: Flow Exceedance Calculations for Site 3L

Site 3L	Percent of Erosion		
	95%	50%	5%
	Flow (cfs)		
Year	98,234	78,682	37,098
2000	NA	NA	5.20%
2001	NA	NA	5.10%
2002	NA	NA	2.70%
2003	NA	NA	6.50%
2004	NA	NA	1.70%
2005	NA	NA	9.00%
2006	NA	NA	7.40%
2007	NA	NA	5.00%
2008	NA	NA	11.60%
2009	NA	NA	4.00%
2010	NA	NA	6.30%
2011	0.20%	0.60%	10.40%
2012	NA	NA	0.50%
2013	NA	NA	1.80%
2014	NA	NA	3.90%

NA: Not Applicable since flows did not reach this value

Figure 5.4.3.6-1 Photos at site 3L

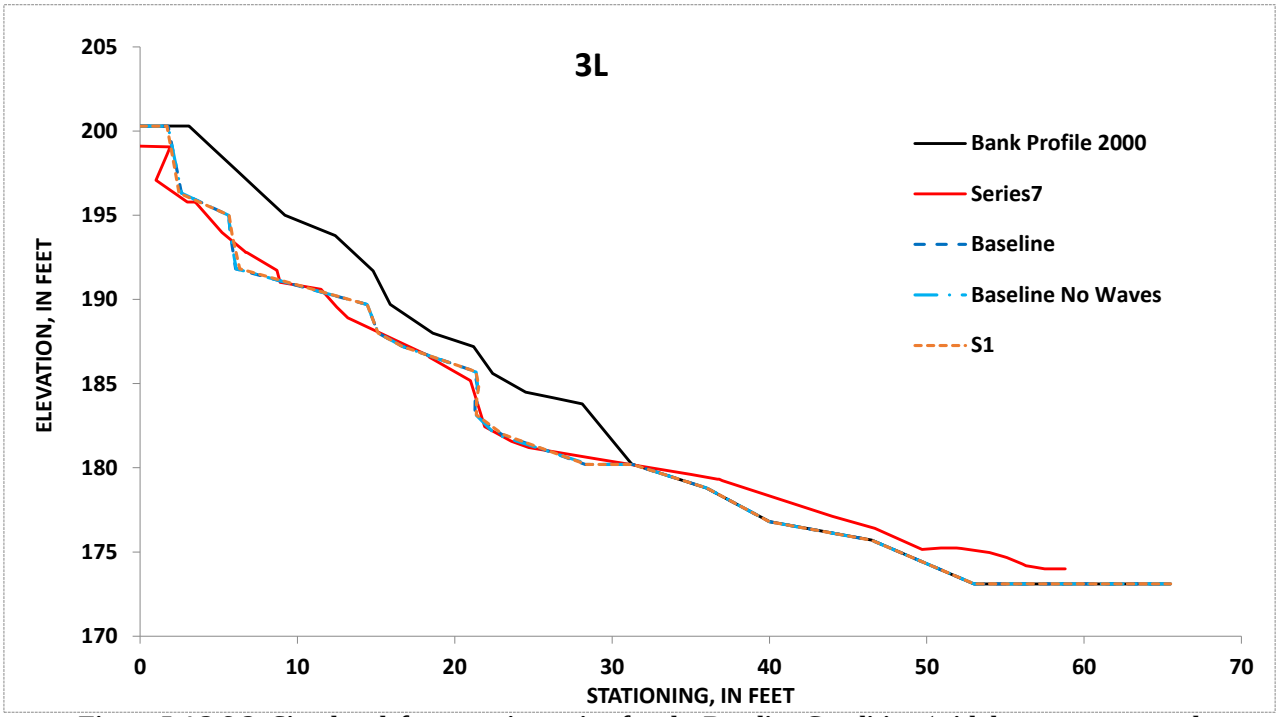

Figure 5.4.3.6-2: Simulated, future unit-erosion for the Baseline Condition (with boat waves on and off) and Scenarios 1 at site 3L for the period 2000-2014

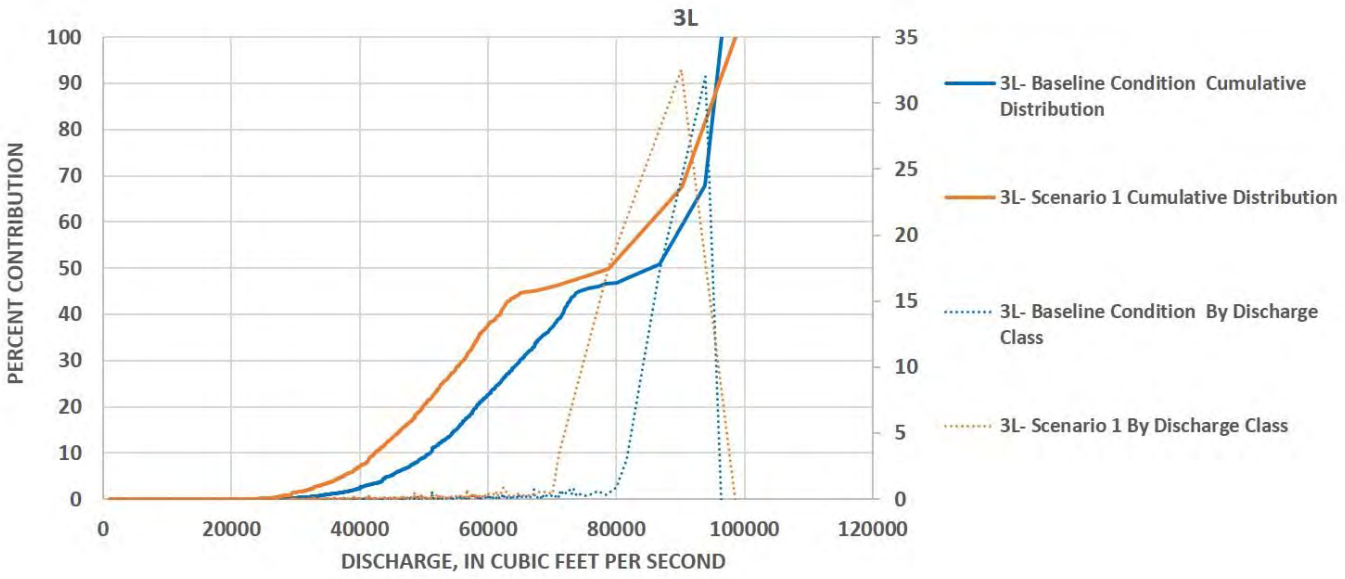

Figure 5.4.3.6-3: Simulated, percent contribution of total erosion by discharge for the Baseline Condition and Scenarios 1 at site 3L for the period 2000-2014

5.4.3.7 Site 3R Pre-Restoration

The river at site 3R Pre-Restoration has steep to vertical, very sparsely vegetated banks and is the same stationing (79,500) as site 3L, above. The bank is roughly 26 feet tall, with a silty-sand bank and beach. Observations from 1998 indicate active and extensive erosion with overhanging banks and notches (Figure 5.4.3.7-1).

BSTEM runs at this site show that under the Baseline Condition, about 100 ft^3 of erosion occurred per foot of bank, during the 2000 to 2006 flow period prior to restoration, averaging 15.4 $ft^3/ft/y$ (Table 5.4.3-1). This results in the highest erosion rate for the Baseline Condition, placing it between the 95^{th} and 100^{th} percentiles of erosion rates along the reach. The modeling also indicates that 42% (6.51 $ft^3/ft/y$) of the erosion is due directly to hydraulic processes, whereas the other 58% (8.91 $ft^3/ft/y$) is the result of geotechnical processes and associated mass failures.

The Baseline Condition (Waves off) resulted in 15.4 $ft^3/ft/y$, with 15.5 $ft^3/ft/y$ for Scenario 1. This resulted in the following percent reductions in erosion rates: 0.113% and -0.219% for Baseline Wave off and Scenario 1, respectively (Figure 5.4.3.7-2). Baseline simulations with waves off showed very little reduction in erosion indicating that boat waves have little effect on erosion processes at this site. Because of this, all of the remaining scenarios were simulated with boat waves on.

For the Baseline Condition, 95% of the total erosion occurs at flows of about 32,000 cfs or greater (Figure 5.4.3.7-3). The hydraulic erosion occurs across the range of flows between 32,000 cfs and 61,000 cfs, at which point a large geotechnical failure occurs resulting in roughly 65% of the total erosion at site 3R prior to restoration activities. Through this analysis we can conclude that those flows greater than the hydraulic capacity at Vernon are accounting for most of the total erosion.

Table 5.4.3.7-1 denotes the flows above which 95%, 50%, and 5% of all erosion occurs at the site as well as the amount of time those flows were exceeded for each year in the modeling period.

Table 5.4.3.7-1: Flow Exceedance Calculations for Site 3R Pre-Restoration

Site 3R	Percent of Erosion		
	95%	50%	5%
	Flow (cfs)		
Year	**87,760**	**54,420**	**36,411**
2000	NA	1.20%	5.30%
2001	NA	2.70%	5.40%
2002	NA	0.40%	2.90%
2003	NA	1.70%	6.90%
2004	NA	0.30%	1.90%
2005	NA	2.20%	9.40%
2006	NA	1.50%	7.80%
2007	NA	2.70%	5.20%
2008	NA	3.30%	12.00%
2009	NA	0.80%	4.20%
2010	NA	1.00%	6.60%
2011	0.30%	4.50%	11.10%
2012	NA	NA	0.50%
2013	NA	0.10%	2.00%
2014	NA	2.10%	4.20%

NA: Not Applicable since flows did not reach this value

Right bank, 1998

Figure 5.4.3.7-1 Photos from 1998 at site 3R Pre Restoration (Labeled as 1998 FRR/ECP-Site 9)

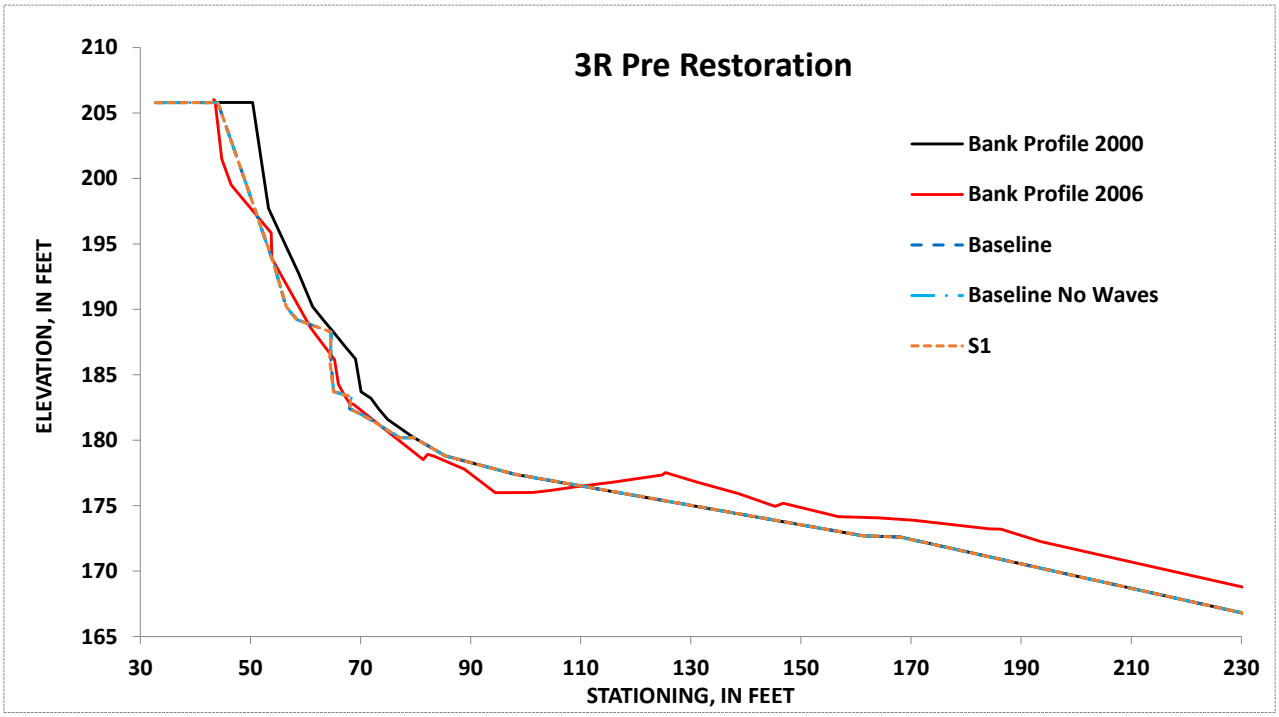

Figure 5.4.3.7-2: Simulated, future unit-erosion for the Baseline Condition (with boat waves on and off) and Scenarios 1 at site 3R for the period 2000-2006

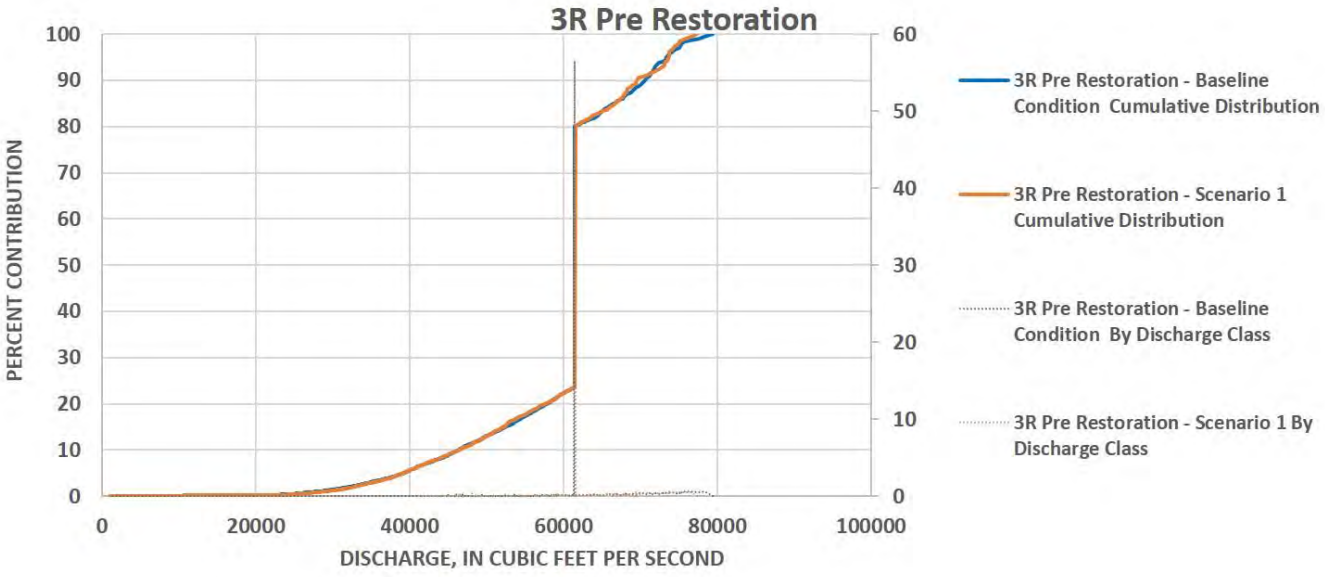

Figure 5.4.3.7-3: Simulated, percent contribution of total erosion by discharge for the Baseline Condition and Scenario 1 at site 3R for the period 2000-2006

5.4.3.8 Site 3R Post Restoration

The river at site 3R Post Restoration has slightly more gradual, heavily vegetated banks, located at station 79,500, north of the Massachusetts-Vermont border, just north of site 21R. The bank is roughly 26 feet tall, with a placed rock toe designed to reduce hydraulic erosion (d_{50} = 55 mm) and a silt loam bank. The replanted bank is heavily vegetated with large shrubs and the bank top is planted in corn (Figure 5.4.3.8-1).

BSTEM runs at this site show that under the Baseline Condition, 1.75 ft^3 of erosion occurred per foot of bank, during the 2006 to 2014 flow period after restoration activities, averaging 0.285 $ft^3/ft/y$ (Table 5.4.3-1). This results in the 8th lowest erosion rate for the Baseline Condition, placing it between the 10th and 15th percentiles of erosion rates along the reach. The modeling also indicates that all 100% (0.285 $ft^3/ft/y$) of the erosion is due directly to hydraulic processes, and none of the bank erosion is the result of larger geotechnical failures. The minimal amount of hydraulic erosion that is occurring is within the level of the placed rock at the toe, indicating that the rock may be slightly undersized for the flows.

The Baseline Condition (Waves off) resulted in 0.281 $ft^3/ft/y$, with 0.282 $ft^3/ft/y$ for Scenario 1 (Note- while this site did show a small reduction in erosion between the BL and S1 Scenarios the total reduction in erosion is well below the measureable/significant rate of 0.161 $ft^3/ft/yr$). This resulted in the following percent reductions in erosion rates: 1.4% and 1.1% for Baseline Wave off and Scenario 1, respectively (Figure 5.4.3.8-2). Baseline simulations with waves off showed very little reduction in erosion, it was concluded that boat waves have little effect on erosion processes at this site. Because of this, all of the remaining scenarios were simulated with boat waves on.

For the Baseline Condition, 97.5% of the total erosion occurs at flows of 17,130 cfs or greater (Figure 5.4.3.8-3). The minimal hydraulic erosion that did occur was between 36,000 cfs and 70,000 cfs. As there is almost no erosion below the operating capacity of Vernon, those flows above the peaking operations look to be the cause of the minimal erosion at this site. Based on the reduction in erosion rates from pre-restoration to post-restoration conditions, we can conclude that the restoration work was highly successful. In general there is currently no active erosion taking place at this site. Table 5.4.3.8-1 denotes the flows above which 95%, 50%, and 5% of all erosion occurs at the site as well as the amount of time those flows were exceeded for each year in the modeling period.

Table 5.4.3.8-1: Flow Exceedance Calculations for Site 3R Post Restoration

Site 3R	Percent of Erosion		
	95%	50%	5%
	Flow (cfs)		
Year	**87,760**	**54,420**	**36,411**
2000	NA	1.20%	5.30%
2001	NA	2.70%	5.40%
2002	NA	0.40%	2.90%
2003	NA	1.70%	6.90%
2004	NA	0.30%	1.90%
2005	NA	2.20%	9.40%
2006	NA	1.50%	7.80%
2007	NA	2.70%	5.20%
2008	NA	3.30%	12.00%
2009	NA	0.80%	4.20%
2010	NA	1.00%	6.60%
2011	0.30%	4.50%	11.10%
2012	NA	NA	0.50%
2013	NA	0.10%	2.00%
2014	NA	2.10%	4.20%

NA: Not Applicable since flows did not reach this value

Figure 5.4.3.8-1 Photos at site 3R Post Restoration

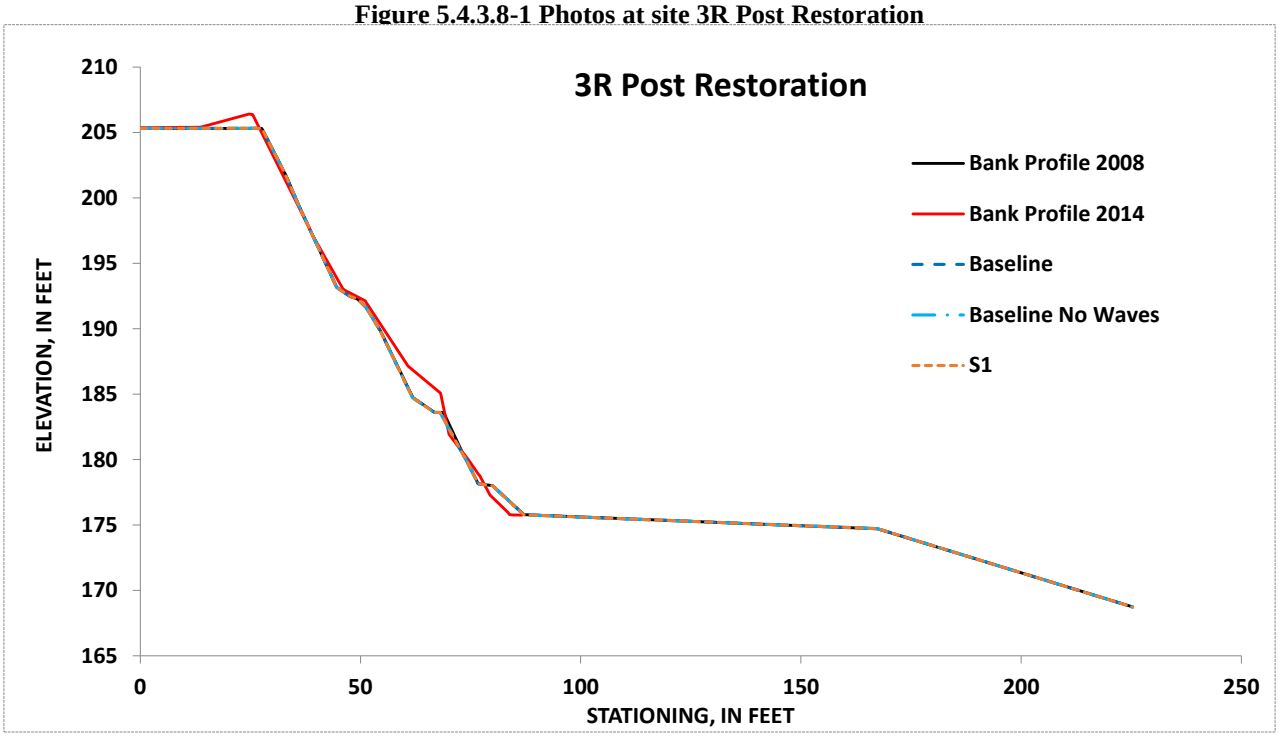

Figure 5.4.3.8-2: Simulated, future unit-erosion for the Baseline Condition (with boat waves on and off) and Scenarios 1 at site 3R for the period 2006-2014

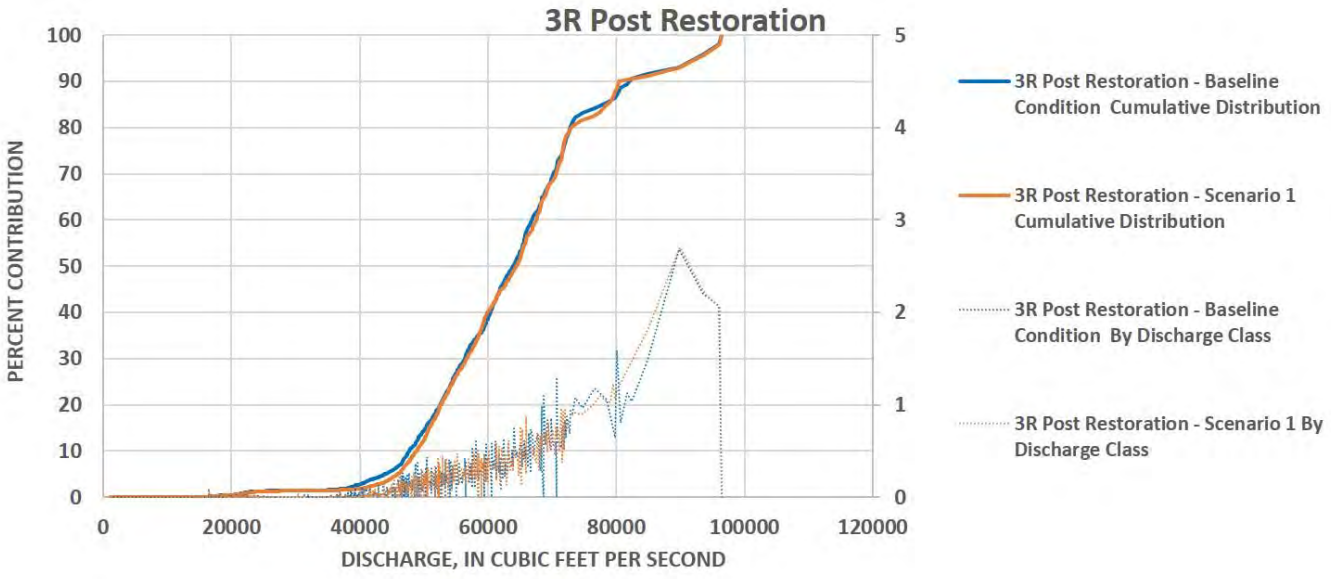

Figure 5.4.3.8-3: Simulated, percent contribution of total erosion by discharge for the Baseline Condition and Scenarios 1 at site 3R for the period 2006-2014

5.4.3.9 Site 21R

The river at site 21R has a steep bank face, sparsely vegetated banks, and is located at station 79,250, just north of the Massachusetts-Vermont Border. The bank is roughly 27 feet tall, with a sandy-loam bank toe and upper bank. The bank is vegetated mostly with grasses and small shrubs, but contains a few American basswood, Green ash, and Northern red oak trees. A significant amount of bare soil was noted on the bank face. No historical cross sections existed for this site. A survey conducted in 2014 was used as the initial bank geometry for the model runs (Figure 5.4.3.9-1).

BSTEM runs at this site show that under the Baseline Condition, 34.6 ft^3 of erosion occurred per foot of bank, during the 2000-2014 flow period, averaging 2.36 $ft^3/ft/y$ (Table 5.4.3-1). This results in the 13^{th} highest erosion rate for the Baseline Condition, placing it at the 50^{th} percentile of erosion rates along the reach. The modeling also indicates that all 100% (2.36 $ft^3/ft/y$) of the erosion is due directly to hydraulic processes, and that none of the bank erosion is the result of larger geotechnical failures.

The Baseline Condition (Waves off) resulted in 2.29 $ft^3/ft/y$, with 2.35 $ft^3/ft/y$ for Scenario 1 (Note- while this site did show a small reduction in erosion between the BL and S1 Scenarios the total reduction in erosion is well below the measureable/significant rate of 0.161 $ft^3/ft/yr$). This is a reduction in erosion of 2.9% for Baseline Wave off and 0.2% for Scenario 1(Figure 5.4.3.9-2 to Figure 5.4.3.9-3). As Baseline Condition (Waves off) scenario illustrated a very little reduction in erosion, it was concluded that boat waves are not having a significant impact on bank stability, and the remaining scenarios were not considered with boat waves off.

For the Baseline Condition, 96.8% of the total erosion occurs at flows of about 17,130 cfs or greater (Figure 5.4.3.9-4). Though there is some small amount of hydraulic erosion at site 21R below about 12,000 cfs, the rate of hydraulic erosion drastically increases at about 23,000 cfs, climbing steadily until 65,000 cfs, and then dropping off at the extreme high flows. Table 5.4.3.9-1 denotes the flows above which 95%, 50%, and 5% of all erosion occurs at the site as well as the amount of time those flows were exceeded for each year in the modeling period. Through this analysis we can conclude that high flows above the hydraulic capacity of Vernon are accounting for most of the total erosion.

Table 5.4.3.9-1: Flow Exceedance Calculations for Site 21R

Site 21R	Percent of Erosion		
	95%	50%	5%
	Flow (cfs)		
Year	**63,852**	**46,345**	**22,928**
2000	0.20%	2.60%	15.10%
2001	1.70%	3.80%	8.20%
2002	0.10%	1.20%	10.60%
2003	0.60%	3.40%	18.50%
2004	NA	0.80%	8.40%
2005	0.70%	5.10%	23.20%
2006	0.40%	2.80%	21.00%
2007	0.80%	3.50%	13.30%
2008	0.60%	6.10%	22.10%
2009	NA	2.20%	13.90%
2010	NA	3.10%	15.30%
2011	2.50%	6.80%	25.20%
2012	NA	0.30%	7.80%
2013	NA	0.30%	12.10%
2014	0.90%	2.90%	15.80%

NA: Not Applicable since flows did not reach this value

Figure 5.4.3.9-1: Photos at site 21R

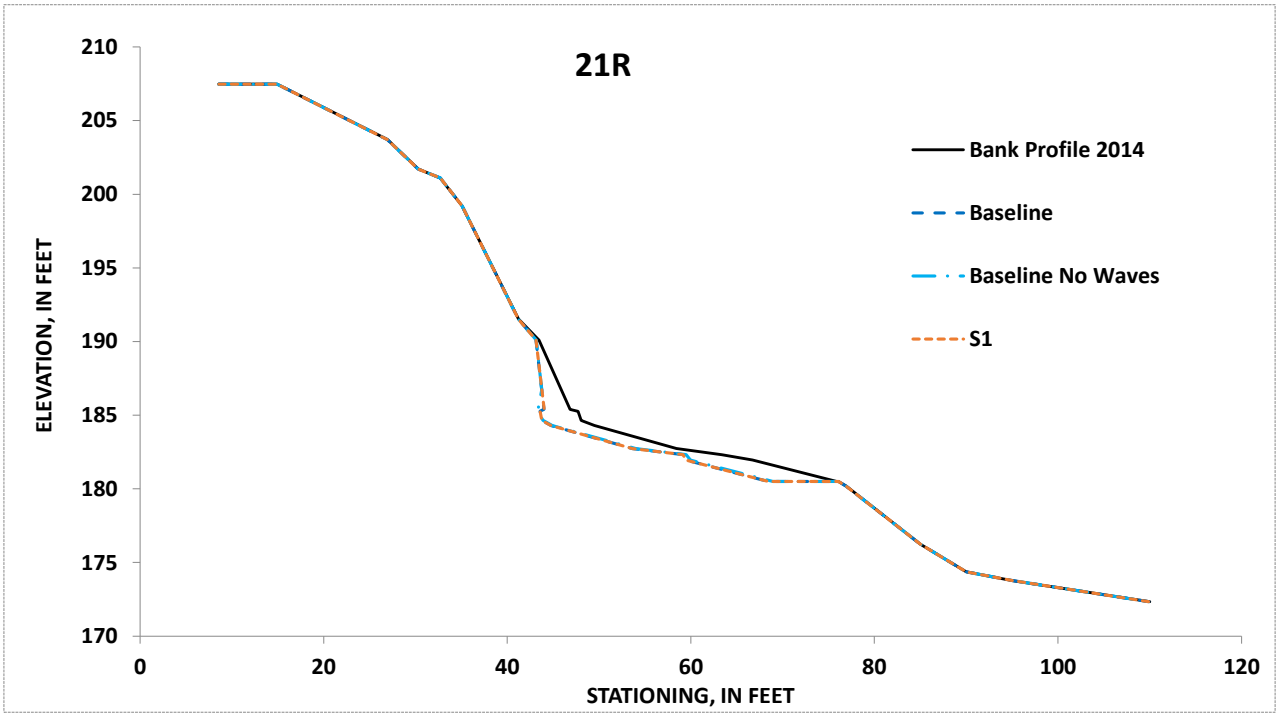

Figure 5.4.3.9-2: Simulated, future unit-erosion for the Baseline Condition (with boat waves on and off) and Scenarios 1 at site 21R for the period 2000-2014

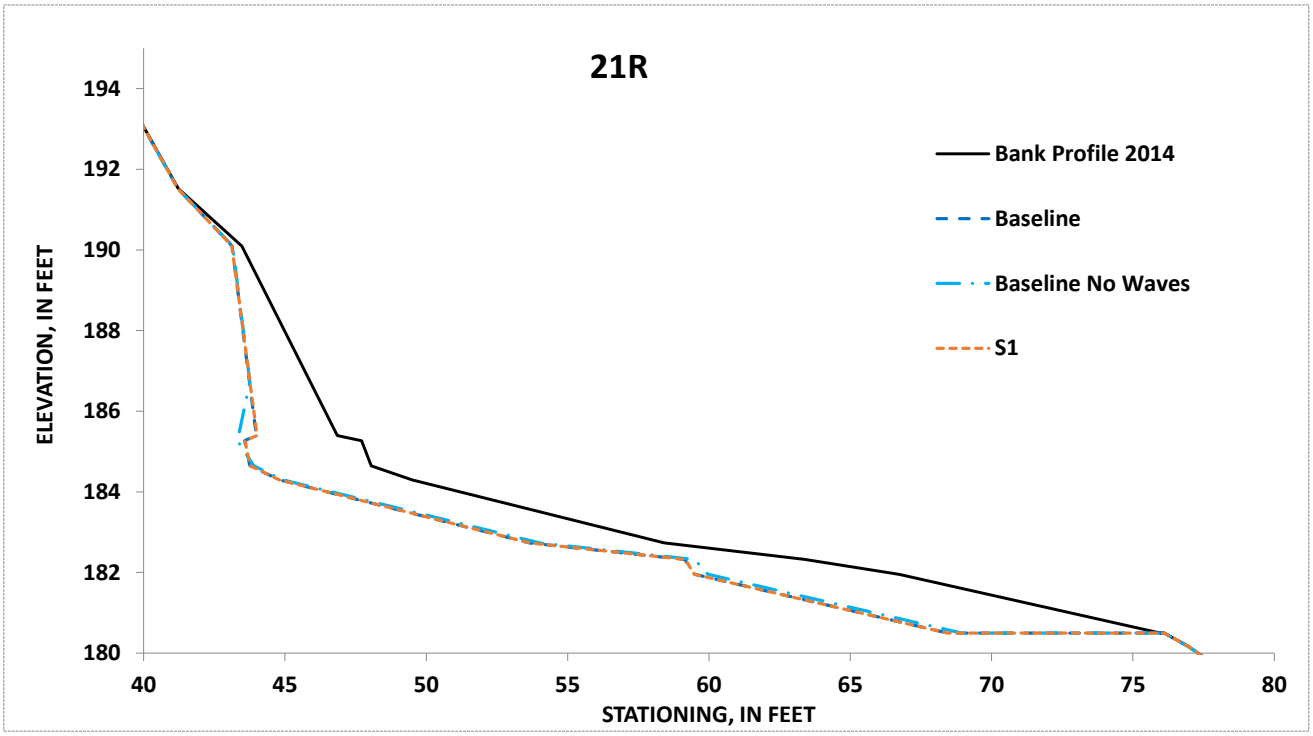

Figure 5.4.3.9-3: Simulated, future erosion for the Baseline Condition (with boat waves on and off) and Scenarios 1 at site 21Rfor the period 2000-2014. Zoomed in at area of erosion for illustrative purposes.

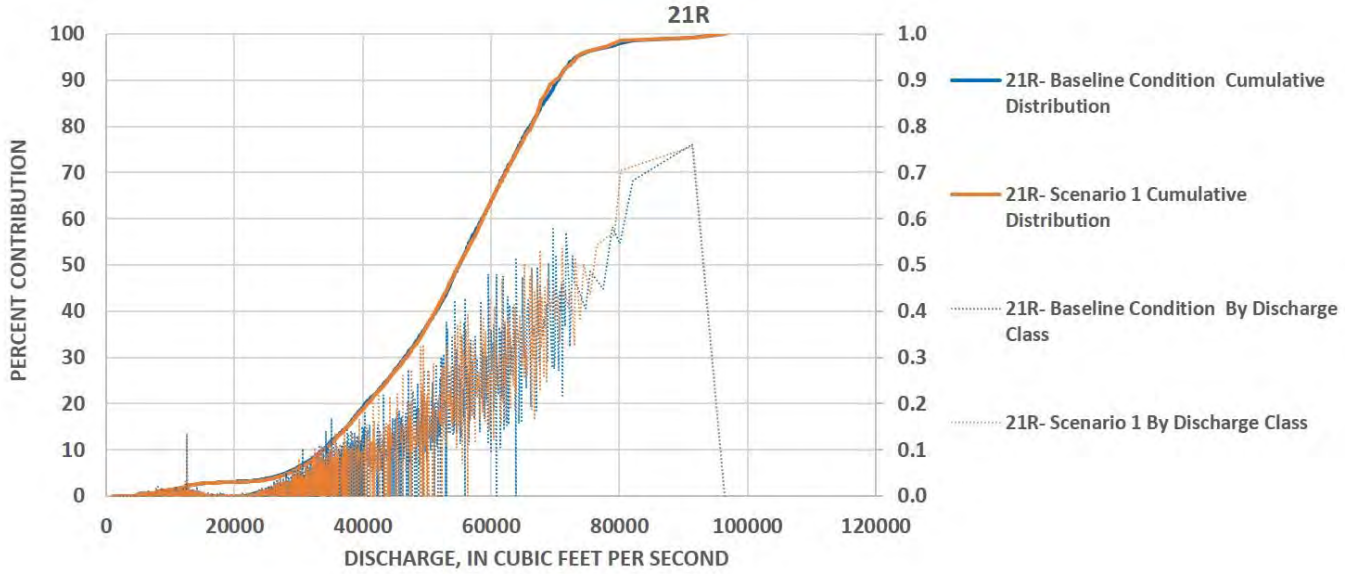

Figure 5.4.3.9-4: Simulated, percent contribution of total erosion by discharge for the Baseline Condition and Scenarios 1 at site 21R for the period 2000-2014

5.4.3.10 Site 4L

The river at site 4L, located at station 74,000 has a gradual bank face, sparsely vegetated banks, and is immediately upstream of the Pauchaug Boat Ramp. The bank is roughly 16 feet tall, with deposits of sandy-loam at the bank toe. The surface of the upper bank is also composed of sandy loam and the bank is vegetated predominantly with grasses and small shrubs, but contains a few American elm, Ashleaf and Silver maple trees (Figure 5.4.3.10-1).

BSTEM runs at this site show that under the Baseline Condition, 0.25 ft^3 of erosion occurred per foot of bank, during the 2000-2014 flow period, averaging 0.017 $ft^3/ft/y$ (Table 5.4.3-1). This results in the 3rd lowest erosion rate for the Baseline Condition, placing it between the 1st and 5th percentiles of erosion rates along the reach. The modeling also indicates that all 100% (0.0173 $ft^3/ft/y$) of the erosion is due directly to hydraulic processes, and that none of the bank erosion is the result of geotechnical failures.

The Baseline Condition (Waves off) resulted in 0.0136 $ft^3/ft/y$, with 0.017 $ft^3/ft/y$ for Scenario 1. This resulted in reduction in erosion rates of 21.4% and 0.6% for Baseline Wave off and Scenario 1 (Figure 5.4.3.10-2). Although erosion rates are quite low at this site as it is in a depositional environment, comparison of the "waves on" and "waves off" conditions under Baseline hydraulics shows that boat waves are a factor at this site. This is not surprising given its proximity to the boat ramp. Still, because of the generally low erosion rates, the remaining scenarios were not considered with boat waves off.

The erosion modeled at this site does not account for the depositional material that has been placed at the toe. The model does not recognize depositional material, and the slight erosion that is happening under the Baseline Condition, is happening at the toe. As material from the bank toe is being eroded, the river is re-depositing additional sediment to compensate. In general though, very little erosion is occurring at this site.

For the Baseline Condition, 95% of the total erosion occurs at flows of only 7,000 cfs or greater (Figure 5.4.9.10-3). This number is again misleading because of the material deposited since the original survey in 2000. However the greater percentage of erosion is occurring at those extreme high flows, and might indicate that material is being eroded during those high flow events, and re-deposited during more normal flow periods. Though the model output is indicating that some slight erosion is occurring within operation flows, the beach has been continually aggrading over the modeling period with increased roughness from establishing grasses at the bank toe.

Table 5.4.3.10-1 denotes the flows above which 95%, 50%, and 5% of all erosion occurs at the site as well as the amount of time those flows were exceeded for each year in the modeling period.

Table 5.4.3.10-1: Flow Exceedance Calculations for Site 4L

Site 4L	Percent of Erosion		
	95%	50%	5%
	Flow (cfs)		
Year	95,042	83,527	6,991
2000	NA	NA	52.90%
2001	NA	NA	35.00%
2002	NA	NA	51.60%
2003	NA	NA	60.60%
2004	NA	NA	59.90%
2005	NA	NA	67.40%
2006	NA	NA	80.80%
2007	NA	NA	61.90%
2008	NA	NA	80.10%
2009	NA	NA	76.70%
2010	NA	NA	67.40%
2011	0.20%	0.30%	73.00%
2012	NA	NA	53.20%
2013	NA	NA	62.40%
2014	NA	NA	63.40%

NA: Not Applicable since flows did not reach this value

Figure 5.4.3.10-1 Photos at site 4L

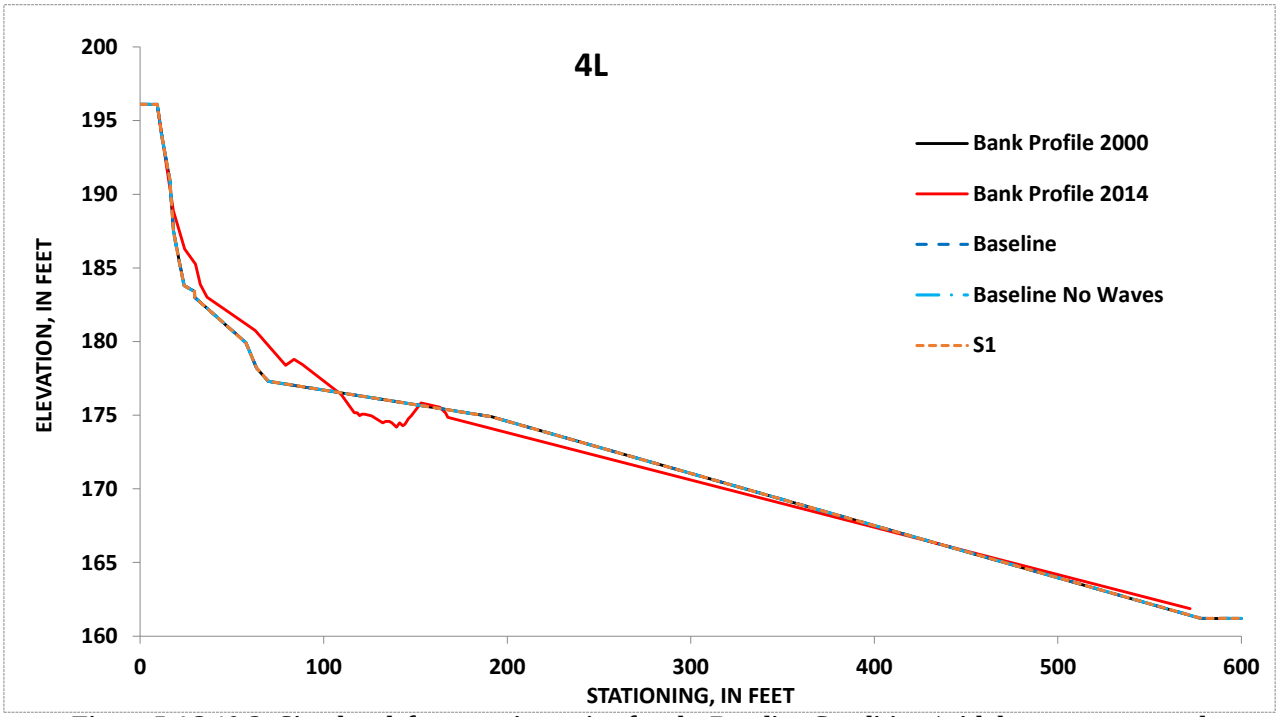

Figure 5.4.3.10-2: Simulated, future unit-erosion for the Baseline Condition (with boat waves on and off) and Scenarios 1 at site 4L for the period 2000-2014

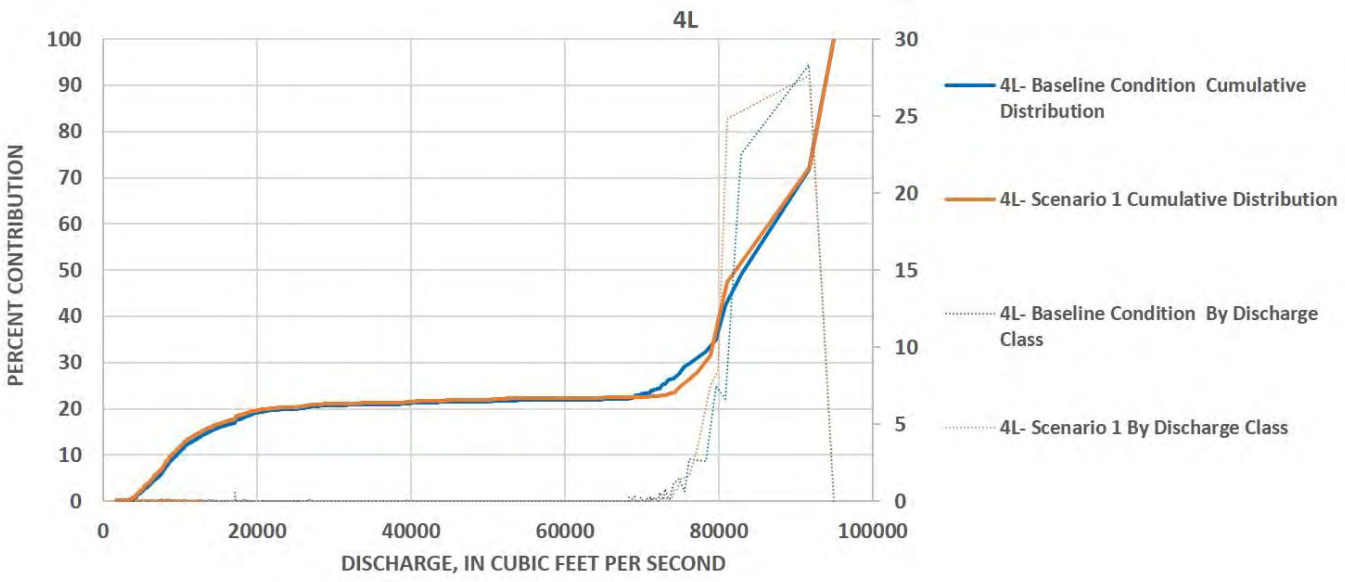

Figure 5.4.3.10-3: Simulated, percent contribution of total erosion by discharge for the Baseline Condition and Scenarios 1 at site 4L for the period 2000-2014

5.4.3.11 Site 29R

The river at site 29R (at station 66,000) has a steep bank face, sparsely vegetated banks, and is located between Mallory Brook and the Pauchaug Boat Ramp. The bank is roughly 26 feet tall, with a sandy loam toe and upper bank slope. The bank contains only patchy vegetation with Green ash and Silver maple trees. A significant amount of bare soil was noted on the bank face. No historical cross sections exist for this site, however this site was surveyed in 2014 and this was used as the initial geometry for the model runs (Figure 5.4.3.11-1).

BSTEM runs at this site show that under the Baseline Condition, 25.2 ft^3 of erosion occurred per foot of bank during the 2000-2014 flow period, averaging 1.72 $ft^3/ft/y$ (Table 5.4.3-1). This results in the 16^{th} highest erosion rate for the Baseline Condition, placing it between the 35^{th} and 40^{th} percentiles of erosion rates along the reach. The modeling also indicates that only 1% (about 0.009 $ft^3/ft/y$) of the erosion is due directly to hydraulic processes, whereas the other 99% (1.71 $ft^3/ft/y$) is the result of geotechnical processes and associated mass failures. Looking at the starting cross section, with the existing undercut, it becomes obvious that a large geotechnical failure is imminent (Figure 5.4.3.11-2). In fact, failure of the upper bank here represents the single, significant erosion event at this site that occurred early on in the simulation period.

The Baseline Condition (Waves off) resulted in 1.71 $ft^3/ft/y$, with 1.72 $ft^3/ft/y$ for Scenario 1. As Baseline Condition (Waves off) scenario illustrated a very little reduction in erosion, it was concluded that boat waves are not having a significant impact on bank stability, and the remaining scenarios were not considered with boat waves off. Under all scenarios, the same soil block failed, indicating that this was likely to occur with minor additional undercutting under any flow scenario. For the Baseline Condition, 95% of the total erosion occurs at flows of 12,000 cfs or greater (Figure 5.4.3.11-3). This coincides with the previous analysis of the results, indicating that there is an imminent bank failure due at site 29R in the near future. Once this block fails, additional undercutting could further destabilize the upper part of the bank.

Table 5.4.3.11-1 denotes the flows above which 95%, 50%, and 5% of all erosion occurs at the site as well as the amount of time those flows were exceeded for each year in the modeling period.

Table 5.4.3.11-1: Flow Exceedance Calculations for Site 29R

Site 29R	Percent of Erosion		
	95%	50%	5%
	Flow (cfs)		
Year	**11,968**	**11,968**	**11,923**
2000	31.10%	31.10%	31.20%
2001	11.40%	11.40%	11.50%
2002	27.60%	27.60%	27.70%
2003	37.60%	37.60%	37.80%
2004	26.30%	26.30%	26.40%
2005	43.80%	43.80%	44.00%
2006	58.10%	58.10%	58.30%
2007	32.80%	32.80%	32.90%
2008	50.10%	50.10%	50.40%
2009	54.50%	54.50%	54.80%
2010	47.40%	47.40%	47.60%
2011	55.30%	55.30%	55.50%
2012	32.00%	32.00%	32.20%
2013	38.10%	38.10%	38.40%
2014	37.50%	37.50%	37.70%

NA: Not Applicable since flows did not reach this value

Figure 5.4.3.11-1 Photos at site 29R

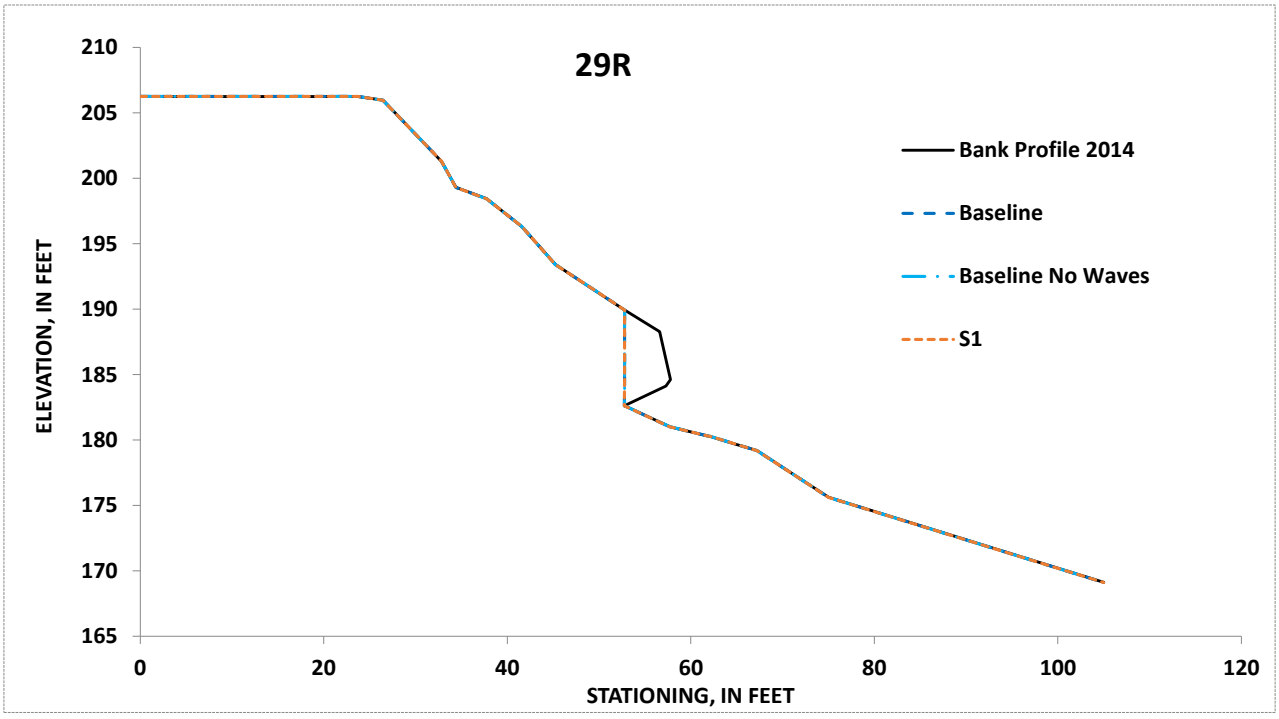

Figure 5.4.3.11-2: Simulated, future unit-erosion for the Baseline Condition (with boat waves on and off) and Scenarios 1 at site 29R for the period 2000-2014

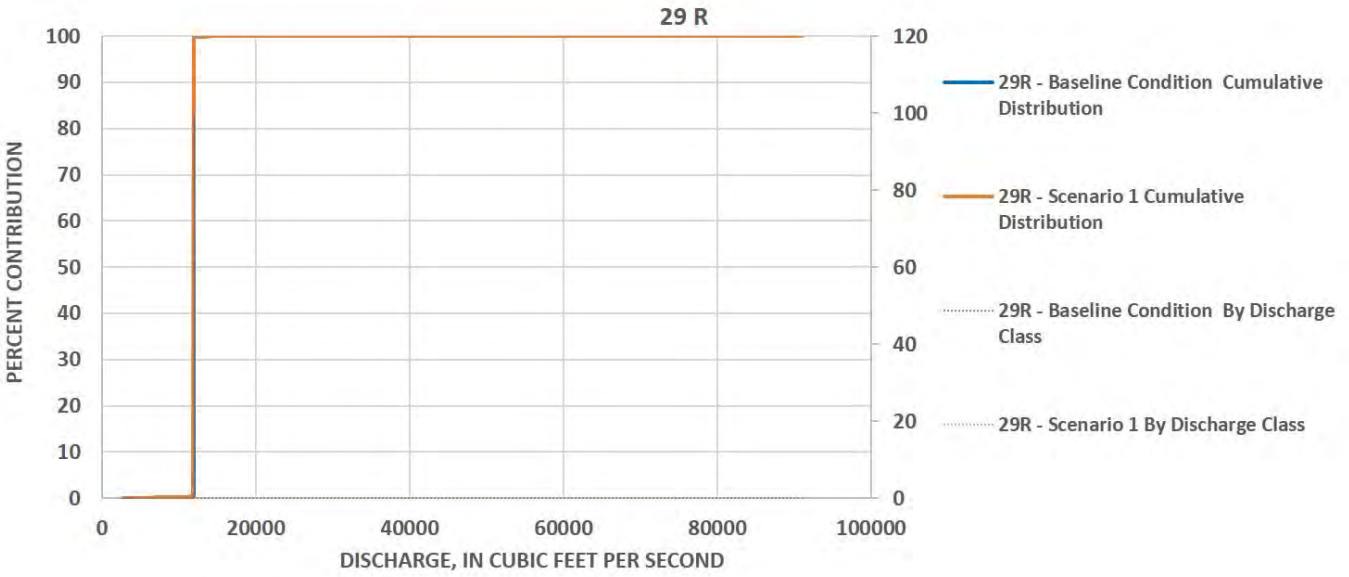

Figure 5.4.3.11-3: Simulated, percent contribution of total erosion by discharge for the Baseline Condition and Scenarios 1 at site 29R for the period 2000-2014

5.4.3.12 Site 5CR

The river at site 5CR (station 57,250) has a steep bank face, which is sparsely vegetated, and is located immediately downstream of the Route 10 Bridge. The bank is roughly 23 feet tall, with a loamy sand toe and bank, and the upper part of the bank consisting of a sandy loam. The bank is vegetated with small shrubs, American basswood, Green ash, and Red and Sugar maple trees. The first historic cross section for site 5CR was taken on 7/8/2002, and was, therefore, used as the initial geometry for modeling (Figure 5.4.3.12-1).

BSTEM runs at this site show that under the Baseline Condition, 105 ft^3 of erosion occurred per foot of bank, during the 2002-2014 flow period, averaging 8.61 $ft^3/ft/y$ (Table 5.4.3-1). This results in the 2nd highest erosion rate for the Baseline Condition, placing it between the 95th and 99th percentiles of erosion rates along the reach. The modeling also indicates that roughly 35% (about 3.0 $ft^3/ft/y$) of the erosion is due directly to hydraulic processes, whereas the other 65% (5.6 $ft^3/ft/y$) is the result of geotechnical processes and associated mass failures.

The Baseline Condition (Waves off) resulted in 8.50 $ft^3/ft/y$, with 8.57 $ft^3/ft/y$ for Scenario 1 (Figure 5.4.3.12-2 to Figure 5.4.3.12-3). This resulted in the following percent reductions in erosion rates: 1.23% and 0.46% for Baseline Wave off and Scenario 1 (Note- while this site did show a small reduction in erosion between the BL and S1 Scenarios the total reduction in erosion is well below the measureable/significant rate of 0.161 $ft^3/ft/yr$). Since waves accounted for only about 1% of the total erosion under the Baseline Condition the remaining scenarios were not considered with boat waves off.

For the Baseline Condition, 95% of the total erosion occurs at flows of about 48,000 cfs or greater (Figure 5.4.3.12-4). Although there is some limited hydraulic erosion at flows below 37,000 cfs, a significant geotechnical failure occurs at 48,000 cfs, with additional hydraulic erosion occurring through 76,000 cfs. At this flow, a large geotechnical failure occurs resulting in roughly 65% of the total erosion at site 5CR. Through this analysis we can conclude that those flows greater than the hydraulic capacity of Vernon and Northfield Mountain are accounting for most of the total erosion. Table 5.4.3.12-1 denotes the flows above which 95%, 50%, and 5% of all erosion occurs at the site as well as the amount of time those flows were exceeded for each year in the modeling period.

Table 5.4.3.12-1: Flow Exceedance Calculations for Site 5CR

Site 5 CR	Percent of Erosion		
	95%	50%	5%
	Flow (cfs)		
Year	**76,391**	**76,391**	**47,867**
2000	NA	NA	2.30%
2001	NA	NA	3.70%
2002	NA	NA	1.10%
2003	NA	NA	2.90%
2004	NA	NA	0.70%
2005	NA	NA	4.30%
2006	0.10%	0.10%	2.30%
2007	NA	NA	3.30%
2008	NA	NA	5.70%
2009	NA	NA	1.80%
2010	NA	NA	2.80%
2011	0.80%	0.80%	6.20%
2012	NA	NA	0.20%
2013	NA	NA	0.20%
2014	NA	NA	2.70%

NA: Not Applicable since flows did not reach this value

Figure 5.4.3.12-1 Photos at site 5CR

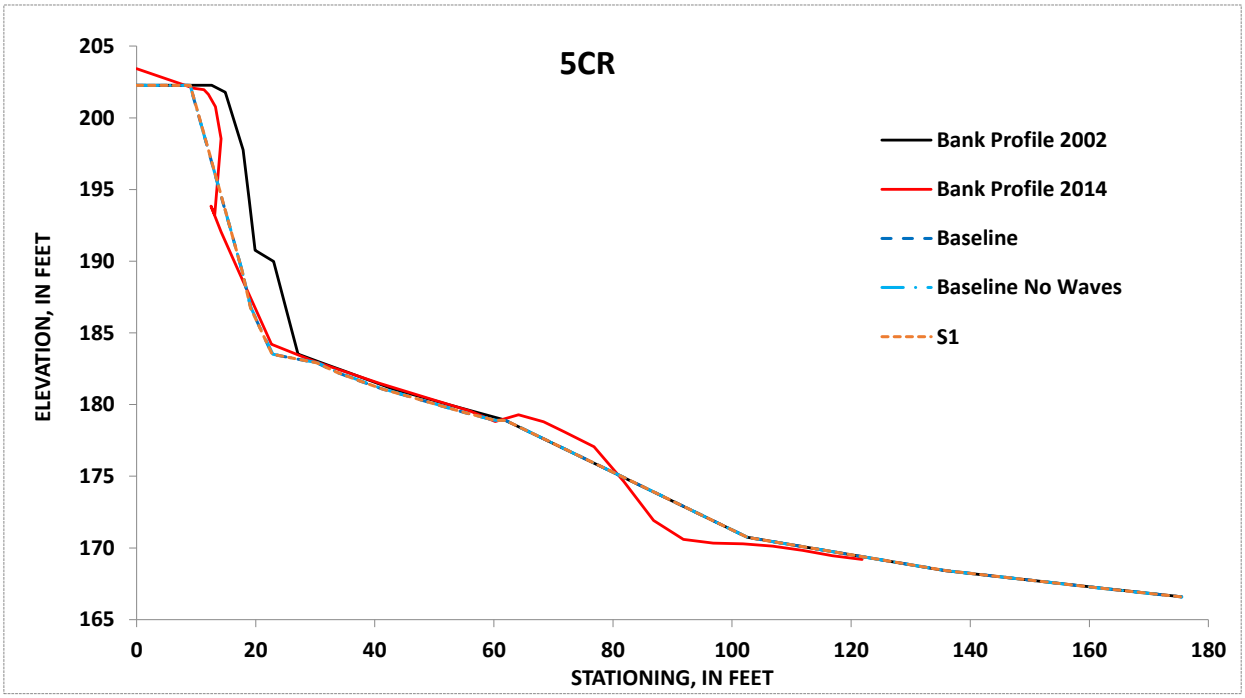

Figure 5.4.3.12-2: Simulated, future unit-erosion for the Baseline Condition (with boat waves on and off) and Scenarios 1 at site 5CR for the period 2002-2014

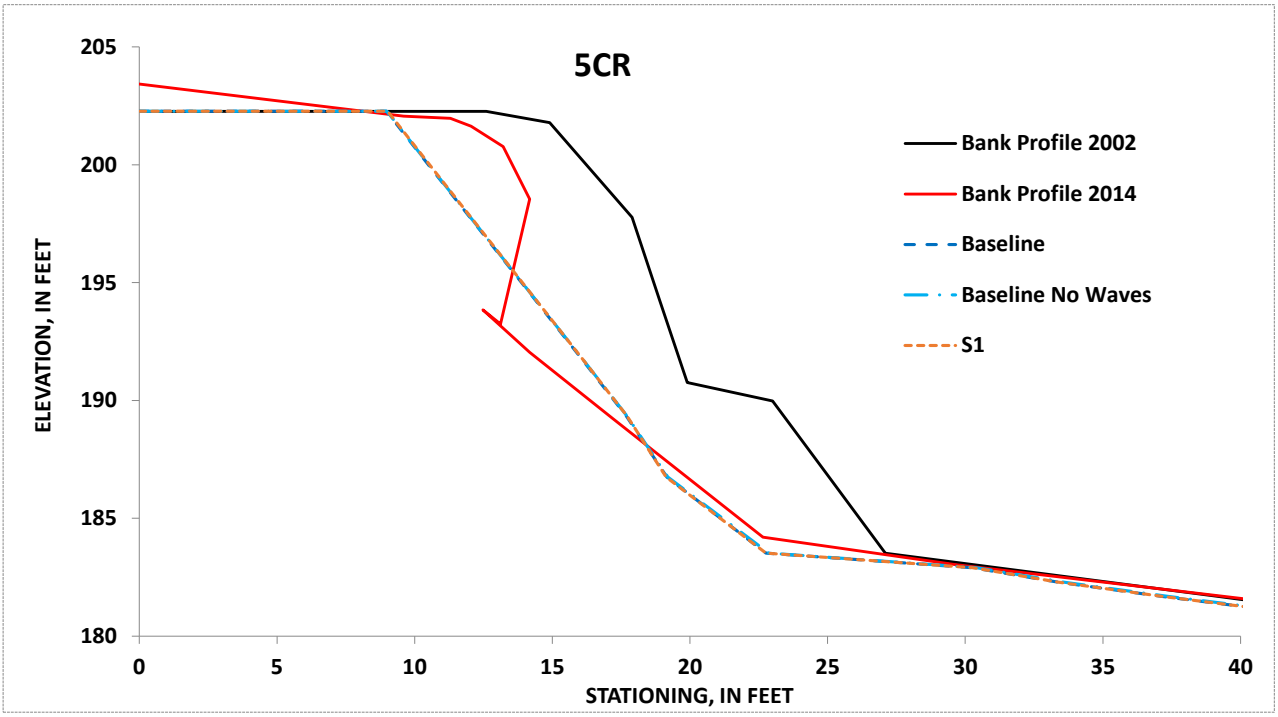

Figure 5.4.3.12-3: Simulated, future erosion for the Baseline Condition (with boat waves on and off) and Scenarios 1 at site 5CR for the period 2002-2014. Zoomed in at area of erosion for illustrative

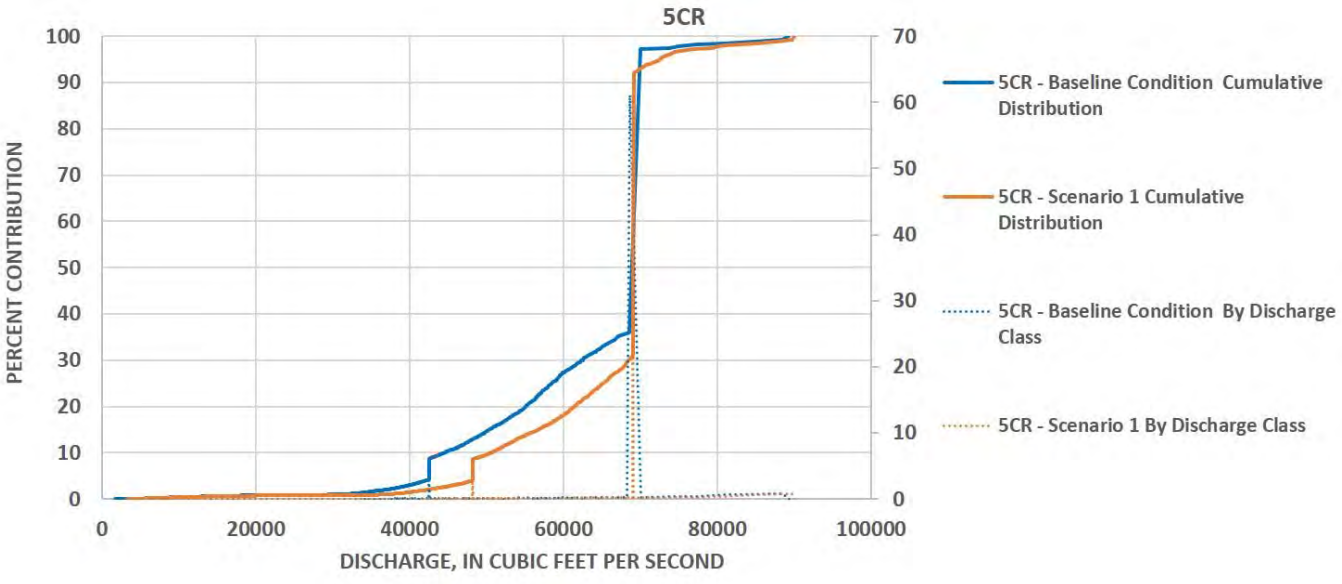

Figure 5.4.3.12-4: Simulated, percent contribution of total erosion by discharge for the Baseline Condition and Scenarios 1 - 3 at site 5CR for the period 2002-2014

5.4.3.13 Site 26R

The river at site 26R (station 50,000) has a steep bank face which is sparsely vegetated. The site is located between Kidds Island and the mouth of Bennett Brook. The bank is roughly 28 feet tall, with a loamy-sand toe and bank, and the upper portion of the bank consisting of a sandy loam. The bank is vegetated with Hickory, Northern red oak, Sugar and Red maples, and White birch trees. No historical cross sections exist for this site, requiring the 2014 survey to be used as the initial geometry for the model runs (Figure 5.4.3.13-1).

BSTEM runs at this site show that under the Baseline Condition, 17.5 ft^3 of erosion occurred per foot of bank, during the 2000-2014 flow period, averaging 1.194 $ft^3/ft/y$ (Table 5.4.3-1). This results in the 14th lowest erosion rate for the Baseline Condition, placing it between the 30th and 35th percentiles of erosion rates along the reach. The modeling also indicates that all 100% (1.19 $ft^3/ft/y$) of the erosion is due directly to hydraulic processes, and none of the bank erosion is the result of larger geotechnical failures.

The Baseline Condition (Waves off) resulted in 1.145 $ft^3/ft/y$, with 1.196 $ft^3/ft/y$ for Scenario 1 (Figure 5.7.13-2 to Figure 5.7.13-3). This resulted in the following percent reductions in erosion rates: 4.1% and -0.123%, for Baseline Wave off and Scenario 1 respectively. These differences are relatively small indicting little difference in erosion rates across all operational scenarios. As Baseline Condition (Waves off) scenario illustrated a very little reduction in erosion, it was concluded that boat waves are not having a significant impact on bank stability, and the remaining scenarios were not considered with boat waves off.

For the Baseline Condition, 96% of the total erosion occurs at flows of about 37,000 cfs or greater (Figure 5.4.3.13-4). Though there is some limited hydraulic erosion at flows below 37,000 cfs, the erosion rate (albeit moderate) drastically increases at 43,000 cfs and is maintained through 70,000 cfs. Through this analysis we can conclude that those flows greater than the combined hydraulic capacity of Vernon and Northfield Mountain are accounting for most of the total erosion. Table 5.4.3.13-1 denotes the flows above which 95%, 50%, and 5% of all erosion occurs at the site as well as the amount of time those flows were exceeded for each year in the modeling period.

Table 5.4.3.13-1: Flow Exceedance Calculations for Site 26R

Site 26R	Percent of Erosion		
	95%	50%	5%
	Flow (cfs)		
Year	**80,503**	**60,282**	**43,294**
2000	NA	0.40%	3.20%
2001	NA	2.20%	4.00%
2002	NA	0.10%	1.70%
2003	NA	0.80%	4.50%
2004	NA	NA	1.00%
2005	NA	0.90%	6.10%
2006	NA	0.70%	4.00%
2007	NA	1.80%	3.80%
2008	NA	1.10%	7.70%
2009	NA	0.20%	2.80%
2010	NA	0.20%	3.80%
2011	0.40%	3.20%	7.50%
2012	NA	NA	0.30%
2013	NA	NA	0.60%
2014	NA	1.40%	3.20%

NA: Not Applicable since flows did not reach this value

Figure 5.4.3.13-1 Photos at site 26R

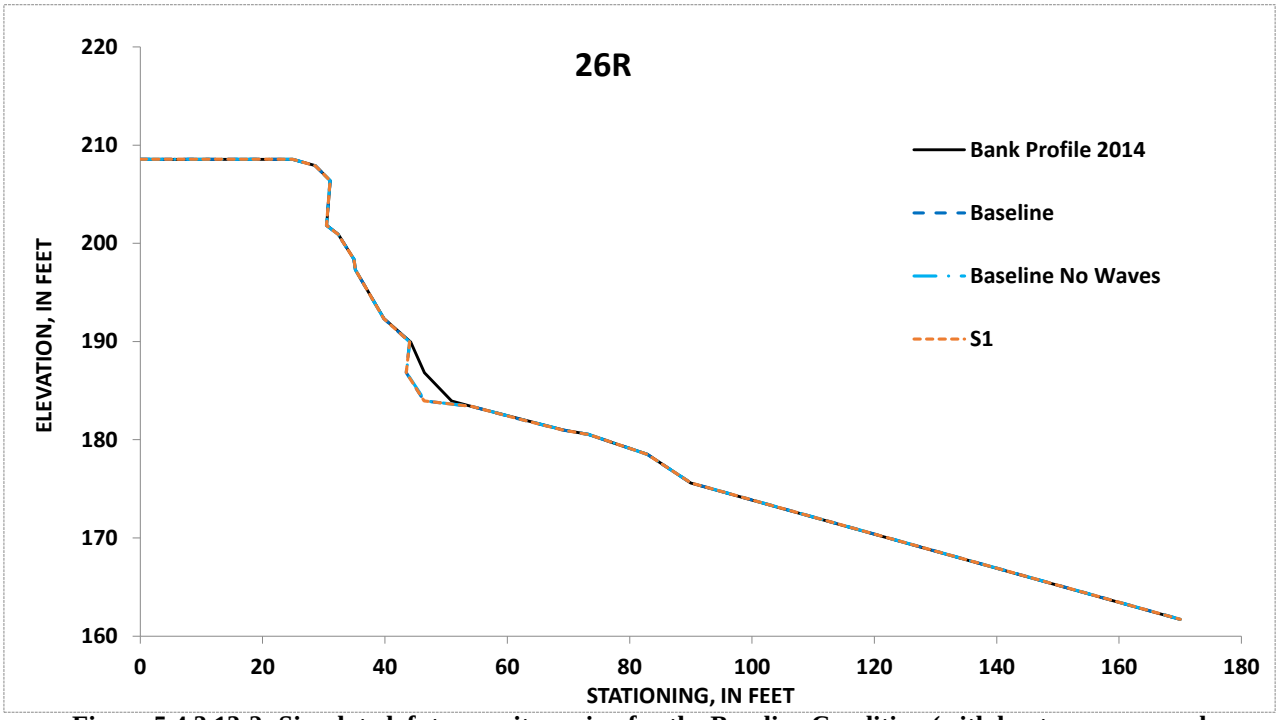

Figure 5.4.3.13-2: Simulated, future unit-erosion for the Baseline Condition (with boat waves on and off) and Scenarios 1 at site 26R for the period 2000-2014

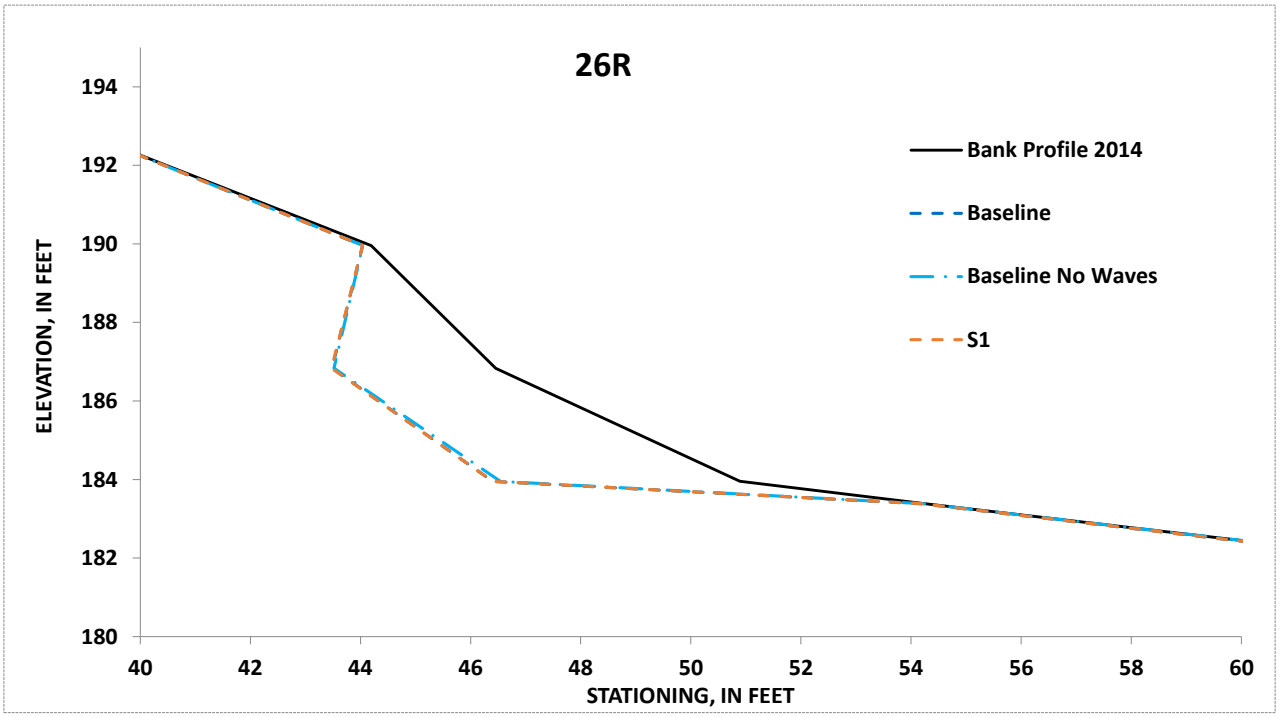

Figure 5.4.3.13-3: Simulated, future erosion for the Baseline Condition (with boat waves on and off) and Scenarios 1 at site 26Rfor the period 2000-2014. Zoomed in at area of erosion for illustrative purposes.

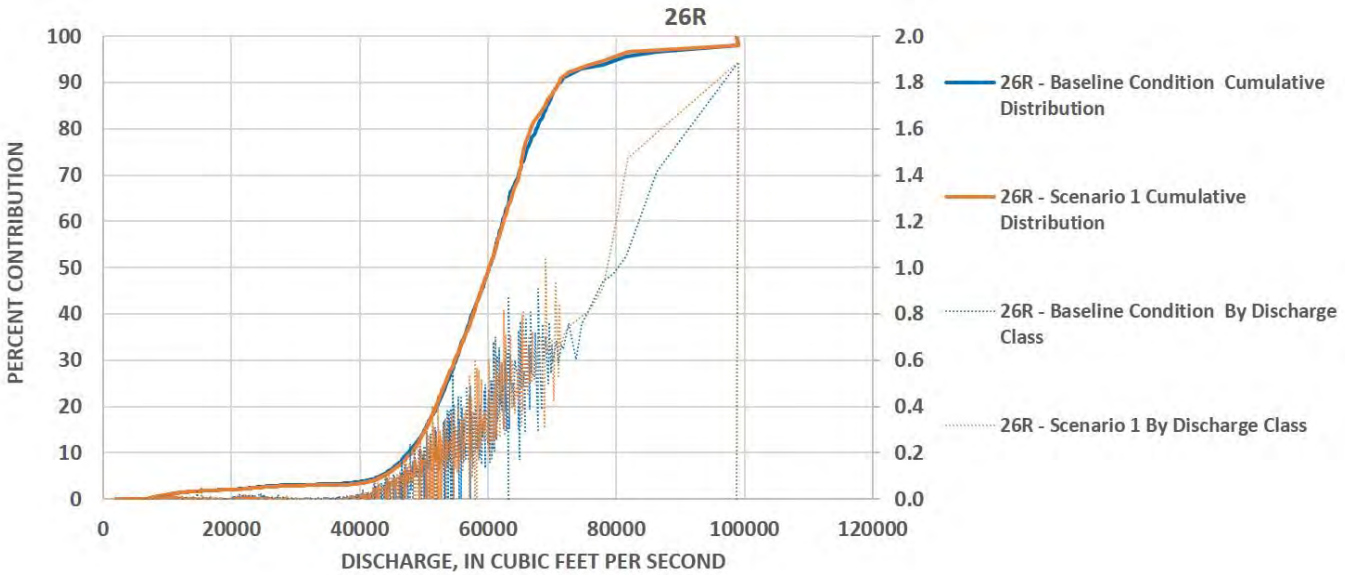

Figure 5.4.3.13-4: Simulated, percent contribution of total erosion by discharge for the Baseline Condition and Scenarios 1 at site 26R for the period 2000-2014

5.4.3.14 Site 10L

The river at site 10L has a gradual bank face, moderately vegetated banks and is located at station 49,000, roughly 6,000 ft upstream of Kidds Island. The bank is roughly 14 feet tall, with a deposited sandy-loam toe and a bank comprised of sand and sandy loam. The bank is vegetated mostly with grasses and shrubs, with large Green ash and Silver maple trees. Behind the upper bank lies a corn field (Figure 5.4.3.14-1).

BSTEM runs at this site show that under the Baseline Condition, 2.34 ft^3 of erosion occurred per foot of bank, during the 2002-2014 flow period, averaging 0.160 $ft^3/ft/y$ (Table 5.4.3-1). This results in the 5^{th} lowest erosion rate for the Baseline Condition, placing it between the 1^{tst} and 5^{th} percentiles of erosion rates along the reach. The modeling also indicates that all 100% (0.160 $ft^3/ft/y$) of the erosion is due directly to hydraulic processes, and none of the bank erosion is the result of geotechnical failures.

The Baseline Condition (Waves off) resulted in 0.1583 $ft^3/ft/y$, with 0.1579 $ft^3/ft/y$ for Scenario 1 (Figure 5.4.3.14-2 to Figure 5.4.3.14-3). This resulted in the following percent reductions in erosion rates: 0.87% and 1.10%, for Baseline Wave off and Scenario 1. As the Baseline Condition (Waves off) scenario illustrated a very little reduction in erosion, it was concluded that boat waves are not having a significant impact on bank stability, and the remaining scenarios were not considered with boat waves off.

Predicted erosion at this site does not account for the deposition of material at the bank toe (Figure 5.4.3.14-4). Since BSTEM is not a sediment-routing model and as such, it does not predict fluvial deposition. Still, the small amount of erosion that is simulated under the Baseline Condition, represents undercutting at the bank toe. As material from the toe is eroded, however, additional sediment is re-deposited. Thus, little net erosion occurs at this site. Differences in predicted erosion rates are minor given the low rates. For the Baseline Condition, 95% of the total erosion occurs at flows of 59,000 cfs or greater (Figure 5.4.3.14-5). Table 5.4.3.14-1 denotes the flows above which 95%, 50%, and 5% of all erosion occurs at the site as well as the amount of time those flows were exceeded for each year in the modeling period. Though there is some minor erosion within operational flow limits, this number is somewhat misleading because of the net deposition of material since the original survey in 2000 (Figure 5.4.3.14-2). The beach has been generally aggrading continually during the modeled period.

Table 5.4.3.14-1: Flow Exceedance Calculations for Site 10L

Site 10 L	Percent of Erosion		
	95%	50%	5%
	Flow (cfs)		
Year	**98,882**	**79,003**	**58,922**
2000	NA	NA	0.60%
2001	NA	NA	2.30%
2002	NA	NA	0.10%
2003	NA	NA	0.90%
2004	NA	NA	NA
2005	NA	NA	1.20%
2006	NA	NA	0.80%
2007	NA	NA	2.40%
2008	NA	NA	1.70%
2009	NA	NA	0.30%
2010	NA	NA	0.30%
2011	0.20%	0.50%	3.40%
2012	NA	NA	NA
2013	NA	NA	0.10%
2014	NA	NA	1.40%

NA: Not Applicable since flows did not reach this value

Figure 5.4.3.14-1 Photos at site 10L

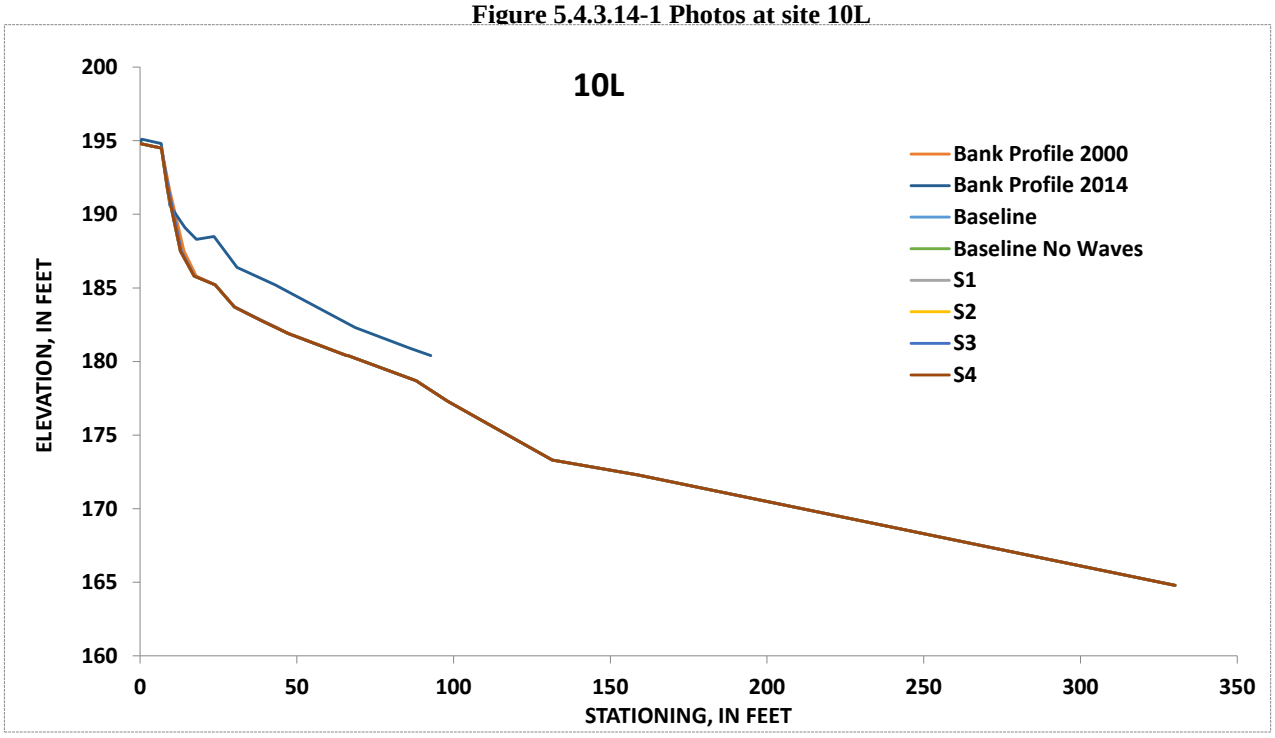

Figure 5.4.3.14-2: Simulated, future unit-erosion for the Baseline Condition (with boat waves on and off) and Scenarios 1 at site 10L for the period 2000-2014

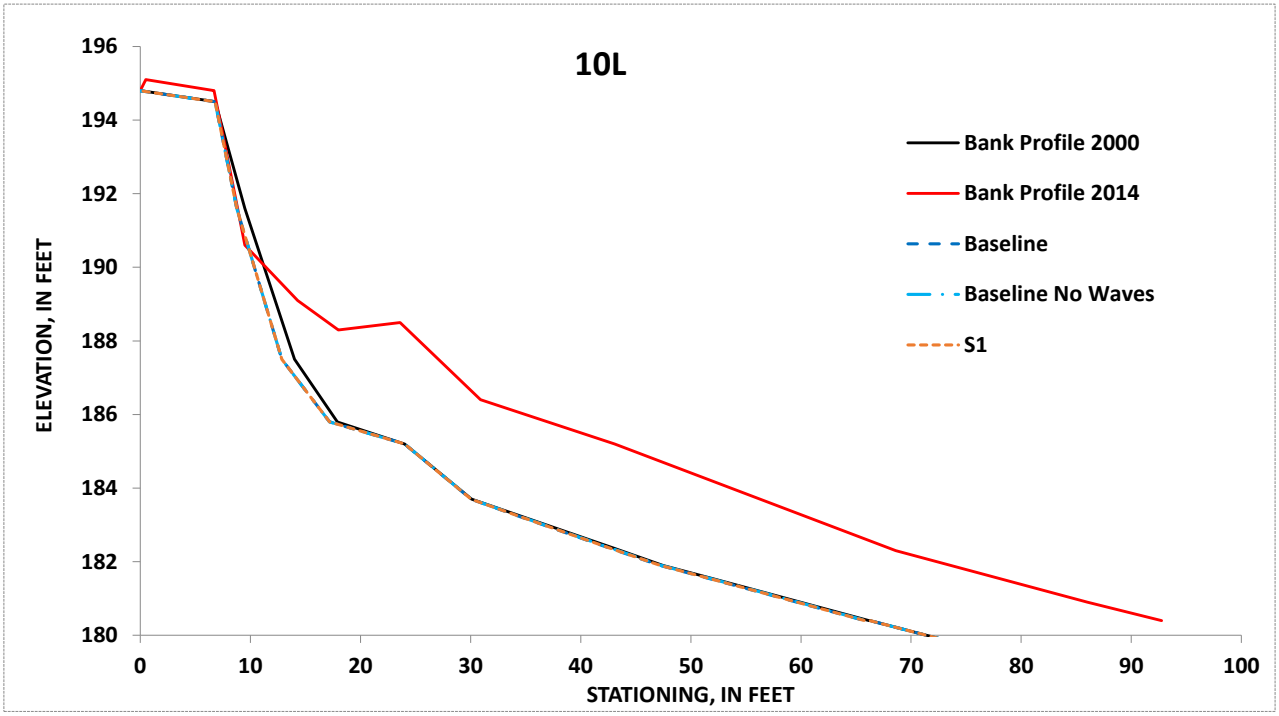

Figure 5.4.3.14-3: Simulated, future erosion for the Baseline Condition (with boat waves on and off) and Scenarios 1 at site 10Lfor the period 2000-2014. Zoomed in at area of erosion for illustrative purposes.

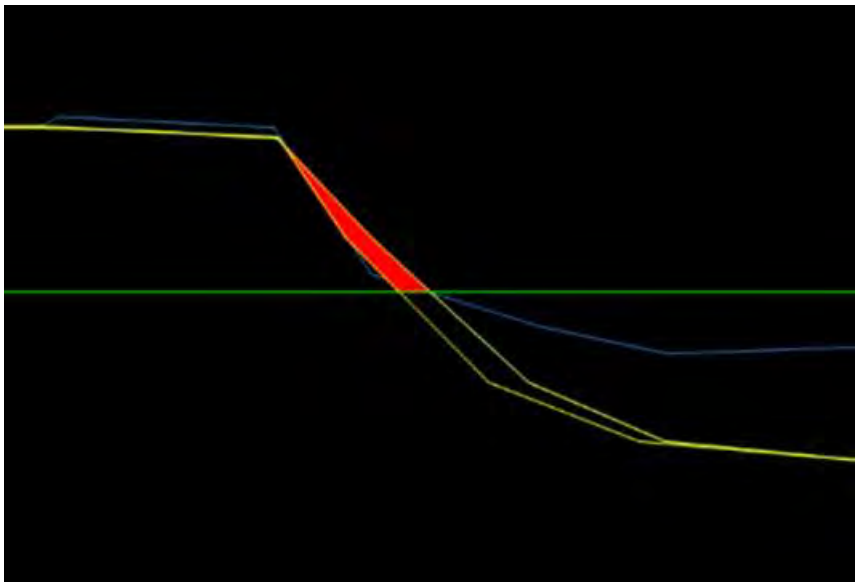

Figure 5.7.14-4 Calculated Erosion above Depositional Layer

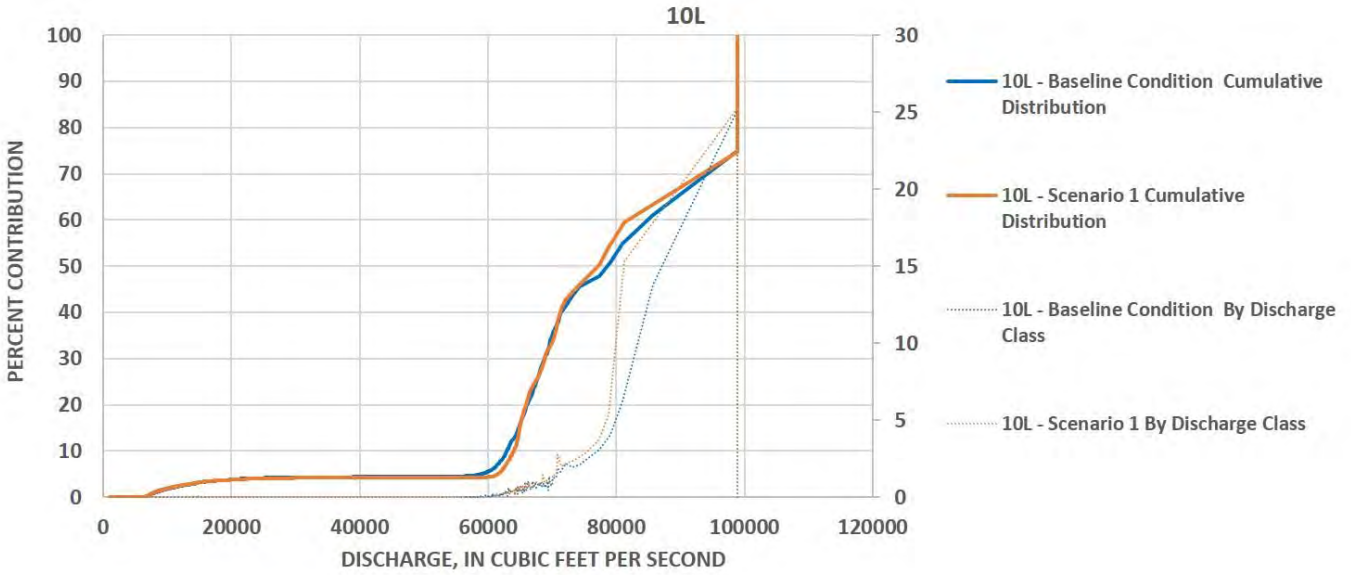

Figure 5.3.3.14-5: Simulated, percent contribution of total erosion by discharge for the Baseline Condition and Scenarios 1 at site 10L for the period 2000-2014

5.4.3.15 Site 10R

The river at site 10R has steep, heavily vegetated banks. The site is located at station 49,000, nearly 6,000 ft upstream of Kidds Island. The bank is roughly 31 feet tall, with a rock toe (d_{50}=59 mm) and a sandy-loam bank. The replanted bank is heavily vegetated with large shrubs, Northern red oak, and Eastern cottonwood. As 10R was restored in 2001, no Pre-Restoration simulation was conducted for this site (Figure 5.4.3.15-1).

BSTEM runs for the Post Restoration condition at this site show that under the Baseline Condition, 3.7E-03 ft^3 of erosion occurred per foot of bank, during the 2001 to 2014 flow period after restoration, averaging 2.8E-04 $ft^3/ft/y$ (Table 5.4.3-1). This represents virtually no erosion and is the 2th lowest erosion rate for the Baseline Condition. The modeling also indicates that all 100% (2.82E-04 $ft^3/ft/y$) of the erosion is due directly to hydraulic processes, and that there are no geotechnical failures.

The Baseline Condition (Waves off) resulted in 2.83E-04 $ft^3/ft/y$, with 3.96E-07 $ft^3/ft/y$ for Scenario 1 (Figure 5.4.3.15-2). This resulted in reductions in erosion rates of -0.4% for Baseline Wave off and 99.9% for Scenario 1. Baseline simulations with waves off showed virtually no reduction in erosion, it was concluded that boat waves have little effect on erosion processes at this site. Because of this, all of the remaining scenarios were simulated with boat waves on.

Erosion values at this site are so low that comparisons of rates are meaningless. Fundamentally, there is no bank erosion at this site and the restoration works have been very successful. For the Baseline Condition, 95% of the total erosion occurs at flows of about 47,000 cfs or greater (Figure 5.4.3.15-3). Table 5.4.3.15-1 denotes the flows above which 95%, 50%, and 5% of all erosion occurs at the site as well as the amount of time those flows were exceeded for each year in the modeling period.

Table 5.4.3.15-1: Flow Exceedance Calculations for Site 10R

Site 10R	Percent of Erosion		
	95%	50%	5%
	Flow (cfs)		
Year	49,015	48,156	46,944
2000	2.10%	2.20%	2.40%
2001	3.70%	3.70%	3.80%
2002	1.10%	1.10%	1.10%
2003	2.60%	2.80%	3.20%
2004	0.60%	0.70%	0.80%
2005	4.00%	4.20%	4.70%
2006	2.20%	2.30%	2.60%
2007	3.20%	3.30%	3.50%
2008	5.20%	5.50%	5.90%
2009	1.60%	1.80%	2.00%
2010	2.40%	2.70%	2.90%
2011	5.80%	6.00%	6.50%
2012	0.20%	0.20%	0.20%
2013	0.10%	0.20%	0.30%
2014	2.70%	2.70%	2.80%

NA: Not Applicable since flows did not reach this value

Figure 5.4.3.15-1 Photos at site 10R Post Restoration

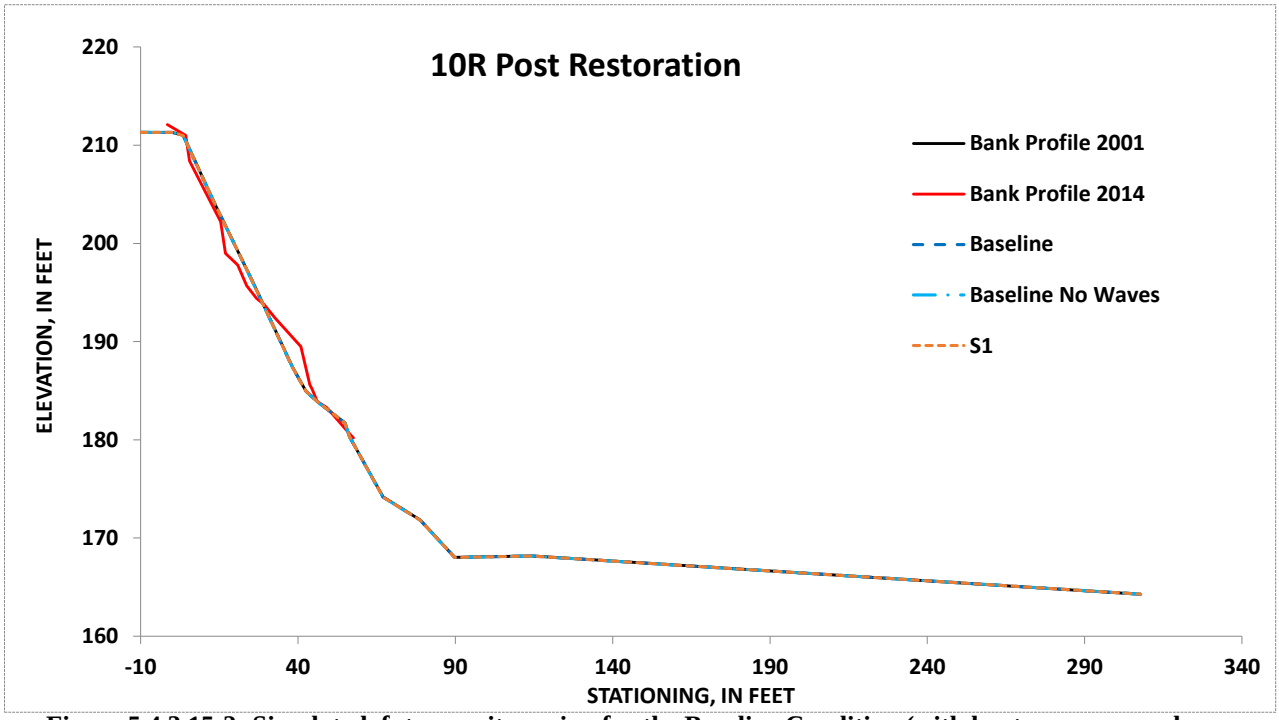

Figure 5.4.3.15-2: Simulated, future unit-erosion for the Baseline Condition (with boat waves on and off) and Scenarios 1 at site 10R for the period 2001-2014

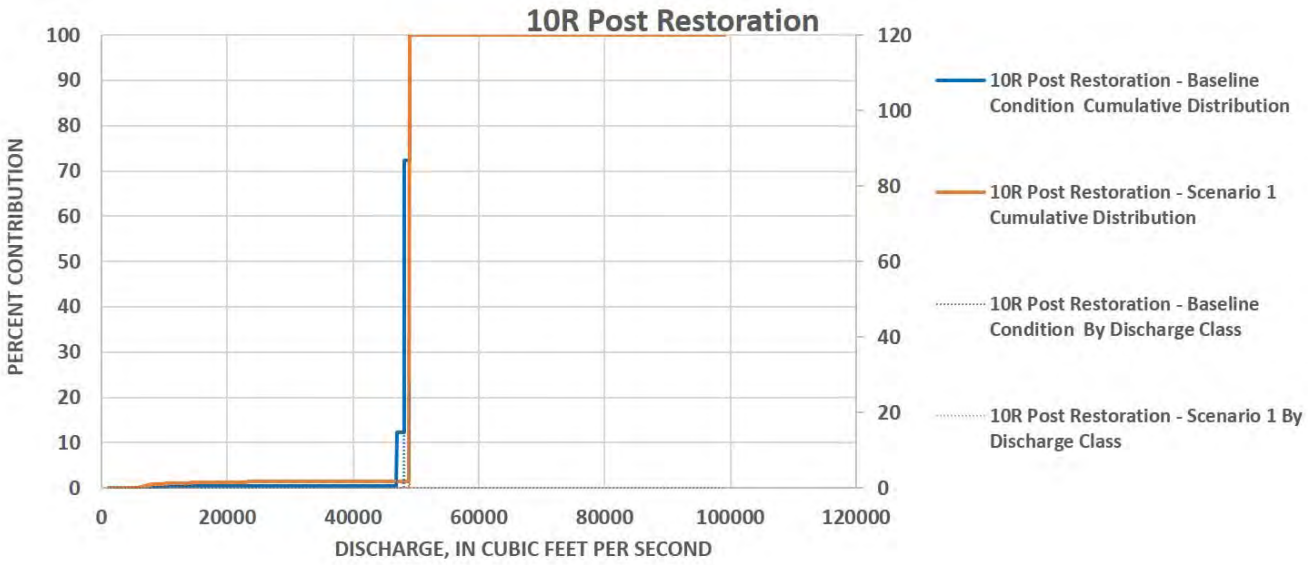

Figure 5.4.3.15-3: Simulated, percent contribution of total erosion by discharge for the Baseline Condition and Scenarios 1 at site 10R for the period 2001-2004

5.4.3.16 Site 6AL – Pre-Restoration

The river at site 6AL Pre-Restoration has steep, to overhanging banks with little vegetation. The site is located at station 41,750, roughly halfway up Kidds Island. The bank is about 37 feet tall, with a silty-sand bank and beach. Observations from 1998 indicate active and extensive erosion with exposed roots, overhanging bank, and leaning trees (Figure 5.4.3.16-1).

BSTEM runs at this site for the Pre-Restoration Condition show that under the Baseline Condition, 12.0 ft^3 of erosion occurred per foot of bank, during the 2000 to 2004 flow period prior to restoration, averaging 2.67 $ft^3/ft/y$ (Table 5.4.3-1). This results in the 12^{th} highest erosion rate for the Baseline Condition, placing it between the 50^{th} and 55^{th} percentiles of erosion rates along the reach. The modeling also indicates that all 100% (2.67 $ft^3/ft/y$) of the erosion is due directly to hydraulic processes, and none of the bank erosion is the result of larger geotechnical failures.

The Baseline Condition (Waves off) resulted in 2.64 $ft^3/ft/y$, with 2.74 $ft^3/ft/y$ for Scenario 1 (Figure 5.4.3.16-2 to Figure 5.4.3.16-3). This resulted in the following percent reductions in erosion rates: 1.2% and -2.57% for Baseline Wave off and Scenario 1 respectively. Baseline simulations with waves off showed virtually no reduction in erosion, it was concluded that boat waves have little effect on erosion processes at this site. Because of this, all of the remaining scenarios were simulated with boat waves on.

For the Baseline Condition, 95% of the total erosion occurs at flows of about 56,000 cfs or greater (Figure 5.4.3.16-4). Table 5.4.3.16-1 denotes the flows above which 95%, 50%, and 5% of all erosion occurs at the site as well as the amount of time those flows were exceeded for each year in the modeling period. The hydraulic erosion occurs across the range of flows above 56,000 cfs. Through this analysis we can conclude that those flows greater than the combined hydraulic capacity of Vernon and Northfield Mountain were accounting for most of the total erosion.

.Table 5.4.3.16-1: Flow Exceedance Calculations for Site 6L Pre-Restoration

Site 6AL	Percent of Erosion		
	95%	50%	5%
	Flow (cfs)		
Year	65,167	63,310	62,287
2000	0.10%	0.20%	0.30%
2001	1.60%	1.90%	1.90%
2002	0.10%	0.10%	0.10%
2003	0.20%	0.60%	0.60%
2004	NA	NA	NA
2005	0.70%	0.80%	0.80%
2006	0.30%	0.40%	0.50%
2007	0.50%	1.00%	1.30%
2008	0.50%	0.60%	0.70%
2009	NA	NA	0.10%
2010	NA	NA	0.10%
2011	2.20%	2.60%	3.00%
2012	NA	NA	NA
2013	NA	NA	NA
2014	0.80%	1.00%	1.10%

NA: Not Applicable since flows did not reach this value

Left bank, 1998

Figure 5.4.3.16-1 Photos at site 6AL Pre Restoration (Labeled as 1998 FRR/ECP-Site 6)

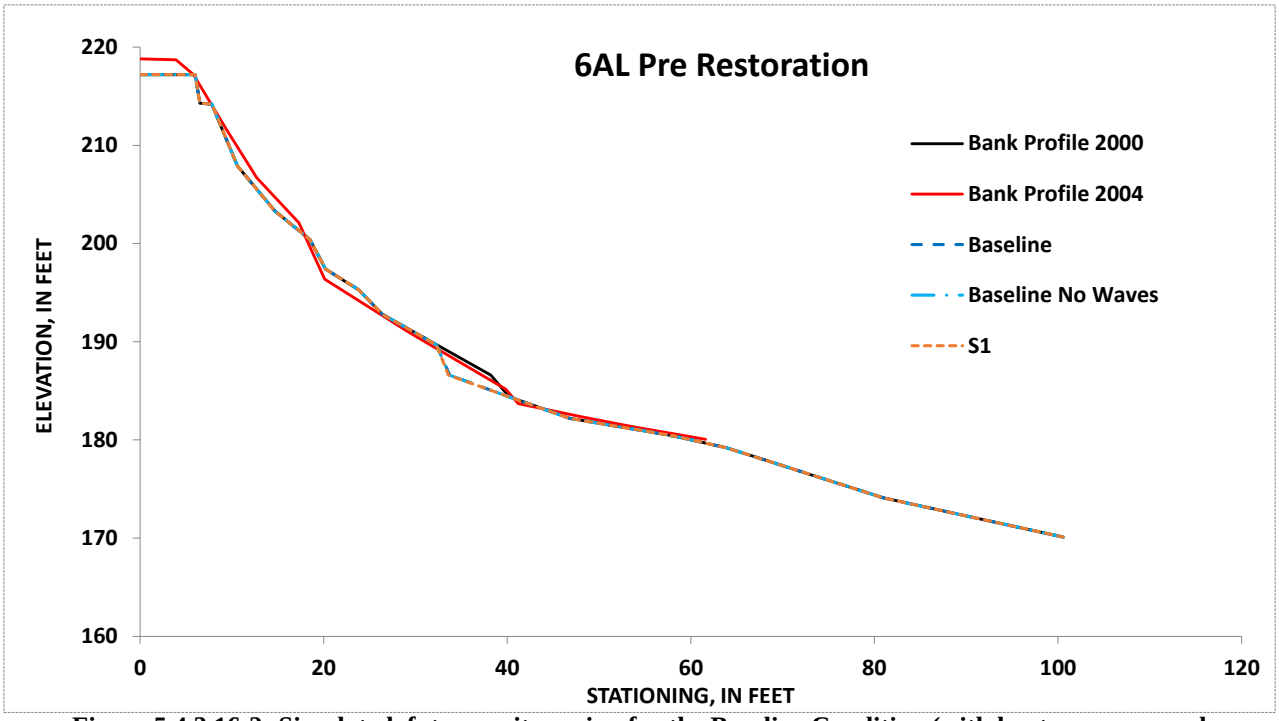

Figure 5.4.3.16-2: Simulated, future unit-erosion for the Baseline Condition (with boat waves on and off) and Scenarios 1 at site 6AL for the period 2000-2004

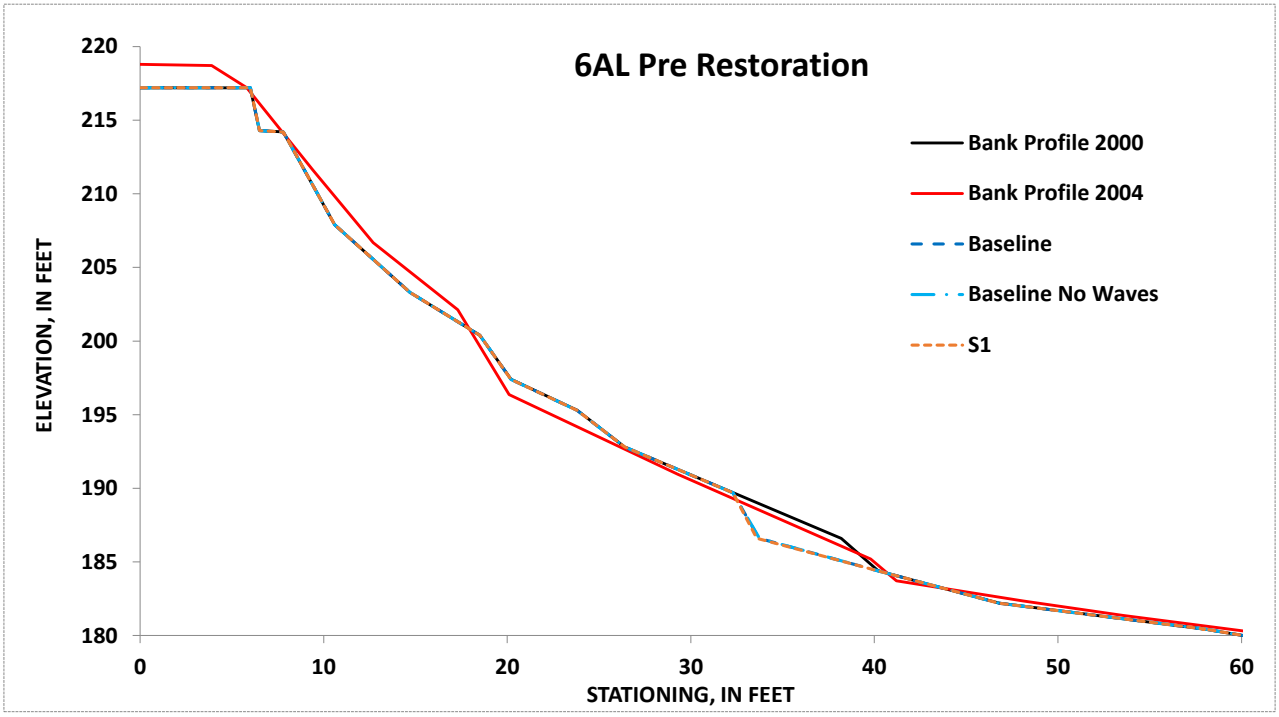

Figure 5.4.3.16-3: Simulated, future erosion for the Baseline Condition (with boat waves on and off) and Scenarios 1 at site 6AL for the period 2000-2004. Zoomed in at area of erosion for illustrative purposes.

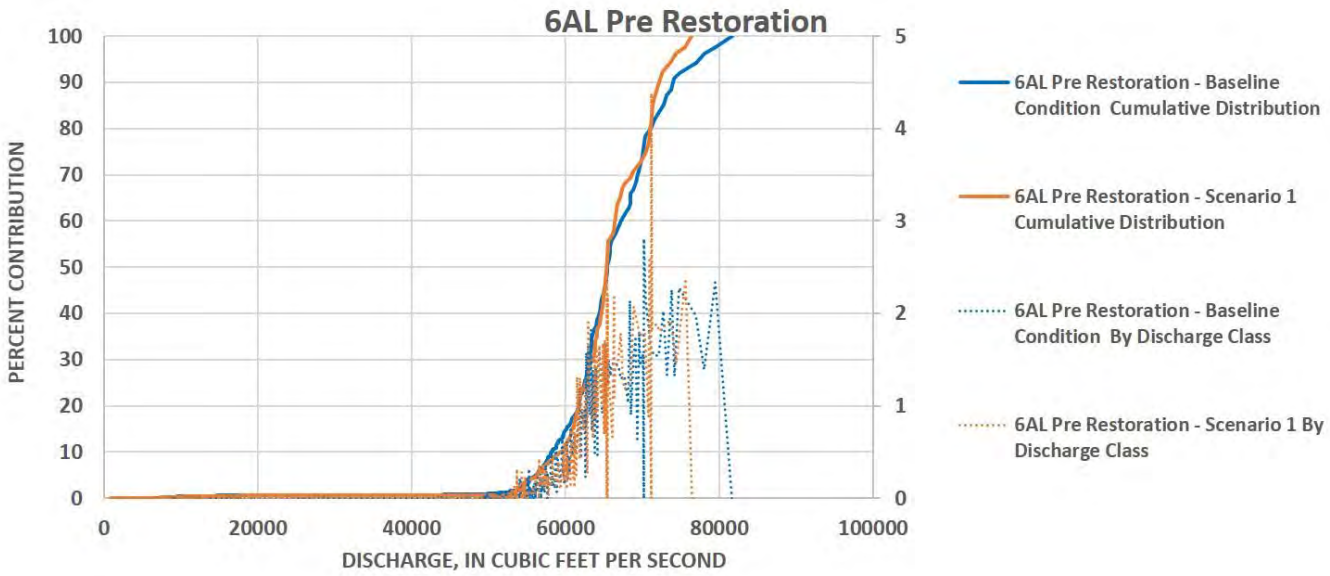

Figure 5.4.3.16-4: Simulated, percent contribution of total erosion by discharge for the Baseline Condition and Scenarios 1 at site 6AL for the period 2000-2004

5.4.3.17 Site 6AL – Post Restoration

The Post Restoration condition at site 6AL is characterized by steep, heavily vegetated banks. The bank is roughly 37 feet tall, with a rock toe (d_{50}=55 mm) and a silt loam bank. The replanted bank is heavily vegetated with large shrubs, Northern red oak, and Sugar maple (Figure 5.4.3.17-1).

BSTEM runs at this site show that the restoration activities have been highly successful with erosion rates under the Baseline Condition of 5.5E-05 ft^3 per foot of bank, during the 2004 to 2014 flow period, averaging 5.45E-06 ft^3/ft/y (Table 5.4.3-1). This results in the lowest erosion rate for the Baseline Condition. The modeling also indicates that all 100% (5.45E-06 ft^3/ft/y) of the erosion is due directly to hydraulic processes, and there are no geotechnical failures.

The Baseline Condition (Waves off) resulted in 0.00E+00 ft^3/ft/y, with 4.42E-06 ft^3/ft/y for Scenario 1 (Figure 5.4.3.17-2). Baseline simulations with waves off showed virtually no reduction in erosion, it was concluded that boat waves have little effect on erosion processes at this site. Because of this, all of the remaining scenarios were simulated with boat waves on.

For the Baseline Condition, 95% of the total erosion occurs at flows of about 62,000 cfs or greater (Figure 5.4.3.17-3). The minimal hydraulic erosion that did occur was between 62,000 cfs and 66,000 cfs. Table 5.4.3.17-1 denotes the flows above which 95%, 50%, and 5% of all erosion occurs at the site as well as the amount of time those flows were exceeded for each year in the modeling period. In summary, there is virtually no erosion at this site.

Table 5.4.3.17-1: Flow Exceedance Calculations for Site 6AL Post Restoration

Site 6AL	Percent of Erosion		
	95%	50%	5%
	Flow (cfs)		
Year	**65,167**	**63,310**	**62,287**
2000	0.10%	0.20%	0.30%
2001	1.60%	1.90%	1.90%
2002	0.10%	0.10%	0.10%
2003	0.20%	0.60%	0.60%
2004	NA	NA	NA
2005	0.70%	0.80%	0.80%
2006	0.30%	0.40%	0.50%
2007	0.50%	1.00%	1.30%
2008	0.50%	0.60%	0.70%
2009	NA	NA	0.10%
2010	NA	NA	0.10%
2011	2.20%	2.60%	3.00%
2012	NA	NA	NA
2013	NA	NA	NA
2014	0.80%	1.00%	1.10%

NA: Not Applicable since flows did not reach this value

Figure 5.4.3.17-1 Photos at site 6AL Post Restoration

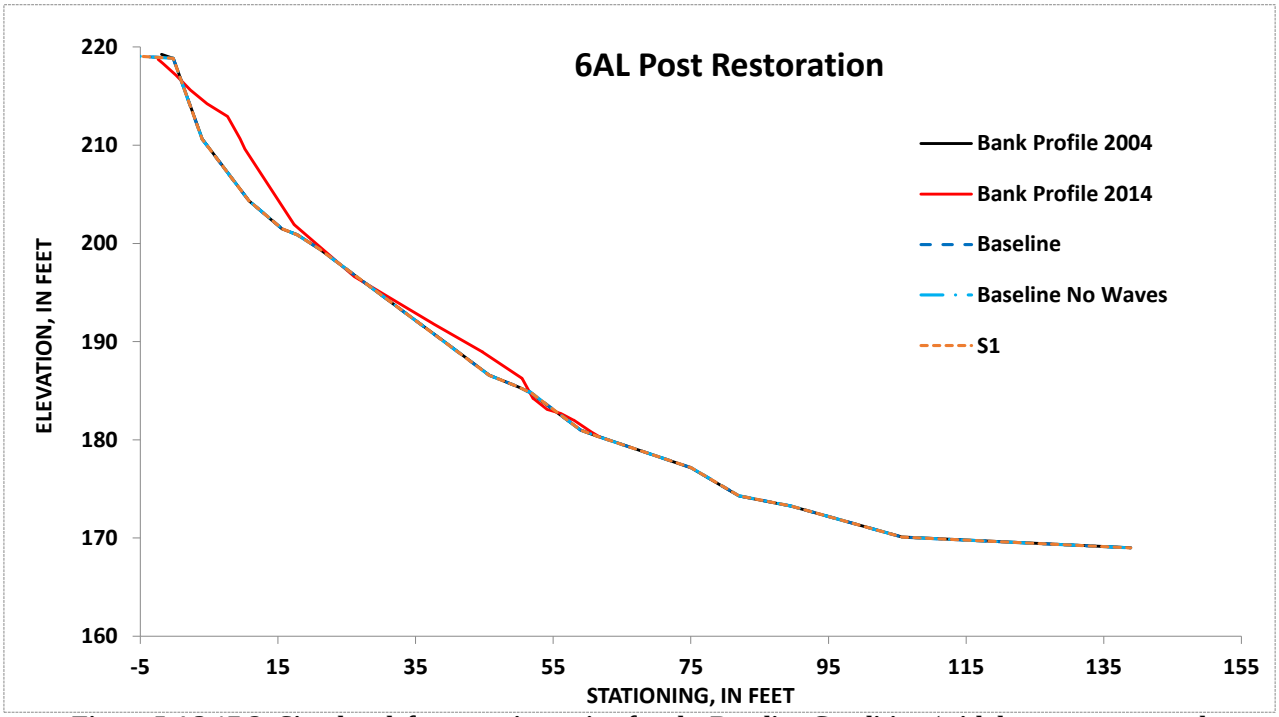

Figure 5.4.3.17-2: Simulated, future unit-erosion for the Baseline Condition (with boat waves on and off) and Scenarios 1 at site 6AL for the period 2004-2014

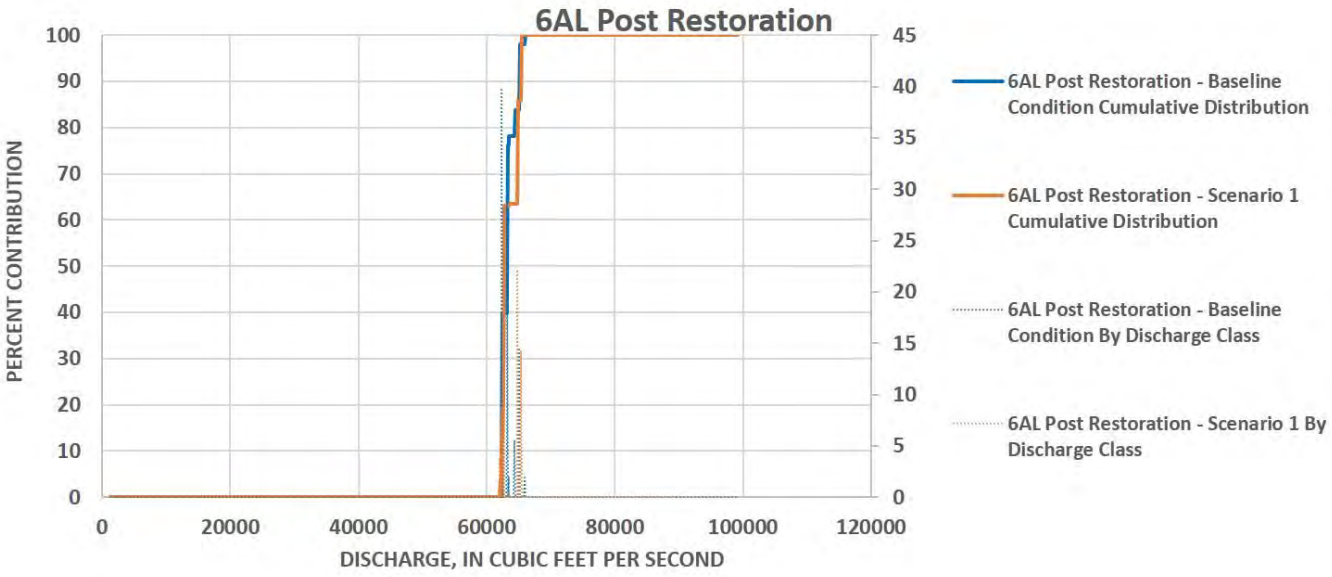

Figure 5.4.3.17-3: Simulated, percent contribution of total erosion by discharge for the Baseline Condition and Scenarios 1 at site 6AL for the period 2004-2014

5.4.3.18 Site 6AR

The river at site 6AR is across the channel from 6AL at station 41,750. The silt-loam bank is about 25 feet tall, and is characterized by steep, heavily vegetated banks and a rock toe (d_{50}=55 mm) that was part of the restoration works undertaken in 2000. The replanted bank is heavily vegetated with large shrubs, Northern red oak, and Sugar maple. As 6AR was restored in 2000, no Pre-Restoration simulation was conducted for this site (Figure 5.4.3.18-1).

BSTEM runs for the Post Restoration Condition at this site show that under the Baseline Condition, 0.295 ft^3 of erosion occurred per foot of bank, during the 2000 to 2014 flow period after restoration, averaging 0.0209 $ft^3/ft/y$ (Table 5.4.3-1). This results in the 4th lowest erosion rate for the Baseline Condition, placing it below the 5th percentile of erosion rates along the reach. The modeling also indicates that all 100% (0.021 $ft^3/ft/y$) of the erosion is due directly to hydraulic processes, and none of the bank erosion is the result of larger, geotechnical failures.

The Baseline Condition (Waves off) resulted in 0.000201 $ft^3/ft/y$, with 0.0204 $ft^3/ft/y$ for Scenario 1 (Figure 5.4.3.18-2). This resulted in a reduction in erosion of 2.0% for Scenario 1. Baseline simulations with waves off showed a large % reduction in erosion but overall the amount of erosion at 6AR is so small that it was concluded that boat waves have little effect on erosion processes at this site. Because of this, all of the remaining scenarios were simulated with boat waves on.

Although the vast majority of the simulated bank erosion occurs at flows within the combined operational range of Vernon Dam and Northfield Mountain, with 95% of the total erosion for the Baseline Condition occurring at flows of 7,000 cfs or greater (Figure 5.4.3.18-3), this does not indicate that Project operations are causing significant bank erosion. Erosion rates here are very low and represent hydraulic scour of deposited material at the bank toe. Observations indicate that there is a net deposition of material here from fluvial deposition. Table 5.4.3.18-1 denotes the flows above which 95%, 50%, and 5% of all erosion occurs at the site as well as the amount of time those flows were exceeded for each year in the modeling period.

Table 5.4.3.18-1: Flow Exceedance Calculations for Site 6AR

Site 6AR	Percent of Erosion		
	95%	50%	5%
	Flow (cfs)		
Year	**29,662**	**11,191**	**7,051**
2000	8.80%	33.40%	52.70%
2001	7.10%	12.50%	34.70%
2002	5.70%	29.60%	51.00%
2003	10.40%	39.90%	60.30%
2004	4.40%	28.00%	59.40%
2005	14.50%	45.90%	66.40%
2006	13.60%	62.40%	80.30%
2007	7.30%	34.70%	60.70%
2008	15.50%	53.80%	79.80%
2009	6.30%	58.70%	76.50%
2010	10.00%	50.90%	67.30%
2011	18.60%	58.80%	72.70%
2012	2.60%	35.70%	53.00%
2013	5.50%	40.90%	62.00%
2014	9.40%	42.10%	63.10%

NA: Not Applicable since flows did not reach this value

Figure 5.4.3.18-1 Photos at site 6AR Post Restoration

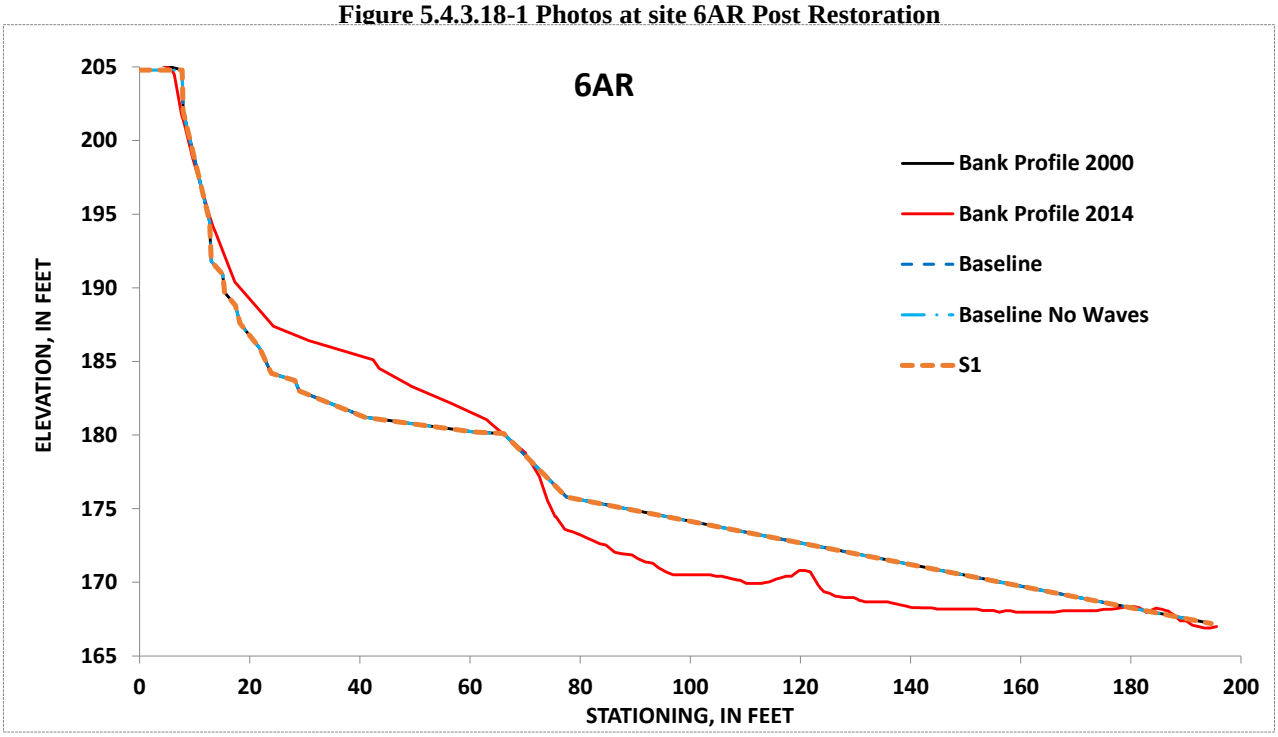

Figure 5.4.3.18-2: Simulated, future unit-erosion for the Baseline Condition (with boat waves on and off) and Scenarios 1 at site 6AR for the period 2000-2014

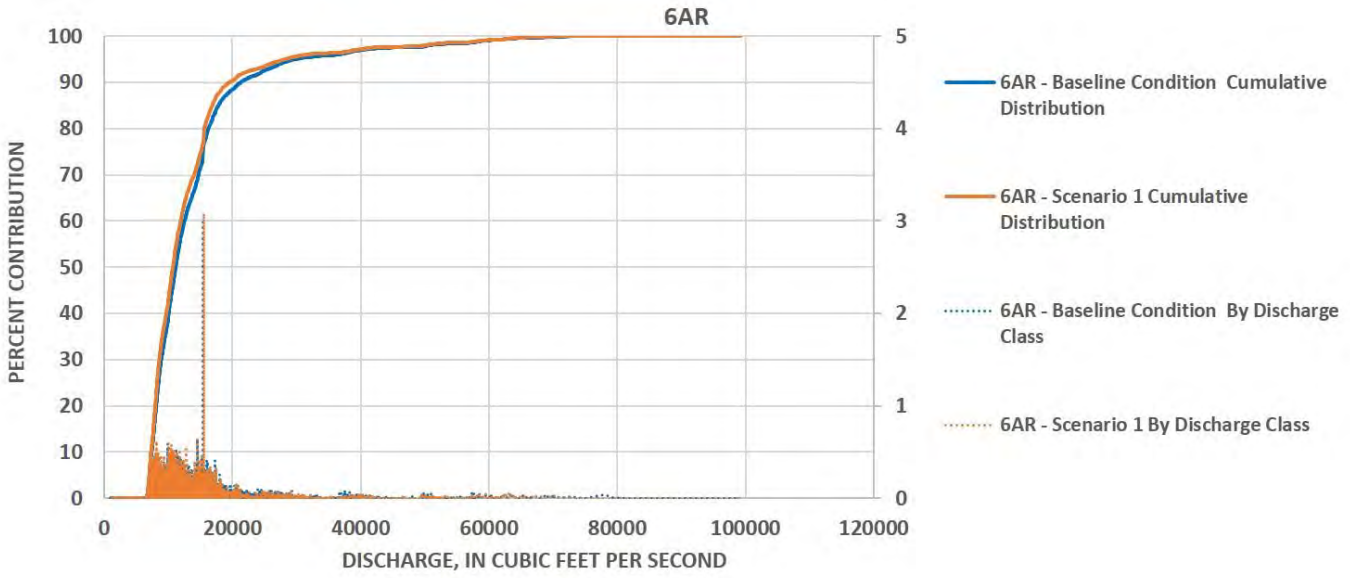

Figure 5.4.3.18-3: Simulated, percent contribution of total erosion by discharge for the Baseline Condition and Scenarios 1 at site 6AR for the period 2000-2014

5.4.3.19 Site 119BL

The river at site 119BL (station 41,000) has steep, partially vegetated banks, located near the downstream limit of Kidds Island. The bank is just under 30 feet tall, with silty-sand toe material with a d_{50} of 0.068 mm. Large Ashleaf maples spread out over most of the upper bank, with short grasses under the canopy. The lower bank, though highly vegetated, shows signs of erosion, with exposed roots, and soft saturated soils. No historical cross sections exist for this site. As a result, the 2014 survey was used as the initial geometry for the model runs (Figure 5.4.3.19-1).

BSTEM runs at this site show that under the Baseline Condition 86.1 ft^3 of erosion occurred per feet of bank, during the 2000 to 2014 flow period modeled, averaging 5.88 $ft^3/ft/y$ (Table 5.4.3-1). This results in the 6th highest erosion amongst the model sites, placing it between the 75th and 80th percentiles of erosion rates along the reach. The modeling also indicates that roughly 73% (4.26 $ft^3/ft/y$) of erosion is due to hydraulic processes, whereas the other 27% (1.62 $ft^3/ft/y$) is due to geotechnical processes and mass failures. This is also shown in the Percent Contribution of Total Erosion by Discharge plot for Site 119BL (Figure 5.4.3.19-4), as the graph has a very gradual smooth shape, with few large spikes indicating mass wasting.

The Baseline Condition (Waves off) resulted in 5.72 $ft^3/ft/y$, with 5.79 $ft^3/ft/y$ for Scenario 1 (Figure 5.4.3.19-2 and Figure 5.4.3.19-3). This resulted in the following percent reduction in erosion rates as compared to the Baseline Condition: 2.61% and 1.47%, for Baseline Wave off and Scenario 1. As the Baseline Condition (Waves off) scenario illustrated a very little reduction in erosion, it was concluded that boat waves are not having a significant impact on bank stability, and the remaining scenarios were not considered with boat waves off.

During the Baseline Condition, 83% of the total erosion occurs at flows of 37,000 cfs or greater (Figure 5.4.3.19-4). The plot shows erosion throughout the range of flows above 37,000 cfs, greater than the combined hydraulic capacity of Vernon and Northfield Mountain. This supports the conclusion that naturally occurring high flows are the biggest factor in bank erosion at Site 119BL. The resulting bank geometry is such that a 4-foot vertical face is developed that could continue to retreat, leading to collapse of the upper part of the bank in the future (Figure 5.4.3.19-2 and Figure 5.4.3.19-3). Moderate flows (17,000 – 37,000 cfs) contribute 13.1% of erosion. Evaluating the moderate flow contribution to the total erosion it was determined that Northfield Mountain operations occurred 7% of the time over the modeled period of record. This equates to 0.9% of the total erosion during the moderate flows. The Northfield Mountain contribution was adjusted by this 0.9% to better estimate contributions from the Project and resulting in a total erosion of 2.4%.

Table 5.4.3.19-1 denotes the flows above which 95%, 50%, and 5% of all erosion occurs at the site as well as the amount of time those flows were exceeded for each year in the modeling period.

Table 5.4.3.19-1: Flow Exceedance Calculations for Site 119BL

Site 119BL	Percent of Erosion		
	95%	50%	5%
	Flow (cfs)		
Year	**70,557**	**53,969**	**24,796**
2000	0.10%	1.30%	14.10%
2001	0.90%	2.90%	7.80%
2002	NA	0.60%	10.00%
2003	0.10%	1.90%	16.60%
2004	NA	0.30%	7.70%
2005	0.50%	2.40%	20.70%
2006	0.20%	1.40%	19.20%
2007	0.20%	2.70%	12.80%
2008	0.30%	3.60%	22.80%
2009	NA	1.10%	14.70%
2010	NA	1.20%	15.00%
2011	1.10%	4.70%	24.10%
2012	NA	NA	7.20%
2013	NA	0.10%	11.40%
2014	0.20%	2.20%	14.80%

NA: Not Applicable since flows did not reach this value

Figure 5.4.3.19-1 Photos at site 119BL

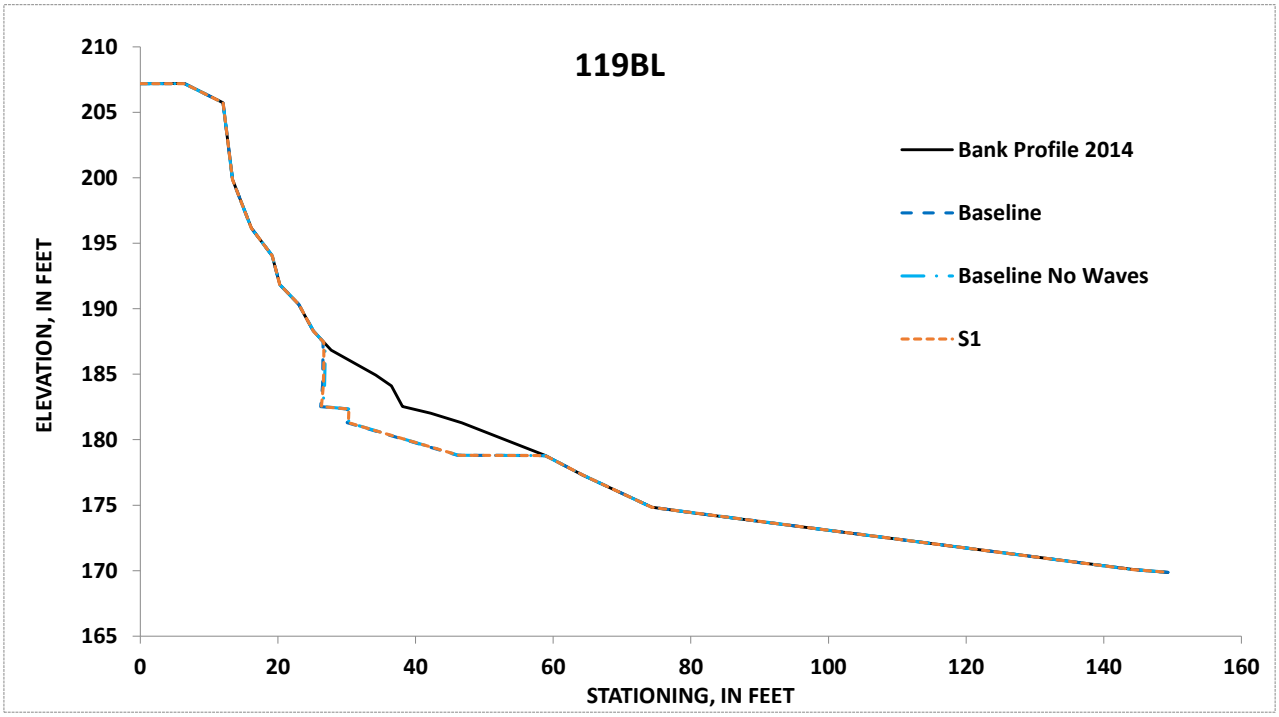

Figure 5.4.3.19-2: Simulated, future unit-erosion The Baseline Condition and Scenario 1(both with boat waves on and boat waves off) at site 119BL for the period 2000-2014

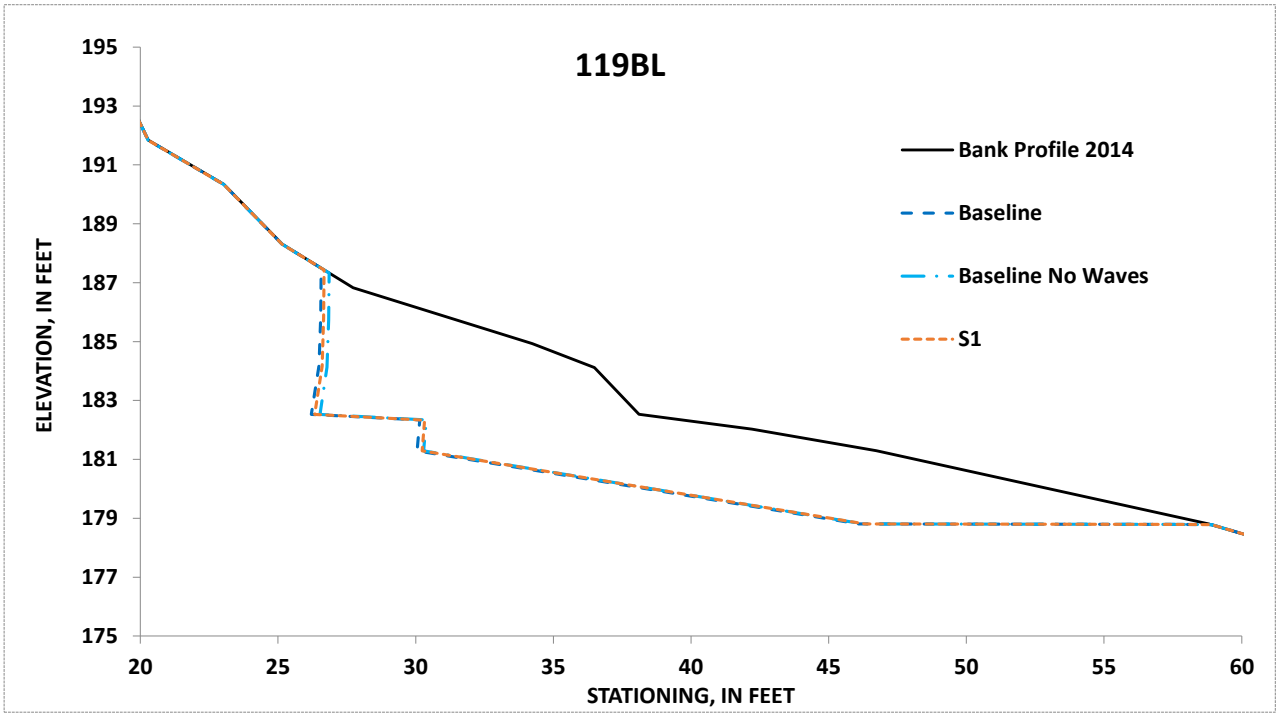

Figure 5.4.3.19-3: Simulated, future unit-erosion The Baseline Condition and Scenario 1 (both with boat waves on and boat waves off) at site 119BL for the period 2000-2014. Zoomed in at area of erosion for illustrative purposes

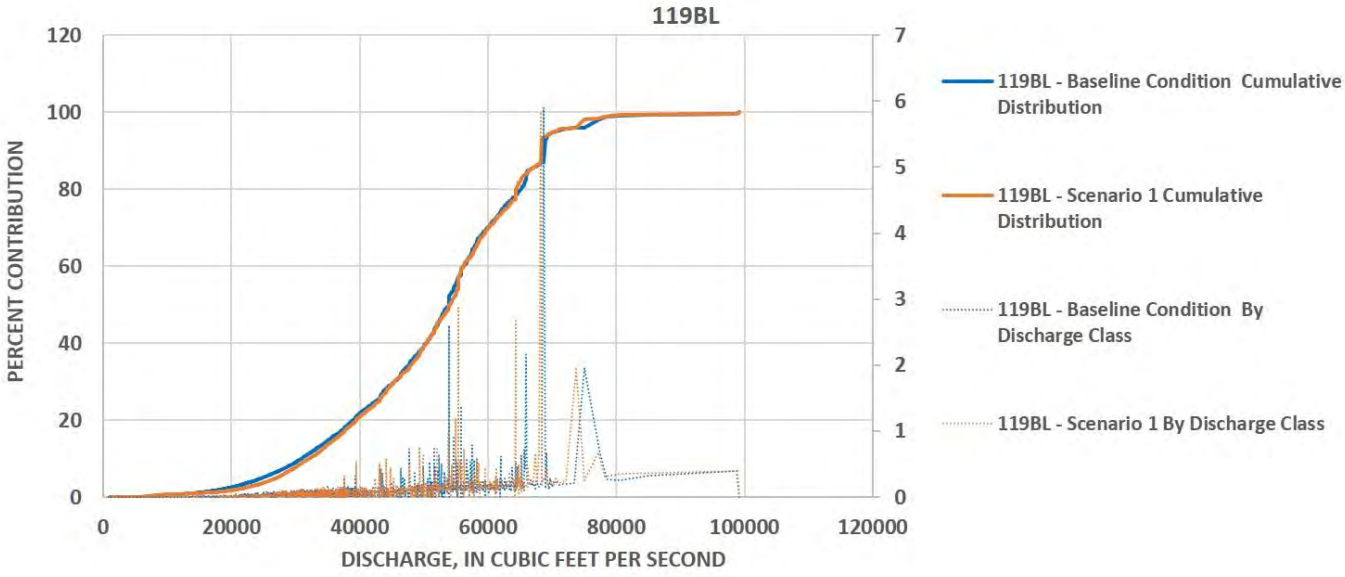

Figure 5.4.3.19-4: Simulated, future percent contribution of total erosion by discharge for Baseline Condition and Scenario 1 at site 119BL for the period 2000-2014

5.4.3.20 Site 7L

The river at site 7L has steep, partially vegetated banks. Located at station 37,500, between Kidds Island and the Northfield Mountain Tailrace, the bank is roughly 28 feet tall, with a sandy toe and a sandy-loam upper bank. The bank slope is highly vegetated with American basswood and Northern red oak. The bank top is similarly vegetated with the addition of small grasses growing under the canopy (Figure 5.4.3.20-1).

BSTEM runs at this site show that under the Baseline Condition, 62.9 ft^3 of erosion occurred per foot of bank, during the 2000 to 2014 flow period, averaging 4.29 $ft^3/ft/y$ (Table 5.4.3-1). This results in the 9th highest erosion rate for the Baseline Condition, placing it between the 65th and 70th percentiles of erosion rates along the reach. The modeling also indicates that roughly 81% (3.48 $ft^3/ft/y$) of the erosion is due directly to hydraulic processes, whereas the other 19% (0.81 $ft^3/ft/y$) is the result of geotechnical processes and associated mass failures.

The Baseline Condition (Waves off) resulted in 4.24 $ft^3/ft/y$, with 4.13 $ft^3/ft/y$ for Scenario 1 (Figure 5.4.3.20-2 to Figure 5.4.3.20-3). This resulted in the following percent reductions in erosion rates: 1.15% and 3.89% for Baseline Wave off and Scenario 1 respectively. As the Baseline Condition (Waves off) scenario illustrated only a 1% reduction in erosion from the waves on condition, it is clear that boat waves have little to no effect on erosion rates at this site. Because of this, the remaining scenarios were not considered with boat waves off.

For the Baseline Condition, 95% of the total erosion occurs at flows of about 47,700 cfs or greater (Figure 5.4.3.20-4). Table 5.4.3.20-1 denotes the flows above which 95%, 50%, and 5% of all erosion occurs at the site as well as the amount of time those flows were exceeded for each year in the modeling period. Hydraulic erosion is fairly consistent across the range of flows above 40,000 cfs, with 75% occurring between about 40,000 cfs and 80,000 cfs, and 25% of the total erosion happening above 80,000 cfs. Through this analysis we can conclude that high flows greater than the combined hydraulic capacity of Vernon Dam and Northfield Mountain are accounting for most of the total erosion.

Table 5.4.3.20-1: Flow Exceedance Calculations for Site 7L

Site 7L	Percent of Erosion		
	95%	50%	5%
	Flow (cfs)		
Year	**98,753**	**65,338**	**47,731**
2000	NA	0.20%	2.30%
2001	NA	1.40%	3.70%
2002	NA	0.10%	1.20%
2003	NA	0.50%	3.20%
2004	NA	NA	0.70%
2005	NA	0.70%	4.50%
2006	NA	0.40%	2.60%
2007	NA	0.80%	3.30%
2008	NA	0.90%	5.80%
2009	NA	0.10%	2.00%
2010	NA	0.10%	2.80%
2011	0.20%	2.20%	6.50%
2012	NA	NA	0.20%
2013	NA	0.10%	0.40%
2014	NA	0.80%	2.70%

NA: Not Applicable since flows did not reach this value

Figure 5.4.3.20-1 Photos at site 7L

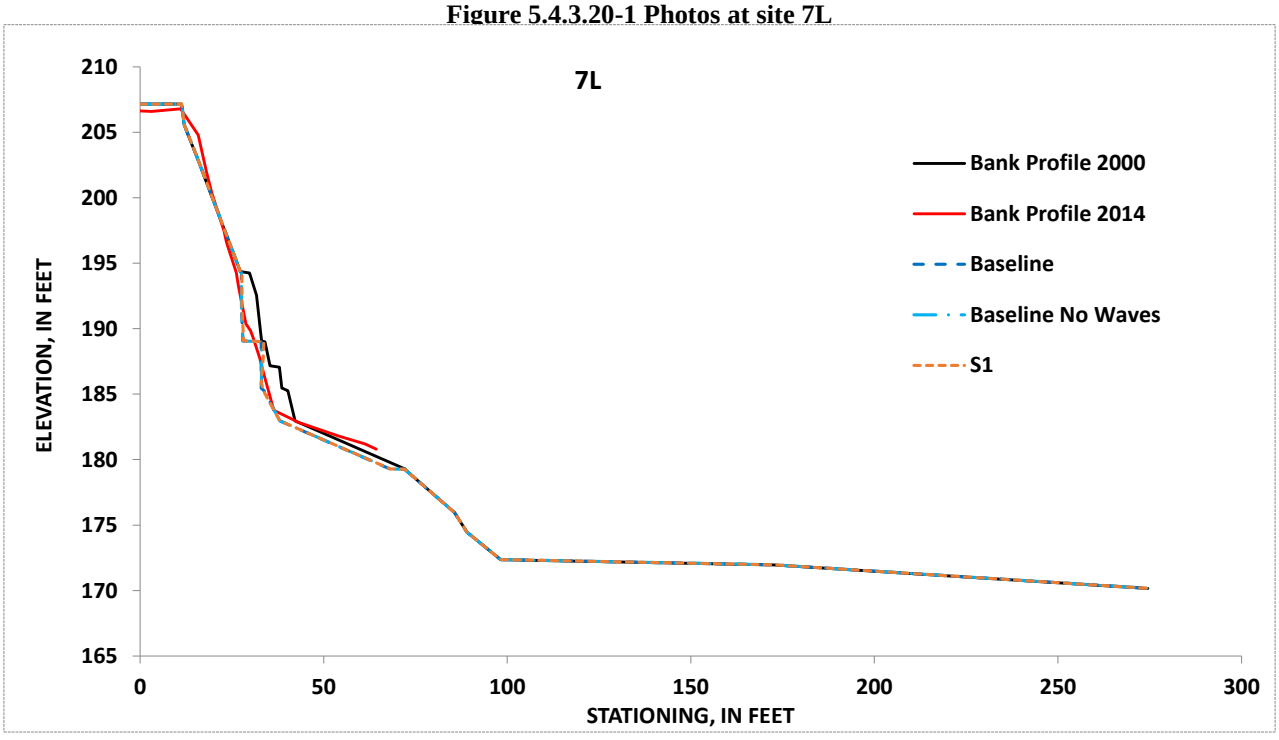

Figure 5.4.3.20-2: Simulated, future unit-erosion for the Baseline Condition (with boat waves on and off) and Scenario 1 at site 7L for the period 2000-2014

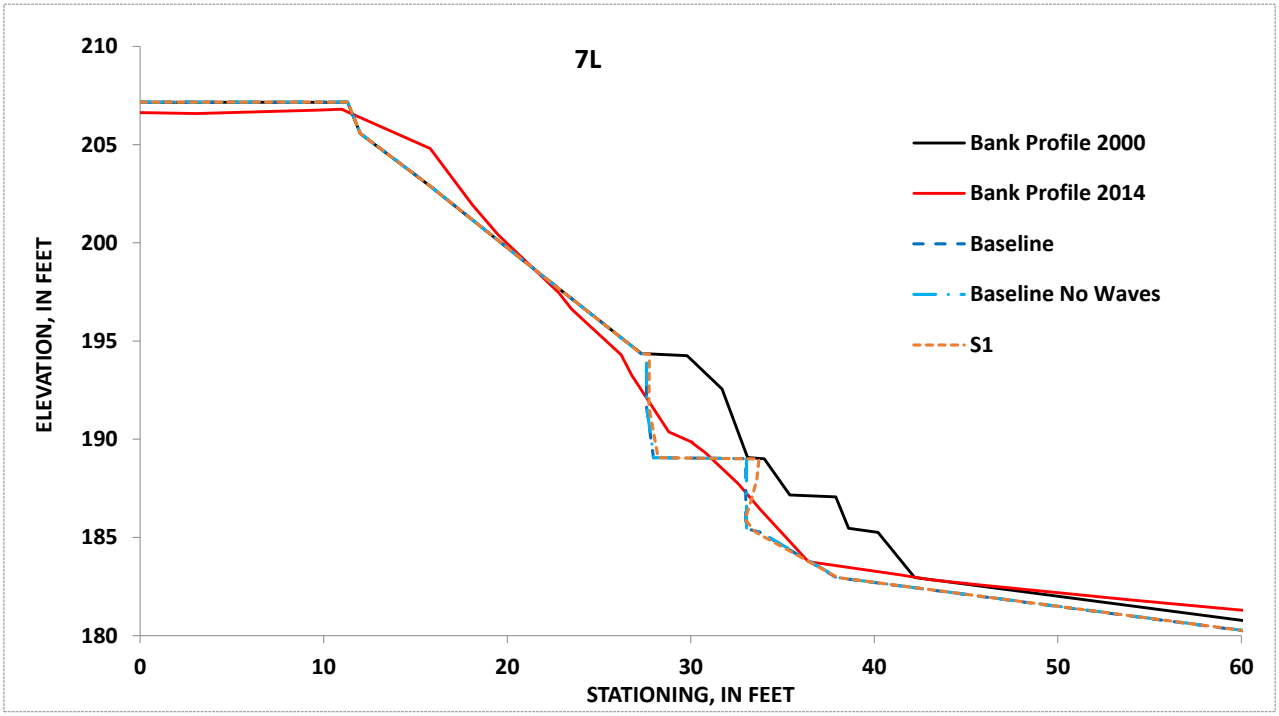

Figure 5.4.3.20-3: Simulated, future erosion for the Baseline Condition (with boat waves on and off) and Scenario 1 at site 7L for the period 2000-2014. Zoomed in at area of erosion for illustrative purposes

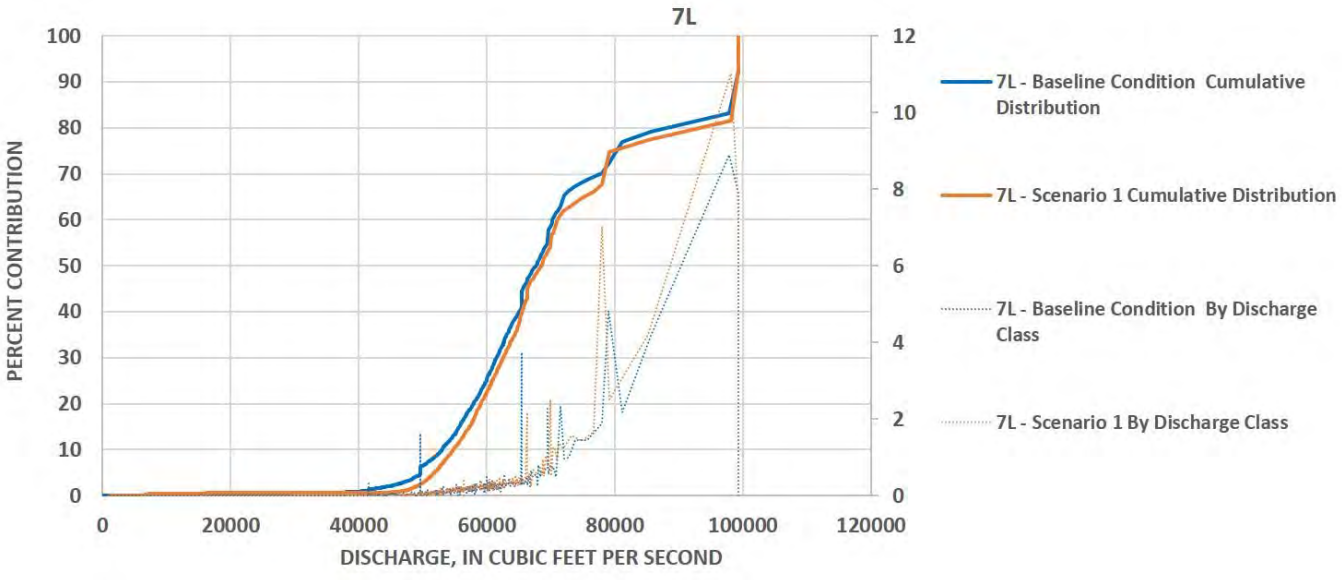

Figure 5.4.3.20-4: Simulated, percent contribution of total erosion by discharge for the Baseline Condition and Scenario 1 at site 7L for the period 2000-2014

5.4.3.21 Site 7R

Site 7R (station 37,500) is located between Kidds Island and the Northfield Mountain Tailrace, just upstream of Dry Brook. The site has steep, partially vegetated banks that are roughly 24 feet tall, with a sandy toe and a sandy-loam upper bank. The bank is vegetated with 20 to 50 year-old Hemlock, Pine, and Silver maple. There was a significant amount of bare soil noted on the upper bank, likely due to the dense tree canopy (Figure 5.4.3.21-1).

BSTEM runs at this site show that under the Baseline Condition, 30.1 ft^3 of erosion occurred per foot of bank, during the 2000 to 2014 flow period, averaging 2.06 $ft^3/ft/y$ (Table 5.4.3-1). This results in the 15th highest erosion rate for the Baseline Condition, placing it between the 40th and 45th percentiles of erosion rates along the reach. The modeling also indicates that all 100% (2.06 $ft^3/ft/y$) of the erosion is due directly to hydraulic processes, and none of the bank erosion is the result of larger, geotechnical failures.

The Baseline Condition (Waves off) resulted in 2.04 $ft^3/ft/y$, with 2.05 $ft^3/ft/y$ for Scenario 1 (Figure 5.4.3.21-2 to Figure 5.4.3.21-3). This resulted in reductions in erosion rates of 1.0% and 0.53% for Baseline Wave off and Scenario 1 respectively. As Baseline simulations with waves off showed virtually no reduction in erosion, it was concluded that boat waves have little effect on erosion processes at this site.

To further support the important role of high flows in bank-erosion rates, for the Baseline Condition, 95% of the total erosion occurs at flows of about 53,500 cfs or greater (Figure 5.4.3.21-4). Table 5.4.3.21-1 denotes the flows above which 95%, 50%, and 5% of all erosion occurs at the site as well as the amount of time those flows were exceeded for each year in the modeling period. The hydraulic erosion looks to be fairly consistent across the range of flows above 40,000 cfs, with 75% occurring between 40,000 cfs and 75,000 cfs, and 25% of the total erosion occurring above 75,000 cfs. Through this analysis we can conclude that those flows greater than the combined hydraulic capacity of Vernon and Northfield Mountain are accounting for most of the total erosion.

Table 5.4.3.21-1: Flow Exceedance Calculations for Site 7R

Site 7R	Percent of Erosion		
	95%	50%	5%
	Flow (cfs)		
Year	98,463	65,880	53,614
2000	NA	0.20%	1.30%
2001	NA	1.40%	3.00%
2002	NA	0.10%	0.60%
2003	NA	0.40%	2.00%
2004	NA	NA	0.30%
2005	NA	0.60%	2.50%
2006	NA	0.30%	1.50%
2007	NA	0.70%	2.70%
2008	NA	0.80%	3.80%
2009	NA	0.10%	1.10%
2010	NA	0.10%	1.30%
2011	0.20%	2.00%	4.80%
2012	NA	NA	NA
2013	NA	0.10%	0.10%
2014	NA	0.70%	2.20%

NA: Not Applicable since flows did not reach this value

Figure 5.4.3.21-1 Photos at site 7R

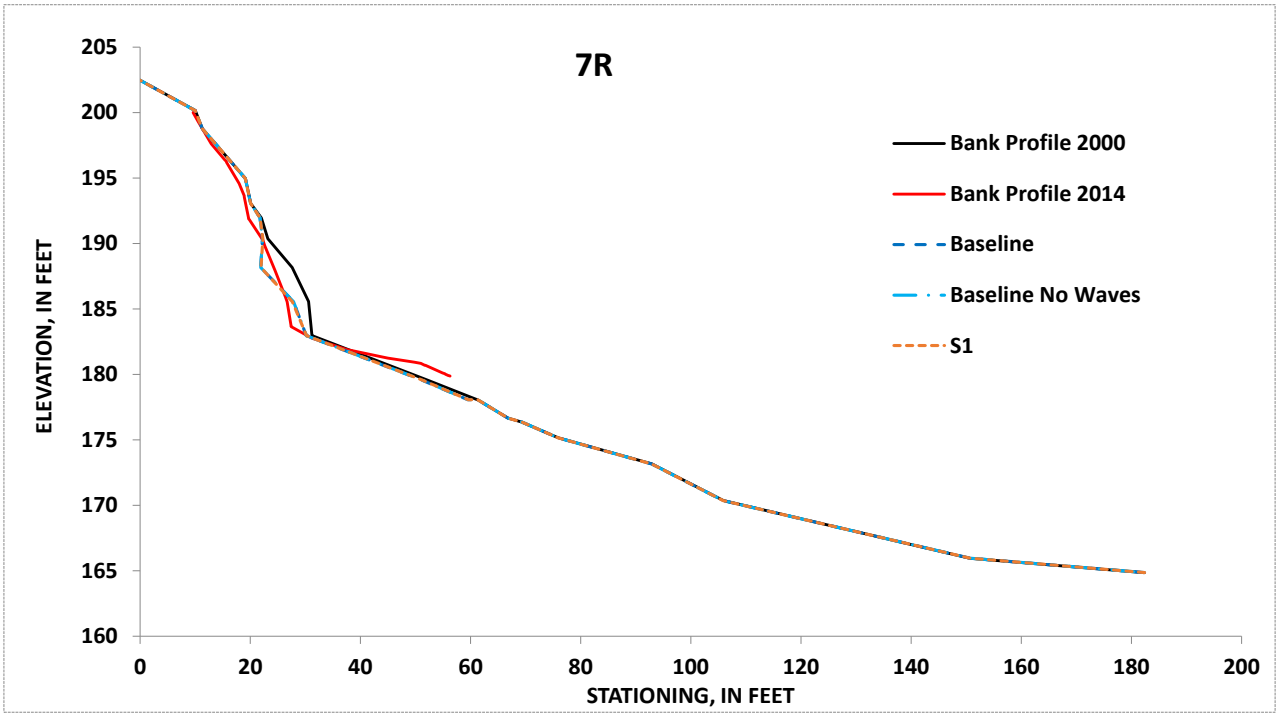

Figure 5.4.3.21-2: Simulated, future unit-erosion for the Baseline Condition (with boat waves on and off) and Scenario 1 at site 7R for the period 2000-2014

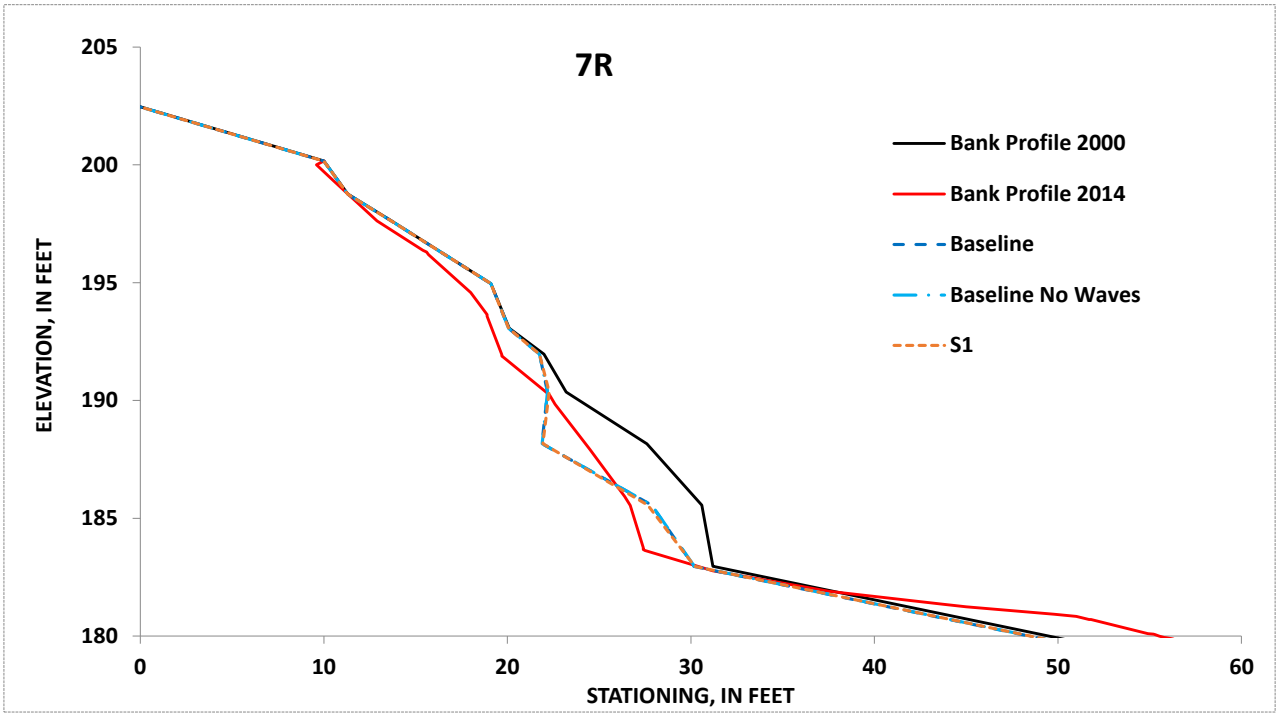

Figure 5.4.3.21-3: Simulated, future erosion for the Baseline Condition (with boat waves on and off) and Scenario 1 at site 7R for the period 2000-2014. Zoomed in at area of erosion for illustrative purposes

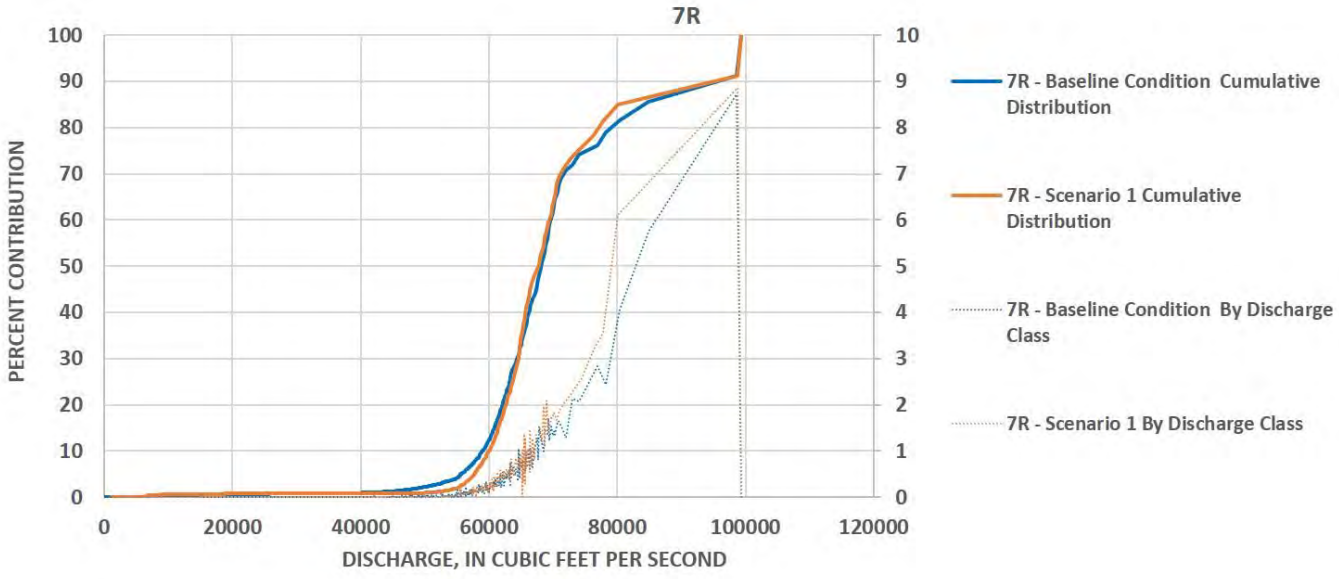

Figure 5.4.3.21-4: Simulated, percent contribution of total erosion by discharge for the Baseline Condition and Scenario 1 at site 7R for the period 2000-2014

5.4.3.22 Site 8BL

The river at site 8BL (station 32,750) has steep, vegetated banks and is located between Kidds Island and the Northfield Mountain Tailrace, just upstream of Pine Meadow Brook. The bank is roughly 24 feet tall, with a sandy toe and a sandy-loam upper bank. The bank is highly vegetated with 20 to 50 year old Hemlock, Pine, and Silver maple. There was a significant amount of bare soil noted, likely due to the dense tree canopy (Figure 5.4.3.22-1).

BSTEM runs at this site show that under the Baseline Condition, 6.09 ft^3 of erosion occurred per foot of bank, during the 2000 to 2014 flow period, averaging 0.43 $ft^3/ft/y$ (Table 5.4.3-1). This results in the 11th lowest erosion rate for the Baseline Condition, placing it between the 15th and 20th percentiles of erosion rates along the reach. The modeling also indicates that all 100% (0.428 $ft^3/ft/y$) of the erosion is due directly to hydraulic processes, and none of the bank erosion is the result of geotechnical processes and associated mass failures.

The Baseline Condition (Waves off) resulted in 0.43 $ft^3/ft/y$, with 0.40 $ft^3/ft/y$ for Scenario 1(Figure 5.4.3.22-2 to Figure 5.4.3.22-3). This resulted in the following percent differences in erosion rates relative to the Baseline Condition: 0.09% and 6.6%, for Baseline Wave off and Scenario 1, respectively. As the Baseline Condition (Waves off) scenario illustrated a very little reduction in erosion, it was concluded that boat waves are not having a significant impact on bank stability, and the remaining scenarios were not considered with boat waves off.

The important role of high flows in bank-erosion rates can be seen in the Baseline Condition erosion results, 93% of the total erosion occurs at flows of 37,000 cfs or greater (Figure 5.4.3.22-4). Table 5.4.3.22-1 denotes the flows above which 95%, 50%, and 5% of all erosion occurs at the site as well as the amount of time those flows were exceeded for each year in the modeling period. Through this analysis we can conclude that those flows greater than the combined hydraulic capacity of Vernon and Northfield Mountain are accounting for most of the total erosion with a small percent of erosion (6.6%) contributed by Northfield Mountain Project operations.

Table 5.4.3.22-1: Flow Exceedance Calculations for Site 8BL

Site 8BL	Percent of Erosion		
	95%	50%	5%
	Flow (cfs)		
Year	**84,451**	**84,138**	**77,997**
2000	NA	NA	NA
2001	0.10%	0.10%	0.30%
2002	NA	NA	NA
2003	NA	NA	NA
2004	NA	NA	NA
2005	NA	NA	0.10%
2006	NA	NA	NA
2007	NA	NA	NA
2008	NA	NA	0.10%
2009	NA	NA	NA
2010	NA	NA	NA
2011	0.40%	0.40%	0.60%
2012	NA	NA	NA
2013	NA	NA	NA
2014	NA	NA	NA

NA: Not Applicable since flows did not reach this value

Figure 5.4.3.22-1 Photos at site 8BL

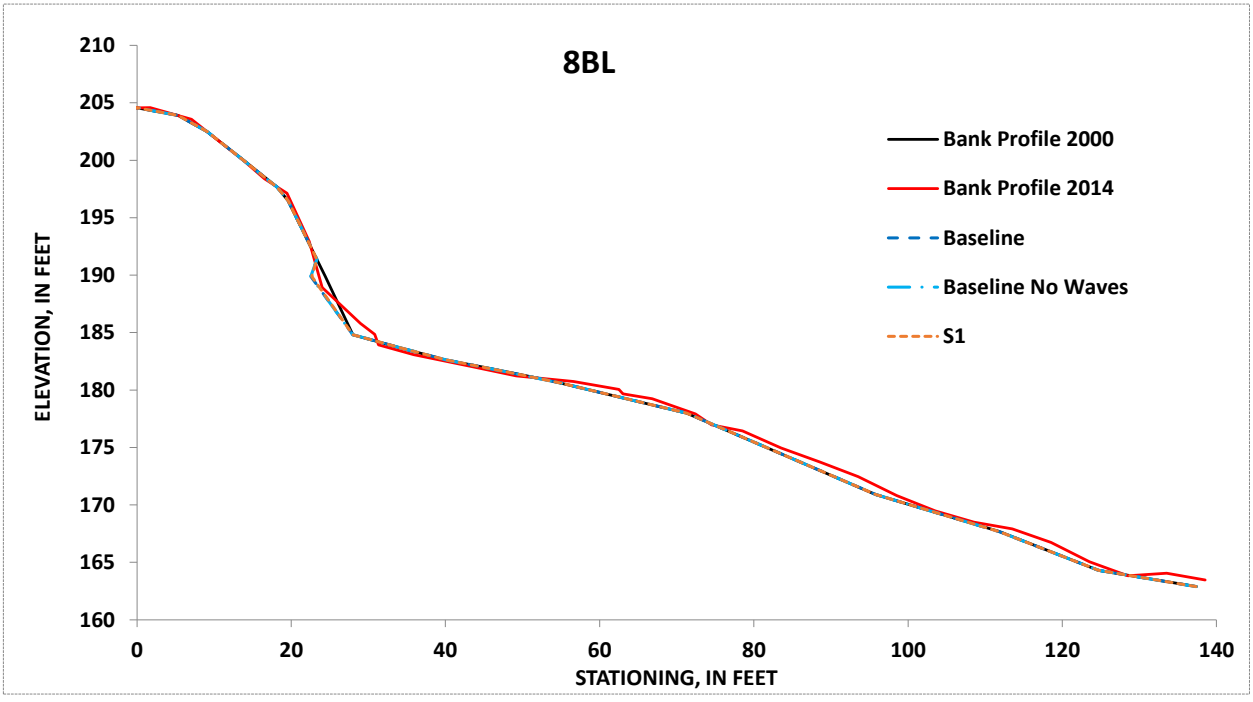

Figure 5.4.3.22-2: Simulated, future unit-erosion for the Baseline Condition (with boat waves on and off) and Scenario 1 at site 8BL for the period 2000-2014

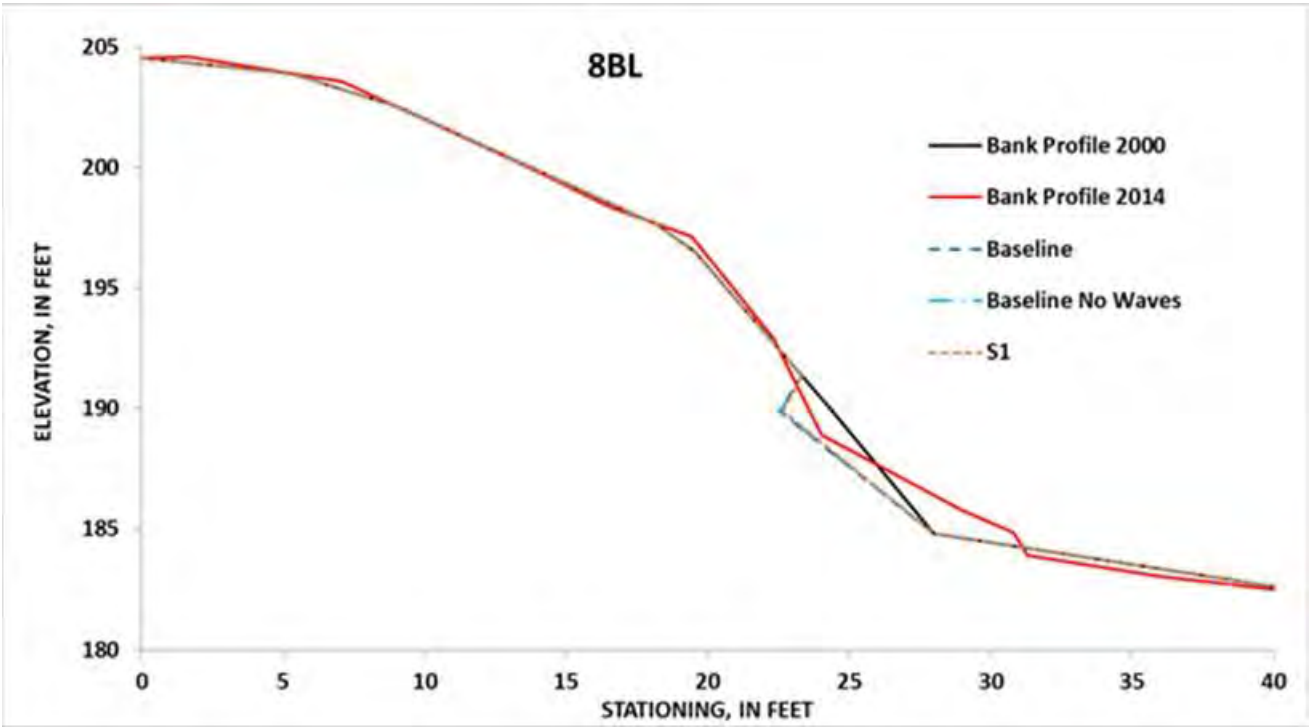

Figure 5.4.3.22-3: Simulated, future erosion for the Baseline Condition (with boat waves on and off) and Scenario 1 at site 8BL for the period 2000-2014. Zoomed in at area of erosion for illustrative purposes

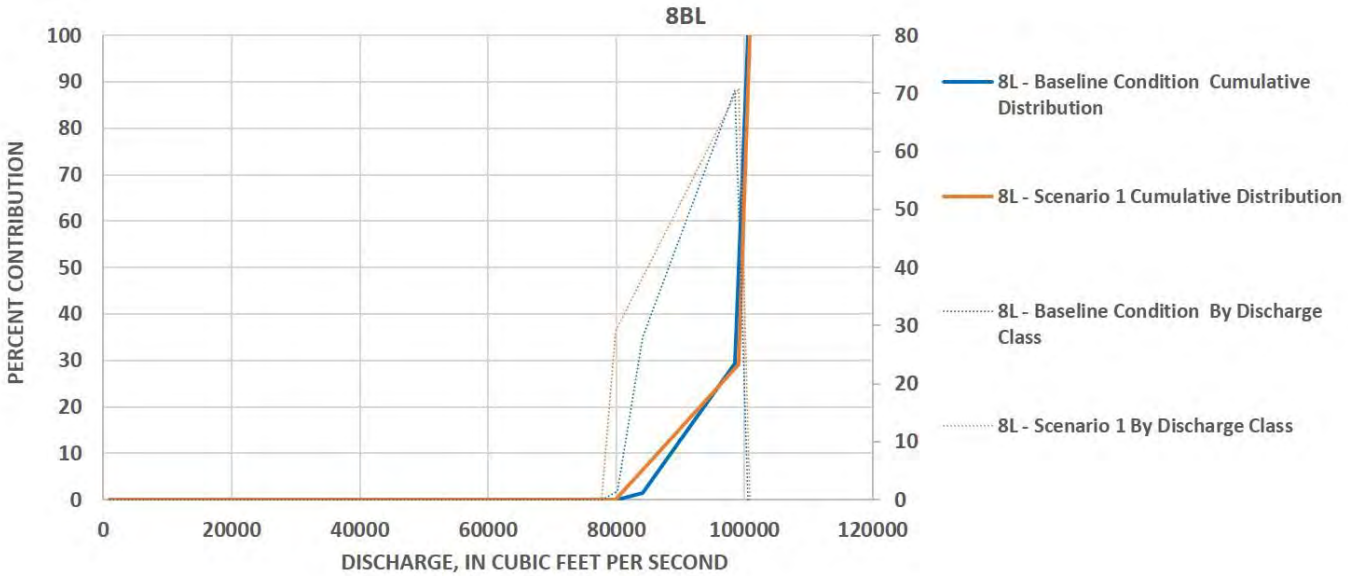

Figure 5.4.3.22-4: Simulated, percent contribution of total erosion by discharge for the Baseline Condition and Scenario 1 at site 8BL for the period 2000-2014

5.4.3.23 Site 8BR – Pre-Restoration

The river at site 8BR (station 32,750) has steep, sparsely vegetated banks and is located between Kidds Island and Northfield Mountain Tailrace, just upstream of Pine Meadow Brook. The bank is roughly 19 feet tall, with a sandy toe and a sandy-loam upper bank. The bank is thinly vegetated with Northern red oak and Green ash. There was also significant amount of bare soil noted (Figure 5.4.3.23-1).

BSTEM runs for the Pre-Restoration Condition at this site show that under the Baseline Condition, 89.6 ft^3 of erosion occurred per foot of bank, during the 2000 to 2012 flow period prior to restoration, averaging 7.42 $ft^3/ft/y$ (Table 5.4.3-1). This results in the 4th highest erosion rate for the Baseline Condition, placing it between the 85th and 90th percentiles of erosion rates along the reach. The modeling also indicates that roughly 30% (2.23 ft^3/y) of the erosion is due to hydraulic processes, whereas the other 70% (5.19 ft^3/y) is the result of geotechnical processes and associated mass failures.

The Baseline Condition (Waves off) resulted in 7.39 $ft^3/ft/y$, with 1.95 $ft^3/ft/y$ for Scenario 1 (Figure 5.4.3.23-2 to Figure 5.4.3.23-3). This resulted in the following percent reductions in erosion rates: 0.28% and 73.6% for Baseline Wave off and Scenario 1, respectively. The drastic difference between bank-erosion rates for the Baseline Condition and Scenarios 1, can be attributed to what happened at 8R during Hurricane Irene in 2011. As this site is in the Northfield Mountain reach, it appears that a significant failure occurs during Baseline Conditions that does not occur during the other Operational scenario when the effects of Northfield Mountain are not included. This difference is attributed to the lack of rapid fluctuations in water-surface elevations for Scenario 1 (because Northfield Mountain is idle) (Figure 5.4.3.23-4). The figure shows that a large failure occurs here under the Baseline Condition, when peaking operations are combined with extreme high flows.

As the Baseline Condition (Waves off) scenario illustrated a very small reduction in erosion compared to waves on, it was concluded that boat waves are not having a significant impact on bank stability, and the remaining scenarios were not considered with boat waves off.

For the Baseline Condition, 95% of the total erosion occurs at flows of about 64,000 cfs or greater (Figure 5.7.23-5). Table 5.4.3.23-1 denotes the flows above which 95%, 50%, and 5% of all erosion occurs at the site as well as the amount of time those flows were exceeded for each year in the modeling period. There is a significant geotechnical failure at extreme high flow (near 99,000 cfs) which accounts for the bulk of the geotechnical erosion, whereas hydraulic erosion is fairly consistent across the range of flows above 50,000 cfs. This large geotechnical failure happens at the extremely high flow during Hurricane Irene but is not present in the Scenario 1 results suggesting that 73.6% of the erosion at this site is due to Northfield Mountain operations.

Table 5.4.3.23-1: Flow Exceedance Calculations for Site 8BR Pre-Restoration

Site 8BR	Percent of Erosion		
	95%	50%	5%
	Flow (cfs)		
Year	**72,009**	**69,312**	**66,504**
2000	NA	0.10%	0.20%
2001	0.80%	1.00%	1.30%
2002	NA	NA	0.10%
2003	0.10%	0.20%	0.40%
2004	NA	NA	NA
2005	0.50%	0.50%	0.60%
2006	0.10%	0.20%	0.30%
2007	0.10%	0.30%	0.50%
2008	0.20%	0.40%	0.70%
2009	NA	NA	0.10%
2010	NA	0.10%	0.10%
2011	0.90%	1.30%	1.90%
2012	NA	NA	NA
2013	NA	NA	0.10%
2014	0.10%	0.40%	0.60%

NA: Not Applicable since flows did not reach this value

Figure 5.4.3.23-1 Photos at site 8BR Pre Restoration (Labeled as 1998 FRR/ECP-Site 16)

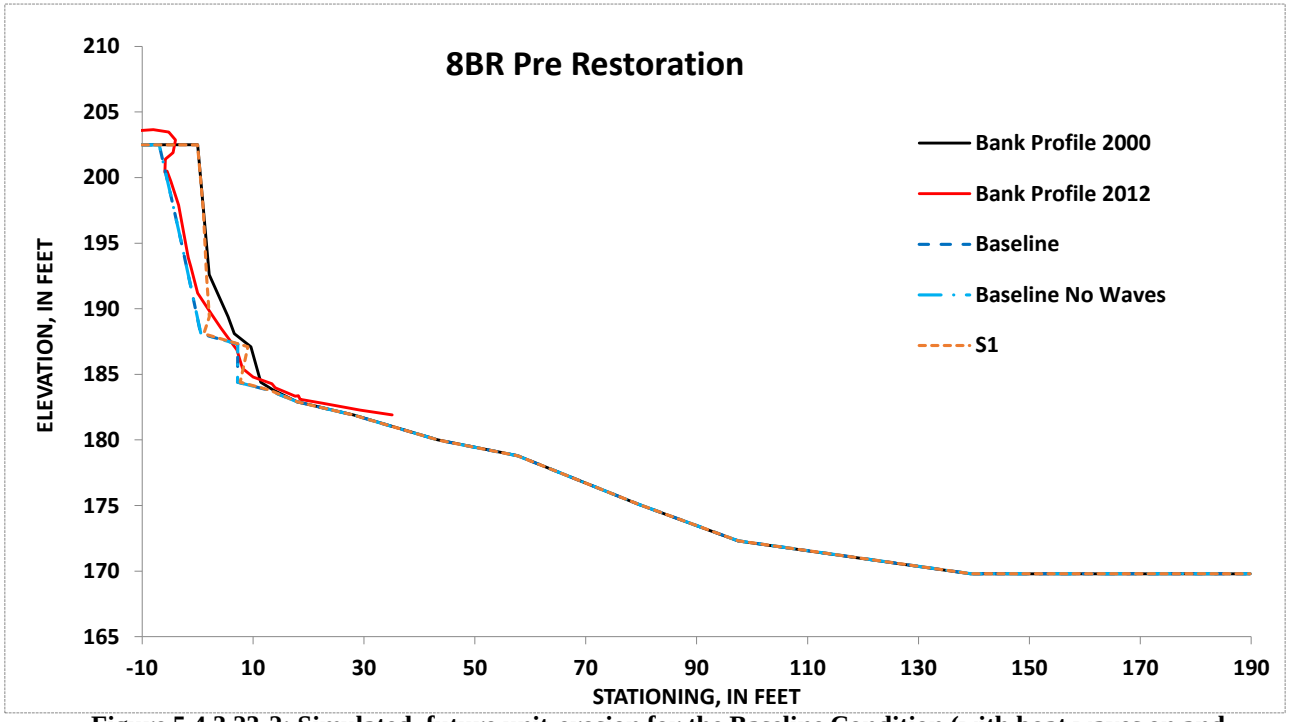

Figure 5.4.3.23-2: Simulated, future unit-erosion for the Baseline Condition (with boat waves on and off) and Scenario 1 at site 8BR for the period 2000-2012

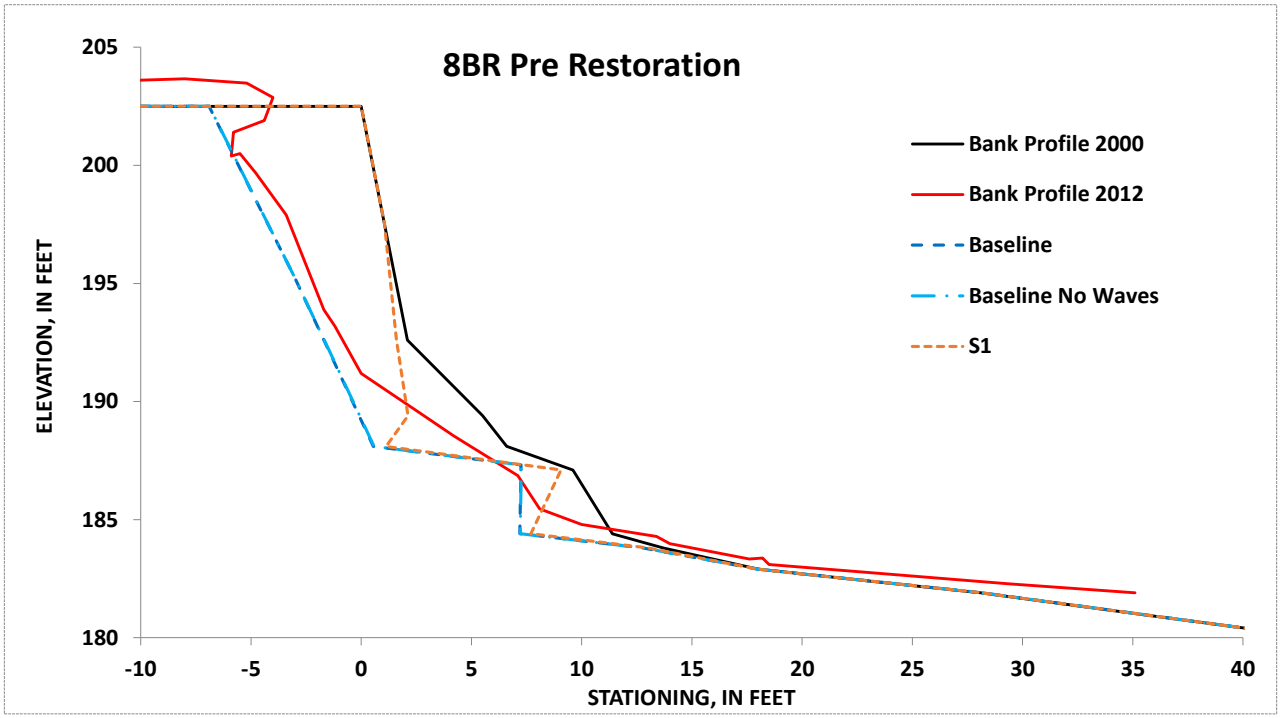

Figure 5.4.3.23-3: Simulated, future erosion for the Baseline Condition (with boat waves on and off) and Scenario 1 at site 8BR for the period 2000-2012. Zoomed in at area of erosion for illustrative purposes

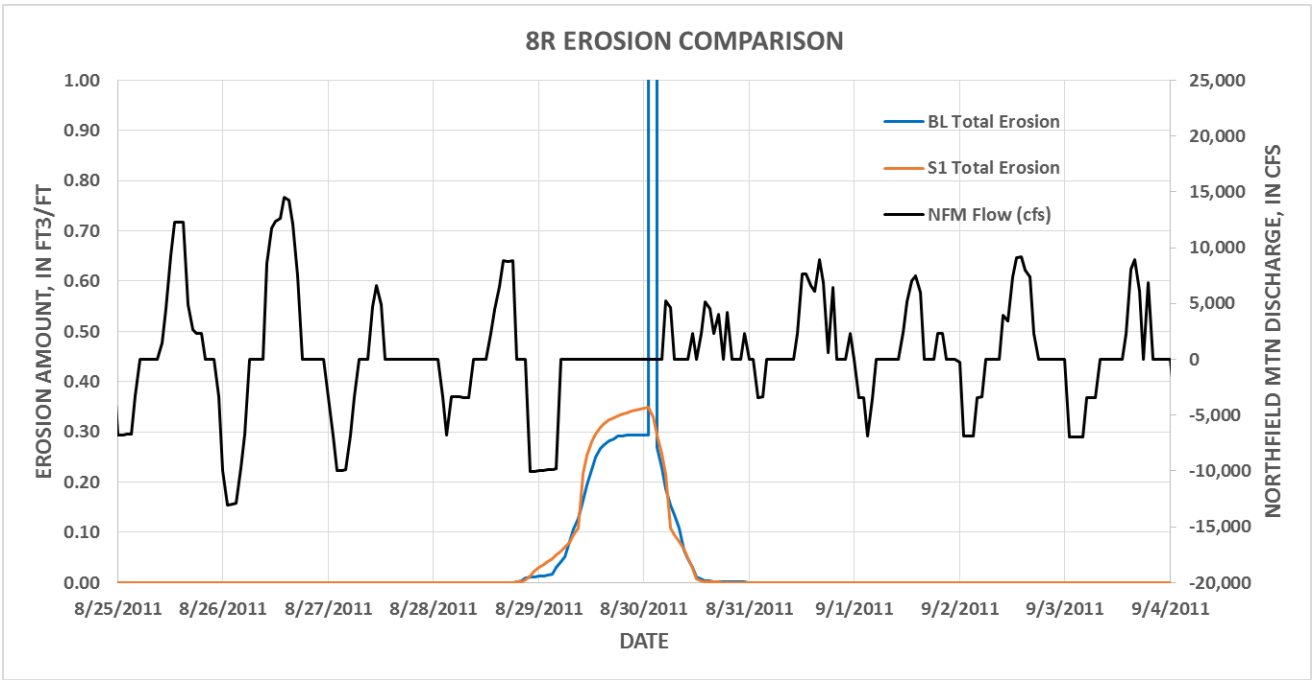

Figure 5.4.23-4 – Timing of large, geotechnical failure during Hurricane Irene for the Baseline Condition but not during Scenario 1 when NFM is idle.

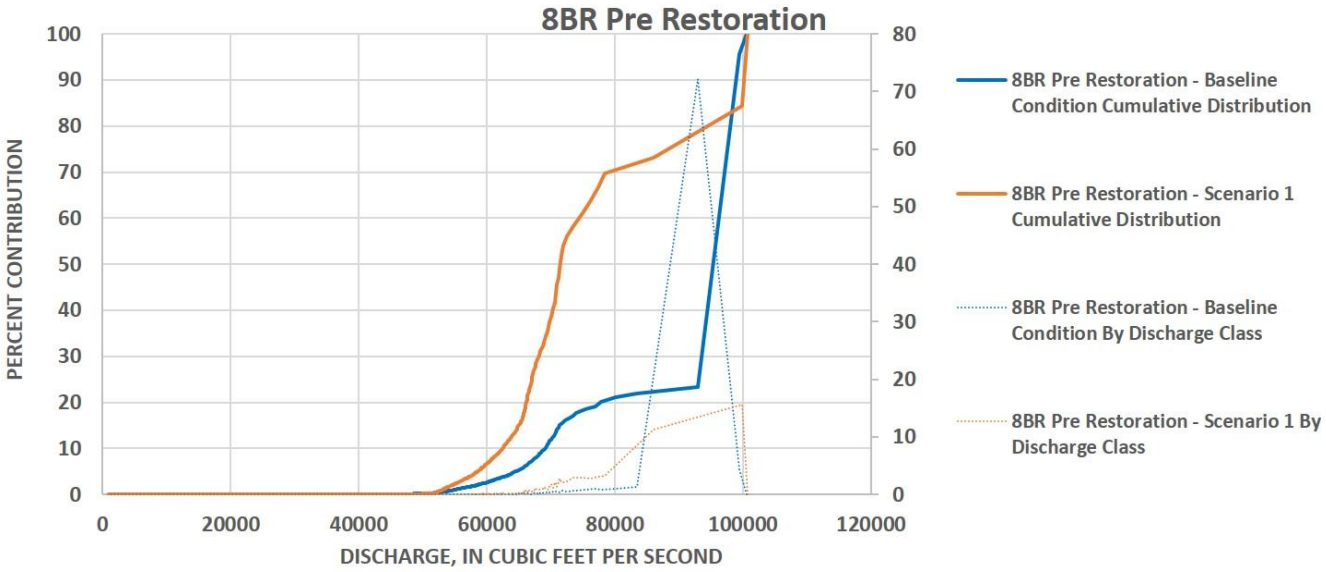

Figure 5.4.3.23-5: Simulated, percent contribution of total erosion by discharge for the Baseline Condition and Scenario 1 at site 8BR for the period 2000-2012

5.4.3.24 Site 8BR – Post Restoration

For the Post Restoration condition at site 8R gravel materials (d_{50} = 13 mm) were placed on the bank toe along with anchored, large woody debris. Vegetation was also added to the lower bank (Figure 5.4.3.24-1).

BSTEM runs at this site show that under the Baseline Condition, 0.671 ft^3 of erosion occurred per foot of bank, during the 2012-2014 flow period post restoration, averaging 0.312 ft^3/ft/y (Table 5.4.3-1). This results in the 10th lowest erosion rate for the Baseline Condition, placing it between the 10th and 15th percentiles of erosion rates along the reach. The modeling also indicates that all 100% (0.31 ft^3/ft/y) of the erosion is due directly to hydraulic processes that are occurring just above the placed materials. None of the bank erosion appears to be the result of geotechnical processes and associated mass failures.

The Baseline Condition (Waves off) resulted in 0.312 ft^3/ft/y, with 0.248 ft^3/ft/y for Scenario 1 (Figure 5.4.3.24-2 to Figure 5.4.3.24-3). This resulted in the differences in erosion rates relative to the Baseline Condition of 0.0% and 20.4%, for Baseline Wave off and Scenario 1 respectively. As Baseline Condition (Waves off) scenario illustrated no reduction in erosion, it was concluded that boat waves are not having a significant impact on bank stability, and the remaining scenarios were not considered with boat waves off.

For the Baseline Condition, 95% of the total erosion occurs at flows of about 66,000 cfs or greater (Figure 5.4.3.24-4). Table 5.4.3.24-1 denotes the flows above which 95%, 50%, and 5% of all erosion occurs at the site as well as the amount of time those flows were exceeded for each year in the modeling period. The hydraulic erosion is fairly consistent across the range of flows above 50,000 cfs. Through this analysis we can conclude that those flows greater than the combined hydraulic capacity of Vernon and Northfield Mountain are accounting for most of the total erosion. Scenario 1 contributes 20.4% of the erosion and suggests that Northfield Mountain is a contributing factor to the total erosion.

Table 5.4.3.24-1: Flow Exceedance Calculations for Site 8BR Post Restoration

Site 8BR	Percent of Erosion		
	95%	50%	5%
	Flow (cfs)		
Year	72,009	69,312	66,504
2000	NA	0.10%	0.20%
2001	0.80%	1.00%	1.30%
2002	NA	NA	0.10%
2003	0.10%	0.20%	0.40%
2004	NA	NA	NA
2005	0.50%	0.50%	0.60%
2006	0.10%	0.20%	0.30%
2007	0.10%	0.30%	0.50%
2008	0.20%	0.40%	0.70%
2009	NA	NA	0.10%
2010	NA	0.10%	0.10%
2011	0.90%	1.30%	1.90%
2012	NA	NA	NA
2013	NA	NA	0.10%
2014	0.10%	0.40%	0.60%

NA: Not Applicable since flows did not reach this value

Figure 5.4.3.24-1 Photos at site 8BR Post Restoration

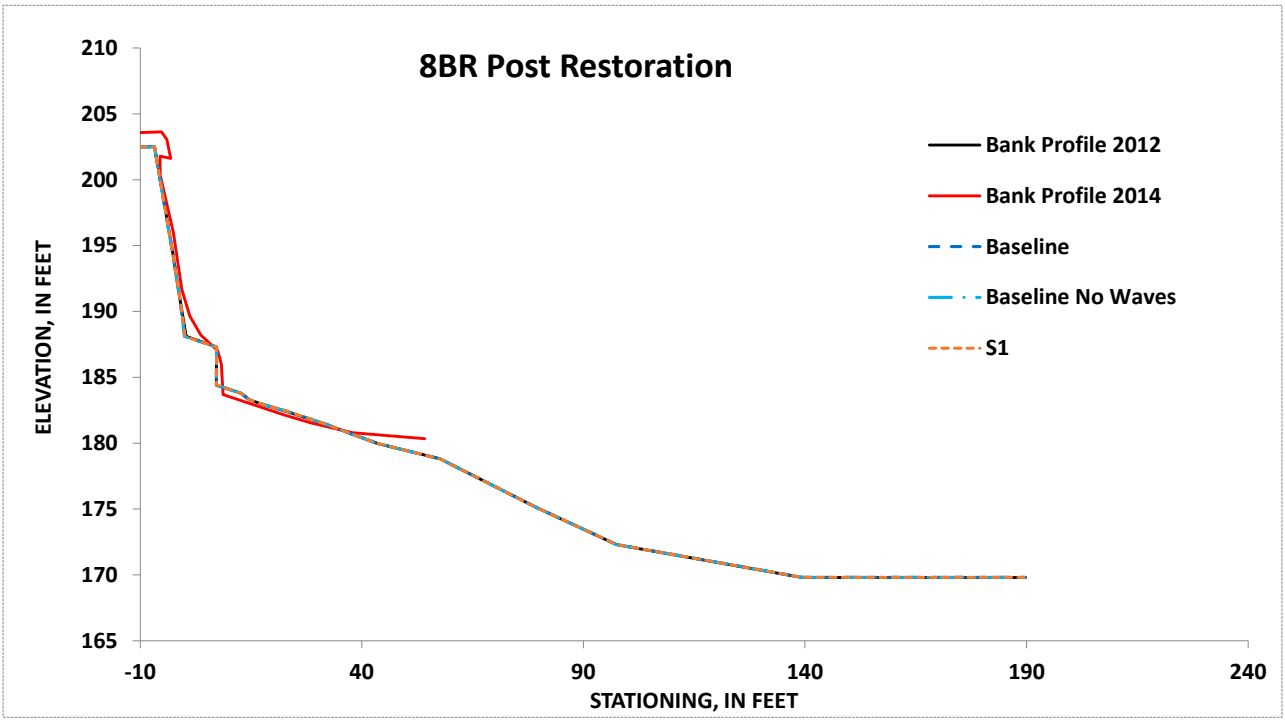

Figure 5.4.3.24-2: Simulated, future unit-erosion for the Baseline Condition (with boat waves on and off) and Scenario 1 at site 8BR Post Restoration for the period 2012-2014

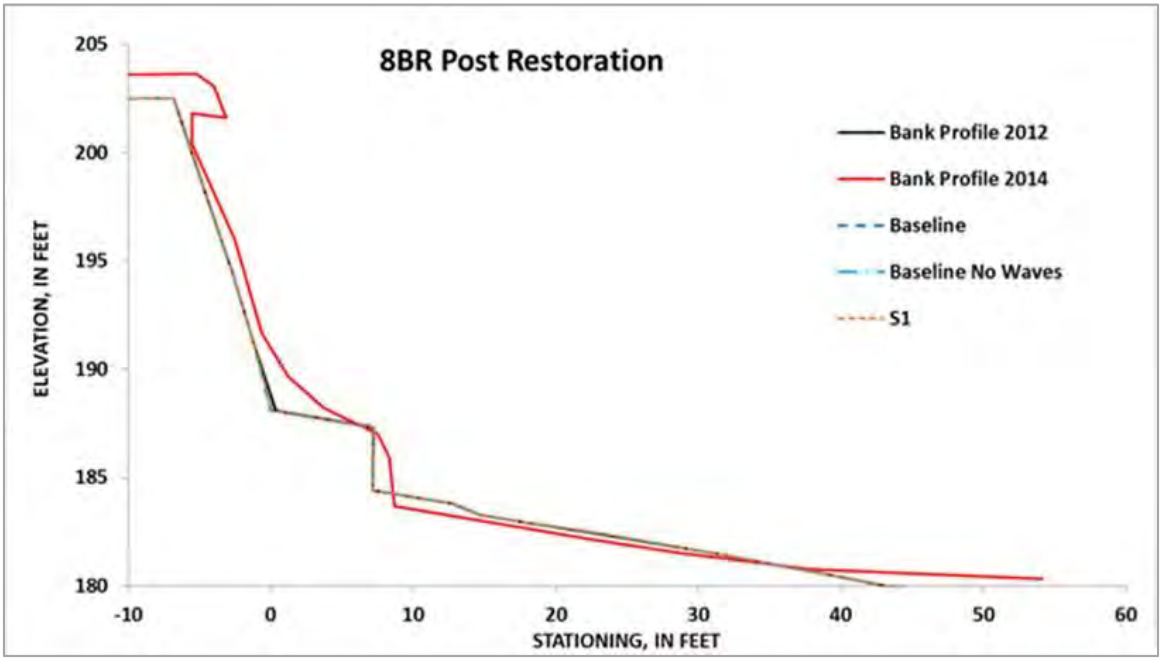

Figure 5.4.3.24-3: Simulated, future erosion for the Baseline Condition (with boat waves on and off) and Scenario 1 at site 8BR Post Restoration for the period 2012-2014. Zoomed in at area of erosion for illustrative purposes

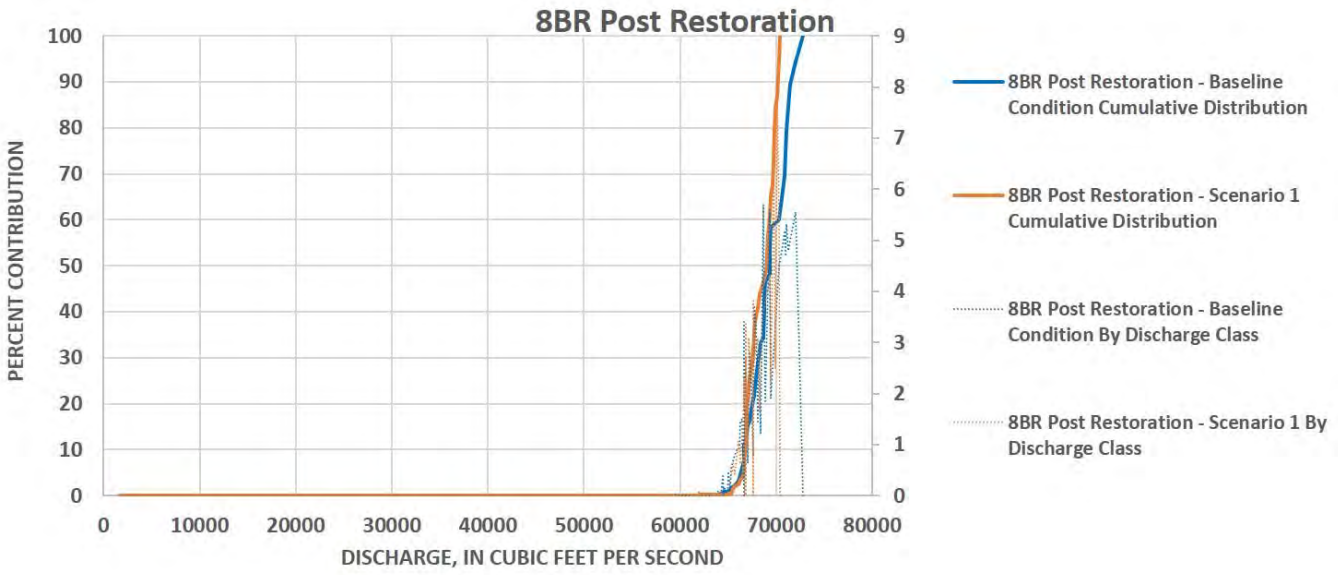

Figure 5.4.3.24-4: Simulated, percent contribution of total erosion by discharge for the Baseline Condition and Scenario 1 at site 8BR Post Restoration for the period 2012-2014

5.4.3.25 Site 87BL

The river at site 87BL (station 30,750) has a steep bank face with an extensive beach, sparsely vegetated banks (Figure 5.4.3.25-1). The site is located between Kidds Island and Northfield Mountain Tailrace, just downstream of Pine Meadow Brook. The bank is roughly 20 feet tall, with a sandy-loam toe and a silt-loam bank. The bank is vegetated with tall grasses and a few American elms. There was a significant amount of bare soil noted. The toe material appears to be depositional. No historical cross sections existed for this site and a 2014 survey was used, therefore, as the initial bank geometry for modeling.

BSTEM runs at this site show that under the Baseline Condition, 52.3 ft^3 of erosion occurred per foot of bank, during the 2000-2014 flow period, averaging 3.57 $ft^3/ft/y$ (Table 5.4.3-1). The modeling also indicates that roughly 73% (2.6 ft^3/y) of the erosion is due directly to hydraulic processes, whereas the other 27% (0.96 ft^3/y) is the result of geotechnical processes and associated mass failures. This reach had higher energy grade line slopes than reach 1 and reach 3. We can see that 87BL has the 11^{th} highest erosion rate and is in the 55^{th} to 60^{th} percentile of erosion rates.

The Baseline Condition (Waves off) resulted in 3.61 $ft^3/ft/y$, with 3.60 $ft^3/ft/y$ for Scenario 1 (Figure 5.4.3.25-2 to Figure 5.4.3.25-3). This resulted in the following percent differences in erosion rates relative to the Baseline Condition: -1.01% and -0.76% for Baseline Wave off and Scenario 1, respectively. As Baseline Condition (Waves off) scenario and Scenario 1 resulted in a slightly higher erosion rate (about 1%) that is certainly within model limitations and does not indicate that erosion would be greater without boat waves and Northfield Mountain operations.

Erosion rates for all Operational scenarios are similar. For the Baseline Condition, 80% of the total erosion occurs at flows of about 37,000 cfs or greater (Figure 5.4.3.25-4). Table 5.4.3.25-1 denotes the flows above which 95%, 50%, and 5% of all erosion occurs at the site as well as the amount of time those flows were exceeded for each year in the modeling period. The geotechnical failures that account for the 27% of the total erosion, occur at the extreme high flows, whereas hydraulic erosion is fairly consistent across the range of flows above 10,000 cfs, resulting in undercutting of the lower bank (Figures 5.4.3.25-2 and Figures 5.4.3.25-3). Evaluating the moderate flow contribution to the total erosion it was determined that Northfield Mountain operations occurred about 17% of the time over the modeled period of record. This equates to about 3.5% of the total erosion during the moderate flows. The Northfield Mountain contribution was adjusted by this 3.5% to better estimate contributions from the project resulting in a total contribution of about 3%.

Table 5.4.3.25-1: Flow Exceedance Calculations for Site 87BL Post Restoration

Site 87BL	Percent of Erosion		
	95%	50%	5%
	Flow (cfs)		
Year	**63,968**	**42,875**	**17,849**
2000	0.30%	3.80%	24.40%
2001	1.60%	4.50%	12.60%
2002	0.10%	1.80%	20.00%
2003	0.60%	4.40%	28.20%
2004	0.10%	1.20%	17.80%
2005	0.70%	6.50%	33.10%
2006	0.50%	4.50%	36.70%
2007	1.00%	3.90%	23.90%
2008	1.20%	8.10%	36.20%
2009	0.10%	2.90%	32.30%
2010	0.20%	4.30%	25.50%
2011	2.30%	8.00%	36.80%
2012	NA	0.40%	18.10%
2013	0.10%	0.80%	22.90%
2014	0.90%	3.30%	27.50%

NA: Not Applicable since flows did not reach this value

Figure 5.4.3.25-1 Photos at site 87BL Post Restoration

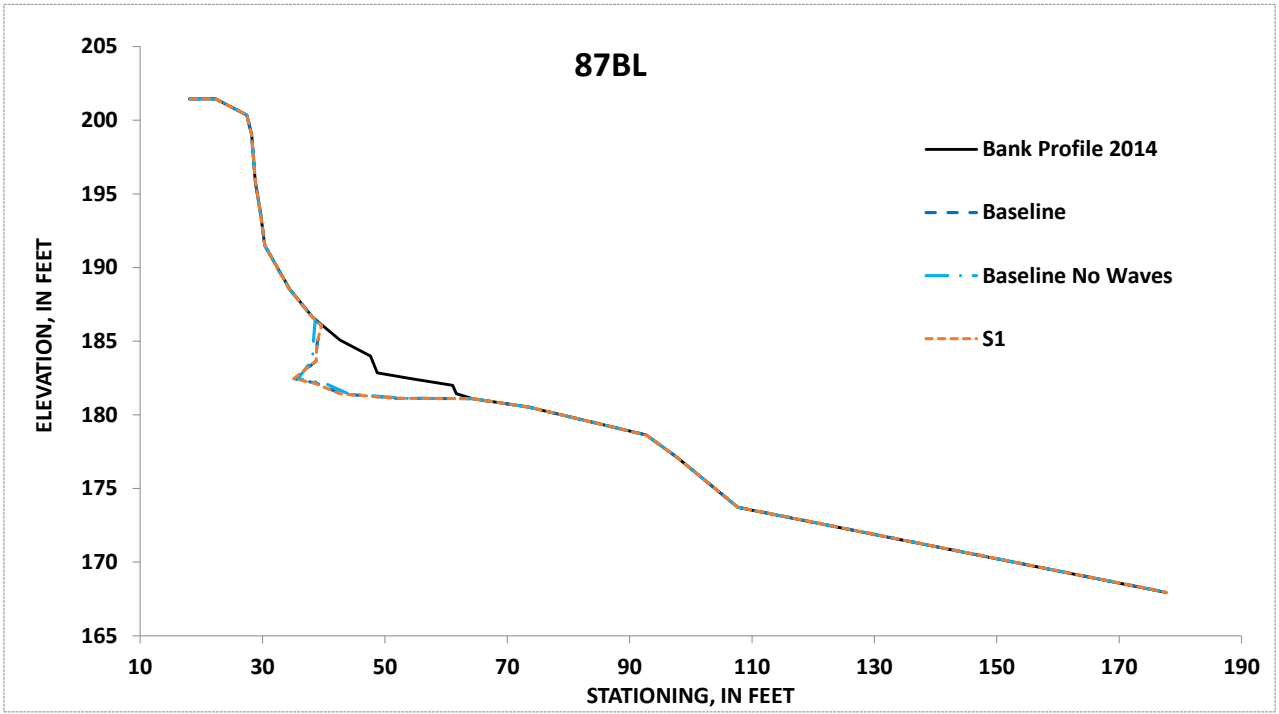

Figure 5.4.3.25-2: Simulated, future unit-erosion for the Baseline Condition (with boat waves on and off) and Scenario 1 at site 87BL for the period 2000-2014

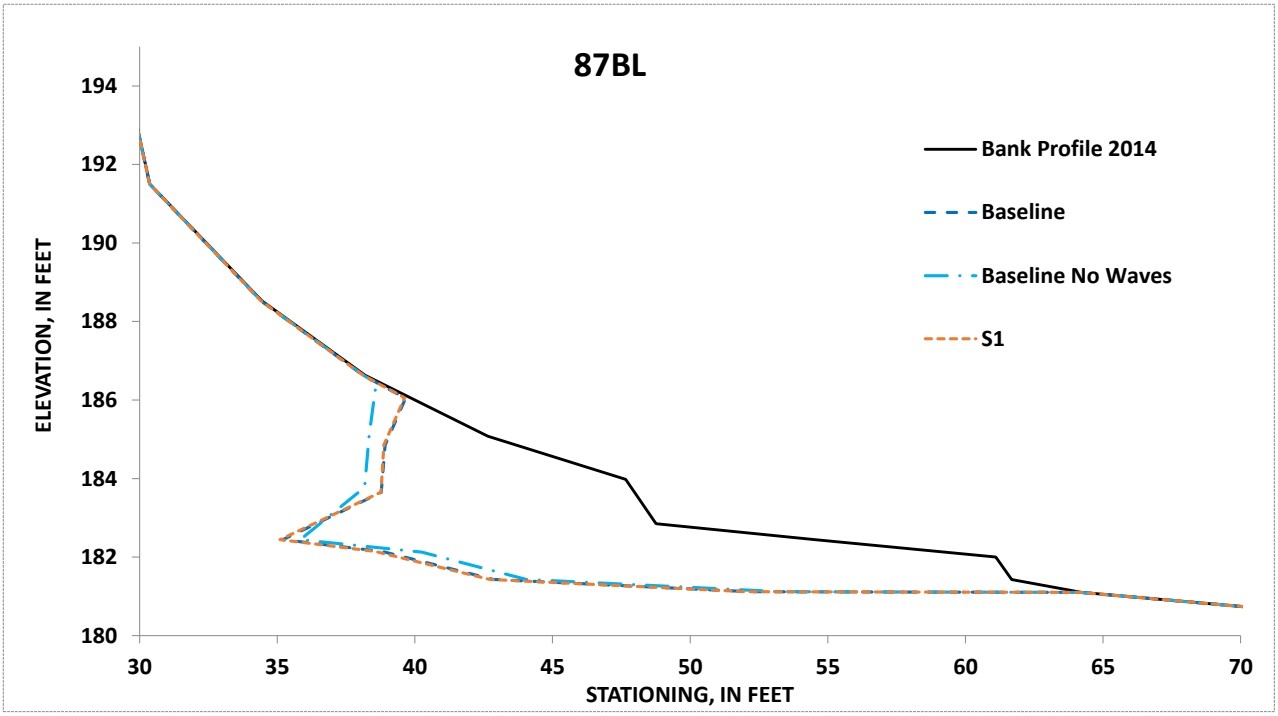

Figure 5.4.3.25-3: Simulated, future erosion for the Baseline Condition (with boat waves on and off) and Scenario 1 at site 87BL for the period 2000-2014. Zoomed in at area of erosion for illustrative purposes

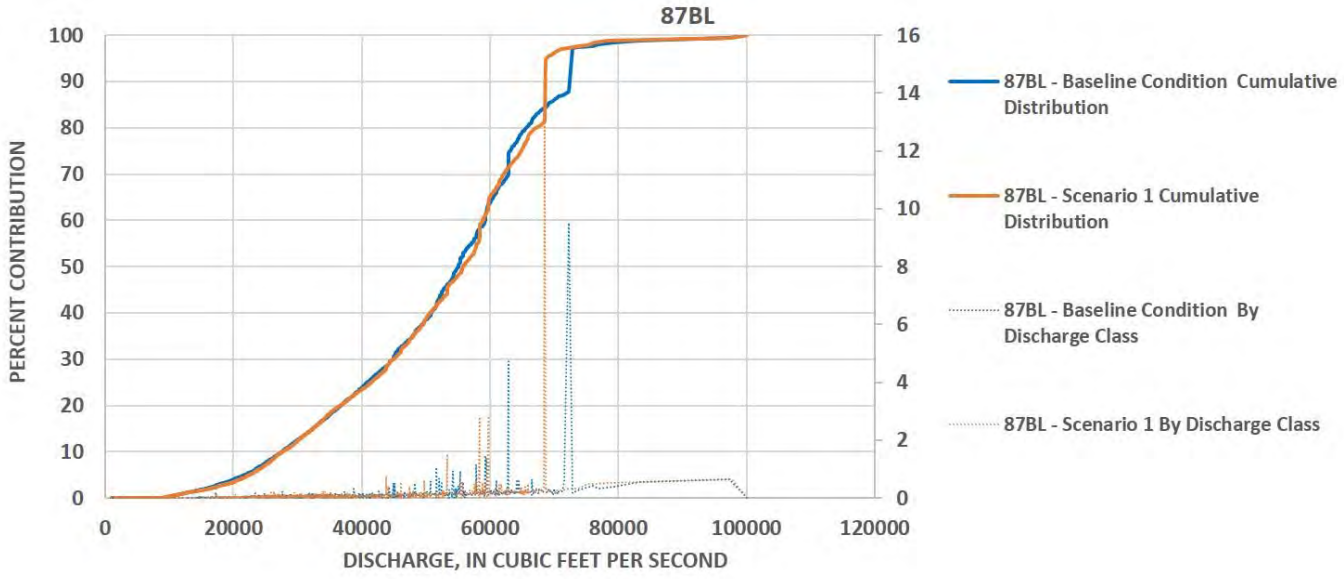

Figure 5.4.3.25-4: Simulated, percent contribution of total erosion by discharge for the Baseline Condition and Scenario 1 at site 87BL for the period 2000-2014

5.4.3.26 Site 75BL

The river at site 75BL (station 27,000) has steep, partially vegetated banks and is located immediately downstream of the Northfield Mountain Tailrace. The bank is roughly 65 feet tall, and the toe material ranges from coarse sand to large cobbles. Large Eastern hemlocks cover most of the upper bank, however the lower bank, shows signs of erosion, with lots of exposed roots. No historical cross sections exist for this site, however this site was surveyed in 2014 as a starting point for the model runs (Figure 5.4.3.26-1).

BSTEM runs at this site show that under the Baseline Condition, 55.0 ft^3 of erosion occurred per foot of bank, during the 2000 to 2014 flow period, averaging 3.76 $ft^3/ft/y$ (Table 5.4.3-1). This results in the 10^{th} highest erosion rate for the Baseline Condition, placing it between the 60^{th} and 65^{th} percentiles of erosion rates along the reach. The modeling also indicates that roughly 56% (2.10 ft^3/y) of the erosion is due directly to hydraulic processes, whereas the other 44% (1.66 ft^3/y) is the result of geotechnical processes and associated mass failures.

For Scenario 1, 3.93 $ft^3/ft/y$ of erosion occurred (Figure 5.4.3.26-2 to Figure 5.4.3.26-3) resulting in a percent difference in erosion rate relative to the Baseline Condition of -4.6%. The Baseline Condition (Waves off) resulted in 3.48 $ft^3/ft/y$. Bank-erosion rates for the Baseline Condition with boat waves was 7.5% greater than without waves, a small, but measurable amount. Because of this, Scenario 1 was also run without the effects of boat waves. With waves off Scenario 1 resulted in 3.72 $ft^3/ft/y$. A comparison of results showed that bank-erosion rates were about 5.3% greater with boat waves than without for Scenario 1. As these numbers are not drastically different from the runs with the boat waves turned on, this location is likely at or near the upstream limit of where boat waves are having a significant impact on bank stability.

For the Baseline Condition, 79.5% of the total erosion occurs at flows of about 37,000 cfs or greater (Figure 5.4.3.26-4). Table 5.4.3.26-1 denotes the flows above which 95%, 50%, and 5% of all erosion occurs at the site as well as the amount of time those flows were exceeded for each year in the modeling period. There are two significant geotechnical failures that account for the bulk of the geotechnical erosion, whereas hydraulic erosion is fairly consistent across the range of flows above 37,000 cfs, with a larger peak between 48,000 and 72,000 cfs. Through this analysis we can conclude that those flows greater than the combined hydraulic capacity of Vernon and Northfield Mountain are accounting for most of the total erosion. The same additional moderate flow analysis completed for site 119BL and 87BL was performed on this site. Moderate flows at 75BL contribute about 13% of the total erosion. Northfield Mountain operations were reviewed and determined to occur about 1.2% of the time over the period of record under moderate flows. This equates to about 0.16% additional contribution by Northfield Mountain resulting in no significate change to the Scenario 1 results.

It should be noted that at this site, the Baseline Condition flows did not result in the greatest amount of erosion. One possible cause for this is that the peaking operations at Northfield Mountain are creating greater fluctuations in water surface elevations than would be created under a run-of-river scenario. By elimination of these fluctuations as seen in Scenario 1 this causes the shear stresses to be focused on a narrower band of the bank cross section, resulting in slightly higher hydraulic erosion which could cause an increase in the size of the individual bank failures.

Table 5.4.3.26-1: Flow Exceedance Calculations for Site 75BL

Site 75BL	Percent of Erosion		
	95%	50%	5%
	Flow (cfs)		
Year	**71,586**	**48,054**	**33,822**
2000	0.10%	2.30%	7.00%
2001	0.80%	3.70%	5.90%
2002	NA	1.20%	4.20%
2003	0.10%	3.10%	8.60%
2004	NA	0.70%	3.10%
2005	0.50%	4.40%	11.40%
2006	0.10%	2.50%	10.50%
2007	0.10%	3.20%	5.90%
2008	0.30%	5.70%	13.70%
2009	NA	1.90%	5.40%
2010	NA	2.70%	7.80%
2011	1.00%	6.40%	14.20%
2012	NA	0.20%	1.30%
2013	NA	0.30%	3.80%
2014	0.20%	2.60%	6.30%

NA: Not Applicable since flows did not reach this value

Figure 5.4.3.26-1 Photos at site 75BL

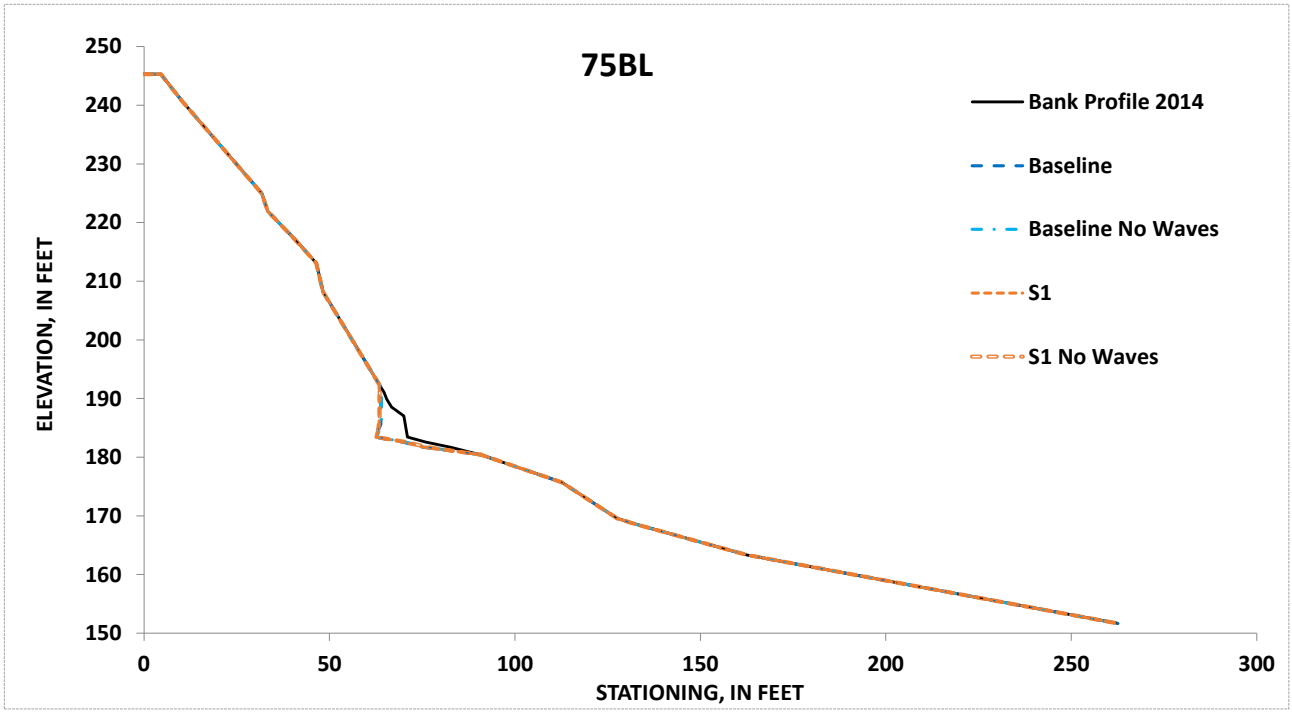

Figure 5.4.3.26-2: Simulated, future unit-erosion for the Baseline Condition (with boat waves on and off) and Scenario 1 at site 75BL for the period 2000-2014

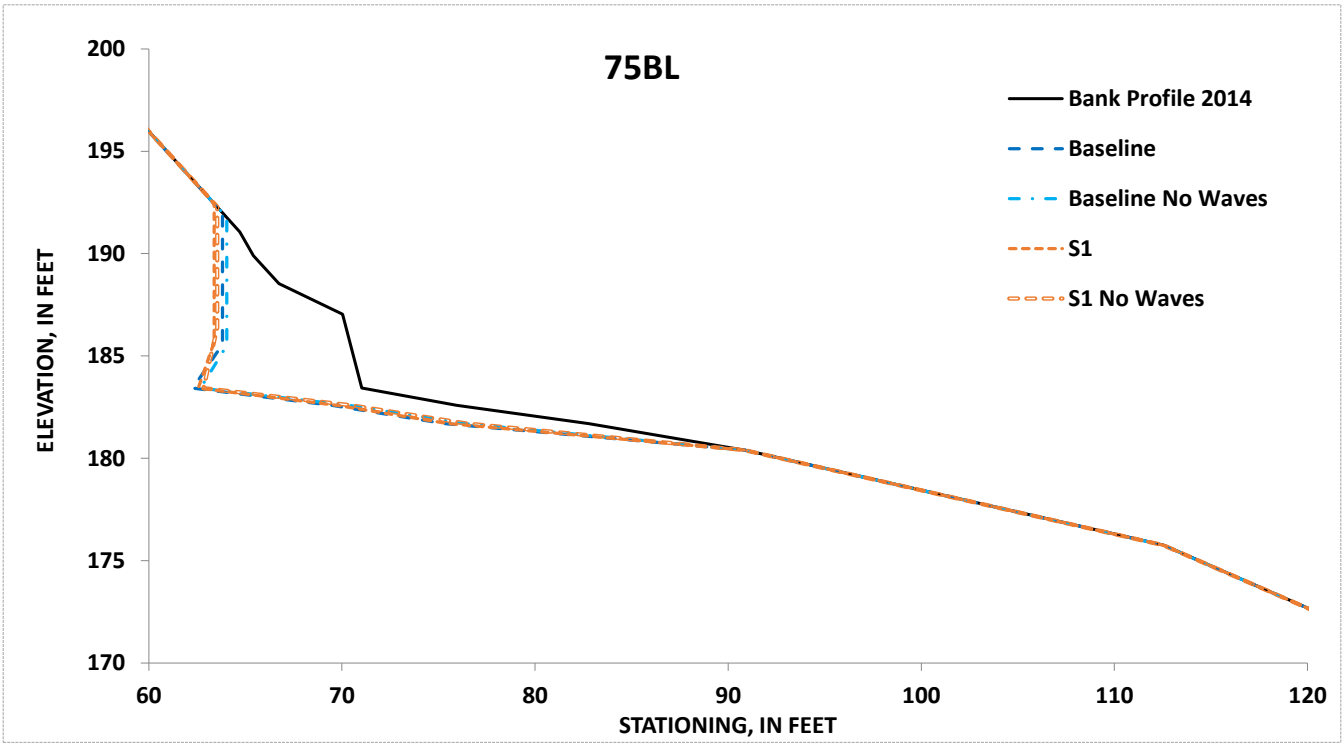

Figure 5.4.3.26-3: Simulated, future erosion for the Baseline Condition (with boat waves on and off) and Scenario 1 at site 75BL for the period 2000-2014. Zoomed in at area of erosion for illustrative purposes

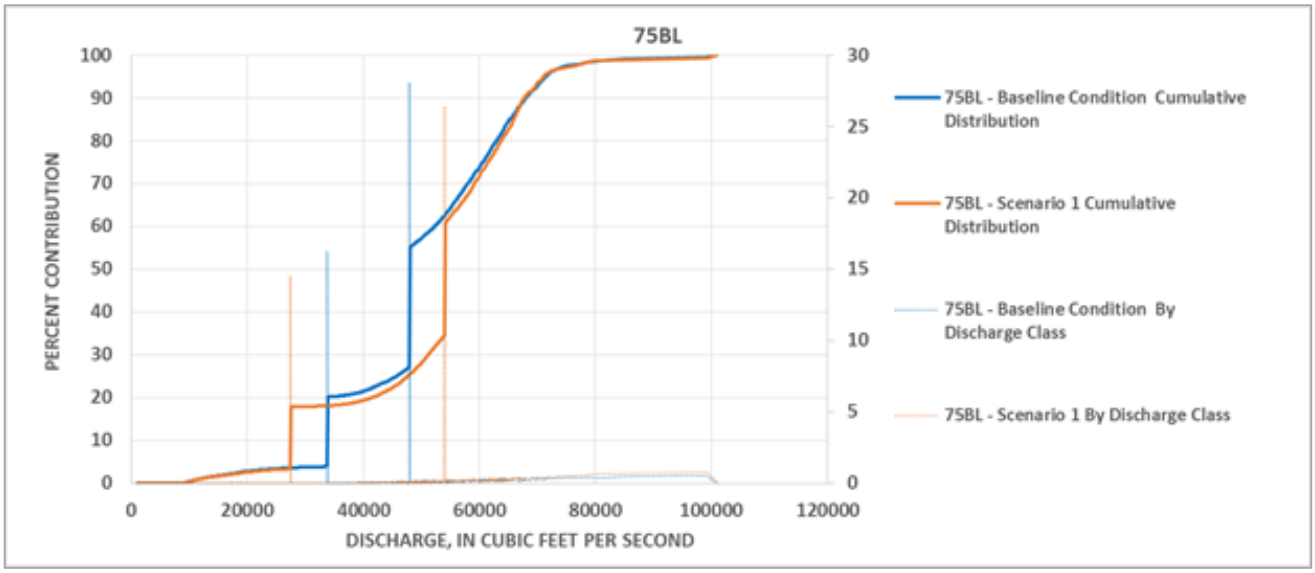

Figure 5.4.3.26-4: Simulated, percent contribution of total erosion by discharge for the Baseline Condition and Scenario 1 at site 75BL for the period 2000-2014

5.4.3.27 Site 9R Pre-Restoration

The river at site 9R (station 6,750) has moderately steep, sparsely vegetated banks and is located on the south side of the Barton Cove Campground. The bank is roughly 61 feet tall, with a sandy toe and a sandy-loam upper bank. The bank is thinly vegetated with Northern red oak, American basswood, and Green ash trees. There was a significant amount of bare soil noted on the bank face, likely due to the large trees and canopy cover (Figure 5.4.3.27-1).

BSTEM runs at this site for the Pre-restoration condition show that under the Baseline Condition, 43.8 ft^3 of erosion occurred per foot of bank, during the 2000 to 2008 flow period prior to restoration, averaging 5.43 $ft^3/ft/y$ (Table 5.4.3-1). This results in the 7th highest erosion rate for the Baseline Condition, placing it between the 70th and 75th percentiles of erosion rates along the reach. The modeling also indicates that all of the erosion is due directly to hydraulic processes.

Scenario 1 produced an erosion rate of 5.19 $ft^3/ft/y$ (Figure 5.4.3.27-2 to Figure 5.4.3.27-4) resulting in a difference in an erosion rate relative to the Baseline Condition of 4.3%. Without the impact of boat waves, erosion rates for the Baseline Condition (Waves off) resulted in 0.967 $ft^3/ft/y$, indicating that boat-generated waves are an important contributor to erosion at this site. As there was a large difference between the Baseline Condition (Waves on) and Baseline Condition (Waves off), Scenario 1 was also investigated for the waves-off condition. With waves off the bank-erosion rate for Scenario 1 was 0.77 $ft^3/ft/y$. While the Baseline Condition had 82% more erosion with boat waves, Scenario 1 showed that bank-erosion rates were greater by 85% with waves.

Overall the difference between Baseline and S1 was found to be 4%; however, determining the causes of erosion at this site is not as simple as subtracting Baseline and S1, as was done at other sites. The difference in impact from boat waves between the Baseline Condition (82%) and S1 (85%) demonstrates how waves influence the erosion in this reach. When Northfield Mountain is set to idle (S1), erosion due to boat waves is 3% greater than if Northfield Mountain is online. In other words, it would appear that the effect of waves on the bank is reduced with Northfield Mountain operating. When taking boat waves into consideration, the actual percent reduction in erosion with the S1 Scenario is likely closer to 1%. This results in an S1 erosion amount of 0.075 $ft^3/ft/y$, which is lower than the measurable/significant rate of 0.161 $ft^3/ft/y$. Another factor compounding the S1 results in this area is the downstream boundary condition used to simulate the Turner Falls Dam. The historic dam operations were used as the boundary condition for S1 which resulted in potentially more TFI fluctuations than may have occurred had Northfield Mountain actually been idle. The increased water level fluctuations modeled in S1 may have actually led to less hydraulic erosion than would have occurred had the TFI been fluctuated less given that the location of the water surface on the bank varied more than it would have historically which would have prevented the repeated undercutting of the bank at the same location.

The proximity of the site to Turner Falls Dam precluded the development of a reliable stage-discharge relation. Because of this the high flow analysis which is based on the erosion amounts within a given range of discharges was not run for this site. Instead, stage was used (Figure 5.4.3.27-4). Still, it is clear that boat-generated waves are a dominant factor in erosion rates in the lower TFI producing 82% of the erosion. While moderate to high flow erosion rates could not be determined for this site, based on the trend throughout the TFI in reaches 2, 3, and 4 it is likely that moderate to high flows still play a role in total erosion.

Figure 5.4.3.27-1 Photos at site 9R Pre Restoration (Photo from 2013 FRR)

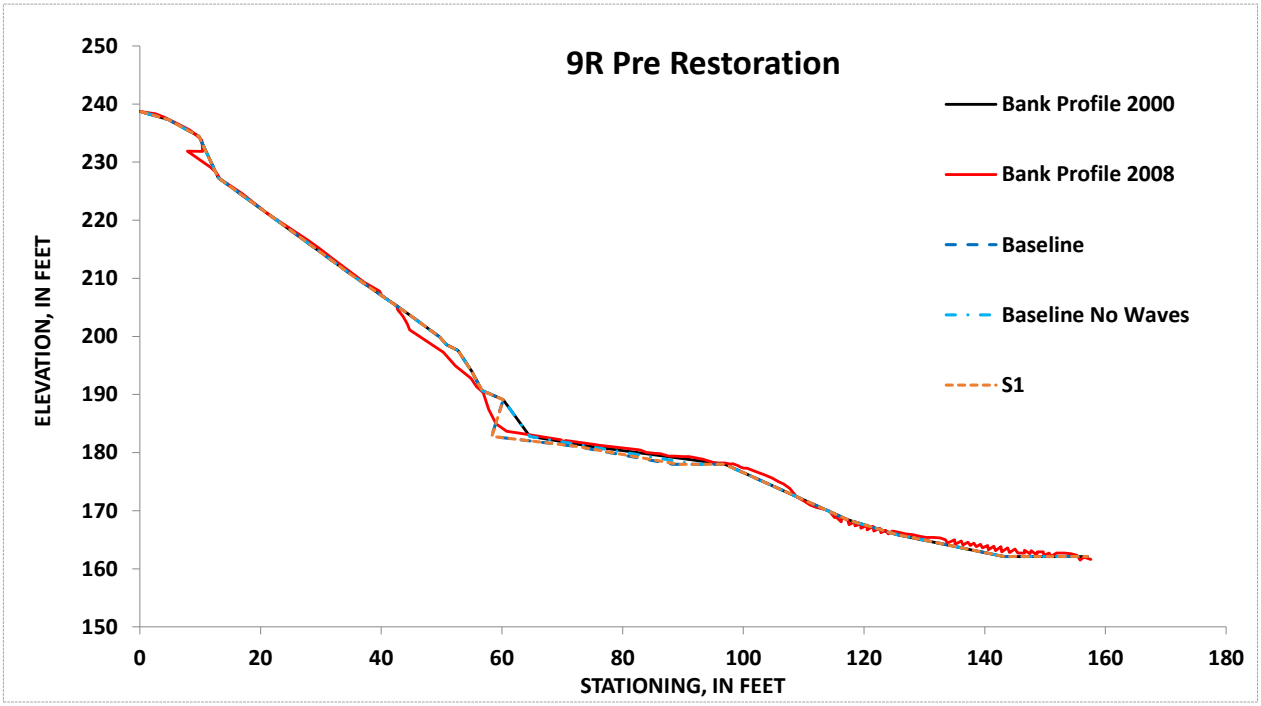

Figure 5.4.3.27-2: Simulated, future unit-erosion for the Baseline Condition and Scenario 1 (with boat waves on) at site 9R Pre Restoration for the period 2000-2008

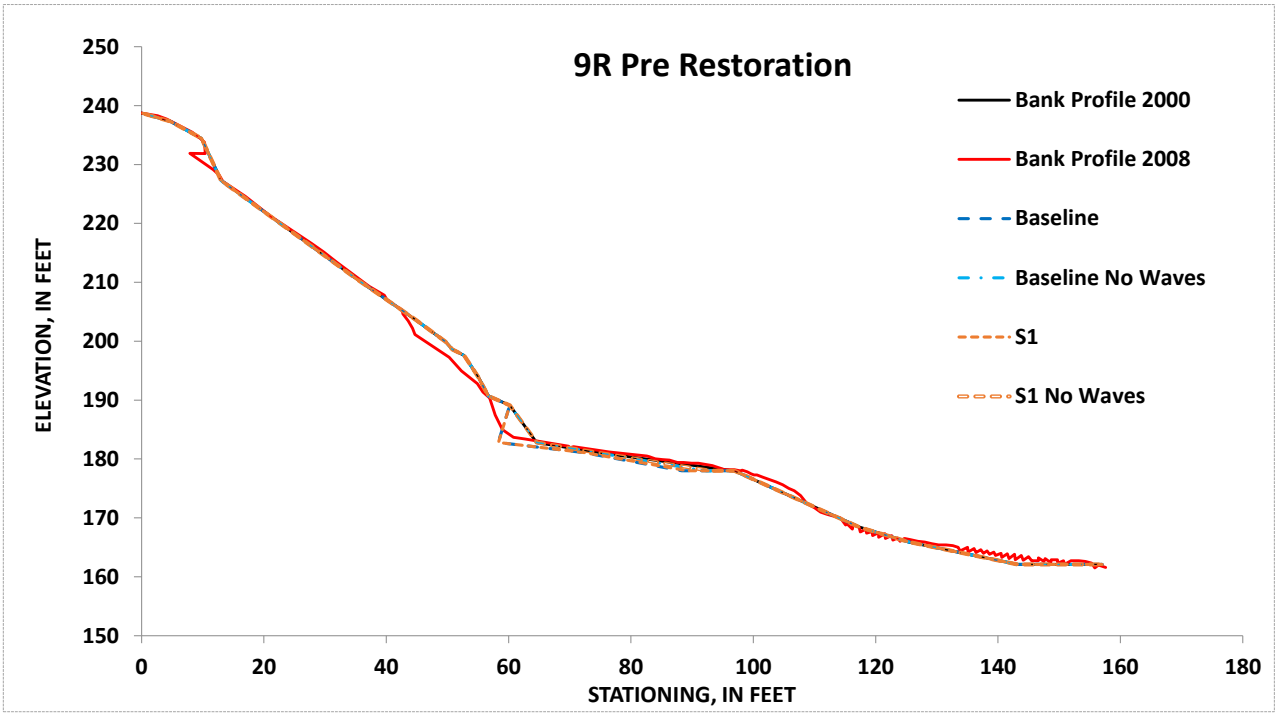

Figure 5.4.3.27-3: Simulated, future unit-erosion for the Baseline Condition (with boat waves on and off) and Scenario 1 at site 9R Pre Restoration for the period 2000-2008

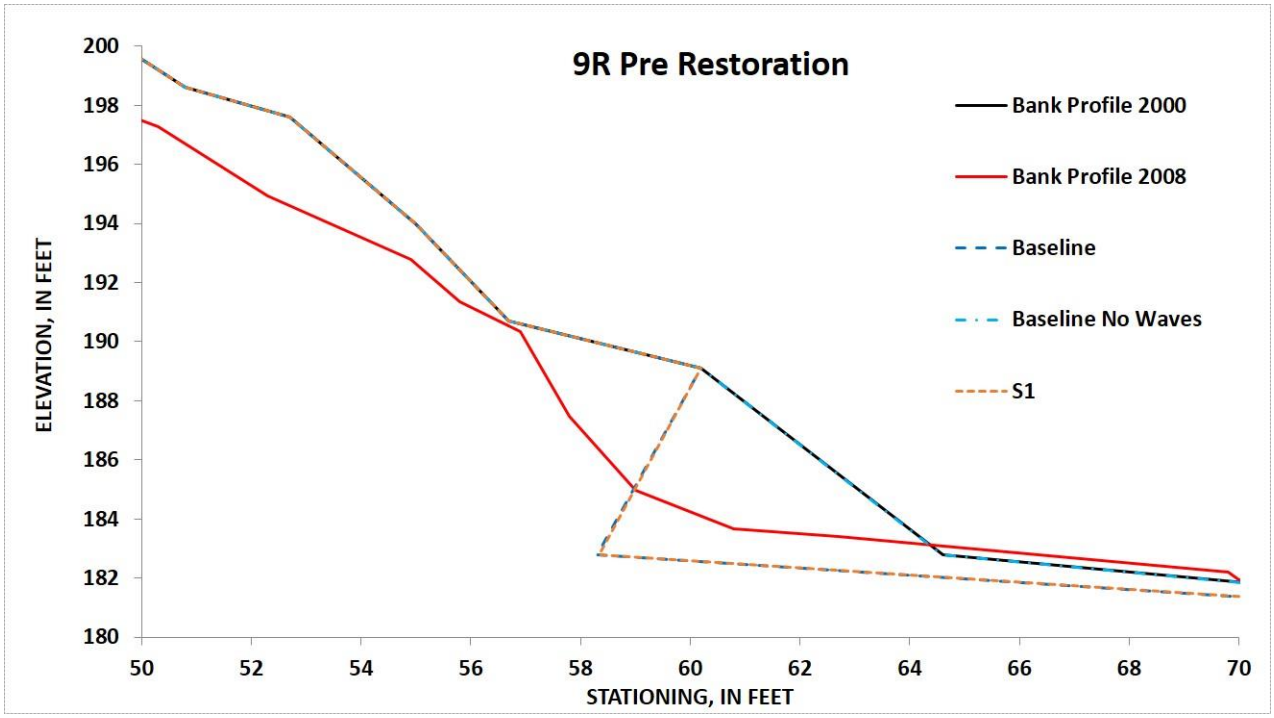

Figure 5.4.3.27-4: Simulated, future erosion for the Baseline Condition and Scenario 1 (with boat waves on) at site 9R Pre Restoration for the period 2000-2008. Zoomed in at area of erosion for illustrative purposes

Figure 5.4.3.27-5: Simulated, percent contribution of total erosion by stage for the Baseline Condition and Scenario 1 at site 9R Pre Restoration for the period 2000-2008. As no stage-discharge relationship could be developed, stage was used

5.4.3.28 Site 9R Post Restoration

As part of the site restoration in 2008, coir or other logs were anchored at the bank toe. Vegetation was also planted on the upper bank (Figure 5.4.3.28-1). As there was no bank reshaping at this site as part of the restoration, the model inputs were only adjusted to account for the toe protection and vegetation. The output cross section from the 9R Pre-Restoration model was used as the starting section for the 9R Post Restoration model.

BSTEM runs at this site show that for Post-restoration under the Baseline Condition, 1.40 ft^3 of erosion occurred per foot of bank, during the 2008 to 2014 flow period, averaging 0.227 $ft^3/ft/y$ (Table 5.4.3-1). This results in the 7^{th} lowest erosion rate for the Baseline Condition, placing it between the 10^{th} and 15^{th} percentiles of erosion rates along the reach. The modeling also indicates that all of the erosion is due directly to hydraulic processes.

Scenario 1 had a resulting erosion amount of 0.224 $ft^3/ft/y$ (Figure 5.4.3.28-2). The Baseline Condition (Waves off) resulted in 0.002 $ft^3/ft/y$, indicating a substantial reduction in bank-erosion rates with the removal of the impacts from boat-generated waves. As there was a large difference between the Baseline Condition (Waves on) and Baseline Condition (Waves off), Scenario 1 was investigated for the waves off condition as well. This resulted in 1.50 x10-3 $ft^3/ft/y$ of erosion for Scenario 1 (Note- while this site did show a small reduction in erosion between the BL and S1 Scenarios the total reduction in erosion is well below the measureable/significant rate of 0.161 $ft^3/ft/yr$). The highest water surface elevation for this period occurred at 184.5 ft. Most of the measured erosion for this site appears to occur above 190 feet. This erosion does not appear to be a function of the TFI hydraulics. For erosion to be present above the high water line, toe erosion would need to occur and then a geotechnical failure would occur above. The toe for this site, based on survey data, has not eroded significantly since the restoration to the point where a geotechnical failure would occur.

As a stage-discharge relation could not be developed for site 9R the high flow analysis is presented according to stage data only (Figure 5.4.3.28-3). Boat-generated waves are a dominant factor in erosion rates at this site producing 99% of the erosion.

Figure 5.4.3.28-1 Photos at site 9R Post Restoration

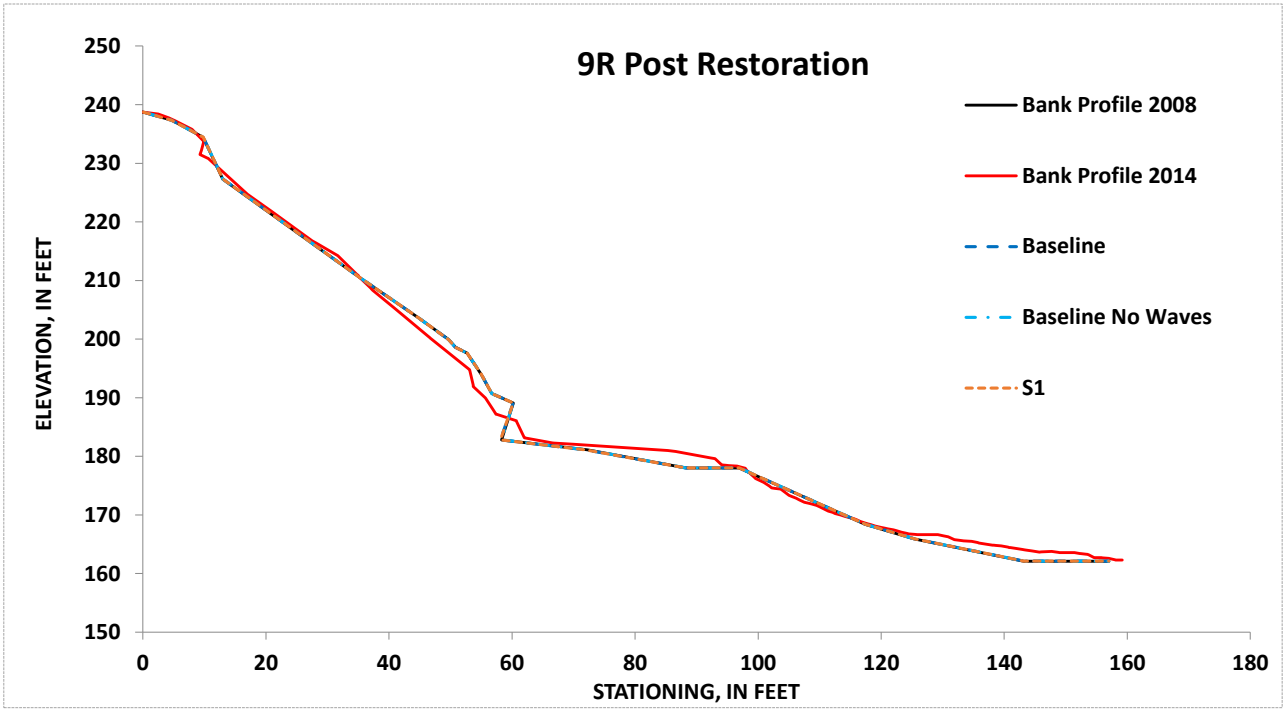

Figure 5.4.3.28-2: Simulated, future unit-erosion for the Baseline Condition (with boat waves on and off) and Scenario 1 at site 9R Post Restoration for the period 2008-2014, with a minimum water surface elevation of 176.9 feet and a maximum water surface elevation of 184.5 feet.

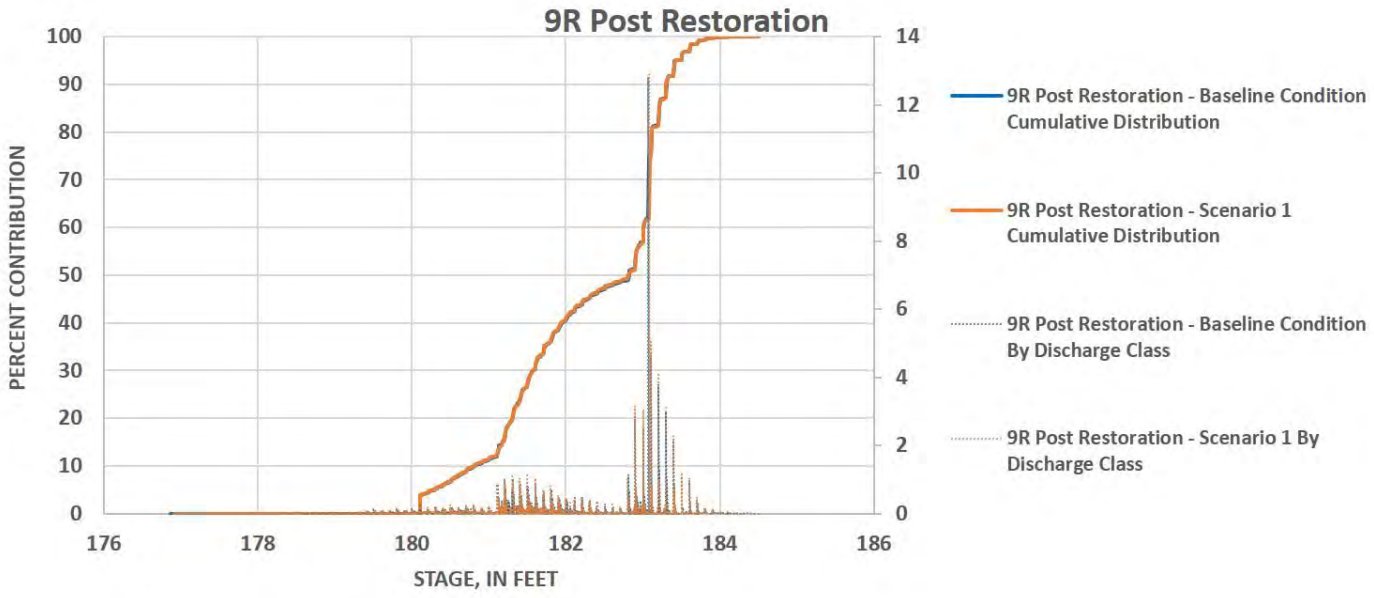

Figure 5.4.3.28-3: Simulated, percent contribution of total erosion by stage for the Baseline Condition and Scenario 1 at site 9R Post Restoration for the period 2008-2014. As no stage-discharge relationship could be developed, stage was used.

5.4.3.29 Site 12BL

The river at site 12BL (station 6,500) has steep, heavily vegetated banks, and is located slightly downstream and across the river from site 9R. The bank is roughly 51 feet tall, and the toe material consists of coarse sand. Large Birch, Oak, and Hemlock cover most of the upper bank. Parts of the lower bank, however, show signs of erosion, with sloughed material against the in-situ bank face (Figure 5.4.3.29-1). No historical cross sections exist for this site thus a 2014 survey was used as the initial geometry for the model runs.

BSTEM runs at this site show that under the Baseline Condition, 32.6 ft^3 of erosion occurred per foot of bank, during the 2000 to 2014 flow period, averaging 2.22 $ft^3/ft/y$ (Table 5.4.3-1). This results in the 14^{th} highest erosion rate for the Baseline Condition, placing it between the 45^{th} and 50^{th} percentiles of erosion rates along the reach. The modeling also indicates that roughly 74% (1.65 ft^3/y) of the erosion is due directly to hydraulic processes, whereas the other 26% (0.57 ft^3/y) is the result of geotechnical processes and associated mass failures.

For Scenario 1, 2.15 $ft^3/ft/y$ of erosion occurred (Figure 5.4.3.29-2 to Figure 5.4.3.29-4) resulting in about 3% of the total erosion (Note- while this site did show a small reduction in erosion between the BL and S1 Scenarios the total reduction in erosion is well below the measureable/significant rate of 0.161 $ft^3/ft/yr$). With the lower variability in water surface fluctuations at this site we see a bigger wave influence. The Baseline Condition (Waves off) resulted in 0.239 $ft^3/ft/y$ representing about 89% of the total erosion, attesting to the important role of boat-generated waves in inducing erosion at this site. As Baseline Condition (Waves off) scenario illustrated a significant reduction in erosion, Scenario 1 was also run without the effects of boat waves. With waves off the model run for Scenario 1 resulted in 0.194 $ft^3/ft/y$. Clearly, boat waves are significant for all Operational scenarios and, therefore, protection of the bank-toe region could limit further bank erosion at this site.

As a stage-discharge relation could not be developed for site 12BL, the high flow analysis is presented according to stage data only (Figure 5.4.3.29-5). Boat-generated waves are a dominant factor in erosion rates at this site producing 89% of the erosion. While moderate to high flow erosion rates could not be determined for this site, based on the trend throughout the impoundment in reaches 2, 3, and 4 it is likely that moderate to high flows still play a contributing role in total erosion.

Figure 5.4.3.29-1 Photos at site 12BL

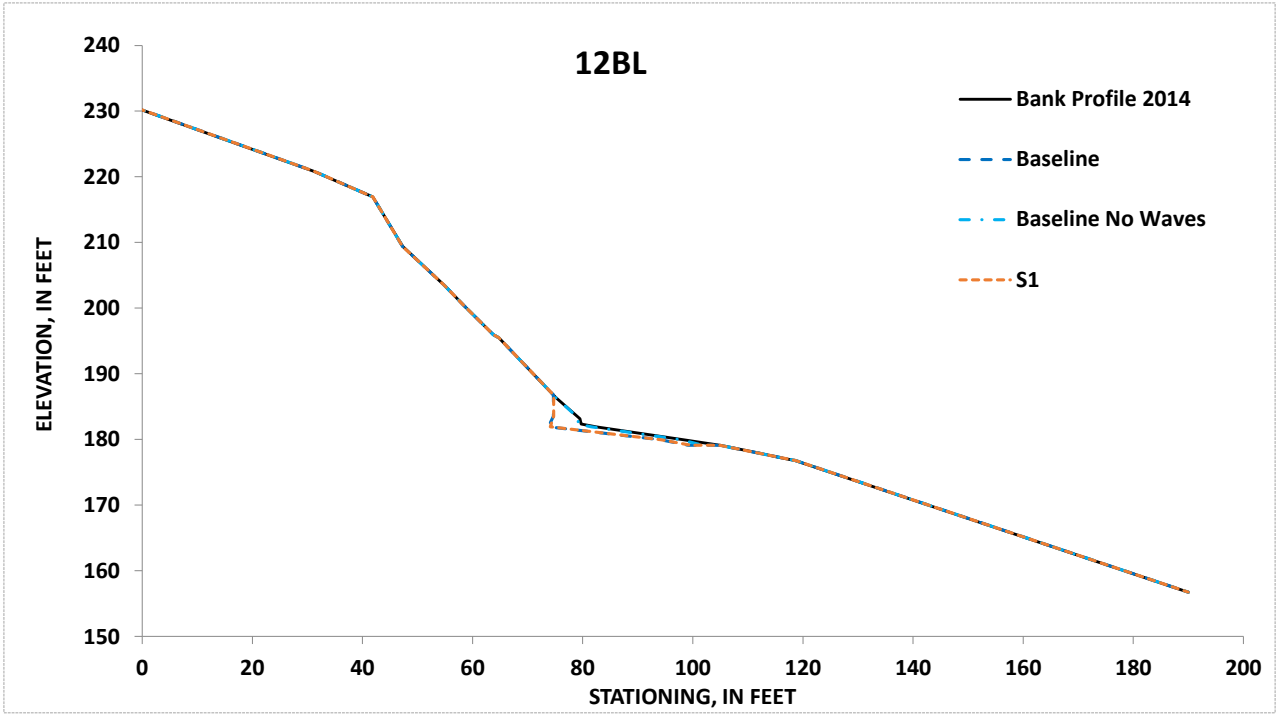

Figure 5.4.3.29-2: Simulated, future unit-erosion for the Baseline Condition and Scenario 1 (with boat waves on) at site 12BL for the period 2000-2014

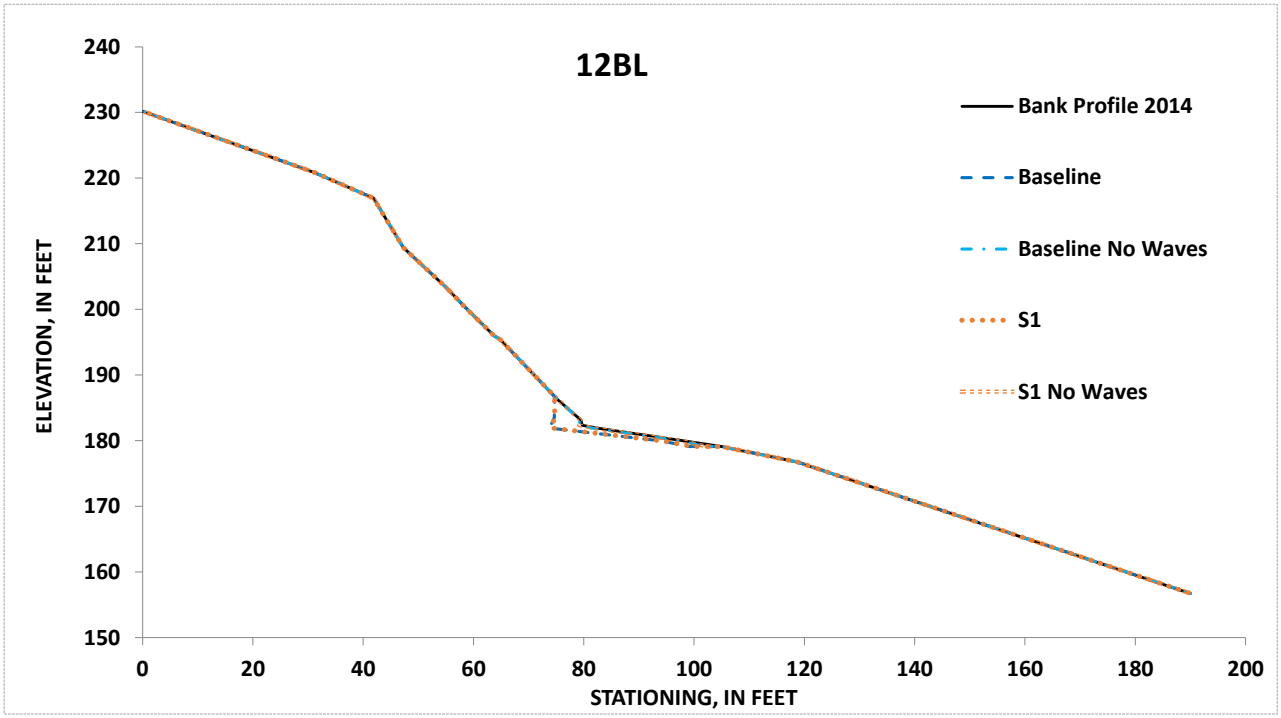

Figure 5.4.3.29-3: Simulated, future unit-erosion for the Baseline Condition (with boat waves on and off) and Scenario 1 at site 12BL for the period 2000-2014

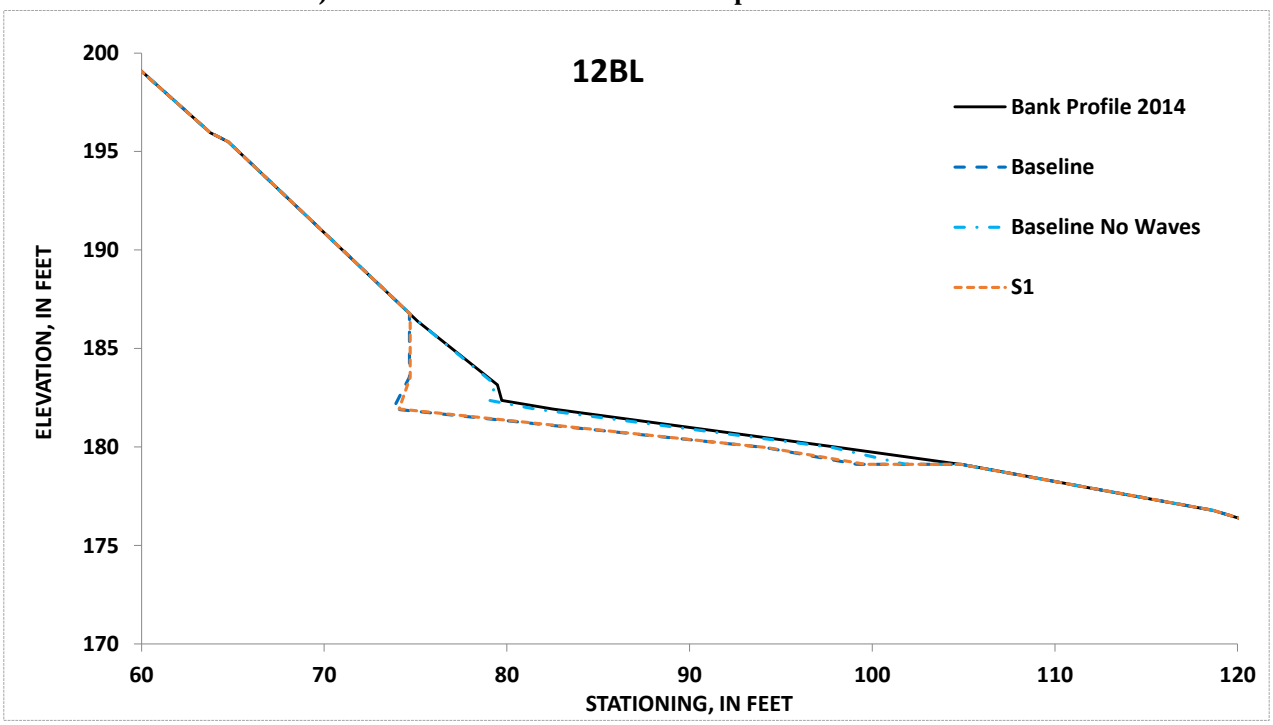

Figure 5.4.3.29-4: Simulated, future erosion for the Baseline Condition and Scenario 1 (with boat waves on) at site 12BL for the period 2000-2014. Zoomed in at area of erosion for illustrative purposes.

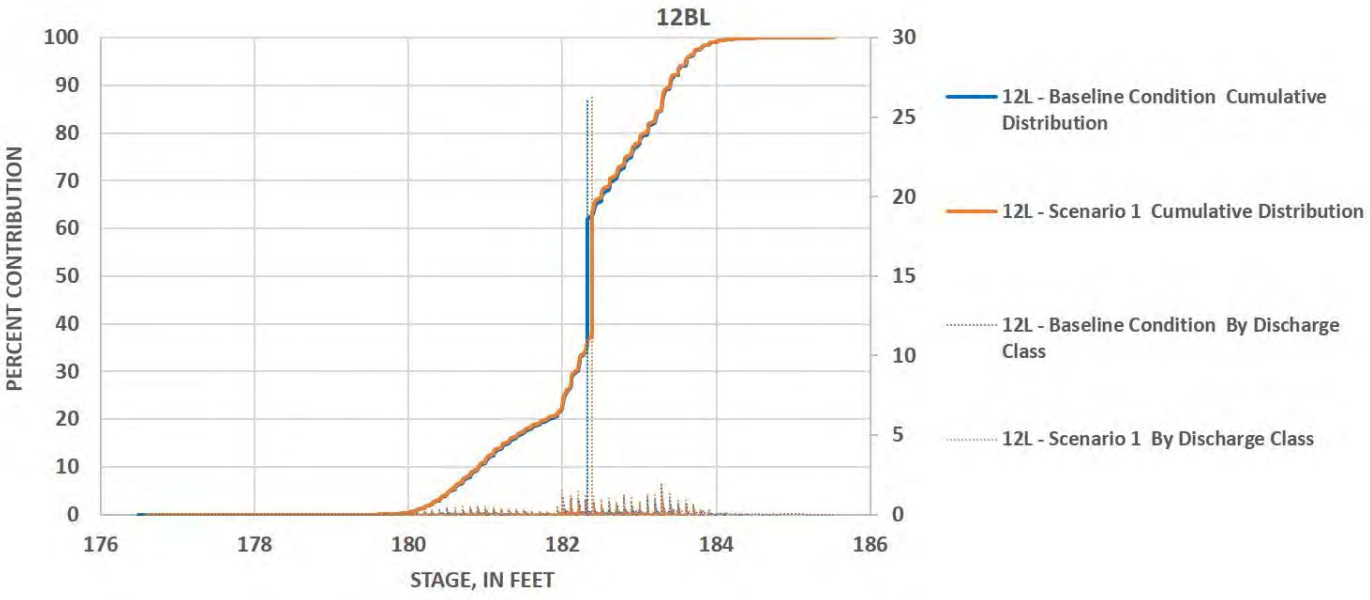

Figure 5.4.3.29-5: Simulated, percent contribution of total erosion by stage for the Baseline Condition and Scenario 1 at site 12BL for the period 2000-2014. As no stage-discharge relationship could be developed, stage was used.

5.4.3.30 Site BC-1R

The river at site BC-1R (station 4,750) has moderately steep, heavily vegetated banks and is located on the north side of the Barton Cove Campground, immediately upstream of the Turners Falls Dam. The bank is roughly 8.5 feet tall, with a silty-loam toe and a sandy upper bank. The bank face and bank top are heavily vegetated with Black birch, Eastern hemlock, Eastern white pine, and Northern red oak. There was a significant amount of bare soil noted on the bank face, likely due to the shade from the canopy cover from large trees (Figure 5.4.3.30-1).

BSTEM runs at this site show that under the Baseline Condition, 2.39 ft^3 of erosion occurred per foot of bank during the 2000 to 2014 flow period, averaging 0.168 $ft^3/ft/y$ (Table 5.4.3-1). This results in the 6^{th} lowest erosion rate for the Baseline Condition, placing it between the 5^{th} and 10^{th} percentiles of erosion rates along the reach. The modeling also indicates that 100% of the bank erosion is due directly to hydraulic processes, and that none of the bank erosion is the result of mass failures.

For Scenario 1, 0.01 $ft^3/ft/y$ less erosion than the Baseline occurred (0.167 $ft^3/ft/y$), (Figure 5.4.3.30-2 to Figure 5.4.3.30-3), resulting in a percent reduction of 0.45%. With the lower variability in water surface fluctuations at this site we see a larger influence from boat-generated waves. As there was a large difference between the Baseline Condition (Waves on) and Baseline Condition (Waves off) resulting in a 100% reduction in erosion, Scenario 1 was investigated for the waves-off condition as well. This resulted in no erosion. Thus, boat-generated waves are the dominant cause (almost 100%) of the small amount of bank erosion at this site.

As a stage-discharge relation could not be developed for site BC-1R, the high flow analysis is shown with stage data only (Figure 5.4.3.30-4).

Figure 5.4.3.30-1 Photos at site BC1R

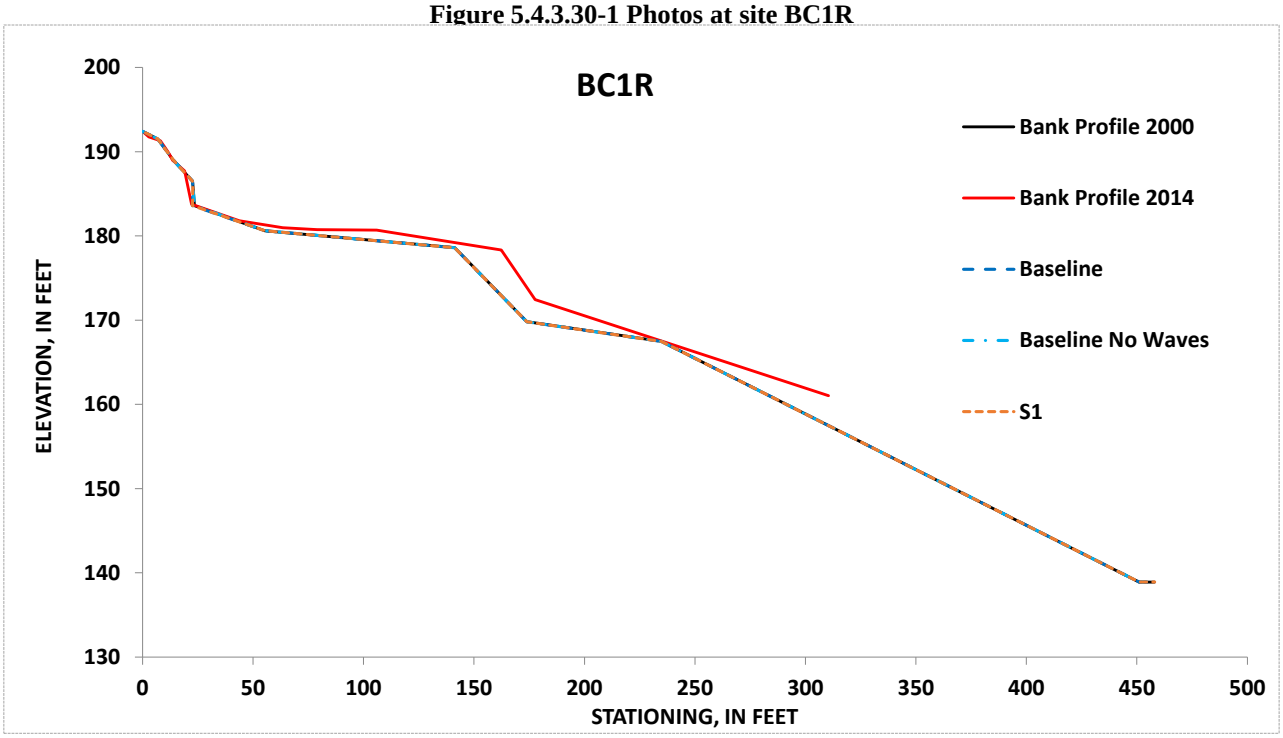

Figure 5.4.3.30-2: Simulated, future unit-erosion for the Baseline Condition (with boat waves on and off) and Scenario 1 at site BC-1R for the period 2000-2014

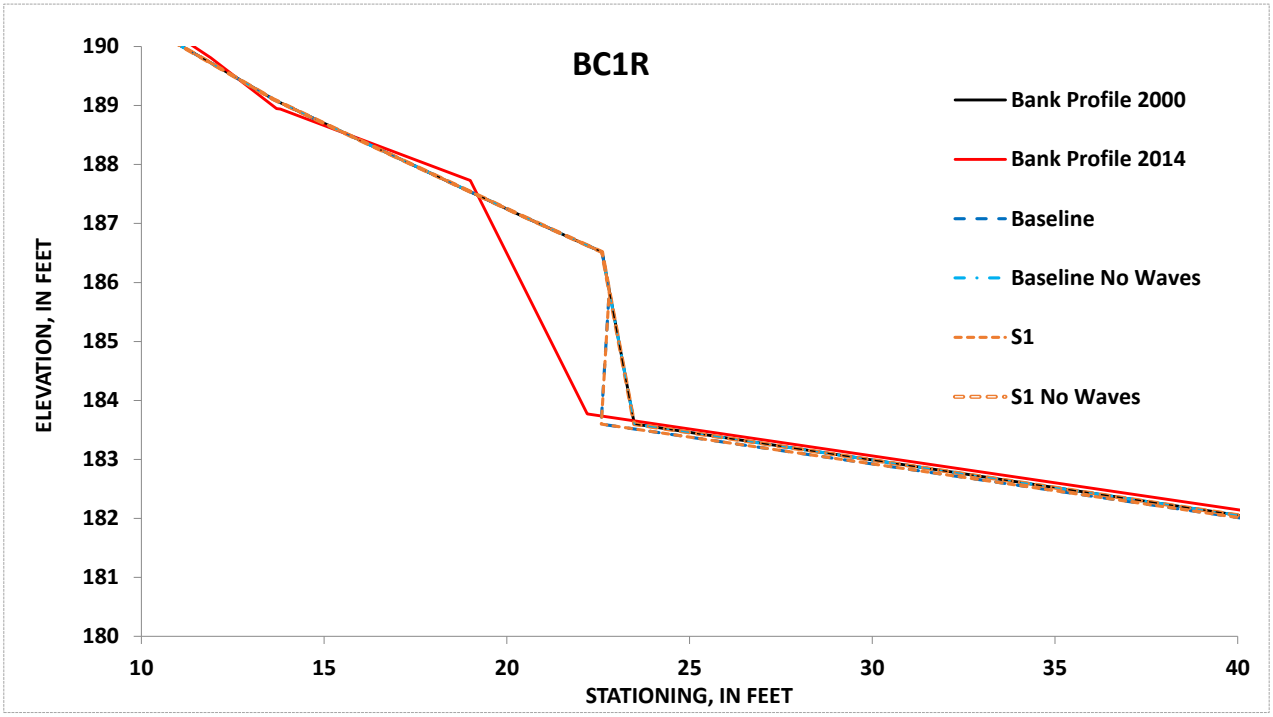

Figure 5.4.3.30-3: Simulated, future erosion for the Baseline Condition (with boat waves on and off) and Scenario 1 at site BC-1R for the period 2000-2014. Zoomed in at area of erosion for illustrative purposes

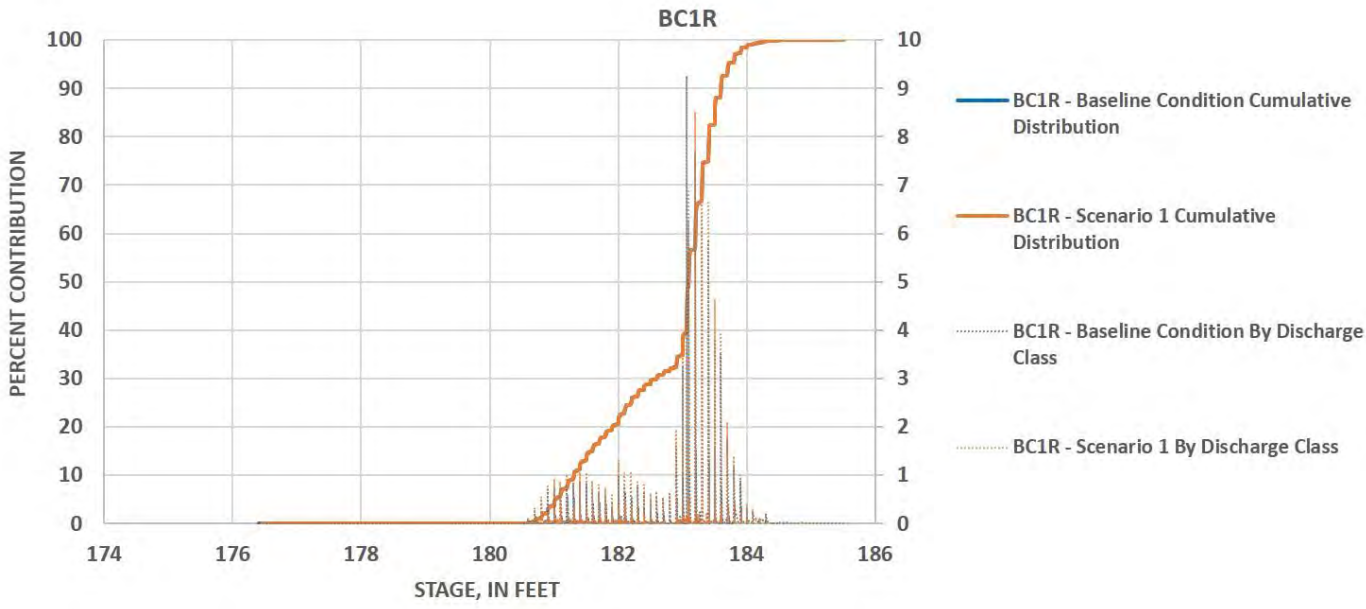

Figure 5.4.3.30-4: Simulated, percent contribution of total erosion by stage for the Baseline Condition and Scenario 1 at site BC-1R for the period 2000-2014. As no stage-discharge relationship could be developed, stage was used.

5.5 Analysis of the Causes of Erosion – Supplemental Analyses

Supplemental analyses discussed in this section served three primary purposes: (1) to serve as a means of comparison against the BSTEM results discussed in the previous section; (2) to investigate the potential primary causes of erosion not included in the BSTEM analysis (i.e. land management practices and ice); and (3) to examine secondary causes of erosion present in the TFI (i.e. animals and unique hydraulic and/or geomorphic conditions).

5.5.1 Hydraulic Shear Stress

Flowing water imparts a force on the river banks (i.e. hydraulic shear stress) which is counteracted by forces which resist sediment movement (i.e. primarily the weight of the soil particles in non-cohesive sediment, or physiochemical inter-particle forces in cohesive sediment). The comparison of these forces dictates if hydraulic erosion and sediment transport occur. Hydraulic erosion occurs on a particle by particle basis when the hydraulic shear stress (i.e. boundary shear stress) exceeds a threshold resistive force (i.e. critical shear stress), causing sediment particles to be dislodged and transported downstream. Further discussion on the estimation of the critical shear stress (τ_c) was provided in Section 4 (i.e. Sections 4.2.6.2 and 4.2.6.6), while the bed shear stress (τ_o) can be computed as follows:

$$\tau_o = \rho * u_*^2 \quad (3)$$

Where τ_o is the boundary shear stress (i.e. hydraulic shear stress), ρ is the density of water, and u_* is the shear velocity.

5.5.1.1 Analysis of velocity and shear stress data – Detailed Study Sites

Table 5.5.1.1-1 provides a comparison of τ_c with τ_o at 23 of the detailed study sites for the six River2D production runs discussed earlier in Section 5 (i.e. Section 5.2.2). The critical shear stress presented in this table represents the median τ_c obtained from the jet test data for each site as presented in Table 4.2.6.6-1. For the computation of the bed shear stress, this analysis assumed a water density appropriate for water with a temperature of approximately 60 degrees Fahrenheit (i.e. 998.9 kg/m^3), while the shear velocity was obtained from the River2D production runs discussed in earlier in Section 5. The River2D results indicate that the hydraulic shear stress is only sufficient to cause erosion when flows at Turners Falls Dam exceed approximately 30,000 cfs (i.e. Operation Rule Threshold A), and may be insufficient to cause erosion at approximately half of the detailed study sites under a 100-year return period event. It should be noted that the River2D results are being compared to the median critical shear value, which means that some erosion may still occur.

Table 5.5.1.1-1: Comparison of Critical Shear Stress and River2D Bed Shear Stress at Detailed Study Sites[42]

Detailed Study Site	Critical Shear Stress, τ_c	Bed Shear Stress, τ_o					
		Generating Capacity at Turners Falls Dam	Operation Rule Threshold A	Operation Rule Threshold B	10-Year Return Period	50-Year Return Period	100-Year Return Period
2L	0.137	0.00	0.00	0.30	0.78	2.00	2.95
3L	0.777	0.00	0.01	0.32	0.26	0.01	0.18
3R	0.639	0.00	0.00	0.03	0.06	0.43	1.33
4L	0.106	0.00	0.09	0.80	2.58	3.44	3.74
5CR	1.03	0.00	0.00	0.06	0.17	0.45	0.98
6AL	0.64	0.00	0.00	0.04	0.13	0.13	0.08
6AR	0.475	0.01	0.09	1.50	1.82	2.29	2.46
7L	0.748	0.05	0.25	0.81	1.38	1.86	2.34
7R	7.14	0.00	0.00	0.01	0.11	0.18	0.22
8BL	3.33	0.00	0.00	0.04	0.14	0.56	0.88
8BR	0.627	0.01	0.06	0.13	0.21	0.59	0.88
9R	10.3	0.00	0.00	0.02	0.14	0.74	1.34
10L	0.585	0.00	0.00	0.11	0.41	0.06	0.17
10R	3.47	0.00	0.01	0.23	0.59	1.37	1.71
11L	2.91	0.00	0.02	0.89	0.58	0.01	0.03
18L	3.27	0.00	0.00	0.03	0.07	0.15	0.22
21R	0.1945	0.00	0.00	0.18	0.30	0.71	1.66
26R	0.024	0.00	0.00	0.14	0.20	0.39	0.48
29R	1.51	0.00	0.00	0.05	0.19	0.73	1.09
75BL	3.41	0.00	0.00	0.12	0.02	0.08	0.14
87BL	0.082	0.00	0.00	0.01	0.01	0.04	0.23
119BL	0.0025	0.00	0.00	0.00	0.05	0.29	0.61
303BL	2.49	0.00	0.00	0.12	0.08	0.08	0.45

[42] Refer to Table 5.2.2-1 for flow thresholds associated with the six bed shear stress categories.

5.5.1.2 Analysis of velocity and shear stress data – Unique Hydraulic Conditions

A one dimensional model assumes that flow is evenly distributed, however, this only holds true for a straight channel with symmetrical cross section geometry and roughness which is not typically the case in a natural river system. The River2D results provided insight into the distribution of flow within the channel, leading to unique hydraulic characteristics which can impact the potential for erosion.

When a channel changes direction, the velocity is higher on the outside of the bend as opposed to the inside of a bend. This leads to a higher chance for erosion on the outside of the bend, and a higher chance for sediment to be deposited on the inside of the bend. Sometimes the distribution of flow in a channel can vary with the magnitude of the flow, as shown in Figure 5.5.1.2-1. Access to other flow paths (e.g. the island in the figure) redistributes flow within the river, which in this case resulted in lower velocities along the bank near Site 11L. Such occurrences help to explain how the bed shear stress can be lower despite a higher total flow in the river. The ultimate impact to bank erosion caused by flow distribution may depend on the severity of bends in the river, channel geometry (e.g. alternate flow paths), the magnitude of flow, nearby bank materials, and other factors.

Additionally, significant changes in channel geometry, whether natural (e.g. rock outcrops or deep chasms) or manmade (e.g. bridge abutments and piers) can impact the flow distribution. Natural chasms exist within the Connecticut River, such as the more than 120 foot deep King Philip's Abyss and French King Hole located approximately 3 miles upstream of the Turners Falls Dam. The River2D model indicates that eddies are formed due to these chasms, as shown in Figure 5.5.1.2-2. Similarly, the model indicates that eddies form approximately 5 miles downstream of Vernon Dam, immediately downstream of an old bridge (i.e. whose deck has been removed, but abutments and piers remain), as shown in Figure 5.5.1.2-3. This figure shows that the magnitude and presence of recirculation can also be impacted by the magnitude of flow in the river.

Previous reports submitted to FERC have documented eddying downstream of Vernon Dam and near the Route 10 Bridge. Figure 5.5.1.2-4 shows an example of eddying in these areas despite the model using a coarser mesh resolution (i.e. as discussed in Section 5.2.2) near Vernon Dam and upstream of the Route 10 Bridge. The eddying downstream of Vernon Dam was noted to be more significant with increased flow, while the eddying in the vicinity of the Route 10 bridge was noted both upstream and downstream of the bridge depending on the flow. While other locations along the Connecticut River also exhibited eddying, only select examples were included for reporting purposes. The ultimate impact to bank erosion caused by changes in channel geometry (i.e. natural or manmade) may depend on the eddy location, the magnitude of flow, nearby bank materials, and other factors.

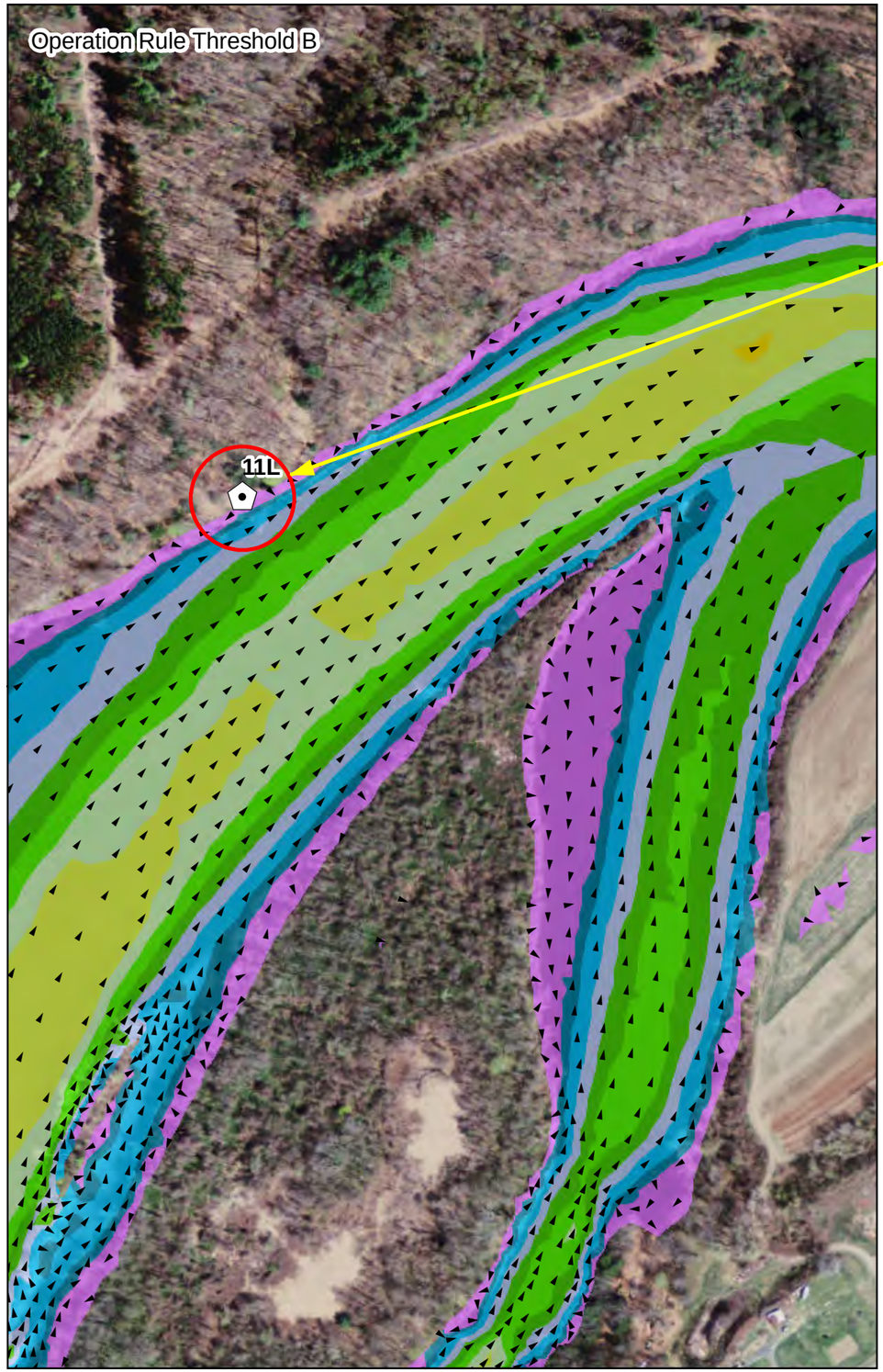

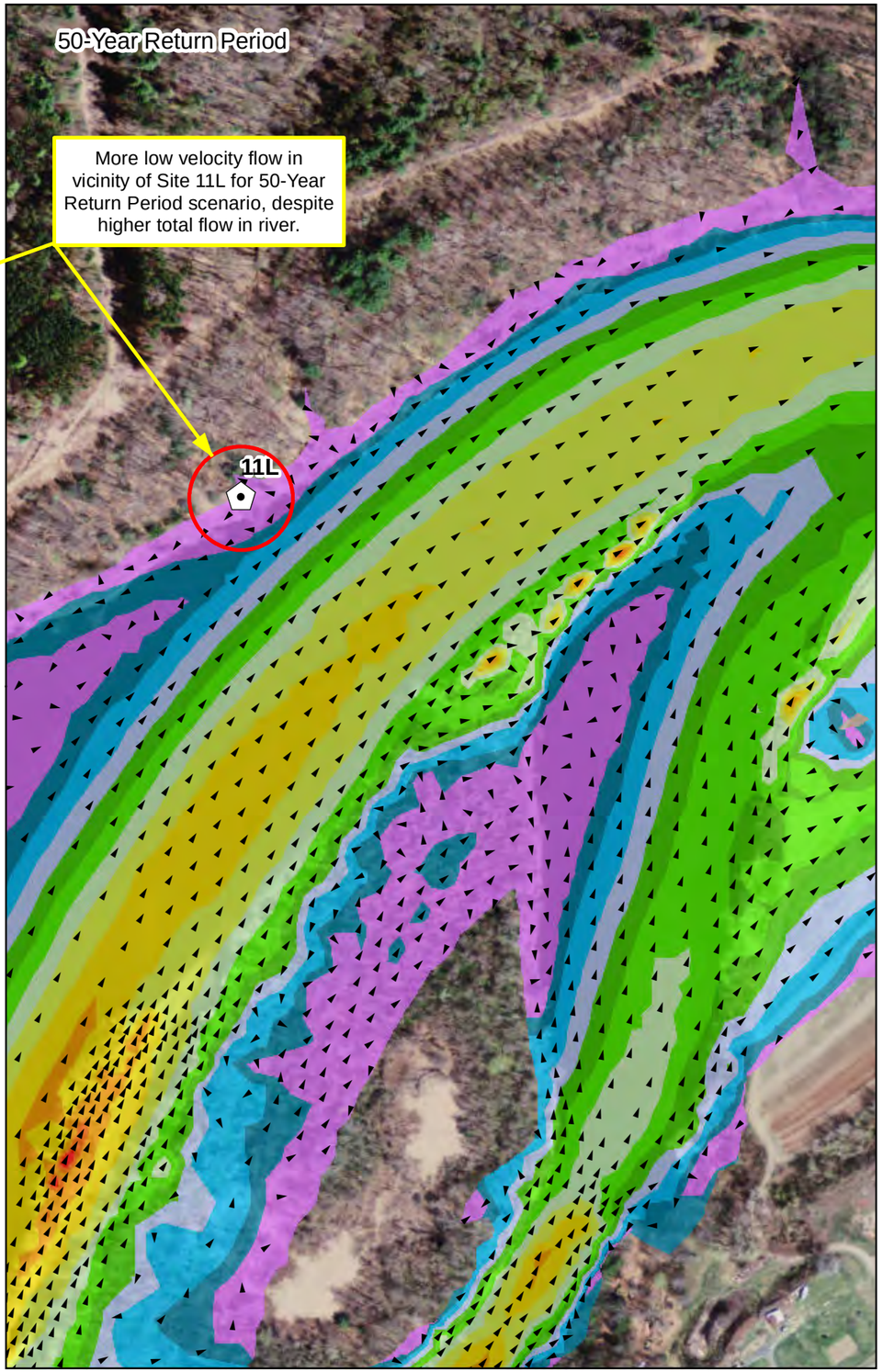

FIRSTLIGHT HYDRO GENERATING COMPANY
Northfield Mountain Pumped Storage Project No. 2485
Turners Falls Hydroelectric Project No. 1889

STUDY 3.1.2

Figure 5.5.1.2-1:
Impact of Flow Magnitude
on Flow Distribution

Legend

N

Erosion Study Site

Velocity Direction

Velocity Magnitude

- >10 (ft/s)
- 9 - 10 (ft/s)
- 8 - 9 (ft/s)
- 7 - 8 (ft/s)
- 6 - 7 (ft/s)
- 5 - 6 (ft/s)
- 4 - 5 (ft/s)
- 3 - 4 (ft/s)
- 2 - 3 (ft/s)
- 1 - 2 (ft/s)
- 0.5 - 1 (ft/s)
- 0 - 0.5 (ft/s)

Service Layer Credits: Sources: Esri, HERE, DeLorme, Intermap, increment P Corp., GEBCO, USGS, FAO, NPS, NRCAN, GeoBase, IGN, Kadaster NL, Ordnance Survey, Esri Japan, METI, Esri China (Hong Kong), swisstopo, MapmyIndia, © OpenStreetMap

0 150 300 600 Feet

1 inch = 300 feet

FirstLight Power Resources

Path: W:\gis\studies\3_1_2\maps\final_report\figure_5_5_1_2-1.mxd

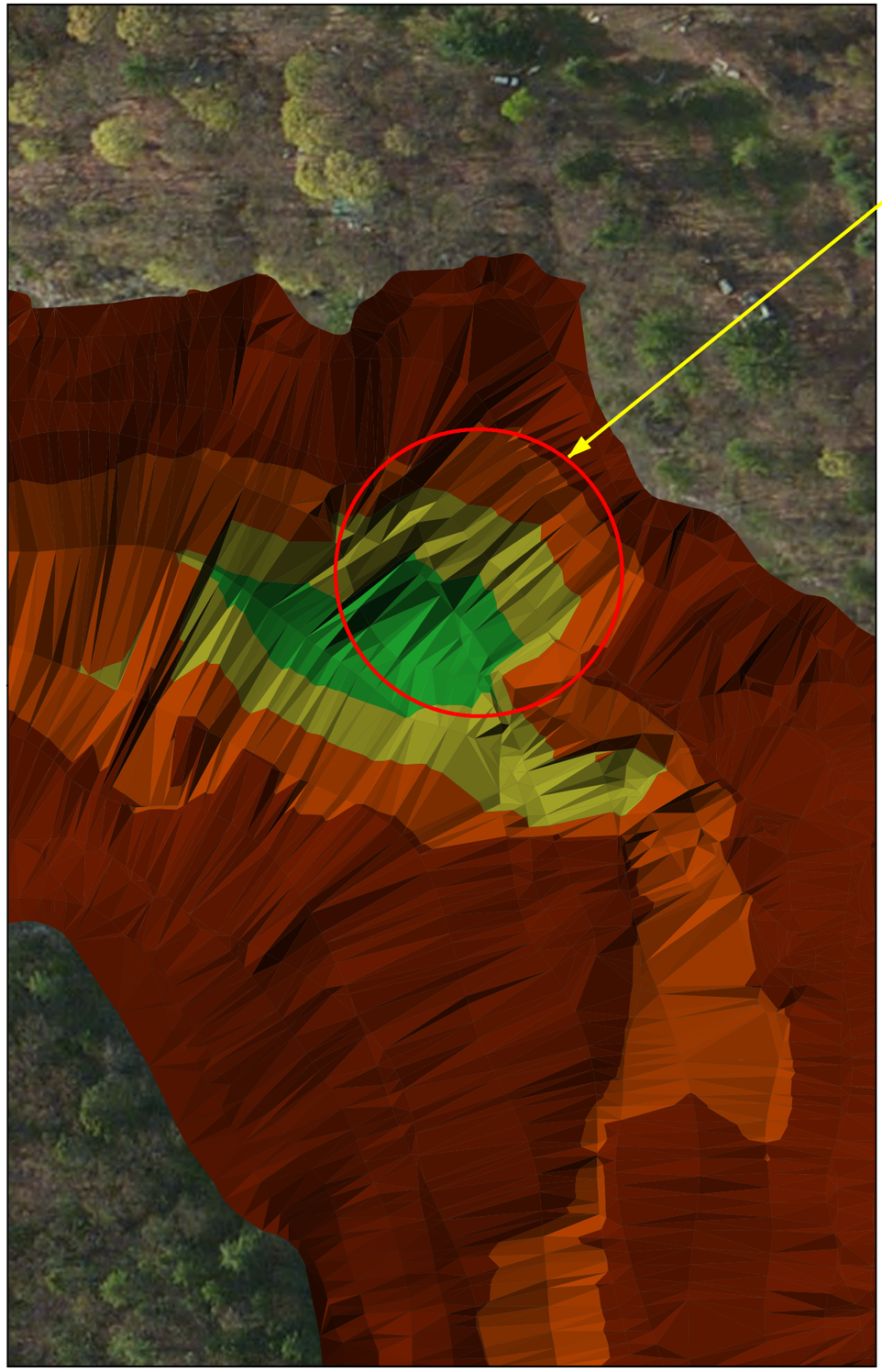

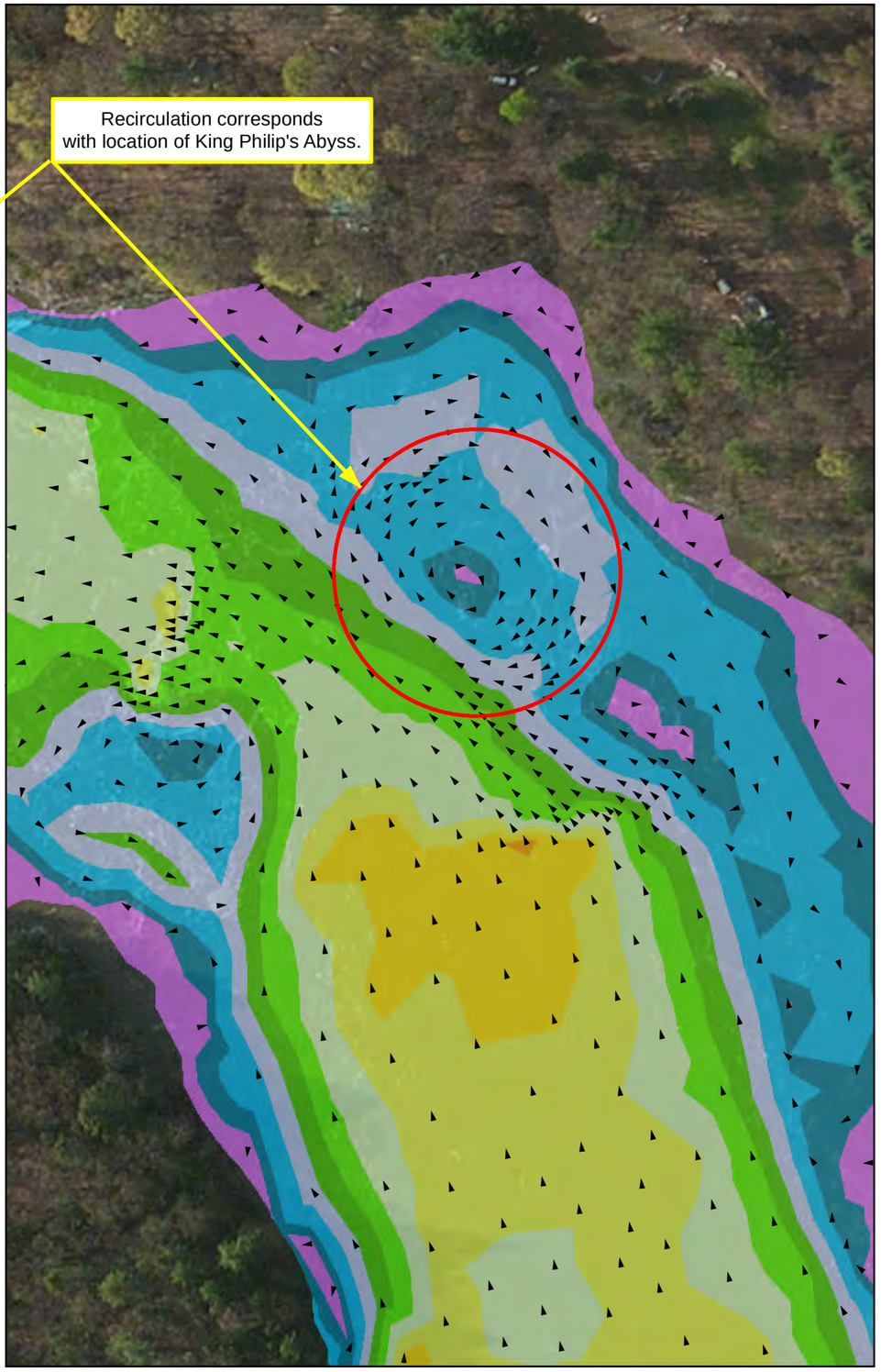

FIRSTLIGHT HYDRO GENERATING COMPANY
Northfield Mountain Pumped Storage Project No. 2485
Turners Falls Hydroelectric Project No. 1889

STUDY 3.1.2

Figure 5.5.1.2-2:
Eddy Formation in
King Philip's Abyss

Legend

- Erosion Study Site
- Velocity Direction

Velocity Magnitude

- >10 (ft/s)
- 9 - 10 (ft/s)
- 8 - 9 (ft/s)
- 7 - 8 (ft/s)
- 6 - 7 (ft/s)
- 5 - 6 (ft/s)
- 4 - 5 (ft/s)
- 3 - 4 (ft/s)
- 2 - 3 (ft/s)
- 1 - 2 (ft/s)
- 0.5 - 1 (ft/s)
- 0 - 0.5 (ft/s)

Bathymetry

- 240 - 272.309
- 210 - 240
- 180 - 210
- 150 - 180
- 120 - 150
- 90 - 120
- 60 - 90
- 30 - 60
- 0 - 30

N

Service Layer Credits: Sources: Esri, HERE, DeLorme, Intermap, increment P Corp., GEBCO, USGS, FAO, NPS, NRCAN, GeoBase, IGN, Kadaster NL, Ordnance Survey, Esri Japan, METI, Esri China (Hong Kong), swisstopo, MapmyIndia, © OpenStreetMap

0 50 100 200 Feet

1 inch = 100 feet

FirstLight Power Resources

Path: W:\gis\studies\3_1_2\maps\final_report\figure_5_5_1_2-2.mxd

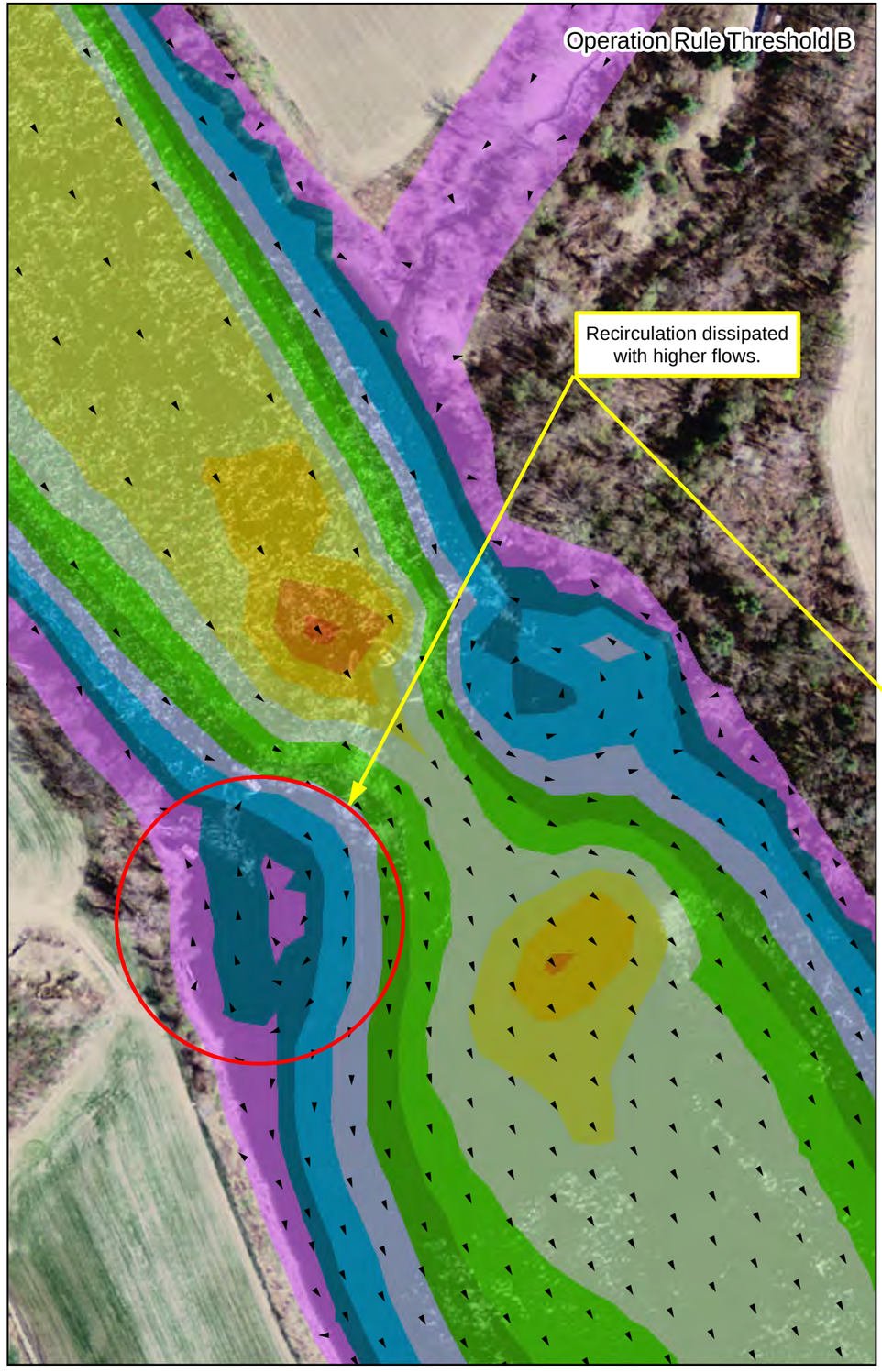

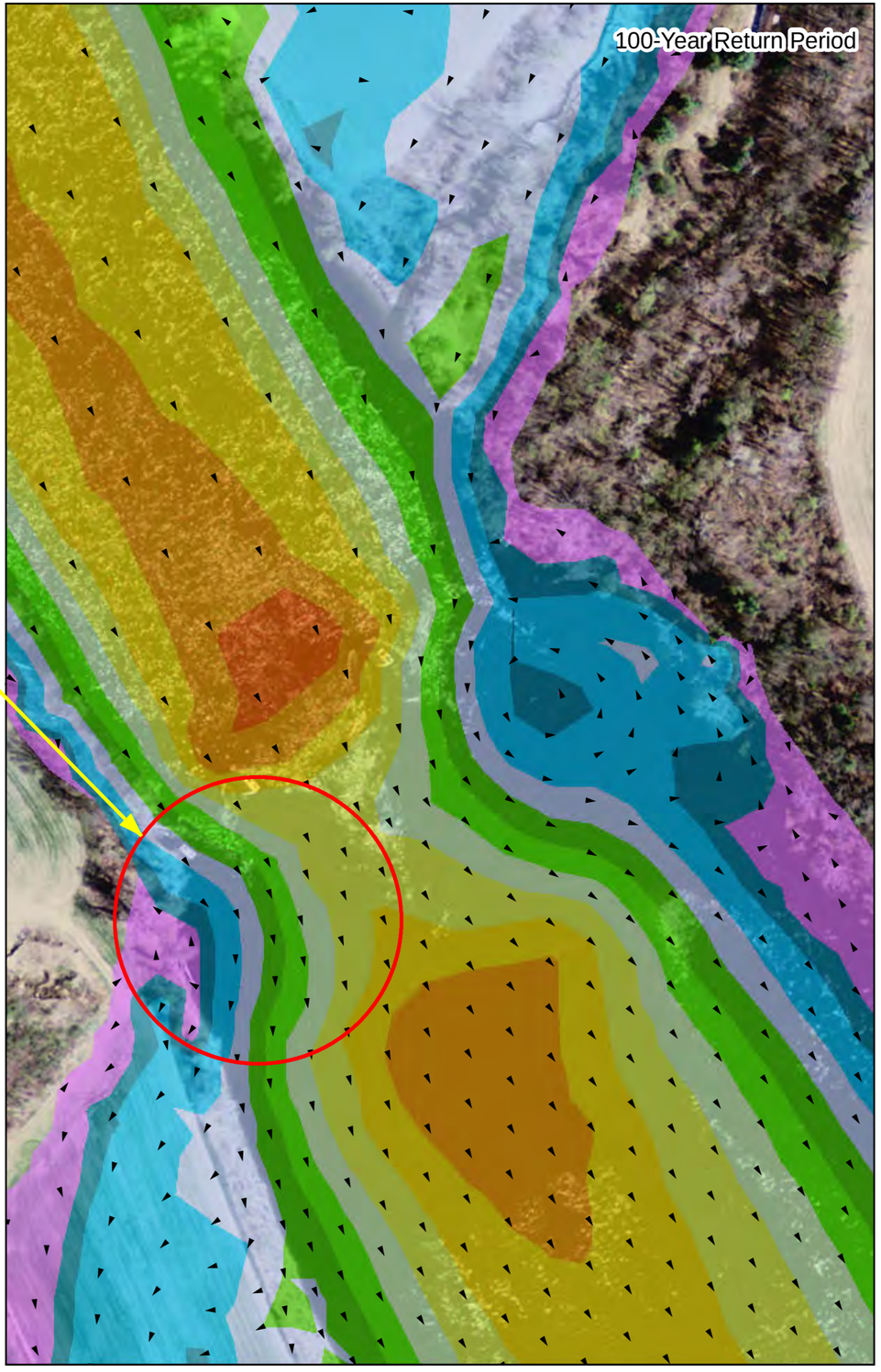

FIRSTLIGHT HYDRO GENERATING COMPANY
Northfield Mountain Pumped Storage Project No. 2485
Turners Falls Hydroelectric Project No. 1889

STUDY 3.1.2

Figure 5.5.1.2-3:
Impact of Flow Magnitude
on Eddies

Legend

- Erosion Study Site
- Velocity Direction

Velocity Magnitude

- >10 (ft/s)
- 9 - 10 (ft/s)
- 8 - 9 (ft/s)
- 7 - 8 (ft/s)
- 6 - 7 (ft/s)
- 5 - 6 (ft/s)
- 4 - 5 (ft/s)
- 3 - 4 (ft/s)
- 2 - 3 (ft/s)
- 1 - 2 (ft/s)
- 0.5 - 1 (ft/s)
- 0 - 0.5 (ft/s)

N

Service Layer Credits: Sources: Esri, HERE, DeLorme, Intermap, increment P Corp., GEBCO, USGS, FAO, NPS, NRCAN, GeoBase, IGN, Kadaster NL, Ordnance Survey, Esri Japan, METI, Esri China (Hong Kong), swisstopo, MapmyIndia, © OpenStreetMap

0 90 180 360 Feet

1 inch = 180 feet

FirstLight Power Resources

Path: W:\gis\studies\3_1_2\maps\final_report\figure_5_5_1_2-3.mxd

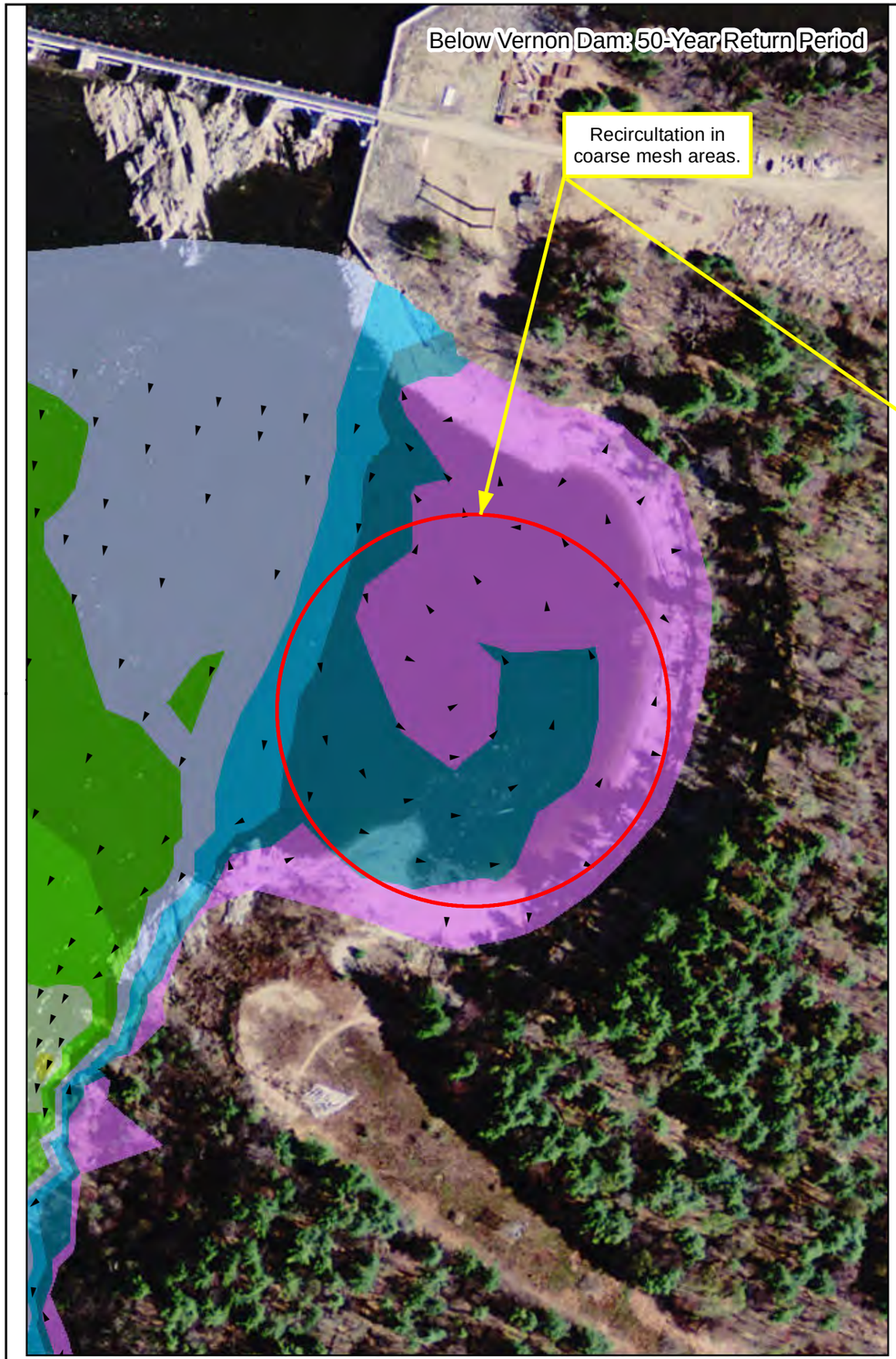

FIRSTLIGHT HYDRO GENERATING COMPANY
Northfield Mountain Pumped Storage Project No. 2485
Turners Falls Hydroelectric Project No. 1889

STUDY 3.1.2

Figure 5.5.1.2-4:
Eddying in Areas of
Coarse Resolution

Legend

- Erosion Study Site
- Velocity Direction

Velocity Magnitude

- >10 (ft/s)
- 9 - 10 (ft/s)
- 8 - 9 (ft/s)
- 7 - 8 (ft/s)
- 6 - 7 (ft/s)
- 5 - 6 (ft/s)
- 4 - 5 (ft/s)
- 3 - 4 (ft/s)
- 2 - 3 (ft/s)
- 1 - 2 (ft/s)
- 0.5 - 1 (ft/s)
- 0 - 0.5 (ft/s)

N

Service Layer Credits: Sources: Esri, HERE, DeLorme, Intermap, increment P Corp., GEBCO, USGS, FAO, NPS, NRCAN, GeoBase, IGN, Kadaster NL, Ordnance Survey, Esri Japan, METI, Esri China (Hong Kong), swisstopo, MapmyIndia, © OpenStreetMap

0 75 150 300 Feet

1 inch = 150 feet

FirstLight Power Resources

Path: W:\gis\studies\3_1_2\maps\final_report\figure_5_5_1_2-4.mxd

5.5.2 Water Level Fluctuations

Water level fluctuations associated with hydropower operations was one of the potential primary causes of erosion identified in the RSP. Section 5.1, and more specifically Section 5.1.3, presented an in-depth look at the complex hydrologic characteristics of the TFI and the hydrologic impacts the Vernon, Northfield Mountain, and Turners Falls hydropower projects have on TFI water levels. The results of the BSTEM modeling discussed in Section 5.4 also took into consideration the impact that water level fluctuations can have on bank stability and erosion processes. Analysis of supplemental groundwater data is presented in this section to examine what impact, if any, water level fluctuations have on groundwater levels and bank stability. The information presented in this section, combined with the information presented in Sections 5.1 and 5.4, provides a comprehensive understanding of water level fluctuations in the TFI and their potential role in bank stability and erosion processes.

The water surface elevation of a river varies depending on the magnitude of flow as a result of typical hydrologic factors including rainfall events and snowmelt. In addition, TFI water levels fluctuate on a shorter term basis as a result of four primary reasons:

1. Natural variability in inflows from upstream as well as from tributary inputs including key tributaries such as the Ashuelot and Millers Rivers;

2. Variable releases from the Vernon Hydroelectric Project;

3. Variable releases from the Turners Falls Hydroelectric Project resulting in water level fluctuations upstream of the Turners Falls Dam; and/or

4. Pumping and generation associated with the Northfield Mountain Project

As previously discussed, when flows are below the hydraulic capacity of the Turners Falls Project (15,938 cfs) and Vernon Project (17,130 cfs), the projects operate in a peaking power mode. During this mode of operation impoundment levels are allowed to rise upstream of the dam(s) during off-peak hours temporarily storing water for power production during peak hours. Power production during peak hours increases the flows through the power plants thus increasing the water level in the river downstream of the dam(s) while also decreasing the impoundment level upstream of the dam(s). When flow in the river is greater than the hydraulic capacity of the hydropower projects, the projects tend to generate at capacity in a run-of-river mode (i.e., inflow equals outflow) with the remaining water being passed over the dam(s). Additionally, Northfield Mountain can operate virtually independent of the flow through the TFI with a maximum generating capacity of 20,000 cfs and pumping capacity of 15,200 cfs, but common operations are not at the maximum capacities.

As discussed in Section 5.1.3, depending on flows and hydropower project operating conditions, water level management at the Turners Falls Dam and operation of Northfield Mountain can impact water levels and flows as far upstream as Vernon. Similarly, Vernon operations can impact water levels and flows as far downstream as the Turners Falls Dam. While some impacts from these projects can be observed a significant distance upstream or downstream from their location, the most significant hydrologic influences are typically localized within the general proximity to a given project with that projects impact dampening in the upstream or downstream direction. This is especially true at high flows (i.e., flows greater than the erosion thresholds observed in BSTEM) where it was observed that water level fluctuations due to hydropower operations at Northfield Mountain were typically on the order of 1.2 ft. at Site 75BL yet only 0.5 ft. at Site 303BL.

5.5.2.1 Groundwater Analysis

The relationship between groundwater levels and river water levels can affect the movement of water through the riverbank via seepage/piping in a narrow zone adjacent to the river. When the groundwater level is higher than the river water level, there is a gradient causing water in the ground to move towards the river. Water tends to move from the river into the ground when river water levels exceed adjacent groundwater levels. The hydraulic conductivity of the soil and the extent of voids or larger spaces between soil particles dictates the speed of water traveling through the soil matrix. Groundwater and river water level data were collected and analyzed in order to better understand these processes.

As discussed in Section 4.2.10, groundwater data were collected in the river as well as at 3 groundwater monitoring wells adjacent to the river in the vicinity of the Rt. 10 Bridge. The groundwater monitoring wells were setback from the edge of water approximately 52, 65, and 210 feet. The complete set of data was plotted and graphs of the entire period from July 13, 1997 through February 28, 1998 are found in Volume III (Appendix I). The corresponding flow for this period of time at the Montague gage shows that the flow ranged from approximately 2,000 to 75,000 cfs, covering periods of low flow with typical hydropower operations as well as a high flow event (Figure 5.5.2.1-1).

Examples of the data from a period of relatively low water and higher water show the response of the groundwater levels to the variations in river water level (Figures 5.5.2.1-2 and 5.5.2.1-3). As observed in the figures, the data show that the ground water closely follows the pattern of water level variations in the river at the two monitoring wells closest to the river. At the well further away from the river, the pattern of hourly fluctuations is damped out but follows the overall rising and falling trends in the river. For the vast majority of the time, the ground water level is higher than water levels in the river indicating a general gradient of groundwater flow towards the river. During the high flow event, the water level in the river rises above the groundwater levels, temporarily reversing the groundwater gradient from the river into the riverbank.

Observation of the data presented above indicates that water moves quite freely into and out of the riverbank. This demonstrates a limited opportunity for significant drawdown effects, particularly during “normal” operations since the water drains out of the soil at essentially the same rate as the decrease in river level. There are no field observations to suggest that groundwater seepage effects due to fluctuating water levels cause failure of riverbanks to any significant degree. In addition to the groundwater analysis described above, soil moisture data were collected and analyzed at the detailed study sites in support of the BSTEM modeling. BSTEM modeling also analyzed the potential impact of water level fluctuations on bank stability via its built-in near bank groundwater model. The findings of the supplemental analysis described above are generally consistent with the findings from the BSTEM modeling efforts and data analysis that showed very limited drawdown effects.

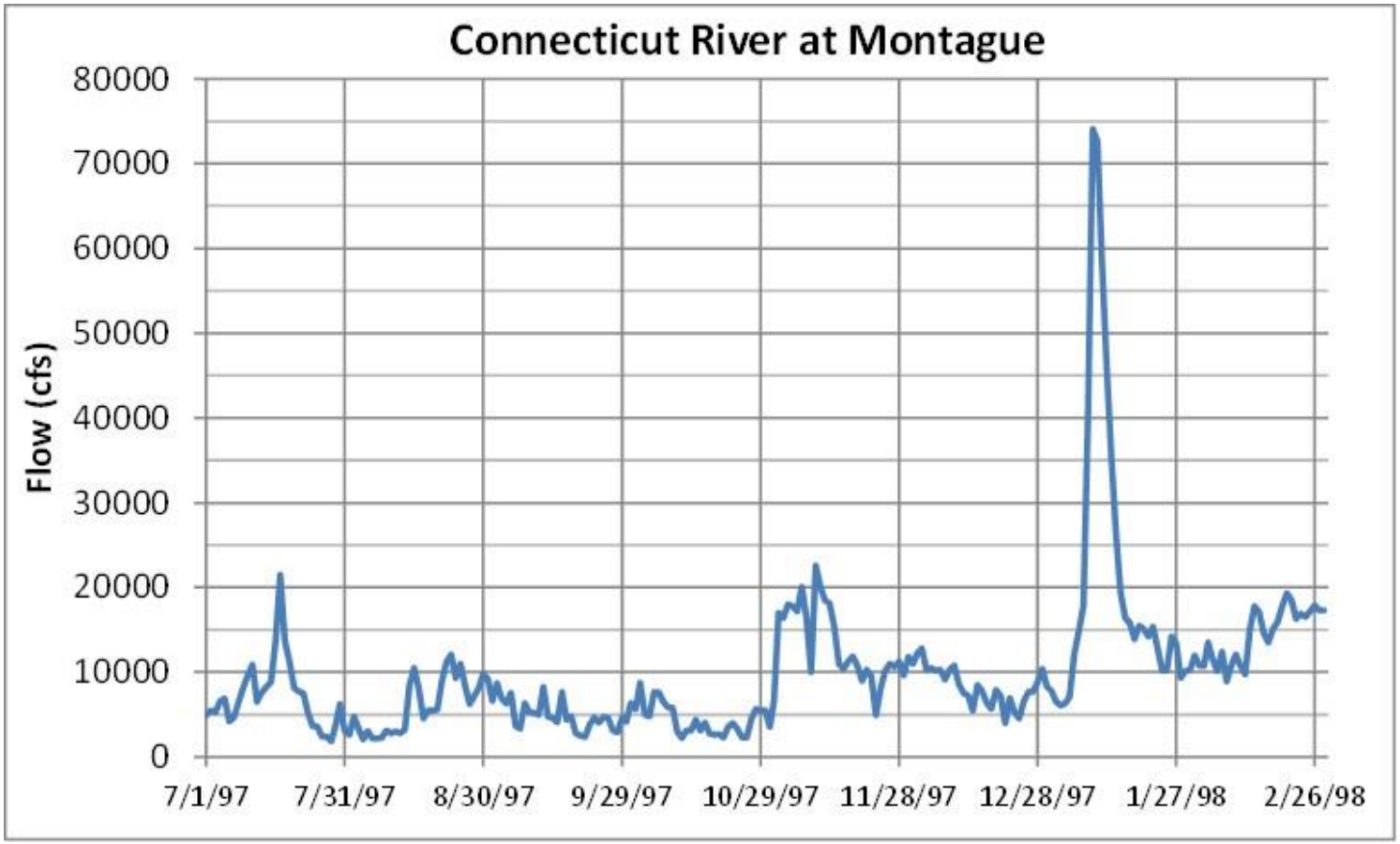

Figure 5.5.2.1-1: Connecticut River at Montague, July 1, 1997 – February 28, 1998

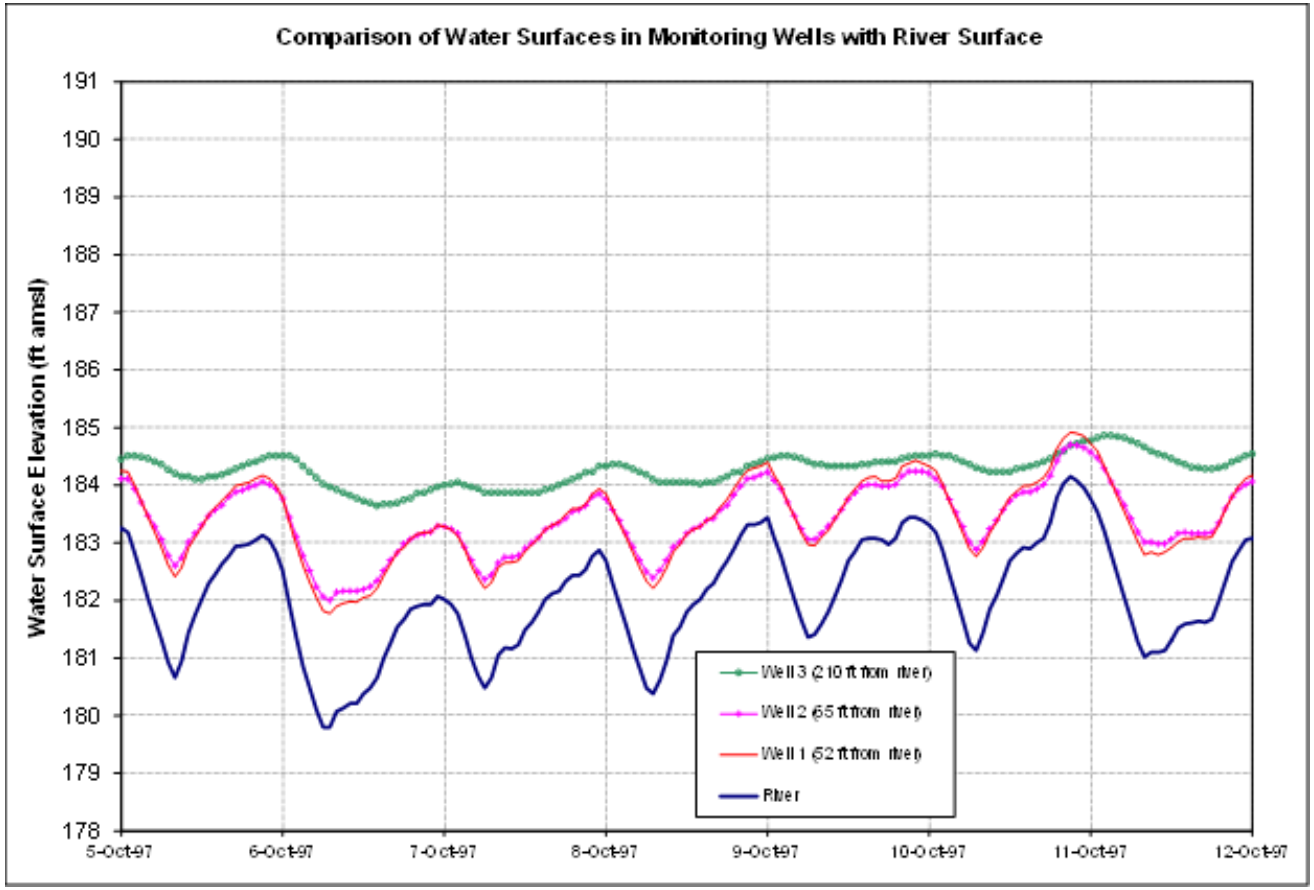

Figure 5.5.2.1-2: Water Level Monitoring Data, October 5-12, 1997

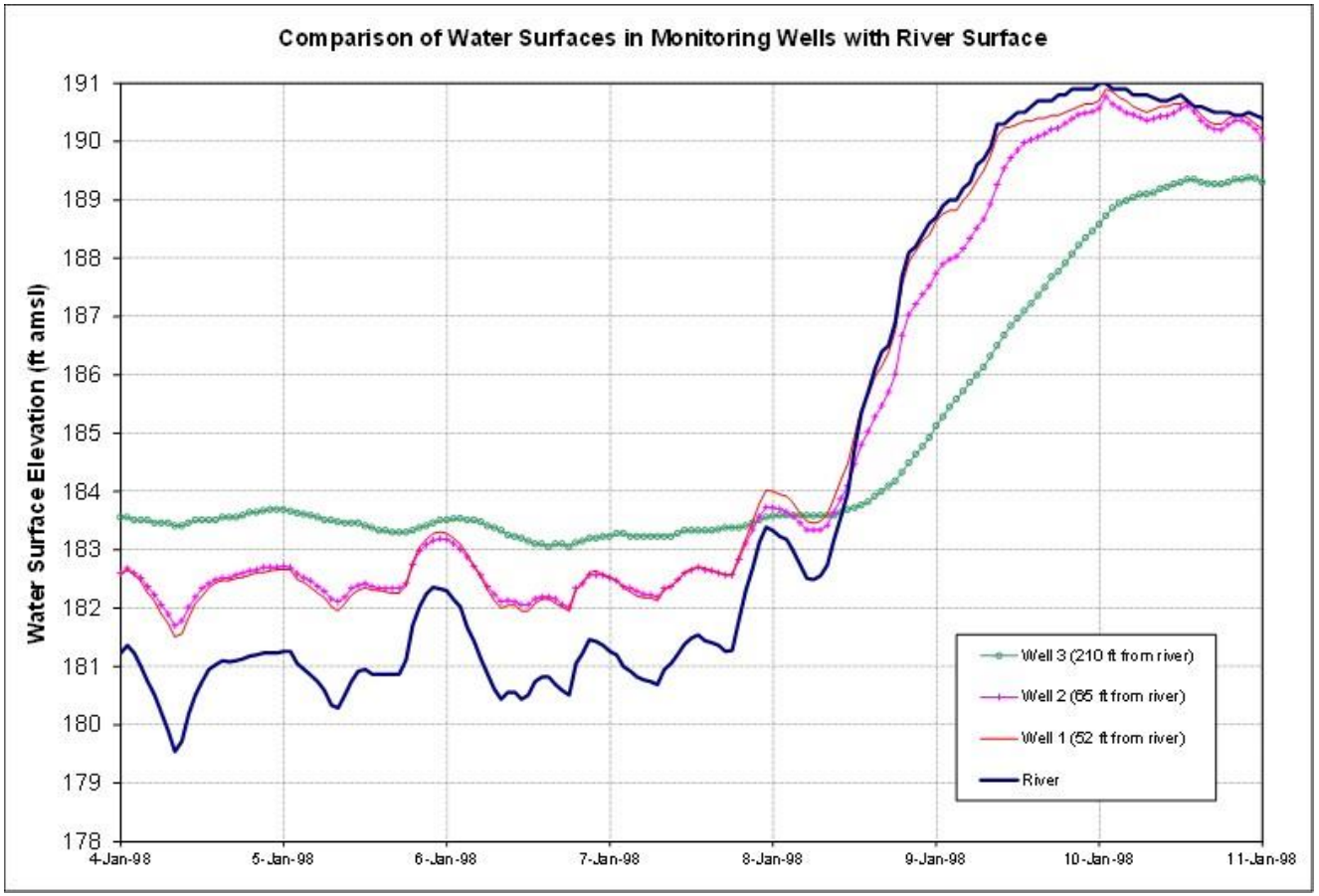

Figure 5.5.2.1-3: Water Level Monitoring Data, January 4-11, 1998

5.5.3 Boat Waves

As discussed in Section 4.2.8 and again in Section 5.4.2, boat waves were investigated in-depth and incorporated for analysis in BSTEM during the study period. In addition to the BSTEM related analysis of boat waves, supplemental boat wave data collected in the 1990's were analyzed as part of this study. This section discusses the results of the non-BSTEM boat wave analysis in order to provide additional context regarding the impact boat waves have on riverbank erosion in the TFI.

The adverse effect of boat wakes and associated waves as they impact the riverbank is acknowledged by the Connecticut River Joint Commissions, supported by Rivers and Trails Conservation Assistance Program of the National Park Service, through the Connecticut River Valley Partnership Program in a guide entitled, "River Dynamics and Erosion." This document states, *"Waves or wakes washing away soil at the base of the bank will undercut it, particularly if it is unvegetated, allowing the unsupported bank material above to collapse into the stream."* The effect of waves is also documented in the scientific literature, an example of which is found in "Experimental measurements of river-bank erosion caused by boat-generated waves on the Gordon river, Tasmania," 1993, Gerald C. Nanson, Axel Von Krusenstierna, Edward A. Bryant and Martin R. Renilson in which they acknowledge that erosion of natural river banks by boat-generated waves is an increasingly serious problem on the navigable reaches of many rivers (Nanson *et al*., 1993).

Episodes of erosion as a result of boat waves are readily observable on the Connecticut River. Furthermore, boat waves have been observed to play a role in creating instability and causing erosion in the TFI. In July 1997, and again in July 1998, S&A investigated the role boat wakes have on riverbank erosion in the TFI. The findings of that investigation are presented in the sections below.

July 1997 Observations

Data on boat waves and their effect on the riverbank were collected on July 12th and 13th, 1997 on the right bank across from Kidds Island and on the right bank downstream of the Route 10 Bridge. The water level in the TFI ranged from about El. 182 down to about El. 180 over the course of the day. The flows released from Vernon ranged from approximately 1,000 to 10,000 cfs. These flow and TFI conditions placed the water level on the lower bank or beach area rather than on the upper bank. At several locations, a temporary staff gage was installed in the water to document wave amplitude and frequency by video tape. Suspended sediment samples were also collected in the area where the waves impacted the riverbank. Figure 5.5.3-1 shows the temporary staff gage and video camera set up to record wave activity. Additional video was taken focusing on the wave activity and bank response.

The rate of rise and fall of the water level due to water level fluctuations was compared to the rate of rise and fall of the water level due to boat waves. Data collected show that boat waves impact the shore at a frequency of once every 1.2 to 1.95 seconds. The maximum amplitude of the initial boat waves recorded by the video camera was generally on the order of several tenths of a foot (approximately 0.2 to 0.4 feet). Timing and amplitude data were determined from analysis of the video of the waves on the staff gage. Some waves that were not recorded on video tape were estimated to have amplitudes as large as about one foot. Based on these data, the rate of rise and fall of the water level based on boat waves is approximately 0.2 to 0.66 feet per second (or 720 to 2400 feet per hour over the limited range of wave from crest to trough). This can be compared with the rate of rise and fall of the TFI fluctuations that are generally on the order of a few tenths of a foot per hour. The rate of change in water level for boat waves therefore ranges from about 1,000 to 10,000 times larger than for TFI fluctuations caused by variability in flow or hydropower operations. Compared against high rates of water level fluctuation that occur less frequently, the ratio of boat wave induced change to TFI level induced change would be smaller than the factor of 1,000 times. Compared against the low rates of TFI water level change that occurs more frequently, the ratio would be even greater than the factor of 10,000. This demonstrates that boat waves are orders of magnitude more

intense in terms of rapidity of change of water level than TFI fluctuations caused by variability of flow or hydropower operations.

In addition, water level fluctuations cause no horizontal impact to the riverbank; the water level simply rises and falls slowly. Boat waves, on the other hand, are traveling toward the riverbank at a significant rate of speed causing an impact against the bank as well as an intense rise and fall of water level. Hours of video tape have been collected showing the slow rise and fall of water level associated with hydropower fluctuations without any observable erosion. In contrast, hours of video tape have been collected showing significant erosion due to boat waves.

A series of six photos showing the sequence of a wave impacting the lower riverbank over a period of about 2 seconds is found in Figure 5.5.3-2a through c. Given that the general water level that day was on the lower riverbank, as the waves moved towards the bank they would break on the lower bank and erode a short notch into the bank. As each progressive wave would impact this small notch, some of the vertical face would frequently break off and collapse onto the beach where the water would move sediment particles back down the beach where they would generally deposit. During these low flow conditions the downstream velocity of the flow was negligible so no significant downstream transport of the detached and mobile sediment occurred. Even during this period of relatively low flow and water surface elevation, there was evidence of larger notches cut by the waves in the transition area between the lower and upper riverbanks (Figure 5.5.3-3).

Suspended sediment samples were collected by dip sampling near the water surface at the bank line when boat waves were impacting against the riverbank. These samples represent sediment concentrations in this limited area in the brief window of time when boat waves directly impacted against the riverbanks causing erosion. Near-bank SSC values when boat waves impacted the riverbank ranged from a few hundred to 20,000 mg/L and averaged approximately 9,800 mg/L. By contrast, average near-bank SSC values during non-boat conditions over a wide range of flows (including much higher flow events up to approximately 80,000 cfs) was approximately 66 mg/L (with a range from <5 to 280 mg/L). Based on these data, SSC values observed during boat events is about 148 (9,800/66=148) times greater than suspended sediment samples collected during non-boat events.

Comparisons between the near-bank sediment concentrations affected by boats and without boats are shown in Figures 5.5.3-4 and 5.5.3-5. The first graph is plotted on an arithmetic scale. Because the sediment concentrations are so high for the samples collected during boat events, the sediment concentrations during non-boat events are located very near the axis as if they were virtually zero (even though they range from 5 to 280 mg/L). Plotting the data using this scale shows the dramatic difference between sediment concentrations collected during boat and non-boat events. The second graph (Figure 5.5.3-5) shows the same data plotted with sediment concentrations on a semi-logarithmic scale. This way, the magnitudes of the concentrations for boat and non-boat events can be distinguished.

The majority of the samples collected during the July 1997 field investigation were collected from within the breaking waves where sediment concentrations are highest. These samples represent: (1) the immediate impact of the breaking waves on the lower bank, (2) the resulting erosion of sediment as the wave impacts against and breaks away segments of bank, and (3) the eroded sediment churning into suspension in the immediate area of the breaking wave. Samples collected from within the breaking wave are shown in the vertical row at flows in the range of approximately 7,400 to 9,300 cfs in Figure 5.5.3-4. Also observed in this figure are the two samples collected on 5/7/97 when the flow ranged from about 29,000 to 30,000 cfs. These samples were not collected directly from within the breaking boat waves but in the general vicinity of the wave. As a result the concentrations were in the few hundred mg/L range as opposed to in the thousands or tens of thousands range. While not as high as the values collected in the breaking wave, they were on the same order of magnitude or higher than those samples collected during non-boat events at significantly higher flows.

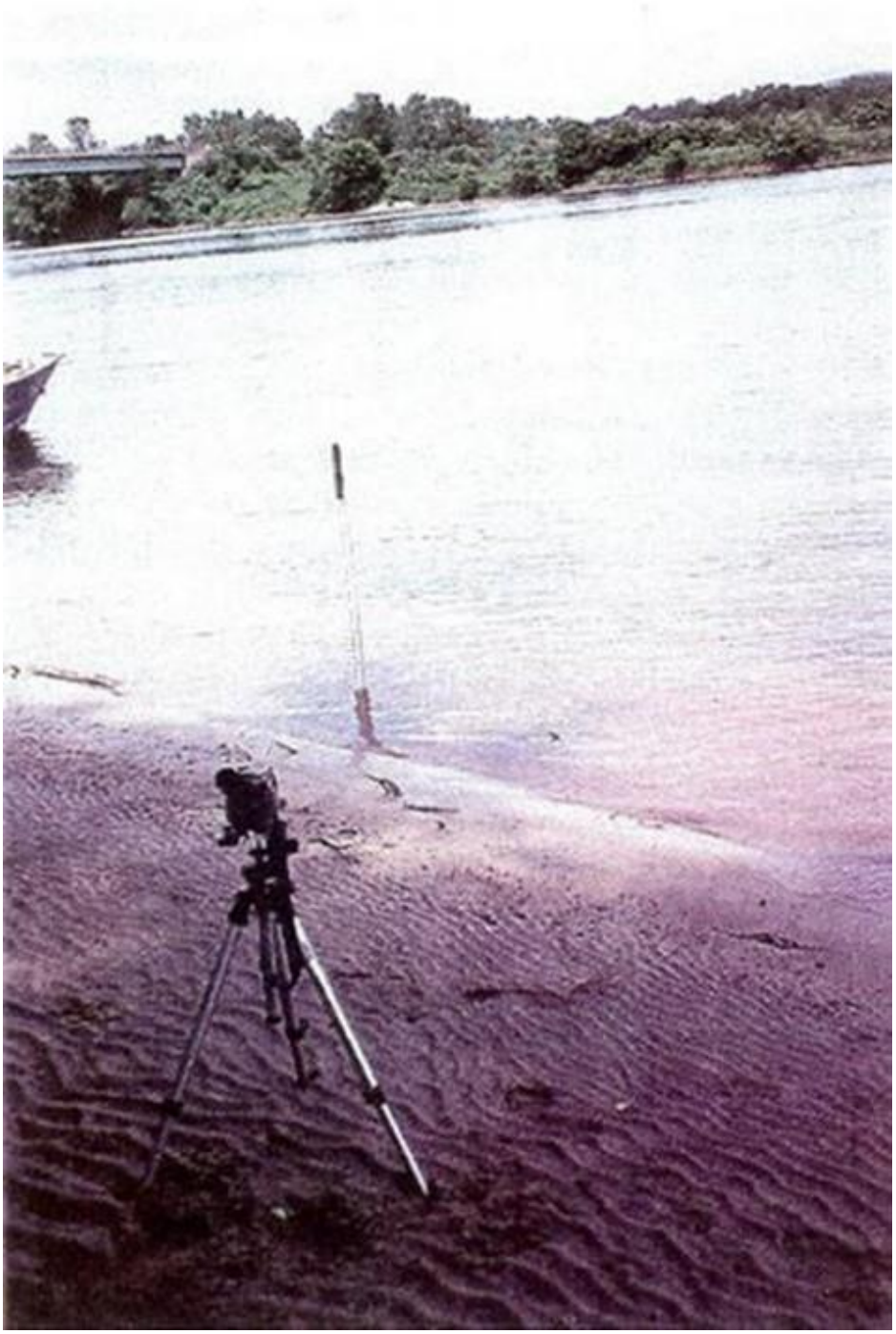

Figure 5.5.3-1: Video Camera and Temporary Staff Gage

Figure 5.5.3-2a: Boat Wave Data Collection, July 1997

Figure 5.5.3-2b: Boat Wave Data Collection, July 1997

Figure 5.5.3-2c: Boat Wave Data Collection, July 1997

Figure 5.5.3-3: Notching Due to Boat Waves

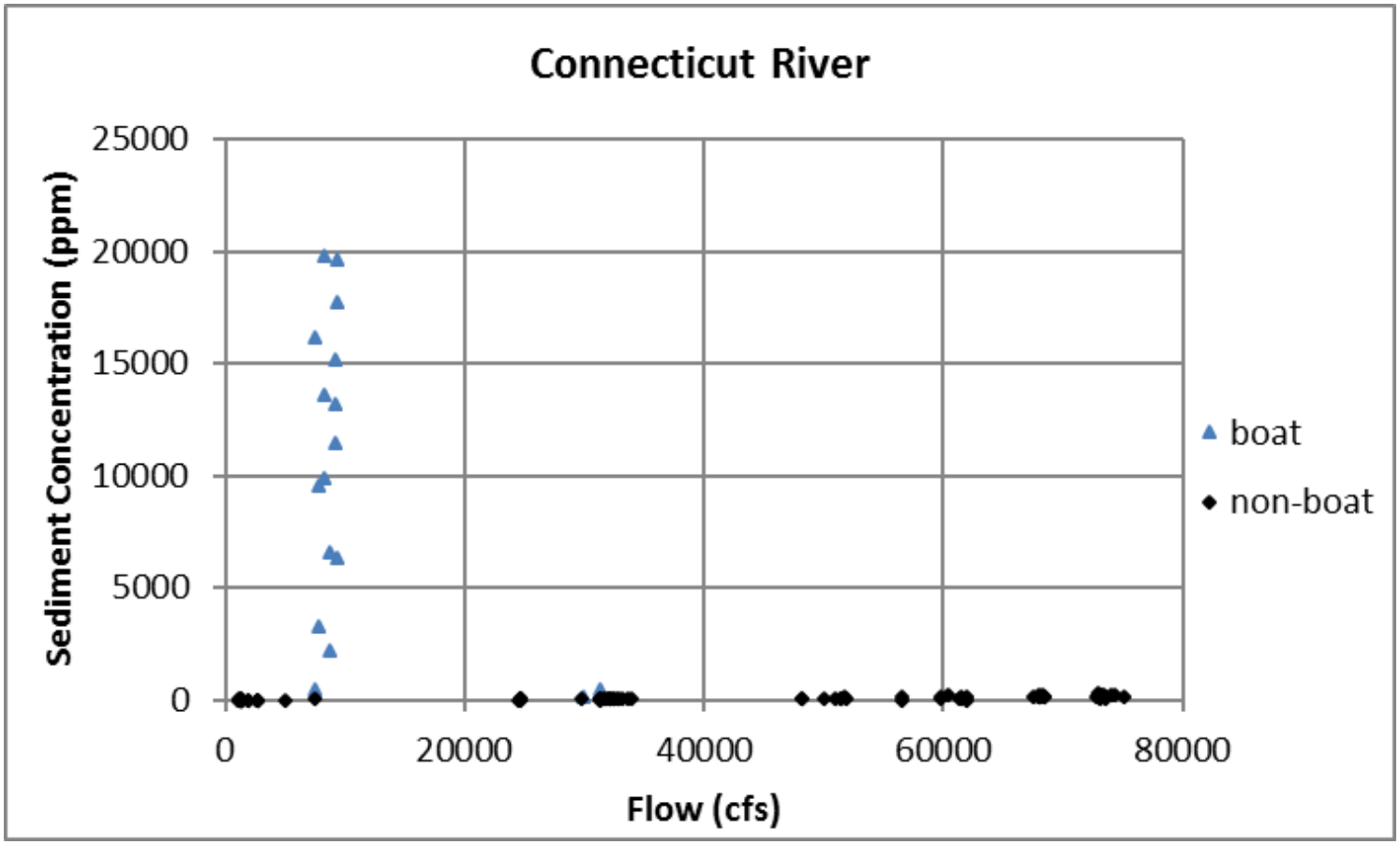

Figure 5.5.3-4 Comparison of Boat vs. Non-Boat Suspended Sediment Concentrations (arithmetic)

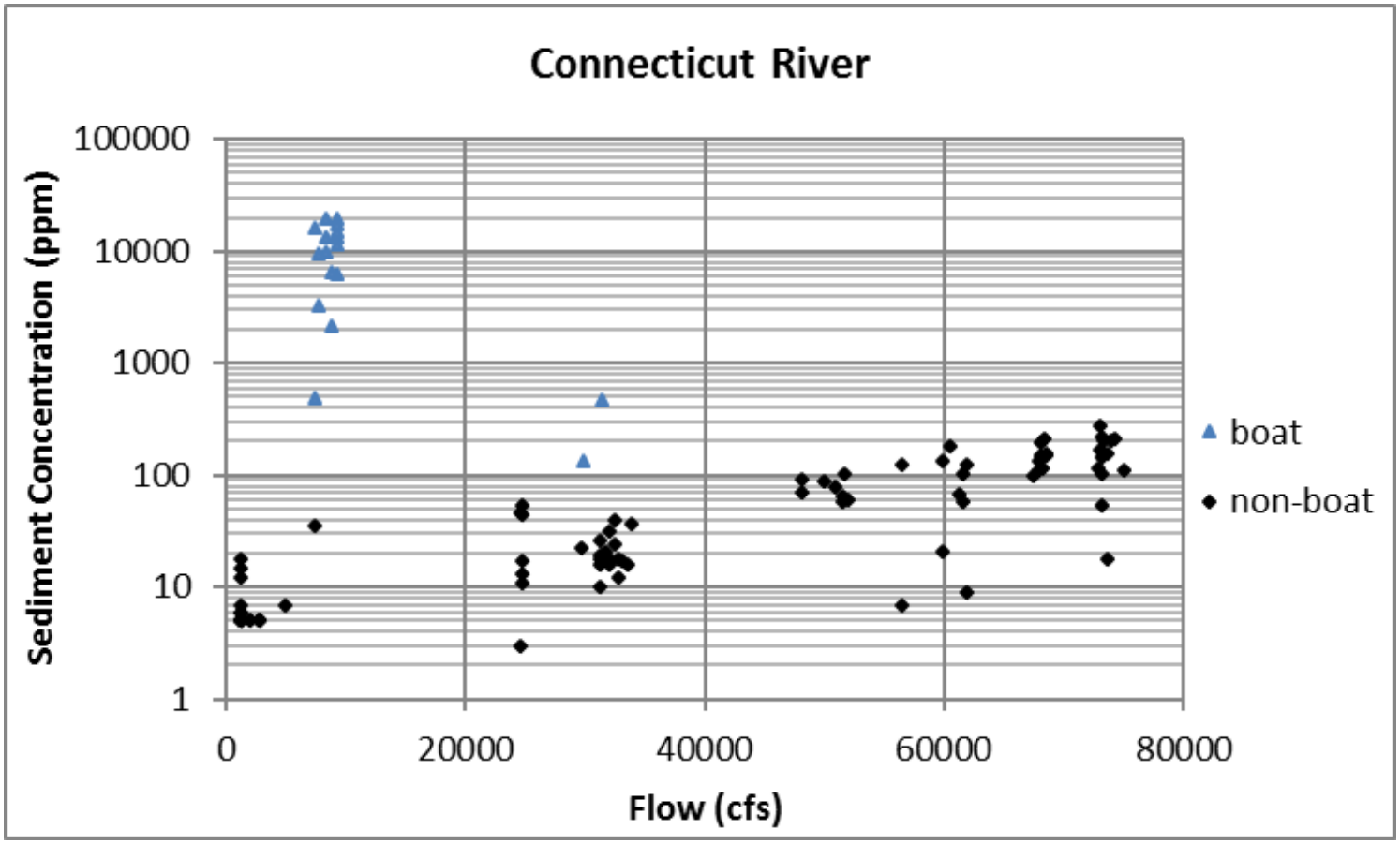

Figure 5.5.3-5 Comparison of Boat vs. Non-Boat Suspended Sediment Concentrations (log)

July 2008 Observations

Boat waves were again monitored during July 26th and 27th, 2008 on the right bank across the river from the Northfield Mountain Tailrace utilizing the same approach with a staff gage and video to analyze the effect of boat waves on riverbank erosion. During these days the flow was relatively high, with Vernon discharge between 48,000 to 50,000 cfs during the day and dropping to about 41,000 cfs at night on July 26th. On July 27th, the flow continued receding from a high of about 42,000 cfs to 34,000 cfs. The water level at Turners Falls Dam was kept between El. 178.8 to 181 during the survey. Thus, the water level at the dam was kept low during this relatively high flow event. The water level at the Northfield tailrace ranged from El. 184.2 to 187.2, dictated by the natural riverine constriction at the French King Gorge. There was no hydropower generation for several hours each day around the middle of the day and no peaking power operations at Vernon or Turners Falls since the flow exceeded the hydraulic generating capacity. As a result of the relatively high flows, the water level was generally above the lower riverbank or beach area for most of these two days and was therefore located on the upper riverbank.

The boat traffic was relatively light for a weekend in July due to cool temperatures and occasional rain. Despite the light boat traffic, significant erosion was observed due to boat waves. Figures 5.5.3-6a and 5.5.3-6b) show a sequence of boat wave impact and erosion photos captured from the video taken these two days. This sequence of photos covers a period of about 10 seconds. The first photo in the sequence shows that a piece of riverbank about 4 to 6 inches in thickness and about a foot or more in height was being undercut by waves at its base had begun to crack loose from the riverbank. As the waves continue to impact the base of this riverbank the crack widens and then the piece falls into the turbulent water. Because the water level was on the upper bank, boat waves undercut the bank and easily caused pieces of bank to fail. As a result, erosion was quite significant over this two day period at the observation site. Hours of video tape are available showing the significant and progressive erosion that resulted from boat waves that impacted the upper bank during a moderately high flow event in July 2008. During these two days, no significant erosion was observed due to the current or the slow rise and fall of the water surface. Significant erosion was observed consistently, however, whenever boat waves impacted and undercut the riverbank. This can be clearly seen in the DVD documenting the study.

After the water had receded further, a photograph of this same area shows that about 4 vertical benches were eroded into the riverbank as waves impacted the bank at different levels as the water level varied with flow (Figure 5.5.3-7). Note that tree roots are observed dangling beneath the overhanging bank at the top of the photograph. It is apparent that other higher flow events have eroded this riverbank resulting in the overhanging bank. A view from a little farther out shows the notches cut into the riverbank by boat waves and the hanging roots from the undercut tree above the portion of the bank recently impacted by boat waves (Figure 5.5.3-8).

Figure 5.5.3-6a: Boat Wave Erosion Sequence

Figure 5.5.3-6b: Boat Wave Erosion Sequence

Figure 5.5.3-7: Example of Boat Wave Erosion

Figure 5.5.3-8: Example of Boat Wave Erosion

Summary of Boat Wave Observations

When the water level is on the lower bank (beach) and boat waves occur, erosion limited in size and damage to the overall riverbank occurs (as shown in Figures 5.5.3-2 a through c). Under conditions with waves breaking on the beach, erosion is typically on the order of an inch or two high and may move on the order of an inch up to a foot in an episode of erosion up the beach. The sediment movement, in this scenario; is from wherever on the beach the wave breaks, down to lower portions of the beach. Since the waves break on the beach, the upper riverbank is not undercut to any significant degree.

On the other hand, when the water level is on the upper bank, boat waves break against a much steeper slope on the upper bank and waves, under this scenario; can and do cause significant erosion and damage to the riverbank. As shown in Figures 5.5.3-6a through b, blocks of sediment on the order of a foot high and several inches back into the bank are broken loose from the upper bank which then fall and disintegrate into individual particles as they hit the turbulent water below. A portion of this eroded material may stay on the upper beach, but when flows are high, the velocity of flow is correspondingly higher than low flow conditions and some of the sediment that is produced by wave action on the upper bank is then transported downstream and away from the beach. Again, no direct erosion of the upper riverbank was observed due to the current or the slowly rising or falling water levels. Significant erosion was observed whenever boat waves impacted and undercut the upper riverbank.

In 2015 detailed boat traffic and wave data were collected as discussed in Section 4.2.8. As part of this data collection effort, cameras were placed on three bridges throughout the TFI to document boat traffic over time. Images from this effort provide further perspective into the fact that boat waves cause some erosion along the riverbanks of the TFI. Figures 5.5.3-9 through 5.5.3-12, taken from the French King Bridge, provide evidence of the impact boat waves can have on erosion. As illustrated by the arrow in the figures, the waves breaking on the shore from the recently passed boat appear to result in a sediment plume emanating from the riverbank. As time progresses so too does the size of the plume.

Figure 5.5.3-9: Plume of Suspended Sediment Begins from Bank Erosion Induced by Waves

Figure 5.5.3-10: Suspended Sediment Plume Expands

Figure 5.5.3-11: Further Expansion of Suspended Sediment Plume

Figure 5.5.3-12: Suspended Sediment Plume Expands Farther Out From Banks

5.5.4 Land Management Practices and Anthropogenic Influences to the Riparian Zone

As part of the 2013 FRR, land-use practices within 200 ft. of adjacent riverbanks throughout the TFI were identified and classified through a combination of desktop GIS analysis and field investigation/validation. In advance of field investigation, preliminary analysis of aerial photographs (2011) was conducted to: (1) determine the width of the riparian buffer; (2) develop a list of predetermined land-use categories that would be used during the field classification; and (3) identify other pertinent land-use information that would be useful during the field survey. Land-use GIS layers from MassGIS were also referenced to complement the preliminary analysis.

Following completion of preliminary analysis land-uses adjacent to TFI riverbanks were identified for an area of approximately 200 feet horizontally from the top of the slope. Land-use categories identified during this process included:

- Agriculture (intensive (e.g., row crops) and pasture/hay)
- Barren (little or no vegetation growth)
- Developed (houses or other impermeable land uses)
- Riparian Buffer Forest (statistics for different widths (0-25 ft., 25-50 ft., 50-100 ft., 100-200 ft., and >200 ft.))
- Wetland (non-forested)
- Restored Banks
- Transportation (roads, bridges, railroad)

Table 5.5.4-1 provides a summary of the land-use classifications identified in the TFI while Table 5.5.4-2 includes summary statistics regarding the width of the forested riparian buffer throughout the TFI. Maps denoting the various land-use classifications throughout the TFI can be found in Figure 5.5.4-1.

Various types and degrees of erosion found in the TFI can be observed at locations with a wide variety of adjacent land-uses. The strongest correlation between land-use and erosion has been observed in agricultural areas. Agriculture along the river typically is located on relatively flat floodplain terraces with only a narrow or virtually non-existent zone of riparian vegetation (Figure 5.5.4-2). Riparian vegetation along a river corridor plays a significant role in riverbank stability as it damps out or attenuates hydraulic forces of flowing water or waves as well as providing structure to bind soils together through its root system. To the extent that riparian vegetation is adversely affected, riverbank stability is likewise adversely affected.

As observed in Tables 5.5.4-1 and 5.5.4-2, 27.5% of TFI riverbanks were classified as either cropland or pasture with 38% of riverbanks exhibiting a riparian buffer less than 50 ft. Frequently riverbanks in areas with narrow or non-existent riparian buffers consist of steep to overhanging banks consisting of silty/sandy soils that are easily erodible unless sufficient vegetation is present to reinforce the soil and provide some buffering of hydraulic forces. An example of erosion that has occurred where the agricultural land-use exists can be seen in Figure 5.5.4-3.

In addition to narrow riparian zones, agricultural irrigation practices can impact riverbank processes. In relatively recent years, irrigation has been increasingly utilized on a number of agricultural fields adjacent to the Connecticut River (Figures 5.5.4-4 and 5.5.4-5). Some irrigation water comes from groundwater pumping and some comes directly from the river (Figures 5.5.4-6a -c). Water is applied on relatively flat terraces adjacent to the river where agricultural fields have been developed. Irrigation water is used to

supplement rainfall which adds to wetter soil conditions. Some of the irrigation water provides water to crops and in this process a portion of the water goes to evapo-transpiration while some of it infiltrates deeper into the soil and flows back towards the river. Irrigation therefore increases soil moisture and the quantity of water that may seep through the banks which could adversely affect riverbank stability in these localized areas.

When significant rainfall occurs, water may pond on relatively flat agricultural fields and infiltrate into the ground (Figures 5.5.4-7 through 5.5.4-13, 9/30/2015). This adds to soil saturation (compared to hillslopes where more rainfall tends to occur as runoff and less infiltration into the soil). A greater degree of saturation in these soils would then result in additional seepage through the riverbank and back to the river.

In addition to agriculture, erosion has also been observed in areas where houses and other associated development are located in close proximity to the river. An example of erosion in close proximity to a house is shown in Figure 5.5.4-14. As shown in the figure undercutting, overhanging bank, and exposed roots were observed at this location in close proximity to the structure. In several instances where houses have been built close to the river, riparian vegetation has also been cleared which can adversely affect riverbank stability. An example of this is shown in Figure 5.5.4-15.

As observed in Figure 5.5.4-1, many of the eroded sites where stabilization has occurred in accordance with the ECP are found at locations where the adjacent land-use is classified as either agricultural or some other type of development. This indicates the adverse effect land-use and land management practices can have on riverbank stability.

Table 5.5.4-1: Summary of Turners Falls Impoundment Land-use (200-ft Buffer)

Land-use	Acres	Percentage of Total
Cropland	275	26
Pasture	15	1.5
Barren	1	<0.5
Developed	86	8
Transportation	22	2
Forest	631	60
Non-forested wetland	4	0.5
Restored	11	1

Table 5.5.4-2: Forested Riparian Buffer Widths (within 500 ft.)

Width (ft.)	Length (mi)	Percentage of Total
0-25	14	31
25-50	3	7
50-100	5	11
100-200	7	15
200-500	16	36

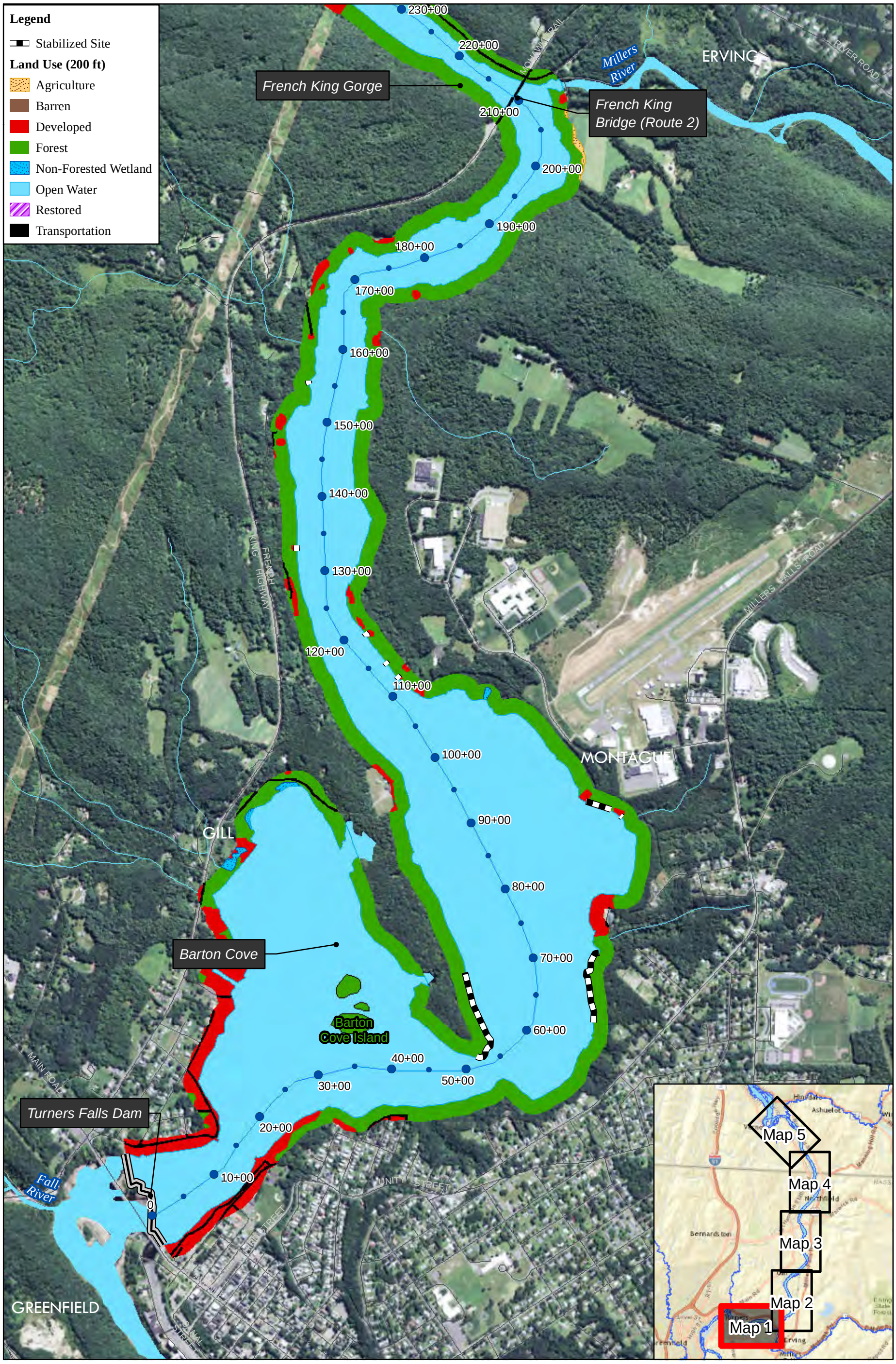

FIRSTLIGHT HYDRO GENERATING COMPANY
Northfield Mountain Pumped Storage Project No. 2485
Turners Falls Hydroelectric Project No. 1889

STUDY 3.1.2

0 625 1,250 2,500 Feet

Figure 5.5.4-1:
Turners Falls Impoundment
Land-use (2013 FRR)
Map 1

Service Layer Credits: Sources: Esri, HERE, DeLorme, USGS, Intermap, increment P Corp., NRCAN, Esri Japan, METI, Esri China (Hong Kong), Esri (Thailand), MapmyIndia, © OpenStreetMap contributors, and the GIS User Community
Source: Esri, DigitalGlobe, GeoEye, Earthstar Geographics, CNES/Airbus DS, USDA, USGS,

Path: W:\gis\studies\3_1_2\maps\final_report\figure_5_5_4-1.mxd

Legend

Stabilized Site

Land Use (200 ft)

Agriculture
Barren
Developed
Forest
Non-Forested Wetland
Open Water
Restored
Transportation

Ashuela Brook
Kidds Island
420+00
410+00
400+00
390+00
380+00
370+00
360+00
350+00
340+00
330+00
320+00
310+00
300+00
290+00
280+00
270+00
260+00
250+00
240+00
230+00
220+00
210+00
200+00
NORTHFIELD
MILLERS FALLS ROAD
Pine Meadow Brook
GILL
Fourmile Brook
Northfield Tailrace
NORTHFIELD ROAD
ERVIN
FRENCH KING HIGHWAY
French King Gorge
French King Bridge (Route 2)
MONTAGUE
Map 5
Map 4
Map 3
Map 2
Map 1

FIRSTLIGHT HYDRO GENERATING COMPANY
Northfield Mountain Pumped Storage Project No. 2485
Turners Falls Hydroelectric Project No. 1889
STUDY 3.1.2

N

0 625 1,250 2,500 Feet

Figure 5.5.4-1:
Turners Falls Impoundment
Land-use (2013 FRR)
Map 2

Path: W:\gis\studies\3_1_2\maps\final_report\figure_5_5_4-1.mxd

Legend

- Stabilized Site

Land Use (200 ft)

- Agriculture
- Barren
- Developed
- Forest
- Non-Forested Wetland
- Open Water
- Restored
- Transportation

620+00
610+00
600+00
590+00
580+00
570+00
560+00
550+00
540+00
530+00
520+00
510+00
500+00
490+00
480+00
470+00
460+00
450+00
440+00
430+00
420+00

Route 10 Bridge
(Bennett's Meadow Bridge)

Bennett Brook
Millers Brook
Bailey Brook
Ashuela Brook
Otter Run
Roaring Brook
Connecticut River
Kidds Island

MOUNTAIN
ROUTE 10
GILL CENTER ROAD
MAIN ROAD
MAIN STREET
MAPLE STREET
WARWICK ROAD
MILLERS FALLS ROAD

NORTHFIELD
BERNARDSTON
GILL

Map 5
Map 4
Map 3
Map 2
Map 1

FIRSTLIGHT HYDRO GENERATING COMPANY
Northfield Mountain Pumped Storage Project No. 2485
Turners Falls Hydroelectric Project No. 1889

STUDY 3.1.2

N

0 625 1,250 2,500 Feet

Figure 5.5.4-1:
Turners Falls Impoundment
Land-use (2013 FRR)
Map 3

Service Layer Credits: Sources: Esri, HERE, DeLorme, USGS, Intermap, increment P Corp., NRCAN, Esri Japan, METI, Esri China (Hong Kong), Esri (Thailand), MapmyIndia, © OpenStreetMap contributors, and the GIS User Community
Source: Esri, DigitalGlobe, GeoEye, Earthstar Geographics, CNES/Airbus DS, USDA, USGS,

Path: W:\gis\studies\3_1_2\maps\final_report\figure_5_5_4-1.mxd

Legend

- Stabilized Site

Land Use (200 ft)

- Agriculture
- Barren
- Developed
- Forest
- Non-Forested Wetland
- Open Water
- Restored
- Transportation

830+00
820+00
810+00
800+00
790+00
780+00
770+00
760+00
750+00
740+00
730+00
720+00
710+00
700+00
690+00
680+00
670+00
660+00
650+00
640+00
630+00

VERNON
HINSDALE
WINCHESTER
VERMONT
MASSACHUSETTS
NEW HAMPSHIRE
MASSACHUSETTS
NORTHFIELD

Newton Brook
Bottom Brook
Mallory Brook
Pauchaug Brook
Louisiana Brook
Connecticut River
Mill Brook

FORT BRIDGMAN RD
MOUNT HERMON STATION ROAD
WEST NORTHFIELD ROAD
EAST NORTHFIELD ROAD
PAUCHAUG RAMP ROAD
HINSDALE ROAD
WANAMAKER ROAD
Northfield Rd
South Parrish Rd
South Scofield Mt Rd
Bolton Rd
Staddle Hill Rd
Gosselin Rd
Mine Rd
Avery Cir
Valley View Dr
Homestead Dr

Map 5
Map 4
Map 3
Map 2
Map 1

FirstLight Power Resources

N

FIRSTLIGHT HYDRO GENERATING COMPANY
Northfield Mountain Pumped Storage Project No. 2485
Turners Falls Hydroelectric Project No. 1889

STUDY 3.1.2

0 625 1,250 2,500 Feet

Figure 5.5.4-1:
Turners Falls Impoundment
Land-use (2013 FRR)
Map 4

Service Layer Credits: Sources: Esri, HERE, DeLorme, USGS, Intermap, increment P Corp., NRCAN, Esri Japan, METI, Esri China (Hong Kong), Esri (Thailand), MapmyIndia, © OpenStreetMap contributors, and the GIS User Community
Source: Esri, DigitalGlobe, GeoEye, Earthstar Geographics, CNES/Airbus DS, USDA, USGS,

Path: W:\gis\studies\3_1_2\maps\final_report\figure_5_5_4-1.mxd

Legend

- Stabilized Site

Land Use (200 ft)

- Agriculture
- Barren
- Developed
- Forest
- Non-Forested Wetland
- Open Water
- Restored
- Transportation

Vernon Dam

1060+00
1050+00
1040+00
1030+00
1020+00
1010+00
1000+00
990+00
980+00
970+00
960+00
950+00
940+00
930+00
920+00
910+00
900+00
890+00
880+00
870+00
860+00
850+00
840+00
830+00

Stebbins Island

Upper Island

Ashuelot River

Newton Brook

VERNON

GOVERNOR HUNT RD
RIVERET DR
FORT BRIDGMAN RD
Strawberry Ln
Prospect St
School St
Hinsdale Heights St
Mohawk St
Indian Acres Dr
Butler Ave
No Name
Old Sledge Rd
River Rd
STEBBINS RD
MARY RD
BLODGETT RD
NEWTON RD
NEWTON HILLS
BRETTY ACRES DR
LINDY LN
MEADOW RD
WOODLAND RD
FOX HILL RD
S ORTWELL RD
POND RD
VALLEY VIEW DR
Transfer Station Rd
Northfield Rd
CENTRAL PK RD
OAK CT
PINE RDG
POPLAR LN
WASHBURN LN
WEST RD
ROAD RD
THIRD DR

Map 5
Map 4
Map 3
Map 2
Map 1

FIRSTLIGHT HYDRO GENERATING COMPANY
Northfield Mountain Pumped Storage Project No. 2485
Turners Falls Hydroelectric Project No. 1889

STUDY 3.1.2

0 625 1,250 2,500 Feet

Figure 5.5.4-1:
Turners Falls Impoundment
Land-use (2013 FRR)
Map 5

Service Layer Credits: Sources: Esri, HERE, DeLorme, USGS, Intermap, increment P Corp., NRCAN, Esri Japan, METI, Esri China (Hong Kong), Esri (Thailand), MapmyIndia, © OpenStreetMap contributors, and the GIS User Community
Source: Esri, DigitalGlobe, GeoEye, Earthstar Geographics, CNES/Airbus DS, USDA, USGS,

Path: W:\gis\studies\3_1_2\maps\final_report\figure_5_5_4-1.mxd

Figure 5.5.4-2 Agricultural development on the terraces of the Turners Falls Impoundment

Figure 5.5.4-3: Erosion Adjacent to Agricultural Land-use

Figure 5.5.4-4: Irrigation on agricultural field adjacent to the Connecticut River and Location on Google Earth, Photo 48

Figure 5.5.4-5: Irrigation pumping from the Connecticut River and Location on Google Earth, Photo 255

Figure 5.5.4-6a: Irrigation pumping from the Connecticut River, Photo 359

Figure 5.5.4-6b: Irrigation pumping from the Connecticut River, Photo 364

Figure 5.5.4-6c: Location of Photos 359 and 364 (Google Earth)

Figure 5.5.4-7: Ponding on agricultural fields from rainfall event, September 30, 2015 (a)

Figure 5.5.4-8: Ponding on agricultural fields from rainfall event, September 30, 2015 (b)

Figure 5.5.4-9: Ponding on agricultural fields from rainfall event, September 30, 2015 (c)

Figure 5.5.4-10: Ponding on agricultural fields from rainfall event, September 30, 2015 (d)

Figure 5.5.4-11: Ponding on agricultural fields from rainfall event, September 30, 2015 (e)

Figure 5.5.4-12: Ponding on agricultural fields from rainfall event, September 30, 2015 (f)

Figure 5.5.4-13: Ponding on Agricultural Fields from Rainfall Event, September 30, 2015 (g)

Figure 5.5.4-14: Erosion adjacent to seasonal Camp 2-W

Figure 5.5.4-15: Development thinning or removing riparian vegetation

5.5.5 Ice

Ice can cause damage to riverbanks and effect erosion processes in a number of ways, including:

- During break-up when moving ice can impact or push against and gouge into the bank disrupting or dislodging segments of the bank;
- Damaging or removing vegetation as it is moving along the bank shearing off or scraping against vegetation; and
- Ripping roots out of the ground when vegetation frozen into the ice is pulled up when the ice begins to move during break-up

For decades (since the early 1970s) when VY began using the Connecticut River for cooling water there has been little ice formation. With the decommissioning of this facility at the end of 2014, water temperatures in the Connecticut River downstream of VY have decreased; thus, increasing the potential presence of ice in the TFI. As discussed in Section 4.2.11, in order to account for the fact that ice may play a more significant role in riverbank erosion processes in the future a number of additional analyses were conducted. The results of these analyses are presented in this section.

5.5.5.1 TFI Photo Documentation – Winter 2015/2016

Photos were taken on eight occasions during the winter of 2015/2016 (December 15, 2015 to March 8, 2016) at eight locations spanning the geographic extent of the TFI to document ice conditions (Figure 4.2.11-1). The goal of the photo monitoring was to observe: (1) when sheet ice developed; (2) during formation of sheet ice; (3) during ice break-up; and (4) after ice break-up occurred. The winter of 2015/2016 was unseasonably mild and did not produce significant ice formation in the TFI. Documentation of ice conditions (or lack thereof) during the winter 2015/2016 are found in Volume III (Appendix J).

In preparation for the 2015-2016 ice season, some photographs were taken of ice conditions that occurred the preceding winter (2014-2015) when conditions were more conducive to the formation of ice. Examples of this effort are presented in Figures 5.5.5.1-1 through 5.5.5.1-10. The full set of photos are included in Volume III (Appendix J). While much of the river in the TFI was covered with ice during the winter of 2014-2015, ice break-up was uneventful and no significant damage or erosion was noted after the ice had melted in the spring of 2015.

Staff from USGS in Vermont and New Hampshire indicated in discussions with FirstLight that they have observed that ice typically does not cause erosion if the ice simply melts in place without significant break-up and if ice floes moving down river causing ice jams and impacting the banks do not occur. If, on the other hand, there is significant break-up, ice floes moving down river with the potential for ice jams that are pushed against and scrape along the banks; then such an event could potentially cause erosion and damage to the riverbanks. Ice formation and accompanying freeze/thaw cycles can weaken the soil matrix by developing cracks and spalling of the soil surface; however, the process of ice break up plays the most significant role in determining the potential for erosion caused by ice.

Figure 5.5.5.1-1: Barton Cove 1/5/2015

Figure 5.5.5.1-2: Barton Cove 3/3/2015

Figure 5.5.5.1-3: Northfield Mountain Tailrace 1/5/2015

Figure 5.5.5.1-4: Northfield Mountain Tailrace 3/3/2015

Figure 5.5.5.1-5: Route 10 Bridge 1/5/2015

Figure 5.5.5.1-6: Route 10 Bridge 1/5/2015

Figure 5.5.5.1-7: Route 10 Bridge 3/3/2015

Figure 5.5.5.1-8: Route 10 Bridge 3/3/2015

Figure 5.5.5.1-9: Pauchaug Boat Launch 1/5/2015

Figure 5.5.5.1-10: Pauchaug Boat Launch 3/3/2015

5.5.5.2 Analysis of Available Historic Ice Information

TransCanada was contacted to conduct database research of available ice information on upstream reaches of the Connecticut River. Primarily this information focused on the Vernon, Bellows Falls, and Wilder Impoundments, but some information from the TFI was also found. Additional research into USACE Cold Regions Research and Engineering Laboratory (CRREL) information on ice was also conducted. As part of this research, a trip was made to TransCanada's Bellows Falls office where TransCanada staff had organized files in boxes for review. Hundreds of individual documents were reviewed and numerous files scanned which contained relevant information. A list of the scanned files and associated type of information is provided in Volume III (Appendix J). Included in the TransCanada files were several documents, papers, and reports regarding ice from CRREL.

Much of the information contained in the TransCanada files consisted of photographs of ice jams, ice damage and erosion that occurred as a result of ice. One of the earliest set of photos from TransCanada showing ice was taken in 1915 at Brattleboro, VT (Figure 5.5.5.2-1), which is located in the Vernon Impoundment and just downstream of the West River confluence. Ice had moved a boat house adjacent to the river and ice had been forced over the riverbanks causing damage to trees as shown in Figures 5.5.5.2-2 and 5.5.5.2-3.

Sets of photographs showing ice found in the TransCanada files include the following years: 1915, 1935, 1940, 1941, 1942, 1943, 1945, 1946, 1959, 1968, 1989, 1992, and 1994. Figure 5.5.5.2-4 provides an example of historic ice photos taken in 1915. In addition to a number of sets of photographs of ice, some data was also available in the TransCanada files including ice thickness at several locations along the river. An example of such data is shown in Figure 5.5.5.2-5. Another example of the type of ice data that are available is found in Figure 5.5.5.2-6. Similar types of data were found in the TransCanada files for the following years: 1940, 1944, 1945, 1946, 1948, 1951, 1952, 1953, 1955, 1956, 1957, and 1958. While some observations, are available before and after these years, actual measurements of ice in the available files were concentrated in the 1940s and 1950s. In addition, maps of the extent of ice were occasionally developed based on observations along the river (Figure 5.5.5.2-7). A review of the files also found that tributaries to the Connecticut River are a significant contributor of ice. When ice jams occur, they form as a result of constrictions or shallow areas associated with tributaries.

The fact that ice can and has caused significant damage and erosion to riverbanks and riparian vegetation is clearly documented photographically as shown in various images from TransCanada. One of the years when ice data, notes, and photographs were all taken during ice formation and after it had melted was 1946. This set of information provides insight into ice observations (Figure 5.5.5.2-8), ice photographs (Figures 5.5.5.2-9 through 5.5.5.2-11), ice measurements (Figure 5.5.5.2-12), and damage to riverbanks caused by ice (Figures 5.5.5.2-13 through 5.5.5.2-20). While photographs were either not taken or not available from reaches farther downstream along the Connecticut River in 1946; notes of observations clearly document that ice moved through the river farther downstream, including the TFI (Figure 5.5.5.2-21).

Damage to riverbanks near Cornish, NH in 1946 look very similar to what was observed farther downstream in the Bellows Falls Impoundment in the study conducted by Simons & Associates, 1992, *"Analysis of Bank Erosion at the Skitchwaug Site in the Bellows Falls Pool of the Connecticut River."* The destruction of vegetation and the jagged nature of the top of bank in 1946 (Figure 5.5.5.2-22) following the ice event that year look similar to the lack of vegetation and ice pushed into the banks in 1992 (Figure 5.5.5.2-23). We believe the impacts at this location in 1992 were similar to that depicted in the 1946 photo.

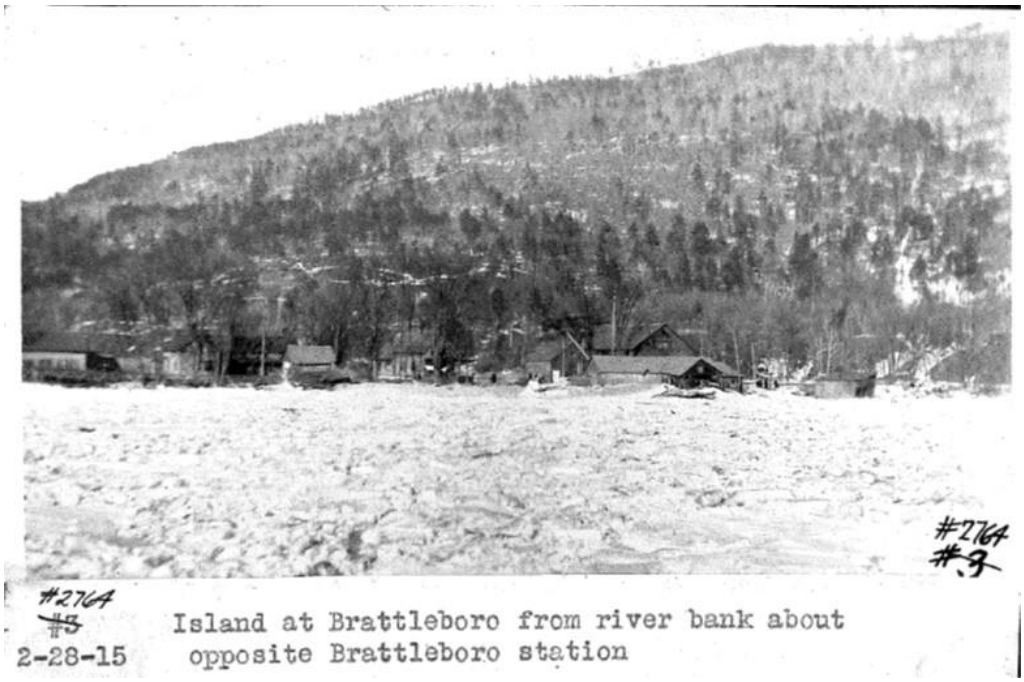

Figure 5.5.5.2-1 Ice on the Connecticut River at Brattleboro, VT – 1915 (TransCanada)

Figure 5.5.5.2-2 Connecticut River Boat House Moved by Ice – 1915 (TransCanada)

Figure 5.5.5.2-3 Ice along riverbanks showing damage to trees, 1915 (after TransCanada)

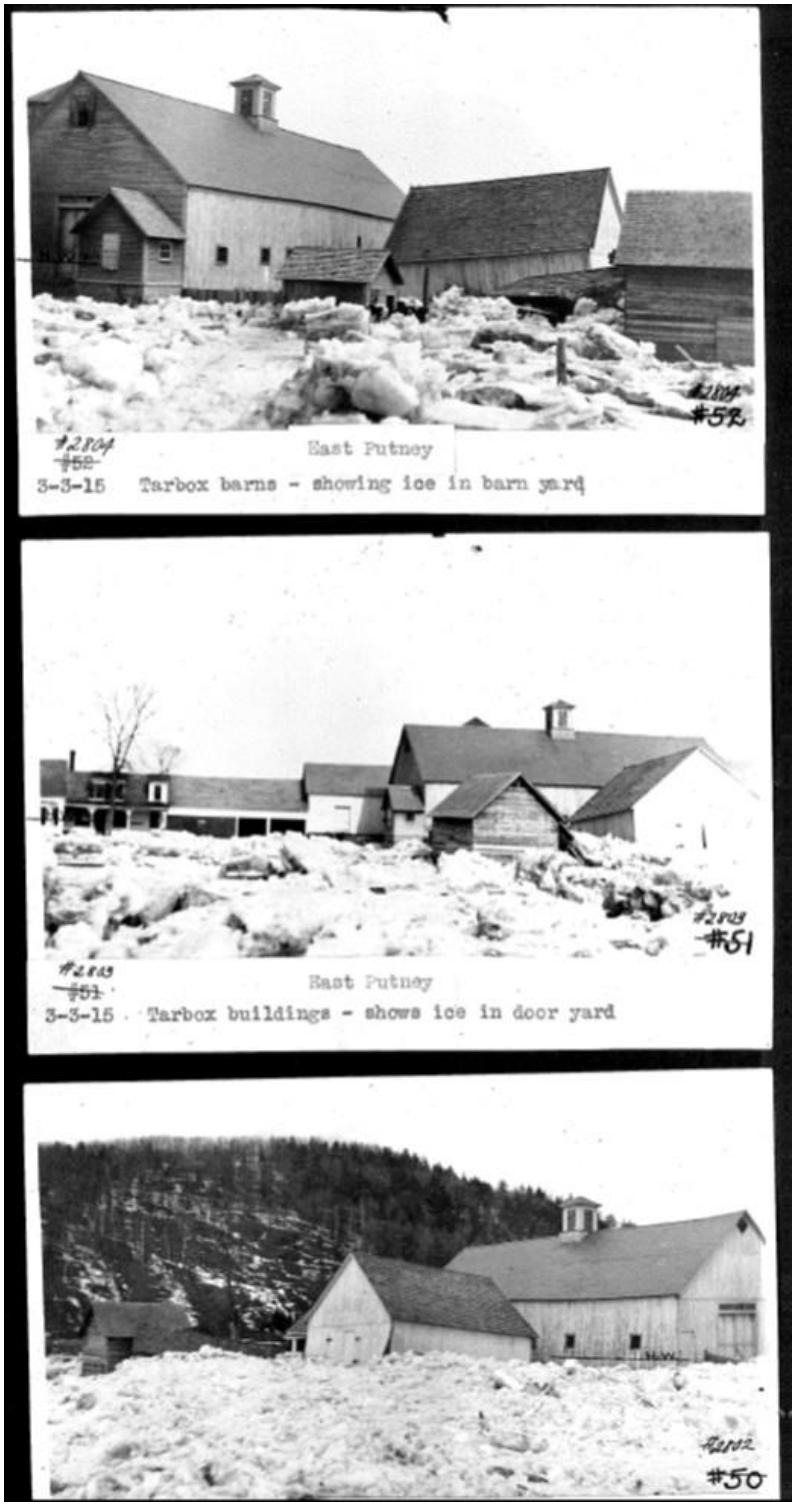

Figure 5.5.5.2-4 Ice at East Putney – 1915 (TransCanada)

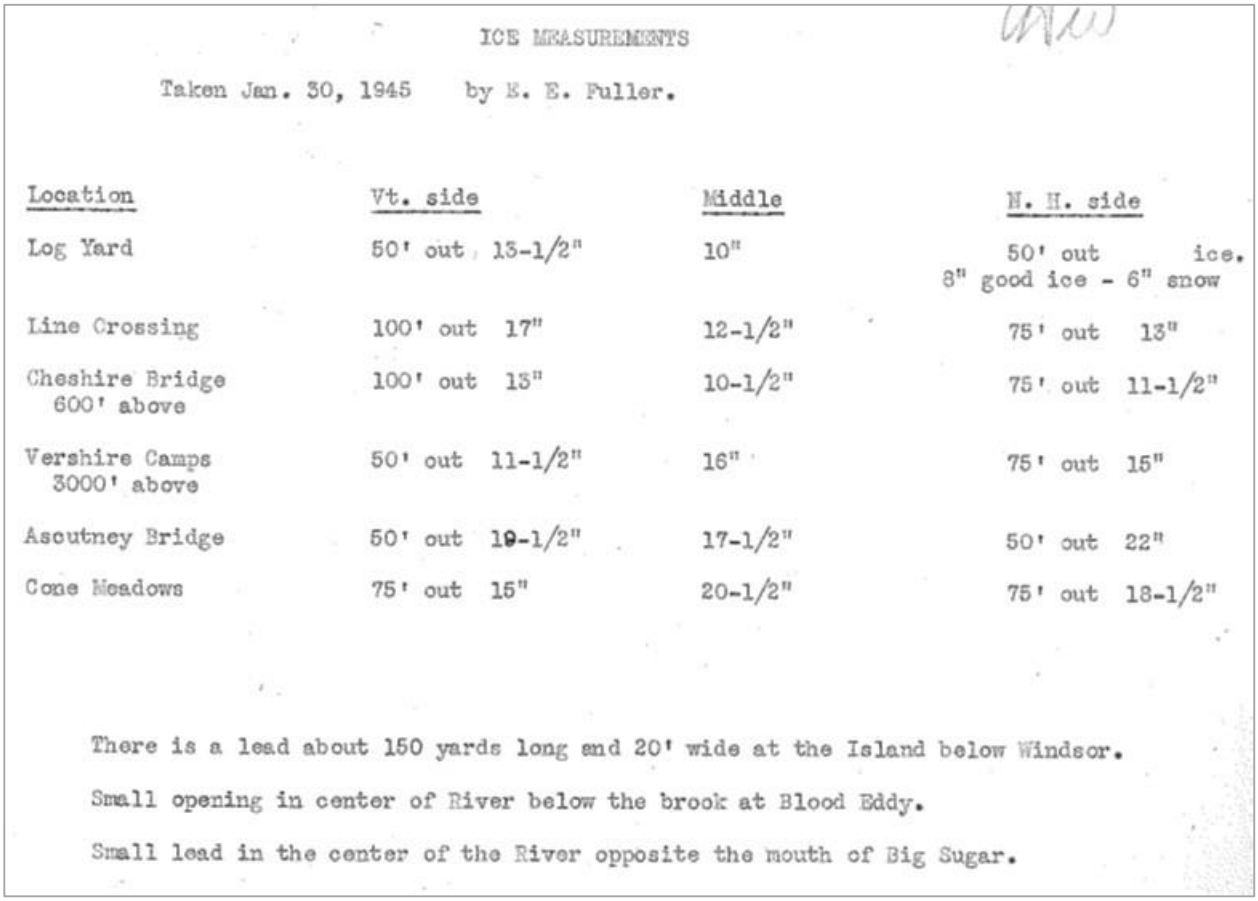

ICE MEASUREMENTS

Taken Jan. 30, 1945 by E. E. Fuller.

Location	Vt. side	Middle	N. H. side
Log Yard	50' out 13-1/2"	10"	50' out ice. 8" good ice - 6" snow
Line Crossing	100' out 17"	12-1/2"	75' out 13"
Cheshire Bridge 600' above	100' out 13"	10-1/2"	75' out 11-1/2"
Vershire Camps 3000' above	50' out 11-1/2"	16"	75' out 15"
Ascutney Bridge	50' out 19-1/2"	17-1/2"	50' out 22"
Cone Meadows	75' out 15"	20-1/2"	75' out 18-1/2"

There is a lead about 150 yards long and 20' wide at the Island below Windsor.

Small opening in center of River below the brook at Blood Eddy.

Small lead in the center of the River opposite the mouth of Big Sugar.

Figure 5.5.5.2-5 Example of Ice Measurements – 1945 (TransCanada)

CONNECTICUT RIVER

1946 ICE SURVEY

WELLS RIVER TO WILDER, VERMONT

Index.	River Mileage above Wilder	No. 1 Test Hole	No. 2 Test Hole	No. 3 Test Hole	No. 4 Test Hole	Average.	Location.
		(Thickness of Ice in Inches)					
1	46.6	37	28½	25½	27	29½	Ingalls Eddy.
2	43.9	23½	16	21	19	19-7/8	Ox-Bow off Chas. Dodge Prop.
3	42.2	34	19	17½	17½	22	Middle of Ox-Bow, Newbury.
4	39.3	37½	17½	18	17½	22-5/8	Newbury Bridge, upstream side.
5	36.5	29	14	17	16	19	S. Newbury Bridge downstream.
6	34.0	28½	16	17	24½	21½	Roaring Brook downstream.
7	32.8	20	17	16	25	19½	Off Judson Clark property.
8	29.0	28½	14½	16	17½	19-1/8	Piermont Bridge downstream.
9	27.8	(No measurements - road drifted)					Off M. A. Jenkins property.
10	26.0	26½	15½	23	18	20-3/4	Orford-Piermont Town Line.
11	24.0	22	13½	16½	12½	15-7/8	Adjacent to Jas. Cummings prop.
12	21.5	26	22½	14	14	19-1/8	Orford Bridge downstream.
13	18.0	28	12	17	20½	19-3/8	Clay Brook upstream at Town Line.
14	15.2	30½	20½	16	23	22½	No. Thetford Bridge upstream.
15	13.1	24	14	20	21	19-3/4	E. Thetford-Lyme Bridge down.
16	10.3	30½	23½	15½	13	20-5/8	Above Huggetts Island.
17	8.2	11	9½	13	10½	11	Kendall R.R. Station.
18	6.0	22½	13	14	11	15-1/8	Above Island at Camp Brook.
19	3.0	31½	23	19½	18½	23-1/8	Above Hanover Bridge.
20	2.4	24	18½	14	18	18-5/8	Above Mink Brook.
21	1.4	(No readings due to wind and cold.)					Chase Island.
22	.9	30	18	15	21½	21-1/8	Wilder Pond above boom piers.
Average		27.2"	17.3"	17.2"	18.3"	20"	

Note: River mileages are taken from River Print R-1661[10] and zero mileage is at the proposed New Wilder Dam Site.

Figure 5.5.5.2-6 Example Ice Survey (TransCanada)

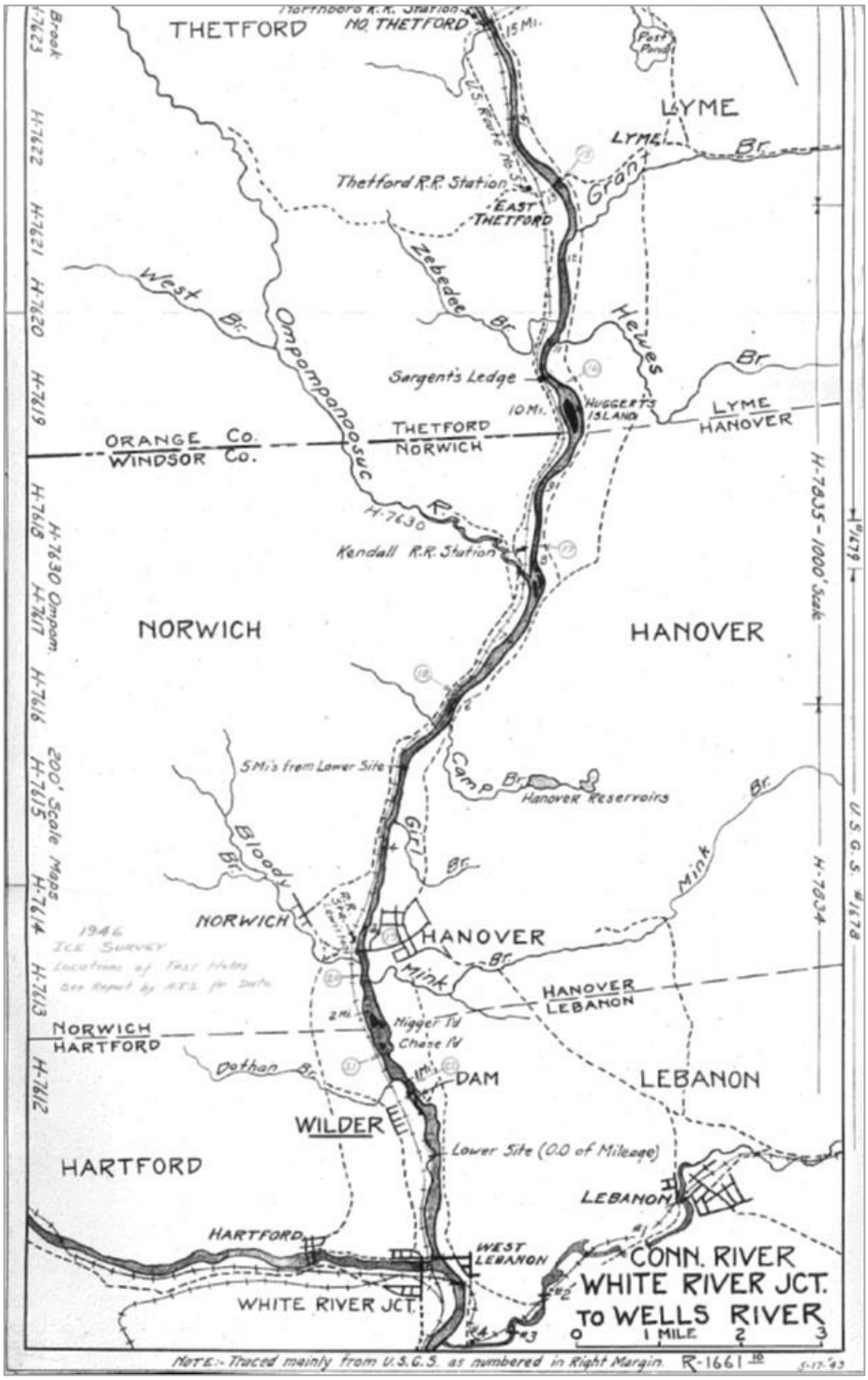

Figure 5.5.5.2-7 Map of Ice Survey and Test Holes – 1946 (TransCanada)

Connecticut River Ice

(Field Notes - C. S. Brewer)

Date	Time	Remarks
3-8-46	3:30 P.M.	Signs of little sugar expelling ice.
3-8-46	3:35 P.M.	Slight lead at Blood Eddy - debris may block culvert.
3-8-46	3:45 P.M.	At Rose Gardens lead 75' wide by 1/4 mile long on New Hampshire shore, ice from January movement intact.
3-8-46	4:25 P.M.	Ottauqueechee open between bridge and dam.
3-8-46	4:45 P.M.	On White River Junction R.R. Bridge, no ice movement - open water in Connecticut under highway bridge. W.R. is filled with ice to about 3/4 mile above R.R. bridge across W.R.
3-8-46	5:30 P.M.	Observed ice jam on highway about 2 miles above Hartford on W.R.-road cleared at this time.
3-8-46	7:30 P.M.	Called Bellows Falls and told Pollard that we were at Windsor House and gave him Windsor at 7:20 P.M. W.R. @ 4:00 P.M. = 20.31
3-9-46	7:20 A.M.	At Windsor gauge - hard rain - but no ice movement since last night.
3-9-46	7:30 A.M.	Clearing sky - rain stopped.
3-9-46	8:30 A.M.	Talked to A.S.Walker and got W.R. readings $7\frac{48}{A}$ = 20.81 $8\frac{05}{A}$ = 19.33. Instructions are to watch Windsor for this slug.
3-9-46	11:10 A.M.	Started to rain and blow at Windsor.
3-9-46	11:45 A.M.	Stopped raining.
3-9-46	1:30 P.M.	Shore lead on Vt. side running more briskly and boiling over on channel ice - ice cracked for few seconds.
3-9-46	4:45 P.M.	Ice started moving - whole river in motion.
3-9-46	5:00 P.M.	Head of previous jam now at Windsor.
3-9-46	5:10 P.M.	Ice motion stopped.
3-9-46	5:15 P.M.	Ice across road North of bridge on N.H. side at Pole #16 Tree on bank scarred and spiked at water high mark.
3-9-46	5:30 P.M.	High water mark 37" below top of sewer behind garage of old toll house on Vt. shore.

Figure 5.5.5.2-8 Connecticut River Ice Observations and Field Notes (TransCanada)

Figure 5.5.5.2-9 Connecticut River at White River Junction, VT – March 8, 1946 (TransCanada)

Figure 5.5.5.2-10 Connecticut River Downstream of Windsor Bridge – March 10, 1946 (TransCanada)

Figure 5.5.5.2-11 Connecticut River at Windsor Bridge – March 10, 1946 (TransCanada)

CONNECTICUT RIVER

1946 ICE SURVEY

WELLS RIVER TO WILDER, VERMONT

Index.	River Mileage above Wilder	No. 1 Test Hole	No. 2 Test Hole	No. 3 Test Hole	No. 4 Test Hole	Average.	Location.
		(Thickness of Ice in Inches)					
1	46.6	37	28½	25½	27	29½	Ingalls Eddy.
2	43.9	23½	16	21	19	19-7/8	Ox-Bow off Chas. Dodge Prop.
3	42.2	34	19	17½	17½	22	Middle of Ox-Bow, Newbury.
4	39.3	37½	17½	18	17½	22-5/8	Newbury Bridge, upstream side.
5	36.5	29	14	17	16	19	S. Newbury Bridge downstream.
6	34.0	28½	16	17	24½	21½	Roaring Brook downstream.
7	32.8	20	17	16	25	19½	Off Judson Clark property.
8	29.0	28½	14½	16	17½	19-1/8	Piermont Bridge downstream.
9	27.8	(No measurements - road drifted)					Off M. A. Jenkins property.
10	26.0	26½	15½	23	18	20-3/4	Orford-Piermont Town Line.
11	24.0	22	13½	16½	12½	15-7/8	Adjacent to Jas. Cummings prop.
12	21.5	26	22½	14	14	19-1/8	Orford Bridge downstream.
13	18.0	28	12	17	20½	19-3/8	Clay Brook upstream at Town Line.
14	15.2	30½	20½	16	23	22½	No. Thetford Bridge upstream.
15	13.1	24	14	20	21	19-3/4	E. Thetford-Lyme Bridge down.
16	10.3	30½	23½	15½	13	20-5/8	Above Huggetts Island.
17	8.2	11	9½	13	10½	11	Kendall R.R. Station.
18	6.0	22½	13	14	11	15-1/8	Above Island at Camp Brook.
19	3.0	31½	23	19½	18½	23-1/8	Above Hanover Bridge.
20	2.4	24	18½	14	18	18-5/8	Above Mink Brook.
21	1.4	(No readings due to wind and cold.)					Chase Island.
22	.9	30	18	15	21½	21-1/8	Wilder Pond above boom piers.
Average		27.2"	17.3"	17.2"	18.3"	20"	

Note: River mileages are taken from River Print R-1661[10] and zero mileage is at the proposed New Wilder Dam Site.

Figure 5.5.5.2-12 Ice Survey, Connecticut River (TransCanada)

Figure 5.5.5.2-13 Connecticut River near Windsor, VT – April 24, 1946 (TransCanada)

Figure 5.5.5.2-14 Connecticut River near Windsor, VT – April 24, 1946 (TransCanada)

Figure 5.5.5.2-15 Connecticut River near Windsor, VT – April 24, 1946 (TransCanada)

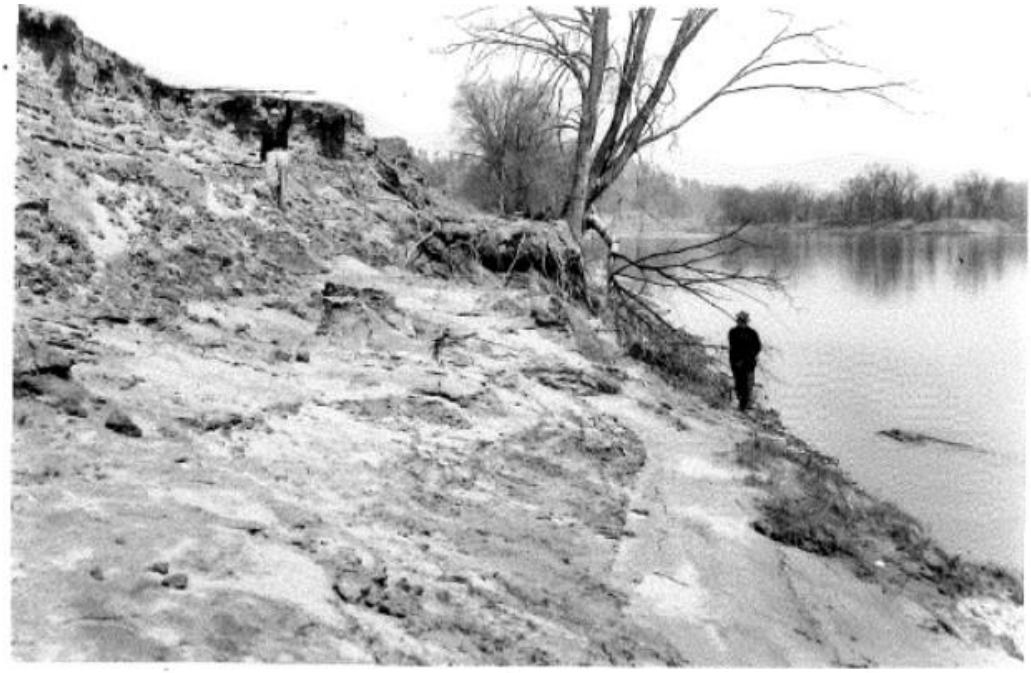

Figure 5.5.5.2-16 Connecticut River near Windsor, VT – April 24, 1946 (TransCanada)

Figure 5.5.5.2-17 Connecticut River near Windsor, VT – April 24, 1946 (TransCanada)

Figure 5.5.5.2-18 Connecticut River near Windsor, VT – April 24, 1946 (TransCanada)

Figure 5.5.5.2-19 Connecticut River near Cornish, NH – April 23, 1946 (TransCanada)

Figure 5.5.5.2-20 Connecticut River near Windsor, VT – April 23, 1946 (TransCanada)

NOTES OF THE 1946 SPRING RUNOFF
By P. C. Pray-In Boston Office

3/8/46
Friday

Observations from French King Bridge reveal breakup in vicinity of Bridge. River just above Turners Falls pond unbroken. No disturbance at Meadow Bridge. Northfield Shell Bridge, there is no disturbance.
Vernon Tail Race cleaned out to line crossing.
No leads from side brooks on Vernon Pond. At Route 9 bridge, there is unbroken ice.
Salmon - Canoe - E. Putney, brook beds are cut open.
Connecticut River cleaned from Bellows Falls tail race to just below Cobb Br. - ice is gathered here.

Monday, Mar. 11-46

Lake went from Gilman to Cannan and ice intact and too solid to go out. From West Stewartston up, river is clear of ice, due to Pittsburg flow.

Simmonds reports ice in Wilder Basin too solid to move out on present flows. Ice has lifted in some places and some evidence of water pressure but no movement.

A. S. W. called - no change in ice conditions.-J.A.C. to Hadley.

Mr. Nullish called - gave him temps and ppt. from 3-8-46 - 3-11-46 at 15 M. F. He commented on Montague City having turned over and Springfield still rising. I told him Vernon turned over between 3-10-46, 4:00 P.M. and 3-11-46, 8:00 A.M. and that would bear out Montegue and Springfield might be expected to turn over a little later. He commented on some trouble at the Northampton. Hadley Bridge but seemed to have no details, other than dyke work was done. He said he presumed it was the White River ice that had jammed up at Hadley and caused only a little trouble. I pointed out that the White River ice had not got down that far and that it had not passed B. F. or was not quite past Windsor.

C.R.B.-P.C.P

C.R.Bliss reports ice moving in Conn. River below Vernon, passing under Schell Bridge about 2:45 P. M., 3-12-46. He then went back over meadow, down Gill Road and across French King. Main body passed thru meadow while there and it appears that the river is clear from Vernon tail race to French King Br.

Figure 5.5.5.2-21 Notes of the 1946 Spring Runoff (TransCanada)

C.R.B.-P.C.P — C.R.Bliss reports ice moving in Conn. River below Vernon, passing under Schell Bridge about 2:45 P. M., 3-12-46. He then went back over meadow, down Gill Road and across French King. Main body passed thru meadow while there and it appears that the river is clear from Vernon tail race to French King Br.

2:30 P. M. — Informed Col. Dalton that ice was passing over Vernon dam. Flows had not increased. This was not an unusual thing, but we were keeping him informed as we said. He asked how soon it would get down river and this was answered by saying it had to go thru Turners Falls pond, etc., before getting to Whateley and we were not familiar with river timing down the river. He replied by saying he would say about 18 hours.

Friday, 3-15-46 — About 12:00 Noon Vernon reported they had lost the remaining 300' of their boards and that ice in the Vernon Pond had started out.

Figure 5.5.5.2-21 Notes of the 1946 Spring Runoff (TransCanada) continued

Figure 5.5.5.2-22 Connecticut River near Cornish, NH – April 25, 1946 (TransCanada)

Figure 5.5.5.2-23 Ice-Riverbank Interaction in Bellows Falls Impoundment – 1992 (TransCanada)

5.5.5.3 Analysis of the Effects of Ice

A review of the effect of ice on rivers was published in the Journal of Cold Regions Engineering, *"Review of Alluvial-channel Responses to River Ice,"* (Ettema, 2002). The review acknowledges that general concepts regarding the interaction between ice and rivers are understood to some degree but much remains for further study and analysis. The review discusses the fact that riverbanks are weakened due to ice-related processes.

One such ice-related process that is discussed is freeze-thaw. The report states that, freeze-thaw dynamics *"may locally weaken bank soils* (Ettema, 2002)*."* Water is found in at least some of the pore spaces between soil particles in riverbanks. During sufficiently cold weather (in terms of temperature and duration), some of the water in riverbanks can freeze. As water freezes it expands thereby loosening soil particles, causing an expansion of the space between particles, or causing cracks in the soil matrix. Additional water can find its way into larger spaces and with additional freeze-thaw cycles more disruption of the soil matrix can occur. In cold climates, freeze-thaw can adversely affect riverbank stability allowing flow-related forces or gravity to have an enhanced erosive effect on riverbanks.

Inspection of riverbanks during winter conditions sometimes reveals cracks in the bank that may be related to freeze-thaw. Cracks that form as a result of this dynamic encourage more water to infiltrate into the crack because there is less resistance to flow than through the general soil matrix. As a result of subsequent freeze-thaw cycles, cracks in the soil may grow and eventually could lead to pieces of sediment breaking loose (spalling) and falling or sliding down the riverbank slope. Figure 5.5.5.3-1 shows ice on the river as well as icicles hanging down the riverbank, which is indicative of water moving through the riverbank and freezing. Figure 5.5.5.3-2 is an example of the small cracks forming in riverbanks that may be due to freeze-thaw. No actual data exist that allows quantification of the effect of freeze-thaw cycles on riverbank stability in the TFI. Freeze-thaw is a natural process that is primarily influenced by weather and climatic cycles and is not considered a primary factor in riverbank erosion processes in the TFI, nonetheless it is likely to contribute to riverbank instability to some lesser degree.

Another phenomenon discussed in R. Ettema, 2002 was that ice may cause erosion to riverbanks by abrasion or gouging. The review specifically noted that "*during heavy ice runs resulting from ice-cover breakup or ice-jam release, large pieces of ice potentially may gouge and abrade channel banks. There exists significant evidence showing that ice runs may substantially affect riverbank morphology (Marusenko 1956; Hamelin 1979; Smith 1979; U.S. 1983; Doyle 1988; Wuebben 1995; Uunila 1997)"* (R. Ettema, 2002). Ice flowing downstream, or being forced into the banks, was clearly seen in historic and recent photographs shown previously in this report (see Figures 5.5.5.2-1 through 5.5.5.2-4, 5.5.5.2-9 through 5.5.5.2-11, and 5.5.5.2-23). Damage associated with these ice events can be observed in previous figures (Figure 5.5.5.2-13, 5.5.5.2-15 through 5.5.5.2-18, and 5.5.5.2-22 through 5.5.5.2-23).

Ice also has an adverse effect on riparian vegetation (as shown in previously referenced Figure 5.5.5.2-14, 5.5.5.2-19, and 5.5.5.2-20). As noted in R. Ettema, 2002:

> *"Ice-run gouging and abrasion have an important, though as of yet not quantified, effect on riparian vegetation that, in turn, may affect bank erosion and channel shifting. Where ice runs occur with about annual frequency, riparian vegetation communities have difficulty getting established. Ice abrasion and ice jam flooding may suppress certain vegetation types along banks . . . possibly exacerbating bank susceptibility to erosion. This aspect of river ice has yet to be further investigated."*

The effects of ice on riparian vegetation were investigated on the Platte River in Nebraska. A comprehensive vegetation demography study was conducted over a period of numerous years where thousands of seedlings were tagged and tracked through stages of germination, establishment, and growth; as well as numerous modes of mortality including scour, desiccation, ice, and inundation. W.C. Johnson, a vegetation biologist, was the primary investigator of the vegetation demography studies. S&A provided

hydrologic and hydraulic support and then utilized the data to develop computer models simulating the interaction between rivers and riparian vegetation. Additional information about this study can be found in the reports: *Analysis of Ice Formation on the Platte River (S&A, 1990a); Physical Process Computer Model of Channel Width and Woodland Changes on the North Platte, South Platte and Platte Rivers* (S&A, 1990b); and *Calibration of SEDVEG Model Based on Specific Events from Demography Data* (S&A, 2002).

A summary of aspects of this work was presented in *"Physical History of the Platte River in Nebraska: Focusing upon Flow, Sediment Transport, Geomorphology, and Vegetation,"* (S&A, 2000). The report found that ice frequently formed along the Platte River during the winter with the ability to remove or damage vegetation as it breaks up and begins to move downstream. Seedling mortality was observed to be highest in the winter due to the fact that ice can block flow and raise river stage, cause sediment movement, and physically damage living vegetation. Mortality rates were observed to be as high as 98% due to ice. The vegetation monitoring studies presented clear evidence of the significant impact ice-scour has in controlling vegetation in the Platte River (S&A, 2000).

While these studies focused on relatively early stages of life from germination through several years old, it confirms the concept in R. Ettema, 2000 regarding the adverse effects of ice on riparian vegetation. It provides a reasonable explanation of why eroded segments of river found in the Vernon and Bellows Falls Impoundments in 1997 remain in the same eroded state in 2008 and; in contrast, significant establishment and growth of new riparian vegetation has been observed in the TFI in both the 2008 and 2013 FRRs where no significant ice formed due to VY.

Although data pertaining to the forces that ice imposes on riverbanks or riparian vegetation is not available, it is evident that ice forces are larger than those imposed by the flow alone as documented photographically and descriptively where trees being snapped off by ice are described and damage to vegetation is readily observed. Figure 5.5.5.3-3 shows ice damage to riparian vegetation along a forested riverbank of the Connecticut River in the Bellows Falls Impoundment. The photograph shows scarring of trees and downed or leaning trees that might have been damaged by the ice. Ice can remove significant vegetation along segments of the river exposing the banks to the erosive forces of water without protective vegetation. Ice may also damage or stress vegetation such that it can die or be weakened such that the vegetation provides reduced or limited protection against erosion.

A number of reports have been published over time investigating the impacts of ice on erosion processes along the banks of the Connecticut River. One such paper was developed by CRREL and included conducting analysis of historic ice events on the Connecticut River. This analysis focused on the reach of river in the vicinity of Windsor, VT where the Cornish-Windsor Bridge is located. In a paper entitled, *"Dynamic Ice Breakup Control for the Connecticut River near Windsor, Vermont,"* M.G. Ferrick, Lemieux, G.E., Weyrick, P.B., and Demont, W.(1988), information is given regarding historic ice events in this part of the river. As the report states, this bridge *"is the longest covered bridge in the United States and has significant historical value."* The report then cites historic ice events that have damaged or destroyed this bridge.

> *Initially constructed in 1796, the Cornish-Windsor covered bridge was destroyed by the Connecticut River in the spring of 1824, in 1849, and again on 3-4 March 1866 (Childs 1960). The loss of the third bridge in 1866 was specifically attributed to ice breakup. The present structure was constructed in 1866 at a higher elevation above the river than previous bridges. Rawson (1963) reports that ice jam floods damaged this bridge in the spring of 1925, 1929, 1936 and 1938, and significant damage from ice impacts occurred again on 14 March 1977. The water levels associated with ice damage to the bridge also caused flood damage in Windsor, Vermont.*

In their analysis, CRREL characterized ice events into three categories of breakup since it is during the process of ice breakup when most damage occurs. Table 5.5.5.3-1 summarizes CRREL's assessment of ice

breakup and associated damage to the bridge. CRREL defined the various categories of ice breakup with the following discussion (Ferrick, *et al*., 1988):

- The first group of events (1927, 1929, 1945, 1968, and 1981) exhibited high discharge with only gradual variations, and concurrent ice movement over a period of several days. A gradual and simultaneous breakup at several locations characterizes reduced energy gradient breakup behavior. The breakup was in an advanced stage when the peak discharge occurred, and water levels were generally moderate.

- The events in the second group (1946, 1964, and 1979) each included the formation of a persistent upstream ice jam. The eventual release of the White River ice jam in 1964 produced the highest water levels since at least the 1920s at White River Junction, Vermont. . . This short-duration, extremely high flow input was not supplemented by a rising Connecticut River and experienced significant attenuation prior to arriving at Windsor. In 1946 and 1979 ice jams near the Connecticut River gaging station persisted for about 35 and 48 hr, respectively. The delay of ice from the White River and upstream reach of the Connecticut River provided an opportunity for breakup downstream to proceed with a smaller ice volume, effectively increasing the channel capacity.

- The third group of events (1925, 1936, 1938, and 1977) includes most years of reported bridge damage and the highest water levels at Windsor. In each case an abrupt White River rise deposited large quantities of ice in the Connecticut River. The intact and competent ice on the Connecticut River then began to fail as the discharge continued to increase rapidly, and the breakup traveled downstream. The largest quantities of ice together with a high peak discharge produce the highest river levels at breakup.

According to the *"Flood of March 1936"* (Grover, 1937), the 1936 flood was the result of a warm, moisture-laden front which moved into and stalled over New England resulting in increased temperatures and heavy rainfall during the period March 11-13. For most of the Connecticut River watershed, this was a two-peak event. The first peak (as discussed in this section) was due to a rain-on-snow and ice jam event in mid-March while the second peak was more of a rain caused event later in March. Rainfall amounts as much as 5 inches were reported in some areas of New Hampshire. The combination of heavy rain and melting snow resulted in flooding throughout New England, including on the Connecticut River. The movement of ice, including ice jams and breaks, resulted in significant damage along the Connecticut River. An example of the magnitude of damage occurred at the Holyoke Dam where an ice jam formed above the dam resulting in the Connecticut River cutting a new channel on the east side of the river to get around the dam. Once the ice jam broke, over 9 ft. of water passed over the dam shearing off a 1,000 ft. wide by 5 ft. high section of the dam (Grover, 1937).

CRREL's analysis of historic ice events utilized climatic data including temperature and precipitation during the "warm period" in categorizing and understanding these events. Through this process, the 1936 event was evaluated to have a breakup category of 3 (the highest level where ice damage occurs with a combination of high flow and large quantities of competent ice), with a #1 ranking in terms of peak flow and a #3 ranking in terms of cold. Regarding precipitation during the warm period, no ranking was given but it was one of the highest listed in Table 5.5.5.3-1 with only 2 years having higher values.

Table 5.5.5.3-1: Assessment of Ice Break-up and Associated Damage to the Cornish-Windsor Bridge (CRREL)

Year	Peak flow date of breakup event	Peak daily avg. discharge		Discharge rank	Hydrothermal melting (m^3/s-days)	Freezing (°C) days	Cold rank	Melting °C-days through peak Q	Precip. in warm period (cm)	Breakup category
		(ft^3/s)	(m^3/s)							
Reported bridge damage										
1925	12-Feb	36,000	1020	6	100	625	20	18.3	0.20	3
1929	24-Mar	31,100	881	11	4600	445	48	28.1	0.69	1
1936	13-Mar	45,100	1280	1	600	790	3	20.0	4.80	3
1938	25-Mar	34,800	985	8	1900	585	26	56.8	0.05	3
1977	14-Mar	43,100	1220	2	900	741	7	59.4	3.89	3
No reported bridge damage										
1927	20-Mar	34,000	963	9	3900	580	29	59.7	0.53	1
1945	22-Mar	40,200	1140	3	4600	712	12	50.6	2.62	1
1946	9-Mar	31,000	878	12	800	744	6	34.4	2.92	2
1964	6-Mar	35,000	991	7	400	618	23	24.7	4.14	2
1968	22-Mar	34,000	963	9	2100	736	8	36.7	3.73	1
1979	7-Mar	40,000	1130	4	1000	671	18	37.5	6.48	2
1981	21-Feb	38,400	1090	5	4500	565	31	43.9	1.52	1
1986	27-Jan	19,700	558	28	100	641	19	0.0	6.99	2

Figure 5.5.5.3-1 Icicles Hanging from Upper Bank

Figure 5.5.5.3-2 Cracks in a Riverbank Potentially Associated with Freeze-Thaw

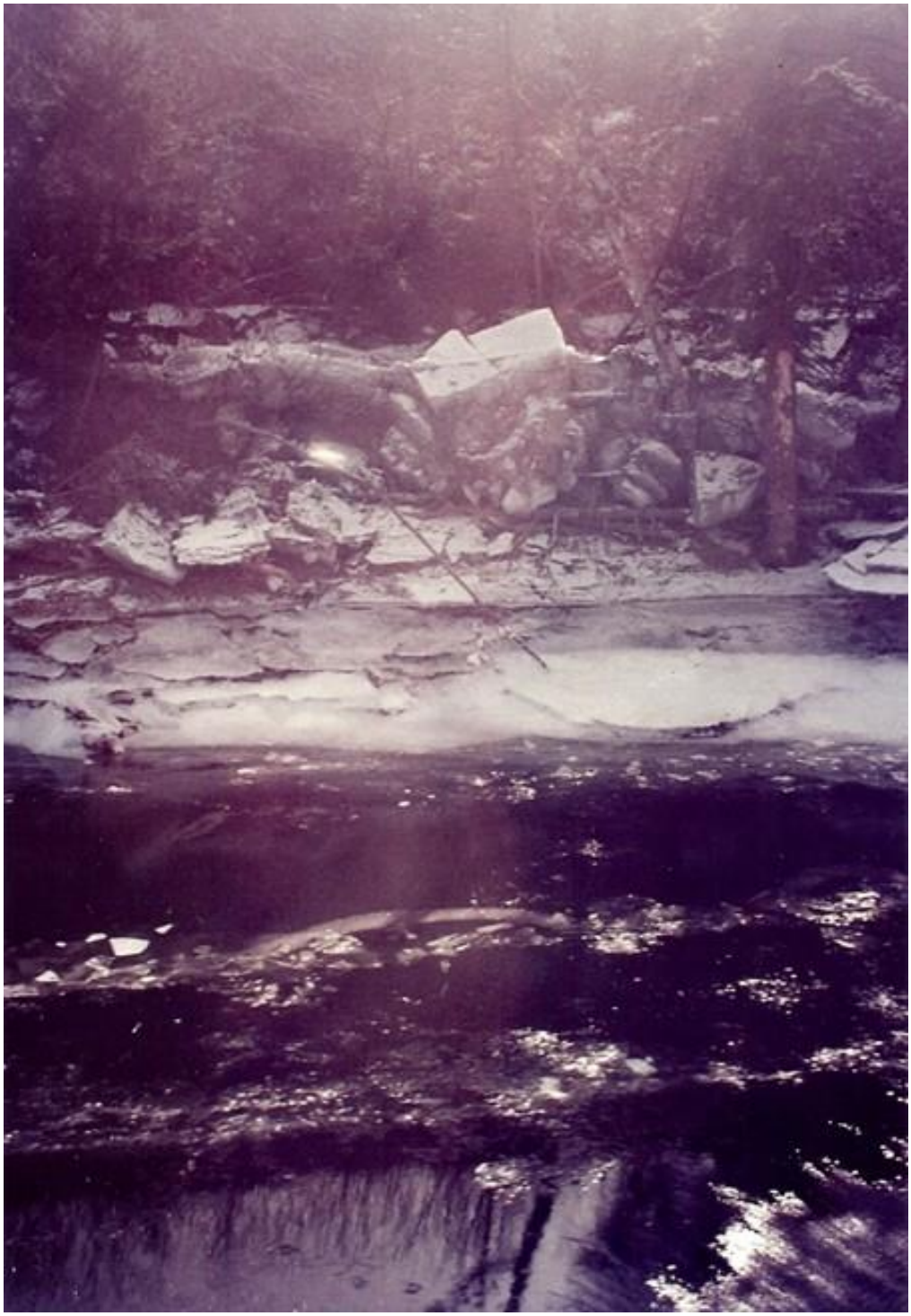

Figure 5.5.5.3-3 Ice Damage to Riparian Vegetation in the Bellows Falls Impoundment – 1992

5.5.5.4 Correlations between Ice and Temperature

The RSP Addendum outlining the study of ice calls for correlations between ice formation and breakup to be developed. As such, the correlation process begins by evaluating years of data where the greatest amount of information exists in order to determine what type of correlations are possible given the specific types of information available. Weather data for this analysis was obtained from monitoring stations in Amherst, MA; Vernon, VT; Keene, NH; and Hanover, NH. Table 5.5.5.4-1 provides an overview of the available information.

A considerable volume of material was found to be available for 1946 regarding ice. Available information includes photographs of ice and damage to riverbanks and vegetation after ice out, ice measurements and notes on observations, a map where ice measurements were taken, and notes of high flow during the spring runoff. In addition, air temperature and flow data are available. Information from January 7-12, 1946 does not discuss ice formation, but rather a thaw and ice movement at various locations. This indicates that ice formed prior to January 7, 1946 since there was an early winter thaw and ice movement event. Ice measurements were taken in February (15-19), with the next set of information being notes discussing ice break up and movement starting on March 8-14 and later in the spring. The minimum and maximum air temperatures at Amherst, MA, Vernon, VT, Keene, NH and Hanover, NH for December 1, 1935 through March 31, 1936 are displayed on Figures 5.5.5.4-1 through 5.5.5.4-4. Table 5.5.5.4-2 provides information correlating ice related events to days on the figures.

All of these graphs show a very similar pattern over time. The graphs of temperature over time indicate that since there was an ice thaw and movement event on January 7-12 (38-41), ice formed before this time; likely during the time when temperatures were low between days 21 – 25. For days 21 – 25, the minimum daily temperatures were primarily between 0 and 10°F with one day below zero (Amherst). The maximum daily temperatures for these days were in the teens and twenties and therefore below freezing. During the January thaw (days 38 – 41), minimum daily temperatures were at or above 30° and maximum daily temperatures ranged from 40 to 50°. During March (days 98-99 and 104-108), the minimum daily temperatures again rose above 30° with maximum temperatures rising into the 50's to over 70° for the days when ice breakup and movement were occurring. Similar temperature patterns were observed at Vernon, Keene, and Hanover.

The fact that ice must have formed when minimum temperatures ranged from below zero up to 10° with maximum daily temperatures less than 30°; and that ice thawed and began breaking up and moving occurred when minimum temperatures were above 30° with maximum temperatures into the 40s, 50s or significantly higher is not surprising.

Another known year with ice data occurred in the winter of 1943/1944. Graphs of temperature over time were prepared for these same stations (Figures 5.5.5.4-5 through 5.5.5.4-8). For the winter of 1943/1944, again no specific information is given regarding ice formation. Available information discusses some ice "shoving" and movement on February 8-10. Ice had to have formed before this time, probably on days 11 through 17 (December 11-17). Additional cold periods occurred through the winter, but as previously mentioned there was some type of ice movement on February 8-10 (days 70-72). The temperature data show a relatively warm period on days 50-60 and another small spike in temperature on about day 69. Minimum daily temperatures dropped again on approximately days 60-80. Notes indicate ice breakup on March 14-17 (days 105-108) and March 26 through April 1 (days 117-123). Minimum daily temperatures during this time period approached and sometimes exceeded freezing and daily maximum temperatures started getting into the 40° to over 60° range. Again, no specific information is available for this year regarding ice formation and ice melt/breakup provides a simple look at a complex issue given that other hydrologic variables of precipitation and flow must be considered.

Ice formation, melting/break-up, and potential ice jam flooding are dictated by climatic conditions that govern these processes. Similar to the CRREL study, climatic data were summarized over the period record

to compare and correlate conditions that caused the ice related flooding of 1936 and other years to the rest of the historic record using the Amherst, MA weather station. Ice formation is governed by the number of days that are below freezing or colder during the winter months. Ice melting/break-up is governed by temperatures above freezing in the early spring. Potential flooding is governed by the amount of precipitation that occurs during the early spring concurrently with ice melt as well as snow melt. Table 5.5.5.4-3 summarizes these key data for the historic period. Columns 2-5 are the number of days during the winter months (from December of the preceding year through March of the current year) when the minimum daily temperature is less than 32°, 20°, 10° and 0°F. Columns 6 and 7 are average maximum daily temperature during March and the total precipitation for March (inches). There is an indication of ice occurring in the last column based on the scanned files from TransCanada. The same information is provided for Vernon, VT, Keene, NH and Hanover, NH in Tables 5.5.5.4-4 through 5.5.5.4-6. For the stations that go back into the 1800s, it is noted that 1896 is a year with significant numbers of cold days coupled with one of the larger values of precipitation in March.

For those years where the TransCanada files indicated ice on the Connecticut River, the maximum, average and minimum numbers of days below the selected temperatures are summarized in Table 5.5.5.4-7 through 10 for these four stations. For years when ice formed (as indicated by the TransCanada files and other information) the number of days below the various temperature ranges (<32°, <20°, <10°, <0°) when ice was indicated shows the types of temperature conditions that form ice. These summaries provide a general correlation of the range of temperature conditions under which ice historically formed on the Connecticut River. Ice formation could be expected during those years when ice observations were not available or for future prediction when the number of days below the various levels of temperatures falls within the ranges when ice was documented to have occurred as shown by this summary correlation.

It is instructive to compare temperature and flow conditions for some ice events for which some erosion information is available. The number of days below the various temperature levels for 1936 and 1946 are summarized in Table 5.5.5.4-11. 1936 had the fewest number of days <32° but somewhat above average number of days <20° through <0°. 1946 ranged from slightly below to somewhat above average number of days for the range of temperatures compared to all years indicated as having ice, but did not approach the maximum number of days in any temperature category. Regarding ice break up, the average maximum temperature in March for both 1936 and 1946 were above average, with 1946 actually being the maximum average March temperature. March precipitation for 1936 was well above average and near the maximum while for 1946, March precipitation was near the minimum for all ice years. Referring back to CRREL's evaluation of various ice events, 1936 was ranked in the maximum damage category while 1946 was in the middle or 2nd of the 3 levels of ice/break up events.

Given that 1936 resulted in devastating flooding and damage caused by flooding associated with ice, it can be assumed that a repeat of similar climatic conditions could potentially cause similar results. During the winter of 1936 there were 47 days of minimum temperatures less than 10ºF and 25 days of minimum temperatures less than 0ºF at Vernon. This caused significant ice formation. The average maximum temperature during March was 50ºF and there was 8.45 inches of precipitation which combined to cause melting/break-up of ice and sufficient flow in the river to cause ice-jam flooding and associated flooding and damage. The same information is available at the other weather stations. The question then becomes how unusual were the combination of climatic conditions in 1936 and could they be expected to recur in the future.

At Keene, NH, which has a record of climatic data from 1893 to 2016, the number of days less than 10ºF ranged from 19 to 55, averaging 39.3. The number of days less than 0ºF ranged from 0 to 38, averaging 17.9. Conditions in 1936 were above average in terms of numbers of days below the range of various temperatures but are exceeded several times during the more than 100 year period of available data. In terms of number of days less than 10ºF, 1936 ranks 2nd highest. For the number of days less than 0°, 1936 ranks 3rd highest. Based on the Hanover data, 1936 ranks 7th highest number of days <10ºF and 3rd highest

<0ºF. Conditions that caused formation of ice during 1936 were somewhat unusual, but not the most extreme. Regarding melting/break-up which is dictated by warmer temperatures, during March of 1936 the average maximum temperature was 50ºF (at Keene). This temperature was exceeded 4 times plus during the 1893-2016 record. March precipitation during 1936 totaled 7.60 inches which ranked first for the period of record. At Hanover, 1936 March precipitation ranked 2nd, but was significantly smaller (5.63 inches compared to 9.25 inches) than 1896. While 1936 ranks in the upper ranges regarding cold during the winter and a warm, wet spring; 1896 stands out as a significant ice event along with a number of other years for which no records of ice exist but for which ice is indicated based on the tables showing numbers of days for which temperatures are below the range of selected values. There are numerous years in these tables that exceed the number of days below 10° or 0° from 1936 for which there was no ice indicated. There are numerous years where ice was indicated with fewer cold days than years with no indication of ice. This indicates that the available record of ice is incomplete.

While 1936 represents the greatest flood of record, the individual climatic conditions leading to this event are not extreme and are within the realm of possibility to repeat. Consideration must also be given to the fact that ice related issues causing erosion occur during climatic conditions that occur much more frequently than just 1936 as documented in the CRREL analysis (Ferrick, *et al*, 1988) as well as numerous ice surveys and photographic documentation presented in this section. These conditions can now extend farther downstream through the TFI as a consequence of the closure of VY, as it had in the past.

The variation in temperature at Keene, NH, in terms of the number of days <10° and <0° as well as the average March maximum temperature is shown in Figure 5.5.5.4-9. March precipitation over the available period of record (1893 – 2016) is presented in Figure 5.5.5.4-10. These data plotted over time do not reveal any significant temporal trends.

These graphic and tabular correlations between known existence of ice and break up of ice yield the expected conclusion that ice forms when it is sufficiently cold and it breaks up when it is sufficiently warm. Due to the fact that actual ice formation data were not available (since those collecting the data and observations were focused on ice break up rather than ice formation), no specific criteria can be developed for ice formation. While ice does not necessarily form every year, whenever ice does form in the winter; as surely as night follows day, ice which forms in the winter melts in the spring (noting that spring in this context is considered to be based on climatic season rather than strictly the calendar). The fact ice necessarily melts in the spring of every year following the formation of ice from the previous winter (under the recent historic climatic regime); complicates the development of specific criteria regarding the consequences of ice break up as this is further complicated by the influence of precipitation, snow melt, and flow. More detailed analysis, beyond the scope of this investigation, would be required to develop more complex and specific criteria regarding ice break up that were not outlined in the study addendum. The general correlation, however, from the summary tables provides guidance as to the potential for damaging ice break up.

Table 5.5.5.4-1 Weather and Temperature Data Analyzed

Station	Weather Data Availability	Temperature Data
Amherst, MA	1893-2015	1893-2015
Vernon, VT	1893-1998	1912-1998
Keene, NH	1893-2016	1893-2016
Hanover, NH	1884-2016	1895-2016

**Columns for temperature data were included in the data files but contained no temperature data*

Table 5.5.5.4-2 Correlation of ice related events to dates (days), 1946

Date (day)	Observation
January 7-12 (38-41)	January thaw – ice thaw, breakup and movement
February 15-19 (77-78)	Ice measurements taken
March 8-9 (98-99)	Ice breakup and movement
March 14-18 (104-108)	Ice breakup and movement

Table 5.5.5.4-3 Summary of climatic data – Amherst, MA 1930-2015

Year	No. Days below Temperature Threshold				March Temperature (average max, °F)	March Precipitation (in.)	Ice indicated by TransCanada files*
	<32°	<20°	<10°	<0°			
1893	81	56	33	12	40	3.25	
1894	101	59	26	8	51	1.45	
1895	114	73	36	15	40	2.62	
1896							x
1897	99	59	24	7	44	3.31	
1898	91	46	25	9	50	1.18	
1899	108	62	26	9	40	6.96	
1900	105	61	22	4	39	6.11	
1901	85	52	23	4			
1902	88	50	18	5	51	5.47	
1903	92	49	25	10	53	5.58	
1904	114	80	51	21	40	4.48	
1905	112	84	48	15	44	3.66	
1906	106	55	24	7	37	3.92	
1907	104	69	37	17	45	1.82	
1908	107	59	22	9	44	2.86	
1909	104	51	18	2	41	3.01	
1910	104	54	22	12	51	1.37	
1911	110	69	26	2	42	3.8	
1912	107	66	35	14	41	5.7	
1913	87	38	14	3	48	6.3	
1914	106	56	30	15	42	5.52	
1915	108	48	19	6	43	0.12	
1916	113	71	26	8	37	3.97	
1917	103	60	29	8	42	4.09	
1918	115	83	50	25	47	2.91	
1919	101	36	10	3	48	4.22	
1920	112	79	49	17	45	2.9	
1921	89	47	17	5	53	3.57	
1922	107	58	32	10	45	5.34	
1923	113	82	48	20	40	2.28	
1924	101	49	22	6	44	1.05	
1925	98	50	23	6	50	4.62	x
1926	102	65	24	2	38	3.95	
1927	107	63	34	8	36	2.62	x
1928	105	54	21	3	42	1.17	
1929	98	49	18	3	47	3.2	x
1930	68	35	16	4	43.3	3.95	
1931	105	55	23	7	44.2	3.79	
1932	98	43	7	0	39.8	4.24	
1933	99	32	13	2	39.3	4.79	
1934	114	74	43	20	40.9	3.6	
1935	102	63	30	13	45.4	1.48	x
1936	88	63	40	12	49.6	7.04	x
1937	98	34	6	0	39.4	3.38	
1938	102	53	20	3	47.5	2	x
1939	103	58	18	1	38.9	4.49	

Year	No. Days below Temperature Threshold				March Temperature (average max, °F)	March Precipitation (in.)	Ice indicated by TransCanada files*
	<32°	<20°	<10°	<0°			
1940	109	71	28	3	37.4	5.58	x
1941	108	70	24	3	39	1.63	x
1942	97	44	23	5	48.1	7.89	x
1943	111	57	30	11	41.4	3.07	x
1944	106	65	32	5	41.1	4.36	x
1945	105	63	34	11	56.2	2.16	x
1946	100	62	37	8	57.5	1.6	x
1947	111	53	17	1	42.6	3.29	
1948	111	72	42	15	46.2	2.92	x
1949	92	35	11	1	48.5	1.67	
1950	98	48	16	9	41	2.67	
1951	93	37	14	5	45	5.13	x
1952	100	44	12	5	44.1	3.17	x
1953	91	32	3	0	46.2	8.24	x
1954	97	32	18	5	46.1	3.93	
1955	104	42	11	1	42.4	4.39	x
1956	106	59	16	6	37.1	4.94	x
1957	101	46	18	7	47.1	1.55	x
1958	99	40	21	6	43.9	2.62	x
1959	113	70	33	7	44.4	2.83	x
1960	104	44	11	0	36.5	3.32	
1961	106	77	52	29	42.9	3	
1962	107	63	36	8	45.1	1.84	
1963	116	76	50	27	44.1	3.61	
1964	113	63	44	13	47.2	2.71	x
1965	118	74	33	17	42.6	1.1	
1966	105	59	24	5	44.7	2.93	
1967	109	64	33	11	42.1	3.27	
1968	107	63	36	15	48.9	4.47	x
1969	108	67	36	5	44.3	1.97	
1970	110	74	41	24	44.2	3.52	
1971	114	68	39	18	43.3	2.53	
1972	107	54	30	6	43.6	4.85	
1973	96	40	20	5	52.6	3.45	
1974	106	55	20	11	46.6	4.34	
1975	102	53	17	6	45.5	3.97	
1976	102	57	33	12	51	2.15	
1977	102	70	46	12	54	5.88	x
1978	110	70	34	13	43.2	2.65	
1979	72	38	18	8	49.6	3	x
1980	100	62	26	1	41.2	6.42	
1981	106	65	41	18	47.3	0.24	x
1982	117	72	37	17	46.6	2.26	
1983	95	47	19	8	43	4.95	
1984	108	60	28	16	38.9	3.68	
1985	103	52	26	5	53	2.65	
1986	107	63	30	5	50.5	3.69	x
1987	110	59	29	11	50.4	4.58	
1988	102	52	27	11	49.5	2.13	

Year	No. Days below Temperature Threshold				March Temperature (average max, °F)	March Precipitation (in.)	Ice indicated by TransCanada files*
	<32°	<20°	<10°	<0°			
1989	106	66	22	3	50	2	x
1990	94	63	25	7	53	3.13	
1991	98	36	8	2	51.2	4.73	
1992	105	72	27	1	41.7	3.25	x
1993	113	67	30	9	42.5	5.44	
1994	110	78	55	29	43.2	5.6	x
1995	93	54	17	6	48.1	1.68	
1996	112	70	42	18	42.7	2.19	
1997	94	50	9	4	42.1	3.19	
1998	95	44	8	0	47.8	4.53	
1999	105	48	20	5	46.1	4.82	
2000	98	57	31	12	51.9	3.82	
2001	118	79	39	6	41.2	6.16	
2002	105	40	7	0	46.7	3.8	
2003	110	77	51	23	47.9	2.83	
2004	106	64	26	12	48.2	2.11	
2005	110	62	30	15	42.7	3.13	
2006	110	54	17	3	46.4	0.5	
2007	100	55	26	1	43.8	5.01	
2008	116	58	21	4	43	6.04	
2009	112	66	34	14	45.7	4.2	
2010	101	48	18	0	52.5	5.78	
2011	112	70	32	12	44.7	5.33	
2012	90	31	7	0	55.2	1.45	
2013	111	48	11	5	43.6	1.82	
2014	114	80	43	16	39.7	4.25	
2015	110	79	44	24	39.3	1.77	x

**Note that the indication of ice is incomplete in these scanned files; since for example, there was ice in 2015 and not in the files as well as numerous other years where the files did not contain ice information, yet temperatures were colder than for some years in the files where ice was observed.*

Table 5.5.5.4-4 Summary of climatic data – Vernon, VT 1912-1998

Year	No. Days below Temperature Threshold				March Temperature (average max, °F)	March Precipitation (in.)	Ice indicated by TransCanada files*
	<32°	<20°	<10°	<0°			
1912	102	58	33	18	39	5.29	
1913	80	36	6	1	46	6.31	
1914	97	55	27	14	42	2.77	
1915	106	58	19	6	40	0.09	
1916	114	78	35	14	36	1.74	
1917	113	66	35	18	40	2.63	
1918	115	80	60	40	44	1.61	
1919	103	47	13	8	45	4	
1920	107	79	46	19	46	2.09	
1921	82	46	18	4	53	8.23	
1922	111	60	41	14	41	4.8	
1923	110	82	52	27	38	2.01	
1924	94	50	25	5	41	0.74	
1925	101	61	41	15	44	4.55	x
1926	111	73	45	13	34	2.52	
1927	92	55	31	7	52	1.75	x
1928	103	59	24	5	43	2.07	
1929	89	53	21	5	51	2.43	x
1930	70	50	26	8			
1931	95	50	15	4	46	3.86	
1932	55	29	10	4	43	3.65	
1933	108	47	18	6	40	4.94	
1934	112	76	47	31	44	2.65	
1935	107	74	49	23	48	1.54	x
1936	97	67	47	25	50	8.45	x
1937	111	74	23	0	39	3.74	
1938	111	80	41	14	47	1.89	x
1939	115	79	51	20	38	4.04	
1940	118	85	52	28	38	4.38	x
1941	105	79	45	22	38	1.6	x
1942	111	57	38	14	47	5.67	x
1943	118	76	45	28	40	3.03	x
1944	117	83	57	18	40	4.6	x
1945	111	82	54	36	54	1.95	x
1946	110	77	57	26	42	3.11	x
1947	117	77	42	13	46	2.79	
1948	116	89	64	40			x
1949	0	0	0	0		1.88	
1950	0	0	0	0		3.15	
1951	52	19	11	4	43	5.01	x
1952	114	75	39	13	43	2.82	x
1953	106	61	22	0	46	8.35	x
1954	114	45	28	12	46	3.79	
1955	116	72	23	4	42	4.46	x
1956	117	82	41	17	39	4.36	x
1957	114	73	32	16	48	1.71	x

Year	No. Days below Temperature Threshold				March Temperature (average max, °F)	March Precipitation (in.)	Ice indicated by TransCanada files*
	<32°	<20°	<10°	<0°			
1958	114	73	32	16	46	1.99	x
1959	121	98	60	36	44	4.21	x
1960	117	77	37	4	38	2.36	
1961	112	87	66	42	44	3.09	
1962	114	73	50	25	45	1.84	
1963	112	83	54	32	44	3.16	
1964	117	83	46	25	45	3.81	x
1965	117	70	36	18	43	1.54	
1966	115	62	32	12	45	3.57	
1967	114	80	50	23	40	2.84	
1968	111	79	52	18	45	4.32	x
1969	112	76	40	16	42	2.41	
1970	114	91	53	27	42	3.69	
1971	121	80	54	26	42	3.11	
1972	113	69	44	20	39	5.77	
1973	106	53	31	17	48	4.65	
1974	111	61	33	14	43	4.83	
1975	111	66	30	13	42	3.38	
1976	109	68	39	18	47	3.18	
1977	112	77	51	20	49	6.59	x
1978	109	75	45	25	43	2.71	
1979	104	70	40	16	49	3.3	x
1980	108	68	42	4	43	5.62	
1981	107	74	50	26	45	0.73	x
1982	116	80	48	23	42	2.97	
1983	95	50	23	7	45	6.08	
1984	105	61	38	18	39	5.19	
1985	109	63	32	6	49	3.74	
1986	110	82	42	11	47	4.68	x
1987	111	72	35	10	48	2.46	
1988	112	73	35	16	47	2.76	
1989	114	70	24	3	45	2.62	x
1990	107	71	39	19	49	3.51	
1991	105	49	18	5	47	3.9	
1992	106	70	32	2	42	4.16	x
1993	110	62	32	7	41	5.45	
1994	104	69	43	22	42	5.11	x
1995	97	50	18	4	44	2.35	
1996	120	82	46	19	43	2.29	
1997	70	36	10	2	43	3.65	
1998	103	39	8	2	47	4.05	

Table 5.5.5.4-5 Summary of climatic data – Keene, NH 1893-2016

Year	No. Days below Temperature Threshold				March Temperature (average max, °F)	March Precipitation (in.)	Ice indicated by TransCanada files*
	<32°	<20°	<10°	<0°			
1893	85	65	42	21	40	1.97	
1894	112	66	40	12	48	1.21	
1895	116	87	50	29	37	1.89	
1896	112	77	46	19	35	6.19	x
1897	113	73	41	18	41	4.08	
1898	102	59	30	13	49	0.97	
1899	111	73	46	20	39	6.02	
1900	113	78	43	14	37	4.28	
1901	115	74	45	20	41	4.61	
1902	102	65	45	13	50	3.86	
1903	99	66	39	19	52	4.67	
1904	118	90	63	32	40	2.21	
1905	117	92	65	36	43	2.73	
1906	113	73	39	17	37	3.4	
1907	109	79	55	26	45	1.68	
1908	113	74	38	16	44	2.67	
1909	110	69	29	11	40	2.15	
1910	110	66	36	21	51	1.02	
1911	116	74	48	17	41	3.55	
1912	107	75	43	25	40	4.64	
1913	101	51	25	7	49	5.76	
1914	112	70	51	23	42	4.05	
1915	112	74	28	14	42	0.04	
1916	116	82	44	21	37	2.78	
1917	114	72	46	19	42	2.97	
1918	119	92	66	40	46	1.95	
1919	104	60	22	6	48	4.93	
1920	112	88	57	32	46	4.21	
1921	100	54	29	12	54	3.94	
1922	113	70	45	24	45	5.24	
1923	115	86	53	34	40	2.01	
1924	111	63	35	15	42	1.13	
1925	103	66	38	23	49	4.18	x
1926	108	79	44	19	38	2.44	
1927	106	72	44	18	48	1.61	x
1928	104	62	30	6	42	1.99	
1929	106	63	27	10	46	3.59	x
1930	100	65	31	12	45	4.49	
1931	112	69	36	21	43	3.99	
1932	111	61	26	3	39	3.21	
1933	106	55	26	6	39	4.18	
1934	116	84	58	34	43	2.18	
1935	109	78	55	27	45	1.29	x
1936	104	69	53	30	50	7.6	x
1937	110	62	26	2	39	3.71	

Year	No. Days below Temperature Threshold				March Temperature (average max, °F)	March Precipitation (in.)	Ice indicated by TransCanada files*
	<32°	<20°	<10°	<0°			
1938	108	70	33	11	48	1.47	x
1939	107	68	42	19	37	3.87	
1940	117	82	49	22	38	3.67	x
1941	108	76	39	12	39	1.42	x
1942	103	49	30	11	47	5.4	x
1943	113	66	33	22	41	2.36	x
1944	112	76	48	16	48	4.01	x
1945	105	70	37	18	56	1.91	x
1946	103	68	39	16	58	0.98	x
1947	110	59	26	7	42	3.36	
1948	112	82	50	26	46	2.93	x
1949	100	50	20	8	48	2.01	
1950	104	62	38	15	41	2.25	
1951	99	46	28	7	44	5.07	x
1952	105	58	26	10	43	2.46	x
1953	103	51	19	0	46	6.6	x
1954	100	49	19	7	46	3.7	
1955	109	61	21	5	42	4.1	x
1956	112	74	38	14	39	4.85	x
1957	110	62	31	14	47	2.84	x
1958	106	48	31	11	45	2.35	x
1959	117	89	50	23	44	3.65	x
1960	111	61	29	6	37	3.27	
1961	111	78	55	36	45	2.25	
1962	111	64	40	22	47	1.36	
1963	117	79	51	33	46	2.33	
1964	115	71	44	23	46	3.7	x
1965	110	75	36	19	42	1.34	
1966	106	60	31	14	46	2.54	
1967	109	66	45	17	41	2.14	
1968	107	69	45	21	48	4.18	x
1969	109	72	36	16	41	2.11	
1970	111	78	50	26	42	3.14	
1971	118	78	42	22	41	2.87	
1972	109	66	34	20	39	5.11	
1973	103	51	28	15	48	3.09	
1974	108	64	25	11	42	4.31	
1975	111	52	23	10	41	2.67	
1976	110	66	39	15	48	2.81	
1977	107	70	47	23	52	4.98	x
1978	117	78	47	23	42	1.77	
1979	101	65	35	19	49	3.23	x
1980	105	62	37	10	45	5.53	
1981	102	73	44	26	46	0.66	x
1982	82	59	40	17	44	2.43	
1983	90	52	23	10	45	4.01	
1984	108	61	34	18	39	3.17	
1985	100	62	32	13	49	2.85	
1986	106	72	34	15	47	4.39	x

Year	No. Days below Temperature Threshold				March Temperature (average max, °F)	March Precipitation (in.)	Ice indicated by TransCanada files*
	<32°	<20°	<10°	<0°			
1987	109	63	32	11	48	1.61	
1988	108	64	35	11	46	1.78	
1989	109	67	29	6	45	2.17	x
1990	105	74	34	16	50	3.01	
1991	109	56	22	4	45	3.47	
1992	114	82	48	21	40	3.68	x
1993	116	86	49	23	41	4.86	
1994	115	86	54	38	41	4.68	x
1995	106	67	28	10	46	2.59	
1996	114	77	48	30	41	1.74	
1997	108	66	32	8	40	3.66	
1998	110	59	23	7	46	3.79	
1999	112	68	29	16	44	4.1	
2000	106	62	39	21	50	2.86	
2001	110	56	14	0			
2002	86	69	47	26	45	3.95	
2003	109	74	43	15			
2004	115	73	41	23	47	1.28	
2005	113	64	34	7	42	4.57	
2006	107	67	42	8	44	1.18	
2007	117	81	32	12	44	3.47	
2008	114	84	45	21	42	5.62	
2009	110	58	23	9	45	3.31	
2010	114	83	45	16	50	5.39	
2011	98	48	14	5	43	5.33	
2012	112	60	22	9	54	1.56	
2013	112	85	60	27	43	1.98	
2014	112	85	60	27	38	3.99	
2015	113	84	52	34	39	1.36	x
2016	94	47	15	5	50	3.22	

Table 5.5.5.4-6 Summary of climatic data – Hanover, NH 1895-2016

Year	No. Days below Temperature Threshold				March Temperature (average max, °F)	March Precipitation (in.)	Ice indicated by TransCanada files*
	<32°	<20°	<10°	<0°			
1895	116	84	46	26	35	1.99	
1896	108	78	45	21	33	9.25	x
1897	109	73	47	23	39	3.05	
1898	101	65	38	18	48	1.17	
1899	115	80	58	32	35	5.34	
1900	115	87	60	25	35	3.69	
1901	118	85	58	25	37	3.72	
1902	106	77	48	22	47	3.8	
1903	100	70	47	26	51	4.9	
1904	119	92	68	42	38	1.71	
1905	115	100	79	43	42	2.51	
1906	112	82	50	22	34	2.19	
1907	117	87	69	39	42	2.08	
1908	111	81	48	23	41	1.24	
1909	111	84	51	16	38	2.07	
1910	110	73	42	24	48	0.92	
1911	120	95	70	32	49	3.3	
1912	115	84	54	31	38	3.23	
1913	105	60	28	11	47	6.02	
1914	107	76	52	35	39	4.35	
1915	112	83	39	15	38	0.03	
1916	117	84	48	22	36	3.01	
1917	112	80	53	29	40	2.4	
1918	121	95	76	46	42	1.44	
1919	121	95	76	46	44	3.41	
1920	115	89	64	34	43	3.39	
1921	104	62	31	16	50	4.12	
1922	112	83	54	30	41	4.61	
1923	118	93	62	42	37	2.41	
1924	108	74	45	22	42	0.78	
1925	108	77	54	30	47	2.95	x
1926	111	86	58	29	35	1.65	
1927	111	78	54	21	45	0.88	x
1928	111	75	41	18	39	1.97	
1929	107	72	35	14	42	1.91	x
1930	109	73	42	18	41	2.87	
1931	113	67	38	18	43	1.98	
1932	107	67	30	4	36	3.24	
1933	112	56	18	6	37	3.4	
1934	116	89	69	39	40	1.9	
1935	112	78	61	34	42	1.43	x
1936	100	70	56	35	47	5.63	x
1937	115	70	29	5	35	3.49	
1938	112	76	48	16	44	1.37	x
1939	112	81	51	24	35	2.36	

Year	No. Days below Temperature Threshold				March Temperature (average max, °F)	March Precipitation (in.)	Ice indicated by TransCanada files*
	<32°	<20°	<10°	<0°			
1940	119	88	59	27	37	3.9	x
1941	113	85	54	23	36	2.03	x
1942	113	60	34	20	44	4.16	x
1943	117	78	47	30	37	1.75	x
1944	120	87	65	38	37	2.94	x
1945	109	79	55	25	53	1.57	x
1946	107	75	56	29	56	1.26	x
1947	115	76	42	21	40	2.43	
1948	118	91	65	43	44	2.41	x
1949	104	60	28	7	43	1.7	
1950	107	76	41	14	36	3.01	
1951	103	56	29	10	39	4.07	x
1952	110	64	41	18	40	2.07	x
1953	100	59	31	7	43	4.98	x
1954	108	63	29	17	40	3.54	
1955	113	69	34	11	39	2.83	x
1956	116	80	45	20	36	4.44	x
1957	110	70	39	17	43	1.47	x
1958	110	54	36	18	43	2.09	x
1959	118	91	61	32	41	3.16	x
1960	116	66	34	11	35	2.37	
1961	115	82	60	31	42	2.2	
1962	114	70	47	25	44	2.65	
1963	115	77	48	28	42	2.5	
1964	114	79	47	25	42	4.67	x
1965	86	68	42	20			
1966	106	72	36	15	42	2.45	
1967	113	80	52	25	37	1.39	
1968	108	75	56	34	45	3.28	x
1969	114	74	48	21	39	2.04	
1970	111	87	49	32	40	2.55	
1971	116	82	54	23	39	3.35	
1972	112	75	50	27	38	3.89	
1973	111	57	38	20	48	2.13	
1974	110	67	33	15	40	3.27	
1975	111	67	35	14	37	2.09	
1976	115	79	46	19	44	3.49	
1977	110	79	55	27	49	4.03	x
1978	114	88	61	30	40	1.68	
1979	99	70	44	25	45	1.73	x
1980	103	67	43	13	42		
1981	101	68	47	25	46	0	x
1982	116	75	49	26	43	2.27	
1983	105	58	30	12	43	4.74	
1984	99	67	40	18	35	5.19	
1985	107	72	40	16	47	2.75	
1986	111	81	62	29	47	2.27	x
1987	112	69	46	20	48	2.57	
1988	114	67	43	23	45	1.04	

Year	No. Days below Temperature Threshold				March Temperature (average max, °F)	March Precipitation (in.)	Ice indicated by TransCanada files*
	<32°	<20°	<10°	<0°			
1989	115	82	43	19	42	2.43	x
1990	108	78	49	29	48	2.45	
1991	99	48	27	9	43	2.1	
1992	111	78	47	19	39	2.59	x
1993	112	82	49	23	41	5.57	
1994	115	76	49	30	40	3.46	x
1995	72	47	25	11	46	2.79	
1996	108	75	38	16	42	1.87	
1997	105	61	33	7	39	4.59	
1998	78	41	20	5	45	2.54	
1999	67	38	23	9	42	4.09	
2000	100	54	28	18	48	2.98	
2001	110	82	34	7	38	5.56	
2002	106	49	17	4	43	3.46	
2003	110	82	55	31	44	2.15	
2004	115	74	44	18	44	1.15	
2005	111	77	45	14	39	4.1	
2006	109	59	23	5	41	1.84	
2007	105	66	39	14	41	3.13	
2008	114	71	31	7	40	4.59	
2009	110	78	43	15	44	2.96	
2010	103	47	18	6	50	4.66	
2011	106	76	36	14	40	3.61	
2012	99	48	17	4	53	1.77	
2013	104	49	24	7	43	1.18	
2014	103	73	48	23	36	3.93	
2015	109	81	47	25	39	0.8	x
2016	86	39	16	6	50	2.63	

Table 5.5.5.4-7 Temperature and precipitation statistics (Amherst, MA) for years having ice based on TransCanada files

Year	No. Days below Temperature Threshold				March Temperature (average max, °F)	March Precipitation (in.)
	<32°	<20°	<10°	<0°		
Minimum	72	32	3	0	36	0.24
Mean	102.7	58.5	28.3	8.5	45.8	3.61
Maximum	113	79	55	29	57.5	8.24

Table 5.5.5.4-8 Temperature and precipitation statistics (Vernon, VT) for years having ice based on TransCanada files

Year	No. Days below Temperature Threshold				March Temperature (average max, °F)	March Precipitation (in.)
	<32°	<20°	<10°	<0°		
Minimum	52	19	11	0	38	0.7
Mean	107.8	72.4	41.4	17.7	45.0	3.8
Maximum	121	98	64	40	54	8.45

Table 5.5.5.4-9 Temperature and precipitation statistics (Hanover, NH) for years having ice based on TransCanada files

Year	No. Days below Temperature Threshold				March Temperature (average max, °F)	March Precipitation (in.)
	<32°	<20°	<10°	<0°		
Minimum	99	54	29	7	33	0
Mean	110.5	75.3	48.5	24.2	42.5	2.84
Maximum	120	91	65	43	56	9.25

Table 5.5.5.4-10 Temperature and precipitation statistics (Keene, NH) for years having ice based on TransCanada files

Year	No. Days below Temperature Threshold				March Temperature (average max, °F)	March Precipitation (in.)
	<32°	<20°	<10°	<0°		
Minimum	99	46	19	0	35	0.66
Mean	108.2	69.5	39.3	17.9	45.4	3.44
Maximum	117	89	55	38	58	7.60

Table 5.5.5.4-11 Temperature and precipitation statistics (Vernon, VT) for 1936 and 1946

Year	No. Days below Temperature Threshold				March Temperature (average max, °F)	March Precipitation (in.)
	<32°	<20°	<10°	<0°		
1936	97	67	47	25	50	8.45
1946	117	77	57	26	42	3.11

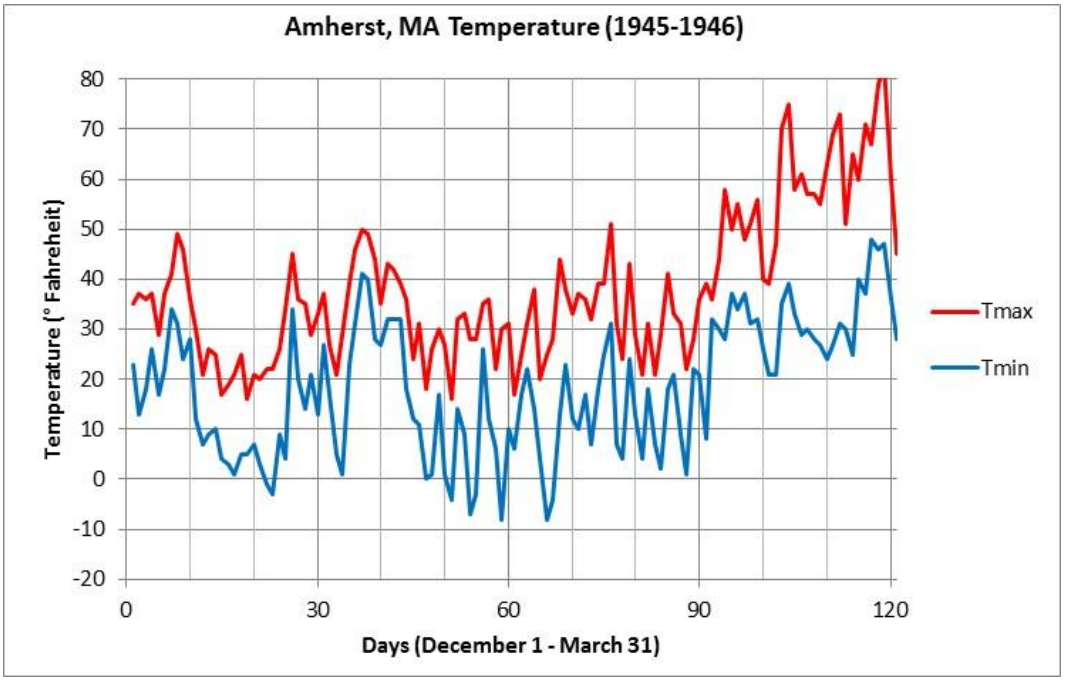

Figure 5.5.5.4-1 Temperatures at Amherst, MA December 1, 1945 – March 31, 1946

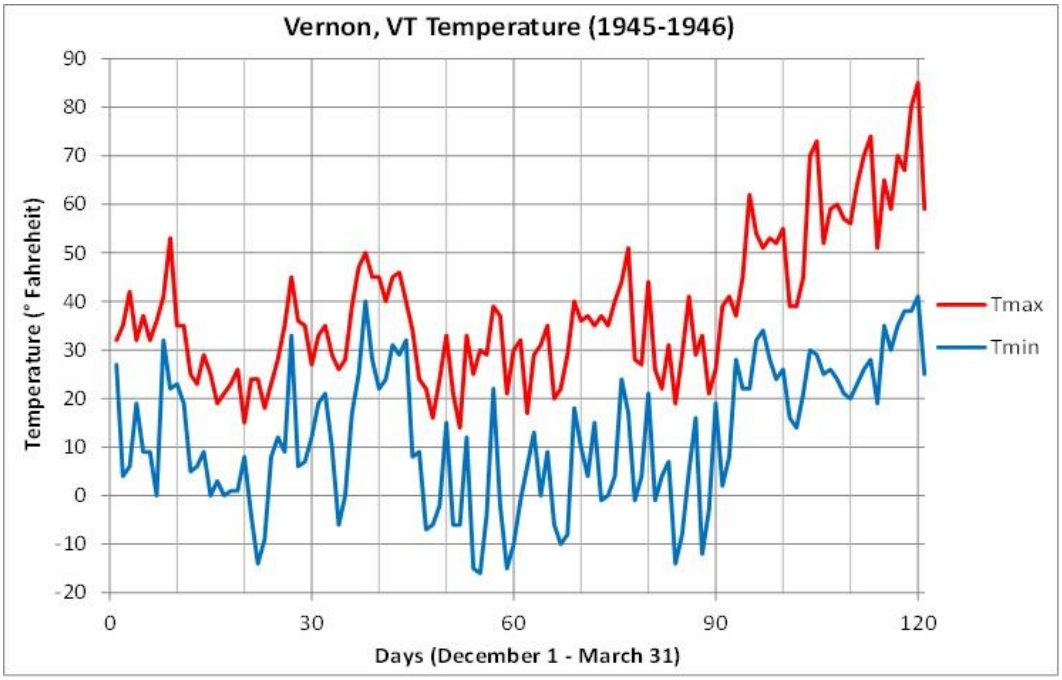

Figure 5.5.5.4-2 Temperatures at Vernon, VT December 1, 1945 – March 31, 1946

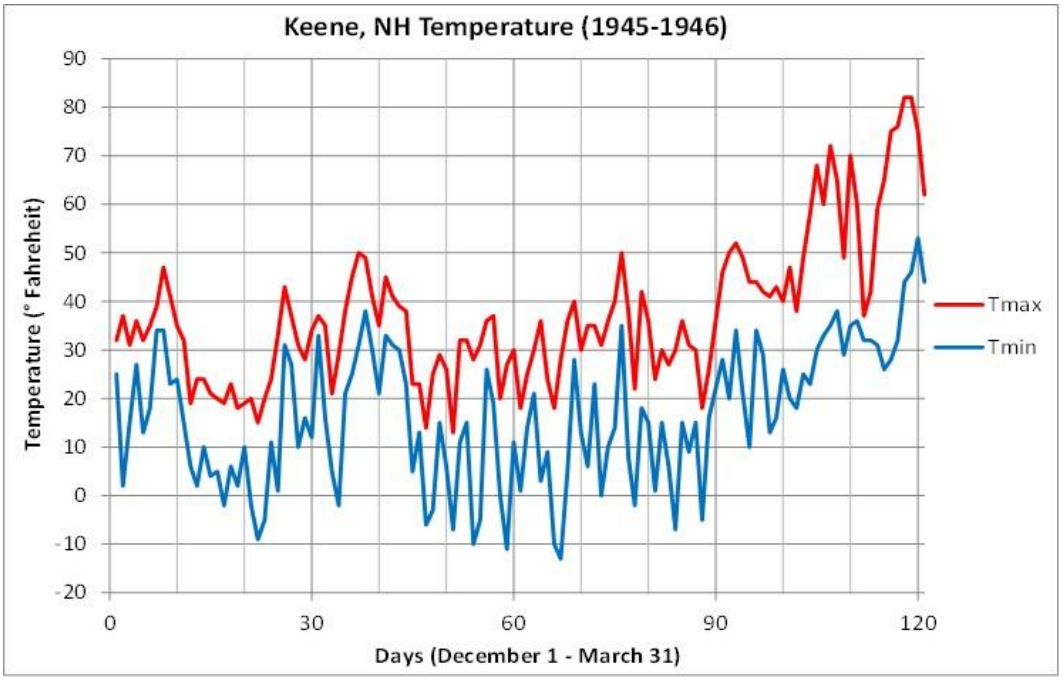

Figure 5.5.5.4-3 Temperatures at Keene, NH December 1, 1945 – March 31, 1946

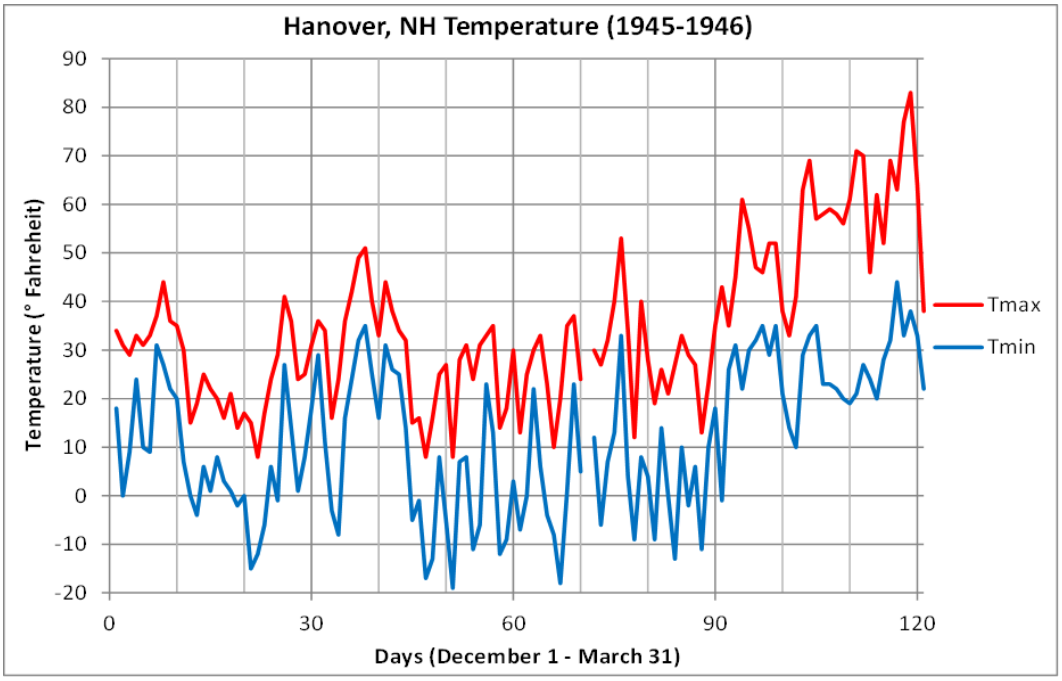

Figure 5.5.5.4-4 Temperatures at Hanover, NH December 1, 1945 – March 31, 1946

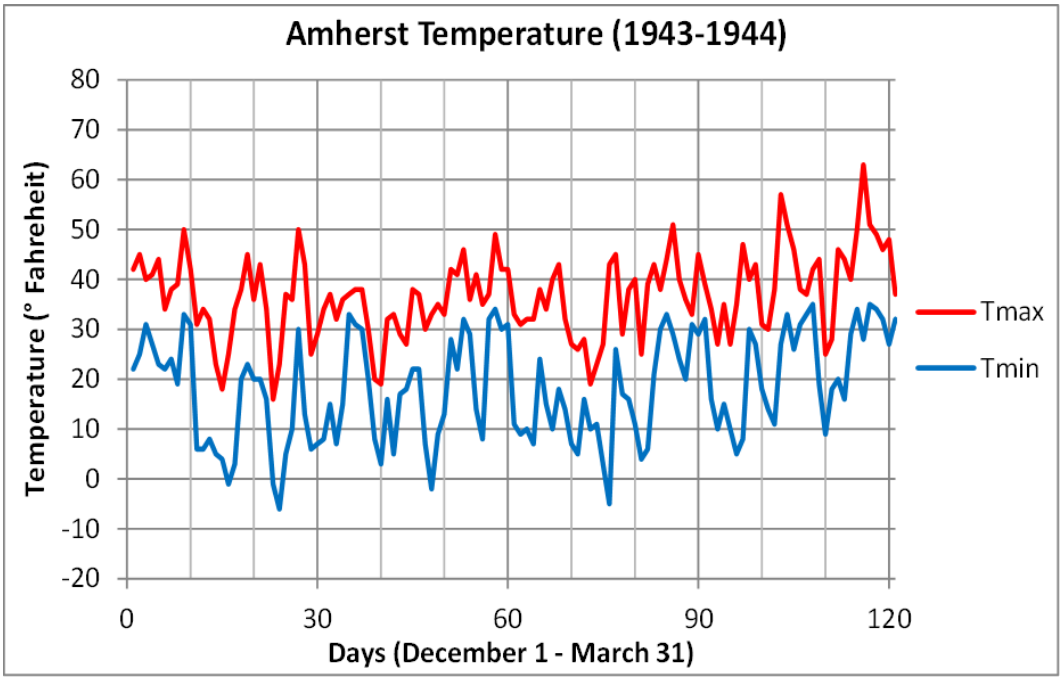

Figure 5.5.5.4-5 Temperatures at Amherst, MA December 1, 1943 – March 31, 1945

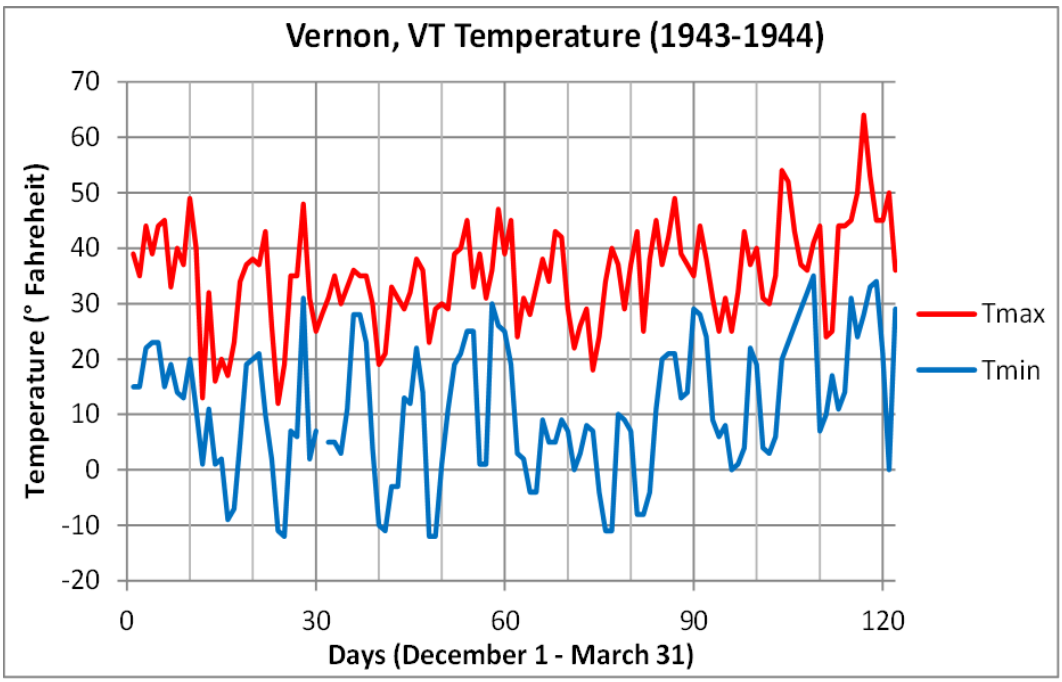

Figure 5.5.5.4-6 Temperatures at Vernon, VT December 1, 1943 – March 31, 1944

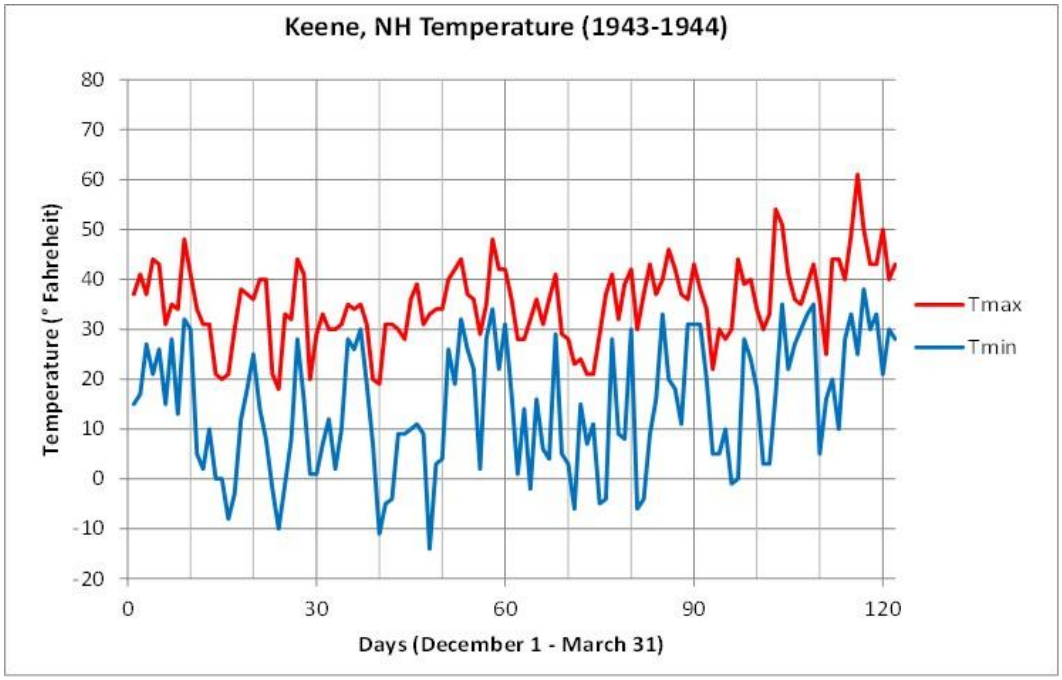

Figure 5.5.5.4-7 Temperatures at Keene, NH December 1, 1943 – March 31, 1944

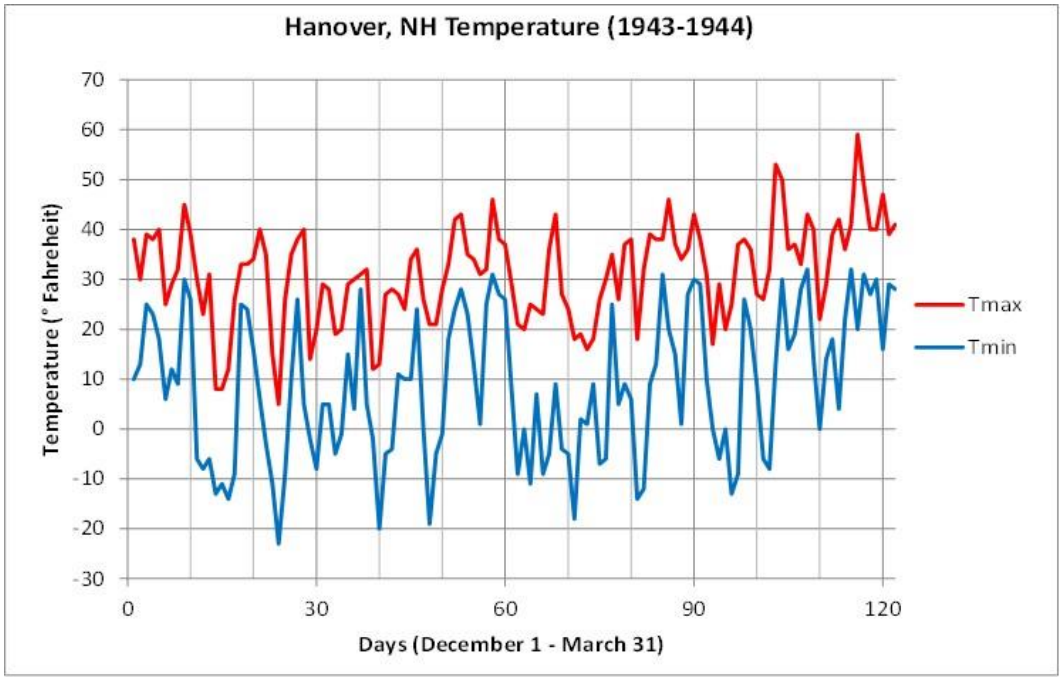

Figure 5.5.5.4-8 Temperatures at Vernon, VT December 1, 1943 – March 31, 1944

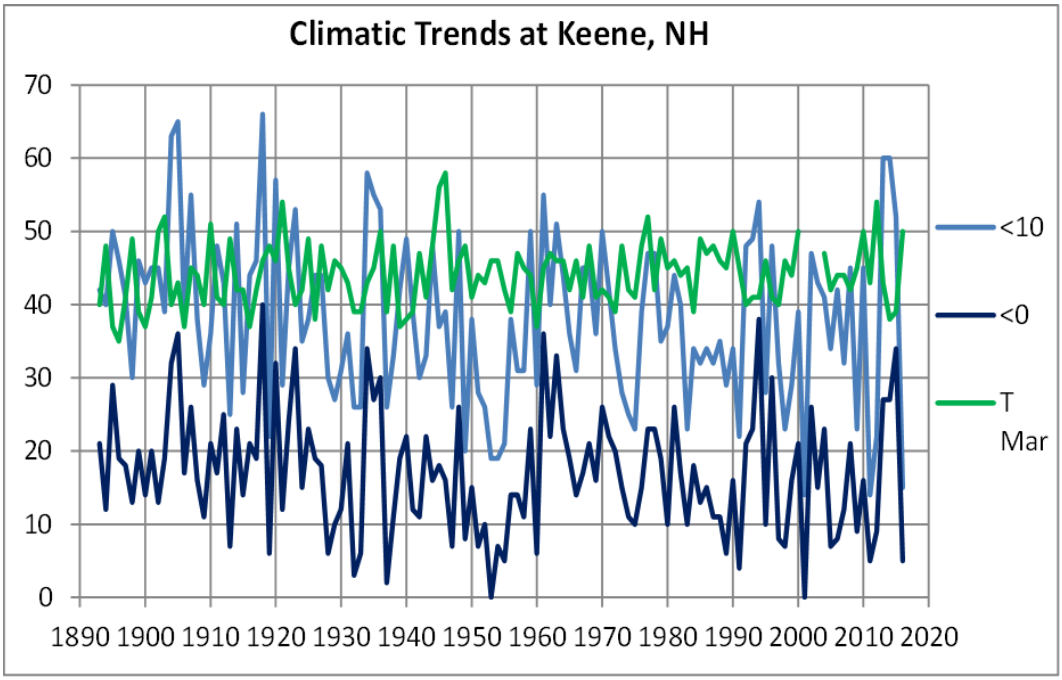

Figure 5.5.5.4-9. Climatic trends – Keene, NH

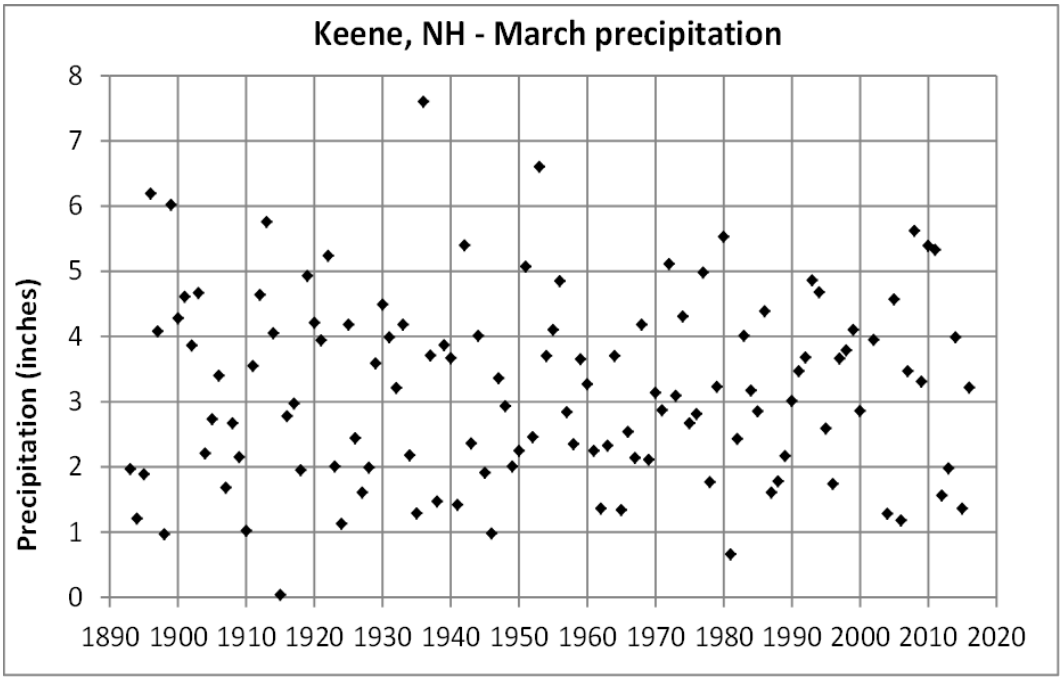

Figure 5.5.5.4-10 March precipitation – Keene, NH

5.5.5.5 Discussion of Key Questions, Summary, and Conclusions

The key questions before all those interested in understanding the causes of erosion in the TFI are: to what extent might erosion due to ice have occurred in the past, what were the effects of VY, and now that VY is no longer operating – to what extent might ice impact the riverbanks in the future. Much can be learned in answering these key questions by evaluating and analyzing the available information and applying scientific inductive and deductive processes to the available information.

While most photographs related to ice and riverbank conditions after ice events are concentrated in reaches of the Connecticut River upstream of Vernon Dam, some information exists regarding ice in the TFI and farther downstream. In the notes of the 1946 Spring Runoff (Figure 5.5.5.2-21), the following statements were made:

> 3/8/1946 – *Observation from French King Bridge reveal breakup in vicinity of bridge. River just above Turners Falls pond unbroken. No disturbance at Meadow Bridge. Northfield Schell Bridge, there is no disturbance.*
>
> 3/11/1946 – *some trouble at the Northampton. Hadley Bridge but seemed to have no details…. presumed it was the White River ice that had jammed up at Hadley and caused only a little trouble.*
>
> 3/12/1946 – *C.R. Bliss reports ice moving in Conn. River below Vernon, passing under Schell Bridge about 2:45 P.M., 3-12-46. He then went back over meadow, down Gill Road and across French King. Main body passed thru meadow while there and it appears that the river is clear from Vernon tailrace to French King Br.*

Another wave of ice was discussed later in the notes passing over Vernon Dam and through the TFI:

> *Informed Col. Dalton that ice was passing over Vernon dam…He asked how soon it would get down river and this was answered by saying it had to go thru Turners Falls Pond, etc., before getting to Whateley and we were not familiar with river timing down the river.*
>
> 3/15/1946 – *About 12:00 Noon Vernon reported they had lost the remaining 300' of their boards and that ice in the Vernon Pond had started out.*

The fact that there is significant information related to ice in the Vernon, Bellows Falls and Wilder Impoundments is due to the power companies' historic focus on these impoundments and does not necessarily indicate that ice is historically more prevalent in the upstream reaches or that there was a lack of ice in the TFI. The fact that ice formed and flowed through the TFI is confirmed by the 1946 observations (in a year that is near the average for ice related temperature conditions) and is supplemented by previous observations of ice and significant damage occurring even farther downstream than Turners Falls.

Historic accounts provide background information regarding the fact that ice events cause erosion along the Connecticut River. An account of the 1896 flood (Charles Thayer) stated the following about what he observed.

> *I thought someone fired off a gun over across the river, but in a minute it began roar, crash, snap, crackle, bang. The fog was so thick that I couldn't see the riverbank but pretty soon it lifted and we could see the trees go down like cornstalks, as the big cakes of ice struck them.*
>
> *In the afternoon we went down to Titans Pier to see the ice go fast. It did go fast with a vengeance and so did the hencoops, trees, barrels, beams, and such. The noise was enough to make you deaf.*

Titans pier is a rock formation on the Connecticut River near Northampton, MA; downstream of the TFI. This account provides observations of ice moving down river shearing off trees and destroying adjacent structures accompanied by deafening noise. This observation demonstrates that historically ice has flowed farther downstream than the TFI.

The CRREL report categorized the 1936 flood as the highest level of damage due to ice breakup. Erosion damage due to the 1936 event is similar to damage shown on the 1946 photographs (Figure 5.5.5.5-1). Field (2007) discussed erosion resulting from the 1936 flood in the form of avulsions in the TFI. He stated that *"The flood of 1936 spread across the floodplain with sufficient force to scour a new channel 20 feet deep across Moose Plain around Schell Bridge in part the result of floating debris that had accumulated under the bridge."* Since ice was a significant factor in the 1936 event, it is likely that ice was the primary component of the floating debris observed at the Schell Bridge (especially since there are only two widely spaced bridge piers at a narrow section of the river where there is also a sharp bend and a significant mid-channel bar downstream of Schell Bridge, see Figure 16 from Field). Ice jams frequently occur as a result of constrictions, bends, and shallow areas of a river where ice floes are restricted. An avulsion occurs when a river abandons (or partially abandons) an existing river channel and forms a new channel through a process of rapid erosion (see Figure 5.5.5.5-2). Field described several avulsion channels that resulted from rapid and significant erosion as a result of floods such as the 1936 flood. Potential erosion scars from the flood of 1936 are visible on a 1939 aerial photograph (Figure 5.5.5.5-3).

The notes from 1946 and the information presented from the 1936 event show that ice has affected the TFI. Historic accounts from 1896 discuss the dramatic effect of ice farther downstream on the Connecticut River near Northampton. In addition to this direct evidence, there is additional information to be considered regarding the condition of riverbanks in the TFI before the influence of VY.

An eroded bank affected by ice is shown in the 1946 photograph in Figure 5.5.5.5-4. This photograph is similar to photographs of eroded banks in the TFI adjacent to an agricultural field downstream of Vernon Dam taken the same time of year (April) in 1913 (Figure 5.5.5.5-5 and 5.5.5.5-6). The reach of the Connecticut River in the TFI downstream of Vernon Dam shows a farm on the *"Vermont side,"* or right bank (Figure 5.5.5.5-7) which may be the area depicted in the previous figures (Figures 5.5.5.5-5 and 5.5.5.5-6). The river in the vicinity of this field is shown in a 1929 aerial photograph (Figure 5.5.5.5-8). The bank along this field is eroded and devoid of riparian vegetation (as is the opposite bank near the downstream tip of Stebbins Island). Ice events occurred in 1866, 1896, 1915, 1925 and 1929. It is possible that these ice events played a significant role in the eroded condition of this riverbank as shown in the 1913 photos and in the 1929 aerial photograph since such erosion is typical of what has been observed on photos showing ice damage. The eroded condition of this reach of the river continues on the aerial photograph taken in 1952 (Figure 5.5.5.5-8), but by the 2008-2010 aerial imagery, a narrow zone of riparian vegetation had become established in this same part of the river.

This area of the river was noted in the 2008 FRR when it was compared to the 1998 image showing that this area was naturally revegetating and becoming more stable over time. These photos, as well as a photo from 2013 show this area over the past 15 years (Figures 5.5.5.5-9 through 5.5.5.5-14). The comparison over time, from 1998 through 2013, show increasing vegetation over this period indicating increasing riverbank stability in this area of the river and significant improvement compared to the barren, eroded conditions seen in the 1929 and 1952 photographs. Other areas that were eroded and lacked riparian vegetation, but now support a zone of riparian vegetation through natural stabilization processes were documented in Section 2.3.4. Documentation of the establishment and growth of new riparian vegetation is provided in Volume III (Appendix J).

As shown by the analysis of historic aerial photographs (Section 2.3), numerous areas of significant erosion were evident in the TFI in the 1950s and 1960s. The study comparing riverbank erosion along the Connecticut River (*"Riverbank Erosion Comparison along the Connecticut River,"* Simons & Associates, 2012) concluded that the segment of river with the greatest extent of eroding riverbanks is the un-impounded northern reach, erosion sites have been stabilizes in the TFI with evidence of natural stabilization, and during the same period of time erosion sites in other impoundments (Bellows Falls, Vernon, and Holyoke) have continued eroding. Given this, the question can and should be raised as to what extent ice may play in the disparate erosion responses occurring in various reaches of river.

Erosion is more extensive in the reaches of river upstream of the TFI (3 times more extensive in the un-impounded reach compared to the TFI based on S&A, 2012). The un-impounded reach does not experience hydropower water level fluctuations but is not dammed and hence somewhat steeper and flows at higher velocities. It is farther north with a potentially somewhat colder climate and has experienced numerous episodes of ice throughout recent history. Historic aerial imagery taken prior to the construction and beginning of operation of both VY and Northfield Mountain which occurred in the 1970s, show that there were significant areas of erosion in the TFI during these years. As a result of VY operations (1972-2014), the TFI has experienced warmer water and very limited episodes of ice. In recent years, segments of river within the TFI have experienced natural stabilization processes with increased vegetation (see 2008 and 2013 FRRs). In contrast, observations in 1998 and 2008 showed that riverbank segments that were eroded over this time period remain in essentially the same eroded condition in Vernon and Bellows Falls Impoundments where the effects of ice has continued (S&A, 2012). Due to the fact that (1) numerous severely eroded areas (consistent with erosion observations in upstream reaches due to ice) were present before 1972 in the TFI; (2) natural stabilization processes have been ongoing in the TFI in recent years during a period of limited ice; and (3) erosion is greatest in a reach of river that is impacted by ice and the TFI has not been significantly affected by ice for a period of more than 30 years it can be concluded that ice plays a significant role as a cause of erosion and lack of ice has played a role in the natural stabilization processes.

The effect of ice is further evaluated by comparing erosion that occurred during 1946 and 2011 in both the TFI and upstream impoundments. The flow hydrographs (at Montague) for these two years are presented in Figure 5.5.5.5-15. The peak flow for 1946 occurred during March with a maximum mean daily flow of 67,000 cfs. There was also a peak flow in March of 2011 of 58,800 cfs. While flows during the remainder of 1946 did not exceed the March peak, there were several higher peak flows during 2011 including a peak of 82,500 cfs in April and 118,000 cfs (mean daily) in August due to Tropical Storm Irene. Flows were much higher in 2011 compared to 1946, with multiple high peaks including the highest peak flow in recent years. If high flows alone caused the most significant erosion, it would be expected that erosion during 2011 would be significantly greater than 1946. Riverbanks were observed by boat in 2011 just after the peak flow due to Tropical Storm Irene. In traveling through the TFI in 2011 only a couple of areas of erosion were observed. Examples of erosion that occurred due to the high flow event in 2011 are shown in Figures 5.5.5.5-16 and 5.5.5.5-17. These areas of erosion are relatively small. In contrast, erosion during 1946 as shown in previous set of figures (Figures 5.5.5.2-13 through 5.5.5.2-20) as well as Figure 5.5.5.5-18, below, is much greater than erosion observed in 2011.

The contrast between extensive and dramatic erosion due to ice in 1946, despite much lower peak flows, compared to quite limited erosion due to a much higher peak flow in 2011 is dramatic. Erosion due to ice is much greater and more extensive than erosion due to a much higher peak flow event without ice.

While the erosion photos from 1946 are quite dramatic and severe, the question of whether this erosion is due to ice or perhaps high flow should be considered. The previously presented photos in 1946 showed ice floes in the river and ice pushing up, into and over the riverbanks on March 8th and 10th, 1946 (Figures 5.5.5.2-9 through 5.5.5.2-11). A series of photos were taken shortly thereafter on April 23rd through 25th, 1946 (Figures 5.5.5.2-13 through 5.5.5.2-20 and 5.5.5.2-22). These photos show the eroded banks and damaged vegetation with evidence of ice gouging and scarring of trees as a result of ice. This combination of ice survey data, photographs of ice on the river, followed by photos of riverbank damage about a month after the ice event show that ice and associated damage was the focus of this set of information. The peak flow of 71,000 cfs (at Montague) in 1946 is below the long-term (1904-1960) average peak flow (97,600 cfs). For a number of years prior to 1946, the peak flows were likewise quite low (Table 5.5.5.5-1).

The fact that an effort was made to document riverbank conditions immediately after the ice event of 1946, coupled with flow data showing that for a period of 6 consecutive years from 1941 through 1946 peak flows

were below average; indicate that the eroded and damaged condition of the riverbanks and riparian vegetation shown in the April 1946 photographs resulted primarily from ice.

The observations of the significance of damage to riverbanks due to ice compared to high flow on the Connecticut River is supported by studies on other rivers. The importance of ice as a cause of erosion was discussed in an analysis of erosion on the Missouri River in Montana (Simon *et al*., 1999):

> *The cycle of river-ice formation, presence, and breakup affects bank erosion, sediment transport, and channel morphology in numerous ways. The mechanisms whereby river ice locally may accelerate bank erosion and change in channel morphology are as follows:*

- Elevated ice-cover level;
- Elevated flow rates after freeze up;
- Local scour in regions of locally high flow velocity at ice accumulations or flow
- Deflected by ice accumulations;
- Ice-run gouging and abrasion of channel banks and bars;
- Channel avulsion attributable to ice jams; and,
- Ice-cover influence on bank-material strength and bank stability.

> *Two of the most important issues regarding streambank erosion along the Missouri River in the study reach are pore-water pressure effects from sustained high flows, ice-related effects, and the direct effects of an ice cover.*

While quantitative analysis of the effect of ice on riverbank erosion is not possible with the available information (since riverbank surveys in the TFI occurred during a period of no ice and no known historic cross-section surveys are available over a period of years at upstream reaches), observations of ice on the Connecticut River (from photographs, notes, ice data, temperature and climatic data, flow data, and direct observations of ice), analysis of ice on other rivers (Platte, and Missouri) all strongly indicate that ice has the potential to be one of the dominant primary causes of erosion, on a level similar to or even greater than high flow events, in the TFI.

Another important question of interest is to what extent water level fluctuations may adversely affect young riparian or other vegetation when the TFI is covered with ice. During the winter of 2014/2015, as shown in Figures 5.5.5.1-2, 5.5.5.1-4, 5.5.5.1-7, 5.5.5.1-8, and 5.5.5.1-10 (taken on March 3, 2015), ice formed on the Connecticut River through much of the TFI. Photographs taken on January 5, 2015 showed that there was some ice on the river but that most of the river was open water (Figures 5.5.5.1-3, 5.5.5.1-5, 5.5.5.1-6 and 5.5.5.1-9). Based on these photographs, the river may have been covered with ice later in January or February and then into March. As indicated in the literature, ice may adversely affect riparian vegetation. It has been clearly demonstrated that when ice breaks up rapidly, potentially jams, and moves downstream in floes; riparian vegetation including trees can be sheared off, otherwise severely damaged or scarred. In addition, young riparian vegetation may be impacted by ice in the earliest stages of life including establishment and survival from the seedling to sapling phase of growth (Ettema, 2002). As noted in R. Ettema, 2002:

> *Where ice runs occur with about annual frequency, riparian vegetation communities have difficulty getting established. Ice abrasion and ice jam flooding may suppress certain vegetation types along banks…possibly exacerbating bank susceptibility to erosion.*

High seedling mortality was further documented in (S&A, 2000).

> *In Johnson's report (1994a), he states that, "seedling mortality is usually highest in winter". In both the Johnson reports covering 1993-94 and 1994-95, he concludes with essentially the same information, "seedling mortality is usually highest in the winter associated with ice; ice is an effective mortality factor because it can block flow and raise river stage, cause sediment movement,*

and physically damage living vegetation". Johnson recorded mortality rates as high as 98 percent due to ice. Furthermore, he states that "ice remains the only factor with much potential to kill older seedlings, at least within the flow ranges that we have experienced during the course of this study."

In the TFI with the continual fluctuations due to hydropower operations, there could be some adverse impact primarily on young vegetation when ice moves up and down with the water level fluctuations. Water level fluctuations are shown during February and March of 2015 at the Northfield Mountain Tailrace in Figures 5.5.5.5-19 and 5.5.5.5-20. During these months, daily water level fluctuations ranged from approximately 1 to 3 feet with fluctuations over a week's time as large as approximately 5 feet. Overall water levels during this time period ranged from about El. 179 to 185 feet. This range of fluctuation which occurred during February and March of 2015 is considered as being typical of Northfield operations.

Photographs were taken later in 2015 showing riverbank vegetation focusing on aquatic, herbaceous and young woody riparian vegetation. Figure 5.5.5.5-21 shows a maple seedling that survived the winter ice of 2014/2015 (Note that maples seeds drop in the fall of the year as can be seen lying on the ground in this photograph that was taken in September). Figure 5.5.5.5-22 shows cottonwood seedlings/saplings that are 2 or more years old and survived the winter ice of 2014/2015. Ice-out in 2015 did not include a significant break-up event as the ice essentially melted in place. The fact that seedlings and other vulnerable vegetation, which can be seen in these photographs taken later in 2015, survived the 2014/2015 winter ice demonstrates that the typical water level fluctuations which occurred when ice covered the TFI during this winter did not cause significant adverse impacts to even the most sensitive vegetation. Observations of ice in 2014/2015 and subsequent observation of vegetation later in the year suggest that ice cover which experiences typical water level fluctuations and that subsequently melts without a significant break up event does not cause significant damage to young riparian vegetation in the TFI.

Several key points regarding ice are made based on photographs, aerial photographs, notes, measurements and observations of ice on the Connecticut River:

- Ice has caused erosion of riverbanks and damage to riparian vegetation on the Connecticut River as documented by photographs, observations and measurements from the 1800s to the present, upstream of Vernon Dam;

- Ice both destroys riparian vegetation and limits its establishment and growth as demonstrated by various analyses and observations (and has been quantitatively demonstrated by vegetation demography studies, analysis and computer modeling that ice plays a *"significant, if not dominant"* role in removing and limiting riparian vegetation on the Platte River). As shown in the erosion causation study, riparian vegetation plays a significant role in riverbank stability;

- Ice has been observed flowing through the TFI as well as downstream on several occasions along with damage likely due to ice jam flooding and an avulsion in 1936 in the vicinity of the Schell Bridge;

- Eroded riverbanks and lack of riparian vegetation has been documented in the TFI before VY that is similar to the condition of riverbanks eroded by ice in reaches upstream of Vernon Dam as documented by historic aerial and ground photographs;

- Areas that were eroded and lacked riparian vegetation in the TFI have been experiencing a natural stabilization process and associated increase in vegetation as documented by aerial photographs taken over time when VY was in operation and little ice occurred. Riparian vegetation and aquatic vegetation have been increasing in the TFI as documented by the 2008 and 2013 FRR's and subsequent observations;

- The river upstream of Vernon Dam has experienced more significant erosion over recent decades than the TFI as documented in *"Riverbank Erosion Comparison along the Connecticut River,"* Simons & Associates, 2012):

> Several erosion sites were identified and photographed in the Bellows Falls, Vernon, Turners Falls, and Holyoke Impoundments in 1997, and again in 2008. All of the erosion sites in 1997 in the Bellows Falls and Holyoke Impoundments and all but one of the 1997 erosion sites in the Vernon Impoundment remain in essentially the same state of erosion when photographed in 2008, many of which are significant in both size and severity.

These observations are consistent with: (1) the scientific literature regarding the adverse effects of ice; (2) studies on other rivers which show that ice plays a significant role in causing erosion (on the same order of magnitude as high flows) and a significant, if not dominant, role in riparian vegetation processes; and (3) the fact that ice has affected the Connecticut River upstream of VY on an ongoing basis over centuries of time but that the effects of ice were essentially eliminated for the period from the early 1970s until the end of 2014 in the TFI due to the operation of VY. Given that VY has ceased operation and will no longer warm the waters of the TFI, ice is expected to once again affect riverbanks and riparian vegetation in the TFI as dictated by climatic and hydrologic processes as has been seen in other areas along the river (Figures 5.5.5.5-23 and 5.5.5.5-24).

Conclusions

Ice has the potential to be a naturally occurring dominant primary cause of erosion in the TFI in the future given the right climatic and hydrologic conditions. Furthermore, based on (1) the results of the ice analysis conducted as part of this study; (2) observations made during the 2014/2015 winter when ice formed over much of the TFI; and (3) the results of the various hydrologic analyses previously discussed it appears unlikely that Project operations will exacerbate the impact of ice on erosion processes. The most significant erosion associated with ice is due to ice break-up, floes, and jams and the corresponding damage which occurs as the ice scrapes along the bank while moving downstream. Based on analysis of historic information, these processes occur as a result of moderate to high flows which typically exceed the high flow threshold previously discussed (i.e. 37,000 cfs). At flows greater than 37,000 cfs (or 17,130 cfs in the upper reach) hydropower operations typically have minimal hydrologic impact in the TFI. While ice is the ultimate cause of erosion in these instances, it is not until sufficiently high flows persist for damage to the riverbanks to occur. This is a naturally occurring process independent of hydropower operations.

Sheet ice can also impact riverbank stability by scraping along the bank when water levels fluctuate. As previously demonstrated from the results of the various hydrologic analyses, for the vast majority of the time the water surface (and therefore the ice) rests on the lower riverbank. In the TFI, the lower bank is typically a flat, beach like feature with minimal to no vegetation or erosion. It is not until the water surface (and therefore the ice) reaches the upper bank that erosion could potentially occur. It is typically not until flows approach or exceed the natural high flow threshold that the water level reaches the upper bank. As such, based on the results of the hydrologic analyses conducted, it is unlikely that water level fluctuations associated with typical hydropower operations could result in ice damage to the banks.

These processes were observed during the winter/spring of 2014/2015 when ice formed over much of the TFI. During this time Northfield Mountain operated in a typical manner. Water levels at the Northfield Mountain Tailrace fluctuated approximately 1 to 4 feet on a daily basis, with an average of about 2 feet, and about 5 feet over a week's time through the winter and early spring. For the vast majority of the time the water level rested, and fluctuated, on the lower bank. Based on observations of ice through this period, these fluctuations did not cause ice break-up or floes as the ice persisted into March. There was no significant ice break-up event and ice primarily melted in place, probably partly due to inflow from Vernon not exceeding 17,130 cfs until April 4th. Observations of the riverbank later in the year did not exhibit

damage due to ice erosion and young riparian vegetation (seedlings and saplings) that had been established prior to the winter of 2014/2015 were observed at various locations in the TFI. Typical Project operations and associated water level fluctuations did not appear to cause or exacerbate ice related erosion or damage.

Although a quantitative analysis of the impact of ice as a cause of erosion was not possible given weather conditions during the monitoring period and the available historic data, the results of the analyses which were conducted indicate that ice has the potential to be a naturally occurring dominant cause of erosion in the TFI in the future if the right climatic and hydrologic conditions persist. Available information and observations indicate that Project operations do not cause an ice break-up event to occur, as ice break-up events occur as a result of climatic and hydrologic conditions (i.e. moderate to high flows, rapid melting, and rainfall) which are independent of Project operations.

Table 5.5.5.5-1 Peak Flows immediately preceding and including 1946 (Connecticut River at Montague)

Year	Peak Flow
1941	46,300
1942	70,600
1943	71,100
1944	69,600
1945	85,600
1946	71,000

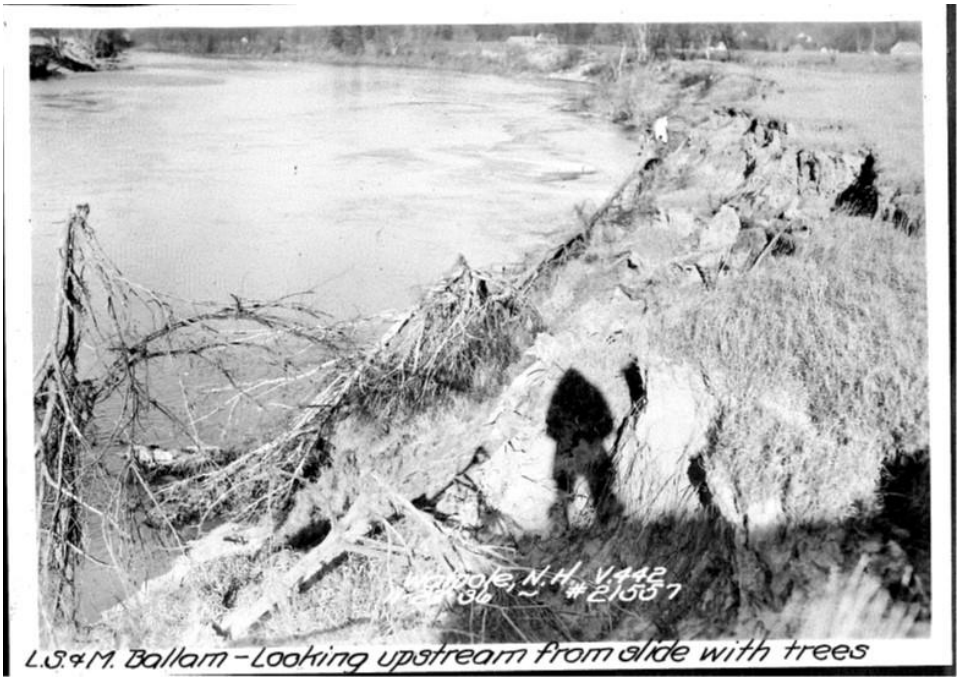

Figure 5.5.5.5-1 Erosion Damage – 1936 Flood

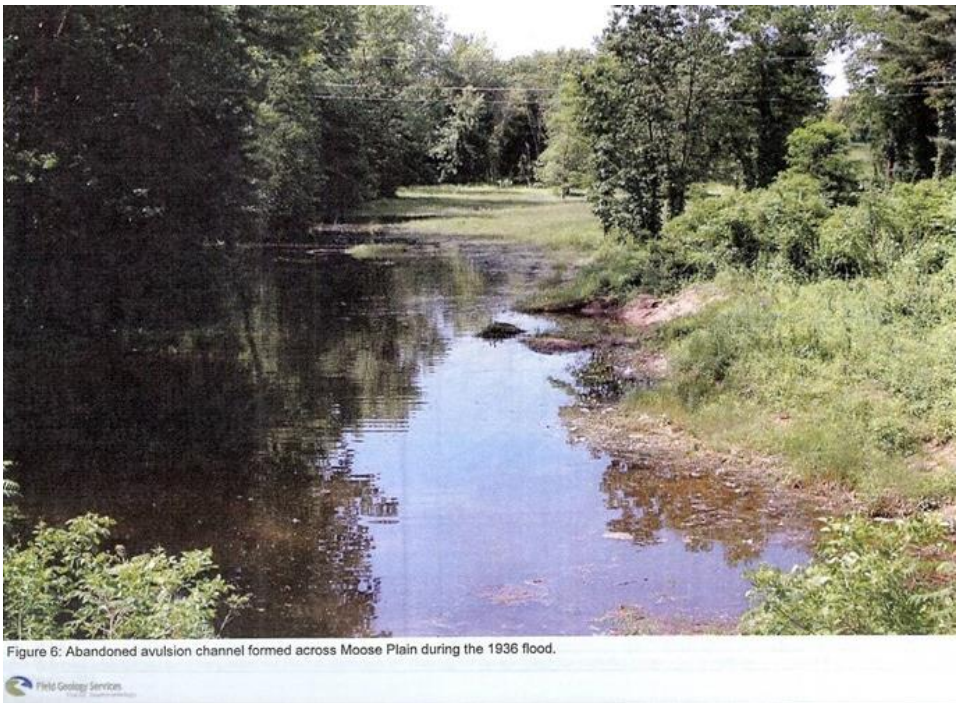

Figure 5.5.5.5-2 Abandoned Avulsion Channel – 1936 Flood (Field, 2007)

Figure 5.5.5.5-3 Aerial Photo Showing Erosion Scars on Floodplain - 1939

Figure 5.5.5.5-4 Connecticut River near Windsor, VT – April 28, 1946 (TransCanada)

Figure 5.5.5.5-5 Eroded Bank in Turners Falls Impoundment Downstream of Vernon Dam – April 5, 1913 (TransCanada)

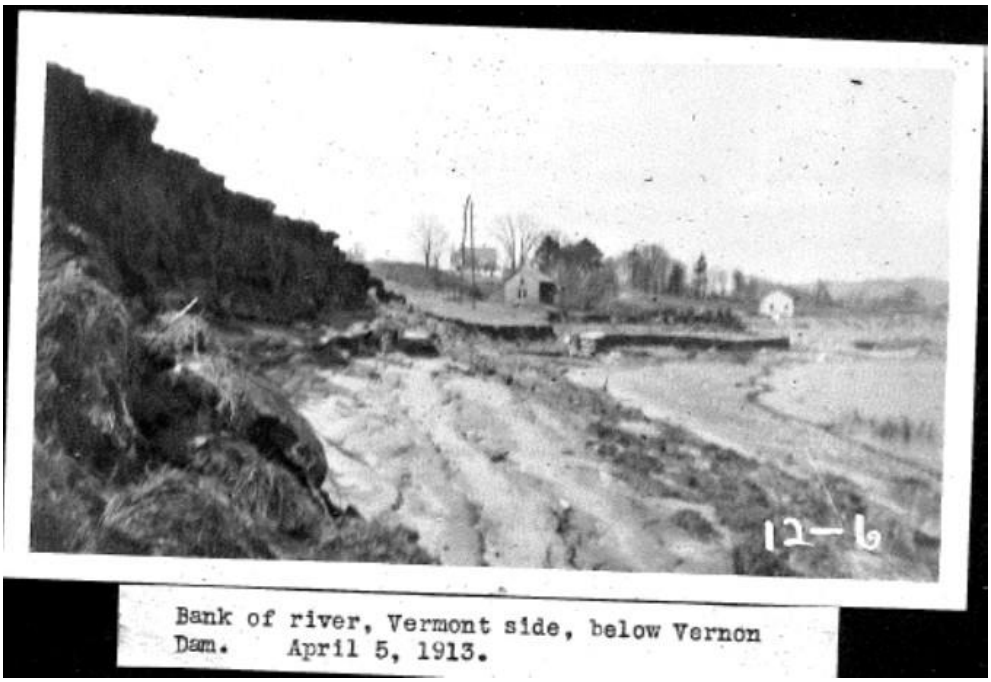

Figure 5.5.5.5-6 Eroded Bank in Turners Falls Impoundment Downstream of Vernon Dam – April 5, 1913 (TransCanada)

Figure 5.5.5.5-7 Connecticut River Downstream of Vernon Dam (Google Earth)

Figure 5.5.5.5-8 Field Downstream of Vernon Dam – 1929

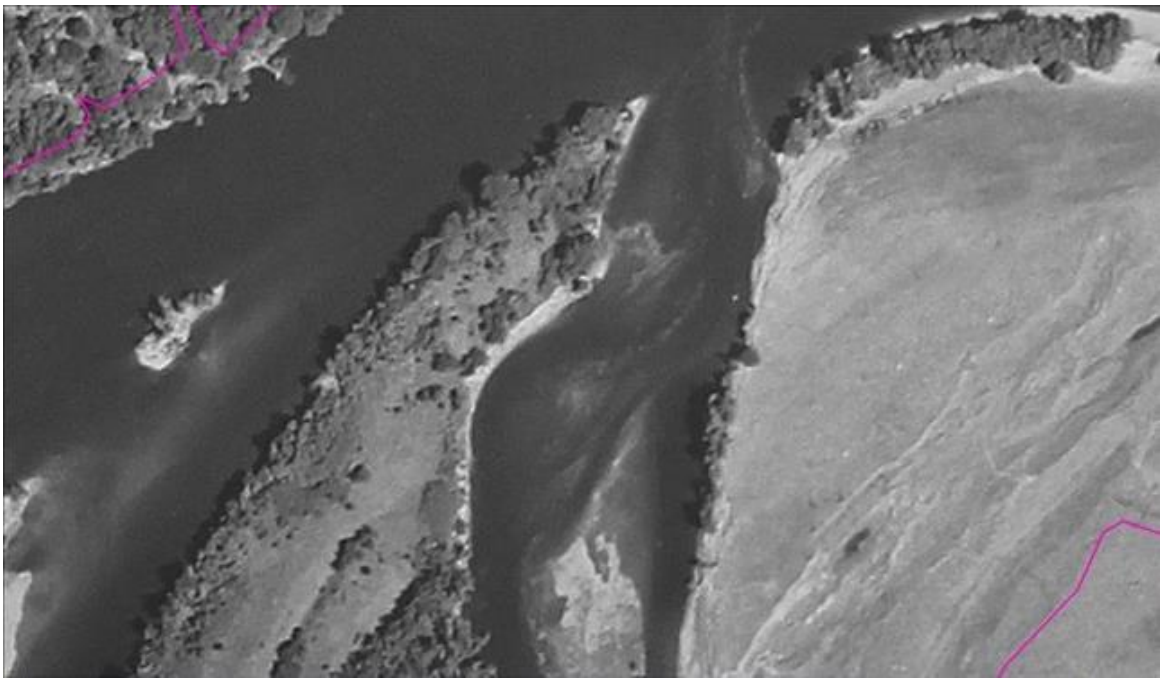

Figure 5.5.5.5-9 Field Downstream of Vernon Dam – 1952

Figure 5.5.5.5-10 Field Downstream of Vernon Dam – 2008-2010

Figure 5.5.5.5-11 Right Bank Near Downstream End of Stebbins Island – 1998

Figure 5.5.5.5-12 Right Bank Near Downstream End of Stebbins Island – 2008

Figure 5.5.5.5-13 Right Bank near Downstream End of Stebbins Island – 2013

Figure 5.5.5.5-14 Location of Photos Taken Downstream of Stebbins Island (Google Earth)

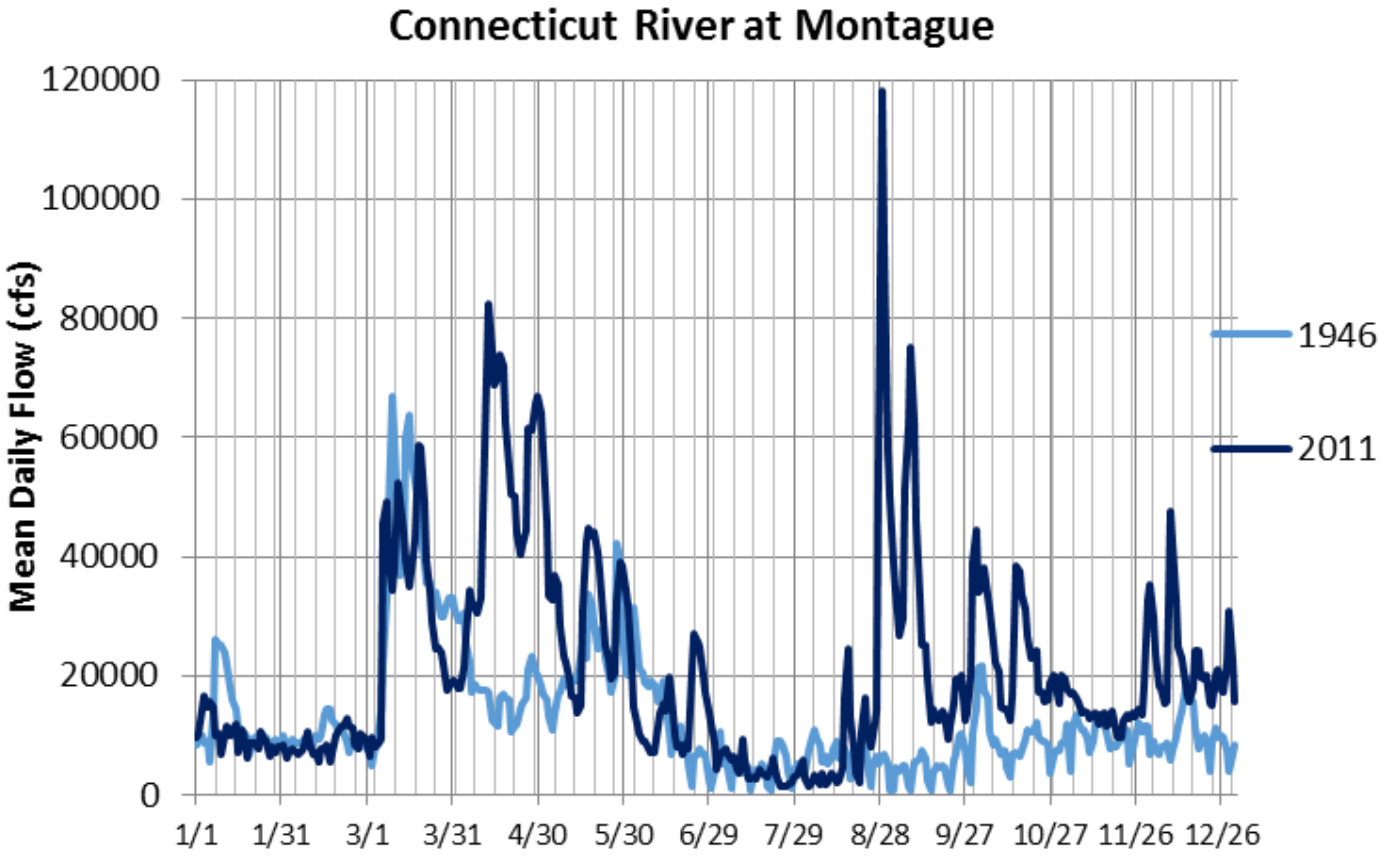

Figure 5.5.5.5-15: Connecticut River at Montague, MA – 1946 and 2011 (USGS)

Figure 5.5.5.5-16 Erosion Due to High Flow in 2011

Figure 5.5.5.5-17 Erosion Due to High Flow in 2011

Figure 5.5.5.5-18 Erosion in 1946 Due to Ice (TransCanada)

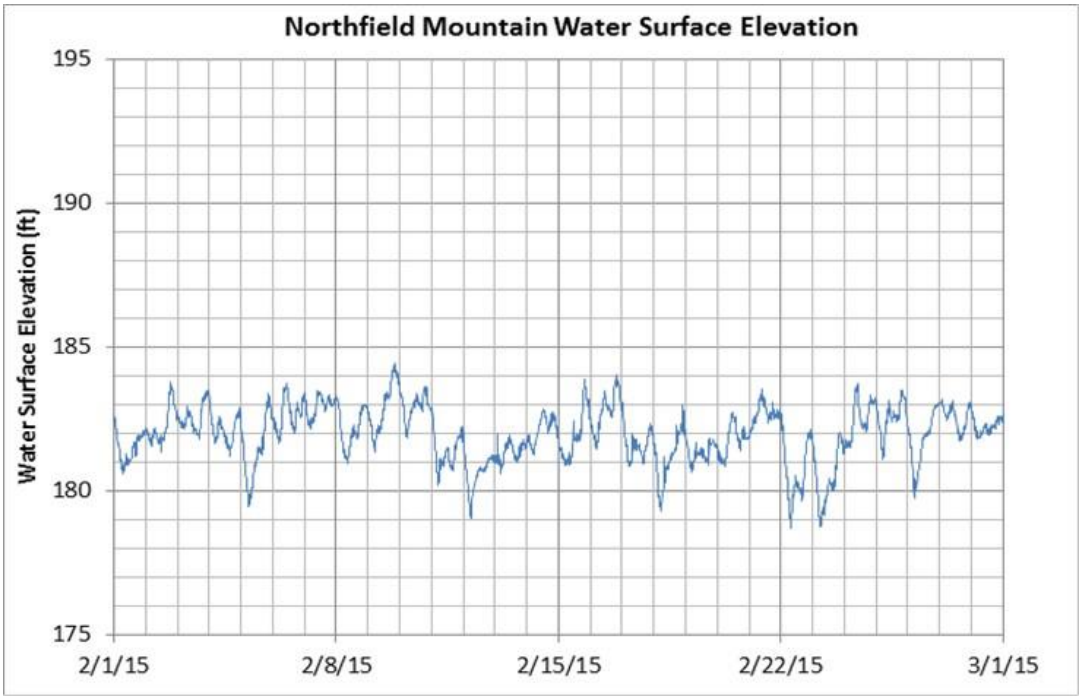

Figure 5.5.5.5-19 Water Level Fluctuations at Northfield Mountain Tailrace, February 2015

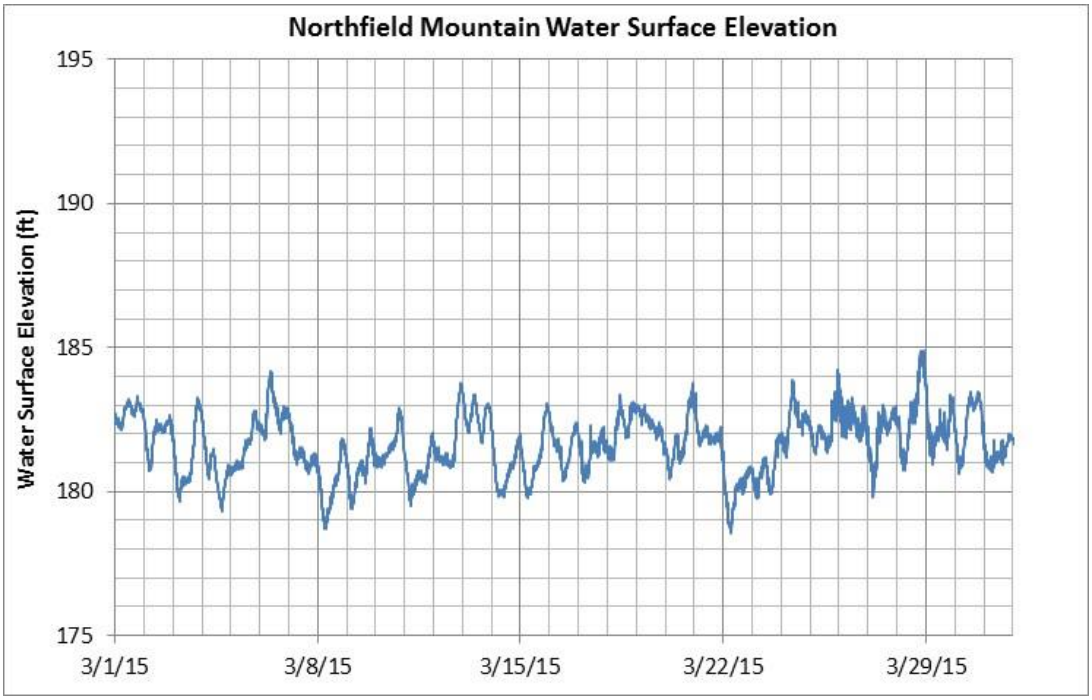

Figure 5.5.5.5-20: Water Level Fluctuations at Northfield Mountain Tailrace, March 2015

Figure 5.5.5.5-21: Maple seedling (9/28/2015)

Figure 5.5.5.5-22: Cottonwood seedlings (9/28/2015)

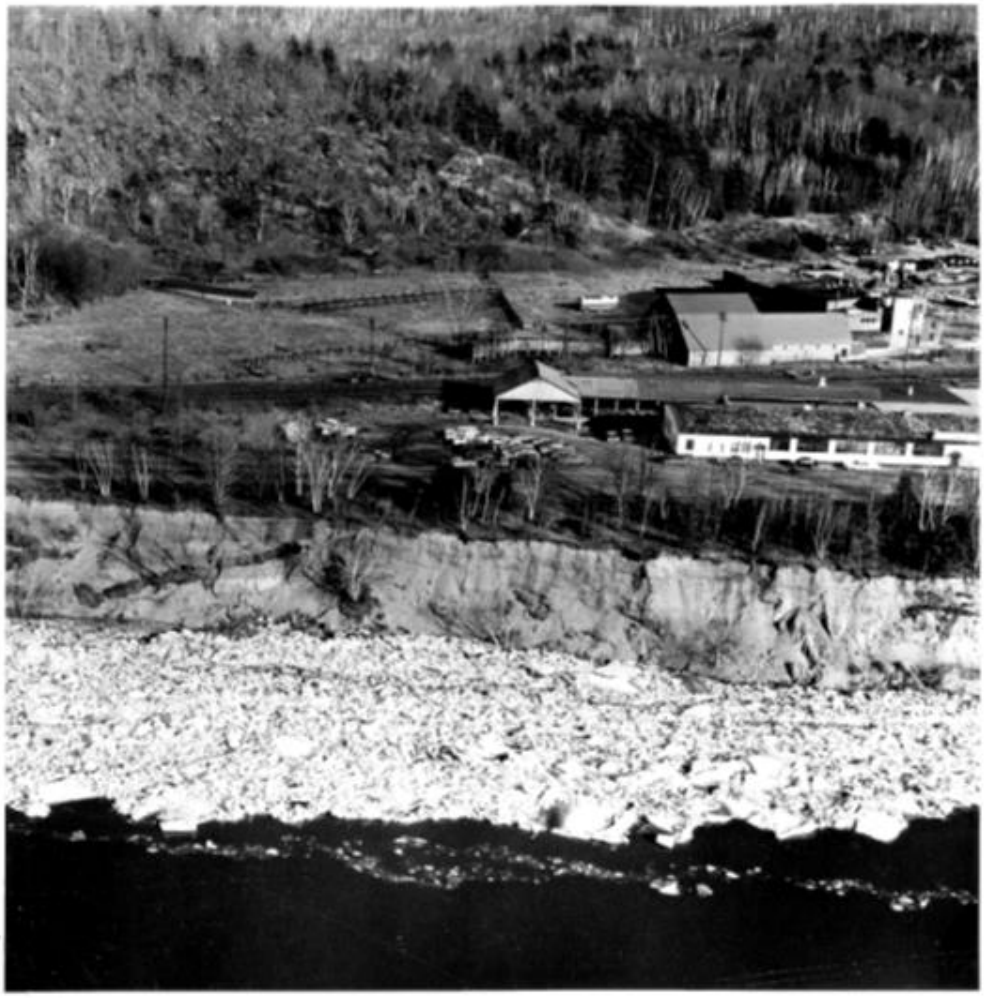

A - 3

March 25, 1968 - Eroded banks on N.E.P. property just north of Cray banks.

Figure 5.5.5.5-23 Ice and erosion damage, 1968

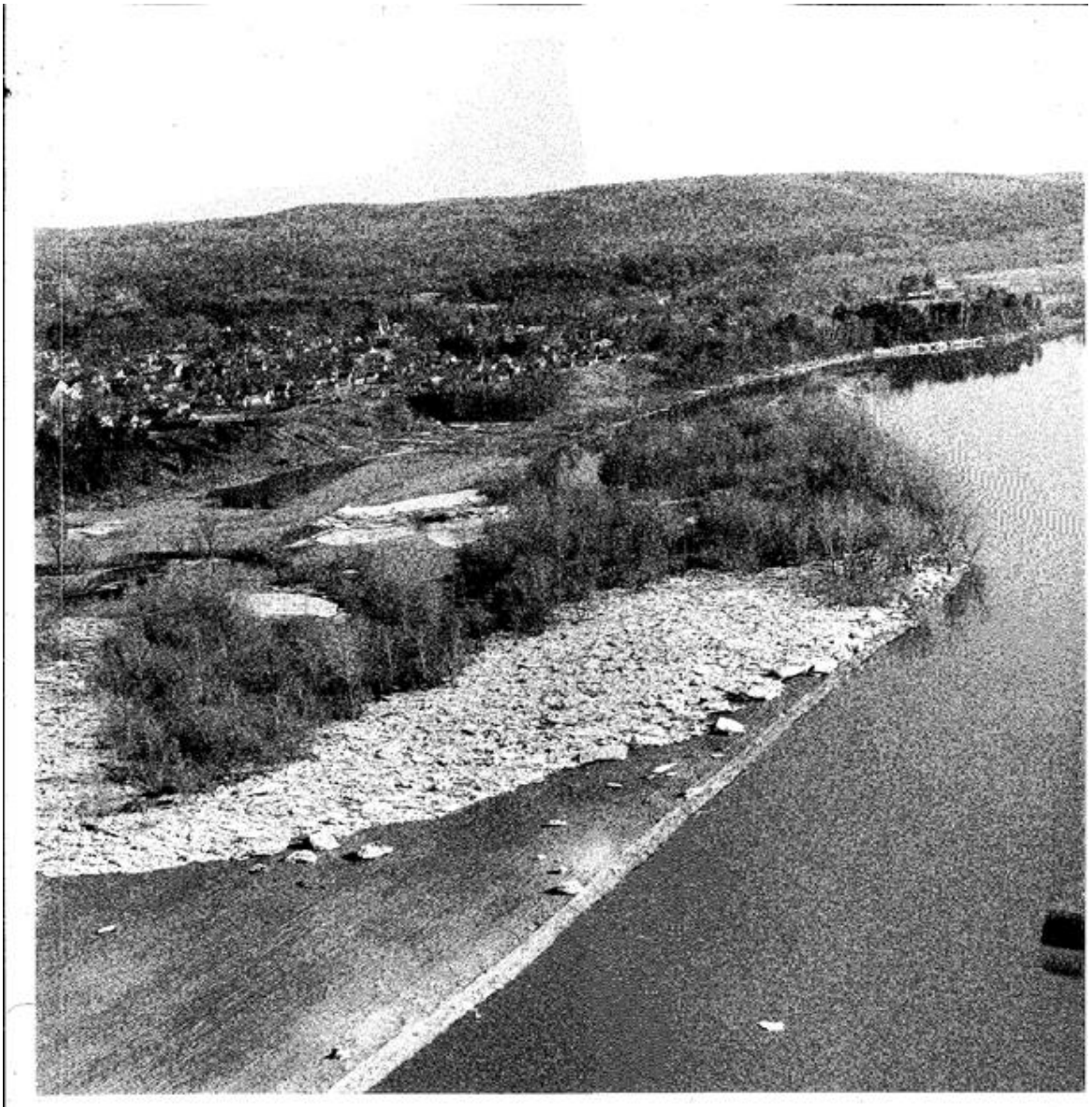

A - 15

Evidence of low bank erosion opposite Charlestown.

Figure 5.5.5.5-24 Ice and erosion damage, 1968

5.5.6 Animals

Animals cause damage to riverbanks in a number of ways. Animal trails leading to the river can create concentrated runoff that cause gullies to form along the trail. Removal or damage to vegetation above ground reduces the protective effect against erosion that vegetation offers which, in turn, can result in root damage and decrease in the binding effect that roots have on the soil matrix. Burrowing of animals or birds into the riverbank can also create disturbance to the riverbank or can create points where seepage may more easily develop resulting in concentration of such flows down the riverbank slope and corresponding erosion.

As part of the 2013 FRR, the locations of sensitive receptors found along or near the TFI riverbanks were mapped. A sensitive receptor was defined as important wildlife habitat located at or near the riverbank. Many wildlife features were observed during this survey including bank swallow and belted kingfisher nesting sites and bald eagle nest and perch sites. Of particular interest to this study were the bank swallow and belted kingfisher nesting sites since they are reliant on eroding banks for habitat. Belted kingfishers and bank swallows excavate cavities to use as nests in sheer banks lacking vegetation and containing appropriate soil conditions. Figure 5.5.6-1 depicts the locations of the sensitive receptors identified during the 2013 FRR. An example of a bank swallow nesting site is found in Figure 5.5.6-2.

Along agricultural fields, paths are frequently created by animals traveling between fields and the river. Examples of this activity are shown in Figure 5.5.6-3 and again in Figures 5.5.6-4 through 5.5.6-12. Figure 5.5.6-13 shows the location where each of the photos in Figures 5.5.6-4 through 5.5.6-12 were taken. At the agricultural field found in Figures 5.5.6-4 through 5.5.6-12 it was observed that there were a number of animal paths over the length of the field. Based on the width of the riparian zone adjacent to this particular field, the animal paths were found where the riparian zone was narrow while no animal paths were observed where the riparian zone was wider.

While the types of animal activities discussed above have been observed to occur along the riverbanks of the TFI, they are found only in a few discrete areas along the river.

Legend

- 1000' River Marker
- 500' River Marker

Sensitive Receptor

BASW - Bank Swallows
BEKI - Belted Kingfishers
BAEA - Bald Eagles

French King Gorge

French King Bridge (Route 2)

Barton Cove

Turners Falls Dam

230+00
220+00
210+00
200+00
190+00
180+00
170+00
160+00
150+00
140+00
130+00
120+00
110+00
100+00
90+00
80+00
70+00
60+00
50+00
40+00
30+00
20+00
10+00
0

ERVING
GILL
MONTAGUE
GREENFIELD

Millers River
Fall River

FRENCH KING HIGHWAY
MOHAWK TRAIL
RIVER ROAD
MILLERS FALLS ROAD
GILL-MONTAGUE BRIDGE
TURNERS FALLS ROAD
UNITY STREET
L STREET

Barton Cove Island
BEKI & BASW
BEKI & BASW

Map 5
Map 4
Map 3
Map 2
Map 1

FirstLight Power Resources

FIRSTLIGHT HYDRO GENERATING COMPANY
Northfield Mountain Pumped Storage Project No. 2485
Turners Falls Hydroelectric Project No. 1889
STUDY 3.1.2

0 625 1,250 2,500 Feet

Figure 5.5.6-1
Sensitive Receptor Locations
Map 1

Service Layer Credits: Sources: Esri, HERE, DeLorme, USGS, Intermap, increment P Corp., NRCAN, Esri Japan, METI, Esri China (Hong Kong), Esri (Thailand), MapmyIndia, © OpenStreetMap contributors, and the GIS User Community
Source: Esri, DigitalGlobe, GeoEye, Earthstar Geographics, CNES/Airbus DS, USDA, USGS, AEX, Getmapping, Aerogrid, IGN, IGP, swisstopo, and the GIS User Community

Path: W:\gis\studies\3_1_2\maps\final_report\figure_5_5_6-1.mxd

Legend

- 1000' River Marker
- 500' River Marker

Sensitive Receptor

- BASW - Bank Swallows
- BEKI - Belted Kingfishers
- BAEA - Bald Eagles

BASW (historic colony site)
Ashuelot Brook
420+00
410+00
Kidds Island
BAEA
BEKI
400+00
BEKI & BASW
390+00
MILLERS FALLS ROAD
380+00
370+00
Pine Meadow Brook
360+00
350+00
340+00
NORTHFIELD
330+00
BEKI & BASW
GILL
320+00
BASW
BEKI
Fourmile Brook
BEKI & BASW
310+00
BEKI
300+00
290+00
280+00
Northfield Tailrace
270+00
potential nest site (BASW & BEKI)
260+00
BASW (historic colony site)
250+00
240+00
ERVING
230+00
FRENCH KING HIGHWAY
NORTHFIELD ROAD
French King Gorge
220+00
French King Bridge (Route 2)
200+00
MONTAGUE

Map 5
Map 4
Map 3
Map 2
Map 1

FirstLight Power Resources

N

0 625 1,250 2,500 Feet

FIRSTLIGHT HYDRO GENERATING COMPANY
Northfield Mountain Pumped Storage Project No. 2485
Turners Falls Hydroelectric Project No. 1889
STUDY 3.1.2

Figure 5.5.6-1
Sensitive Receptor Locations
Map 2

Path: W:\gis\studies\3_1_2\maps\final_report\figure_5_5_6-1.mxd

Legend

- 1000' River Marker
- 500' River Marker

Sensitive Receptor

BASW - Bank Swallows
BEKI - Belted Kingfishers
BAEA - Bald Eagles

620+00
610+00
600+00
590+00
580+00
570+00
560+00
550+00
540+00
530+00
520+00
510+00
500+00
490+00
480+00
470+00
460+00
450+00
440+00
430+00
420+00

BEKI
BEKI & BASW
BEKI
BEKI
BEKI

Route 10 Bridge
(Bennett's Meadow Bridge)

Bennett Brook
Bailey Brook
Millers Brook
Ashuela Brook
Connecticut River
Roaring Brook
Otter Run
Merriam Brook
Ashuela Brook

MOUNT HERMON STATION ROAD
WARWICK ROAD
MAPLE STREET
ROUTE 10
MAIN ROAD
MILLERS FALLS ROAD
MAIN ROAD

NORTHFIELD
BERNARDSTON
GILL

Kidds Island

Map 5
Map 4
Map 3
Map 2
Map 1

FIRSTLIGHT HYDRO GENERATING COMPANY
Northfield Mountain Pumped Storage Project No. 2485
Turners Falls Hydroelectric Project No. 1889

STUDY 3.1.2

N

0 625 1,250 2,500 Feet

Figure 5.5.6-1
Sensitive Receptor Locations
Map 3

Service Layer Credits: Sources: Esri, HERE, DeLorme, USGS, Intermap, increment P Corp., NRCAN, Esri Japan, METI, Esri China (Hong Kong), Esri (Thailand), MapmyIndia, © OpenStreetMap contributors, and the GIS User Community
Source: Esri, DigitalGlobe, GeoEye, Earthstar Geographics, CNES/Airbus DS, USDA, USGS, AEX, Getmapping, Aerogrid, IGN, IGP, swisstopo, and the GIS User Community

Path: W:\gis\studies\3_1_2\maps\final_report\figure_5_5_6-1.mxd

Legend

- 1000' River Marker
- 500' River Marker

Sensitive Receptor

BASW - Bank Swallows
BEKI - Belted Kingfishers
BAEA - Bald Eagles

HINSDALE
VERNON
VERMONT
MASSACHUSETTS
WINCHESTER
NEW HAMPSHIRE
MASSACHUSETTS
NORTHFIELD

830+00
820+00
810+00
800+00
790+00
780+00
770+00
760+00
750+00
740+00
730+00
720+00
710+00
700+00
690+00
680+00
670+00
660+00
650+00
640+00
630+00

BEKI
BEKI
BEKI
BEKI & BASW
BEKI

Newton Brook
Bottom Brook
Mallory Brook
Mill Brook
Pauchaug Brook
Louisiana Brook
Connecticut River

POND RD
FORT BRIDGMAN RD
South Parish Rd
South Scofield Mtn Rd
Bolton Rd
Bolton Woods
Northfield Rd
Staddle Hill Rd
Saczawa Dr
South Parish Rd
Gosselin Rd
Avery Cir
Walker's Ln
Conner Cir
Mine Rd
HINSDALE ROAD
WANAMAKER ROAD
WEST NORTHFIELD ROAD
MOUNT HERMON STATION ROAD
MAIN ST

Map 5
Map 4
Map 3
Map 2
Map 1

FirstLight Power Resources

N

0 625 1,250 2,500 Feet

FIRSTLIGHT HYDRO GENERATING COMPANY
Northfield Mountain Pumped Storage Project No. 2485
Turners Falls Hydroelectric Project No. 1889

STUDY 3.1.2

Figure 5.5.6-1
Sensitive Receptor Locations
Map 4

Path: W:\gis\studies\3_1_2\maps\final_report\figure_5_5_6-1.mxd

Legend

- 1000' River Marker
- 500' River Marker

Sensitive Receptor

BASW - Bank Swallows
BEKI - Belted Kingfishers
BAEA - Bald Eagles

1060+70
1060+00
1050+00
1040+00
1030+00
1020+00
1010+00
1000+00
990+00
980+00
970+00
960+00
950+00
940+00
930+00
920+00
910+00
900+00
890+00
880+00
870+00
860+00
850+00
840+00
830+00

Vernon Dam
BEKI & BASW
BAEA
BEKI & BASW
BASW
BEKI & BASW
BASW
Upper Island
BASW
BEKI
Stebbins Island
HINSDALE
VERNON
Ashuelot River
Newton Brook
Map 5
Map 4
Map 3
Map 2
Map 1

FIRSTLIGHT HYDRO GENERATING COMPANY
Northfield Mountain Pumped Storage Project No. 2485
Turners Falls Hydroelectric Project No. 1889
STUDY 3.1.2

0 625 1,250 2,500 Feet

Figure 5.5.6-1
Sensitive Receptor Locations
Map 5

Service Layer Credits: Sources: Esri, HERE, DeLorme, USGS, Intermap, increment P Corp., NRCAN, Esri Japan, METI, Esri China (Hong Kong), Esri (Thailand), MapmyIndia, © OpenStreetMap contributors, and the GIS User Community
Source: Esri, DigitalGlobe, GeoEye, Earthstar Geographics, CNES/Airbus DS, USDA, USGS, AEX, Getmapping, Aerogrid, IGN, IGP, swisstopo, and the GIS User Community

Path: W:\gis\studies\3_1_2\maps\final_report\figure_5_5_6-1.mxd

Figure 5.5.6-2: Bank swallow nests – Flagg erosion site near Kidds Island, Turners Falls Impoundment

Figure 5.5.6-3: Cattle using riverbank area along Connecticut River – Flagg erosion site near Kidds Island, Turners Falls Impoundment

Figure 5.5.6-4: Animal path from river to field, Photo 101

Figure 5.5.6-5: Animal path from river to field, Photo 109

Figure 5.5.6-6: Animal path from river to field, Photo 117

Figure 5.5.5-6-7: Animal path from river to field, Photo 119

Figure 5.5.6-8: Animal path from river to field, Photo 120

Figure 5.5.6-9: Animal path from river to field, Photo 124

Figure 5.5.6-10: Animal path from river to field, Photo 128

Figure 5.5.6-11: Animal path from river to field, Photo 130

Figure 5.5.6-12: Animal path from river to field, Photo 135

Figure 5.5.6-13: Location of Animal Paths along Field